Comprendre les périodes chaudes pendant et après la transition du Pléistocène moyen (MIS 31 et MIS 11) dans la péninsule Ibérique

Dulce Oliveira

université de BORDEAUX

THÈSE PRÉSENTÉE

POUR OBTENIR LE GRADE DE

DOCTEUR DE

L'UNIVERSITÉ DE BORDEAUX

ÉCOLE DOCTORALE: SCIENCES ET ENVIRONNEMENTS

SPÉCIALITÉ: SEDIMENTOLOGIE MARINE ET PALEOCLIMATS

Par Dulce OLIVEIRA

COMPRENDRE LES PERIODES CHAUDES PENDANT ET APRES LA TRANSITION DU PLEISTOCENE MOYEN (MIS 31 ET MIS 11) DANS LA PENINSULE IBERIQUE

Sous la direction de: María Fernanda SANCHEZ GOÑI

Soutenue le 23 Mai 2017

Membres du jury:

M. MCMANUS Jerry, Professeur, University of Columbia	Rapporteur
M. FLETCHER William, Senior Lecturer, University of Manchester	Rapporteur
Mme ABRANTES Fátima, Directrice de Recherche, Instituto Português do Mar e da Atmosfera	Examinatrice
Mme DESPRAT Stéphanie, Maître de Conférences, EPHE PSL Research University, Université de Bordeaux	Examinatrice
Mme NAUGHTON Filipa, Chargé de Recherche, Instituto Português do Mar e da Atmosfera	Co-encadrante
M. TRIGO Ricardo, Professeur/Directeur de Recherche, Instituto Dom Luiz-IDL, Universidade de Lisboa	Co-encadrant et Président du Jury
Mme SANCHEZ GOÑI María Fernanda, Professeur/Directrice d'Etudes, EPHE PSL Research University, Université de Bordeaux	Directrice de thèse

Titre: Comprendre les périodes chaudes pendant et après la transition du Pléistocène moyen (MIS 31 et MIS 11) dans la péninsule Ibérique

Résumé: L'étude des interglaciaires passés qui sont des périodes chaudes avec un volume de glace réduit comme l'interglaciaire actuel, l'Holocène, est cruciale pour comprendre le climat futur. Ce travail apporte de nouvelles informations sur le climat des interglaciaires clés, les stades isotopiques marins (MIS) 11 et 31, considérés comme des analogues au réchauffement global projeté. Une analyse pollinique des sédiments du Site IODP U1385 (marge sud-ouest ibérique) a été effectuée à haute résolution, ce qui permet de comparer directement les variations de la végétation (atmosphère) avec celles de la température des eaux de surface océaniques. Nos données montrent qu'à l'échelle orbitale, la forêt du sud-ouest de l'Europe pendant le MIS 11 est principalement influencée par la précession alors que pendant le MIS 31, malgré des valeurs de précession extrêmes, le forçage dominant est l'obliquité, favorisant une végétation moins méditerranéenne et un régime climatique tempéré. De plus, la variabilité millénaire apparaît comme une caractéristique persistante mais les épisodes de refroidissement varient en intensité et durée en fonction des conditions limites qui favorisent un forçage prédominant des hautes ou basses latitudes. Enfin, nous examinons l'expression régionale de l'Holocène et de ses analogues orbitaux, les MIS 11c et 19c dans le sud-ouest de l'Europe. Ceci révèle que l'optimum Holocène se distingue par un plus fort développement forestier et donc que les MIS 11c et 19c ne sont pas des analogues à l'Holocène pour notre zone d'étude. Grâce à une comparaison modèle-données, nous montrons aussi que la forêt interglaciaire dans cette région est principalement contrôlée par la précession en influençant les précipitations hivernales, facteur critique pour le développement de la forêt méditerranéenne, tandis que le CO_2 joue un rôle négligeable.

Mots clés: Climat interglaciaire, MIS 11, MIS 31, Analogues potentiels de l'Holocène, Végétation méditerranéenne, Analyse pollinique des archives marines.

Title: Understanding warm periods within and after the Mid Pleistocene Transition (MIS 31 and 11) in the Iberian Peninsula

Abstract: The study of past interglacials, periods of reduced ice volume like our present interglacial, the Holocene, is crucial for understanding the future climate. This work provides new insights into the intensity and climate variability of key interglacials, namely Marine Isotopic Stages (MIS) 11 and 31, considered as analogues for the projected global warming. A high resolution pollen analysis at IODP Site U1385 off SW Iberia was performed, which enables a direct comparison between atmospheric-driven vegetation changes and sea surface temperature variability. At orbital timescale, this thesis shows that the dominant orbital forcing on the SW European forest was different between the interglacials of the 100-ky (MIS 11) and 41-ky (MIS 31) worlds. While during MIS 11 its weak precessional forcing predominates, during MIS 31 its extreme precession forcing is dwarfed by the prevailing influence of obliquity leading to a temperate climate regime as shown by a less Mediterranean character of the vegetation. This work also shows that millennial-scale variability was a pervasive feature and suggests that the different intensity and duration of the cooling events in SW Iberia was related to different atmospheric and oceanic configurations modulated by high or low-latitude forcing depending on the baseline climate states. Finally, this study examines the dominant forcing underlying the regional expression of the Holocene and its orbital analogues, MIS 11c and 19c, over SW Iberia using a data-model comparison approach. This comparison reveals that the Holocene optimum stands out for its higher forest development and therefore these interglacials cannot be considered as analogues for the Holocene vegetation and climate changes in Iberia. Additionally, it shows that the SW Iberian forest dynamics during these interglacials were primarily controlled by precession through its influence on winter precipitation, which is critical for the Mediterranean forest development whereas CO_2 played a negligible role.

Keywords: Interglacial climate, MIS 11, MIS 31, Potential Holocene analogues, Mediterranean vegetation, Marine pollen analysis.

EPOC UMR 5805, Université de Bordeaux, Allée Geoffroy St Hilaire, 33615 Pessac

Para ti Gabriel

For a billion years the patient Earth amassed documents and inscribed them with signs and pictures which lay unnoticed and unused. Today, at last, they are waking up, because man has come to rouse them. Stones have begun to speak, because an ear is there to hear them. Layers become history and, released from the enchanted sleep of eternity, life's motley, never-ending dance rises out of the black depths of the past into the light of the present.

– Hans Cloos from Conversations with the Earth –

ACKNOWLEDGMENTS / AGRADECIMENTOS

This dissertation would not have been possible without the support of many people and institutions. It is a pleasure to express my sincere gratitude to all who contributed to this work and made my dream of doing this doctoral research come true…

Tudo começou com um sonho no final da licenciatura… e depois de percorrida uma longa e atribulada viagem chego a esta fase final de "weee, terminei o doutoramento!!!" Ciente de que as melhores viagens só se fazem em boa companhia, quero expressar a minha gratidão às várias pessoas e instituições que, de diferentes formas, contribuíram para a concretização deste sonho…

First, I would like to thank my exceptional team of French supervisors, Prof. Dr. Maria F. Sánchez Goñi and Dr. Stéphanie Desprat, and Portuguese co-supervisors, Dr. Filipa Naughton and Prof. Dr. Ricardo Trigo. Each of you was very important on its own way and this PhD project would not have been possible without your guidance, encouragement and friendship. Thank you all for your help through constructive comments and reviews on the numerous abstracts, presentations and manuscripts. I sincerely hope that this PhD research has been only the beginning of a series of successful collaborations.

- Merci Maria for giving me the opportunity to do my PhD in the University of Bordeaux and with the excellent "paleo" team. Merci Stéphanie for accepting me as a PhD student, even if it was not official. Maria and Stéphanie, throughout these years your enthusiasm for debating anything related to paleoclimate and your love for palynology has been truly contagious. It has been a great pleasure working with you. This PhD research would not have become a reality without your vision, teaching and much appreciated scientific and personal support.

- À Filipa e ao Dr. Ricardo Trigo, agradeço por todo o apoio e confiança depositada em mim desde o mestrado em 2011 na FCUL. As palavras serão sempre poucas para vos agradecer pela experiência e sabedoria partilhados que sempre me deixaram (e deixam!) vontade de fazer mais e melhor! Filipa, és sem dúvida uma investigadora de alma e coração e serás sempre a minha Amiga *coach*… obrigado por tudo mas principalmente por me "apresentares" os *pollens* e a *paleo*! Ao Dr. Ricardo Trigo não posso deixar de agradecer as suas observações construtivas que sempre me incentivaram a "ir mais longe" e me tanto me ajudaram na reconstrução dos padrões de circulação atmosférica.

I am deeply grateful to all members of the jury for agreeing to revise my PhD thesis and for their positive and helpful feedback and discussions in the defense. Moreover, I would like to acknowledge to all the people who worked with me on the different manuscripts of this PhD research.

Special thanks to the scientists and technicians of the Integrated Ocean Drilling Program (IODP) Expedition 339: The Mediterranean outflow, the crew of the *JOIDES Resolution* and the Bremen Core Repository staff without whom studying Site U1385 would not have been possible.

Financial support from the Fundação para a Ciência e a Tecnologia (FCT) through the doctoral grant awarded SFRH/BD/9079/2012, the project CLIMHOL (PTDC/AAC-CLI/100157/2008) and CCMAR (FCT Research Unit - UID/Multi/04326/2013) are gratefully acknowledged. Additional funding for participation in the 11th Urbino Summer School in Paleoclimatology in Italy and in several international scientific meetings was provided by the LEFE-INSU IMAGO WarmClim project, PAGES (Past Global Changes), AFEQ-CNF INQUA (Association Française pour l'Etude du Quaternaire - CNF INQUA), INQUA (International Union for Quaternary Research), APLF (Association des Palynologues de Langue Française) and ECORD (European Consortium for Ocean Research Drilling). Funds provided by the project PHC STAR MEDKO allowed my training on different lipid biomarkers from the Mediterranean cores at the University of Hanyang, South Korea.

I am indebted to my main host institutions, the University of Bordeaux and Instituto Português do Mar e da Atmosfera (IPMA, former LNEG) for providing me the opportunity to perform my PhD research in a great human and scientific environment.

- Un grand merci à toutes les membres de l'équipe paleo, l'équipe technique du laboratoire EPOC and PhD students from the Unv. of Bordeaux that somehow supported me and made my time in Bordeaux a very enjoyable one, namely: Johan, Anne-Laure, Josue, Cesar, Frédérique, Philippe, Giovanni, Ludovic, Marie-Hélène, Vicent, Melanie, Léo, Léa, Mathylde, Salomé, Coralie, Bárbara, Amna, Clement, Calypso, Anna and Melina.

- Special thanks go out to all the members of the "PhD survivors" group for their friendship, help and support. MERCI for all the nice moments during the every day lunches, breaks and several nights. My stay in Bordeaux would not have been such a great experience without you – *my best french friends* – Léo, Melanie, Léa, Salomé and Childeric.

- Um muito obrigado com carinho a todo o pessoal da Divisão de Geologia e Georecursos Marinhos do IPMA pela partilha de experiências, dúvidas, questões e saberes desde o mestrado no LNEG, e que, de alguma forma, me ajudaram a chegar ao final desta etapa do meu percurso académico. Um agradecimento especial à Dra. Fátima Abrantes, a "mentora" do nosso departamento, e a todos os que demonstraram interesse e apoiaram o meu trabalho: Teresa, Antje, Emilia, Cristina Lopes, Isabelle, Susana, Montse, Zuzia, Pedro, Ana Rodrigues, Dona Apolónia, Daniel, Warley e Cremilde.

- Muito obrigada, de coração, ao pessoal "da sala das lupas" - Andreia, Catarina, Ana, Cristina, Lélia, Sandra, Célia e Isabel - pelo constante apoio e incentivo nas diversas fases desta viagem….e por muitas outras razões que não cabem nestas breves palavras. Muito muito obrigado por tudo, sobretudo pela Amizade preciosa.

Não diretamente envolvidos no meu trabalho científico, mas naturalmente imprescindíveis no meu bem-estar, essenciais para conseguir realizar as tarefas propostas, cumprir prazos estabelecidos e terminar o meu doutoramento, quero agradecer sinceramente:

À Andreia, amiga de sempre e para sempre. Obrigada pela ininterrupta e incansável ajuda, a qualquer hora do dia e noite, quer chova ou faça sol. Sem ti, este trabalho não teria sido sequer começado! Obrigada por tudo e mais um "cadito"!!

À Celina, "irmã" construída desde infância e que me faz acreditar que as ligações e afinidades são efetivamente transversais ao tempo e à distância. Obrigada por estares sempre comigo.

À minha "família da Amadora", Alexandra, Dona Lúcia e Leandro, que partilhou e viveu comigo as angústias e alegrias deste projeto. Obrigado por todo o genuíno apoio, encorajamento, incentivo e carinho. Muito obrigada por serem tão especiais!

À minha “família de Bordéus", Roger, Claudine e os seus lindos filhos Tiago e Luís, faltam palavras para agradecer tudo o que fizeram por mim. O meu muito obrigada por me terem acolhido na vossa casa, me terem recebido tão bem e por toda a Amizade!

Um sincero obrigado a todos os meus amigos, especialmente à Lúcia, Mónica, Susana M., Ana Inglês, Dina, Ana L. e todo o pessoal do Carreira, que nunca deixaram de me incentivar e apoiar e que suportaram ao longo deste período numerosas ausências e estados de humor no mínimo duvidosos.

A todos os outros, não declarados aqui, mas que sabem que constituíram pilares importantes e decisivos em muitos momentos.

Por fim, mas não menos importantes, aqueles que estão sempre em primeiro plano, a minha família:

Na família tenho a feliz companhia dos meus queridos pais, irmã e sobrinha, pilares da minha vida, que sempre apoiaram sem restrições e de forma incondicional o meu trabalho, sentindo também que nele se projetava algo mais que um simples trabalho. Obrigado pelo suporte emocional e pela segurança que me proporcionaram ao longo de toda a minha vida. Obrigado por serem a melhor família do mundo :) OBRIGADO POR TUDO!

- tenho também a companhia da minha avó, tios e primas, que como segundos pais e irmãs são uma presença continua e profunda na minha vida. Um obrigado especial à Suzi pelo apoio a todos os níveis. Dedico, também, esta dissertação à memória do meu querido avô Joaquim que é um dos meus maiores exemplos de humildade e resistência às dificuldades.

- obrigado ainda aos meus sogros por todo o apoio que me (nos) têm dado.

A ti Marco, companheiro inigualável, tão diferente de mim e tão dedicado em ser tudo para mim, expresso o meu maior reconhecimento, que não cabe em tão poucas palavras. Obrigado por seres a âncora de toda a minha vida ao longo destes 12 anos que, oficialmente:), nos unem. Obrigado pela força, energia e amor que me transmites em todos os momentos da nossa vida. Obrigado pelo incansável apoio nas pequenas e grandes tarefas do dia-a-dia, sem o qual não teria sido possível este percurso, não só académico, mas também pessoal. Obrigado por acreditares sempre em mim e me ajudares a tornar os meus sonhos realidade. Obrigada, meu amor, por toda a tua dedicação a mim e a nosso filho.

Ao meu querido filho Gabriel, sentido essencial da minha existência, dedico este trabalho, na esperança de que consiga ser para ti um exemplo de força, determinação e de que podemos conseguir tudo, basta querer!! Não podia ter mais orgulho em ti e no que conseguiste construir na convivência diária com uma mãe muitas vezes ocupada e em muitos momentos ausente. Obrigada, meu “bebé”, por dares um novo sentido à minha vida e me relembrares diariamente o que verdadeiramente tem valor.

A todos o meu sincero e profundo OBRIGADO!

TABLE OF CONTENTS

CHAPTER 3

Unexpected weak seasonal climate in the western Mediterranean region in response to MIS 31, a high-insolation forced interglacial

Oliveira, D., Sánchez Goñi, M.F., Naughton, F., Polanco-Martínez, J.M., Jimenez-Espejo, F.J., Grimalt, J.O., Martrat, B., Voelker, A.H.L., Trigo, R., Hodell, D., Abrantes, F., Desprat, S. (2017) Quaternary Science Reviews 161, 1–17

CHAPTER 4

Unraveling the forcings controlling the magnitude and climate variability of the best orbital analogues for the present interglacial in SW Europe

Oliveira, D., Desprat, S., Yin, Q., Naughton, F., Trigo, R., Rodrigues, T., Abrantes, F., Sánchez Goñi, M.F., under review, Climate Dynamics

CHAPTER 5

REFERENCES

APPENDIX A

APPENDIX B

RÉSUMÉ / FRENCH SUMMARY

Au cours du Quaternaire, soit les derniers 2.58 millions d'années, la Terre a connu de grands changements environnementaux se traduisant par des oscillations entre périodes glaciaires et interglaciaires. Ces oscillations qui sont cycliques sont forcées à l'origine par les variations de l'insolation, dit forçage orbital, régies par les paramètres astronomiques que sont l'excentricité, la précession et l'obliquité, qui définissent la position de la Terre par rapport au Soleil. Les interglaciaires du Quaternaire sont tous des périodes chaudes comme celle dans laquelle nous vivons, l'Holocène, durant lesquelles les calottes de glace de l'hémisphère nord sont réduites. Ils sont néanmoins très variables en termes d'intensité, de durée, de variabilité millénaire et de forçage. Certains d'entre eux présentent de fortes analogies avec le réchauffement actuel et futur et leur étude pourrait apporter des informations clés permettant de distinguer les changements climatiques « naturels » de ceux d'origine anthropique durant notre interglaciaire, et évaluer comment ce dernier pourrait évoluer en l'absence de gaz à effet de serre générés par les activités humaines.

Cette thèse est dédiée à l'étude de ces périodes interglaciaires particulières afin de documenter la réponse des composantes du système climatique telles que la cryosphère, l'océan, l'atmosphère et la biosphère ainsi que leurs interactions face à un réchauffement climatique important d'origine naturelle. Notre intérêt s'est porté sur deux stades interglaciaires en particulier, le MIS (Stade Isotopique Marin) 31, situé entre 1.082 et 1.062 ka et le MIS 11, entre 425 et 374 ka, l'un se produisant pendant la Transition du Pléistocène Moyen (MPT) alors que les cycles glaciaires-interglaciaires sont encore dominés par l'obliquité (« monde de 41-ky »), et l'autre après cette transition lorsque les cycles glaciaires-interglaciaires sont dominés par l'excentricité (« monde de 100-ky » auquel appartient aussi notre interglaciaire). Au-delà d'appartenir à un monde de variabilité climatique différent, ces deux stades présentent un forçage orbital contrasté, les variations d'insolation (et précession) pendant le MIS 11 sont faibles dues à une faible excentricité alors qu'elles sont particulièrement importantes pendant le MIS 31. Lors de ces deux interglaciaires, l'ampleur du réchauffement atteint aux hautes latitudes est pourtant similaire ; elle était telle que la dénomination de « super interglaciaire » leur a été attribuée. De plus, la fonte quasi-totale des calottes groenlandaise et ouest antarctique aurait entraîné un niveau marin bien plus élevé qu'à l'heure actuelle (Pollard and DeConto, 2009; DeConto et al., 2012;

Melles et al., 2012). Cependant, l'intensité et l'extension géographique de ce réchauffement restent sujet à débat car dans d'autres régions du globe, ces interglaciaires ne se démarquent pas des autres interglaciaires du Quaternaire, sachant tout de même que l'expression régionale du MIS 31 est à ce jour très peu connue. Par ailleurs, le MIS 11 présente un autre intérêt majeur, il est considéré avec le MIS 19 (~800 ka) comme un analogue orbital de notre interglaciaire (Yin and Berger, 2012, 2015). En effet, la configuration orbitale de la Terre pendant ces trois interglaciaires présente de fortes similitudes, se traduisant par une distribution annuelle et saisonnière de l'insolation comparable. Toutefois, le couvert forestier simulé pour les latitudes subtropicales pendant le MIS 19 (Yin and Berger, 2012) ne coïncide pas avec celui observé (Sanchez Goñi et al., 2016), ce qui indique que les mécanismes contrôlant l'expression régionale du climat durant les analogues orbitaux ne sont pas encore bien contraints.

La recherche présentée dans cette thèse a premièrement pour objectif de mieux comprendre les changements de la végétation et du climat dans le sud-ouest de l'Europe, une région subtropicale particulièrement sensible au réchauffement climatique actuel surtout en terme de disponibilité en eau, pendant les interglaciaires clés que sont les MIS 31 et MIS 11. En deuxième lieu, cette recherche s'intéresse aux forçages dominants pouvant expliquer l'intensité et la variabilité climatique de ces interglaciaires aux latitudes subtropicales. Identifier les processus responsables de la variabilité climatique des MIS 11 et MIS 31 permet une nouvelle compréhension de la nature, rapidité et causes des changements climatiques passés avec des conditions climatiques de base différentes, avant et après ~1 million d'années, i.e. les cyclicités de 41- et 100-ky. Finalement, la recherche des facteurs contrôlant le climat interglaciaires dans les subtropiques se focalisera en dernier lieu sur les analogues orbitaux de l'Holocène dans le monde de 100-ky.

Cette thèse présente l'analyse pollinique à haute résolution (~ 400 ans) des sédiments du site IODP U1385, situé sur la marge Ibérique en face de l'estuaire du Tage, qui permet de reconstituer la végétation du proche continent, soit du sud-ouest de la péninsule Ibérique. L'analyse pollinique de sédiments marins permet de comparer directement, c'est-à-dire sans incertitudes chronologiques, les variations de la végétation régionale et du climat continental, avec celles de la température des eaux de surface de l'océan. Cette approche est donc un sérieux atout dans l'étude des réponses et interactions du système océan-atmosphère.

Les résultats majeurs obtenus à partir de l'analyse pollinique du site U1385 sont tout d'abord pour le MIS 11 (Oliveira et al., 2016, QR), une caractérisation des variations de la végétation et du climat dans le sud-ouest de l'Europe à l'échelle orbitale. Notre enregistrement pollinique reflète les trois phases classiques d'expansion de la forêt marquant une augmentation des températures et des précipitations, chacune étant associée à un minimum de précession. Néanmoins, le couvert forestier et en particulier le maquis méditerranéens restent limités au cours du MIS 11 probablement en réponse au faible forçage de la précession caractérisant ce stade. De plus, grâce à une résolution temporelle inédite, l'enregistrement pollinique du site U1385 révèle des oscillations marquées de la forêt tout au long du MIS 11, indiquant que des changements climatiques millénaires ont eu lieu quel que soit le volume de glace. La comparaison directe entre les changements océaniques et de la végétation a permis de mettre en évidence que l'amplitude et la durée des événements millénaires froids sur le continent sont variables et qu'ils ne sont pas toujours couplés à des variations de la température des eaux de surface. Nous montrons que cette diversité d'épisodes de refroidissement est le reflet des différents processus atmosphériques et océaniques en jeu dont le rôle varie en fonction des conditions limites et en particulier du volume de glace. Une configuration atmosphérique induisant la sécheresse dans le sud-ouest de la péninsule Ibérique sans changement simultané de la température des eaux de surface, ce qui rappelle le mode positif de l'Oscillation Nord-Atlantique (NAO), semble prévaloir lorsque le volume de glace est faible. Par contre, quand le volume de glace devient relativement élevé, les mécanismes associés à la dynamique des calottes glaciaires, tels que la perturbation de la circulation méridionale atlantique (AMOC) associée aux décharges d'icebergs et son impact sur les précipitations régionales, génèreraient des épisodes froids et secs de forte intensité et de longue durée dans le sud-ouest de l'Europe.

L'étude de la variabilité climatique entre 1100 et 1050 ka qui comprend le « super interglaciaire » du MIS 31 appartenant au « monte de 41-ky », révèle que malgré un forçage de la précession très important le réchauffement atmosphérique et des eaux de surface n'étaient pas exceptionnel dans cette région fortement sensible à la précession (Oliveira et al., 2017, QSR). En effet, l'enregistrement pollinique montre que cet intervalle se distingue par un régime tempéré et humide avec une saisonnalité réduite. Contrairement aux résultats obtenus pour le MIS11 (« monde de 100-ky ») qui montraient que bien que faible le forçage de la précession module le

développement de la forêt lors de ce stade, ici nous trouvons que le forçage dominant contrôlant l'expansion de la forêt tempérée est l'obliquité, ce paramètre favorisant une sécheresse estivale et un contraste saisonnier des précipitations moindres.

De plus, cette étude fournit pour la première fois des données qui montrent l'existence d'une variabilité atmosphérique millénaire pendant les MIS 31 et MIS 32 et le début du MIS 30. L'enregistrement pollinique U1385 atteste de nombreux déclins de la forêt reflétant une succession d'épisodes de refroidissement et de sècheresse prolongée dans le sud-ouest de la péninsule Ibérique. La comparaison directe continent-océan montre, comme pour le MIS 11, que l'expression des évènements de refroidissements suborbitaux est variable en fonction des conditions limites. Lorsque le volume de glace est plus élevé, c'est-à-dire, pendant les glaciaires MIS 32 et MIS 30, les événements de refroidissement se ressentent sur le continent et dans l'océan de surface et sont associés à une sècheresse marquée. Les épisodes les plus intenses, qui apparaissent comparables aux évènements de Heinrich de par leur empreinte climatique, sont probablement liés à une perturbation de l'AMOC associée à l'instabilité des calottes de glace. Au contraire, les déclins répétés de la forêt tempérée pendant le MIS 31 ne sont associés ni à des baisses de la température des eaux de surface sur la marge ibérique, ni à un forçage d'eau douce aux hautes latitudes. L'analyse statistique des séries temporelles révèle que les variations de la forêt tempérée pendant le MIS 31 sont marquées par une cyclicité de 6 000 ans. Cette cyclicité se retrouve dans l'insolation des basses latitudes en lien avec le quatrième harmonique de la précession, ce qui suggère un lien potentiel avec le forçage tropical. Ces résultats démontrent donc que dans le sud-ouest l'Europe les variations climatiques millénaires du MIS 31 sont modulées par le forçage des hautes ou des basses latitudes dont la prédominance dépend respectivement de l'état de base du climat glaciaire ou interglaciaire.

Dans sa dernière partie, cette thèse s'est concentrée sur les MIS 19, MIS 11 et MIS 1 qui sont des périodes présentant une configuration orbitale de la Terre semblable. Nous avons tout d'abord évalué la pertinence de considérer les MIS11c et MIS19c comme analogues de l'interglaciaire actuel dans le sud-ouest de l'Europe, puis nous avons cherché à déterminer les facteurs dominants qui contrôlent l'intensité de ces interglaciaires, en particulier en termes de végétation et précipitations, ainsi que l'évolution du climat au cours de ces périodes (Oliveira et al., under review, Clim. Dyn.). Pour cela, une comparaison modèle-données a été réalisée en

confrontant les simulations du climat régional obtenues avec le modèle LOVECLIM, avec les enregistrements climatiques atmosphériques et océaniques du site IODP U1385 pour les trois interglaciaires. Les expériences de modélisations utilisées sont des simulations « instantanées » des optima climatiques (au maximum d'insolation d'été dans l'hémisphère nord) et les simulations transitoires de l'intégralité de chaque période interglaciaire (insolation et CO_2 variant en fonction du temps).

Les reconstructions polliniques révèlent des divergences importantes entre l'optimum de forêt du MIS1 et ceux des MIS11c et MIS19c, ce qui remet en cause leur potentiel à être des analogues pour l'optimum climatique de notre interglaciaire dans le sud-ouest de l'Europe. Les enregistrements polliniques et les simulations climatiques suggèrent tous deux un couvert forestier plus faible au MIS11 qu'à l'Holocène probablement dû à des précipitations hivernales moindres, facteur critique pour le développement de la forêt dans notre zone d'étude. Bien que la configuration orbitale de la Terre pendant ces deux stades soit proche, l'insolation d'été et donc la température présentent un gradient latitudinal sensiblement plus important pendant l'optimum du MIS 11. Ce gradient a probablement induit une trajectoire plus méridionale des vents d'ouest, diminuant par conséquent la quantité des précipitations arrivant dans le sud-ouest de la péninsule Ibérique en hiver. Par contre, le maximum de forêt du MIS 19c indiqué par les données polliniques est substantiellement plus faible que celui reproduit par les simulations. Nous proposons que cette différence entre simulations et données est liée à la paramétrisation du volume de glace dans le modèle qui est fixé au niveau pré-industriel. En effet, les expériences de modélisation ne prennent pas en compte que le volume de glace était relativement plus important pendant le MIS 19, et notamment que la calotte glaciaire eurasiatique était plus étendue, alors que la taille et la localisation des calottes peuvent jouer un rôle important sur le parcours des tempêtes de l'Atlantique nord.

Finalement, la comparaison modèle-données de l'évolution de la végétation dans le sud-ouest de la péninsule Ibérique au cours de l'Holocène, du MIS 11c et du MIS 19c montre tout d'abord un accord entre simulations et données à l'exception notable de la déglaciation. Cette différence est attribuée au manque d'interactions entre la calotte glaciaire et le climat dans les expériences de modélisation qui incluent seulement un volume de glace typique des interglaciaires. Nous trouvons que l'expansion de la forêt dans le sud-ouest de la péninsule Ibérique est fortement corrélée avec des étés chauds et d'importantes précipitations d'hiver, ce

qui est principalement contrôlé par la précession, et que donc le CO_2 joue un rôle négligeable dans l'évolution de la forêt méditerranéenne.

Notre travail met en évidence une concordance entre variabilité millénaire intra-interglaciaire modélisée et observée dans le sud-ouest de la péninsule Ibérique, se traduisant par des réductions répétées de la forêt indiquant des épisodes de sécheresse hivernale sans diminution de la température des eaux de surface. Etant donné que les interactions calottes glaciaires-climat ont été négligées dans le modèle, les simulations transitoires mettent en évidence que le forçage astronomique à lui seul est suffisant pour produire la variabilité millénaire intra-interglaciaire observée. De plus, il est remarquable que la réduction la plus dramatique de la forêt qui a lieu à la fin de l'« optimum » de chaque interglaciaire lorsque le volume de glace est encore faible, soit aussi reproduite dans les expériences transitoires, même si elles présentent une tendance plus graduelle. Cette observation souligne le rôle potentiel de l'interaction entre les variabilités climatiques orbitale et millénaire dans l'amplification des réponses de la végétation et du climat. Néanmoins, une étude plus approfondie est clairement requise pour mieux comprendre cette interaction, ainsi que des expériences de modélisation considérant la configuration des calottes glaciaires et les rétroactions associées au sein du système climatique.

PREFACE

Over the last three million years, the Earth's climate system underwent repeated long-term climatic shifts between cold glacial and warm interglacial periods. These long-term climate changes were originally driven by a combination of changes in precession, obliquity and eccentricity that together determine the insolation at different latitudes and the seasonal distribution. We are presently in an interglacial, the Holocene, which started about 11.700 years ago. It is widely acknowledged that the climate is changing significantly particularly so in the last few decades and that it will be warmer in the coming century (IPCC, 2013). The predicted global warming in response to anthropogenic greenhouse gases increase is accompanied by changes of other components of the climate system that will affect people and the environment worldwide, including widespread melting of ice sheets, global sea-level rise, sea-ice cover decrease and reduced global permafrost cover. As the climate of our planet appears to be heading for high rates of climate change, whether due to natural variability or human activity, a deeper knowledge of the mechanisms that drive the Earth's climate by studying past climate changes is therefore crucial to understand the natural variability for periods stretching back beyond the instrumental record. From this perspective, it is of importance to investigate the climatic evolution of past interglacials, particularly the ones characterized by warmer climates and higher sea-levels than those of the Holocene, as they may provide decisive information about the response of the cryosphere, ocean circulation, and other components of the Earth system during our present warm climate and hopefully its future.

Marine Isotope Stage (MIS) 11 (425-374 ka), MIS 19 (790-761 ka) and MIS 31 (1.082–1.062 ka) are periods of primary interest in this regard as they are considered among the best interglacial analogues for the current interglacial and projected global warming. The levels of warmth achieved during MIS 11 and MIS 31 were so exceptional at high latitudes that they were considered as "super interglacials" (Melles et al., 2012). However, the magnitude and geographical extent of their warming remains debatable as in other regions of the world their thermal optima do not appear warmer than that of any other interglacial of the Quaternary (the past 2.6 million years). MIS 19 in turn features a similar orbital configuration than that of the Holocene resulting in a comparable distribution of annual and seasonal temperatures (Yin and Berger, 2012, 2015). Nonetheless, there is a discrepancy between the simulated forest cover for

the subtropical latitudes (Yin and Berger, 2012) and that observed (Sanchez Goñi et al., 2016a), which highlights the interest of looking at diverse climatic variables, not only temperatures, to understand the diversity of interglacials at regional scale.

The research presented in this thesis seeks first for a better understanding of the relevant mechanisms driving the orbital and suborbital vegetation and climate changes in southwestern (SW) Europe during two different worlds: MIS 11 dominated by eccentricity (100,000-year cyclicity) and the poorly known MIS 31 dominated by obliquity (41,000-year cyclicity), respectively. Secondly it aims to unravel the forcing factors controlling the magnitude and climate variability of the Holocene and its best orbital analogues (MIS 11c and MIS 19c) in the subtropical latitudes. This is attempted by performing high resolution pollen analyses that allow a direct comparison between atmospherically-driven vegetation changes and sea surface temperature variability in the same sediment sample set from the International Ocean Discovery Program (IODP) Site U1385 (Expedition 339). This site, also known as the "Shackleton Site", was recently collected on the SW Iberian margin, which is considered a prime location for tracking past climate changes and, additionally, has been identified as one of the most vulnerable region to the ongoing global climatic changes. Revealing the processes behind the climatic variability of MIS 11 and MIS 31 provides new insights on the nature, timing and causes of past climate changes under the different baseline climate states before and after ~1 million years, i.e. the 41,000 and 100,000-year cyclicity worlds, respectively. In addition, the discussion of Site U1385 paleoclimate records in the light of modelling experiments allows determining the dominant forcing and feedback mechanisms explaining the regional expression of the best orbital analogues of the Holocene.

In this manuscript, a number of fundamental concepts and an overview of the state-of-the-art of past interglacial climate are firstly given in Chapter 1, providing the starting point of the work presented in this thesis. To avoid repetition, this introduction does not include a detailed presentation of the current knowledge of each studied interglacial climate because this information is already provided within the three core chapters of this thesis (Chapter 2 to 4) that correspond to material published (or submitted) in peer-reviewed international journals. The main research questions of this PhD and central issues that will be addressed in Chapter 2, 3 and 4

follows the general overview. In the last part of this chapter, the study region, chronological framework and proxy-based methods are presented.

Chapter 2 focuses on the millennial-scale climate variability during MIS 11 and reveals that climate instabilities are a pervasive feature of MIS 11 in SW Europe, but most importantly it highlights the diverse expression of the cooling events in terms of magnitude, character and duration. We propose that this diversity is related to different atmospheric and oceanic configurations depending on the baseline climate states (Oliveira et al., 2016, QR).

Chapter 3 presents the first direct comparison between oceanic and atmospherically-driven vegetation changes in SW Iberian region between MIS 32 and early MIS 30, including the MIS 31. We show that, despite its extreme precession forcing, MIS 31 was characterized by a temperate and humid climate regime marked by weak seasonality in this region very sensitive to precession during the 100,000-year world. We find that this regional signature was likely due to the prevailing influence of obliquity in controlling the hydroclimate of subtropical latitudes. In addition, this study reveals that the different expression of the climatic instabilities during the glacials and MIS 31 interglacial probably reflect the predominance of high or low-latitude forcing, respectively, on the SW European climate variability (Oliveira et al., 2017, QSR).

In Chapter 4, we examine the vegetation and climate features of the best orbital analogues of the Holocene, i.e. MIS 11c and MIS 19c, in SW Europe and we seek to determine the controlling factors responsible for their regional climatic expression. For that, we used a model-data comparison based on snapshot and transient experiments performed with the LOVECLIM climate model and new and published terrestrial-marine climate profiles from Site U1385 (Holocene: Chapter 4, MIS 11c: Oliveira et al., 2016 and MIS 19c: Sánchez Goñi et al., 2016a). We show that MIS 11c and MIS 19c cannot be considered as straightforward analogues of the Holocene climate "optimum", which was characterized by a much larger forest extent. Our model-data comparison reveals that the differences between the three interglacial peaks and throughout the interglacials were primarily constrained by the winter hydroclimate which is in turn mainly controlled by precession whereas CO_2 played a negligible role in the subtropics forest development. Moreover, we find that the observed intra-interglacial variability and the strong forest reductions marking the end of the interglacial "optimum" is well reproduced in

climate simulations. This finding underlies the potential role of the interactions between long-term and millennial-scale climate dynamics in amplifying the climate and vegetation response (Oliveira et al., under review, Climate Dynamics).

Finally, the main conclusions and future perspectives are summarized in Chapter 5 followed by Appendix A, including the detailed percentage pollen diagrams for MIS 1, MIS 11 and MIS 31, and Appendix B presenting additional publications to which I have substantially contributed.

Chapter 1

Introduction

1. INTERGLACIAL CLIMATES

1.1 Fundamental concepts and general overview

During the Quaternary, global climate has repeatedly changed between cold glacial and warm interglacial conditions primarily due to gradual variations in insolation (e.g. Milankovitch, 1920; Shackleton and Opdyke, 1973; Berger, 1975; Hays et al., 1976; Imbrie et al., 1992; Berger and Loutre, 1994; Ruddiman, 2006). Changes in the amount of incoming solar radiation (insolation) as well as its seasonal and latitudinal distribution are controlled by oscillations in the Earth's orbital geometry modulated by three orbital parameters as first established by Milutin Milankovitch (Milankovitch, 1920, 1941) (Fig. 1):

(1) Eccentricity reflects the shape of Earth's orbit around the Sun, ranging from a quasi-circular (low eccentricity of 0.0006) to a slightly elliptical shape (high eccentricity of 0.0535) and with two periodicities of about 100 and 400 thousands of years (hereafter ky) (Berger and Loutre, 1992; Berger and Loutre, 2004). The eccentricity is the only parameter that changes the mean insolation received globally and annually by the Earth (Berger, 1975).

(2) Obliquity refers to the tilt of Earth's rotation axis relative to a perpendicular to the orbital plane, varying from 22° to 24.5° (current value of ~23.5°) with a periodicity of about 41 ky (Berger and Loutre, 2004). It determines the distribution of insolation between the summer and winter season with a symmetric impact in both hemispheres. Fluctuations in obliquity have less influence at low-latitudes as the strength of its effect decline towards the equator (e.g. Buchdahl, 1999; Berger et al., 2010).

(3) Precession of the equinoxes (change in the orientation of the Earth's rotational axis) is modulated by eccentricity, which splits the precession into two periods of about 23 ky and 19 ky, leading to an average period of 21 ky (Berger, 2001; Berger and Loutre, 2004). This cycle has two components: an axial precession, caused by the gravitational forces exerted on Earth of all other planetary bodies in our solar system, and an elliptical precession, in which the elliptical orbit of the Earth itself rotates about one focus (Buchdahl, 1999). Changes in axial precession modify the times of perihelion and aphelion, and consequently increase the seasonal contrast in one hemisphere and decrease in the other hemisphere. The hemisphere at perihelion experiences an increase in summer solar radiation and a cooler winter, while the opposite hemisphere will have a warmer winter and a cooler summer. Presently, the Earth is

at perihelion in the northern hemisphere (hereafter NH) winter, which makes the winters and summers less severe in this region (Ruddiman, 2001).

The changes in orbital forcing drove the growth and decay of glaciers that together with other feedback processes (e.g. greenhouse gases (GHG), albedo) gave rise to glacial-interglacial (G-I) cycles (Fig. 1). These cycles were clearly observed not only in the records of benthic foraminifera oxygen isotope ratio ($\delta^{18}O$) (e.g. Emiliani, 1955; Shackleton and Opdyke, 1973; Hays et al., 1976; Lisiecki and Raymo, 2005) but also in an extensive range of marine, ice core, lacustrine and terrestrial archives all around the world. Shackleton (1967) demonstrated, based on the $\delta^{18}O$ of benthic foraminifera curve from a deep-sea core covering the last 1 million years (hereafter My), the occurrence of ice volume changes producing long periods of glacial climates during which extensive ice sheets developed (heavy $\delta^{18}O$ values) separated by temperate/warm conditions with restricted ice sheets extent (light $\delta^{18}O$ values). The $\delta^{18}O$ records were later used for stratigraphic purpose and divided into numbered marine isotope stages (MIS; G-I corresponding to even- and odd-numbers, respectively, excepting MIS 3 which is a part of the last glacial period) (Shackleton and Opdyke, 1973). Over the past decades, the chronostratigraphic framework of the Quaternary has been gradually improved based on orbitally tuned $\delta^{18}O$-stack records (e.g. Imbrie et al., 1984; Martinson et al., 1987; Shackleton et al., 1990; Bassinot et al., 1994; Lisiecki and Raymo, 2005). Correlating individual benthic profiles with a global stack, such as the LR04, is a common practice to establish a chronological framework for long marine sedimentary records. However, local deep-water temperatures and hydrography can also influence benthic $\delta^{18}O$ signals predominantly used as an indicator of global ice volume (Skinner and Shackleton, 2005). In addition, a recent work shows that global stacks neglect regional differences that can reach several thousands of years during glacial terminations possibly causing significant deviations (Lisiecki and Stern, 2016). Regional $\delta^{18}O$ stacks may, therefore, provide a better stratigraphic alignment targets than the LR04 global stack, which is older by 1-2 ky throughout the Pleistocene according to these new regional $\delta^{18}O$ tuning targets (Lisiecki and Stern, 2016).

The orbital-scale variability within the MIS may be further divided into interstadials and stadials representing secondary advances or retreats of glaciers, which are referred by the stage number followed by a substage letter (e.g. Shackleton, 1969) or number (e.g. Bassinot et al., 1994). Since the MIS substage and decimal event notation are not interchangeable, as substages refer to intervals and oxygen isotope events refer to individual points in time, a

complete and optimized scheme of substage nomenclature for the last one million years was recently proposed by Railsback et al. (2015) for use henceforth in palaeoclimate studies.

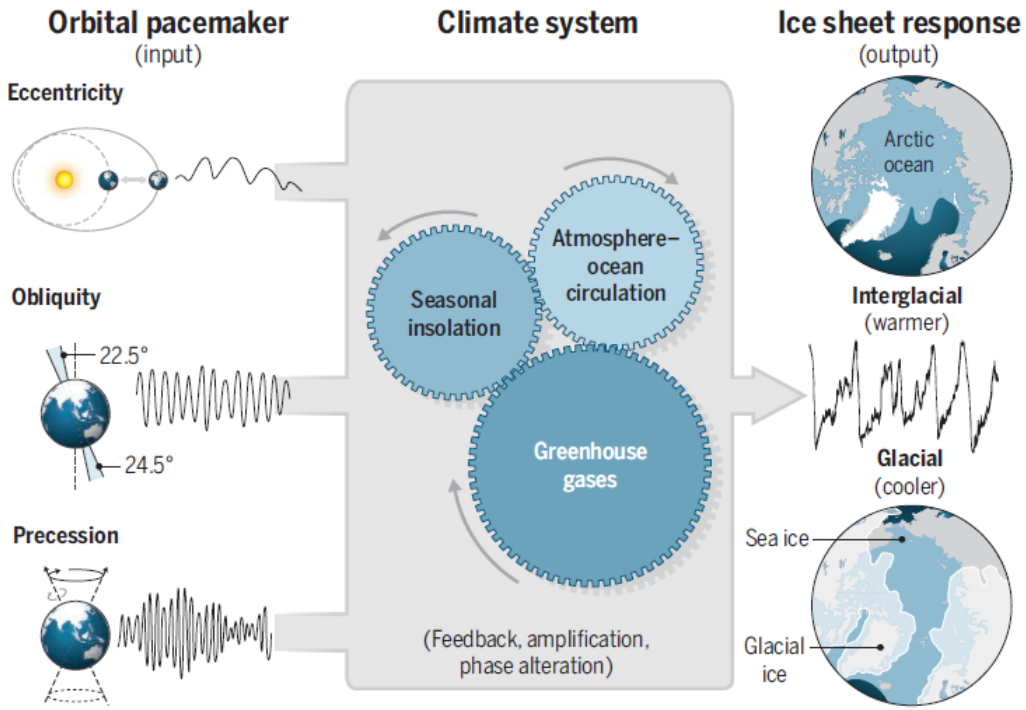

Fig. 1. Schematic representation of the "Pacemaker of the ice ages" mechanism of Hays, Imbrie and Shackleton (1976) that provided strong support for the Milankovitch hypothesis (from Hodell, 2016). In the pacemaker analogy, the pacemaker is the cyclic variations in Earth's orbital geometry, the heart is the climate system, and the heartbeat is the resulting G-I cycles.

It is important to note that as shown by the combination of pollen and isotope analyses in marine sediments, the ice volume and vegetation changes did not occur necessarily simultaneously (for example, regional forest conditions persisted during some intervals of northern hemisphere ice growth) (e.g. Sánchez Goñi et al., 1999; Shackleton et al., 2002, 2003). Therefore, the marine and terrestrial stage boundaries are generally not isochronous. It is also extremely important to note that the term "MIS" and "interglacial complex" is not synonymous with the term interglacial (e.g. Shackleton, 1969; Martinson et al., 1987; Tzedakis et al., 2009a). The term "interglacial" was initially developed based on pollen stratigraphy in western and central Europe and North America to refer to a climate episode at least as warm as the Holocene that allowed the expansion of temperate deciduous forest (e.g. Fairbridge, 1972; Turner, 1970; West, 1984; Gibbard and West, 2000). However, the term "interglacial" has been loosely defined due to the large number of different approaches and criteria used. A review by the Past Interglacials working group of PAGES (2016) recently

forward a working definition of interglacial for the last 800 ky that may be more objectively applied. Based on sea-level close to present, an interglacial would correspond to the interval of minima continental ice volume with a distribution of NH ice similar to the present (0 ± 20 m), i.e. there was litle NH ice outside Greenland, with periods of higher ice volume (~ 50 m below present sea-level) before and after the interglacial period (Past Interglacials working group of PAGES, 2016). This often ends up with the interglacial being the MIS substage after deglaciation, as observed by isotopic minimum, sea-level high stand and/or less positive seawater $\delta^{18}O$. However, the paucity of archives that are currently available hamper the validation of this working definition and, therefore, an accurate and consistent identification of the interglacials intervals (Past Interglacials working group of PAGES, 2016). For simplicity's sake throughout this thesis the term interglacial is generally used to refer to the interglacial complex, i.e. the MIS, while the interglacial as defined by Past Interglacials working group of PAGES (2016) is referred to as the respective lightest $\delta^{18}O$ MIS substage (e.g. MIS 5e, 9e, 11c, 19c).

Despite the large number of studies that exists regarding the orbital variability described by Milankovitch, there is still an extensive debate about the exact contribution of orbital parameters in modulating the Earth's climate, particularly during the Mid Pleistocene Transition (MPT, 1.25-0.7 Ma, Clark et al., 2006), more recently known as the Early Middle Pleistocene Transition (Head and Gibbard, 2015). During this enigmatic transition, the Earth's climate underwent prominent changes in G-I amplitude and periodicity, from dominant symmetrical low-amplitude and high-frequency (41 ky obliquity-driven) climate cycles prior to ~900 ky to increasing long-term average global ice volume and dominant asymmetrical high amplitude and low-frequency (100 ky eccentricity-forced) climate cycles (Fig. 2), under no significant difference in the orbital forcing (e.g. Pisias and Moore, 1981; Lisiecki and Raymo, 2005; Clark et al., 2006; Elderfield et al., 2012; Head and Gibbard, 2015). The exact timing of deglaciations and glaciations, role of orbital forcing and mechanisms of the onset of the 100-ky periodicity represents a major challenge in the palaeoclimate research (Huybers 2007, 2011; Maslin and Brierley, 2015 and references therein; Tzedakis et al., 2017). Various internal processes such as ice sheet size and configuration, GHG, ocean and atmospheric dynamics and vegetation were invoked to explain the observed changes during the MPT.

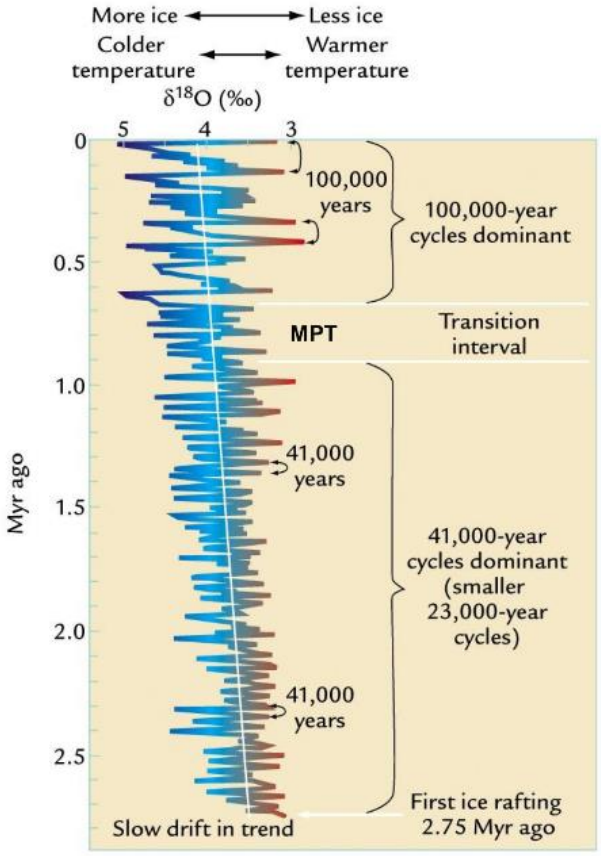

Fig. 2. Orbitally-driven 100-ky and 41-ky climatic oscillations. The North Atlantic benthic foraminiferal $\delta^{18}O$ record shows a general cooling trend in global climate together with an increase in global ice volume over the past 3 My (diagonal white line). The G-I variability changed from symmetrical low-amplitude variations during the early Pleistocene (the "41-ky world") to high-amplitude asymmetrical variations during the middle-to late Pleistocene (the "100-ky world"). MPT: Mid Pleistocene Transition. (from Ruddiman, 2001).

Interglacial climate variability over the MPT has received little attention mainly due to the scarcity of palaeoclimatic records available for this interval (Head and Gibbard, 2015 and references therein). Within the MPT, MIS 31 (~1.07 Ma) stands out as a long lasting interglacial marked by exceptional warmth in the high-latitude records (e.g. Scherer et al., 2008; DeConto et al., 2012; Melles et al., 2012; de Wet et al., 2016). The typical configuration of the ~ 100-ky G-I cycles initiates at MIS 25 (~0.95 Ma), with higher G-I contrasts occurring after this interglacial (e.g. Wright and Flower, 2002; McClymont et al., 2008; Hernández-Almeida et al., 2012, 2013). High-resolution records in the subpolar gyre (IODP Site U1314) between MIS 31 and MIS 19 provide evidence for warmer interglacials temperatures after MIS 25 and larger oscillations in the position of the Arctic Front (Hernández-Almeida et al., 2012, 2013). It is suggested that these oscillations allowed increased northward export of heat and moisture during interglacials, with MIS 21 and MIS

19 displaying substantial northward retreat of the Arctic Front, which favoured the buildup of larger ice sheets during the glacials of the MPT (Ruddiman and McIntyre, 1981; Raymo and Nisancioglu, 2003; Hernández-Almeida et al., 2013). MIS 23 is generally noted as the weakest interglacial of the MPT and interrupts the interval from MIS 24 to MIS 22 (936-866 ka), the "900 ka event" (Clark et al., 2006), marking the first long-duration glaciation of the Pleistocene and a progression to the heaviest $\delta^{18}O$ values of the MPT (e.g. Weirauch et al., 2008; Elderfield et al., 2012). In SW Europe, the small number of available pollen-based vegetation and climate reconstructions that cover the MPT lack the chronological precision and/or required time resolution to investigate in detail the regional interglacial climate variability and its relationship with records of North Atlantic (Tzedakis et al., 2006 and references therein). Yet, on the well-known Tenaghi Philippon sequence, spanning the last 1.35 My, Tzedakis et al. (2006) found that both the obliquity and precession signals persisted into the 100- and 41-kyr worlds, respectively. Other low-resolution SW European pollen studies also provide evidence of both obliquity and precession-driven changes before and across the MPT, highlighting the pervasive influence of precession on the Mediterranean climate, including during the 41-ky world (Joannin et al., 2007, 2008, 2011; Tzedakis 2007 and references therein).

During the last ~800 ky, global climate was dominated by the regular 100-ky driven symmetrical "saw-tooth" pattern of G-I changes (Fig. 2) resulting from a non-linear response of the climate system to orbital forcing (e.g. Hays et al., 1976; Imbrie et al., 1992). This time interval is well represented in marine and terrestrial sequences from a range of locations across the globe and has received a large amount of attention since the recovery of the long Antarctic ice core EPICA Dome C which extends back eight glacial cycles (~last 740 ky) (see Past Interglacials working group of PAGES, 2016 for a recent review). In addition, this period has also been the target of Earth models of intermediate complexity (EMICs) which are focused on several climate cycles and those of full Earth system models (ESMs) that consider varying boundary conditions, including the ones of recent interglacials (e.g. Yin and Berger, 2010, 2012, 2015; Ganopolski and Robinson, 2011; Herold et al., 2012; Bakker et al., 2013, 2014; Milker et al., 2013; Yin, 2013; Capron et al., 2014; Kleinen et al., 2014, 2016; Ganopolski et al., 2016).

Using the LOVECLIM model, Yin and Berger (2010, 2012, 2015) have investigated, the individual contributions of the primary forcings (insolation and GHG) to different climate-related parameters (temperature, tree fraction, sea ice) of the interglacials at the climate "optimum" and also across the entire period of each interglacial. They have found that: a) there is not a straightforward relationship between astronomical forcing and the interglacial intensity, which is not directly related to the closest precession peak or the phase of obliquity maximum and precession minimum; b) the warmest, MIS 5e and MIS 9e, and coolest, MIS 13 and MIS 17 in the high-latitudes results of the combined contribution of insolation and GHG; c) insolation (peak in boreal summer insolation) plays a dominant role on the variation of the tree fraction globally and precipitation, and in particular the North African (southern Mediterranean) tree fraction is highly correlated with precession, with GHG playing a negligible role, d) even if MIS 11 and MIS 19 are considered as the best analogues for the Holocene from an astronomical point of view, they do not show the same variations of annual and seasonal temperatures under the combined effect of the primary forcings. The major difference for MIS 11 is related to its higher GHG concentration and a slightly different insolation pattern (Ganopolski et al., 2016), which leads to a warmer interglacial than that of the Holocene and MIS 19c.

In agreement with data compilations from Lang and Wolff (2011) and Past Interglacials working group of PAGES (2016), Yin and Berger simulations (2012, 2015) also show a strong regional variability in the intensity of interglacial periods across the last 800 ky. In contrast to high-latitude locations, simulated temperatures in southern Europe appear comparable for all interglacials. Nevertheless, the tree fraction in the subtropics is simulated as highly variable from one interglacial to another, which highlights the importance of evaluating precipitation when assessing the regional expression of interglacials in lower latitudes (Yin and Berger, 2012, 2015). These model results are in line with a recent composite SST record showing that the interglacials over the last ~1 My off the Iberian Margin were characterized by similar levels of warmth with SST close to 20ºC (Rodrigues et al., 2016). However, one should keep in mind that the interglacial intensity and its regional expression have been routinely evaluated in terms of thermal regime with little attention paid to precipitation patterns. In regions with landscapes and ecosystems highly susceptible to hydrological changes, such as the Mediterranean, it is therefore crucial to consider precipitation changes. The Mediterranean region, including the SW Iberian Peninsula, has been identified as one of the most vulnerable regions to global warming (Giorgi, 2006).

Climate projections show repeated occurrence of severe drought episodes and a reduction of the mean annual precipitation in the Mediterranean area that will deeply affect the natural landscape systems (Gao and Giorgi, 2008; Solomon et al., 2009; Anav and Mariotti, 2011; Santini et al., 2014; Sousa et al., 2015; Guiot and Cramer, 2016). Future climate changes in the Mediterranean region may lead for example to the expansion of temperate evergreen broadleaved trees in zones previously occupied by temperate deciduous trees and to the collapse of the Mediterranean forest in drier zones (Anav and Mariotti, 2011; Santini et al., 2014). Yet, important biases are found in models used for simulating the Mediterranean climate and ecosystem responses to global climate change (Gao and Giorgi, 2008), which emphasizes the need to integrate proxy-based climate reconstructions in model experiments (Flato et al., 2013).

Another subject of debate in the interglacial climate research of the last 800 ky lies in the presence/absence of differences between the post-MBE (MBE: mid-Brunhes Event, between MIS 13 and MIS 11) and the pre-MBE interglacials (Yin and Berger, 2010; Lang and Wolff, 2011; Candy and McClymont, 2013; Past Interglacials working group of PAGES, 2016). Interglacial periods before this event appeared to be long and characterized by larger ice sheets, lower sea-level, cooler temperatures in Antarctica and reduced CO_2 than the more recent ones (e.g. Lambeck et al., 2002; EPICA, 2004; Bintanja et al., 2005; Lisiecki and Raymo 2005; Lüthi et al., 2008). However the expression of the MBE was neither globally or regionally uniform (Candy and McClymont, 2013; Past Interglacials working group of PAGES, 2016), being only clearly expressed in climatic variables dominated by GHG such as global annual mean temperature, but not in the ones dominated by insolation such as tree fraction and precipitation (Yin and Berger, 2010, 2012).

As far as the length of interglacials is concerned, interglacials have an overall duration ranging between ~10 and 30 ky consistent with orbital forcing timescale, with MIS 7e and MIS 11c being generally the shortest and longest, respectively (Past Interglacials working group of PAGES, 2016). Tzedakis et al. (2012a) suggested that the phasing of precession and obliquity played an important role in the persistence of interglacial conditions over one or two insolation peaks, leading to short (~13 ± 3 ky, MIS 5e, 7e, 9e, 15a and 19c) or long (~28 ± 2 ky, MIS 11c, 13a and 17) interglacials. However, estimating the interglacial duration remains problematic as it is based on the definition and identification of the interglacial onset and termination (Tzedakis et al., 2012a, b). Recently, a simple rule has been proposed based on

the combination of amount of energy integrated over the caloric summer half of the year at 65° N (obliquity) and length of previous glacial for the timing of deglaciations whether in the 41-ky or 100-ky worlds; however, the glacial inceptions were not discussed (Tzedakis et al., 2017).

Superimposed on the long-term G-I variability, the climate of the Quaternary has been characterized by global and pervasive millennial-scale climatic changes, particularly well documented for the last glacial period (Heinrich and Dansgaard-Oeschger events) and past 800 ky in a number of palaeoarchives from marine, ice core and terrestrial sequences (e.g. Dansgaard et al., 1993; Heinrich, 1988; McManus et al., 1999; EPICA, 2004; NGRIP members, 2004; Martrat et al., 2007; Hodell et al., 2008; Wang et al., 2008; Barker et al., 2011; Jouzel et al., 2007; Naafs et al., 2013; Rodrigues et al., 2016; Kawamura et al., 2017). Although the causes of these abrupt changes are not totally understood, they are tightly associated with variations in the ocean thermohaline circulation (Lynch-Stieglitz, 2017; Oppo et al., 2006), global sea-level dynamics (Siddall et al., 2003) and GHG concentration changes (Loulergue et al., 2008). It is generally accepted that millennial-scale climate variability is a recurrent feature of glacial periods and occurs regardless of 41- and 100-ky background climate states (e.g. Oppo et al., 1998; McManus et al., 1999; Weirauch et al., 2008; Hodell et al., 2013a, 2015; Barker et al., 2015; Birner et al., 2016). If the relatively subdued abrupt variability during interglacials is a clue to plausible underlying mechanisms, the extent of NH ice sheets appears as the most important forcing factor. In agreement, much of the work of the last decades has invoked critical ice sheet size thresholds and associated iceberg surges for amplifying the magnitude of cooling episodes (e.g. McManus et al., 1999; Mc Intyre et al., 2001; Wright and Flower, 2002; Grützner and Higgins, 2010; Alonso-Garcia et al., 2011; Hodell et al., 2015), even if they may not be the trigger (Barker et al., 2015). Nevertheless, a growing body of evidence shows that the current interglacial is not climatically stable and, in fact, it is punctuated by abrupt and widespread millennial-scale climatic changes (e.g. Alley and Agustsdottir, 2005; Wanner et al., 2008; Daley et al., 2011; Marcott et al., 2013).

Until recently, it was unclear if past interglacials were also prone to abrupt oscillations. However, high-resolution records from Antarctica, subtropical and subpolar North Atlantic, and northern Europe, have provided convincing evidence for the occurrence of millennial-scale climate change during interglacials periods, namely in what concerns the best studied MIS 5e, 9e, 11c, 19c, despite reduced ice caps (Oppo et al., 1998; Billups et al., 2004;

Tzedakis et al., 2004; Brauer et al., 2007; Desprat et al., 2009; Bigler et al., 2010; Koutsodendris et al., 2011; Pol et al., 2011, 2014; Ferretti et al., 2010, 2015; Sánchez Goñi et al., 2016a; Tye et al., 2016). In addition, some works have proposed that millennial cold spells, related to large and abrupt changes in the strength of the Atlantic Meridional Overturning circulation (AMOC) may have played a determinant role in the timing of the glacial inception primarily forced by astronomical changes (e.g. Tzedakis et al., 2004, 2012a, b; Past Interglacials working group of PAGES, 2016). More recently, the intra-interglacial variability has been associated to the Earth climate system's response to the harmonics of precession driven by low-latitude insolation forcing (Berger et al., 2006; Weirauch et al., 2008; Ferretti et al., 2010, 2015; Billups et al., 2011; Hernández-Almeida et al., 2012; Billups and Scheinwald, 2014), which potentially hastened the glacial inception (Sánchez Goñi et al., 2016a). Notwithstanding the recent palaeodata acquisition, further work on high-resolution palaeoclimate records is clearly needed to document intra-interglacial climate variability, its origin and the interaction with long-term orbital changes to explain G-I cycles (Hodell, 2016).

Summarizing the above, while the understanding of the interglacial climate variability during the 41-ky world remains limited, a number of studies have shown that each interglacial of the last 800 ky has been the result of a specific interplay between the distribution of incoming solar radiation, GHG concentrations and ice volume, leading to a variety of warm periods that differ in terms of intensity, character and duration (e.g. Tzedakis et al., 2009a; Lang and Wolff, 2011; Past Interglacials working group of PAGES, 2006). Nevertheless, important questions regarding the external (insolation) and internal (ice sheet, GHG, ocean and atmospheric dynamics, vegetation) processes controlling the regional expression and the magnitude of the climate optimum (warmest period), length and millennial-scale variability of past interglacials in both 100- and 41-ky worlds remain to be solved. The work presented in this thesis focuses on the climate variability of key past warm periods of the 100-ky and 41-ky worlds, the MIS 11 and MIS 31, respectively (Fig. 3), both described as "super interglacials" as they appear to have been characterized by exceptionally warm conditions at least in the western Arctic (Melles et al., 2012). Another central theme of this thesis is the regional expression of the best orbital analogues (MIS 11c and MIS 19c) (Fig. 3) for the current interglacial in SW Europe and the assessment of the major factors controlling the magnitude and evolution of the Mediterranean tree fraction and climate.

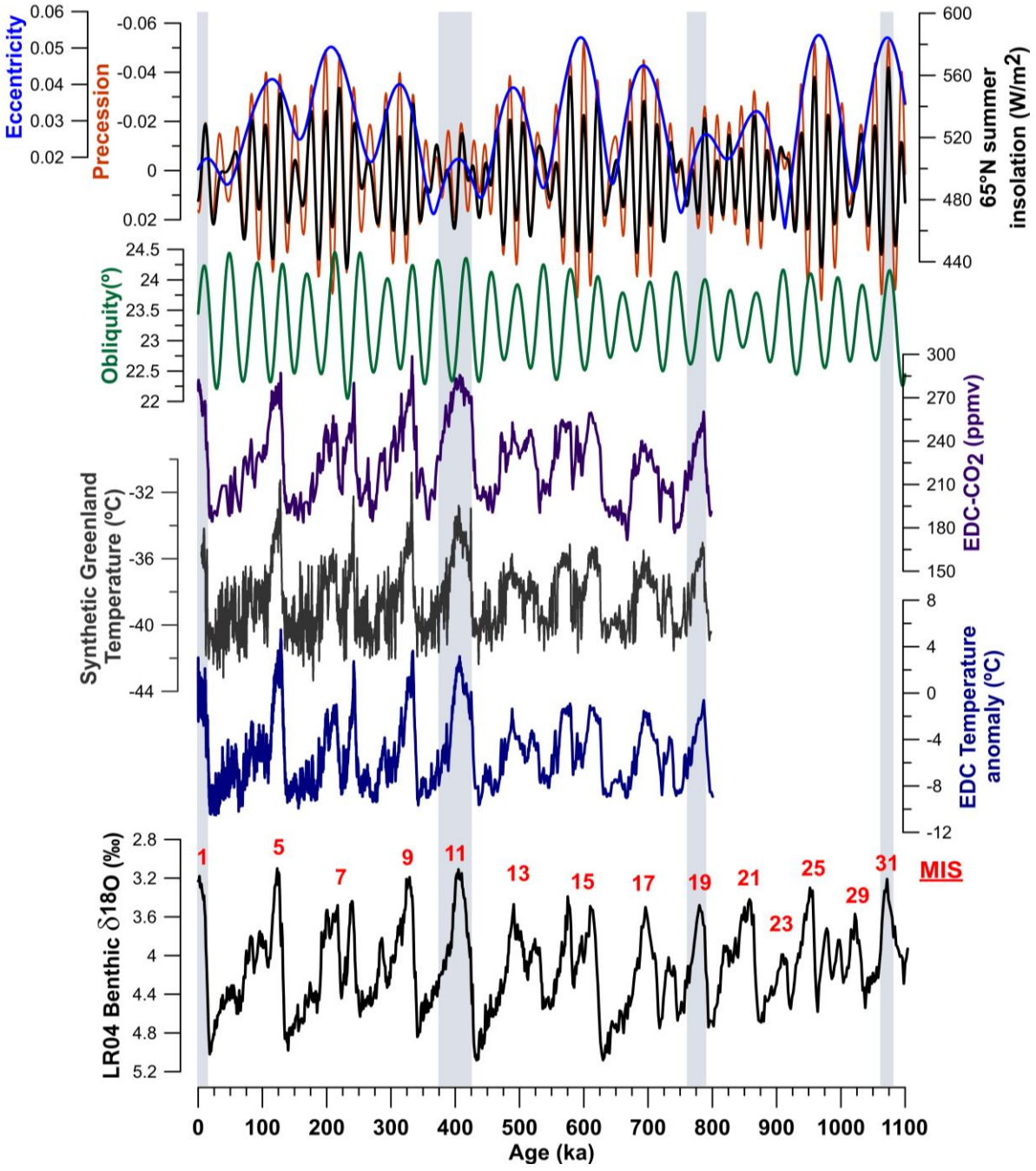

Fig. 3. From bottom to top: LR04 $\delta^{18}O$ benthic record with odd-numbered marine isotopic stages (MIS) following Lisiecki and Raymo (2005) (black); EPICA Dome C temperature anomaly (°C) (Jouzel et al., 2007) (blue); synthetic record of Greenland temperature (Barker et al., 2011) (dark grey); EPICA Dome C atmospheric CO_2 concentration (Lüthi et al., 2008) (purple); 65°N summer insolation (black), obliquity (green), precession (red) and eccentricity (blue) (Berger, 1978). The blue bars indicate the interglacials studied in this thesis, MIS 1 (MIS 1: last 14.5 ky, Holocene: last 11.7 ky following Walker et al. (2008)), MIS 11, MIS 19 and MIS 31.

MIS 11 (425-374 ka) (Lisiecki and Raymo, 2005) has been the subject of great attention in the palaeoclimate community over the past twenty years (synthesis papers and references therein: Droxler et al., 2003; Candy et al., 2014). The wealth of information available for MIS 11 is mostly due to its potential orbital analogy with our present and future climate mainly due to nearly circular orbit and damped precession and subsequent similar latitudinal and seasonal distributions of insolation (e.g. Berger and Loutre, 2002, 2003; Loutre and Berger, 2003; Yin and Berger, 2015). Consequently, a number of studies have focused on MIS 11c exceptional length as it might bring new insight into the duration of the current interglacial in the absence of anthropogenic interference (e.g. Berger and Loutre, 1996, 2002; Droxler et al., 2003; Loutre and Berger, 2003; McManus et al., 2003; EPICA, 2004; Rohling et al., 2010). Yin and Berger (2015) transient simulations have confirmed the long duration of MIS 11c and demonstrated that it is associated to the weak precession together with the nearly opposite in phase between obliquity and precession and the high CO_2 concentration. Based on the orbital analogy with MIS 11c, climate simulations have shown that the current interglacial may naturally last for more than 50 ky (Berger and Loutre, 2002). However, this analogy remains debatable primarily because it depends on which parameter is used in the orbital alignment of the two interglacials (e.g. EPICA, 2004; Ruddiman, 2005; Masson-Delmotte et al., 2006; Tzedakis, 2010). Additional key attributes highlight the importance to investigate MIS 11 palaeoclimate in the context of anthropogenic greenhouse warming, including the dominance of GHG-driven warming, potential higher than present sea-level originated from the collapse of the Greenland and West Antarctica ice sheets, prolonged interglacial conditions and evidence of intra-interglacial variability throughout MIS 11 (Candy et al., 2014 and references therein).

In terms of orbital analogues of the Holocene and its natural future, recent attention has been paid to MIS 19, characterized by weak eccentricity, like MIS 1 and MIS 11, but with an insolation distribution pattern and temperature response closest to the current interglacial than MIS 11 (e.g. Tzedakis et al., 2009a, 2012a, b; Pol et al., 2010; Rohling et al., 2010; Tzedakis, 2010; Yin and Berger, 2012, 2015; Candy et al., 2014; Giaccio et al., 2015; Ganopolski et al., 2016). Following this good analogy with MIS 19c, Tzedakis et al. (2012b) proposed that the Holocene would last 1.5 ky more under pre-industrial CO_2 concentrations. Nevertheless, a recent work also challenges this analogy based on the different millennial-scale climatic cyclicity observed throughout the two interglacials that appears to interact with the long-term variability in triggering the glacial inception (Sánchez Goñi et al., 2016a).

MIS 31 (1081-1062 ka; Lisiecki and Raymo, 2005) also represents a Quaternary interglacial of primary interest and in recent years it has become the focus of much attention from the scientific community. One of the main reasons of this interest stems from the fact that MIS 31 palaeoclimate has the potential to act as analogue of current and predicted anthropogenic warming due to evidence of extreme warmth in some critical regions such as the high-latitudes of both hemispheres (e.g. Scherer et al., 2008; Naish et al., 2009; Melles et al., 2012; Teitler et al., 2015; de Wet et al., 2016). Furthermore, it offers the opportunity to investigate the Earth's climate system during the warm periods dominated by the 41-ky obliquity periodicity within the intriguing MPT. MIS 31 was characterized by exceptionally high values of high-latitude insolation (Laskar et al., 2004) that along with high CO_2 (Tripati et al., 2011) drove the highest model-predicted eustatic sea-level rise of the early Pleistocene (~ 20 m above present, Raymo et al., 2006). Proxy-based and model studies suggest that MIS 31 extreme warmth may have triggered stronger than usual melting of both Greenland and Antarctica ice sheets (e.g. Scherer et al., 2008; Naish et al., 2009; Pollard and DeConto, 2009; DeConto et al., 2012; Melles et al., 2012; Teitler et al., 2015). In addition, recent studies from the high-latitudes indicate that the warming spanned the interval from MIS 31 to MIS 33, with MIS 32 having the character of a stadial rather than a glacial, and suggest that this interval should be re-classified as one exceptionally long interglacial (Teitler et al., 2015; de Wet et al., 2016). However, the study of MIS 31 interglacial climate remains challenging because of the scarcity and poor temporal resolution of palaeoclimatic records that are currently available apart from the ones in polar regions of the northern and southern hemispheres.

1.2 Research questions

The overview of the literature reveals that despite the extensive interglacial climate research, key questions remain to be solved, particularly at the regional-scale. This thesis aims to provide new insights into the climate variability of key Quaternary interglacials, MIS 11 and MIS 31, and the best orbital analogues (MIS 11c and MIS 19c) of the current interglacial in SW Europe, a particularly sensitive region to hydrological changes and predicted anthropogenic warming. To this end, a top-quality marine sequence, the SW Iberian margin Site U1385, was studied using a high-resolution multiproxy approach permitting the direct comparison between pollen-based vegetation and terrestrial climate and marine environmental change. This PhD project sought to answer the following research questions:

(a) What were the impacts of MIS 11 and MIS 31 climate variability on western Mediterranean climate and terrestrial environments?

(b) Were climate and vegetation changes during MIS 11 and MIS 31 imprinted by their muted and extreme orbital forcing, respectively, and also by the climate system of the 100-ky and 41-ky worlds?

(c) How were millennial-scale changes during MIS 11 and MIS 31 modulated by shifts in baseline climate states and remote controlling factors? What was the origin and frequency of the millennial-scale variability during these interglacials?

(d) Were MIS 11c and 19c good analogues of our present interglacial, the Holocene, over the SW Iberia region?

(e) What are the dominant forcing factors driving 1) the interglacial intensity, in terms of forest expansion and precipitation, of the Holocene and its potential analogues in SW Iberia; 2) the evolution of the tree fraction and climate over these specific warm periods, 3) their intra-interglacial variability?

2. MATERIAL AND ENVIRONMENTAL SETTING

2.1 IODP Site U1385 (Shackleton Site)

Scientific drilling by the IODP provides the opportunity to investigate unique palaeo-archives of climate change such as marine sediments. This thesis uses samples from the IODP Site U1385 recovered on the SW Iberian margin off the Portuguese coast during the Expedition 339 "Mediterranean Outflow" in 2011 (Expedition 339 Scientists, 2013; Hodell et al., 2013b) (Fig. 4, Table 1).

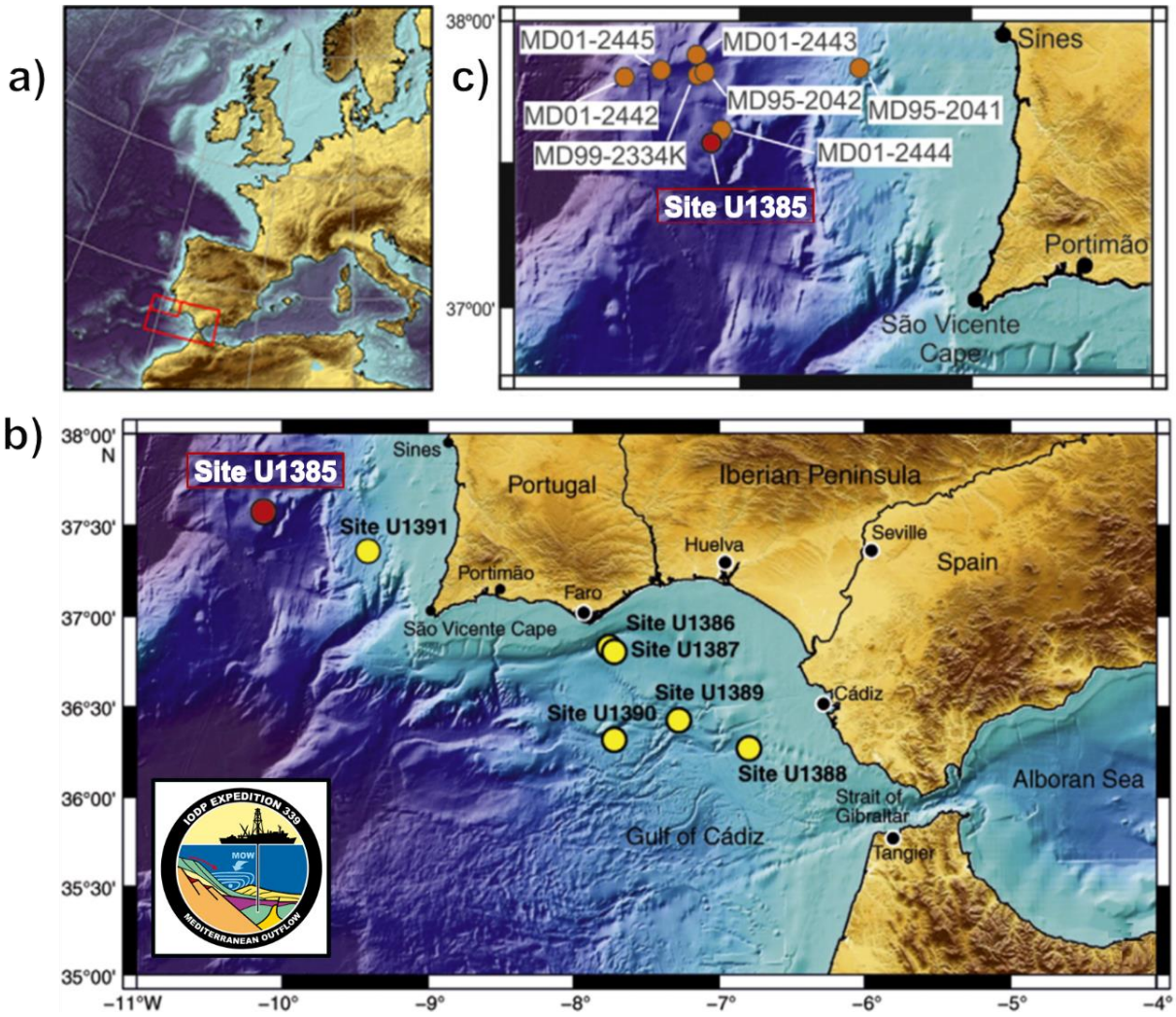

Fig. 4. Maps showing a) Target area of the IODP Expedition 339: the Gulf of Cádiz and SW Iberian margin; b) the drilled sites and the official logo (left inset); c) location of Site U1385 and the *Marion Dufresne* (MD) piston cores recovered on the SW Iberian margin (after Rodríguez-Tovar et al., 2015).

Table 1. Summary description of the studied IODP Site U1385 (Expedition 339 Scientists, 2013; Hodell et al., 2013b).

Core Ref.	IODP Site U1385
Latitude, longitude	37°34.285'N, 10°7.562' W
Expedition	IODP Expedition 339 "Mediterranean Outflow"
Ship	D/V *JOIDES Resolution*
Sampler	Advanced Piston Corer (APC)
Water depth	2578 m below sea-level (b.s.l.)
Penetration	~155.9 m below sea floor (b.s.f.)
Sediment lithology	Uniform, nannofossil muds and clays with varying proportions of biogenic carbonate and terrigenous material

Site U1385 is known as the "Shackleton Site" in honour of Nick Shackleton's seminal study on the nearby site MD95-2042 (Fig. 4), which showed the exceptional ability of the sediments from this margin to record both Greenland and Antarctica global climatic signals in a single archive (Shackleton et al., 2000, 2004). In addition, the proximity of Tagus and Sado hydrographic basins and the narrow continental shelf off Portugal (30–50 km wide) favours the rapid delivery of continental material to the deep-sea sediments, including pollen grains. Marine and terrestrial climate indicators from subtropical latitudes having a common chronology can therefore be compared without chronological ambiguities and linked with polar ice cores of both hemispheres and European terrestrial sequences (e.g. Sánchez-Goñi et al., 1999, 2000, 2008; Shackleton et al., 2000, 2003, 2004; Tzedakis et al., 2004, 2009b; Margari et al., 2010). For all these reasons, the Iberian margin has emerged as a benchmark region for the palaeoclimate research, providing reliable marine-ice-terrestrial comparisons on orbital, millennial and sub-millennial timescales. Site U1385 was drilled at the same location as core MD01-2444 and is close to a series of high-quality cores retrieved from the SW Iberian margin (Fig. 4) which have been extensively studied and have contributed to important breakthroughs in the orbital and millennial-scale variability of the last ~ 424 ky (MIS 11) (e.g. Tzedakis et al., 2004, 2009b; Vautravers and Shackleton, 2006; Martrat et al., 2007; Skinner et al., 2007; Margari et al., 2010; Voelker and de Abreu, 2011 and references therein; Hodell et al., 2013a; Channell et al., 2014). Site U1385 extends the SW Iberian margin records back to the early Pleistocene, and has the potential to become a marine reference section for Milankovitch and sub-Milankovitch climate variability and their

imprints in both terrestrial and marine ecosystems (Expedition 339 Scientists, 2013; Hodell et al., 2013b, 2015).

IODP Expedition 339 drilled five holes (A–E, 67 cores in total) at Site U1385, located on the structural high "Promontorio dos Principes de Avis" to circumvent the disturbance of sediments by turbidity currents. A total of 621.8 m of hemipelagic sediments were recovered and analyzed by core scanning XRF at 1-cm spatial resolution (Expedition 339 Scientists, 2013; Hodell et al., 2013b, 2015). These data allowed a precise hole-to-hole correlation and the construction of a composite spliced stratigraphic section, without gaps or disturbed intervals, to ~166.5 corrected revised meters composite depth (crmcd) that corrects for squeezing and stretching in each core (Hodell et al., 2015). The low-resolution $\delta^{18}O_b$ record of Site U1385 shows a continuous Pleistocene–Holocene sequence covering the last 1.45 My (from MIS 47 to the Holocene), with an average sedimentation rate of ~11 cm/ky (Hodell et al., 2015) (see section 4.1 Chronological framework for more details).

2.2 The southwestern Iberian region

2.2.1 Climate and vegetation

The Iberian Peninsula encompasses two macrobioclimatic/biogeographic regions: the Temperate/Eurosiberian region occupying mostly the north and the northwest of the peninsula and the Mediterranean region that includes the large area of its center and south (Rivas-Martínez et al., 2004) (Fig. 5).

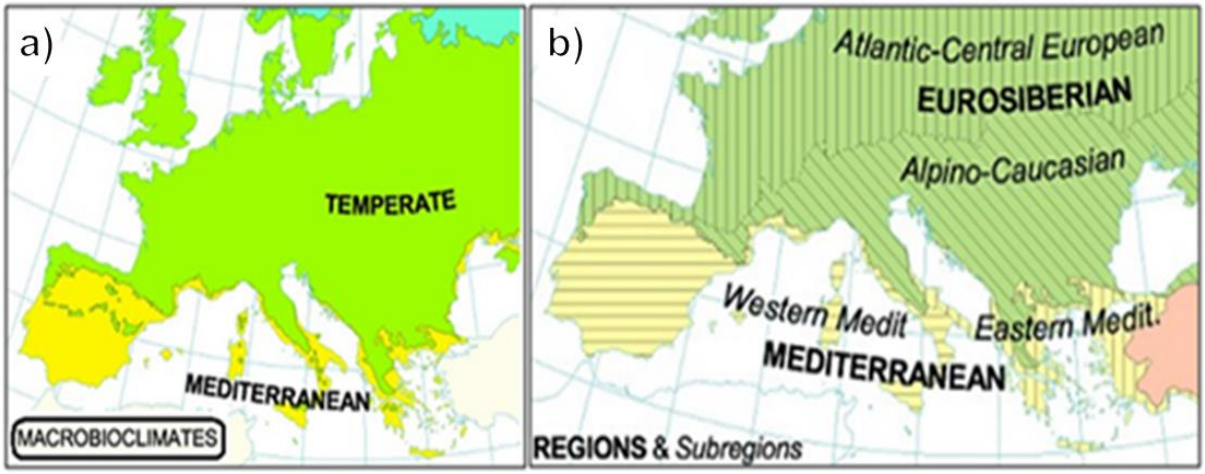

Fig. 5. Bioclimatic a) and biogeographic b) maps of Europe (from Rivas-Martínez, 2007).

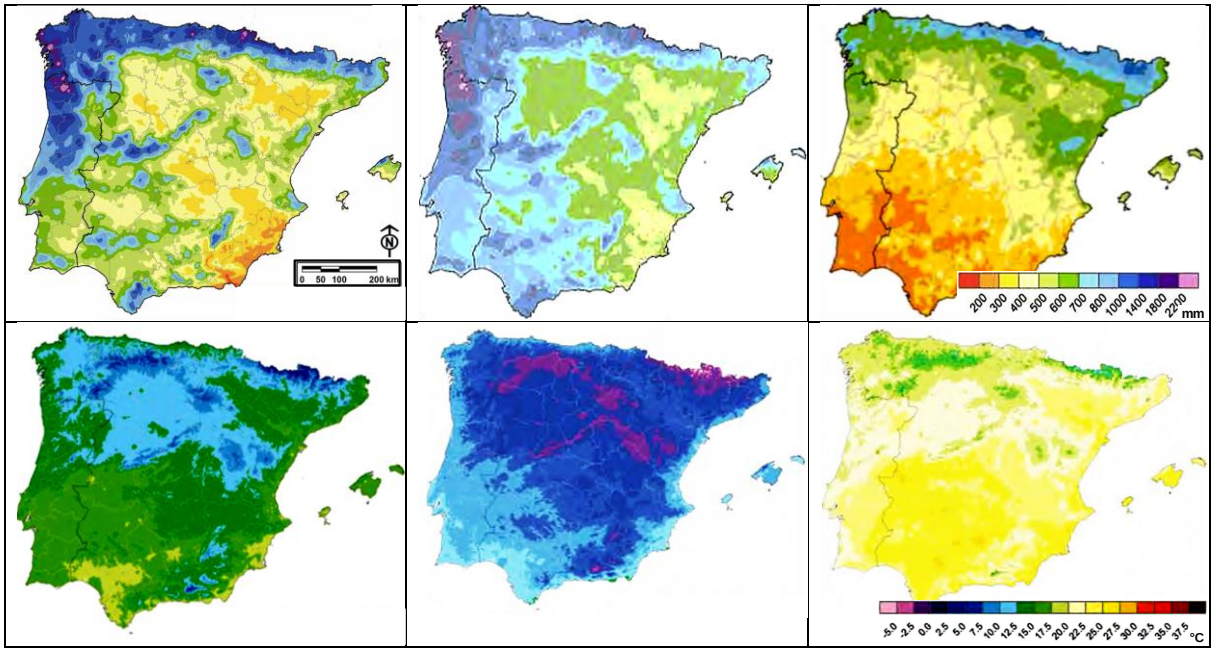

Fig. 6. Annual, coldest and warmest months average total precipitation and temperature in Iberia (1971-2000) (from Iberian Climate Atlas, 2010). Upper panel: Annual, January and August average total precipitation. Lower panel: Annual, January and August average mean temperature.

The present-day climate in SW Iberia is Mediterranean, characterized by warm, dry summers and cool, wet winters (Fig. 6). Mean annual temperature (Tann) ranges from ~17 to 13 ºC and minimal winter temperatures from 5 to -1 °C (Peinado Lorca and Martinez-Parras, 1987). The annual precipitation (Pann) is around 350-600 mm, mostly falling during the winter season (Peinado Lorca and Martinez-Parras, 1987). This characteristic climate seasonality results from the complex interactions between the subtropical and mid-latitude atmospheric circulations (Lionello et al., 2006). While in summer the influence of the northward expansion of the Azores high pressure system dominates, in wintertime this region is directly affected by the position and strength of the North Atlantic westerlies and associated changes in the North Atlantic Oscillation (NAO) (Hurrel, 1995; Trigo et al., 2004; Lionello et al., 2006).

It is widely accepted that NAO corresponds to the dominant mode of atmospheric circulation variability over western Europe in winter, dictating to a large extent the temperature and precipitation variability of the studied region by inducing changes in the activity of the Atlantic storm tracks (e.g. Trigo et al., 2002). This mode is related to the strength of the meridional pressure gradient along the North Atlantic sector. Generally, the NAO Index is determined by the difference between sea-level pressure measured over Iceland

and Ponta Delgada (Azores), although in recent years other stations have been proposed for the southern sector of the pattern, namely Lisbon (Hurrell, 1995) or Gibraltar (Jones et al., 1997). When the NAO is in a positive phase, the Icelandic Low and the Azores High are both enhanced causing a large wintertime meridional pressure gradient over the North Atlantic (Hurrell, 1995) (Fig. 7). In the negative NAO phase both pressure centers are weakened, i.e. weak subtropical high and weak Icelandic Low (Hurrell, 1995) (Fig. 7).

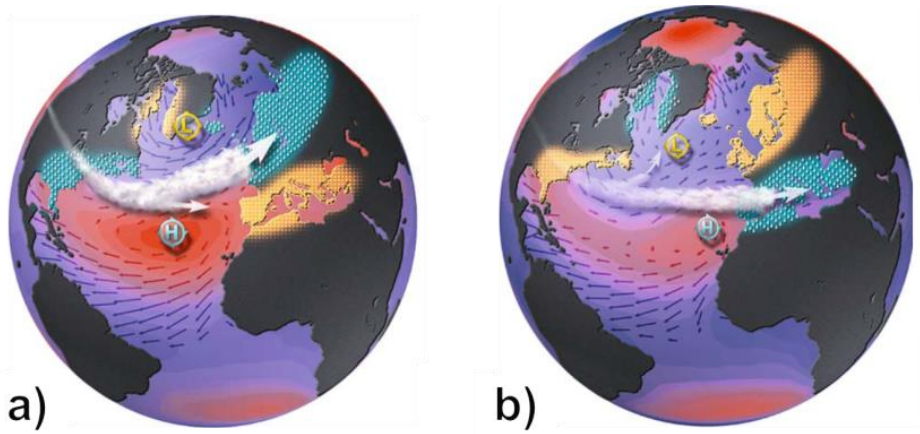

Fig. 7. The two phases of the NAO variability mode. a) Positive phase: stronger than average westerlies, mild and wet winters over N-Europe and dry conditions in the Mediterranean; b) Negative phase: weaker than average westerlies, cold and dry winters in N-Europe and rainy winters in S-Europe (from http://www.ldeo.columbia.edu/NAO by Martin Visbeck).

Fluctuations from one NAO phase to the other produce variations in the position and strength of the westerlies over the North Atlantic, seasonal mean heat and moisture transport over the ocean and the path and number of storms. They can also be responsible for important changes in ocean temperature and heat content, current patterns, and sea ice cover in the Arctic region (Trigo et al., 2002; Hurrell, et al., 2003) (Fig. 7). In western Iberia, a positive phase leads to dry winters and strong coastal upwelling along its margin, while the opposite situation generates an increase in winter precipitation (e.g. Trigo and DaCamara, 2000; Hurrell et al., 2001; Trigo et al., 2004; Abrantes et al., 2005). In addition, a remote sensing study showed that recent (1982-2002) Iberian vegetation dynamics, as estimated using the Normalised Difference Vegetation Index (NDVI), is also largely controlled by the NAO variability (Gouveia et al., 2008). This work found a significant negative correlation between the NAO values and the vegetation activity in the subsequent spring and summer seasons, which is consistent with the critical role of winter precipitation in sustaining the forest growth during the dry season through groundwater recharge (Gouveia et al., 2008, Luque-Espinar et al., 2008). Given the present-day dependence of the vegetation on winter precipitation over

the studied region (Quezel, 2002), past vegetation and climate changes may be explained, at least partly, by prolonged periods of the large-scale atmospheric circulation preferably locked into either an NAO- or NAO+ phase type circulation, i.e. changing the intensity and direction of the westerlies, over longer timescales (e.g. Fletcher et al., 2012).

The vegetation distribution and composition of SW Iberia, and most particularly of the Tagus and Sado watersheds, are closely related to orographic and maritime influences on temperature and precipitation gradients (Peinado Lorca and Martínez-Parras, 1987; Quezel, 1989; Blanco Castro et al., 1997). Thus, even though Mediterranean vegetation dominates the SW and central Iberian landscapes, floristic elements characteristic of the Eurosiberian region are found in sub-humid to humid areas (Pann: 600-1200 mm) (Blanco Castro et al., 1997).

The largest area of the studied region, situated at low altitude (<1000 m above sea-level (a.s.l.)), is currently dominated by evergreen sclerophyllous forests, consisting primarily of holm oak (*Quercus rotundifolia*) and kermes oak (*Quercus coccifera*) (Blanco Castro et al., 1997). Evergreen *Quercus* woodlands (*Quercus rotundifolia* and *Quercus coccifera*) with juniper (*Juniperus communis*) and aleppo pine (*Pinus halepensis*) are found in drier environments, mainly in the eastern part. *Quercus rotundifolia* and *Quercus suber* (cork oak) dominate in the western part with increased moisture availability, associated with some evergreen sclerophyllous plants such as *Phillyrea angustifolia* and *Pistacia terebinthus*. Scattered evergreen sclerophyllous species, such as mastic (*Pistacia lentiscus*) and olive (*Olea sylvestris*), *Phillyrea* and Cistaceae are present in the warmest areas. At mid-altitudes (700–1000 m a.s.l.), the thermal and hydrologic gradients promote the development of Eurosiberian floristic communities, mainly deciduous oak woodlands (*Quercus pyrenaica* and *Quercus faginea*) (Blanco Castro et al., 1997). Coniferous vegetation (*Pinus sylvestris, Pinus nigra* and *Juniperus communis*) occupies areas at higher altitudes (1000–2000 m a.s.l) characterized by cold winter conditions and dry summers (Peinado Lorca and Martínez-Parras, 1987). Mediterranean shrub vegetation are either dominated by heathers (Ericaceae) in zones with wet soils and higher humidity (Pann>600 mm) due to strong oceanic conditions or evergreen aromatic shrubs (Cistaceae) in drier environments (Peinado Lorca and Martínez-Parras, 1987; Loidi et al., 2007).

The distribution of the Mediterranean vegetation in SW Iberia has been affected by fire and human intervention. Olive (*Olea europea*) and introduced tree species, mostly eucalyptus (*Eucalyptus globulus*), only expanded substantially in the last centuries as a result of intense human activity (Alcara Ariza et al., 1987).

2.2.2 Oceanographic conditions

The western Iberian margin is located on the northernmost limit of the seasonal eastern North Atlantic upwelling system (Fiúza, 1984). The modern surface hydrography and coastal upwelling regime are dominated by the Portugal Current System (PCS), which is marked by distinct currents and countercurrents mainly controlled by the strength and direction of the offshore winds (Fiúza et al., 1982; Peliz et al., 2005; Ramos et al., 2013). In winter, the Azores high pressure system migrates southward and decreases in strength, leading to coastal downwelling processes and to a warm and salty surface current flowing northward along the margin, named Iberian Poleward Current (IPC) (Fiúza et al., 1982; Peliz et al., 2005) (Fig. 8). In contrast, in spring and summer as the Azores high intensifies and migrates northward, the slow southward Portugal Current (PC) develops and strong north/north-westerly winds cause upwelling and sea surface cooling (Fiúza et al., 1982; Peliz et al., 2005; Ramos et al., 2013).

Below the surface layer, the Eastern North Atlantic Central Water (ENACW) occupies the depth of the permanent thermocline (Rios et al., 1992; Fiúza et al., 1998) (Fig. 8). It is composed of two branches with different origin and thermohaline characteristics: (1) the poleward flowing ENACWst of subtropical origin, which corresponds to the subsurface component of the IPC, is formed along the Azores front during winter; (2) the equatorward flowing ENACWsp, the subsurface component of the IPC, is formed in the northern Iberian Peninsula. Since the ENACWst is lighter, relatively warmer and saltier, it overlies its subpolar counterpart. Depending on the wind strength either water mass can be upwelled.

The intermediate layer, between ~550 and 1500 m, is dominated by the warm and salty Mediterranean Outflow Water (MOW), which is formed in the Gulf of Cádiz by mixing of Mediterranean Sea with Atlantic water. Due to the mixing, the MOW forms two branches that flow northward as undercurrents (Ambar and Howe, 1979) (Fig. 8). Beneath the MOW, at a depth of ~1800 m, lies the Labrador Sea Water (LSW), the uppermost component of the North Atlantic Deep Water (NADW) (Fiuza et al., 1998) (Fig. 8). The deeper layer is occupied by the NADW, with low stratification and a high oxygen content, and the Lower Deep Water (LDW) (>4000 m) mainly composed of carbonate corrosive Antarctic Bottom Water (AABW) and Labrador Deep Water (LDW) (Fiúza, 1984) (Fig. 8).

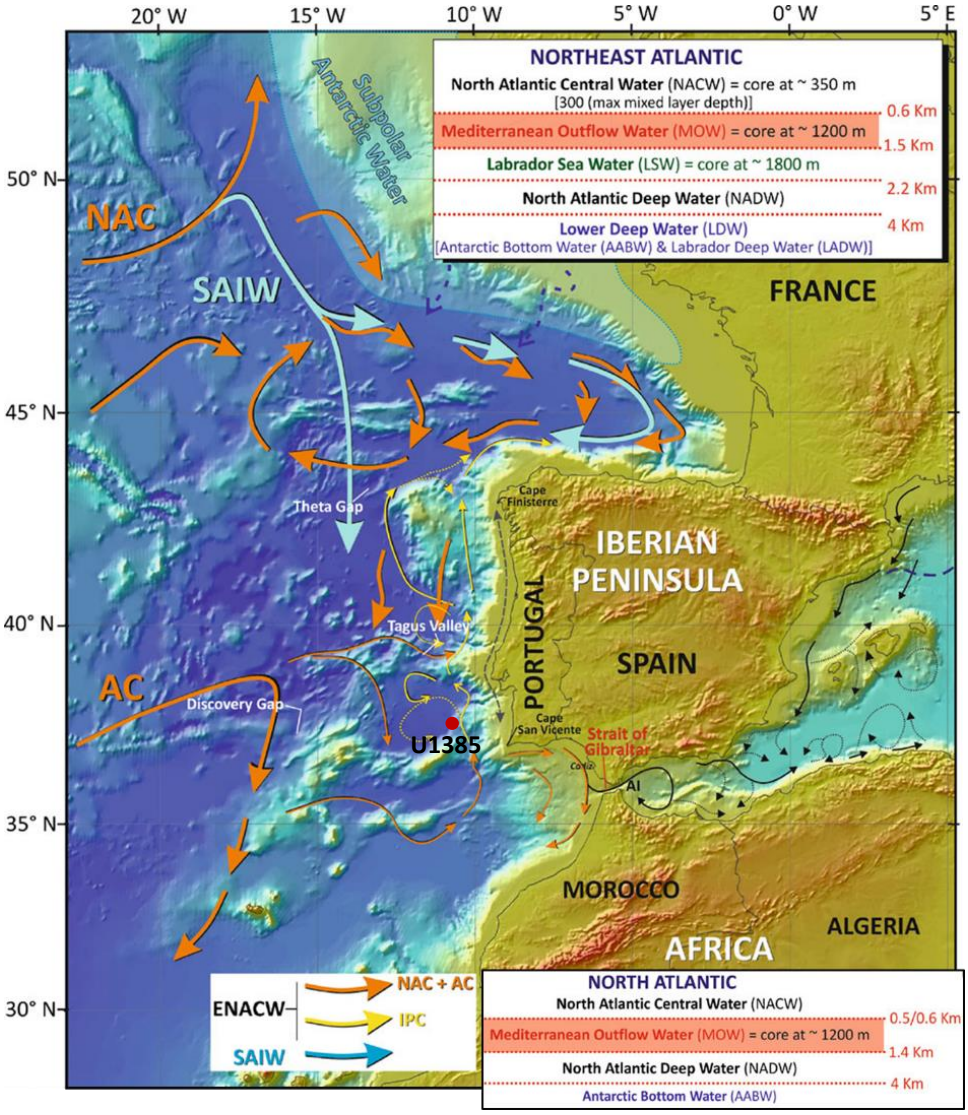

Fig. 8. Surficial water circulation off western Iberia (after Hernández-Molina et al., 2011). AC: Atlantic Current, ENACW: Eastern North Atlantic Current Water, IPC: Iberian Polar Current, NAC: North Atlantic Current, SAIW: Subarctic Intermediate Water. Red dot indicates the location of Site U1385.

At present-day, Site U1385 is located under the trajectory of the surface and subsurface PCS and ENACW (Fig. 8), which provides the opportunity to study past surface circulation variability in connection with atmospheric circulation changes. At the bottom, the site is under the influence of the NADW (Fig. 8), although during glacials and millennial-scale cold periods less ventilated southern sourced waters (AABW) were the predominant bottom waters (Duplessy et al., 1988; Martrat et al., 2007; Skinner and Elderfield, 2007).

3. METHODOLOGY

The main target of palaeoclimatology is to describe and understand Earth's climatic history through as many timescales as possible. Part of this aim can be achieved with climate indicators enclosed in the deep-sea sediments.

IPCC (2013) defined a proxy climate indicator "as a record that is interpreted, using physical and biophysical principles, to represent some combination of climate-related variations back in time". A single deep-sea sediment core can include several proxies (e.g. stable isotopes, trace elements, microfossil assemblages, magnetic and physical properties) that provide reliable and extensive climatic reconstructions with accurate stratigraphy and chronology (Cronin, 1999). These reconstructions may then be integrated with observations of Earth's modern climate to attain a longer temporal perspective. Furthermore, reconstructed time series of basic climatological variables, such as temperature, SST, precipitation can be also compared with the corresponding outputs obtained from coupled ocean-atmosphere model simulations allowing for a more robust characterization of past climate.

The backbone and strength of this thesis relies on a direct comparison between terrestrial and marine climatic indicators at Site U1385 that allows us to compare, without any chronological ambiguity, regional vegetation, precipitation regime and atmospheric and oceanic temperature variability over key past interglacials.

3.1 Chronological framework

Deep-sea sediments constitute a superb archive of palaeoclimate information as they are often undisturbed and accumulate continuously over millions of years. However, in the absence of a robust chronological framework it is inconceivable to achieve the full potential of this information. Establishing accurate timescales is required for almost all aspects of palaeoclimatology, for example to investigate the climatic response driven by external and internal forcings, to infer mechanisms of past environmental and climate changes, or to compare climate signals from different archives which allow marine-ice–terrestrial correlations.

A reference chronological framework was provided by Hodell et al. (2015) to underpin the palaeoclimate studies of Site U1385. The authors developed four depth-age models that can be used according to the goal of the scientific research:

(1) "Age_Depth_Radiocarbon" covers the last 25 ky with an average sedimentation rate of ~20 cm/ky. It is based on the correlation of the log(Ca/Ti) of Site U1385 and the weight %CaCO3 record of the nearby core MD99-2334 (Fig. 4), which has an extremely robust radiocarbon chronology (Skinner et al., 2014). The age model of the upper ~3 crmcd of Site U1385 presented in Chapter 4 was established from five newly obtained radiocarbon dates. We only used one age–depth point from the "Age_Depth_Radiocarbon" age model to constrain the lower part of the sequence (see Chapter 4 for more detail).

(2) "Age_Depth_GreenSyn" results from correlating the log(Ca/Ti) record of Site U1385 to that of nearby cores MD01-2444 and -2443 (Fig. 4) using 55 age–depth control points (Hodell et al., 2013a). This age model was not used in the thesis because it was only reconstructed for the last 400 ky.

(3) "Age_Depth_Iso" extends back to ~1.45 My with a mean sedimentation rate of 10.9 cm/ky. It is an oxygen isotope stratigraphy developed by correlating the low-resolution (20 cm) $\delta^{18}O_b$ record from Site U1385 to the most widely used Pliocene-Pleistocene benthic $\delta^{18}O$ stack, the LR04 stack of Lisiecki and Raymo (2005). Site U1385 $\delta^{18}O_b$ record presents an excellent correlation with the LR04 (Fig. 9), and all marine isotope stages were identified suggesting a complete section from MIS 1 to MIS 47. This age model was used in this thesis (Chapter 2 and 4) for studying the section of Site U1385 covering MIS 11 (50.27-56.02 crmcd).

The interval between Termination V and early MIS 11c (55.45-55.99 crmcd) is, however, marked by extremely low sedimentation rates (<1 cm/ky) which points to a brief hiatus or a small condensed section. Fourteen additional benthic foraminifera $\delta^{18}O$ measurements were performed in order to refine the LR04-derived chronology over this interval (Chapter 2). The new $\delta^{18}O_b$ data strengthened the evidence of a condensed interval/short hiatus and allowed adding two new control points to the LR04-derived age model (Chapter 2).

It is noteworthy that establishing a chronological framework for MIS 11 is not always straightforward. As stressed by some authors (e.g. Desprat et al., 2005; Candy et al., 2014 and references therein), MIS 11 has few clearly defined control points due to the weak oscillations in the benthic $\delta^{18}O$ marine records. Furthermore, the LR04 stack presents a relatively steady climatic deterioration after the MIS 11 interglacial peak, the MIS 11c substage or MIS 11.3

following the decimal event notation Bassinot et al. (1994). This hampers a clear identification of the heavy (11.22–11.24) and light isotopic events (11.23–11.1) observed in some key $\delta^{18}O$ records (e.g. Bassinot et al., 1994; Oppo et al., 1998; Rohling et al., 2009; Elderfield et al., 2012) and other climatic archives (e.g. EPICA, 2004; Desprat et al., 2005; Martrat et al., 2007; Jouzel et al., 2007; Loulergue et al., 2008; Stein et al., 2009; Prokopenko et al., 2010). The chronology in which the MIS 11 section of Site U1385 is shown in the thesis is as precise as the present $\delta^{18}O_b$ data permit. However, future high-resolution palaeoceanographic studies from U1385 may improve MIS 11 chronology and constrain the interval corresponding to the condensed section/brief hiatus.

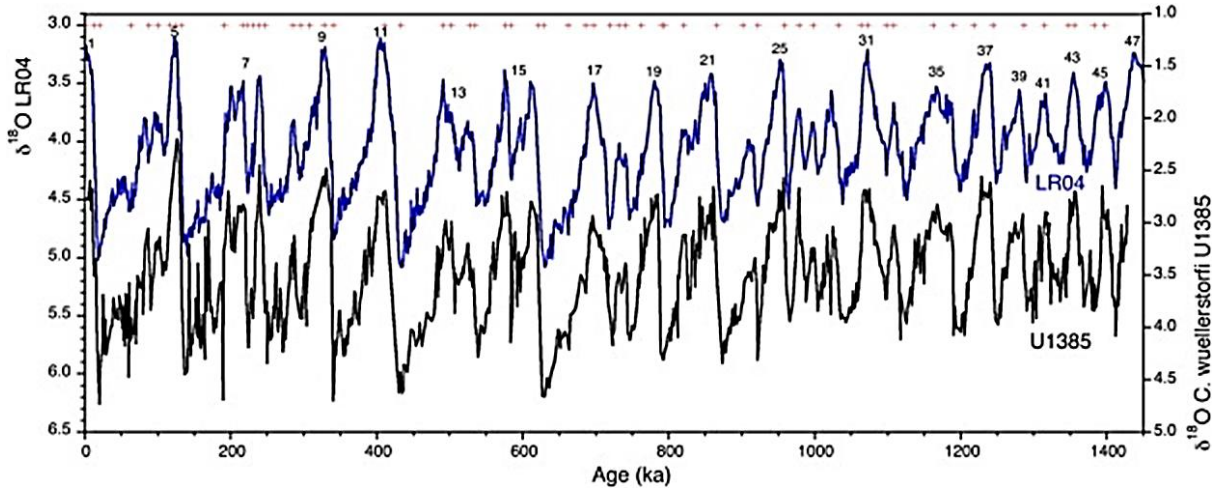

Fig. 9. Correlation of $\delta^{18}O_b$ from Site U1385 (black) with the LR04 stack (blue) of Lisiecki and Raymo (2005) (from Hodell et al., 2015). Numbers and red crosses on top indicate the marine isotope stages and age–depth control points, respectively.

(4) "Age_Depth_Tuned" is an orbitally tuned timescale established by correlating changes in sediment color (lightness - L*) of Site U1385 with precession for the past ~1.45 My. It is based on the two-fold assumption that L* is in phase with local summer insolation and lagged precession minima by 3 ky, as in the nearby and well dated MD99-2334K core (Skinner et al., 2014) (Fig. 4). The amplitude modulation of precession of the L* record in the depth domain supports the validity of the tuning process, which is reinforced by the good age model's correlation agreement with the Mediterranean sapropel cyclostratigraphy (Konijnendijk et al., 2014). Comparison with the timescales of LR04 (Lisiecki and Raymo, 2005), Site 677 (Shackleton et al., 1990), and EDC3 (Parrenin et al., 2007) also reveals a reasonable agreement within the age uncertainties (Lisiecki and Raymo, 2005).

The "Age_Depth_Tuned" age model was applied to the interval spanning MIS 31 (Chapter 3) because: (1) MIS 31 received some of the highest intensity summer insolation of the last 1.5 Ma (Laskar et al., 2004), which enables an accurate correlation between the L* record of Site U1385 and the precession. (2) Contrary to LR04 age model, obliquity was not integrated directly in the precession-tuned timescale of Site U1385, and thus it may be more appropriate to study the early Pleistocene (41-ky world) climate variability in the obliquity band (D. Hodell personal communication).

An overall good agreement was found when comparing the last three independently chronologies listed above and the revised position of polarity reversal boundaries (Hodell et al., 2015) (Fig. 10).

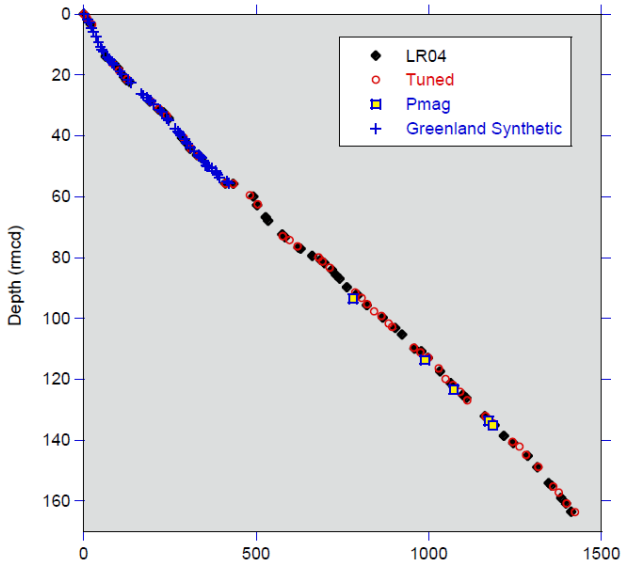

Fig. 10. Comparison of the "Age_Depth_GreenSyn", "Age_Depth_Iso" and "Age_Depth_Tuned" age models and the revised position of polarity reversal boundaries at Site U1385 (from Hodell et al., 2015).

3.2 Pollen-derived vegetation and climate changes

Pollen grains included in the marine sediments are one of the most important tools to track past vegetation and climate changes, being the main proxy-based method used in this dissertation. When comparing to terrestrial pollen records, this approach has the major advantage of providing a direct comparison between terrestrial and marine climatic indicators in the same stratigraphic level (e.g. Heusser and Balsam, 1977; Turon, 1984; Sánchez Goñi et al., 1999; Hooghiemstra et al., 1992, 2006; Tzedakis et al., 2004; Desprat et al., 2007; Naughton et al. 2007). This conjunction of terrestrial and marine indicators allows a more

accurate understanding of the interactions of the atmosphere-ocean-land systems and their impact to a given climate change within a common chronological framework. In addition, marine pollen records generally represent an integrated image of the regional vegetation rather than local, being therefore more appropriate to investigate regional climate and atmospherically-driven vegetation changes (e.g. Groot and Groot, 1966; Manten, 1966; Naughton et al., 2007).

3.2.1 Basic principles of pollen analysis

Palynology is primarily concerned with the study of pollen grains (produced by seed plants, angiosperms and gymnosperms) and spores (produced by pteridophytes, bryophytes, algae and fungi) and the subsequent reconstruction of former vegetation and environment conditions (Moore et al., 1991).

Faegri et al. (1989) describe pollen analysis as "a technique for reconstructing past vegetation by means of the pollen grains it produced". Since palynology embraces the uniformitarian principle, *the present is the key to the past*, it is reliable to use the relationship between modern pollen distribution and climate as a "guide" to understand past pollen patterns and produce palaeoclimatic reconstructions.

The vegetation reconstruction from fossil pollen spectra is based on the following general principles of pollen analysis (Birks and Birks, 1980):

- Pollen grains are abundantly produced during the natural reproductive cycle of plants.

- In the atmosphere pollen grains are mixed by atmospheric mechanisms, causing a uniform pollen rain over a certain area.

- Pollen grains are preserved in anaerobic environments (e.g. bogs, marshes, lakes, fens, ocean floor) and reflect the natural vegetation at the time of pollen deposition. Consequently, the composition of the pollen rain is a function of the vegetation composition.

- Fossil grains can be extracted from sediments and identification is possible at the level of genus or family, and may be achievable to species level.

- Pollen spectra obtained through a sediment sequence provide a picture of vegetation variability over time, which can yield information about past climatic conditions.

However, one should keep in mind that the relationship between pollen assemblages and vegetation is not direct, and interpretation must be based on comprehension of all the different factors influencing the palynological data. These factors range from pollen productivity and dispersability, source area and distance, amenability to wind dispersal, deposition and preservation until sampling and analysis of vegetation dynamics (e.g. Bradshaw and Webb, 1985; Prentice et al., 1987; Faegri et al., 1989). Nevertheless, this does not affect the pollen-vegetation relationships as the pollen tree percentages have been shown to reflect the past tree cover patterns (Williams and Jackson, 2003) and recent studies have shown that changes in vegetation composition are accurately recorded by pollen assemblages (Nieto-Lugilde et al., 2015).

3.2.2 The main features of pollen grains

Pollen grains and spores differ in their function; however, both result from cell division involving a reduction by half of the chromosomes content (meiosis) and need to be dispersed in order to carry out their functions (Moore et al., 1991).

Spores are reproductive structures that contain the necessary genetic material for dispersal and growth of plants. Pollen grains are unicellular and microscopic (10–100 µm for the European pollen flora) organs that contain the male genetic material of the angiosperms and gymnosperms; sexual reproductive success is assured only if this material reaches a female receptacle of the same plant species.

The dispersal of pollen grains to the female reproductive structure – pollination – can occur in different ways depending on the plant taxa. Most pollen is either wind-dispersed (anemophily) or insect-dispersed (entomophily) (Faegri and van der Pijl, 1979), although there are others agents of pollination such as water (hydrophily) and vertebrates (zoophily). In addition, pollen production varies with dispersal strategy; for example, anemophilous species produce much larger quantities of pollen than entomophilous ones.

Both pollen grains and spores comprise an outer layer, the exine, made of a mixture of cellulose and a complex polymer called sporopollenin. Sporopollenin is resistant to most forms of chemical (including enzymatic) and physical degradation, except oxidation (Faegri et al., 1989). As a result, pollen is well preserved in anaerobic environments and strong chemicals can be used to remove other components in laboratory.

Sculptural elements are developed in the exine, which is divided into two sublayers, the inner is the endexine and the outer is the ektexine (Faegri, 1956; Punt et al., 2007) (Fig. 11). While the ektexine consists of a basal foot layer with projecting columellae, that may be free distally (intectate) or partially connected by a tectum (semitectate); the endexine is an unstructured layer (Hesse et al., 2009). The interior wall that surrounds the cytoplasm, identified as intine, is largely composed of cellulose and other substances that are easily destroyed and thus hardly fossilized.

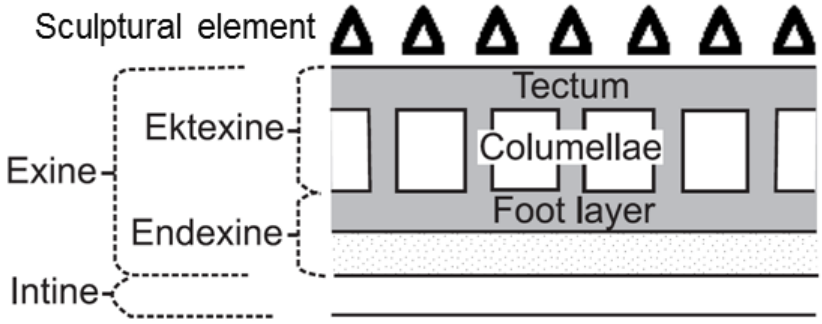

Fig. 11. Details of angiosperm pollen wall structure as defined by Faegri (1956) (after Heusser, 2005).

Pollen grains have different morphology depending on the taxa (or morphotype); therefore, they can be distinguished by their size, shape, apertures, surface sculpture and wall structure. The surface sculpture, wall structure and apertures are considered the most important features for pollen identification.

An aperture is a region of the pollen that is thinner than the remainder of the sporoderm and generally differs in ornamentation and/or in structure (Erdtman, 1947). There are two types of apertures, the pores (isodiametric apertures) and colpi (elongate or furrow aperture). Fig. 12 shows the several groups of pollen according to the number, type and position of apertures (Moore et al., 1991).

The structure (internal construction of the pollen wall) and ornamentation of the exine are also extremely important in pollen identification. LO analysis is used to detect patterns of exine organization with a light microscopy; "L" means lux/light and "O" means obscuritas/darkness (Erdtman, 1952; Punt et al., 2007). A variation of the focus allows the understanding of all the sculptural and structural elements of a pollen grain; at high focus

raised exine elements appear bright and at low focus they become dark. Fig. 13 represents the main sculpture and ornamentations forms that can be found in Palynology: psilate, verrucate, echinate, striate, reticulate, fossulate, baculate and clavate.

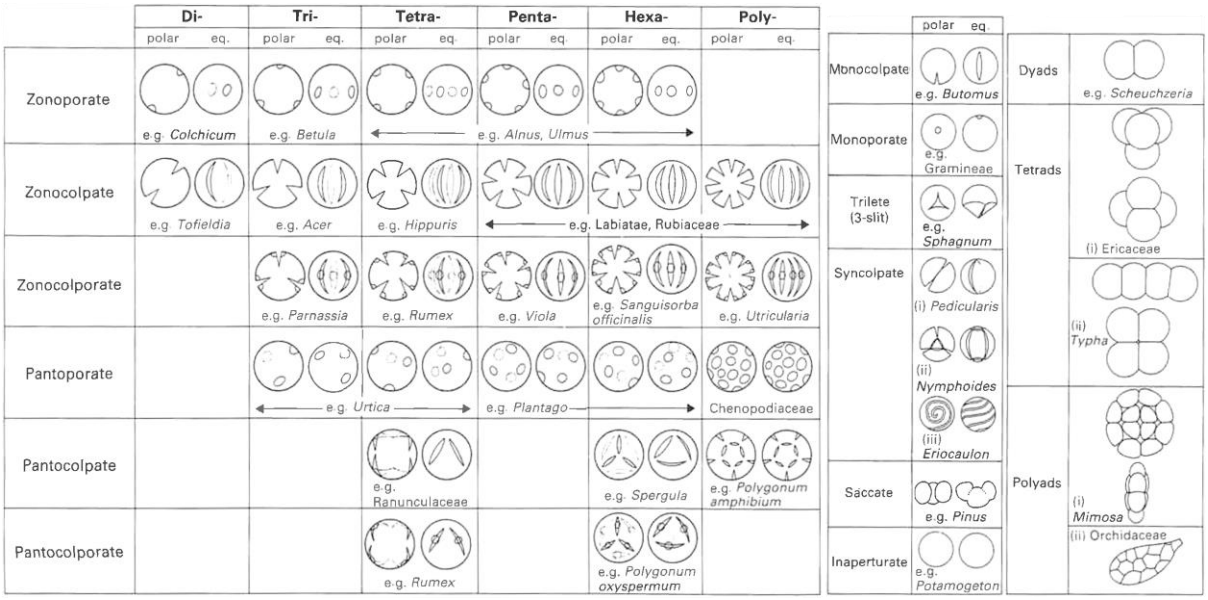

Fig. 12. Classification of pollen types according to the number, type and position of apertures (from Moore et al., 1991). Examples are shown in equatorial view (view of a pollen grain where the equatorial plane is directed towards the observer) and polar view (the polar axis is directed towards the observer).

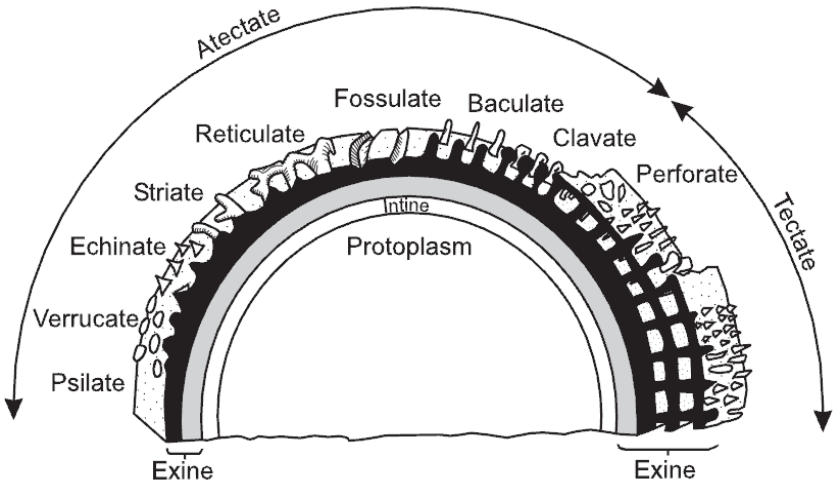

Fig. 13. Wall structure and ornamentation of angiosperm pollen (from Heusser, 2005).

3.2.3 Dispersal and source of pollen from marine sediments

There are different transport vectors for pollen to the sea depending essentially on the environmental conditions of each region (e.g. Groot and Groot, 1966; Dupont et al., 2000; Hooghiemstra et al., 2006). Arid zones with small hydrological systems, like NW of Africa, reveal a main role of wind in the pollen transfer to the marine environments (e.g. Mudie and McCarthy, 1994; Hooghiemstra et al., 2006). Other zones such as the Gulf of Guinea (Lézine and Vergnaud-Grazzini, 1993) have shown a mixture of stream- and wind-borne pollen transport. In zones with large drainage basins and prevailing offshore winds, such as western Iberian margin, pollen grains are primarily transported by rivers and streams to the sea (Naughton et al., 2007).

Once the pollen grains have entered the water column, they behave similarly to fine sedimentary particles, and processes such as flocculation, agglomeration and incorporation into fecal pellets enable pollen to settle down in the deep-sea floor (Muller, 1959; Hooghiemstra et al., 1992; Chmura and Eisma, 1995; Mudie and McCarthy, 2006). In particular, Naughton et al. (2007) has proposed that the pattern of pollen dispersion in the western Iberian margin is similar to well-known conceptual models of fine particle dynamics of this region. Nevertheless, pollen quantity and preservation in marine sequences can be influenced by several factors related to the regional/local marine environment (e.g. marine currents, oxygen content and temperature of water, sedimentary rate) and to pollen features (e.g. pollen productivities, amenability to wind dispersal, resistance to degradation) (Bottema and Van Straaten, 1966; Hooghiemstra et al., 1986). Hooghiemstra et al. (1992) have shown, however, that the velocity of settling of fine particles, including pollen, in the Atlantic water column reaches values up to 100 m per day and is not significantly affected by oceanic currents. Moreover, pollen assemblages in marine sequences are usually similar in their general trends to the pollen records of terrestrial deposits allowing a reliable correlation between both pollens signatures (e.g. Heusser and Florer, 1973; Naughton et al., 2007).

The comparison of modern marine and terrestrial pollen samples in the western Iberian region has shown that the marine pollen signature of its margin provides an integrated and regional image of the vegetation from the adjacent landmasses (Naughton et al., 2007). Present-day forest communities from the Eurosiberian and Mediterranean biogeographical zones are clearly differentiated by north and south Iberian margin pollen spectra, respectively (Naughton et al., 2007). Since the Tagus and, to a lesser extent, Sado fluvial systems are the main pollen suppliers to the SW Iberian deep-sea sediments (Naughton et al., 2007), the pollen signal of Site U1385 reflects the regional vegetation from the SW to central Iberian Peninsula.

3.2.4 Pollen analysis procedure

A total of 342 levels were sampled for pollen analysis from the sections of Site U1385 from Holes E and D covering MIS 1, MIS 11 and MIS 31 (Table 2). All the pollen samples were processed at the EPOC (UMR 5805 - University of Bordeaux, CNRS, EPHE).

Table 2. Sections of Site U1385 from Holes E and D used for the pollen analysis.

Depth interval (crmd)	0.05-2.92	50.27-56.01	120.08-125.09
Time interval (ka)	0.209-17.496	363.1-438.1	1049.9-1097.8
Sampling interval (cm)	5 to 10	2 to 4	4
Number of samples	38	170	134
Mean temporal resolution (yr)	455	447	365

Pollen concentration technique

The pollen extraction method followed standard palynological procedures described by de Vernal et al. (1996) and improved at EPOC (Desprat, 2005; detailed protocol available at http://ephe-palaeoclimat.com/ephe/Pollen%20sample%20preparation.htm:

(1) Samples of 2.5 to 5 cm^3 were washed through sieves to recover the fraction inferior to 150 μm. Sieving allows the separation of the lower fraction for the study of pollen and dinocyst while the coarse fraction can be used for the study of other proxies such as foraminifera and ice-rafted debris (IRD). The sediment of the recovered fraction was separated from the supernatant by decantation during a minimum of 48 hours.

(2) The residue was transferred into a polypropylene centrifuge tube and balanced with distilled water. After centrifugation (7 minutes at 2500 r.p.m) and decantation of the supernatant, exotic grain tablets (*Lycopodium* spores) were added to each sample. The purpose of this step is to add a known number of exotic marker grains to a known volume of sample, allowing the estimation of pollen concentration (Stockmarr, 1971). The target is to add about as much exotic as there is fossil pollen, to minimize counting effort and maximize precision of results (Maher, 1981).

(3) To remove carbonates, successive treatments with cold hydrochloric acid (HCl) at increasing strength were carried out successively; first with 10% HCl, then with 25% HCl until complete cessation of effervescence and finally with 50% HCl.

(4) To avoid pollen being obscured when mounted, it is necessary to remove silica and silicates (Moore et al., 1991). Hence, two treatments with cold hydrofluoric acid (HF) were performed, first with 45% HF and the second with 70% HF.

(5) Further two successive treatments with 25% cold HCl were used to eliminate fluorosilicates formed during treatments with HF.

(6) After rinsing, the residue was filtered using a 10 µm nylon mesh screens to recover the fraction between 10 and 150 µm (Heusser and Stock, 1984).

(7) The final residue was mounted with glycerol with phenol, which is a mobile mounting media. This method has the advantage of being optically suitable, and allowing the three-dimensional pollen grains to be rotated below the coverslip by applying a gentle pressure (Moore et al., 1991).

Pollen identification and counting

Pollen slides were observed and counted using a Nikon light microscope at 500× (oil immersion) magnification with routine use of 1000× magnification (oil immersion) for identification of pollen morphotypes. The slides were scanned along parallel equidistant lines and identifications were achieved based in morphological characters and comparison with pollen atlases (Moore et al., 1991 and Reille, 1992) and the modern reference collection available at EPOC.

Pollen grains were identified down to the lowest possible taxonomic level given their preservation. Pollen taxa (or morphotype) includes family, genus and species or a pollen morphological category (referred by suffix '-type') subsidiary to a pollen class and including pollen grains which can be recognized by distinctive characters (Punt, 1971). Since pollen grains can be damaged during the fossilization and laboratorial treatments, pollen grains that were hidden, crumpled, corroded and broken were included in indeterminable group.

A minimum of 100 pollen grains (excluding *Pinus*, *Cedrus*, aquatic plant, indeterminable pollen grains and Pteridophyta spores) and 100 *Lycopodium* grains were counted at each of the 342 levels analyzed. In addition, a minimum of 20 taxa were counted in

each sample to provide a reliable image of the vegetation community and its floristic diversity (McAndrew and King, 1976).

In this thesis, the pollen sum achieved in the pollen analysis, 100 to 166 pollen grains excluding *Pinus* in a total sporo-pollen ranging between 142 and 719 per sample, is lower than the counts usually performed for terrestrial records. However, pollen counts from marine records from the Iberian margin and Alboran Sea typically aim for a minimum of 100 pollen grains excluding *Pinus* (e.g. Sánchez Goñi et al, 1999, 2013, 2016a; Tzedakis et al., 2004, 2015; Desprat et al., 2007; Naughton et al., 2007; Fletcher and Sánchez Goñi, 2008; Combourieu-Nebout et al., 2009; Chabaud et al., 2014). Higher count size is difficult to achieve because pollen and spore concentrations are one order lower, 10^3 to 10^5 pollen grains/cc, than in terrestrial sediments. The reliability of this method was statistically demonstrated following Maher (1972) in a nearby SE Iberian marine pollen record, which found an average error of 7.9% for the calculated pollen percentage values (Fletcher and Sánchez Goñi, 2008).

Pollen percentage

The relative frequencies (pollen percentages) of different pollen types were calculated as follows:

$$\%\ \text{pollen type “Y”} = \frac{\text{nº of pollen type “Y” counted}}{\text{main sum}} \times 100$$

Results were expressed as percentages of the main sum, which corresponds to the pollen sum excluding *Pinus*, *Cedrus* and aquatic plant pollen, Pteridophyta spores and indeterminable and unknown pollen grains.

Pinus pollen was excluded from the main sum because, as expected, it was over-represented in the pollen assemblage. Pine trees produce a large amount of pollen, which is highly resistant to corrosion and oxidation and easily transported by wind, rivers or ocean currents because of its bisaccate morphology. These factors favor *Pinus* pollen over-representation in the marine sediments (Heusser and Balsam, 1977; Turon, 1984), including those from the western Iberian margin (Naughton et al., 2007). *Cedrus* (cedar) pollen was also excluded from the main sum because its abundance is suggested to reflect long-distance transportation from North Africa rather than past vegetation dynamics in western Iberia (Sánchez Goñi et al., 1999; Chabaud et al., 2014). Such an interpretation is based on the

evidence of cedar absence from Iberia during the Quaternary (Magri, 2012) and its current distribution in northern Africa in cool and moist habitats, between 1300 and 2600 m a.s.l. (Cheddadi et al., 1998).

Percentages of aquatic plant pollen and spores were calculated using the total sum including all pollen (main sum + *Cedrus* + *Pinus* + aquatics + indeterminable + unknown) and spores. *Pinus* and *Cedrus* percentages were based on the main pollen sum plus their individual counts.

Pollen diagram

Pollen data is classically displayed graphically through a vertical sequence of samples in a form of a pollen diagram. This diagram is composed of pollen spectra, expressed as relative frequencies or concentrations of the different morphotypes, from each sampled level. The pollen diagram is divided into pollen zones to obtain a pollen assemblage zone that reflects a vegetation unit or collection of units of local and/or regional significance (West, 1970). According to Birks and Birks (1980) the pollen zones can be established using qualitative fluctuations with a minimum of two curves of ecologically important taxa varying significantly. However, the definition of what constitutes a zone is a subjective concept that depends of the researcher and the purpose of the study (Tzedakis, 1994). The pollen data can be displayed through detailed and/or or synthetic pollen diagrams. While a detailed pollen diagram includes all taxa, a synthetic pollen diagram only displays selected taxa and ecological groups comprising taxa with similar modern ecological requirements (Suc, 1984).

In this dissertation, PSIMPOLL program (Bennett, 2000) was used to draw the detailed (Appendix A) and synthetic pollen percentage diagrams (Chapter 2: Fig. 2; Chapter 3: Fig. 2; Chapter 4: Fig. S1). Pollen zones were established by visual inspection based on fluctuations of at least two ecologically different morphotypes (Birks and Birks, 1980), independently of other proxy data. Identification of pollen zones was statistically confirmed using constrained hierarchical cluster analysis based on Euclidean distance between samples. Analysis of pollen percentages of morphotypes included in the main sum was performed in the R environment v. 3.1.1 (R Core Team, 2014) using the *chclust* function from package *Rioja* (Juggins, 2009).

Conventionally, the pollen diagram is arranged into groups of taxa, with arboreal types followed by non-arboreal pollen types, although the precise arrangement within any group differs subtly between the scientists (Moore et al., 1991). Following previous palynological studies off southern Iberia (e.g. Fletcher and Sánchez Goñi, 2008; Sánchez Goñi et al, 2008, 2009, 2013; Chabaud et al., 2014), the pollen taxa identified in the pollen records of Site U1385 were grouped as follows:

- Mediterranean forest (MF): All temperate tree and shrub taxa excluding *Pinus*, *Cedrus* and Cupressaceae, and Mediterranean taxa.

- Temperate trees and shrubs: *Acer*, *Alnus*, *Betula*, *Carpinus betulus*, *Castanea*, *Corylus*, *Fagus*, *Fraxinus excelsior*-type, *Hedera helix*, *Ilex*, *Juglans*, *Ligustrum*-type, *Myrica*, *Populus*, *Pterocarya*, deciduous *Quercus*-type, *Rhus*-type, *Salix*, *Quercus suber*-type; *Tilia*, *Ulex*-type, *Ulmus* and *Vitis.*

- Mediterranean taxa: *Carpinus orientalis*, *Cistus*, *Fraxinus ornus*-type, *Olea*, *Phillyrea*, *Pistacia* and evergreen *Quercus* -type.

- Semi-desert plants: *Artemisia*, Chenopodiaceae, *Ephedra fragilis*-type and *E. fragilis*-type.

3.3 Alkenone-derived sea surface temperature reconstruction

Molecular biomarkers were selected to reconstruct past oceanic hydrological conditions because the C_{37}-alkenones unsaturation index ($U^{k'}_{37}$) is considered one of the most reliable methods for estimating sea surface temperature (e.g. Eglinton et al, 2001). In addition, the value of the $U^{k'}_{37}$-SST index has been shown in the Iberian margin by a number of high-resolution studies providing important insights into past climate change on both glacial-to-interglacial and millennial timescales for the last 1 My (e.g. Bard et al., 2000; Martrat et al., 2007; Rodrigues et al., 2009, 2011, 2016).

Alkenones are highly resistant long-chain mono-ketones (C_{37-39}) synthesized by marine coccolithophorid algae, mostly the coccolithophores (single-celled phytoplankton) *Emiliania huxleyi* and *Gephyrocapsa oceanica*. The great potential of the alkenones lies in the relationship between the degree of unsaturation of the C_{37} alkenones and the temperature of the environment where these compounds were synthesized (e.g. Prahl and Wakeham, 1987). The widely used $U^{k'}_{37}$-SST index (Prahl and Wakeham, 1987) is based on the di $C_{37:2}$ and tri $C_{37:3}$ -unsatured alkenones ratio, and because of its precision (±0.5ºC) it constitutes one of the

major successes of molecular biogeochemistry research (Eglinton et al, 2001). In this thesis, the conversion of the $U^{k'}_{37}$-SST index was performed with the global core-top calibration of Müller et al. (1998) to provide an accurate reconstruction of mean annual sea surface (0 m) temperatures.

$U^{k'}_{37}$ index = $C_{37:2}$ / ($C_{37:2}$+$C_{37:3}$); Prahl and Wakeham, 1987

$U^{k'}_{37}$ = 0.033 x SST + 0.044, r=0.96; n=370; Müller et al., 1998)

Besides the alkenones used to reconstruct SSTs, the tetra-unsaturated alkenone proportion ($C_{37:4}$) relative to the total C_{37} compounds was used as a proxy for subpolar water influence following modern calibrations (Bendle and Rosell-Melé, 2004; McClymont et al., 2008) and previous work in the Iberian margin (Bard et al., 2000; Martrat et al., 2007; Rodrigues et al., 2011). High $C_{37:4}$ proportions (> 5%) have been mainly described in regions of the North Atlantic influenced by of Polar/Arctic waters and in non-marine environments (e.g. Cranwell, 1985; Rosell-Mele et al., 1998; Schulz et al., 2000). Since marine sediments normally contain negligible or very low abundances of $C_{37:4}$, high percentages of $C_{37:4}$ have been linked to cold and low salinity waters in the North Atlantic region, including the southward deflection of the subpolar front down to the Iberian margin during cold episodes (Bard et al., 2000; Martrat et al., 2007; Rodrigues et al., 2011).

Biomarker analyses of Site U1385 from the Holes E and D (Table 3) covering MIS 1 and MIS 11 were performed at the laboratory of the Division for Geology and Marine Georesources (LSM-DivGM) of IPMA (formerly LNEG, Lisbon) by T. Rodrigues. MIS 31 analyses were carried out at the Institute of Environmental Assessment and Water Research (IDAEA), Barcelona by J.O. Grimalt and B. Martrat.

Table 3. Sections of Site U1385 from Holes E and D used for the biomarker analyses.

Depth interval (crmd)	0.05-2.92	50.29-56.02	120.08-125.44
Time interval (ka)	0.209-17.496	363.2-438.6	1049.9-1100.4
Sampling interval (cm)	5 to 10	1 to 6	1 to 6
Number of samples	38	163	205
Mean temporal resolution (yr)	455	469	251

Extraction and details of the analytical methods used for the determination and purification of the alkenones in deep-sea sediments are described elsewhere (see Villanueva et al., 1997 for details). Alkenones were extracted from sediments, purified using organic solvents and quantified with Varian gas chromatographs (model 3800 at IPMA and model 450 at IDAEA) equipped with a septum programmable injector and a flame ionization detector with a CPSIL-5 CB column. Hydrogen was used as the carrier gas (2.5 ml/min). Alkenone concentrations were determined using n-hexatriacontane as an internal standard.

Chapter 2

The complexity of millennial-scale variability in southwestern Europe during MIS 11

The complexity of millennial-scale variability in southwestern Europe during MIS 11

Dulce Oliveira (1) (2) (3) (4); Stéphanie Desprat (1) (2); Teresa Rodrigues (3) (4); Filipa Naughton (3) (4); David Hodell (5); Ricardo Trigo (6); Marta Rufino (3) (4); Cristina Lopes (3) (4); Fátima Abrantes (3) (4); Maria Fernanda Sánchez Goñi (1) (2)

(1) EPHE, PSL Research University, Laboratoire Paléoclimatologie et Paléoenvironnements Marins, F-33615 Pessac, France

(2) Univ. Bordeaux, EPOC, UMR 5805, F-33615 Pessac, France

(3) Divisão de Geologia e Georecursos Marinhos, Instituto Português do Mar e da Atmosfera (IPMA), Avenida de Brasília 6, 1449-006 Lisboa, Portugal

(4) CCMAR, Centro de Ciências do Mar, Universidade do Algarve, Campus de Gambelas, 8005-139 Faro, Portugal

(5) Godwin Laboratory for Palaeoclimate Research, Department of Earth Sciences, University of Cambridge, UK

(6) Instituto Dom Luiz, Universidade de Lisboa, 1749-016 Lisboa, Portugal

Published in: QUATERNARY RESEARCH 86, 373-387 (2016)

Abstract

Climatic variability of Marine Isotope Stage (MIS) 11 is examined using a new high-resolution direct land-sea comparison from the SW Iberian margin Site U1385. This study, based on pollen and biomarker analyses, documents regional vegetation, terrestrial climate and sea surface temperature (SST) variability. Suborbital climate variability is revealed by a series of forest decline events suggesting repeated cooling and drying episodes in SW Iberia throughout MIS 11. Only the most severe events on land are coeval with SST decreases, under larger ice volume conditions. Our study shows that the diverse expression (magnitude, character and duration) of the millennial-scale cooling events in SW Europe relies on atmospheric and oceanic processes whose predominant role likely depends on baseline climate states. Repeated atmospheric shifts recalling the positive North Atlantic Oscillation mode, inducing dryness in SW Iberia without systematical SST changes, would prevail during low ice volume conditions. In contrast, disruption of the Atlantic meridional overturning circulation (AMOC), related to iceberg discharges, colder SST and increased hydrological regime, would be responsible for the coldest and driest episodes of prolonged duration in SW Europe.

Keywords: Marine Isotope Stage (MIS) 11, Iberian margin, Mediterranean vegetation, Millennial-scale climate variability, Cooling events, Land-sea comparison, Pollen analysis.

Introduction

The Mediterranean region is particularly sensitive to global climate change owing to its geographical position between the mid-latitudes and subtropical climate regimes (Giorgi, 2006; Lionello et al., 2006; IPCC, 2013). Climate projections show repeated occurrence of severe drought episodes in the Mediterranean area, including the Iberian Peninsula, which will deeply affect terrestrial ecosystems (Gao and Giorgi, 2008; Anav and Mariotti, 2011; Santini et al., 2014; Sousa et al., 2015a). During past climatic cycles, it has been demonstrated that similar recurring dry conditions led to drastic forest decline in southern Europe. However, while millennial-scale climate variability has been widely documented mainly for the last glacial period (e.g. Sánchez Goñi et al., 2000, 2008; Combourieu-Nebout et al., 2002; Fletcher and Sánchez Goñi, 2008; Naughton et al., 2009; Fletcher et al., 2010), few available records report abrupt interglacial climate variability prior to the current interglacial.

Specifically, Marine Isotope Stage (MIS) 11 (425-374 ka) represents a period of primary interest to investigate natural abrupt climate variability. Despite its potential astronomical analogy with the Holocene (Loutre and Berger, 2003) remaining complex and controversial (e.g. Tzedakis, 2010; Yin and Berger, 2012), this interglacial presents additional key features, including its higher than present-day sea-level related to the collapse of Greenland and West Antarctica ice sheets (Raymo and Mitrovica, 2012; Roberts et al., 2012; Reyes et al., 2014) and its greenhouse gas-driven climate warming (Raynaud et al., 2005; Yin and Berger, 2012.

MIS 11c generally stands out as a long, warm and relatively stable interglacial in numerous records (e.g. Oppo et al., 1998; McManus et al., 2003; Melles et al., 2012; Bauch, 2012; Milker et al., 2013; Candy et al., 2014), although few high temporal resolution records from Antarctica, subtropical and subpolar North Atlantic, and northern Europe, document pronounced abrupt climate change during MIS 11c despite reduced ice caps (Oppo et al., 1998; Billups et al., 2004; Koutsodendris et al., 2011; Pol et al., 2011; Tye et al., 2016). Comparatively, suborbital climatic variability during MIS 11b (~395-374 ka) is well-documented in records from the North Atlantic, particularly off western Iberia (de Abreu et al., 2005; Martrat et al., 2007; Stein et al., 2009; Voelker et al., 2010; Rodrigues et al., 2011; Amore et al., 2012; Hodell et al, 2013a; Palumbo et al., 2013; Marino et al., 2014; Maiorano et al., 2015). Three marked cooling episodes linked to deep ocean circulation changes and

iceberg discharges into the North Atlantic are commonly reported (e.g. Oppo et al., 1998). Yet, the amplitude of precipitation, changes in temperature and duration of the cold episodes on land associated with these abrupt changes are not well-known. In addition, phase relationship between ocean and terrestrial climatic changes remain to be assessed since air-sea decoupling was identified during some periods of ice sheet growth by European margin records (Sánchez Goñi et al., 2013; Cortina et al., 2015). So far, only two pollen records have been published in the northern and southern parts of the Iberian margin for MIS 11 (Desprat et al., 2005; Tzedakis et al., 2009). However, the temporal resolution of these records precludes a reliable assessment of the regional vegetation-based climate in response to the millennial-scale cooling throughout MIS 11.

Although millennial-scale variability is an inherent pattern of the Pleistocene climate regardless of glacial state (Oppo et al., 1998), ice sheet dynamics is one of the primary factors modulating millennial-scale cooling events. Cooling episodes in the North Atlantic associated with iceberg surges would be amplified when ice sheet size surpasses a critical threshold (McManus et al., 1999). Freshwater from melting icebergs may be responsible for the enhancement and/or prolonged duration of cold conditions through a positive feedback mechanism on AMOC (Atlantic Meridional Overturning Circulation) even if they may not be the trigger of northern stadial events (Barker et al., 2015). However, the duration and intensity of northern cold events may also rely on the background climate, such as the intensity of regional precipitation, modifying the AMOC response to freshwater forcing (Margari et al., 2010). To date, the factors modulating millennial-scale cooling of MIS 11 remain insufficiently understood.

Here we present a new high-resolution record of MIS 11 from Site U1385, also known as the "Shackleton Site", collected recently during the Integrated Ocean Drilling Program (IODP) Expedition 339. Site U1385 is located on the SW Iberian margin (Fig.1), considered as a unique and exceptional area for palaeoclimate research since Nick Shackleton's seminal study of the last climatic cycle recorded at the nearby site MD95-2042 (Shackleton et al., 2000, 2004), and the publication of the first land-sea direct comparison from the same site (Sánchez Goñi et al, 1999, 2000; Shackleton et al., 2003). We provide a detailed record of atmospherically-driven southern European vegetation changes at suborbital timescales that we directly compare with sea surface temperatures in eastern subtropical North Atlantic. Cooling

events, differing in terms of magnitude, character and duration, are discussed in the light of a larger European and North Atlantic context and global ice volume changes. In addition, we discuss the potential atmospheric and oceanic configurations behind this complexity of millennial-scale climate variability during MIS 11.

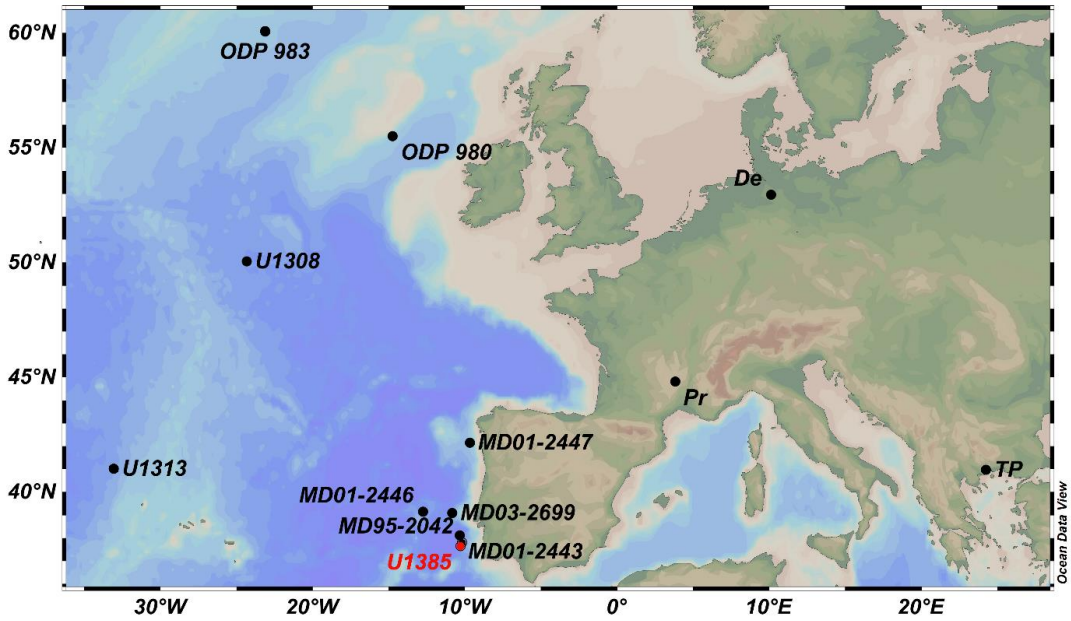

Fig. 1. Location of the IODP Site U1385 and available European and North Atlantic records discussed in the text: ODP Site 983 (Barker et al., 2015); ODP Site 980 (Oppo et al., 1998; McManus et al., 1999); De: Dethlingen (Koutsodendris et al., 2010); Site U1308 (Hodell et al., 2008); Pr: Praclaux (Reille et al., 2000); MD01-2447 (Desprat et al., 2005); Site U1313 (Stein et al., 2009); TP: Tenaghi Philippon (Wijmstra and Smit, 1976); MD01-2446 (Voelker et al., 2010; Marino et al., 2014); MD03-2699 (Voelker et al., 2010; Rodrigues et al., 2011; Amore et al., 2012; Palumbo et al., 2013); MD95-2042 (Sánchez Goñi et al., 1999, 2002; Shackleton et al., 2000; Chabaud et al., 2014) ; MD01-2443 (de Abreu et al., 2005; Martrat et al., 2007; Tzedakis et al., 2009).

Environmental setting and pollen signal

Site U1385 (Fig. 1) is located on the SW Iberian margin (37°34.285'N, 10°7.562' W; 2578 m below sea-level). The modern sea surface circulation of this region is dominated by the Portugal Current System, the descending branch of the eastern North Atlantic subtropical gyre (Fiúza, 1983; Peliz et al., 2005). In spring and summer seasons, the southward flowing Portugal Current (PC) and subsequent coastal upwelling are induced by strong northerly winds, while in winter the northward warm and saltier surface Iberian Poleward Current (IPC) prevails (Fiúza et al., 1982; Peliz et al., 2005).

The present-day SW Iberian climate is Mediterranean, marked by a pronounced seasonality between warm/dry summers and cool/wet winters, with strong influence of moisture from the Atlantic in the westernmost area (Peinado Lorca and Martinez-Parras, 1987; Gimeno et al., 2010). The North Atlantic Oscillation (NAO) is the major atmospheric pattern dictating winter precipitation variability over western Iberia through changes in the position of the North Atlantic jet stream and storm tracks (e.g. Hurrell, 1995; Trigo et al., 2004). Conversely, summer dryness is tied to the northeastward expansion of the Azores subtropical High, associated with the descending branch of the Hadley cell (Lionello et al., 2006).

The Mediterranean vegetation dominates the Tagus watershed landscape, although its composition varies over the basin (Peinado Lorca and Martínez-Parras, 1987; Blanco Castro et al., 1997). At low altitudes, *Quercus rotundifolia* and *Quercus suber* woodlands with evergreen shrubs *Phillyrea angustifolia* and *Pistacia terebinthus* are the main forest components in the western part of the basin, while evergreen oak woodlands (*Quercus rotundifolia* and *Quercus coccifera*) associated with juniper (*Juniperus communis*) and aleppo pine (*Pinus halepensis*) develop in the eastern part due to decreased maritime influence. In the warmest areas, scattered sclerophyllous trees and shrubs, such as mastic (*Pistacia lentiscus*) and olive (*Olea europea*) are present. In the Iberian mountains, orogenic precipitation and an altitudinal thermal gradient promote the dominance of deciduous oak (*Quercus pyrenaica* and *Quercus faginea*) woodlands at middle altitudes, and pinewoods (*Pinus sylvestris, P. nigra*) with juniper at higher altitudes. Heathers (Ericaceae) develop in zones with relatively high humidity due to Atlantic influence while evergreen aromatic shrubs (Cistaceae) are found in drier environments (Peinado Lorca and Martínez-Parras, 1987).

Marine sites located near regions with large drainage basins, such as Site U1385, mainly receive pollen grains supplied by rivers (Heusser and Balsam, 1977; Dupont and Wyputta, 2003). Pollen settles down through the water column and ultimately the deep-sea floor, thanks to physical processes such as flocculation, agglomeration and incorporation in faecal pellets (Mudie and McCarthy, 2006). In particular, the Tagus and, to a lesser extent, Sado fluvial systems are the primary pollen suppliers to the deep-sea off SW Iberia, thus providing a reliable integrated image of the vegetation from the SW Iberian Peninsula (Naughton et al., 2007).

Material and methods

IODP Site U1385

Site U1385 (Fig. 1) was drilled on the spur Promontorio dos Principes de Avis on the continental slope of the SW Iberian margin (Fig. 1) during the IODP Expedition 339 ("Mediterranean Outflow") on board the D/V JOIDES Resolution (Expedition 339 Scientists, 2013; Hodell et al., 2013b). Five holes (A–E) were cored and accurately correlated on the basis of XRF analyses to construct a composite depth scale (Hodell et al., 2015). This depth-scale corrects for distortion in individual cores and is given in corrected revised meters composite depth (crmcd) (Hodell et al., 2015). The sediments are composed of relatively homogeneous hemipelagic mud- and claystones with different proportions of biogenic carbonate and terrigenous sediment (Expedition 339 Scientists, 2013).

Pollen analysis

Holes E and D were sampled for pollen analysis every 4 cm between 50.27 and 56.01 crmcd and every 2 cm between 54.50 and 56.01 crmcd. The pollen sample preparation technique followed standard palynological procedure employed for marine samples at UMR EPOC, University of Bordeaux, including coarse-sieving (150 µm mesh) and successive chemical treatments (cold 10%, 25% and 50% HCl; cold 45% and 70% HF; cold HCl at 25%). The obtained residue was sieved through 10 µm nylon mesh screens and mounted unstained in glycerol (Desprat, 2005).

Pollen analysis was performed on 170 samples using a Nikon light microscope at ×500 and ×1000 (oil immersion) magnifications. A total of 100 to 166 pollen grains without *Pinus* were counted in a total pollen sum ranging between 150 and 719 per sample. Twenty to thirty-three different morphotypes were identified in each pollen sample analyzed to ensure a reliable representation of the vegetation community (McAndrew and King, 1976). Identifications followed Moore et al. (1991) and Reille (1992). Pollen data were expressed as percentages of the main sum, which excludes the over-represented *Pinus* (Heusser and Balsam, 1977; Naughton et al., 2007), aquatic plant, indeterminable pollen grains and Pteridophyta spores. *Cedrus* pollen was also excluded from the main sum because it likely originates from North African montane cedar forest (Sánchez Goñi et al., 1999; Magri., 2012;

Chabaud et al., 2014). *Pinus* and *Cedrus* percentages were calculated using the main sum plus their individual counts. Spore and aquatic percentages were estimated using the total sum (pollen+ spores+indeterminable+unknowns).

Pollen percentages were plotted against depth by using the software Psimpoll (Bennett, 2000) (Fig. 2). Pollen zones were established by visual inspection based on fluctuations of at least two ecologically different morphotypes (Birks and Birks, 1980), and statistically confirmed using constrained hierarchical cluster analysis. Clustering of pollen percentages of morphotypes included in the main sum was performed in R environment v. 3.1.1 (R Core Team, 2014), using the function *chclust* from the R package rioja (Juggins, 2009). All temperate tree and shrub taxa excluding *Pinus, Cedrus* and Cupressaceae (*Acer, Alnus, Betula, Carpinus, Corylus, Fagus, Fraxinus excelsior*-type, *Hedera helix, Ilex, Juglans, Ligustrum*-type, *Myrica, Populus, Pterocarya, Quercus deciduous*-type, *Rhus*-type, *Salix, Tilia, Ulex*-type, *Ulmus* and *Vitis*) and Mediterranean taxa (*Cistus, Fraxinus ornus*-type, *Olea, Phillyrea, Pistacia* and *Quercus evergreen*-type), were included in the Mediterranean forest (MF) group (Fig. 2; Table 1), following previous studies off southern Iberia (e,g. Fletcher and Sánchez Goñi, 2008; Sánchez Goñi et al, 2008, 2009, 2013; Chabaud et al., 2014).

A generalized additive mixed model (GAMM) that incorporates temporal correlation was applied to the percentages of the MF group in order to identify rapid forest decline events (Supplementary Fig. S1). We used the *gamm* function from the *mgcv* R package (Wood, 2006; Zuur et al., 2009) to fit a smoothing curve through the data and remove low-frequency variations. Millennial-scale forest decline events were determined based on the twofold condition that model residuals of at least one sample exceeded one standard deviation (1σ) and that substantial declines in MF percentages (> 10%) occur within at least two consecutive samples (Supplementary Fig. S1).

Analysis of marine climatic indicators

Biomarker analyses were carried out in 163 levels from Holes E and D, most of them coinciding with pollen analysis levels, at intervals of 1, 2, 4 or 6 cm between 50.29 and 56.02 crmcd. Analyses were performed following the analytical procedure described in Villanueva et al. (1997a). Organic compounds were extracted from sediments and separated using organic solvents, then identified using Bruker Mass spectrometer detector and quantified with Varian Gas chromatograph Model 3800 equipped with a septum programmable injector and a

flame ionization detector with a CPSIL-5 CB column. Alkenones concentrations were determined using *n*-hexatriacontane as an internal standard. Alkenone-derived sea surface temperature (Uk'_{37}-SST) was based on the $C_{37:2}$ and $C_{37:3}$ ratio following the global core top calibration (Müller et al.,1998), while the $C_{37:4}$ concentration was used as an indicator for subpolar water influence induced by iceberg melting (Villanueva et al., 1997b; Bard et al., 2000; Martrat et al., 2004, 2007; Rodrigues et al., 2011).

MIS 11 benthic foraminiferal oxygen isotope ($\delta^{18}O_b$) record includes a total of 46 samples between 50.29 and 56.14 crmcd (sampling interval ranging between 1 and 20 cm). It combines the Hodell et al. (2015) dataset and fourteen new levels analyzed to increase the MIS 11c resolution.

Results and interpretations

Chronology

In the light of the new $\delta^{18}O_b$ data, we modified the original chronology from Hodell et al. (2015) for the MIS 12-11 section by using two new control points for correlating the Site U1385 $\delta^{18}O_b$ record to the LR04 benthic stack, which has an uncertainty of ±4 ka (Lisiecki and Raymo, 2005) (Fig. 3, Table 2). Age-depth modeling was based on linear interpolation.

The new $\delta^{18}O_b$ data confirmed the very low sediment rate (0.24 cm/ka) between ~431 and 415 ka (Table 2), which possibly reflects a condensed section or a hiatus between Termination V and early MIS 11c (Hodell et al., 2015). The sedimentation rate increases up to 2.7 cm/ka between ~415 and 401 ka (Table 2) and after the end of MIS 11 $\delta^{18}O_b$ plateau at ~401 ka (Fig. 3) the high sedimentation rates and sampling interval allows for a mean time resolution of ~290 years between pollen samples.

We followed the recent nomenclature recommendation dividing MIS 11 into three substages 11c, 11b and 11a (Railsback et al., 2015) (Fig. 4). However, we also used the decimal event notation of Bassinot et al. (1994) that distinguishes additional isotopic events reflecting orbital-scale variability within MIS 11b. In this context, MIS 11c and MIS 11a encompasses the light isotopic events 11.3 and 11.1, respectively, while MIS 11b incorporates two heavy isotopic events, 11.24 and 11.22, separated by the light isotopic event 11.23 (double peak) (Fig. 4).

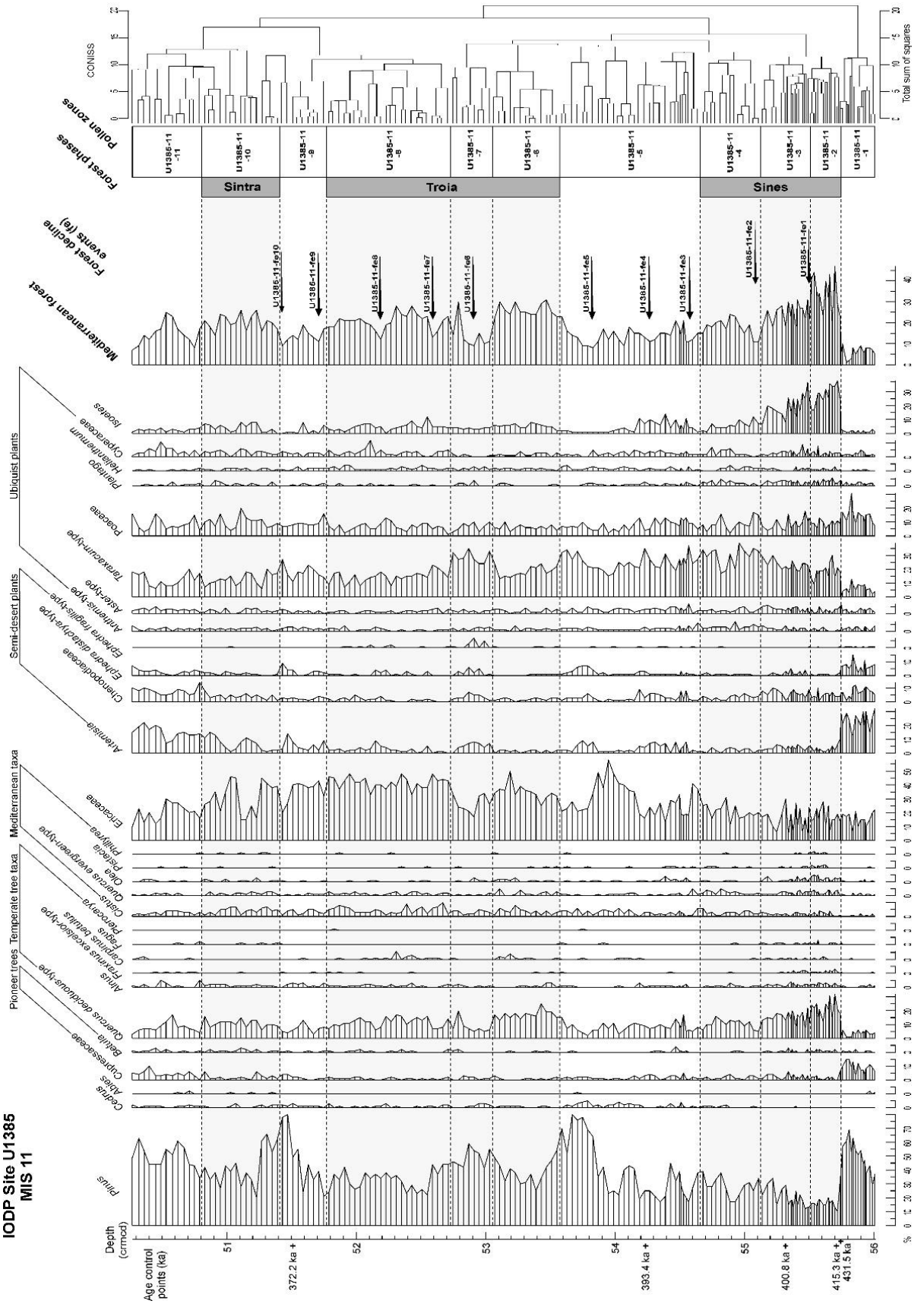
IODP Site U1385
MIS 11
Sintra
Troia
Sines
Mediterranean forest
Forest decline events (fe)
Forest phases
Pollen zones
CONISS
Total sum of squares
Ubiquist plants
Semi-desert plants
Mediterranean taxa
Temperate tree taxa
Pioneer trees
Depth (cmcd)
Age control points (ka)
372.2 ka
393.4 ka
400.8 ka
415.3 ka
431.5 ka

Fig. 2.

Fig. 2. Pollen percentage diagram of selected morphotypes and Mediterranean forest (MF) group at Site U1385 versus depth (crmcd: corrected revised meter composite depth). Position of the control points are indicated with crosses on the left side. MF is composed of all arboreal pollen taxa, mainly deciduous *Quercus* plus Mediterranean taxa, excluding *Pinus*, *Cedrus* and Cupressaceae. Pollen zones and dendrogram showing the results from the hierarchical clustering analysis are represented on the right. Shaded areas indicate forest phases labeled with local names. Arrows underline forest decline events defined using residuals from the GAMM analysis (Supplementary Fig. S1). Pollen zone and event names are designated as following: Site U1385 (site name) and MIS 11 (Marine Isotopic Stage) – followed by the number of the pollen zone and "fe" for forest decline event plus the number of the event, respectively.

Table 2. Description and interpretation of the MIS 11 pollen record at Site U1385. Mediterranean forest (MF) decline events (fe) are indicated in the last column. Grey shaded bar mark the interval during MIS 12/11 transition to early MIS 11 with anomalous low sedimentation rate probably corresponding to a condensed section or hiatus (Hodell et al., 2015).

Forest stages	Pollen zones (Basal depth in crmcd; age in ka)	Duration of intervals (ka) (Number of samples)	Pollen signature	Forest decline events (fe)
	U1385-11-11 (50.83; 367.2)	≥4 (13)	Marked drop of Mediterranean forest (MF), Ericaceae and *Isoetes* values along with high frequencies of semi-desert plants (in particular *Artemisia*, Chenopodiaceae and *Ephedra distachya*-type), *Pinus* and Cupressaceae. Brief but distinct rise of oak percentages at the middle of the zone while semi-desert plants decrease. Continuous presence of *Cedrus* and occurrences of *Abies.*	
Sintra	**U1385-11-10** (51.43; 371.6)	4.4 (15)	Increase of MF taxa values (mainly deciduous and evergreen *Quercus*, *Cistus*, *Olea* and occurrences of *Pistacia* and *Phillyrea*) and *Isoetes*. High percentages of Ericaceae, but showing a distinct decline by the middle of the zone and a decreasing trend by the top mainly in favor of semi-desert plants. Lower abundances of *Pinus*, *Cedrus*, Cupressaceae and *Taraxacum*-type.	
	U1385-11-9 (51.79; 374.4)	2.8 (9)	Important decline of MF taxa percentages and high representation of semi-desert taxa, *Taraxacum*-type, Poaceae, Cupressaceae, *Cedrus* and *Pinus*. Short-lived increase of deciduous *Quercus* by the middle of the zone coupled with a reduction in semi-desert taxa values. By top of the zone, the second deciduous *Quercus* decrease is simultaneous with the drop of Ericaceae values and higher increase of semi-desert plants.	U1385-11-fe10 U1385-11-fe9
Troia	**U1385-11-8** (52.75; 381.8)	7.4 (24)	Percentages of semi-desert plants, *Taraxacum*-type and *Pinus* decrease while those of Mediterranean taxa returns to higher abundances. Highest Ericaceae values. Rise of Cyperaceae, Poaceae and *Isoetes* followed by a decreasing trend by the end of the zone.	U1385-11-fe8 U1385-11-fe7
	U1385-11-7 (53.07; 384.3)	2.5 (8)	Pronounced decline in MF taxa values and Ericaceae associated with an increase of all semi-desert plants, herbs taxa (mainly *Taraxacum*-type), pioneer trees, *Cedrus* and *Pinus*. *Quercus* deciduous sharp increase at the end of the zone coupled with lower percentages of semi-desert plants and *Pinus*.	U1385-11-fe6
	U1385-11-6 (53.59; 388.3)	4 (13)	Rise of MF taxa values (principally deciduous and evergreen *Quercus*, *Alnus*, *Fraxinus excelsior*-type, *Carpinus betulus* and *Olea*), coinciding with higher percentages of Ericaceae and *Isoetes*, and the fall of ubiquist grasses (mainly *Taraxacum*-type). Low semi-desert plants, pioneer trees and *Cedrus* frequencies. *Pinus* percentages decline in lower part of the zone followed by a rise until the top.	
	U1385-11-5 (54.68; 396.4)	8.1 (30)	Lower abundances of MF taxa (mostly deciduous oak) and higher representation of ubiquist plants (in particular *Taraxacum*-type) and *Cedrus*. Ericaceae is detected in moderate to high abundances, with marked fluctuations in favor of semi-desert plants and/or *Taraxacum*-type. By the end of the zone increasing values of MF associated with maximum *Taraxacum*-type are concomitant with decreasing semi-desert taxa and *Pinus* percentages.	U1385-11-fe5 U1385-11-fe4 U1385-11-fe3
Sines	**U1385-11-4** (55.14; 399.6)	3.2 (13)	Intermediate values of deciduous *Quercus* along with reduced percentages of the other temperate trees and high herbaceous abundances (mainly represented by Asteraceae, Poaceae and Ericaceae). Drop of semi-desert taxa and *Isoetes* frequencies.	U1385-11-fe2
	U1385-11-3 (55.52; 408.3)	8.5 (17)	Fall of deciduous oak frequencies and Mediterranean taxa whereas *Taraxacum*-type and semi-desert taxa increase (in particular Chenopodiaceae and *Ephedra distachya*-type). Rise of Poaceae and *Isoetes* at the beginning followed by a decrease along the zone. Lower and oscillating Ericaceae values. Increasing *Pinus* abundances.	U1385-11-fe1
	U1385-11-2 (55.74; 425.9)	14.2 (12)	Abrupt rise in MF taxa percentages (particularly deciduous and evergreen *Quercus*, *Alnus*, *Fraxinus excelsior*-type, *Cistus* and *Olea*). Pronounced decrease in *Pinus*, Cupressaceae, Poaceae and semi-desert plants values, while *Taraxacum*-type and *Isoetes* increase strongly. Highest Mediterranean taxa abundances at the top of the zone coinciding with Ericaceae, *Taraxacum*-type and *Isoetes* drop.	
MIS 12/11 transition	**U1385-11-1** (56.01; 438.1)	>15.9 (16)	Strong dominance of non-arboreal pollen (NAP) taxa, in particular semi-desert plants, grassland taxa (mainly Poaceae and *Taraxacum*-type) and Ericaceae. Low frequencies of all tree taxa, except Cupressaceae and *Pinus*.	

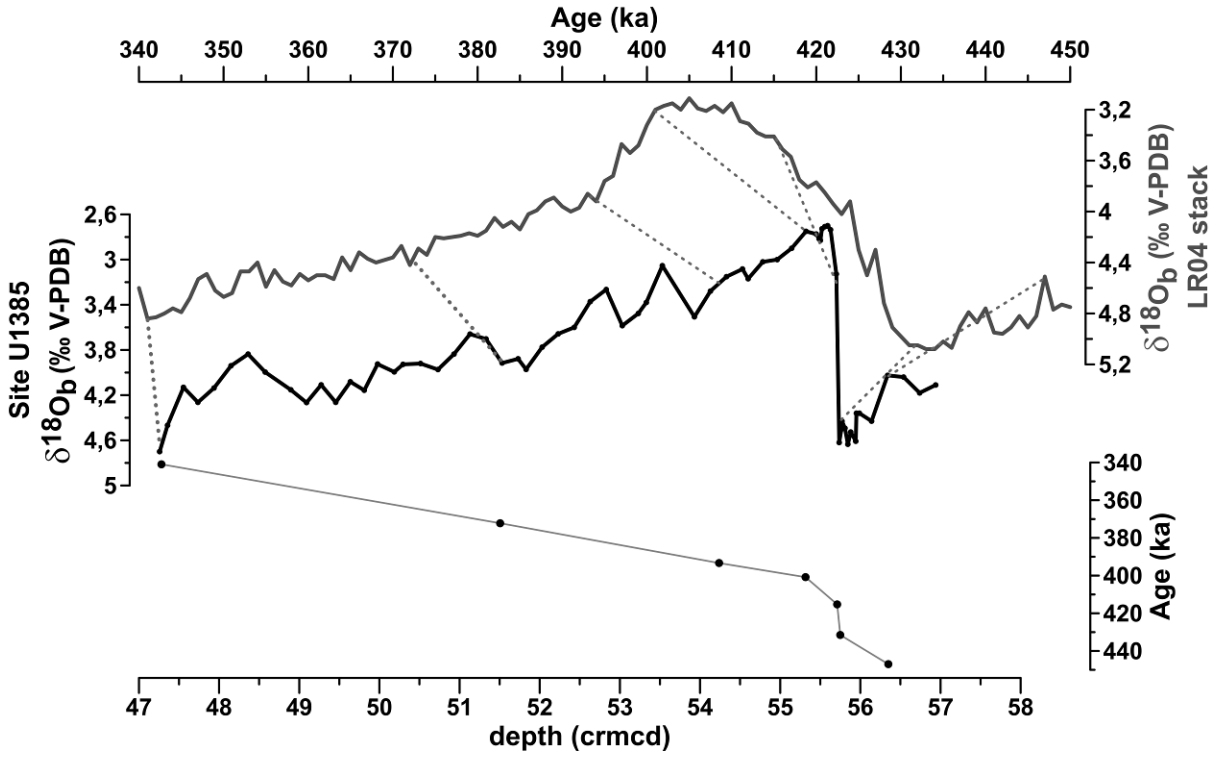

Fig. 3. Age model based on the correlation of Site U1385 $\delta^{18}O_b$ record (black line; in depth scale, crmcd: corrected revised meter composite depth) with the LR04 $\delta^{18}O_b$ stack (grey line; in age scale) of Lisiecki and Raymo (2005). Control points used for the correlation between records are depicted with dashed lines. The age-depth model is presented on the bottom.

Table 2. Age control points used to correlate the Site U1385 $\delta^{18}O_b$ record to the LR04 benthic stack of Lisiecki and Raymo (2005) (Hodell et al., 2015). *New control points used in this study.

Site U1385 Depth (crmcd)	Control points LR04 Age (ka)	Sed. Rate (cm/ka)
47.280	340.95	
51.506	372.21	13.52
54.238*	393.35*	12.92
55.317	400.84	14.41
55.711	415.27	2.73
55.750*	431.53*	0.24
56.349	446.99	3.87

Pollen-derived vegetation reconstruction

Pollen analysis results are displayed in a synthetic pollen percentage diagram (Fig. 2) together with a summary of the main features of the pollen zones in Table 1.

Long-term vegetation trends

The pollen record was divided into eleven pollen zones, generally corresponding to the major shifts between forested and open vegetation intervals (Fig. 2), as summarized in Table 1. The forest phases, named Sines, Troia and Sintra, associated with the light isotopic events MIS 11.3, 11.23 and 11.1, respectively, are characterized by an expansion of the Mediterranean forest (MF) mainly composed of deciduous oak and Mediterranean taxa (Figs. 2 and 4). MF percentages range between ~20 and 50%, indicating atmospheric warmth and moisture availability in SW Iberia (Figs. 2 and 4).

Sines is the longest, warmest and most floristically diverse forest phase documented in our record (Figs. 2 and 4). Sines duration is about 26 ka, although chronological uncertainties during Termination V preclude the precise identification of its onset. The optimal expression of the Mediterranean climate, i.e. warmest conditions with highly seasonal rainfall, is suggested by the highest abundances of Mediterranean taxa between ~414 and 408 ka (Fig. 4). This warmest phase was followed by a progressive contraction of MF and expansion of dry-grasslands (mostly Poaceae, Asteraceae and semi-desert plants, i.e. *Artemisia*, Chenopodiaceae and both *Ephedra* types, as defined by Polunin and Walters (1985)), indicating cooler and drier conditions over the end of Sines forest phase (Figs. 2 and 4). During the second forest phase, Troia (~13.9 ka), deciduous *Quercus* woodland with heathland (Ericaceae) dominated the landscape (Figs. 2 and 4), reflecting more humid and temperate conditions than during Sines interglacial. The MF moderately expanded during the last forest phase, Sintra (~4.4 ka), suggesting a weaker increase in warmth and moisture availability (Figs. 2 and 4).

Open vegetation phases, encompassing the heavy isotopic events 11.24 and 11.22 (Fig. 4), ~396.5 to 388.5 ka and from ~374.5 to 371.5 ka, are represented by MF values below 20%, in accordance with studies on modern samples (e.g. Wright et al., 1967; Prentice, 1978; Petersen, 1983). Such change suggests a shift towards cooler and drier conditions since temperature, and particularly moisture availability, are critical for forest composition and

development in the Mediterranean region (Quezel, 2002). Both open vegetation phases are characterized by alternations between dominance of heathland and dry-grassland (Figs. 2 and 4). The progressive replacement of MF by Ericaceae likely reflects cooling with sustained humidity year-round, although heath requires less water than forest (Walter and Breckle, 1989; Loidi et al., 2007). In contrast, dry-grassland expansion indicates cold and more pronounced dry conditions, with semi-desert plants being an indicator of lower moisture availability than Asteraceae-Poaceae (Polunin and Walters, 1985). The last open vegetation interval, between ~371.5 and 363 ka, is characterized by the dominance of semi-desert plants, including the substantial expansion of *Ephedra*, suggesting the setting of overall dry and cold glacial conditions during the early stages of MIS 10 (Figs. 2 and 4). This interval also depicts a brief expansion of MF at ~365 ka representing an interstadial-type episode during MIS 10.

Suborbital vegetation dynamics

Superimposed on the long-term vegetation changes, the pollen record at Site U1385 provides evidence for repeated short-term climate variations of different character and intensity throughout MIS 11 in SW Iberia. Nine millennial-scale forest decline events (U1385-11-fe-2 to -fe10) were identified using the twofold condition previously described (Figs. 2, 5 and Supplementary S1). We additionally identified one event (U1385-11-fe1) which displays a substantial decrease in MF of ~20%, although marked by only one data-point. This significant abrupt forest contraction with no recovery suggests the occurrence of a millennial-scale event such as that previously inferred from the SW Iberian margin pollen record within MIS 9e and 7e (Tzedakis et al., 2004). Duration of the MF decline events, defined as the interval between the mid-points of the decline and increase in MF values, varies from ~700 yr (U1385-11-fe2 and fe-7) to ~2100 yr (U1385-11-fe5).

The MF decline events U1385-11-fe1, -fe4, -fe8 and -fe9 (at ~408, 393.5, 377.5 and 373.5 ka, respectively) are characterized by an increase in semi-desert plants of up to ~15%, implying cool and dry conditions (Fig. 5). In addition, the associated herbaceous components vary revealing differences in the degree of moisture deficiency between events: U1385-11-fe1 and -fe4 (highest dry-grassland values) appear drier than U1385-11-fe8 and -fe9 (Fig. 5).

During the forest decline events U1385-11-fe2, -fe3, and -fe7 (centered at ~399.5, 396 and 380.5 ka, respectively), semi-desert plants did not expand (Fig. 5). Asteraceae-Poaceae

strongly expanded during U1385-11-fe2 reflecting a weaker shift to cool and dry atmospheric conditions, while Ericaceae dominated over U1385-11-fe3 and -fe7, hence suggesting a cooling with higher annual humidity (Fig. 5).

The most severe forest decline events, U1385-11-fe5, -fe6 and -fe10 (centered at ~390, 383 and 371.5 ka, respectively), are consistently represented by pronounced expansions of semi-desert elements (~20%), minimal MF cover (<10%) and Ericaceae decrease (Fig. 5), suggesting the coldest and driest atmospheric conditions of MIS 11. Interestingly, these events are also associated with high relative abundances of *Cedrus* and *Pinus* (Fig. 5). The few detailed available pollen records suggest that cedar was, however, absent from Iberia throughout the Quaternary (Magri, 2012). Given the current distribution of cedar in cool and moist high altitude habitats of northern Africa (Cheddadi et al., 1998) and its anemophily, peaks in *Cedrus* in the Iberian margin sediments during cold periods likely resulted from enhanced wind-driven pollen supply (Sánchez Goñi et al., 1999; Chabaud et al., 2014). The peaks of pine pollen remain difficult to interpret due to the low taxonomical resolution of the *Pinus* morphotype including pollen from Iberian highland and Mediterranean pine species (Desprat el al., 2015). However, since pine pollen is wind-pollinated and highly buoyant in the air (Birks and Birks, 1980), *Pinus* peaks in the SW Iberian margin during cold events may also result from high intensity winds. These cold, dry and windy events are also noticeably long with a duration between ~1600 and 2100 yr.

Alkenone-sea surface temperature reconstruction

The Uk'_{37}-SST at Site U1385 describe an increasing SST profile from ~9°C to 18°C during Termination V (Fig. 4). Nevertheless, the low sedimentation rates and chronological uncertainties hinder the identification of sea surface water variability during this interval. SSTs remained warm and relatively stable around 18°C up to ~400 ka. At this time, both SST and $\delta^{18}O_b$ initiated a cooling and heavier long-term trend towards MIS 10 glacial conditions (Fig. 4). Three prominent cooling episodes with temperatures close to 10°C interrupted this trend at ~390 ka (MIS 11.24), ~383 ka (mid MIS 11.23) and ~372 ka (MIS 11.22) (Fig. 5). These cooling events are associated with the strongest $\%C_{37:4}$ increases suggesting freshwater/iceberg discharges (Fig. 5). In addition, a moderate cooling event with SST decreasing down to ~13°C and a minor increase in $\%C_{37:4}$ is detected at ~378 ka (Fig. 5).

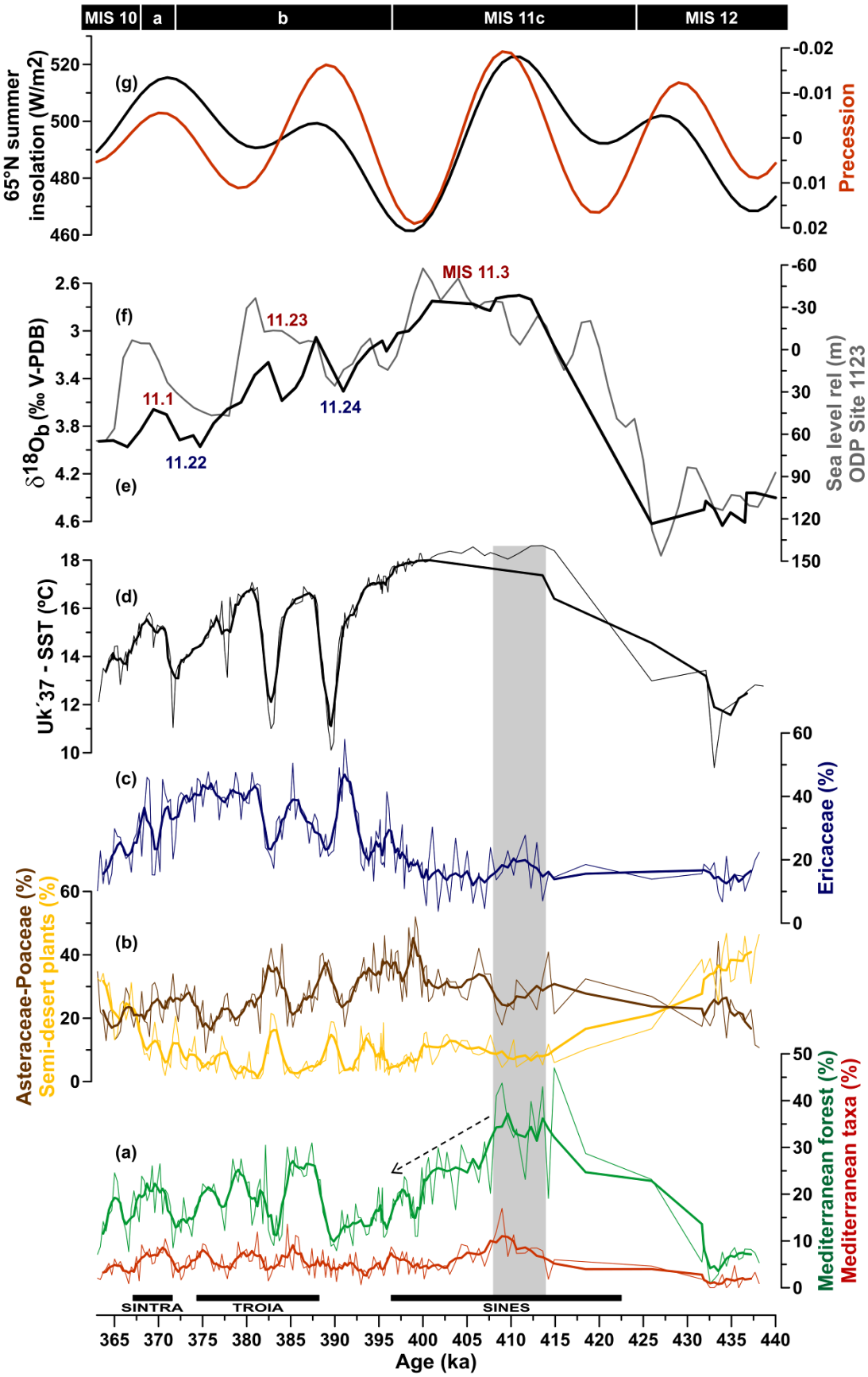
MIS 10
a
b
MIS 11c
MIS 12
65°N summer insolation (W/m2)
(g)
Precession
MIS 11.3
11.23
11.1
11.24
11.22
(f)
(e)
δ18Ob (‰ V-PDB)
Sea level rel (m) ODP Site 1123
(d)
Uk´37 - SST (°C)
(c)
Ericaceae (%)
(b)
Asteraceae-Poaceae (%)
Semi-desert plants (%)
(a)
Mediterranean forest (%)
Mediterranean taxa (%)
SINTRA
TROIA
SINES
Age (ka)

Fig. 4.

Fig. 4. MIS 11 long-term vegetation and climatic changes at Site U1385. From the bottom to the top: Percentages of selected pollen taxa or group of taxa: (a) Mediterranean taxa (*Quercus evergreen*-type, *Cistus*, *Olea*, *Phillyrea*, *Pistacia and Fraxinus ornus*-type) (red line) and Mediterranean forest (MF, all arboreal pollen taxa, mainly deciduous *Quercus* plus Mediterranean taxa, excluding *Pinus*, *Cedrus* and Cupressaceae) (green line), (b) semi-desert plants (*Artemisia*, Chenopodiaceae, *Ephedra distachya*-type and *Ephedra fragilis*-type) (yellow line) and Asteraceae-Poaceae group (brown line), (c) Ericaceae; U1385 marine data: (d) Uk'_{37}-SST and (e) $\delta^{18}O_b$ record (black line) with marine isotope events according to Bassinot et al. (1994); (f) Relative sea-level changes (grey line) based on ODP 1123 $\delta^{18}O_{seawater}$ (Elderfield et al., 2012); (g) 65°N summer insolation (black line) and precession index (red line) (Berger, 1978). Forest phases and marine isotopic substages on bottom and top, respectively. Bold lines represent 5-point moving averages of pollen percentages and Uk'_{37}-SST. The grey bar indicates the MF maximal expansion during Sines forest phase.

Fig. 5. Millennial-scale Mediterranean forest (MF) decline events and oceanic surface changes from Site U1385 direct land-ocean comparison. From the bottom to the top: Selected pollen percentage curves: (a) MF, (b) semi-desert plants (yellow line) and Asteraceae-Poaceae group (brown line), (c) Ericaceae, (d) *Pinus* and *Cedrus*; U1385 marine data: (e) Uk'_{37}-SST and % $C_{37:4}$ – based surface ocean freshwater inputs; (f) $\delta^{18}O_b$ record (black line) with marine isotope events according to Bassinot et al. (1994); (g) Relative sea-level changes (grey line) based on ODP 1123 $\delta^{18}O_{seawater}$ (Elderfield et al., 2012); (h) 65°N summer insolation (Berger, 1978). Forest phases and marine isotopic substages on bottom and top, respectively. Numbered blue bands mark the millennial-scale events of high (5, 6 and 10) (dark blue) and moderate (8, 9) (light blue) intensity, while numbered pink bands (1, 2, 3, 4 and 7) represent the MF decline events without counterpart in the SST record.

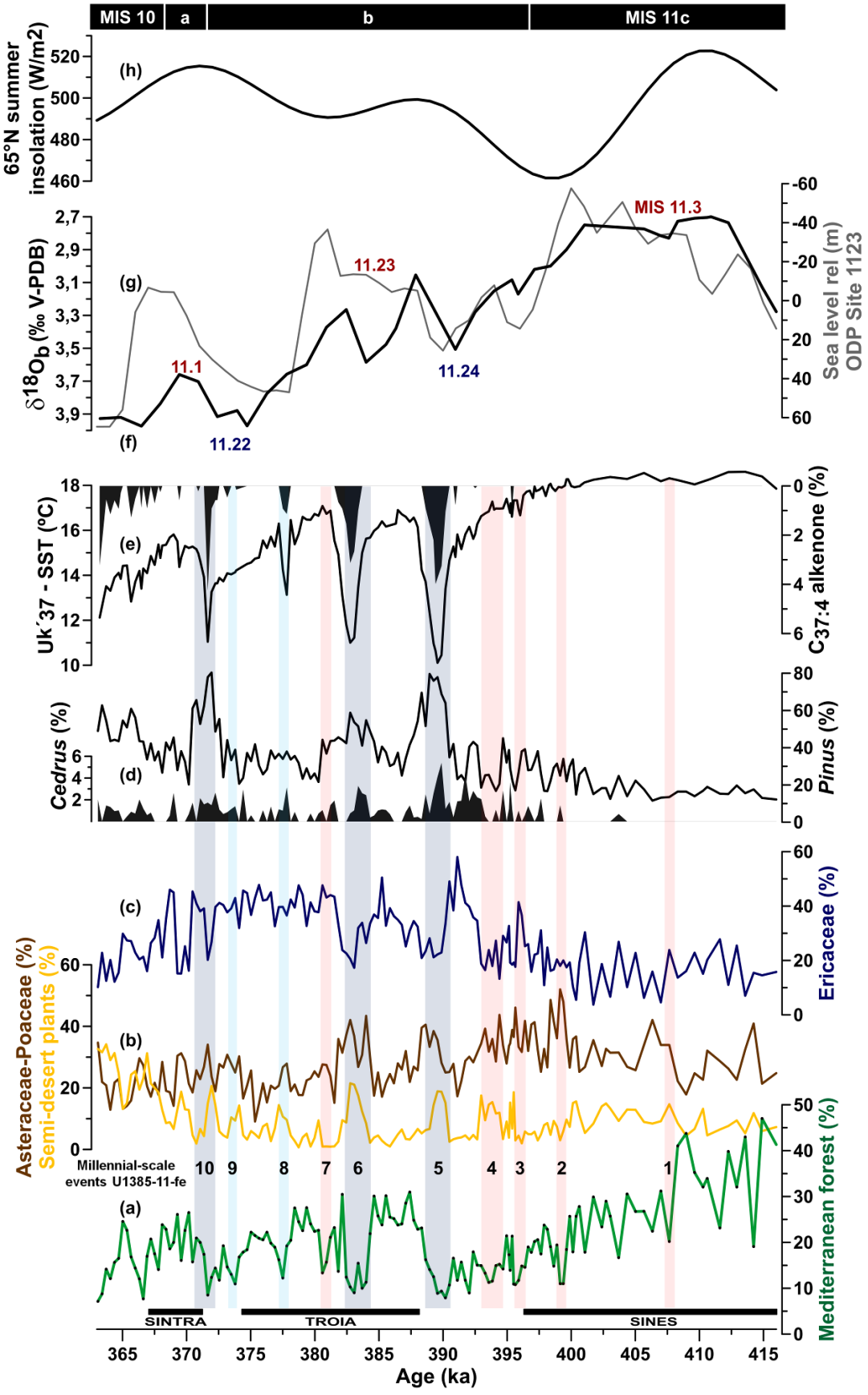
MIS 10
a
b
MIS 11c
65°N summer insolation (W/m2)
(h)
520
500
480
460
MIS 11.3
11.23
11.1
11.24
11.22
(g)
(f)
δ18Ob (‰ V-PDB)
Sea level rel (m) ODP Site 1123
Uk´37 - SST (ºC)
(e)
C37:4 alkenone (%)
Cedrus (%)
(d)
Pinus (%)
(c)
Ericaceae (%)
(b)
Asteraceae-Poaceae (%)
Semi-desert plants (%)
Millennial-scale events U1385-11-fe
10 9 8 7 6 5 4 3 2 1
(a)
Mediterranean forest (%)
SINTRA
TROIA
SINES
Age (ka)

Fig. 5.

Discussion

Long-term vegetation and climatic changes

The MIS 11 long-term vegetation pattern detected at Site U1385 (Fig. 4) has already been documented for NW and SW Iberia (Desprat et al., 2005; Tzedakis et al., 2009), northwestern Greece (Wijmstra and Smit, 1976; Tzedakis et al., 2001) and southern France (Reille et al., 2000; de Beaulieu et al., 2001).

The close correspondence of Sines, Troia and Sintra major forest expansion with maxima in northern hemisphere (NH) summer insolation and low ice volume intervals (Fig. 4) reflects the influence of orbital-scale climatic variability on SW Iberian vegetation. In line with previous works (Desprat et al., 2005; Tzedakis et al., 2009), our pollen record shows the highest degree of warming in Iberia associated with the strongest NH summer insolation maxima of MIS 11c. The three forest extent maxima observed during Sines, Troia and Sintra do not parallel the magnitude of the three insolation maxima but that of precession minima (Fig. 4). In particular, the largest expansion of mixed oak forest and Mediterranean taxa during Sines, reflecting the warmest and strongest rainfall seasonality, occurred during the strongest MIS 11 precession minimum. However, despite the relatively higher sea-level and equivalent CO_2 concentrations during MIS 11c (Dutton et al., 2015), the extent of woodland vegetation remained low in comparison with that of warm stages marked by large precession minima such as MIS 5e (Sánchez Goñi et al., 1999). These observations confirm that precession plays a major role on the forest extent in the Mediterranean region south of 40°N (Sánchez Goñi et al., 2008).

As described for other Iberian margin records (Desprat et al., 2005; Tzedakis et al., 2009), the long-term forest decline during the final phase of MIS 11c, i.e. the end of Sines (~408 to 396 ka), parallels the decrease in NH summer insolation (Fig. 4). This western Iberian long-term vegetation response to insolation forcing is similar to other interglacial periods of the last 400 ka (Tzedakis et al., 2004; Sánchez Goñi et al., 2005; Roucoux et al., 2006; Desprat et al., 2007, 2009; Naughton et al., 2007; Chabaud et al., 2014). However, while conditions on land progressively cooled during the late MIS 11c, SSTs remained relatively warm, experiencing solely a subtle decrease from ~18.5ºC to 17.5°C (Fig. 4). Pervasive relatively warm conditions off SW Iberia may reflect the persistent dominance of the subtropical Azores Current (AzC) and Iberian Poleward Current (IPC) in this area over the final phase of MIS 11c (Voelker et al., 2010), even after the onset of the NH ice sheet growth at ~400 ka (Fig. 4).

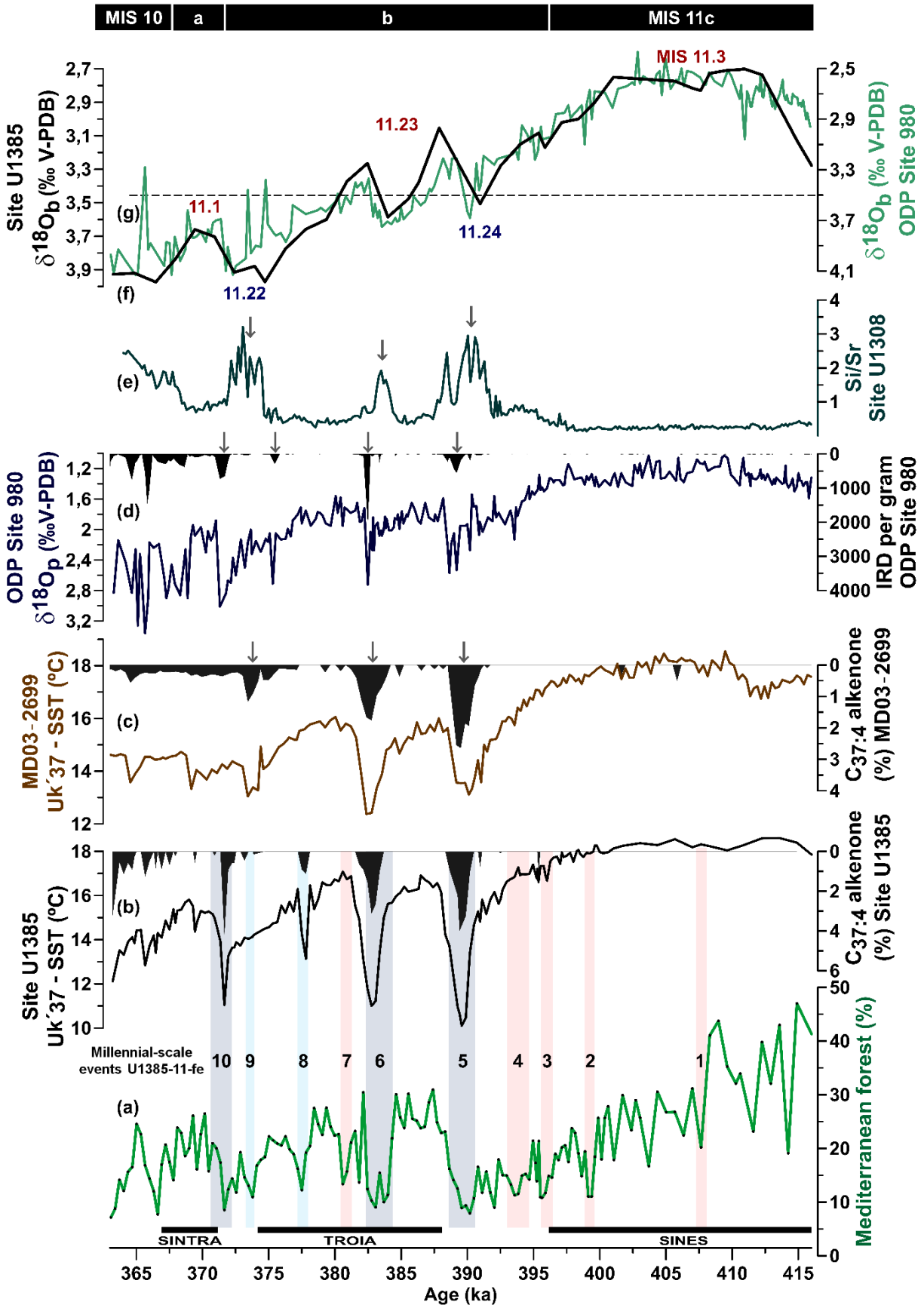
MIS 10
a
b
MIS 11c
MIS 11.3
11.23
11.1
11.24
11.22
Site U1385 $\delta^{18}O_b$ (‰ V-PDB)
$\delta^{18}O_b$ (‰ V-PDB) ODP Site 980
(g)
(f)
(e)
Si/Sr Site U1308
ODP Site 980 $\delta^{18}O_p$ (‰V-PDB)
(d)
IRD per gram ODP Site 980
MD03-2699 Uk´37 - SST (ºC)
(c)
C37:4 alkenone (%) MD03-2699
Site U1385 Uk´37 - SST (ºC)
(b)
C37:4 alkenone (%) Site U1385
Millennial-scale events U1385-11-fe
10 9 8 7 6 5 4 3 2 1
(a)
Mediterranean forest (%)
SINTRA
TROIA
SINES
Age (ka)

Fig. 6.

Fig. 6. Millennial-scale variability derived from Site U1385 direct land-ocean comparison. (a) MF pollen percentage curve and (b) Uk'_{37}-SST and % $C_{37:4}$ – based surface ocean freshwater inputs, in comparison with (c) Uk'_{37}-SST and % $C_{37:4}$ from Iberian margin core MD03-2699 (Voelker et al., 2010; Rodrigues et al., 2011), (d) planktic $\delta^{18}O$ and ice rafted detritus (IRD) concentrations (grains/g) at ODP 980 (Oppo et al., 1998) on its LR04 chronology (Lisiecki and Raymo, 2005), and (e) Si/Sr ratio from Site U1308 (Hodell et al., 2008). (f) $\delta^{18}O_b$ records at Sites U1385 (black line) and ODP 980 (green line) with marine isotope events according to Bassinot et al. (1994). Dashed line designates the ice volume threshold of McManus et al. (1999). Forest phases and marine isotopic substages on bottom and top, respectively. Numbered blue bands mark the millennial-scale events of high (5, 6 and 10) (dark blue) and moderate (8, 9) (light blue) intensity, while numbered pink bands (1, 2, 3, 4 and 7) represent the MF decline events without counterpart in the SST record.

Millennial-scale climate variability

The outstanding features of the multiproxy record at Site U1385 are the pervasive millennial-scale climate instabilities throughout MIS 11 and their diversity as depicted by different regional vegetation and eastern North Atlantic SST changes (Figs. 5 and 6).

Intra-interglacial climate variability during MIS 11c ice volume minimum

The intriguing abrupt MF contraction recorded within MIS 11c at ~408 ka (Fig. 5), event U1385-11-fe1, is also detected, within age uncertainties, in the closest MD01-2443 pollen record at ~406 ka (Tzedakis et al., 2009). Similarly to Site U1385, this event occurred well before the end of the benthic δ18Ob plateau and the forest did not recover afterwards. However, this high amplitude MF change does not have a counterpart in either the SST profile from core MD01-2443, or in other records from the mid-latitude North Atlantic, that consistently report a single cooling event at ~412 ka separating the two MIS 11c warm SST plateaus (Martrat et al., 2007; Stein et al., 2009; Voelker et al., 2010; Rodrigues et al., 2011). This short-term cooling, also observed in the MD01-2443 pollen record (Tzedakis et al., 2009), probably corresponds to the pronounced MF decrease identified at Site U1385 at ~411.6 ka (Figs. 5, 6 and Supplementary S1). Nevertheless, the very low sedimentation rate of Site U1385 during early MIS 11c prevents further discussion about this specific millennial-scale event.

Intra-interglacial vegetation and climate changes during MIS 11c were also detected in northern Europe. In particular, the Dethlingen varved pollen sequence displays an abrupt cooling event during the Holsteinian interglacial named "Older Holsteinian Oscillation" (OHO) (Koutsodendris et al. 2010, 2011, 2012). Although the timing of the OHO is still debated (Koutsodendris et al., 2012; Tye et al., 2016), Koutsodendris et al. (2012) argued that it most probably occurred at ~408 (±0.5) ka based on the assumption that Holsteinian interglacial correlates with the later part of MIS 11c (~415–397 ka), coinciding with the NH summer insolation maximum, low global ice volume, and highest temperatures in the North Atlantic and Antarctica. Relying on this assumption, the U1385-11-fe1 event, which after our chronology is also detected at ~408 ka, would correspond to the OHO widely recognized in pollen records from the British Islands to Poland north of 50° latitude (Koutsodendris et al., 2012 and references therein). However, the impact of this abrupt climatic oscillation on the vegetation of northern Europe strongly differed from that of SW Iberia. In contrast to SW Iberia (Tzedakis et al., 2009; this study), the northern European forest recovered after the rapid climate change. Comparison of the OHO duration (~300 years) and its equivalent events in SW Iberia is prevented by the lower time resolution of the pollen records at Site U1385 and MD01-2443 (Tzedakis et al., 2009).

Koutsodendris et al. (2012) additionally proposed that the OHO is analogous to the early Holocene 8.2 ka event in respect with terrestrial ecosystem changes, boundary conditions (reduced NH ice sheets and high NH summer insolation) and European spatial and climatic patterns. Based on these similarities, the OHO could be triggered by a similar forcing mechanism to the 8.2 ka event (Koutsodendris et al., 2012), i.e. a slowdown of the NADW formation induced by freshwater pulse from proglacial lake discharges (Alley and Ágústsdóttir, 2005). Chronological uncertainties preclude the assessment of the AMOC change at the time of this event (e.g. Oppo et al., 1998). The vegetation changes associated with the U1385-11-fe1 event and the 8.2 ka event recorded in the Iberian margin twin cores U1385 and MD95-2042 (Chabaud et al., 2014) support the hypothesis of an analogous terrestrial response to the intra-interglacial events. They are both associated with a rapid and high-amplitude MF contraction that marked the end of the maximum forest expansion, after which the MF did not recover.

However, the analogy between both events is hampered when comparing Iberian SST patterns. While no corresponding sea surface cooling event is detected on the Iberian margin during the warmest interval of MIS 11c (Martrat et al., 2007; Voelker et al., 2010; Rodrigues, et al., 2011), one is observed during the 8.2 ka event (Rodrigues et al., 2009). Additionally, whereas the 8.2 ka event occurred during the retreat of substantial NH ice sheets, the MIS 11 intra-interglacial event might have occurred after the complete melting of the NH continental ice sheets and consequently not as a result of deglacial processes. As recently argued by Raymo and Mitrovica (2012), MIS 11 sea-level highstand which occurred from 410 to 401 ka, was higher than at present-day, probably resulting from the Greenland Ice Sheet (GIS) and West Antarctic Ice Sheet collapse. Moreover, while the southern GIS persisted through the Holocene (Colville et al., 2011), a nearly ice-free Greenland regime which promoted the regional development of boreal coniferous forest (de Vernal and Hillaire-Marcel, 2008), likely characterized the late MIS 11c (Reyes et al., 2014). Therefore, the U1385-11-fe1 may be more alike to the mid-to-late Holocene events that occurred during minimum NH ice sheets (Combourieu-Nebout et al., 2009; Desprat et al., 2013). Because the MF development is controlled by the wintertime conditions, especially by precipitation (Quezel, 2002; Gouveia et al., 2008), forest contractions without concomitant SST reversals, as observed during U1385-11-fe1, are likely related to a moisture deficiency. Millennial-scale oscillations of the zonal flow recalling the present-day atmospheric patterns tightly linked to blocking episodes in the North Atlantic (NAO) and Europe (Scandinavian pattern) (Sousa et al., 2015b) appear therefore as a cause of these type of forest declines mainly driven by increased dryness. In fact, for the last millennia, atmospheric centennial variability related to NAO-type events was observed despite the small changes in SST (Moffa-Sanchéz et al., 2014; Ortega et al., 2015). NAO-type circulation possibly driven by an internal oscillation in interglacial AMOC strength was also involved in explaining western Mediterranean multi-centennial climate variability of the mid-to-late Holocene (Fletcher et al., 2012). The enhanced dryness associated with U1385-11-fe1 event supports a shift to more persistent positive mode of the NAO-type and, therefore, a weaker influence of the winter mid-latitude North Atlantic westerlies in the SW Iberia.

Decoupled atmospheric and oceanic changes during the glacial inception

The MIS 11c/11 b transition and the late part of MIS 11.23, both characterized by weak ice sheet growth, were punctuated by millennial-scale cooling and drying events on land, U1385-11-fe2 to -fe4 and fe7 (at ~399.5, 396, 393.5 and ~381 ka, respectively). None of these events has a counterpart in the SST record at Site U1385; they are all associated with warm SSTs, between ~18°C and 16.5°C on the margin (Figs. 5 and 6). These observations are also reflected by nearby MD01-2443 palaeoclimatic records (Martrat et al., 2007; Tzedakis et al., 2009) and suggest an air-sea thermal contrast at millennial timescales. The atmospheric processes behind this thermal contrast can be related to a frequent positive mode of NAO-type circulation enhancing dryness in Iberia but impacting weakly local SSTs because of the prevailing influence of subtropical AzC and IPC waters over this time interval (Voelker et al., 2010). The influence of the atmosphere on SST is relatively weak at the local scale due to the large heat capacity of the ocean and very effective heat transport via ocean currents (Oort, et al., 1976). Additionally, it has been demonstrated that correlation between NAO and SST was not stationary over the last half century (Walter and Graf, 2002).

The MIS 11c/11b glacial inception, marked by three millennial-scale cooling events, is associated with a period of subtle SST cooling in our record, also detected in other mid-latitude North Atlantic records (de Abreu et al., 2005; Martrat et al., 2007; Stein et al., 2009; Voelker et al., 2010; Rodrigues et al., 2011) and in the northern North Atlantic ODP Site 980 by increasing polar foraminifera percentages (Oppo et al., 1998). This progressive cooling across the North Atlantic region may have increased the temperature gradient favoring the recurrence of positive mode of the NAO-type circulation. It would also explain that the millennial-scale Mediterranean forest recovery was progressively less successful in SW Iberia. Decoupling at millennial timescales between air temperatures and SST on the European margins was similarly reported during the ice sheet growth of MIS 5a/4 transition (Sánchez Goñi et al., 2013), and for the past four glacial inceptions (Cortina et al., 2015). This analogy, despite differences in boundary conditions, suggests increased regional moisture that is transported northward through intensified storm tracks, thereby contributing to ice-growth. Such thermal contrasts between cold air and warm sea surface temperatures may have also operated during the MIS 11c/11b transition, at millennial timescales, enhancing northward moisture transport and the glacial inception.

Land-sea cooling during large ice volume conditions

The events U1385-11-fe5, -fe6 and -fe10 (at ~390, 383 and 371.5 ka, respectively), associated with the isotopic events 11.24, mid 11.23 and 11.22, respectively, are characterized in SW Iberia by the coldest and driest atmospheric conditions of MIS 11, high intensity winds and a particularly long duration, between 1600 to 2100 yr (Fig. 5). These high intensity events are synchronous with strong and sudden drops in SSTs down to 10°C and the highest $\%C_{37:4}$, suggesting that the site was under the influence of subpolar water.

The nearest MIS 11 pollen record shows close similarities regarding the sequence and intensity of these abrupt forest decline events (Tzedakis et al., 2009), where three major forest contractions related with large SST cooling are observed. Despite their low temporal resolution, the NW Iberian margin and southern France pollen records (Reille et al., 2000; Desprat et al., 2005) also reported three main open vegetation periods associated with the MIS 11 coldest conditions. In the North Atlantic, three major millennial-scale cooling events associated with lithic evidence of iceberg discharges (Fig. 6) are commonly detected and have been linked to changes in AMOC (e.g. Oppo et al., 1998; Martrat et al., 2007; Hodell et al., 2008; Voelker et al., 2010; Rodrigues et al., 2011; Barker et al., 2015). Such suborbital variability is even recorded in other regions of the world, such as Siberia (Prokopenko et al., 2010). By analogy to the last glacial cooling events, specifically to Heinrich Events (HE), enhanced aridity over SW Iberia during these MIS 11 events probably resulted from AMOC changes and further intensification and northward displacement of the westerlies (e.g. Sánchez Goñi et al., 2002). These high intensity events only occurred during the second part of MIS 11 when sea-level substantially lowered (Rohling et al., 2009; Elderfield et al., 2012) (Fig. 6). In particular, our direct land-sea comparison at Site U1385 shows that those events only occurred once surpassing the $\delta^{18}O_b$ 3.5‰ threshold (Figs. 5 and 6), in agreement with the critical ice sheet size threshold suggested by McManus et al. (1999). Changes in $\delta^{18}O_b$ are not only driven by ice volume (Skinner and Shackleton, 2005) albeit this threshold value represents the overall conditions when ice sheets reach a critical size to modify the hydrological cycle, deflect the main atmospheric streams or produce rafting ice (McManus et al., 1999). This threshold value in the $\delta^{18}O_b$ is tied to the amplification of millennial-scale cooling by feedback mechanisms associated with ice sheet dynamics, and has been supported by numerous MIS 11 records along the Iberian margin (de Abreu et al., 2005; Desprat et al.,

2005; Voelker et al., 2010; Rodrigues et al., 2011), as well as elsewhere in the Atlantic Ocean (Poli et al., 2000; Hall and Becker, 2007; Dickson et al., 2008; Stein et al., 2009).

Compared to the Heinrich Stadial (HS) of the last glacial period, the most severe MIS 11 events are marked by weaker MF contractions and moderate semi-desert plant expansion (e.g. Combourieu-Nebout et al., 2002; Sánchez Goñi et al., 2002). However, they present a similar extent of MF than the first and last phases of HS5 and HS4 with an average MF value of 10% (Sánchez Goñi et al., 2000). This percentage of MF suggests that the atmospheric moisture availability and/or temperatures did not reach the critical bioclimatic threshold for major tree decline, although cold and dry conditions prevailed. The less intense dryness during the first and final phases of HS4 and HS5 have been linked to the source of iceberg surges (Sánchez Goñi et al., 2000), and are considered to have been European ice sheets, rather than the Laurentide ice sheet (Grousset et al., 2000). Such IRD source was also proposed for the MIS 11 events (Voelker et al., 2010; Rodrigues et al., 2011). Other sources of iceberg pulses than the Laurentide ice sheet is also supported by XRF data from Site U1308, showing the absence of Ca/Sr peaks but short-lived increases in Si/Sr ratio (Hodell et al., 2008) (Fig. 6). Modeling results using LGM baseline conditions show that depending on its origin, the freshwater flux affects differentially deep-water formation, sea-ice seasonal range and extent and, consequently, the regional response of air temperatures (Roche et al., 2010). As for HS5 and HS4, the main source of freshwater discharges during MIS 11 cooling events probably played an important role on the vegetation and climatic response in SW Europe. Our MIS 11 direct land-sea comparison confirms therefore that the ice sheet dynamics is a key factor modulating the amplitude of precipitation and temperature reduction in SW Europe at millennial timescales.

Our data additionally show that the coldest and driest episodes which are associated with iceberg discharges into the North Atlantic are also particularly long (Figs. 5 and 6). This observation would confirm that besides amplifying the cooling, iceberg discharges may also promote prolonged stadial conditions (Clark et al. 2007; Barker et al., 2015). It is also worthy to note that the Antarctica temperature record displays only three cooling episodes followed by a gradual warming (Jouzel et al., 2007), that likely correlates with the large and long cold episodes recorded in the North Atlantic and SW Europe. The low resolution of the $\delta^{18}O_b$ record from Site U1385 precludes the assessment of the phase relationship between the two

hemispheres in response to climate changes. However, it is likely that as for MIS 19 (Tzedakis et al., 2012), the bipolar see-saw became active when ice volume was large enough to produce ice-rafting episodes and most particularly during events of high magnitude and long duration. During MIS 11, the coldest episodes in the North Atlantic appeared generally longer and more humid in SW Iberia and warmer in Antarctica than those punctuating the last glacial. The MIS 11 coldest episodes are, nevertheless, similar to those characterizing MIS 6 when an enhanced hydrological cycle in the North Atlantic may have contributed to disrupt the AMOC despite the lack of iceberg discharges from the Laurentide (Margari et al., 2010). This similarity suggests that the freshwater forcing threshold was also modified during the coldest episodes of MIS 11 facilitating their extended duration (Margari et al., 2010).

Besides this, two additional events are detected in our pollen record, U1385-11-fe8 and -fe9 (~377.5 and 374 ka, respectively), both characterized by weaker expansion of semi-desert plants and relatively moderate contraction of forest, reflecting less intense cooling and drying episodes on land (Fig. 5). While event -fe8 is coeval with a moderate SST cooling of ~3.3°C and a small peak in $\%C_{37:4}$, event -fe9 does not appear associated with SST and $\%C_{37:4}$ changes (Fig. 5). Despite the low temporal resolution, the MD01-2443 pollen record also documents a forest decline event at the transition MIS 11.23/11.22 that may correlate with event -fe8. Most of the North Atlantic records also display a moderate SST cooling event at the MIS 11.23/11.22 transition (de Abreu et al., 2005; Martrat et al., 2007; Tzedakis et al., 2009) with few IRD grains in the subpolar sediments (Oppo et al., 1998; Barker et al., 2015), possibly suggesting a minor iceberg pulse. Event -fe8 could be assimilated to the group of high intensity events mentioned above although the iceberg discharge, if any, appears too moderate to disrupt the AMOC. The weak and short-lived cold episodes on land and in the ocean as well as the lack of millennial-scale change in Antarctica concomitant with event -fe8, are in line with a still active AMOC. In contrast with event -fe8, no change in the North Atlantic SST appears related with event -fe9, contemporaneous with maximum in ice volume (MIS 11.22). This finding demonstrates that air-sea decoupling may also be a feature of periods with no ice-growth, further illustrating the complexity and diversity of millennial-scale climatic variability.

Conclusions

The new high temporal resolution multiproxy study of MIS 11 at Site U1385 documents SW Iberian vegetation and subtropical eastern North Atlantic sea surface changes at orbital and suborbital timescales.

1. At orbital timescales, our reconstruction shows the three classical forest phases of decreasing extent separated by open vegetation conditions (warm/humid - cold periods). The weak precessional forcing of MIS 11 is reflected in the overall low expansion of the Mediterranean forest (MF) and in particular the Mediterranean taxa, although higher forest expansion coincides with precession minima.

2. At millennial timescales, the Site U1385 pollen record reveals ten MF declines events indicating recurring cool and dry atmospheric episodes throughout MIS 11. The direct comparison between vegetation and oceanic changes allows the characterization of different types of millennial-scale events under distinct boundary conditions, highlighting the key role of ice-ocean-atmosphere interactions in the diversity of suborbital coolings:

- Site U1385 reveals a number of abrupt forest decline events indicating cooler and drier atmospheric conditions with no concurrent SST change. All these events occurred during low ice volume conditions associated with MIS 11c sea-level highstand, and MIS 11c/11b transition and late MIS 11.23, both characterized by weak ice sheet growth. We propose that these events were probably related with a frequent positive mode of the NAO-type, which led to enhanced aridity in SW Iberia but had a minor or unsystematic impact on local SSTs. The observed air–sea decoupling during MIS 11c/11b transition highlights the potential role of the thermal contrast on suborbital timescales on glacial inception by increasing northward transport of moisture, hence accelerating northern ice sheet growth.

- Particularly long, coldest, driest and windy events in SW Europe along with large SST cooling punctuated MIS 11b, an interval with larger ice volume conditions. These high intensity events were contemporaneous with the well-known prominent North Atlantic cooling events associated with iceberg discharges, likely originating from the European ice sheets. Our record supports that dynamics of northern ice sheets was a key factor for amplifying the magnitude of precipitation and temperature reduction in SW Europe and extending the duration of these abrupt climate changes. Modulation of millennial-scale

cooling events likely involves positive feedback mechanisms on AMOC related to freshwater from melting icebergs, changes in regional precipitation and the differential impact of iceberg discharges on deep-water circulation and regional climates depending on their origin. In addition, the sequence of these high intensity events correlates with warming in Antarctica suggesting that the interhemispheric link through the bipolar see-saw was active despite the European origin for iceberg pulses.

Supplementary data

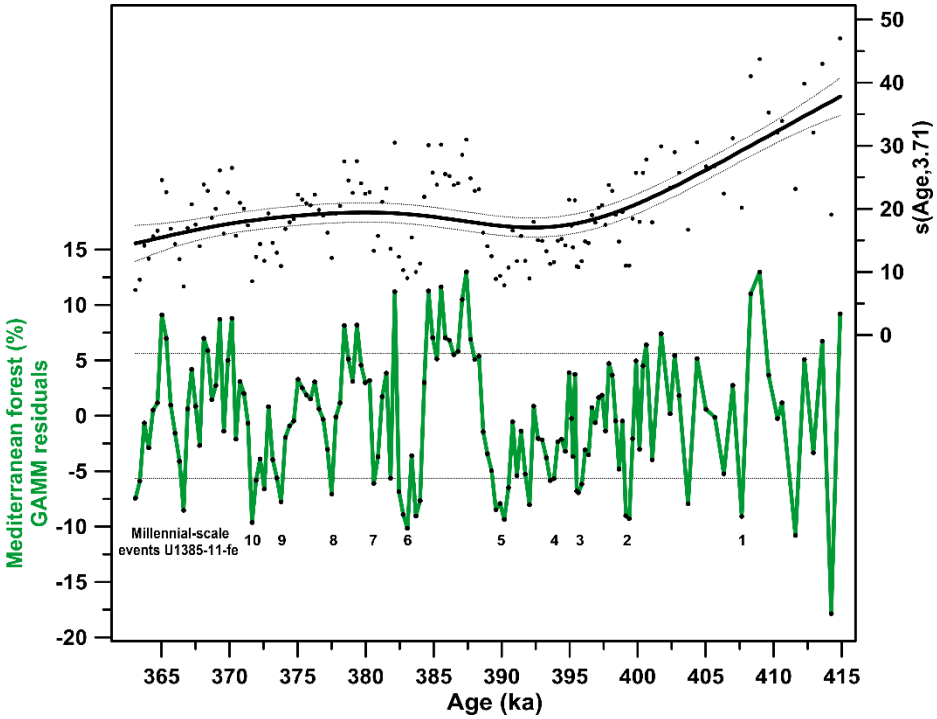

Supplementary Fig. 1. Predictions (bold line) with respective standard error (thin line) (top panel) and residuals (bottom panel) of the generalized additive mixed model (GAMM) of the change in Mediterranean forest data through time (%MF represented by the dots on the top panel). The normality of the residuals has not been rejected by the Shapiro–Wilk test. The millennial-scale forest decline events are considered based on the twofold condition that a minimum of one sample of the model residuals exceeded one standard deviation and that the substantial MF declines (> 10%) occur within at least 2 consecutive samples (events U1385-11-fe2 to fe-10). The forest event U1385-11-fe1 is characterized by a single sample, however it is associated with a pronounced decline in the MF of ~20% without subsequent forest recovery, indicating the occurrence of a millennial vegetation change.

Acknowledgments

This study used samples provided by the IODP Expedition 339. This work was funded by *WarmClim*, a CNRS LEFE-INSU IMAGO project. This research was also supported by the Portuguese Foundation for Science and Technology (FCT) through the project CLIMHOL (PTDC/AAC-CLI/100157/2008) and D. Oliveira's doctoral grant (SFRH/BD/9079/2012). We are very grateful to L. Devaux for technical assistance, as well as J. Etourneau and Z. Stroynowski for their helpful comments and editing. The editor Derek Booth, Terri Lacourse, Adele Bertini, Ian Candy and anonymous reviewer are thanked for their thoughtful suggestions.

References

Alley, R., Ágústsdóttir, A.M., 2005. The 8k event: cause and consequences of a major Holocene abrupt climate change. Quaternary Science Reviews 24, 1123–1149.

Amore, F.O., Flores, J.A., Voelker, A.H.L., Lebreiro, S.M., Palumbo, E., Sierro, F.J., 2012. A Middle Pleistocene Northeast Atlantic coccolithophore record: Paleoclimatology and paleoproductivity aspects. Marine Micropaleontology 90-91, 44–59. doi:10.1016/j.marmicro.2012.03.006.

Anav, A., Mariotti, A., 2011. Sensitivity of natural vegetation to climate change in the Euro-Mediterranean area. Climate Research 46, 277–292. doi:10.3354/cr00993.

Bard, E., Rostek, F., Turon, J. L., Gendreau, S., 2000. Hydrological impact of Heinrich events in the subtropical northeast Atlantic. Science 289(5483), 1321-1324. doi:10.1126/science.289.5483.1321.

Barker, S., Chen, J., Gong, X., Jonkers, L., Knorr, G., Thornalley, D., 2015. Icebergs not the trigger for North Atlantic cold events. Nature 520, 333–336. doi:10.1038/nature14330.

Bassinot, F.C., Labeyrie, L.D., Vincent, E., Quidelleur, X., Shackleton, N.J., Lancelot, Y., 1994. The astronomical theory of climate and the age of the Brunhes-Matuyama magnetic reversal. Earth and Planetary Science Letters 126, 91–108.

Bauch, H.A., 2012. Interglacial climates and the Atlantic meridional overturning circulation: is there an Arctic controversy? Quaternary Science Reviews 63, 1–22. doi:10.1016/j.quascirev.2012.11.023.

Bennett, K.D., 2000. Psimpoll and pscomb: computer programs for data plotting and analysis. Uppsala, Sweden: Quaternary Geology, Earth Sciences, Uppsala University. Software available on the internet at http://www.kv.geo.uu.se.

Berger, A., 1978. Long-Term variations of daily insolation and Quaternary climatic changes. Journal of Atmospheric Science, 35, 2362–2367.

Billups, K., Chaisson, W., Worsnopp, M., Thunell, R., 2004. Millennial-scale fluctuations in subtropical northwestern Atlantic surface ocean hydrography during the mid-Pleistocene. Paleoceanography 19(2), PA2017. doi:10.1029/2003pa000990.

Birks, H., Birks, H., 1980. Quaternary palaeoecology. London: Edward Arnold.

Blanco Castro, E., Casado González, M.A., Costa Tenorio M., Escribano Bombín, R., García Antón, M., Génova Fuster, M., Gómez Manzaneque, F., Moreno Sáiz, J.C., Morla Juaristi, C., Regato Pajares, P., Sáiz Ollero, H., 1997. Los bosques ibéricos: una Interpretación Geobotánica. Editorial Planeta, 572 p., Barcelona.

Candy, I., Schreve, D.C., Sherriff, J., Tye, G.J., 2014. Marine Isotope Stage 11: Palaeoclimates, palaeoenvironments and its role as an analogue for the current interglacial. Earth-Science Reviews 128, 18–51. doi:10.1016/j.earscirev.2013.09.006.

Chabaud, L., Sánchez Goñi, M.F., Desprat, S., Rossignol, L., 2014. Land-sea climatic variability in the eastern North Atlantic subtropical region over the last 14,200 years: atmospheric and oceanic processes at different timescales. The Holocene 24, 787–797. doi:10.1177/0959683614530439.

Cheddadi, R., Lamb, H.F., Guiot, J., Van Der Kaars, S., 1998. Holocene climatic change in Morocco: A quantitative reconstruction from pollen data. Climate Dynamics 14, 883–890. doi:10.1007/s003820050262.

Clark, P.U., Hostetler, S.W., Pisias, N.G., Schmittner, A., Meissner, K.J., 2007. Mechanisms for a ~7-kyr climate and sea-level oscillation during marine isotope stage 3, in Schmittner, A., Chiang, J., and Hemming, S., Eds., Ocean Circulation: Mechanisms and Impacts, American Geophysical Union, Geophysical Monograph 173, Washington, D.C., pp. 209-246.

Colville, E.J., Carlson, A.E., Beard, B.L., Hatfield, R.G., Stoner, J.S., Reyes, A. V, Ullman, D.J., 2011. Sr-Nd-Pb isotope evidence for ice-sheet presence on southern Greenland during the Last Interglacial. Science 333, 620–3. doi:10.1126/science.1204673.

Combourieu-Nebout, N., Peyron, O., Dormoy, I., Desprat, S., Beaudouin, C., Kotthoff, U., Marret, F., 2009. Rapid climatic variability in the west Mediterranean during the last 25 000 years from high resolution pollen data. Climate of the Past 5, 503–521. doi:10.5194/cp-5-503-2009.

Combourieu-Nebout, N., Turon, J.-L., Zahn, R., Capotondi, L., Londeix, L., Pahnke, K., 2002. Enhanced aridity and atmospheric high-pressure stability over the western Mediterranean during the North Atlantic cold events of the past 50 ky. Geology 30, 863–866.

Cortina, A., Sierro, F. J., Flores, J. A., Martrat, B., Grimalt, J. O., 2015. The response of SST to insolation and ice sheet variability from MIS 3 to MIS 11 in the northwestern Mediterranean Sea (Gulf of Lions). Geophysical Research Letters 42, 10, 366–10, 374. doi:10.1002/2015GL065539.

de Abreu, L., Abrantes, F., Shackleton, N.J., Tzedakis, P.C., McManus, J.F., Oppo, D.W., Hall, M.A., 2005. Ocean climate variability in the eastern North Atlantic during interglacial marine isotope stage 11: A partial analogue to the Holocene? Paleoceanography 20, 1–15. doi:10.1029/2004PA001091.

de Beaulieu, J.L., Andrieu-Ponel, V., Reille, M., Grüger, E., Tzedakis, C., Svobodova, H., 2001. An attempt at correlation between the Velay pollen sequence and the Middle Pleistocene stratigraphy from central Europe. Quaternary Science Reviews 20, 1593–1602. doi:10.1016/S0277-3791(01)00027-0.

de Vernal, A., Hillaire-Marcel, C., 2008. Natural variability of Greenland climate, vegetation, and ice volume during the past million years. Science 320, 1622–5. doi:10.1126/science.1153929.

Desprat, S., 2005. Réponses climatiques marines et continentales du Sud-Ouest de l'Europe lors des derniers interglaciaires et des entrées en glaciations. PhD Thesis, Bordeaux University, France, 282 pp.

Desprat, S., Combourieu-Nebout, N., Essallami, L., Sicre, M. A., Dormoy, I., Peyron, O., Siani, G., Bout Roumazeilles, V., Turon, J.L., 2013. Deglacial and Holocene vegetation and climatic changes in the southern central Mediterranean from a direct land-sea correlation. Climate of the Past 9, 767–787. doi:10.5194/cp-9-767-2013.

Desprat, S., Díaz Fernández, P.M., Coulon, T., Ezzat, L., Pessarossi-Langlois, J., Gil, L., Morales-Molino, C., Sánchez Goñi, M.F., 2015. *Pinus nigra* (European black pine) as the dominant species of the last glacial pinewoods in south-western to central Iberia: a morphological study of modern and fossil pollen. Journal of Biogeography 42, 1998–2009. doi:10.1111/jbi.12566.

Desprat, S., Sanchez Goni, M. F., Naughton, F., Turon, J.-L., Duprat, J., Malaize, B., Cortijo, E., Peypouquet, J.-P., 2007. Climate variability of the last five isotopic interglacials: Direct land-sea-ice correlation from the multiproxy analysis of North-Western Iberian margin deep-sea cores, in: The Climate of Past Interglacials, Developments in Quaternary Science, edited by: Sirocko, F., Litt, T., Claussen, M., Sánchez Goñi M. F., Elsevier, 375–386, 2007.

Desprat, S., Sánchez Goñi, M.F., McManus, J.F., Duprat, J., Cortijo, E., 2009. Millennial-scale climatic variability between 340000 and 270000 years ago in SW Europe: evidence from a NW Iberian margin pollen sequence. Climate of the Past 5, 53–72. doi:10.5194/cp-5-53-2009.

Desprat, S., Sánchez Goñi, M.F., Turon, J.L., McManus, J.F., Loutre, M.F., Duprat, J., Malaizé, B., Peyron, O., Peypouquet, J.P., 2005. Is vegetation responsible for glacial inception during periods of muted insolation changes? Quaternary Science Reviews 24, 1361–1374. doi:10.1016/j.quascirev.2005.01.005.

Dickson, A.J., Leng, M.J., Maslin, M.A., 2008. Mid-depth South Atlantic Ocean circulation and chemical stratification during MIS-10 to 12: implications for atmospheric CO_2. Climate of the Past 4, 333–344. doi:10.5194/cp-4-333-2008.

Dupont, L.M., Wyputta, U., 2003. Reconstructing pathways of aeolian pollen transport to the marine sediments along the coastline of SW Africa. Quaternary Science Reviews 22, 157–174.

Dutton, A., Carlson, A.E., Long, A.J., Milne, G.A., Clark, P.U., DeConto, R., Horton, B.P., Rahmstorf, S., Raymo, M.E., 2015. Sea-level rise due to polar ice-sheet mass loss during past warm periods. Science 349, aaa4019. doi:10.1126/science.aaa4019.

Elderfield, H., Ferretti, P., Greaves, M., Crowhurst, S., McCave, N., Hodell, D., Piotrowski, A.M., 2012. Evolution of ocean temperature and ice volume through the Mid- Pleistocene climate transition. Science 377, 704–709. doi:10.1126/science.1221294.

Expedition 339 Scientists, 2013. Site U1385. In: Stow, D.A.V., Hernández-Molina, F.J., Alvarez Zarikian, C.A., the Expedition 339 Scientists (Eds.), Proceedings IODP 339. Integrated Ocean Drilling Program Management International, Inc., Tokyo. http://dx.doi.org/10.2204/iodp.proc.339.103.201.

Fiúza, A. F. G., 1983. Upwelling patterns off Portugal, in Coastal Upwelling, Its Sediment Record, edited by E. Suess and J. Thiede, pp. 85–98, Plenum, New York.

Fiúza, A. F. G., Macedo, M. E., Guerreiro, M.R., 1982. Climatological space and time variation of the Portuguese coastal upwelling. Oceanologica Acta, 5(1), 31–40.

Fletcher, W.J., Debret, Sánchez Goñi, M.F., 2012. Mid-Holocene emergence of a low-frequency millennial oscillation in western Mediterranean climate: Implications for past dynamics of the North Atlantic atmospheric westerlies. The Holocene 23, 153–166. doi:10.1177/095968361246078.

Fletcher, W.J., Sánchez Goñi, M.F., 2008. Orbital- and sub-orbital-scale climate impacts on vegetation of the western Mediterranean basin over the last 48,000 yr. Quaternary Research 70, 451–464. doi:10.1016/j.yqres.2008.07.002.

Fletcher, W.J., Sánchez Goñi, M.F., Peyron, O., Dormoy, I., 2010. Abrupt climate changes of the last deglaciation detected in a Western Mediterranean forest record. Climate of the Past 6, 245–264. doi:10.5194/cp-6-245-2010.

Gao, X., Giorgi, F., 2008. Increased aridity in the Mediterranean region under greenhouse gas forcing estimated from high resolution simulations with a regional climate model. Global and Planetary Change 62, 195–209. doi:10.1016/j.gloplacha.2008.02.002.

Gouveia, C., Trigo, R.M., DaCamara, C.C., Libonati, R., Pereira, J.M.C., 2008. The North Atlantic Oscillation and European vegetation dynamics. International Journal of Climatology, 28, 1835-1847.

Gimeno, L., Nieto, R., Trigo, R.M., Vicente-Serrano, S.M., López-Moreno, J.I., 2010. Where Does the Iberian Peninsula Moisture Come From? An Answer Based on a Lagrangian Approach. Journal of Hydrometeorology 11, 421–436. doi:10.1175/2009JHM1182.1.

Giorgi, F., 2006. Climate change hot-spots. Geophysical Research Letters 33, L08707. doi:10.1029/2006GL025734.

Grousset, F. E., Pujol, C., Labeyrie, L., Auffret, G., Boelaert, A., 2000. Were the North Atlantic Heinrich events triggered by the behavior of the European ice sheets? Geology 28, 2, 123-126.

Hall, I.R., Becker, J., 2007. Deep western boundary current variability in the subtropical northwest Atlantic Ocean during marine isotope stages 12-10. Geochemistry, Geophysics, Geosystems 8, 1–14. doi:10.1029/2006GC001518.

Heusser, L., Balsam, W.L., 1977. Pollen distribution in the northeast Pacific Ocean. Quaternary Research 7, 45–62. doi:10.1016/0033-5894(77)90013-8.

Hodell, D., Crowhurst, S., Skinner, L., Tzedakis, P.C., Margari, V., Channell, J.E.T., Kamenov, G., MacLachlan, S., Rothwell, G., 2013a. Response of Iberian Margin sediments to orbital and suborbital forcing over the past 420 ka. Paleoceanography 28, 185–199. doi:10.1002/palo.20017.

Hodell, D., Lourens, L., Crowhurst, S., Konijnendijk, T., Tjallingii, R., Jimenez-Espejo, F., Skinner, L., Tzedakis, P.C., 2015. A reference time scale for Site U1385 (Shackleton Site) on the SW Iberian Margin. Global and Planetary Change 1385, 49–64. doi:10.1016/j.gloplacha.2015.07.002.

Hodell, D.A., Channell, J.E.T., Curtis, J.H., Romero, O.E., Röhl, U., 2008. Onset of "Hudson Strait" Heinrich events in the eastern North Atlantic at the end of the middle Pleistocene transition (~640 ka)? Paleoceanography 23, 1–16. doi:10.1029/2008PA001591.

Hodell, D.A., Lourens, L., Stow, D. V, Hernández-Molina, J., Alvarez Zarikian, C., Shackleton Site Project Members, 2013b. The "Shackleton Site" (IODP Site U1385) on the Iberian Margin. Proceedings of the Integrated Ocean Drilling Program 16, 13–19. doi:10.5194/sd-16-13-2013.

Hurrell, J.W., 1995. Decadal trends in the North Atlantic Oscillation: regional temperatures and precipitation. Science 269, 676–9. doi:10.1126/science.269.5224.676.

IPCC, 2013. Climate Change 2013: The Physical Science Basis. Contribution of Working Group I to the Fifth Assessment Report of the Intergovernmental Panel on Climate Change [Stocker, T.F., D. Qin, G.-K. Plattner, M. Tignor, S.K. Allen, J. Boschung, A. Nauels, Y. Xia, V. Bex and P.M. Midgley (eds.)]. Cambridge University Press, Cambridge, United Kingdom and New York, NY, USA, 1535 pp. doi:10.1017/CBO9781107415324.

Jouzel, J., Masson-Delmotte, V., Cattani, O., Dreyfus, G., Falourd, S., Hoffmann, G., Minster, B., Nouet, J., Barnola, J.M., Chappellaz, J., Fischer, H., Gallet, J.C., Johnsen, S., Leuenberger, M., Loulergue, L., Luethi, D., Oerter, H., Parrenin, F., Raisbeck, G., Raynaud, D., Schilt, A., Schwander, J., Selmo, E., Souchez, R., Spahni, R., Stauffer, B., Steffensen, J.P., Stenni, B., Stocker, T.F., Tison, J.L., Werner, M., Wolff, E.W., 2007. Orbital and millennial Antarctic climate variability over the past 800,000 years. Science 317, 793–796. doi:10.1126/science.1141038.

Juggins, S., 2009. Package "rioja" – Analysis of Quaternary Science Data. The Comprehensive R Archive Network.

Koutsodendris, A., Brauer, A., Pälike, H., Müller, U.C., Dulski, P., Lotter, A.F., Pross, J., 2011. Sub-decadal- to decadal-scale climate cyclicity during the Holsteinian interglacial (MIS 11) evidenced in annually laminated sediments. Climate of the Past 7, 987–999. doi:10.5194/cp-7-987-2011.

Koutsodendris, A., Müller, U.C., Pross, J., Brauer, A., Kotthoff, U., Lotter, A.F., 2010. Vegetation dynamics and climate variability during the Holsteinian interglacial based on a pollen record from Dethlingen (northern Germany). Quaternary Science Reviews 29, 3298–3307. doi:10.1016/j.quascirev.2010.07.024.

Koutsodendris, A., Pross, J., Müller, U.C., Brauer, A., Fletcher, W.J., Kühl, N., Kirilova, E., Verhagen, F.T.M., Lücke, A., Lotter, A.F., 2012. A short-term climate oscillation during the Holsteinian interglacial (MIS 11c): An analogy to the 8.2ka climatic event? Global and Planetary Change 92-93, 224–235. doi:10.1016/j.gloplacha.2012.05.011.

Lionello, P., Malanotte-Rizzoli, P., Boscolo, R., Alpert, P., Artale, V., Li, L., Luterbacher, J., May, W., Trigo, R., Tsimplis, M., Ulbrich, U., Xoplaki, E., 2006. The Mediterranean climate: An overview of the main characteristics and issues. Developments in Earth and Environmental Sciences 4, 1–26. doi:10.1016/S1571-9197(06)80003-0.

Lisiecki, L.E., Raymo, M.E., 2005. A Pliocene–Pleistocene stack of 57 globally-distributed benthic $\delta^{18}O$ records. Paleoceanography 20, PA1003. http://dx.doi.org/10.1029/ 2004PA001071.

Loidi, J., Biurrun, I., Campos, J. A., Garcıa-Mijangos, I., Herrera, M., 2007. A survey of heath vegetation of the Iberian Peninsula and Northern Morocco: a biogeographical and bioclimatic approach. Phytocoenologia 37, 341-370.

Loutre, M.F., Berger, A.L., 2003. Marine Isotope Stage 11 as an analogue for the present interglacial. Global and Planetary Change 36, 209–217. doi:10.1016/S0921-8181(02)00186-8.

Magri, D., 2012. Quaternary History of *Cedrus* in Southern Europe. Annali Di Botanica 57–66. doi:10.4462/annbotrm-10022.

Maiorano, P., Marino, M., Balestra, B., Flores, J.-A., Hodell, D.A., Rodrigues, T., 2015. Coccolithophore variability from the Shackleton Site (IODP Site U1385) through MIS 16-10. Global and Planetary Change 133, 35–48. doi:10.1016/j.gloplacha.2015.07.009.

Margari, V., Skinner, L. C., Tzedakis, P. C., Ganopolski, A., Vautravers, M., Shackleton, N. J., 2010. The nature of millennial-scale climate variability during the past two glacial periods. Nature Geoscience 3, 127-131.

Marino, M., Maiorano, P., Tarantino, F., Voelker, A., Capotondi, L., Girone, A., Lirer, F., Flores, J.A., Naafs, B.D.A, 2014. Coccolithophores as proxy of seawater changes at orbital-to-millennial scale during middle Pleistocene Marine Isotope Stages 14-9 in North Atlantic core MD01-2446. Paleoceanography 29, 518–532. doi:10.1002/2013PA002574.

Martrat, B., Grimalt, J.O., Lopez-Martinez, C., Cacho, I., Sierro, F.J., Flores, J.A., Zahn, R., Canals, M., Curtis, J.H., Hodell, D.A., 2004. Abrupt Temperature Changes in the Western Mediterranean over the past 250,000 years. Science 306(5702), 1762–1765. doi:10.1126/science.1101706.

Martrat, B., Grimalt, J.O., Shackleton, N.J., de Abreu, L., Hutterli, M. A, Stocker, T.F., 2007. Four climate cycles of recurring deep and surface water destabilizations on the Iberian margin. Science 317, 502–507. doi:10.1126/science.1139994.

McAndrews, JH, King, J., 1976. Pollen of the North American Quaternary: the top twenty. Geoscience and Man 15, 41–49.

McManus, J., Oppo, D., Cullen, J., Healey, S., 2003. Marine Isotope Stage 11 (MIS 11): analog for Holocene and future climate? In: Droxler, A.W., Poore, R.Z., Burckle, L.H. (Eds.), Earth's Climate and Orbital Eccentricity: The Marine Isotope Stage 11 Question. AGU Geophysical Monograph Series No. 137, pp. 61–6.

McManus, J.F., Oppo, D.W., Cullen, J.L., 1999. A 0.5-Million-Year Record of Millennial-Scale Climate Variability in the North Atlantic. Science 283, 971–974.

Melles, M., Brigham-Grette, J., Minyuk, P.S., Nowaczyk, N.R.,Wennrich, V., DeConto, R.M., Anderson, P.M., Andreev, A.A., Coletti, A., Cook, T.L., Haltia-Hovi, E., Kukkonen, M., Lozhkin, A.V., Rosen, P., Tarasov, P., Vogel, H., Wagner, B., 2012. 2.8 million years of Arctic climate change from Lake El'gygytgyn, NE Russia. Science 337, 315–320. doi:10.1126/science.1222135.

Milker, Y., Rachmayani, R., Weinkauf, M.F.G., Prange, M., Raitzsch, M., Schulz, M., Kučera, M., 2013. Global and regional sea surface temperature trends during Marine Isotope Stage 11. Climate of the Past 9, 2231–2252. doi:10.5194/cp-9-2231-2013.

Moffa-Sánchez, P., Born, A., Hall, I.R., Thornalley, D.J.R., Barker, S., 2014. Solar forcing of North Atlantic surface temperature and salinity over the past millennium. Nature Geoscience 7, 275–278. doi:10.1038/ngeo2094.

Moore, P.D., Webb, J.A., Collinson, M.E., 1991. Pollen analysis. Oxford, Blackwell scientific publication, 2nd edition, 216 p.

Mudie, P., McCarthy, F., 2006. Marine palynology: potentials for onshore—offshore correlation of Pleistocene—Holocene records. Transactions of the Royal Society of South Africa 61, 139–157.

Müller, P.J., Kirst, G., Ruhland, G., Von Storch, I., Rosell-Melé, A., 1998. Calibration of the alkenone paleotemperature index Uk'_{37}- based on core-tops from the eastern South Atlantic and the global ocean (60°N-60°S). Geochimica et Cosmochimica Acta 62, 1757–1772.

Naughton, F., Sánchez Goñi, M.F., Desprat, S., Turon, J.L., Duprat, J., Malaizé, B., Joli, C., Cortijo, E., Drago, T., Freitas, M.C., 2007. Present-day and past (last 25 000 years) marine pollen signal off western Iberia. Marine Micropaleontology 62, 91–114. doi:10.1016/j.marmicro.2006.07.006.

Naughton, F., Sánchez Goñi, M.F., Kageyama, M., Bard, E., Cortijo, E., Desprat, S., Duprat, J., Malaizé, B., Joli, C., Rostek, F., Turon, J.-L., 2009. Wet to dry climatic trend in north western Iberia within Heinrich events. Earth and Planetary Science Letters 284, 329–342.

Oort, A. H., Vander Haar, T. H., 1976. On the observed annual cycle in the ocean-atmosphere heat balance over the northern hemisphere. Journal of Physical Oceanography 6, 781-800.

Oppo, D.W., McManus, J.F., Cullen, J.L., 1998. Abrupt climate events 500,000 to 340,000 years ago: Evidence from subpolar North Atlantic sediments. Science 279, 1335–1338.

Ortega, P., Lehner, F., Swingedouw, D., Masson-Delmotte, V., Raible, C.C., Casado, M., Yiou, P., 2015. A model-tested North Atlantic Oscillation reconstruction for the past millennium. Nature 523, 71–74. doi:10.1038/nature14518.

Palumbo, E., Flores, J.-A., Perugia, C., Petrillo, Z., Voelker, A.H.L., Amore, F.O., 2013. Millennial scale coccolithophore paleoproductivity and surface water changes between 445 and 360ka (Marine Isotope Stages 12/11) in the Northeast Atlantic. Palaeogeography, Palaeoclimatology, Palaeoecology 383-384, 27–41. doi:http://dx.doi.org/10.1016/j.palaeo.2013.04.024.

Peinado Lorca, M., Martinez-Parras, J.M., 1987. Castilla-La Mancha. In: Peinado Lorca M and Rivas-Martinez S (eds) La vegetación de España. Alcala de Henares: Universidad de Alcala de Henares, pp. 163–196.

Peliz, Á., Dubert, J., Santos, A. M.P., Oliveira, P.B., Le Cann, B., 2005. Winter upper ocean circulation in the Western Iberian Basin - Fronts, Eddies and Poleward Flows: An overview. Deep-Sea Research Part I, 52(4), 621–646. doi:10.1016/j.dsr.2004.11.005.

Peterson, G. M., 1983. Recent pollen spectra and zonal vegetation in the western USSR. Quaternary Science Reviews 2(4), 281-321.

Pol, K., Debret, M., Masson-Delmotte, V., Capron, E., Cattani, O., Dreyfus, G., Falourd, S., Johnsen, S., Jouzel, J., Landais, A., Minster, B., Stenni, B., 2011. Links between MIS 11 millennial to sub-millennial climate variability and long term trends as revealed by new high resolution EPICA Dome C deuterium data - A comparison with the Holocene. Climate of the Past 7, 437–450. doi:10.5194/cp-7-437-2011.

Poli, M.S., Thunnel, R.C., Rio, D., 2000. Millennial-scale changes in North Atlantic Deep Water circulation during marine isotope stages 11 and 12: Linkage to Antarctic climate. Geology 28, 807–810.

Polunin, O., Walters, M., 1985. A Guide to the Vegetation of Britain and Europe. Oxford University Press, New York 238pp.

Prentice, L.C., 1978. Modern pollen spectra from lake sediments in Finland and Finnmark, north Norway. Boreas 7, 131–153.

Prokopenko, A.A., Bezrukova, E. V., Khursevich, G.K., Solotchina, E.P., Kuzmin, M.I., Tarasov, P.E., 2010. Climate in continental interior Asia during the longest interglacial of the past 500 000 years: the new MIS 11 records from Lake Baikal, SE Siberia. Climate of the Past 6, 31–48. doi:10.5194/cp-6-31-2010.

Quezel, P., 2002. Réflexions sur l'évolution de la flore et de la végétation au Maghreb méditerranéen. Ibis Press, Paris.

R Core Team, 2014. R: A language and environment for statistical computing. R Foundation for Statistical Computing, Vienna, Austria. URL http://www.R-project.org/.

Railsback, L.B., Gibbard, P.L., Head, M.J., Voarintsoa, N.R.G., Toucanne, S., 2015. An optimized scheme of lettered marine isotope substages for the last 1.0 million years, and the climatostratigraphic nature of isotope stages and substages. Quaternary Science Reviews 111, 94–106. doi:http://dx.doi.org/10.1016/j.quascirev.2015.01.012.

Raymo, M.E., Mitrovica, J.X., 2012. Collapse of polar ice sheets during the stage 11 interglacial. Nature 483, 453–456. doi:10.1038/nature10891.

Raynaud, D., Barnola, J.-M., Souchez, R., Lorrain, R., Petit, J.-R., Duval, P., Lipenkov, V.Y., 2005. Palaeoclimatology: the record for marine isotopic stage 11. Nature 436, 39–40. doi:10.1038/43639b.

Reille, M., 1992. Pollen et spores d'Europe et d'Afrique du Nord. Marseille, Laboratoire de botanique historique et palynologie, 520 p.

Reille, M., Beaulieu, J.-L. De, Svobodova, H., Andrieu-Ponel, V., Goeury, C., 2000. Pollen analytical biostratigraphy of the last five climatic cycles from a long continental sequence from the Velay region (Massif Central, France). Journal of Quaternary Science 15, 665–685.

Reyes, A. V, Carlson, A.E., Beard, B.L., Hatfield, R.G., Stoner, J.S., Winsor, K., Welke, B., Ullman, D.J., 2014. South Greenland ice-sheet collapse during Marine Isotope Stage 11. Nature 510, 525–8. doi:10.1038/nature13456.

Roberts, D.L., Karkanas, P., Jacobs, Z., Marean, C.W., Roberts, R.G., 2012. Melting ice sheets 400,000 yr ago raised sea level by 13 m: Past analogue for future trends. Earth and Planetary Science Letters 357–358, 226–237. doi:http://dx.doi.org/10.1016/j.epsl.2012.09.006.

Roche, D.M., Wiersma, A.P., Renssen, H., 2010. A systematic study of the impact of freshwater pulses with respect to different geographical locations. Climate Dynamics 34, 997–1013. doi:10.1007/s00382-009-0578-8.

Rodrigues, T., Grimalt, J.O., Abrantes, F., Flores, J.A., Lebreiro, S., 2009. Holocene interdependences of changes in sea surface temperature, productivity and fluvial inputs in the Iberian continental shelf (Tagus mud patch). Geochemistry, Geophysics, Geosystems, 10 (7). doi:10.1029/2008GC002367.

Rodrigues, T., Voelker, A.H.L., Grimalt, J.O., Abrantes, F., Naughton, F., 2011. Iberian Margin sea surface temperature during MIS 15 to 9 (580–300 ka): Glacial suborbital variability versus interglacial stability. Paleoceanography 26, PA1204. doi:10.1029/2010PA001927.

Rohling, E. J., Grant, K., Bolshaw, M., Roberts, A. P., Siddall, M., Hemleben, C., Kucera, M., 2009. Antarctic temperature and global sea level closely coupled over the past five glacial cycles. Nature Geoscience 2, 500–504. doi:10.1038/ngeo557.

Roucoux, K.H., Tzedakis, P.C., de Abreu, L., Shackleton, N.J., 2006. Climate and vegetation changes 180,000 to 345,000 years ago recorded in a deep-sea core off Portugal. Earth and Planetary Science Letters 249, 307–325. doi:10.1016/j.epsl.2006.07.005.

Sánchez Goñi, M.F., Bard, E., Landais, A., Rossignol, L., d'Errico, F., 2013. Air–sea temperature decoupling in western Europe during the last interglacial–glacial transition. Nature Geoscience 6, 837–841. doi:10.1038/ngeo1924.

Sánchez Goñi, M.F., Cacho, I., Turon, J., Guiot, J., Sierro, F., Peypouquet, J., Grimalt, J., Shackleton, N., 2002. Synchroneity between marine and terrestrial responses to millennial scale climatic variability during the last glacial period in the Mediterranean region. Climate Dynamics 19, 95–105. doi:10.1007/s00382-001-0212-x.

Sánchez Goñi, M.F., Eynaud, F., Turon, J.L., Shackleton, N.J., 1999. High resolution palynological record off the Iberian margin: Direct land-sea correlation for the Last Interglacial complex. Earth and Planetary Science Letters 171, 123–137.

Sánchez Goñi, M.F., Landais, A., Fletcher, W.J., Naughton, F., Desprat, S., Duprat, J., 2008. Contrasting impacts of Dansgaard-Oeschger events over a western European latitudinal transect modulated by orbital parameters. Quaternary Science Reviews 27, 1136–1151. doi:10.1016/j.quascirev.2008.03.003.

Sánchez Goñi, M.F., Loutre, M.F., Crucifix, M., Peyron, O., Santos, L., Duprat, J., Malaizé, B., Turon, J.L., Peypouquet, J.P., 2005. Increasing vegetation and climate gradient in Western Europe over the Last Glacial Inception (122-110 ka): Data-model comparison. Earth and Planetary Science Letters 231, 111–130. doi:10.1016/j.epsl.2004.12.010.

Sánchez Goñi, M.F., Turon, J.L., Eynaud, F., Gendreau, S., 2000. European climatic response to millennial-scale changes in the atmosphere-ocean system during the last glacial period. Quaternary Research 54, 394–403. doi:10.1006/qres.2000.2176.

Sánchez-Goñi, M.F., Landais, A., Cacho, I., Duprat, J., Rossignol, L., 2009. Contrasting intrainterstadial climatic evolution between high and middle North Atlantic latitudes: A close-up of Greenland Interstadials 8 and 12. Geochemistry, Geophysics, Geosystems 10. doi:10.1029/2008GC002369.

Santini, M., Collalti, A., Valentini, R., 2014. Climate change impacts on vegetation and water cycle in the Euro-Mediterranean region, studied by a likelihood approach. Regional Environmental Change 14, 1405–1418. doi:10.1007/s10113-013-0582-8.

Shackleton, N. J, Fairbanks, R. G., Chiu, T.-C., Parrenin, F., 2004. Absolute calibration of the Greenland time scale: implications for Antarctic time scales and for Δ14C. Quaternary Science Reviews 23, 1513–1522. doi:10.1016/j.quascirev.2004.03.006.

Shackleton, N.J., Hall, M.A., Vincent, E., 2000. Phase relationships between millennial-scale events 64,000-24,000 years ago. Paleoceanography 15, 565–569. doi:10.1029/2000PA000513.

Shackleton, N.J., Sánchez-Goñi, M.F., Pailler, D., Lancelot, Y., 2003. Marine Isotope Substage 5e and the Eemian Interglacial. Global and Planetary Change 36, 151–155. doi:10.1016/S0921-8181(02)00181-9.

Skinner, L.C., Shackleton, N.J., 2005. An Atlantic lead over Pacific deep-water change across Termination I: implications for the application of the marine isotope stage stratigraphy. Quaternary Science Reviews 24, 571–580. doi:10.1016/j.quascirev.2004.11.008.

Sousa P., Barriopedro D., Trigo R.M., Ramos A.M., Nieto R. Gimeno L., Turkman K.F., Liberato M.L.R., 2015b. Impact of Euro-Atlantic blocking patterns in Iberia precipitation using a novel high resolution dataset. Climate Dynamics, 1-19. doi 10.1007/s00382-015-2718-7.

Sousa, P., Trigo, R.M., Pereira, M., Bedia, J., Gutierrez, J.M., 2015a. Different approaches to model future burnt area in the Iberian Peninsula. Agricultural and Forest Meteorology 202, 11-25. doi: 10.1016/j.agrformet.2014.11.018.

Stein, R., Hefter, J., Grützner, J., Voelker, A., Naafs, B.D.A., 2009. Variability of surface water characteristics and Heinrich-like events in the Pleistocene midlatitude North Atlantic Ocean: Biomarker and XRD records from IODP Site U1313 (MIS 16–9). Paleoceanography 24, PA2203. doi:10.1029/2008pa001639.

Trigo, R.M., Pozo- Vázquez, D., Osborn, T.J., Castro-Díez, Y., Gamiz-Fortis, S., Esteban-Parra, M.J., 2004. North Atlantic Oscillation influence on precipitation, river flow and water resources in the Iberian Peninsula. International Journal of Climatology 24, 925–944. doi:10.1002/joc.1048.

Tye, G.J., Sherriff, J., Candy, I., Coxon, P., Palmer, A., McClymont, E.L., Schreve, D.C., 2016. The $\delta^{18}O$ stratigraphy of the Hoxnian lacustrine sequence at Marks Tey, Essex, UK: implications for the climatic structure of MIS 11 in Britain. Journal of Quaternary Science 31, 75–92. doi:10.1002/jqs.2840.

Tzedakis, P. C., Channell, J. E. T., Hodell, D. A., Kleiven, H. F., Skinner, L. C., 2012. Determining the natural length of the current interglacial. Nature Geoscience 5, 2, 138-142.

Tzedakis, P. C., Roucoux, K. H., de Abreu, L., Shackleton, N. J., 2004. The Duration of Forest Stages in Southern Europe and Interglacial Climate Variability. Science 306, 2231–2235. doi:10.1126/science.1102398.

Tzedakis, P.C., 2010. The MIS 11 – MIS 1 analogy, southern European vegetation, atmospheric methane and the "early anthropogenic hypothesis". Climate of the Past 6, 131–144. doi:10.5194/cp-6-131-2010.

Tzedakis, P.C., Andrieu, V., De Beaulieu, J.L., Birks, H.J.B., Crowhurst, S., Follieri, M., Hooghiemstra, H., Magri, D., Reille, M., Sadori, L., Shackleton, N.J., Wijmstra, T. A., 2001. Establishing a terrestrial chronological framework as a basis for biostratigraphical comparisons. Quaternary Science Reviews 20, 1583–1592. doi:10.1016/S0277-3791(01)00025-7.

Tzedakis, P.C., Pälike, H., Roucoux, K.H., de Abreu, L., 2009. Atmospheric methane, southern European vegetation and low-mid latitude links on orbital and millennial timescales. Earth and Planetary Science Letters 277, 307–317. doi:10.1016/j.epsl.2008.10.027.

Villanueva, J., Grimalt, J.O., Cortijo, E., Vidal, L., Labeyriez, L., 1997a. A biomarker approach to the organic matter deposited in the North Atlantic during the last climatic cycle. Geochimica et Cosmochimica Acta 61, 4633–4646.

Villanueva, J., Pelejero, C., Grimalt, J.O., 1997b. Clean-up procedures for the unbiased estimation of C_{37} alkenone sea surface temperatures and terrigenous n-alkane inputs in paleoceanography. Journal of Chromatography A 757, 145–151.

Voelker, A.H.L., Rodrigues, T., Billups, K., Oppo, D., McManus, J., Stein, R., Hefter, J., Grimalt, J.O., 2010. Variations in mid-latitude North Atlantic surface water properties during the mid-Brunhes (MIS 9–14) and their implications for the thermohaline circulation. Climate of the Past 6, 531–552. doi:10.5194/cp-6-531-2010.

Walter, H., Breckle, S.-W., 1989. Ecological Systems of the Geobiosphere: 3 Temperate and Polar Zonobiomes of Northern Eurasia, Springer-Verlag Berlin Heidelberg.

Walter, K., Graf, H.-F., 2002. On the changing nature of the regional connection between the North Atlantic Oscillation and sea surface temperature. Journal of Geophysical Research 107(D17), 4338. doi:10.1029/2001JD000850.

Wijmstra, T.A., Smit, A., 1976. Palynology of the middle part (30–78 m) of the 120m deep section in Northern Greece (Macedonia). Acta Botanica Neerlandica 25, 297–312.

Wood, S.N., 2006. Generalized Additive Models: An Introduction with R. Chapman and Hall/CRC Press.

Wright, J.H.E., McAndrews, J.H., van Zeist, W., 1967. Modern pollen rain in western Iran, and its relation to plant geography and Quaternary vegetational history. Journal of Ecology 415–443.

Yin, Q.Z., Berger, A., 2012. Individual contribution of insolation and CO_2 to the interglacial climates of the past 800,000 years. Climate Dynamics 38, 709–724. doi:10.1007/s00382-011-1013-5.

Zuur, A.F., Ieno, E.N., Walker, N., Saveliev, A.A., Smith, G.M., 2009. Mixed effects models and extensions in ecology with R, Statistics for Biology and Health. Springer New York, New York, NY. doi:10.1007/978-0-387-87458-6.

Chapter 3

Unexpected weak seasonal climate in the western Mediterranean region during MIS 31, a high-insolation forced interglacial

Unexpected weak seasonal climate in the western Mediterranean region during MIS 31, a high-insolation forced interglacial

Dulce Oliveira (1) (2) (3) (4); Maria Fernanda Sánchez Goñi (1) (2); Filipa Naughton (3) (4); J.M. Polanco-Martínez (1) (2) (3); Francisco J. Jimenez-Espejo (6); Joan O. Grimalt (7); Belen Martrat (7); Antje H.L. Voelker (3) (4); Ricardo Trigo (8); David Hodell (9); Fátima Abrantes (3) (4); Stéphanie Desprat(1) (2)

(1) EPHE, PSL Research University, Laboratoire Paléoclimatologie et Paléoenvironnements Marins, F-33615 Pessac, France

(2) Univ. Bordeaux, EPOC, UMR 5805, F-33615 Pessac, France

(3) Divisão de Geologia e Georecursos Marinhos, Instituto Português do Mar e da Atmosfera (IPMA), Avenida de Brasília 6, 1449-006 Lisboa, Portugal

(4) CCMAR, Centro de Ciências do Mar, Universidade do Algarve, Campus de Gambelas, 8005-139 Faro, Portugal

(5) Basque Centre for Climate Change – BC3, Edificio Sede No. 1, 1a, Parque Científico de la UPV/EHU, 48940 Leioa, Spain

(6) Department of Biogeochemistry, Japan Agency for Marine-Earth Science and Technology (JAMSTEC), 2-15 Natsushima, Yokosuka 237-0061, Japan

(7) Department of Environmental Chemistry, Institute of Environmental Assessment and Water Research (IDAEA), Spanish Council for Scientific Research (CSIC), 08034 Barcelona, Spain

(8) Instituto Dom Luiz, Universidade de Lisboa, 1749-016 Lisboa, Portugal

(9) Godwin Laboratory for Palaeoclimate Research, Department of Earth Sciences, University of Cambridge, UK

Published in: QUATERNARY SCIENCE REVIEWS 161, 1-17 (2017)

Abstract

Marine Isotope Stage 31 (MIS 31) is an important analogue for ongoing and projected global warming, yet key questions remain about the regional signature of its extreme orbital forcing and intra-interglacial variability. Based on a new direct land-sea comparison in SW Iberian margin IODP Site U1385 we examine the climatic variability between 1100 and 1050 ka including the "super interglacial" MIS 31, a period dominated by the 41-ky obliquity periodicity. Pollen and biomarker analyses at centennial-scale-resolution provide new insights into the regional vegetation, precipitation regime and atmospheric and oceanic temperature variability on orbital and suborbital timescales. Our study reveals that atmospheric and SST warmth during MIS 31 was not exceptional in this region highly sensitive to precession. Unexpectedly, this warm stage stands out as a prolonged interval of a temperate and humid climate regime with reduced seasonality, despite the high insolation (precession minima values) forcing. We find that the dominant forcing on the long-term temperate forest development was obliquity, which may have induced a decrease in summer dryness and associated reduction in seasonal precipitation contrast. Moreover, this study provides the first evidence for persistent atmospheric millennial-scale variability during this interval with multiple forest decline events reflecting repeated cooling and drying episodes in SW Iberia. Our direct land-sea comparison shows that the expression of the suborbital cooling events on SW Iberian ecosystems is modulated by the predominance of high or low-latitude forcing depending on the glacial/interglacial baseline climate states. Severe dryness and air-sea cooling is detected under the larger ice volume during glacial MIS 32 and MIS 30. The extreme episodes, which in their climatic imprint are similar to the Heinrich events, are likely related to northern latitude ice sheet instability and a disruption of the Atlantic Meridional Overturning Circulation (AMOC). In contrast, forest declines during MIS 31 are associated to neither SST cooling nor high-latitude freshwater forcing. Time-series analysis reveals a dominant cyclicity of about 6 ky in the temperate forest record, which points to a potential link with the fourth harmonic of precession and thus low-latitude insolation forcing.

Keywords: Marine Isotope Stage (MIS) 31; Super interglacial; Early Pleistocene; Iberian margin; Mediterranean vegetation; Obliquity and precession forcing; Millennial-scale climate variability; Precession harmonics; Land-sea comparison; Pollen analysis.

1. Introduction

The climate transition occurring between the early Pleistocene 41-ky (obliquity-driven) glacial-interglacial cycles and late Pleistocene 100-ky climate cycles (eccentricity-driven) is known as the Mid Pleistocene Transition (MPT, ~1250–700 ka, Clark et al., 2006), and more recently as the Early Middle Pleistocene Transition (Head and Gibbard, 2015). Within this important and complex transitional interval, but prior to the dominant eccentricity-driven cycles (e.g. Mudelsee and Schulz, 1997), Marine Isotopic Stage 31 (MIS 31; 1081–1062 ka; Lisiecki and Raymo, 2005) stands out for its unusual orbital configuration (high obliquity and eccentricity and minima in precession) leading to some of the highest summer insolation levels of the Pleistocene, with a Northern Hemisphere (NH) maximum at 1070 ka bracketed by two Southern Hemisphere (SH) maxima (Laskar et al., 2004). This strong orbital forcing combined with relatively high CO_2 levels (Hönisch et al., 2009; Tripati et al., 2011) contributed to such a remarkable warmth in the high-latitudes that MIS 31 has been described as a "super interglacial" (Pollard and DeConto, 2009; DeConto et al., 2012; Melles et al., 2012; Coletti et al., 2015). Model-predicted ~20 m of eustatic sea-level rise relative to present (Raymo et al., 2006) would be related to major retreats of Greenland, western (WAIS) and eastern Antarctica ice sheets (EAIS), or some combination of the three (Scherer et al., 2008; Naish et al., 2009; Pollard and DeConto, 2009; DeConto et al., 2012; McKay et al., 2012; Melles et al., 2012; Teitler et al., 2015). The few records currently available provide evidence for MIS 31 warmth across most of the world (Ruddiman et al., 1989; Byrami et al., 2005; Medina-Elizalde and Lea, 2005; McClymont et al., 2008; Weirauch et al., 2008; Herbert et al., 2010; Lawrence et al., 2010; Hillaire-Marcel et al., 2011; Russon et al., 2011; Elderfield et al., 2012; Dyez and Ravelo, 2014; Aubry el al, 2016). However, the magnitude of warmth achieved during MIS 31 varies geographically and the majority of the research has been concentrated in the high-latitudes of the NH and the SH (e.g. Flores and Sierro, 2007; Scherer et al., 2008; Maiorano et al., 2009; Naish et al., 2009; Melles et al., 2012; Villa et al., 2012; Tarasov et al., 2013; Teitler et al., 2015; de Wet et al., 2016). Considerably less information is available from the Mediterranean region, where only three vegetation sequences span MIS 31 (Tenaghi Philippon, NE Greece: Tzedakis et al., 2006; Montalbano Jonico section, southern Italy: Joannin et al., 2008; ODP Site 976, Alboran Sea: Joannin et al., 2011) (Fig. 1). Although these studies show the vegetation response to orbital forcing, they lack the required resolution to provide a detailed assessment of the millennial-scale climatic variability

throughout MIS 31. Due to the scarcity and limited time resolution of studies spanning MIS 31, key questions remain concerning the imprint of its extreme orbital forcing and the climate system of the 41-ky world at lower latitudes in both terrestrial and marine ecosystems, and also the magnitude of warming, the duration of the interglacial and the intra-interglacial variability.

Here we present the first high-resolution (centennial-scale) pollen record from IODP Site U1385 covering the early Pleistocene interval, 1100 ka (MIS 32) to 1050 ka (early MIS 30) including MIS 31, that allows the reconstruction of vegetation and atmospheric changes, in a direct comparison to alkenone-based sea surface temperature (SST). Site U1385 is located on the SW Iberian margin (Fig. 1), considered as an exceptional region for palaeoclimate research (e.g. Shackleton et. al, 2000) and an ideal location for assessing the impact of precession since it plays a major role in the climate of the Mediterranean region south of 40°N (Ruddiman and McIntyre, 1984). The influence of precession on the forest extent and composition in southern Europe is shown by numerous pollen records of the last 400 ky (e.g. Magri and Tzedakis, 2000; Fletcher and Sánchez Goñi, 2008; Sánchez Goñi et al., 2008; Margari et al., 2014; Oliveira et al., 2016). More recently, a pollen-based vegetation record of MIS 19 (~800 ka) from Site U1385 revealed millennial cycles driven by the fourth harmonic of the precessional component of the insolation (Sánchez Goñi et al., 2016). However, the impact of precession forcing on the SW Iberian vegetation during the warm stages of the 41-ky world is, to date, completely unknown because pollen records are only available for interglacials younger than MIS 11 (Sánchez Goñi., 1999; Roucoux et al., 2006; Tzedakis et al., 2009; Chabaud et al., 2014; Oliveira et al., 2016) and for MIS 19 (Sánchez Goñi et al., 2016). This study describes the temperature and precipitation regime during MIS 31 in SW Iberia and discusses its modulation by the extreme orbital forcing and the climatic background state of the 41-ky world. In addition, it provides the first evidence for repeated cooling and drying events throughout the studied interval and explores the potential nature and mechanisms involved in the millennial-scale variability of the early Pleistocene.

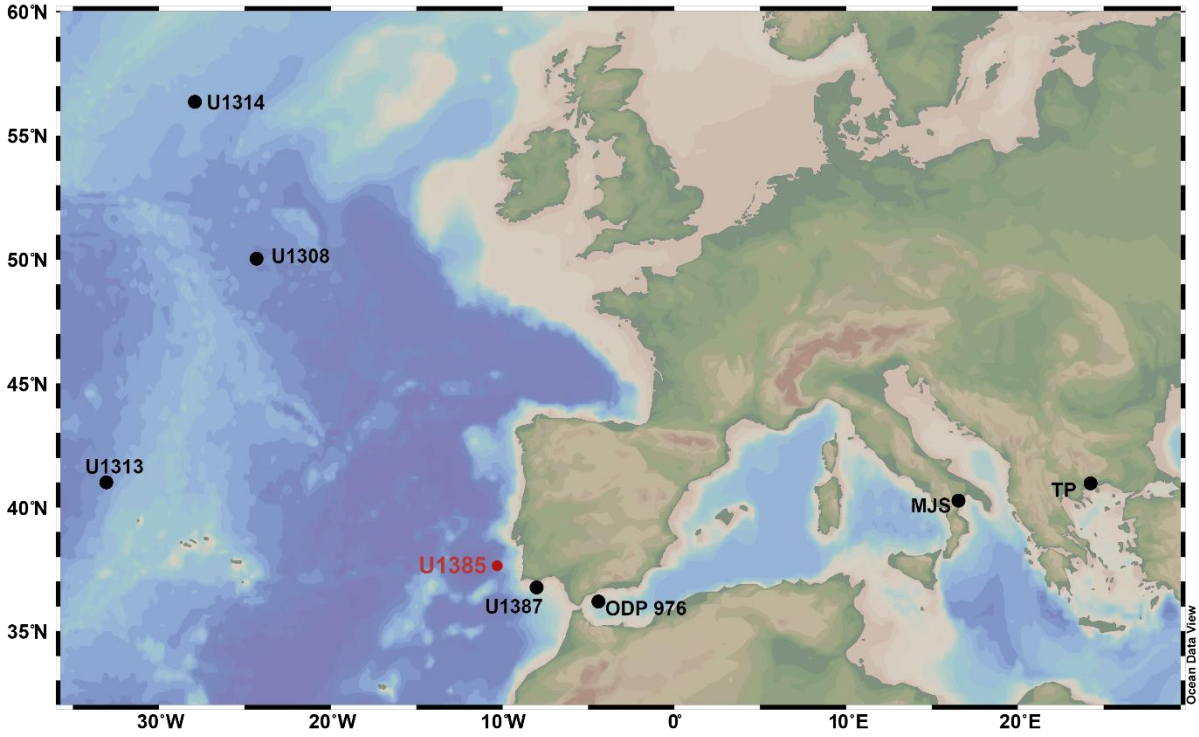

Fig. 1. Location of Site U1385 and available European and North Atlantic records mentioned in the text: Site U1314 (Hernández-Almeida et al., 2012, 2013); Site U1308 (Hodell et al., 2008); Site U1313 (re-drilling of DSDP Site 607, Lawrence et al., 2010; Naafs et al., 2013); Site U1387 (Voelker et al., 2015); ODP Site 976 (Joannin et al., 2011); TP: Tenaghi Philippon (Tzedakis et al., 2006); MJS: Montalbano Jonico (Joannin et al., 2008; Maiorano et al., 2010; Girone et al., 2013).

2. Regional setting

2.1 Core site and hydrographic conditions

IODP Site U1385 (37°34.285′N, 10°7.562′W), or "Shackleton Site", was drilled on the lower slope of the SW Iberian margin at 2578 m below sea-level (Fig. 1) (Expedition 339 Scientists, 2013; Hodell et al., 2013). At present, the site is under the influence of North Atlantic Deep Water (NADW), although during glacials and cold episodes the contribution of southern-sourced Antarctic bottom water increased (Duplessy et al., 1988; Skinner and Elderfield, 2007). Above the NADW, the intermediate depth is dominated by the Mediterranean Outflow Water, and the upper water column by the Portugal Current and the Azores Current, depending on the atmospheric circulation (Fiúza, 1984; Pérez et al., 2001; Peliz et al., 2005). In winter, the northward, warm surface Iberian Poleward Current is

dominant, whereas in spring and summer strong northerly winds induce coastal upwelling and the southward transport of the recently upwelled waters by the Portugal Current. This seasonal surface layer is underlain by the subtropical Eastern North Atlantic Central Water, composed of two branches of subtropical or subpolar origin with the subtropical overlying the subpolar branch (e.g. Rios et al., 1992; Fiúza et al., 1998).

2.2 Modern climate and vegetation

The climate of SW Iberia is Mediterranean with warm/dry summers and cool/wet winters (annual precipitation (Pann): 350-600 mm; annual Temperature (Tann): 13-17°C with minimal winter temperatures between 5 to 1°C), with an important influence of Atlantic moisture on its westernmost side (Peinado Lorca and Martinez-Parras, 1987; Gimeno et al., 2010). The summer dryness is predominantly driven by the northeastward expansion of the subtropical Azores High, which is associated with the descending branch of the Hadley cell (Lionello et al., 2006), while the winter precipitation is directly affected by the position and strength of the North Atlantic westerlies and related changes in the North Atlantic Oscillation and North Atlantic storm tracks (e.g. Hurrell, 1995; Trigo et al., 2004).

The western Iberian margin pollen spectra provide an integrated image of the regional vegetation from the adjacent landmasses because the Tagus and, to a lesser extent, the Sado rivers are the main pollen suppliers to the SW Iberian deep-sea sediments (Naughton et al., 2007). The vegetation distribution and composition of the Tagus and Sado watersheds, which belong to the Mediterranean region, are mainly influenced by precipitation and thermal gradients related to orography and maritime influences (Peinado Lorca and Martínez-Parras, 1987; Quezel, 1989; Blanco Castro et al., 1997). While the lowland areas of the western part of the basin are dominated by deciduous oak (*Quercus*) and cork oak (*Quercus* suber) woodlands due to increased moisture availability, evergreen oak develops (*Quercus* rotundifolia and *Q.* coccifera) towards the east and south. In the montane forests, deciduous *Quercus* dominates areas at mid-altitude and conifers (*Pinus* woodland with *Juniperus)* at the highest elevations. Mediterranean shrub vegetation is characterized by heathers (Ericaceae) in the wettest areas (Pann: >600 mm), and by rockroses (Cistaceae) in drier environments (Peinado Lorca and Martínez-Parras, 1987; Loidi et al., 2007).

3. Material and methods

Deep-sea Site U1385 was retrieved from the structural high "Promontorio dos Principes de Avis", using an advanced piston corer system, during the IODP Expedition 339 (Mediterranean Outflow) on board D/V JOIDES Resolution (Fig. 1) (Expedition 339 Scientists, 2013; Hodell et al., 2013). Five holes (A–E; 67 cores in total) were drilled and correlated on the basis of core scanning XRF at 1-cm resolution to provide a continuous composite section covering the past 1.5 My (Hodell et al., 2015). The recovered sediments form a homogeneous lithologic unit dominated by hemipelagic mud and claystone (Expedition 339 Scientists, 2013).

3.1. Chronostratigraphy

For the studied interval, between MIS 32 and early MIS 30 (120.06-125.09 corrected revised meter composite depth (crmcd)), two age models were produced by Hodell et al. (2015): (1) the oxygen isotope age model derived by correlating the low-resolution (20-cm) benthic oxygen isotope record ($\delta^{18}O_b$) of Site U1385 to the LR04 $\delta^{18}O_b$ stack (Lisiecki and Raymo, 2005), and (2) the astronomically (precession)-tuned timescale produced by tuning sediment lightness (L*) peaks to the precession minima assuming a lag of ~3 ky based on new radiocarbon reconstructions at the nearby core MD99-2334K (Skinner et al., 2014) (Table 1). A third chronology has been proposed based on the revision of the LR04-derived chronology (F. Jimenez-Espejo et al., in progress) through the correlation of the high-resolution $\delta^{18}O_b$ of Site U1385 to the one from IODP Site U1308 (Table 1), which has also an age model related to the LR04 stack (Hodell et al., 2008).

The LR04-derived chronology shows good agreement with the precession-tuned timescale (Hodell et al., 2015; F. Jimenez-Espejo et al., in progress), within the estimated uncertainty for the LR04 stack (±6 ky; Lisiecki and Raymo, 2005). However, since the studied interval is marked by one of the strongest precession cycles of the last 1.5 My (Laskar et al., 2004) the astronomical timescale is probably more accurate than the LR04-derived age model. The good agreement between the Mediterranean sapropel cyclostratigraphy (Konijnendijk et al., 2014) and the precession-tuned age model (Hodell et al., 2015) supports its robustness. Age-depth modeling was based on linear interpolation between four age

control points between ~1048 and 1111 ka (Table 1). High sedimentation rates (Table 1), between 9.4 and 17.8 cm/ky, provide an average temporal resolution of ~350 yr for the pollen record and of ~250 yr for the $U^{k'}_{37}$-SST profile.

Table 1. Site U1385 age-depth control points of the precession-tuned age model (Hodell et al., 2015) and oxygen isotope age model (F. Jimenez-Espejo et al., in progress) and sedimentation rates. crmcd: corrected revised meter composite depth. The palaeoclimatic records presented in this study are plotted on the precession-tuned timescale.

Site U1385 Depth (crmcd)	Precession-tuned age (ky)	Sed. Rate (cm/ky)	Site U1385 Depth (crmcd)	Site U1308 age (ky)	Sed. Rate (cm/ky)
119.89	1047.9	17.75	117.44	1031.9	12.26
121.97	1070.0	9.41	120.26	1054.9	14.29
124.07	1090.2	10.40	120.66	1057.7	18.89
126.94	1111.5	13.38	121.17	1060.4	9.17
			121.39	1062.8	8.96
			121.82	1067.6	8.68
			122.25	1072.6	12.75
			122.41	1073.8	10.72
			124.69	1095.1	10.00
			124.81	1096.3	13.13
			125.11	1098.6	5.57
			123.36	1103	11.4
			125.47	1104	6.1

3.2 Pollen analysis

IODP Site U1385 Holes E and D were subsampled for pollen analysis at 0.02-0.08 crmcd intervals from 120.08 to 125.09 crmcd, except for the transition between the holes where the sample spacing was of ~0.19 crmcd. From each 1-cm thick sample slice, 2.5 to 5 cm^3 of sediment were prepared following the conventional palynological procedure for marine samples (described in detail at http://ephe-paleoclimat.com/ephe/Pollen%20sample%20preparation.htm). After coarse-sieving (150 μm mesh) and carbonate destruction (attack with cold HCl successively at 10%, 25% and 50%), silica and silicates were eliminated by chemical digestion (cold HF at 45% and 70%). Fluorosilicates were removed with a final treatment with cold HCl at 25%. The obtained

residue was sieved through a mesh of 10 μm and mounted unstained in glycerol to allow rotation of the pollen grains.

Pollen analysis on 134 samples was carried out under a Nikon light microscope at x500 and x1000 (oil immersion) magnification and identification followed two well-known European pollen atlases (Moore et al., 1991; Reille, 1992) and the pollen reference collection available at UMR EPOC, University of Bordeaux. Each pollen sample comprised 20 to 29 pollen morphotypes and reached a total sporo-pollen sum between 142 and 487, with a minimum of 100 pollen grains excluding *Pinus*, aquatics and Pteridophyta spores. Due to the *Pinus* over-representation in marine sediments, the genus was excluded from pollen percentage calculations (Heusser and Balsam, 1977; Naughton et al., 2007). Also excluded were *Cedrus*, because it is an exotic pollen grain that likely originates from the North African cedar forest (Magri, 2012), aquatic plants, spores and indeterminable pollen grains. *Pinus* and *Cedrus* percentages were estimated from the main sum plus their individual counts, while spore and aquatic percentages were calculated using the total sum (pollen+spores+indeterminables+unknowns).

A synthetic pollen percentage diagram of major pollen taxa and ecological groups versus depth is presented in Fig. 2. Following previous pollen studies off southern Iberia (e.g. Fletcher and Sánchez Goñi, 2008; Sánchez Goñi et al., 2008, 2016; Chabaud et al., 2014; Oliveira et al., 2016), the pollen types were grouped into three main categories: semi-desert plants (*Artemisia*, Chenopodiaceae and both *Ephedra* types), Mediterranean sclerophylls (*Quercus evergreen*-type, *Cistus*, *Olea*, *Phillyrea* and *Pistacia*) and temperate forest (TF; Mediterranean sclerophylls and all temperate trees and shrub taxa, excluding *Pinus*, *Cedrus* and Cupressaceae). The temperate forest category corresponds to the commonly used Mediterranean forest (MF), however, here we designate it by temperate forest because the vegetation composition displays a marked Atlantic character throughout the pollen record (Fig. 2). Pollen zones were defined by visual inspection of the pollen diagram (Birks and Birks, 1980) and constrained hierarchical cluster analysis (Fig. 2). This analysis was performed using the function *chclust* of the package *rioja* (Juggins, 2009) in R environment v. 3.1.1 (R Core Team, 2014).

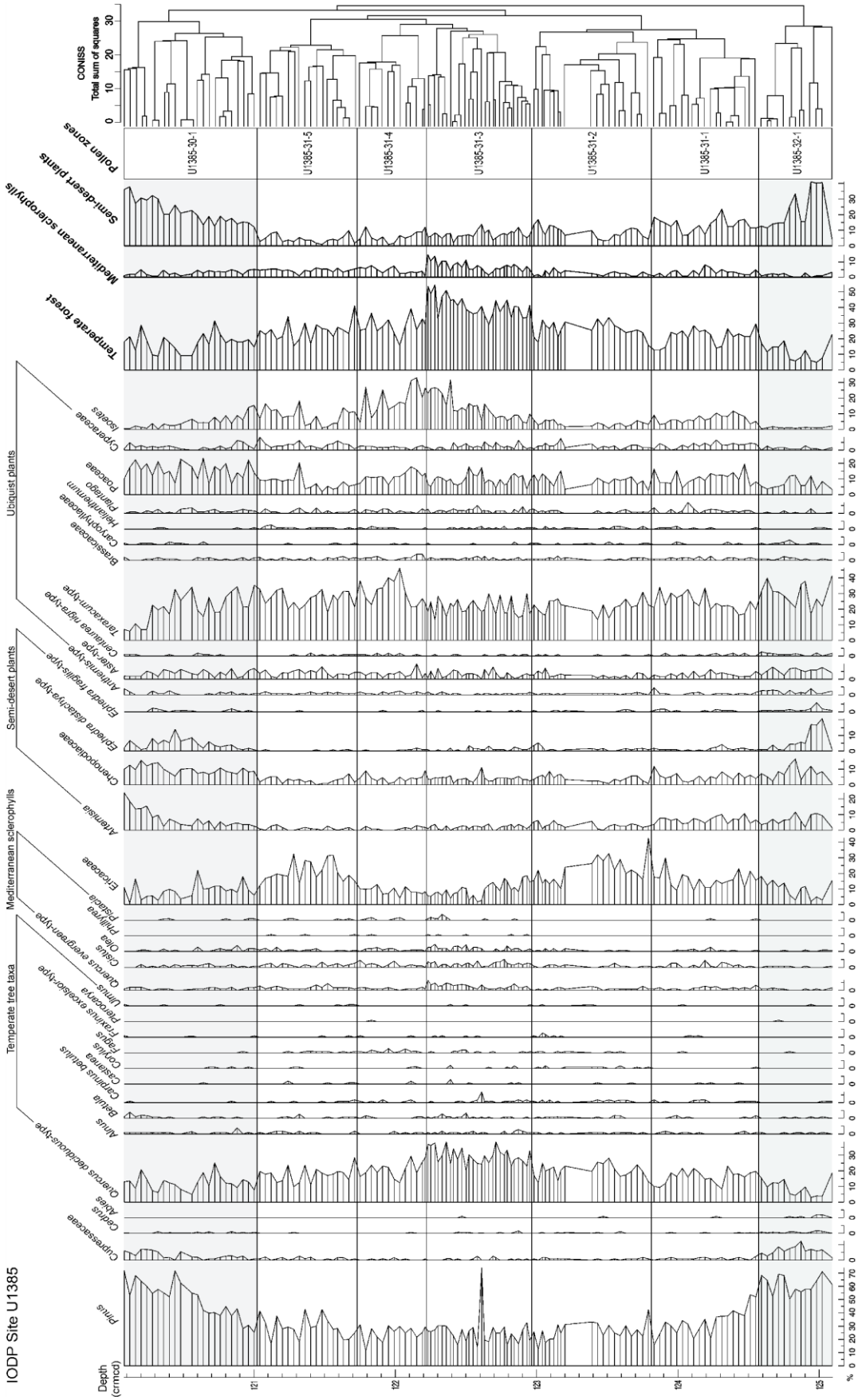
CONISS
Total sum of squares
Pollen zones
U1385-30-1
U1385-31-5
U1385-31-4
U1385-31-3
U1385-31-2
U1385-31-1
U1385-32-1
Semi-desert plants
Mediterranean sclerophylls
Temperate forest
Ubiquist plants
Semi-desert plants
Mediterranean sclerophylls
Temperate tree taxa
Cyperaceae
Poaceae
Asteraceae
Chenopodiaceae
Ephedra distachya-type
Ephedra fragilis-type
Artemisia
Ericaceae
Pistacia
Olea
Quercus evergreen-type
Quercus deciduous-type
Alnus
Betula
Fagus
Corylus
Pinus
Depth (cmcd)
IODP Site U1385

Fig. 2.

Fig. 2. Percentage pollen diagram of selected morphotypes and ecological groups from Site U1385 plotted against depth. Ecological groups include temperate forest (TF) which here includes the Mediterranean sclerophylls and all temperate trees and shrub taxa, excluding *Pinus*, *Cedrus* and Cupressaceae; Mediterranean sclerophylls: *Quercus evergreen*-type, *Cistus*, *Olea*, *Phillyrea* and *Pistacia*; and semi-desert plants: *Artemisia*, Chenopodiaceae, *Ephedra distachya*-type and *Ephedra fragilis*-type. On the right of the diagram are represented the pollen zones and results of the cluster analysis. Pollen zones are labeled as following: Site U1385 - MIS (Marine Isotopic Stage) – number of the pollen zone. Shaded areas indicate open vegetation phases associated with the glacial sections of MIS 32 and MIS 30 bracketing the terrestrial counterpart of MIS 31 in SW Iberia.

3.3 Molecular biomarker analyses

Biomarkers analyses were carried out in 205 levels from Holes E and D between 120.08 and 125.44 crmcd at ~0.01-0.06 crmcd intervals, except in the transition between holes (sample spacing of 0.18 crmcd). Analyses were performed at the laboratory of IDAEA-CSIC, Barcelona, and followed the procedure described in detail in Villanueva et al. (1997). Samples were freeze-dried and extracted with dichloromethane in an ultrasonic bath. After saponification with 10% potassium hydroxide in methanol, the neutral lipids were extracted with hexane and dried under a nitrogen atmosphere, and finally derivatized with bis(trimethylsilyl) trifluoroacetamide. Alkenones were quantified with a Varian gas chromatograph (model 450) equipped with a septum programmable injector, a flame ionisation detector and a CPSIL-5 CB column coated with 100% dimethylsiloxane (film thickness of 0.12 mm). Hydrogen was used as the carrier gas at 50 cm/s. The concentrations of each compound were determined using n-nonadecan-1-ol, n-hexatriacontane and n-dotetracontane as internal standards. Alkenone-based sea surface temperature ($U^{k'}_{37}$-SST) reconstruction was based on the $U^{k'}_{37}$ index (Brassell et al., 1986; Prahl and Wakeham, 1987) and converted into annual mean SST values following the global core-top calibration (Müller et al., 1998). Reproducibility tests show that analytical uncertainty in the alkenone unsaturation index determination is lower than 0.0165 (~ 0.5 °C) (Villanueva et al., 1997).

3.4 Time series analysis

Cross-correlation function (CCF) analysis was implemented using the R package *stats* (R Core Team, 2014) in order to identify and quantify lead/lag relationships between the TF record and orbital parameters. Given the strong response of heathland to precession in the Iberian Peninsula (Roucoux et al., 2006; Margari et al., 2007, 2014; Fletcher and Sánchez Goñi, 2008; Chabaud et al., 2014), the CCF analysis was also applied to these two time series. For this analysis, the unevenly spaced time series were interpolated with the Akima-spline at a regular time step of 300 yr and the linear trend was removed. The correlation coefficients (r) indicate the degree of similarity between two time series with values ranging from -1 to 1. The existence of a lag reveals the time offset between both time series.

Fourier spectral analysis for unevenly spaced palaeoclimate time series was performed to detect potential periodicities in the TF pollen and $U^{k'}_{37}$-SST records. The REDFIT methodology and software package was used for this analysis. REDFIT allows testing for statistically significant spectral peaks that could indicate periodicities in non-constantly sampled time series against a red-noise background (Schulz and Mudelsee, 2002).

4. Results and interpretations

4.1 MIS 31 definition

Following Hodell et al. (2015) who defined the onset of interglacials at the terminal stadial event and its demise where $\delta^{18}O$ drops and millennial variability of log(Ca/Ti) starts, MIS 31 lasted 32 ky, from ~1094 to 1062 ka (Fig. 3). Although the onset of MIS 31 at Site U1385 is 13 ky earlier than defined by Lisiecki and Raymo (2005) for the LR04 stack, it is consistent with recent studies off southern Iberia that used the $\delta^{18}O_p$ and SST records to recognize the beginning of interglacial climate (Voelker et al., 2015) (Fig. 3). This earlier onset of the MIS 31 interglacial also agrees with the benthic foraminifera $\delta^{13}C$ record of North Atlantic Site U1308 that indicates the resumption of strong AMOC (Hodell et al., 2008) within the traditional definition of MIS 32 (Lisiecki and Raymo, 2005). Moreover, recent publications have emphasized the need to reconsider the positioning of the MIS 31 lower boundary defined by Lisiecki and Raymo (2005) due to the unusual weak character of glacial MIS 32 in terms of length and/or intensity (Teitler et al., 2015; de Wet et al., 2016, and references therein).

4.2 Pollen-based reconstruction of vegetation and climate dynamics in SW Iberia

Results of pollen analysis are presented in the percentage pollen diagram (Fig. 2) and Fig. 3. Three pollen superzones are identified and distinguish the two main phases of open vegetation expansion during MIS 32 and MIS 30 glacial stages from the interglacial forest development during MIS 31 (Figs. 2 and 3). These superzones are additionally divided into zones to characterize the dynamics of the vegetation cover and composition (Figs. 2 and 3). Millennial-scale events of forest decline are indicated in Fig. 4 as they are not systematically represented by distinctive pollen zones.

4.2.1 Long-term vegetation and climate change

MIS 32 and MIS 30 are characterized by open vegetation cover (zones U1385-32-1 and U1385-30-1, respectively), dominated by *Pinus*, *Taraxacum*-type, Poaceae and semi-desert plants, while TF and heather are represented by values below 20% (Figs. 2 and 3). Based on the present day ecology of the dominant vegetation types, these intervals were marked by prevailing cold and dry conditions (Polunin and Walters, 1985; Prentice et al., 1996).

The second superzone corresponds to the terrestrial interglacial counterpart of MIS 31 in SW Iberia, which we named Sado, and comprises five zones (zones U1385-31-1 to 5) (Figs. 2 and 3). As documented for SW Iberian interglacials of the middle- to late Pleistocene (Sánchez Goñi et al., 1999, 2016; Tzedakis et al., 2004; Roucoux et al., 2006; Oliveira et al., 2016), a rapid expansion of the TF (pollen percentages above 20%) and *Isoetes* also marks the onset of the Sado interglacial, at ~1094 ka, and ends at ~1060 ka with the dominance of semi-desert plants (Figs. 2 and 3). While the beginning of Sado is contemporaneous with the beginning of MIS 31 as defined by Hodell et al. (2015), its demise occurred two-millennia after the end of MIS 31 (Fig. 3). This 34 ky-long and floristically diverse terrestrial interglacial is characterized by well-developed TF (pollen percentages up to 55%, average 30%) and low expansion of Mediterranean sclerophylls (pollen percentages up 14.8%, average 4.6%), indicating overall warmth and moisture availability in SW Iberia but reduced climate seasonality (Figs. 2 and 3).

The earliest interval of the Sado corresponds to a transition phase from ~1094 to 1087.7 ka (U1385-31-1) marked by a relatively low development of the TF, mainly composed of deciduous *Quercus* woodland, and a characteristic 'M' structure in the TF pollen percentage record. Relatively high values of semi-desert plants, suggest that limited moisture availability may have restricted forest expansion (Figs. 2 and 3). During the ensuing interval, between ~1087.7 and 1079.5 ka (U1385-31-2), semi-desert plants contract and the vegetation cover is dominated by mixed deciduous woodland with small quantities of diverse summer drought-intolerant trees (*Carpinus betulus*, *Castanea*, *Corylus*, *Fagus* and *Fraxinus excelsior*-type) and abundant heathland (Ericaceae) (Figs. 2 and 3). Since these summer drought-intolerant taxa require relatively warm winters and warm–cool but wet summers (Polunin and Walters, 1985; Blanco Castro et al., 1997; Gallardo-Lancho, 2001; Tallantire, 2002) and heath also requires sustained humidity year-round (e.g. Loidi et al., 2007), these vegetation changes reflect the establishment of a temperate and humid climate regime with precipitation distributed evenly all over the year. The weak expansion of *Isoetes* (Figs. 2 and 3), fern ally, further supports the interpretation of reduced seasonal contrast as their optimal development requires periods of flooding alternating with desiccation in wintertime (Prada, 1986; Salvo Tierra, 1990).

During the major forest development (TF% between ~30-55%) (U1385-31-3), from ~1079.5 to 1072.5 ka, a deciduous *Quercus* expansion accompanied by the occurrence of various temperate trees and relatively low representation of the Mediterranean sclerophylls (average 7.8%), reflect a temperate and humid climate regime in SW Iberia with low seasonal contrast (Figs. 2 and 3). Nevertheless, the reduction of Ericaceae, large increase of *Isoetes* and modest expansion of the Mediterranean sclerophylls indicate that this interval was marked by increased warmth and the highest seasonality (slightly warmer and drier summers) within Sado interglacial. A prominent feature of this interval is the asymmetric "M" shape depicted by the TF pollen percentage curve, which points to the occurrence of two warm and humid phases separated by a short-lived and low-amplitude cooling and drying episode between 1076.8 and 1075.2 ka (Fig. 3). This warmest phase ends with a strong and rapid TF decline occurring within ~200 yr. A progressive contraction of the TF (U1385-31-4 to -5) follows suggesting a cooling trend up to the end of Sado interglacial (Fig. 3). The TF long-term decrease was associated with the expansion of dry-grasslands (in particular *Taraxacum*-type and Poaceae) between ~1072.5 and 1067.5 ka (U1385-31-4), and with a distinct heathland

development from ~1067.5 to 1060 ka (U1385-31-5) indicating a climate shift to wetter conditions and lower seasonality (Figs. 2 and 3).

Cross correlation analysis reveals that the TF pollen record is not correlated to the precession (Fig. 5a), but shows a strong positive correlation statistically significant (95% confidence interval) around lag-0 (r=0.78) with obliquity (Fig. 5b). This indicates that, within the chronological uncertainties, the two time series are in phase with no apparent offset. Ericaceae shows a positive correlation with precession statistically significant at lag-0 (r=0.70). The highest correlation coefficient takes place at lag -3 (r=0.75) suggesting that maximum correlation also occurs with nearly no apparent lag (lag of ~1000 yr) within the age model error (Fig. 5c).

4.2.2 Suborbital vegetation and climate variability

The pollen sequence of Site U1385 reveals persistent abrupt climate variability throughout the record with repeated millennial-to-centennial scale vegetation changes superimposed on the long-term evolution (Fig. 4). Ten forest decline events (U1385-32-fe-1 to -30-fe10), reflecting atmospheric cooling and drying, were identified as significant reductions of the TF pollen percentages, between 8 and 24%, occurring at least across two consecutive samples (Fig. 4). These TF setbacks took place over a period of time ranging between ~205 yr (U1385-31-fe7) and ~900 yr (U1385-31-fe2) and lasted between ~600 and 3580 yr (U1385-31-fe3 and -fe10, respectively) (Fig. 4).

The coldest and driest events, U1385-32-fe1 (centered at ~1096.4 ka) and -30-fe10 (~1053.6 ka), occurred during glacial MIS 32 and MIS 30, respectively, and are represented not only by severe forest declines (TF% minima <10%) but also by maximal expansion of semi-desert plants and very low abundances of heaths (Fig. 4). These long-lasting phases, ~2 and 3.6 ky, respectively, are however complex. They both encompass two episodes of forest contraction separated by a short-lived recovery of the TF and heathland at the expense of semi-desert plants. This internal variability reflects a tripartite climatic oscillation marked by cold/dry- warmer/wetter- cold/dry conditions in SW Iberia. Afforestation at the MIS 32/31 transition is briefly interrupted at ~1094.5 ka (U1385-32-fe2 event) revealing a discrete shift to cool and dry conditions on land (Fig. 4).

The interglacial climate variability during the Sado forest stage is marked by six forest decline events, U1385-31-fe3 to -fe8, with TF minima centered at ~1091.7, 1088.3, 1080, 1076.6, 1070.6 and 1063.3 ka, respectively (Fig. 4). The forest setbacks U1385-31-fe3 to -fe5 are characterized by important increases of semi-desert plants (up to ~24%) and relatively low values of TF minima (~15%), implying cool and dry conditions. In contrast, the subsequent forest decline event U1385-31-fe6 is associated with higher TF values (~29%) and weaker expansion of semi-desert plants (to ~14%), indicating that a cool and dry climatic oscillation of low amplitude interrupted the TF maximum development during MIS 31 in SW Iberia. This long-lasting phase of major TF expansion ended abruptly with a strong contraction of the forest (~24% change) comprising a short-lived forest recovery before the minimum percentages of TF, event U1385-31-fe7 (Fig. 4). These changes reflect a rapid vegetation response to colder and drier conditions interrupted by a brief warming and moisture increase. The subsequent long-term decrease in the TF, end of Sado interglacial and the onset of MIS 30, was punctuated by two additional TF setbacks, events U1385-31-fe8 and -30-fe9, associated with similar TF values (~15%) but different changes in herbaceous composition (Fig. 4). During the event U1385-31-fe8 Ericaceae dominance indicates a cooling with higher annual humidity, while during U1385-30-fe9 (TF% minima at ~1059.7 ka) a strong expansion of semi-desert plants suggests a shift to cold and dry conditions at the end of the Sado interglacial.

Spectral analysis of the TF record using the REDFIT method (Schulz and Mudelsee, 2002) shows a peak around 6 ky with significance at 90% on both precession-tuned (Fig. 6a) and LR04-based chronologies (Fig. 6b). These similar results ensure that the identification of ~6 ky cyclicity is independent of the chosen age model.

4.3 Land - sea dynamics

In line with the pollen record, during the first and last intervals of the glacial sections of MIS 32 and early MIS 30, the Uk'_{37}-SST profile shows very cold surface waters off SW Iberia, with absolute SSTs minima of 8.5°C and 10.5°C, respectively (Fig. 3).

The MIS 32/31 transition is marked by an abrupt SST warming up to ~17.5°C coincident with the onset of the Sado interglacial, followed by a progressive SST increase to

its maximum values (20.2°C) until 1079.5 ka, whereas the forest development remained moderate (Fig. 3). In contrast, the following interval between 1079.5 and 1072.5 ka is marked by the major forest development associated with a slight SST cooling. During the subsequent interval, from 1072.5 to 1067.5 ka, the SSTs show persisting warmth contrasting with a rapid and strong decline of the TF to moderate extent, which indicates cooler atmospheric conditions. After ~1067.5 ka, the SSTs continuously decreased from interglacial values towards MIS 30 glacial conditions paralleling the reduction in the TF (Fig. 3).

Superimposed on the long-term SST trends, two prominent cooling episodes occur during MIS 32, at 1098 and 1095.7 ka with SSTs ~8.5°C, and further three during MIS 30, with abrupt SST coolings to ~12°C at 1058.2 ka, and to ~10.5°C at 1053.7 and 1051.8 ka (Fig. 4). These cold spells recorded in the eastern part of the subtropical gyre are synchronously detected in the terrestrial realm (U1385-32-fe1, -30-fe9 and -30-fe10) and concurred with high ice volume baseline conditions (U1385 and U1308 $\delta^{18}O_b > 3.5‰$) (Fig. 4). In contrast, the forest decline events U1385-32-fe2 to -fe8 punctuating the deglaciation and the interglacial do not have counterparts in the SST record (Fig. 4).

Fig. 3. Long-term vegetation and climatic changes (presented on precession-tuned age model) at Site U1385 from MIS 32 to early MIS 30. From bottom to top: Percentages of selected pollen taxa or group of taxa: (a) semi-desert plants (orange), (b) Ericaceae (blue) and *Isoetes* spores (light green), (c) Summer drought-intolerant taxa (*Carpinus betulus*, *Castanea*, *Corylus*, *Fagus*, *Fraxinus excelsior*-type and *Ulmus*) (dark green), Mediterranean sclerophylls (red) and temperate forest (TF) (green); (d) Site U1385 Uk'_{37}-SST (black). Bold lines represent 3-point moving averages of pollen percentages (a-c) and Uk'_{37}-SST (d). (e) $\delta^{18}O_b$ records of Site U1385 (Hodell et al., 2015) (purple), Site U1308 (Hodell et al., 2008) (black) and LR04 (Lisiecki and Raymo, 2005) (light blue); (f) 65°N summer insolation (black), obliquity (green) and precession (red) parameters (Laskar et al., 2004). Marine Isotope Stages (MIS) following Lisiecki and Raymo (2005) and Hodell et al. (2015) are shown at the top. Vertical lines indicate the terrestrial counterpart of MIS 31 in SW Iberia named Sado interglacial (dashed lines) and the major changes in the vegetation composition (dotted lines) based on the zonation of the pollen diagram (Fig. 2) (bottom). The pink bar marks the TF maximal expansion during the Sado interglacial.

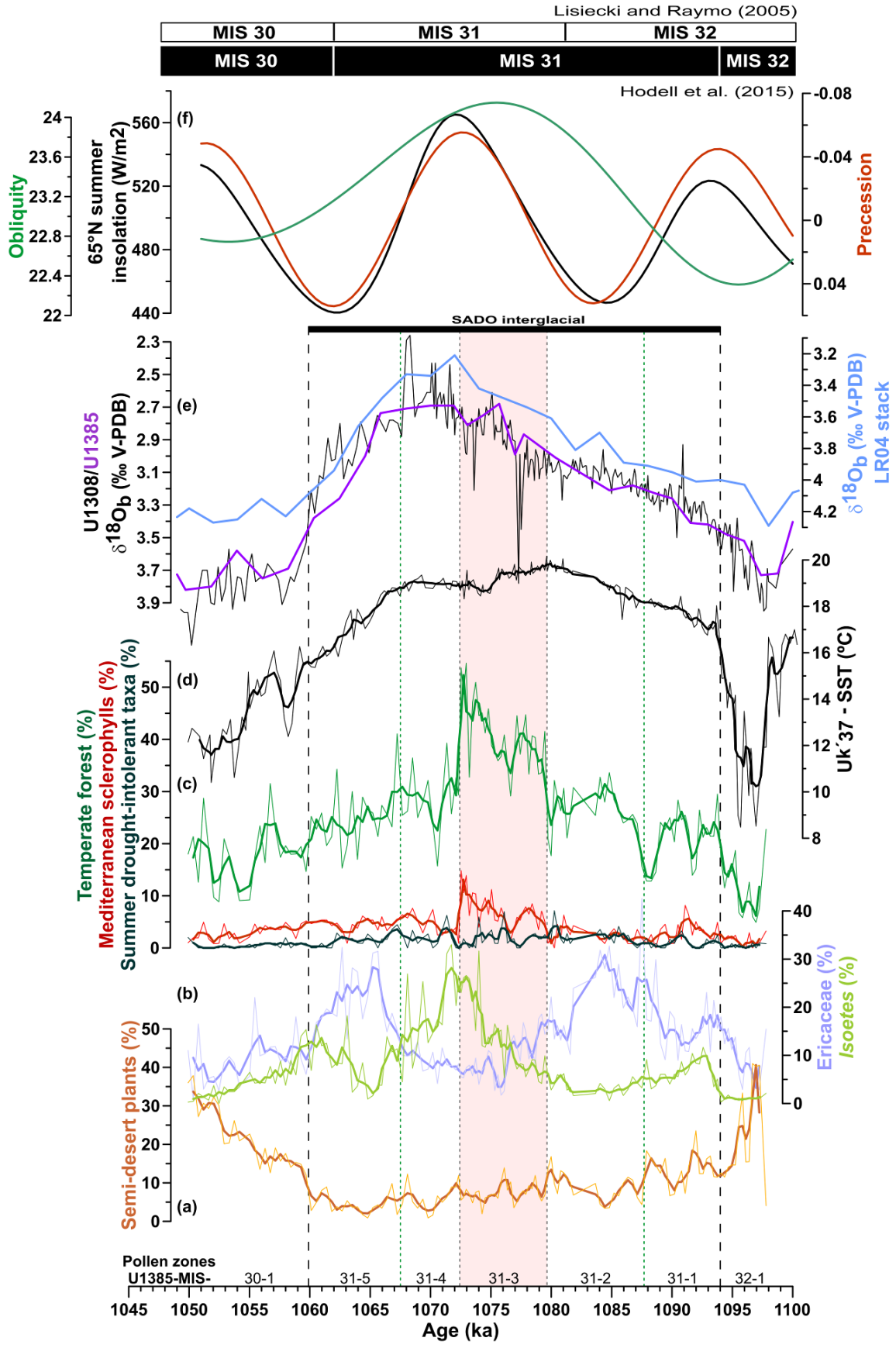
Lisiecki and Raymo (2005)
MIS 30
MIS 31
MIS 32
Hodell et al. (2015)
(f)
Obliquity
65°N summer insolation (W/m2)
Precession
SADO interglacial
(e)
U1308/U1385 δ18Ob (‰ V-PDB)
δ18Ob (‰ V-PDB) LR04 stack
(d)
Uk´37 - SST (ºC)
(c)
Temperate forest (%)
Mediterranean sclerophylls (%)
Summer drought-intolerant taxa (%)
(b)
Ericaceae (%)
Isoetes (%)
(a)
Semi-desert plants (%)
Pollen zones
U1385-MIS-
30-1
31-5
31-4
31-3
31-2
31-1
32-1
Age (ka)

Fig. 3.

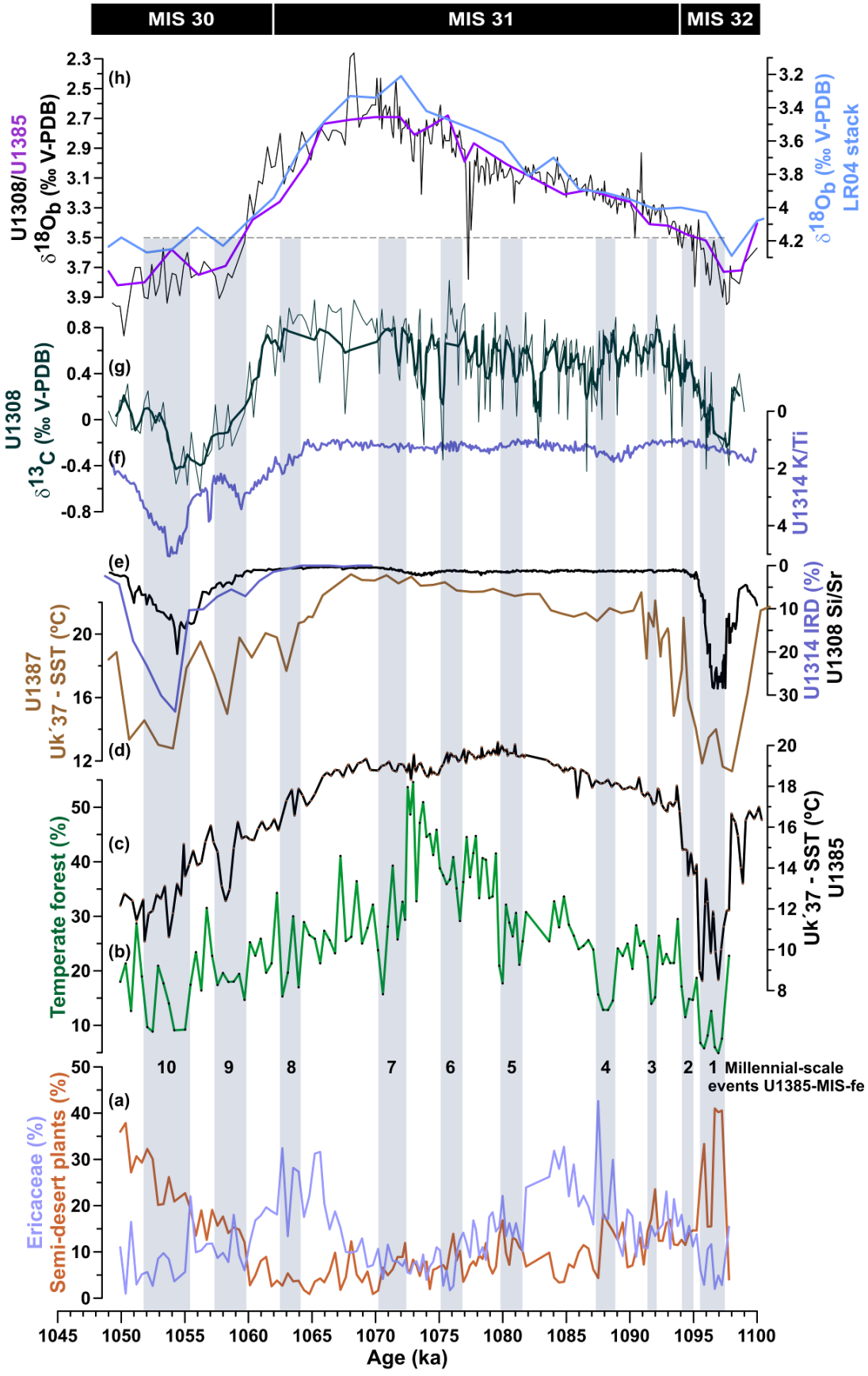
MIS 30
MIS 31
MIS 32
(h)
U1308/U1385 δ18Ob (‰ V-PDB)
δ18Ob (‰ V-PDB) LR04 stack
(g)
U1308 δ13C (‰ V-PDB)
(f)
U1314 K/Ti
(e)
U1387 Uk´37 - SST (°C)
U1314 IRD (%)
U1308 Si/Sr
(d)
(c)
Temperate forest (%)
(b)
Uk´37 - SST (°C) U1385
10 9 8 7 6 5 4 3 2 1 Millennial-scale events U1385-MIS-fe
(a)
Ericaceae (%)
Semi-desert plants (%)
Age (ka)

Fig. 4.

Fig. 4. Site U1385 direct land-ocean comparison between the millennial-scale temperate forest (TF) decline events and oceanic surface changes in the context of eastern North Atlantic changes. From the bottom to the top: Selected pollen percentage curves of (a) semi-desert plants (orange), Ericaceae (blue) and (b) TF (green). Uk'_{37}-SST of (c) Site U1385 (black) and (d) Site U1387 from the Gulf of Cadiz (Voelker et al., 2015) (brown). (e) IRD discharges inferred from the Si/Sr ratio of Site U1308 (Hodell et al., 2008) (black) and IRD% of Site U1314 (Hernández-Almeida et al., 2013) (blue). (f) Iceland–Scotland overflow strength based on the K/Ti record of Site U1314 (Grützner and Higgins, 2010) (blue). (g) Benthic $\delta^{13}C$ of Site U1308 reflecting changes in NADW formation and the AMOC (Hodell et al., 2008) (dark green; bold 3-point moving average). (h) $\delta^{18}O_b$ records of Site U1385 (Hodell et al., 2015) (purple), Site U1308 (Hodell et al., 2008) (black) and LR04 (Lisiecki and Raymo, 2005) (light blue). Dashed line designates the ice volume threshold of McManus et al. (1999). Marine Isotope Stages (MIS) following Hodell et al. (2015) are shown at the top. Numbered blue bands mark the millennial-scale TF decline events labeled as following: Site U1385 - MIS (Marine Isotopic Stage) - number of the event.

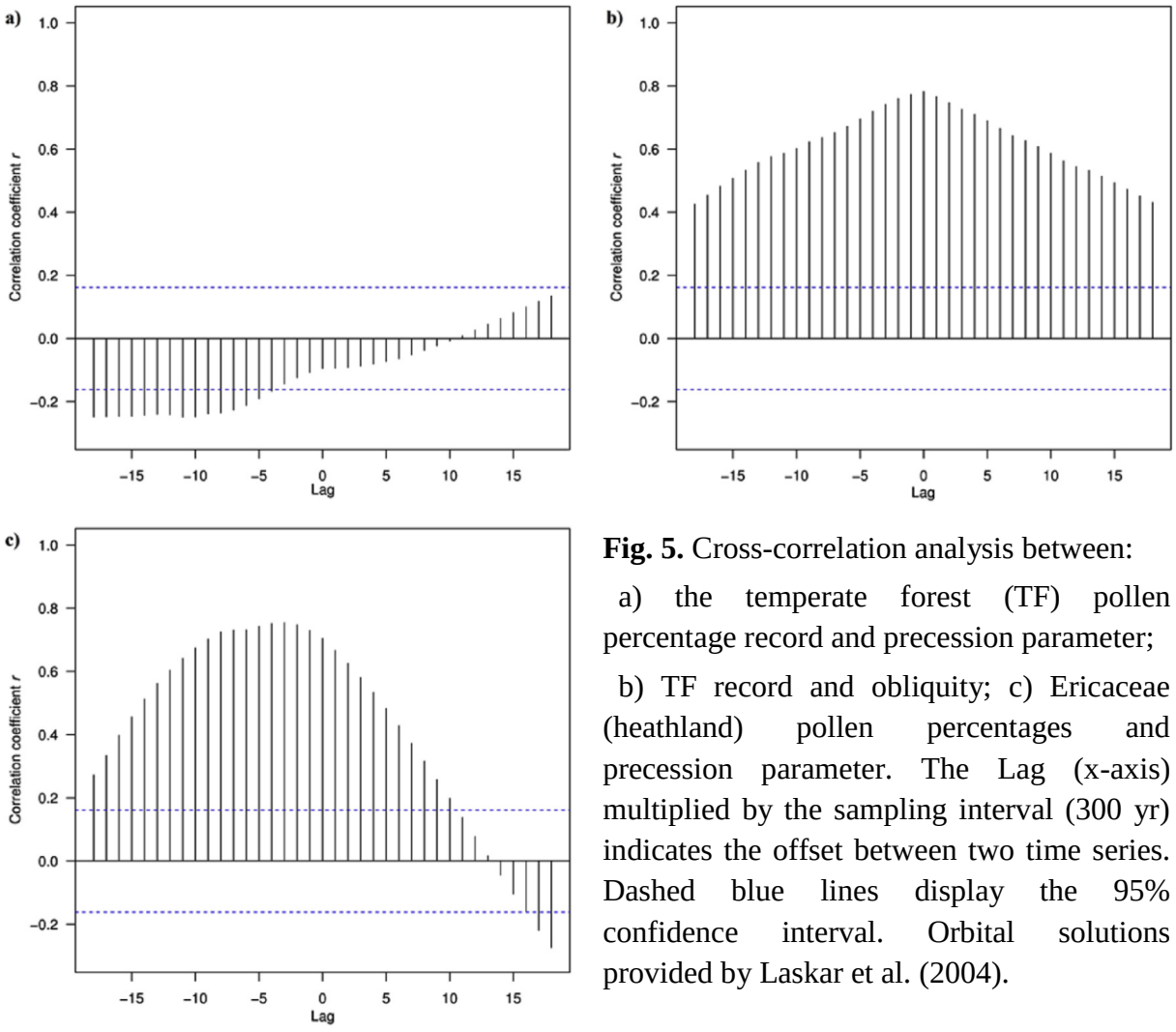

Fig. 5. Cross-correlation analysis between:

a) the temperate forest (TF) pollen percentage record and precession parameter;

b) TF record and obliquity; c) Ericaceae (heathland) pollen percentages and precession parameter. The Lag (x-axis) multiplied by the sampling interval (300 yr) indicates the offset between two time series. Dashed blue lines display the 95% confidence interval. Orbital solutions provided by Laskar et al. (2004).

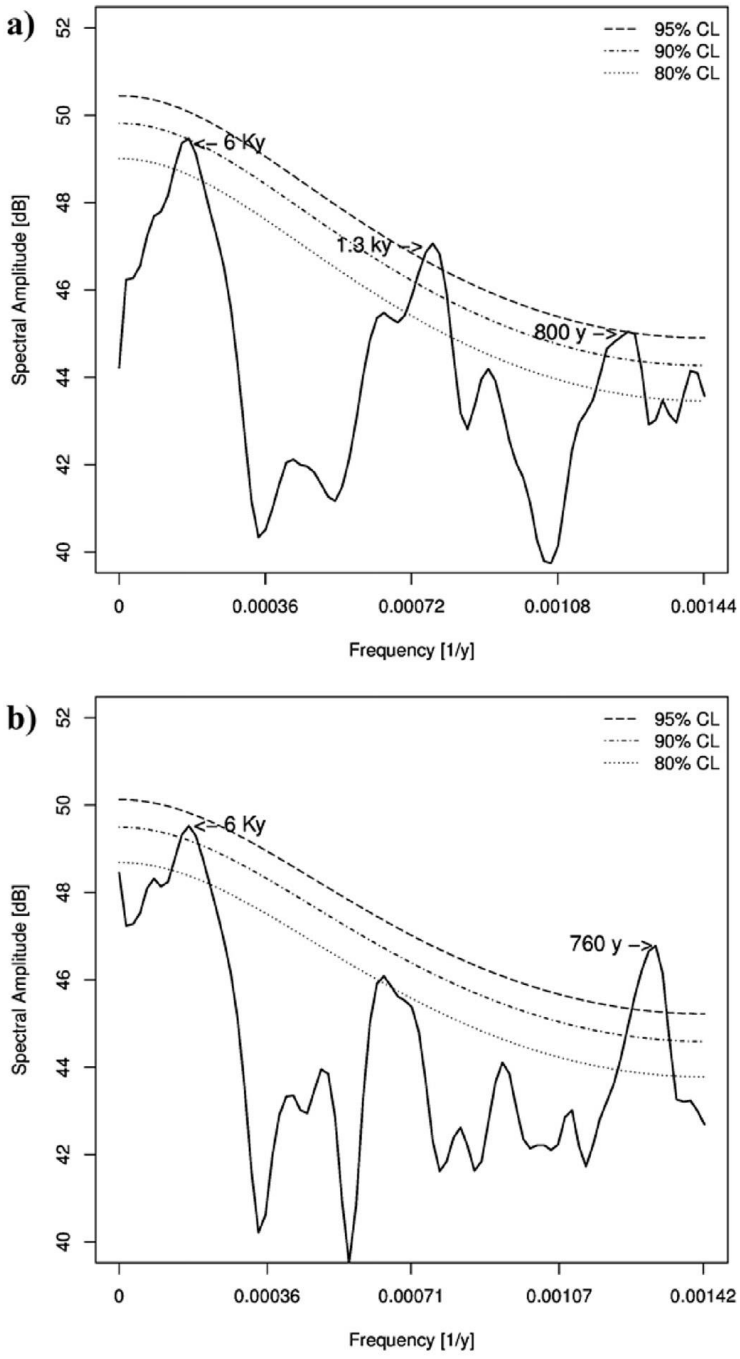

Fig. 6. Spectral analysis (smoothed Lomb–Scargle peridogram with 8 degrees of freedom) (Schulz and Mudelsee, 2002) of the temperate forest (TF) pollen percentages on: a) precession-tuned and b) LR04-based chronologies. Dashed lines represent the significance levels (CL).

5. Discussion

5.1 MIS 31, a "super interglacial" around the world?

The Site U1385 pollen-based vegetation record shows that Sado interglacial was a 34 ky-long forested interval characterized overall by moderate expansion of temperate trees and very reduced development of Mediterranean sclerophylls (Figs. 2 and 3). This interglacial was not extremely warm but rather temperate and humid with reduced seasonal contrast. The MIS 31 conditions found here for the subtropical latitudes of the North Atlantic region were similar to those indicated by the low-resolution western and central Mediterranean pollen records, where the arboreal pollen is not particularly prominent (Joannin et al., 2008, 2011), and the pollen-derived quantitative estimates reveal a peculiar wet character and reduced seasonality in temperature and precipitation (Joannin et al., 2011). Particularly wet MIS 31 conditions are also supported by calcareous nannofossil assemblages at the Montalbano Jonico section from southern Italy (Girone et al., 2013). Comparison of Sado with SW Iberian terrestrial interglacials dominated by 100-ky periodicity shows that the maximum expansion of forest (maximum of 55%) was considerably lower than reported for MIS 5e and the Holocene (maximum ~ 70 and 77%, respectively) and slightly larger than MIS 19c, 11c and 9e (maximum ~ 50, 44 and 53%, respectively) (Sánchez Goñi et al., 1999, 2016; Chabaud et al., 2014; Desprat el al., 2016; Oliveira et al., 2016). In contrast, all these interglacials exhibited higher development of Mediterranean sclerophylls (MIS 19c: 24%, MIS 11c: 17%, MIS 9e: 24% , MIS 5e: 21% and Holocene: 23%) than MIS 31 (% up to 15%). This comparison highlights that the Sado interglacial does not stand out for its forest extent and warmth but rather for the particular weak precipitation seasonality.

In line with the atmospherically driven changes, the Iberian margin SST record is not characterized by exceptionally high temperatures during MIS 31 (Fig. 3). Although the SST optimum is slightly warmer than the Holocene, similar maximum SSTs of 20°C were also recorded at Site U1385 during the last 1.1 My (MIS 19c, 17e, 15e, 9e and 5e) (Rodrigues et al., submitted). These conditions are also reflected in the recently published planktonic $\delta^{18}O$ record of the same site (Hodell et al., 2015) and the nearby Site U1387 Uk'_{37}-SST profile (MIS 34 to 29) (Voelker et al., 2015). Thus, although in the high-latitudes there is consistent proxy data and model evidence of exceptionally high oceanic and atmospheric temperatures during MIS 31 (e.g. Flores and Sierro, 2007; Scherer et al., 2008; Maiorano et al., 2009;

Naish et al., 2009; DeConto et al., 2012; Melles et al., 2012; Tarasov et al., 2013; Coletti et al., 2015; Teitler et al., 2015; de Wet et al., 2016), the land-sea comparison from Site U1385 clearly shows that this interglacial was not unusually warm in the subtropical eastern North Atlantic. Only in a very small number of North Atlantic records does it stand out from the warmest middle- to late Pleistocene interglacials (Ruddiman et al., 1989; McClymont et al., 2008; Hillaire-Marcel et al., 2011). In contrast, most of the records evidence that MIS 31 was warmer than the present interglacial (Helmke et al., 2003; Lawrence et al., 2010; Naafs et al., 2013; Billups and Scheinwald, 2014; Aubry et al., 2016).

Besides highlighting that the warmth magnitude achieved during MIS 31 is not spatially coherent, our study supports the extended duration of this warm stage compared to the oxygen isotope chronology of Lisiecki and Raymo (2005), which places MIS 31 between 1081 and 1062 ka, i.e. lasting for 19 ky (Fig. 3). The precise identification of MIS 31 onset is not straightforward because there is no sharp and rapid glacial-interglacial transition in the $\delta^{18}O_b$ records (Fig. 3). However, it is clear from our combined analyses of marine and terrestrial tracers that the interglacial climate regime started several millennia before 1081 ka in the SW Iberia region (Fig. 3). As in other regions over the globe (Teitler et al., 2015; de Wet et al., 2016 and references therein), western and central Mediterranean palaeoclimate records also show that interglacial conditions were established prior to the LR04-assigned boundary for MIS 31 onset (Joannin et al., 2008; Maiorano et al., 2010; Girone et al., 2013; Hodell et al., 2015; Voelker et al., 2015). Such observations lend support to recent work from the high-latitudes of both northern and southern hemispheres showing that a substantial warming started well before the MIS 32/31 transition as defined in the LR04 stack (Teitler et al., 2015; de Wet et al., 2016). Moreover, our multiproxy reconstruction shows that MIS 31 interglacial conditions persisted for at least 32 ky (Fig. 3), an unusually long duration, but comparable to the one estimated for the longer interglacials of the past 800 ky (28±2 ky; MIS 17, 13a and 11c) (Tzedakis et al., 2012). Tzedakis et al. (2012) suggest that the longer duration of these interglacials could be due to a nearly antiphase relationship between obliquity and precession, with the first summer insolation minimum occurring during maximum obliquity, which is not the case for MIS 31 (Fig. 3). Alternatively MIS 31 prolonged interglacial warmth may be attributed to its unique insolation pattern, with the first SH insolation maxima leading to the weak character of MIS 32 through interhemispheric climate teleconnections related to WAIS melting and consequent changes in the palaeoceanographic and atmospheric circulation (Melles et al., 2012; de Wet et al., 2016).

5.2 Astronomical factors controlling the MIS 31 vegetation and climate in SW Europe

Given the exceptional insolation (precession) forcing during MIS 31, an extensive Mediterranean forest cover in SW Iberia below 40°N with a prominent development of Mediterranean sclerophylls consistent with the precessional influence on seasonal contrast, was likely to be expected. Paradoxically, pollen-based vegetation and atmospheric changes (Fig. 3) and CCF analysis (Fig. 5a) do not show the influence of precession on TF development. The early phases of the Sado interglacial, from ~1094 to 1079.5 ka, provide a clear evidence for this non-linear response with the TF progressive development occurring throughout the descending branch and minima of the summer insolation curve (inverse to precession) (Fig. 3). Moreover, even if there is a slight increase of Mediterranean sclerophylls near the MIS 31 precession minima (Fig. 3), their expansion remains weaker compared to younger interglacials marked by high or low precession forcing such as MIS 5e and MIS 11c, respectively (Sánchez Goñi et al., 1999; Oliveira et al., 2016). The weakness of the Mediterranean sclerophylls response to precession forcing ~1073 ka may be also linked to the impact of millennial-scale climate dynamics in ending the increasing trend of sclerophyll taxa in U1385-31-fe7 (Fig. 4). Interestingly, the major expansion of the forest cover, which corresponds to the strongest expression of the temperate and humid climate regime (pollen zone U1385-31-3), is coincident with the MIS 31 obliquity maxima (Fig. 3). The potential influence of obliquity on TF development, and therefore on the hydrologic conditions of southern Iberia throughout MIS 31 is testified by the unambiguous significant positive correlation without time lag given by the CCF analysis (Fig. 5b). These findings are in agreement with recent climate model simulations for the precession and obliquity forcing on the Mediterranean freshwater budget (Bosmans et al., 2015), using the extreme values of both orbital parameters of the last 1 My (Berger, 1978). These climate simulations suggest increased winter precipitation during obliquity maximum and precession minimum across the Mediterranean basin including adjacent regions such as SW Iberia. However, at times of obliquity maximum the summer precipitation is also relatively high, supporting the low seasonality in precipitation inferred from our pollen record and the predominant role of obliquity on TF development. Bosmans et al. (2015) proposed that the increase of winter precipitation over the Mediterranean basin is primarily due to an air-sea thermal contrast inducing locally convective precipitation, while in southern Iberia and Morocco it is mainly

driven by large scale precipitation, associated to increased storm track activity as it is also in current climate (Sousa et al., 2016). The position and strength of the winter storm track are strongly influenced by the North Atlantic climate dynamics, in particular latitudinal temperature gradients (Brayshaw et al., 2011). Reduced meridional winter temperature gradient (warmer high-latitudes temperatures due to maxima in obliquity) would weaken the flow of the temperate westerlies allowing their southward migration into SW Iberia, and therefore the increase of moisture. Because the summer climate regime in southern Iberia is mainly controlled by subtropical climate dynamics (Lionello et al., 2006), enhanced summer precipitation during obliquity maxima may be related to a more northern position of the North Atlantic Subtropical High which could have led to less summer aridity at subtropical latitudes. We speculate that the unexpected wetter conditions and muted seasonality indicated by SW Iberian vegetation during MIS 31 may also be a result of the higher amount of moisture available in the atmosphere, due to reduced ice sheets, as demonstrated by high-latitudes proxy data and model studies (Scherer et al., 2008; Naish et al., 2009; Pollard and DeConto, 2009; DeConto et al., 2012; Melles et al., 2012; Coletti et al., 2015). This would have produced enough atmospheric humidity in summertime that counterbalanced the strong precession forcing determining high seasonality and allowing for summer drought-intolerant trees to develop in SW Iberia during MIS 31, but constraining the expansion of Mediterranean sclerophylls (Fig. 3).

The pervasive influence of obliquity on the TF development in SW Iberia during MIS 31 is in line with the growing body of evidence that shows an obliquity-forced climate before ~900 ky (e.g. Maasch and Saltzman, 1990; Berger and Jansen, 1994; Mudelsee and Schulz, 1997; Mudelsee and Stattegger, 1997; Maslin and Ridgwell, 2005; Maslin and Brierley, 2015). This obliquity signal is also evident in the western Mediterranean marine pollen record of ODP Site 976, which displays five obliquity-driven botanical successions through MIS 31-23 underlying the eight short-lasting precessional vegetation cycles (Joannin et al., 2011). Pollen analysis from the central Mediterranean region (southern Italy) also show a similar vegetation response to both obliquity and precession parameters during other time intervals of the 41-ky world (MIS 43-40: Joannin et al., 2007; MIS 37-23: Joannin et al., 2008). Similarly, although obliquity plays a dominant role on TF development and composition in the SW Iberian region between MIS 32 and early MIS 30, Ericaceae shows a clear imprint of precession with two major phases of heathland expansion coinciding with precession maxima

(Fig. 3). The precession forcing apparent in the Ericaceae pollen record of Site U1385 is confirmed by the CCF determined statistically significant correlation, even if the highest correlation shows a lag of ~1000 yr (Fig. 5c). The expansion of Ericaceae in southern Iberia during intervals of precession maxima (summer insolation minima) has been documented for glacial and interglacial periods across the late Pleistocene as a taxon-specific response to lower rainfall seasonality (reduced summer dryness) (Roucoux et al., 2006; Margari et al., 2007, 2014; Fletcher and Sánchez Goñi, 2008; Chabaud et al., 2014). This work shows that the influence of precession forcing on heathland development also occurred in the 41-ky world, thereby supporting that this taxon-specific response is pervasive and independent of the climatic background state. The fern spore *Isoetes*, which displays a similar (inverse) trend to the Ericaceae (Fig. 3), also shows a precession signal that may relate to the dependence of *Isoetes* on seasonally flooded ground (Prada, 1986; Salvo Tierra, 1990), as opposed to Ericaceae preference for year-round moisture (e.g. Loidi et al., 2007).

5.3 Land - sea interaction on millennial timescales

5.3.1 Millennial-scale variability during glacials MIS 32 and MIS 30

Site U1385 pollen-based vegetation record reveals that the coldest and driest atmospheric conditions occurred during the MIS 32 and MIS 30 glacial stages, forest decline events U1385-30-fe1 and -32-fe10, concomitantly with abrupt and severe SST cooling at the SW Iberian margin (Fig. 4). Besides their particular long duration, these extreme events display an interesting common tripartite climatic pattern characterized by cold/dry-warmer/wetter- cold/dry conditions (Fig. 4). Cold and dry conditions during both glacial stages are also reported in other western and central Mediterranean (Joannin et al., 2008, 2011; Girone et al., 2013; Hodell et al., 2015; Voelker et al., 2015) and North Atlantic records (e.g. Ruddiman et al., 1989; Toucanne et al., 2009; Lawrence et al., 2010; Naafs et al., 2013; Voelker et al., 2015). Nevertheless, apart from Voelker et al. (2015), those previous studies do not have a sufficiently high temporal resolution to allow for a detailed investigation of the short-lived internal climate variability. Voelker et al. (2015) document a similar tripartite climatic pattern during the extremely cold SST events of MIS 32 and MIS 30 in the Gulf of Cadiz (Fig. 4). This pattern is also evident in the mid-latitude North Atlantic DSDP Site 607

during the abrupt MIS 30 event (Lawrence et al., 2010), however, the SST warming phase is represented by a unique sample, which requires a resolution increase.

The climatic imprint of the most intense MIS 32 and MIS 30 events in the Iberian ecosystems resemble some of the last glacial Heinrich stadials (HS) with regard to the magnitude and duration of the weak forest episodes (TF pollen percentages remain below 10% for ~2-3 ky), severe cooling of surface waters (SSTs absolute minima of 8.5-10°C) and climatic structure (three main phases) (e.g. Bard et al., 2000; Sánchez Goñi et al., 2000; Fletcher and Sánchez Goñi, 2008; Naughton et al., 2009, 2016). Recent studies off western Iberia have also documented the occurrence of Heinrich (H)-type events throughout the middle- to late Pleistocene (Martrat et al., 2007; Voelker et al., 2010; Rodrigues et al., 2011; Palumbo et al., 2013; Marino et al., 2014; Maiorano et al., 2015). However, a complex tripartite climatic pattern was only noticed in the MD03-2699 $U^{k'}_{37}$-SST profile during the cold spell of Termination V (Rodrigues et al., 2011). In analogy to the HS and H-type events displaying a tri-phase climatic pattern, meltwater-induced reduction in AMOC together with rapid southward shifts in the position of the Polar Front and Atlantic jet-stream during the early and late phases (e.g. Naughton et al., 2009, 2016; Rodrigues et al., 2011) appear as plausible underlying mechanisms for explaining the MIS 32 and MIS 30 extreme cold phases. Within age uncertainties, disruption of the AMOC by meltwater discharge is supported by coincident decreases of benthic $\delta^{13}C$ values at Site U1308 and Si-rich IRD events, although these IRD were not derived from the Hudson Strait as the "classic" HS but rather from northern Europe, Greenland and/or Iceland (Hodell et al., 2008) (Fig. 4). Site U1314, located in the subpolar gyre, provides additional evidence for a perturbation of the AMOC during the MIS 30 event, as revealed by an increase in K/Ti that is inferred to reflect a reduction in the Iceland-Scotland Overflow Water (Grützner and Higgins, 2010), and related ice-rafting (Hernández-Almeida et al., 2013). On the contrary, the MIS 32 event is coincident with low K/Ti ratios (Fig. 4). Considering the Site U1385 pollen record of MIS 38 (Tzedakis et al., 2015) and the MIS 41-37 palaeoceanographic study (Birner et. al, 2016) evidence for similar millennial-scale variability during the early Pleistocene and the Dansgaard–Oeschger (D–O) events of the last glacial, we propose that Heinrich-type mechanisms may have been also operating in the 41-ky world, notwithstanding the origin of the iceberg pulses (Hodell et al., 2008; Bailey et al., 2012; Naafs et al., 2013) and the reduced extent of the ice sheets and shorter duration of the glacials (e.g. Lisiecki and Raymo, 2005; Elderfield et al., 2012).

The weak and short-lived event U1385-32-fe2 is associated with a slowdown of the SST increasing rate in the subtropical gyre, but no AMOC change is indicated (Fig. 4). However, it is worth highlighting that a small decrease of the forest before the onset of the terrestrial interglacial, a potential Younger Dryas-type event, has also been documented by other Iberian margin vegetation records from Terminations I to IV (Desprat et al., 2007) and Termination IX (Sanchez Goñi et al, 2016). A substantial drop in SSTs, from 16.3 to 12.4°C, is coeval with event U1385-30-fe9 (Fig. 4). This event is also recorded in the $U^{k'}_{37}$-SST profile of Site U1387 (Voelker et al., 2015) and it may be linked to the progressive AMOC reduction during the MIS 31/30 transition, as suggested by the benthic $\delta^{13}C$ decrease at Site U1308, and the increasing IRD recorded in the subpolar gyre (Hodell et al., 2008; Hernández-Almeida et al., 2013) (Fig. 4).

Our study strengthens previous evidence, from SW Iberian margin (Hodell et al., 2015; Tzedakis et al., 2015; Birner et. al, 2016) and North Atlantic deep-sea sediments (Raymo et al., 1998; Hodell et al., 2008; Grützner and Higgins, 2010), for persistent abrupt climate variability during the glacial climate of the early Pleistocene. Moreover, the present direct land-sea comparison shows that the most intense millennial-scale cooling and drying events in the SW Iberia, events U1385-32-fe1, -30-fe9 and -30-fe10, only occurred when the $\delta^{18}O_b$ exceeded 3.5‰ (Fig. 4). This observation is consistent with the critical ice volume threshold needed to amplify the magnitude of millennial-scale variability after the MPT (McManus et al., 1999) and, most particularly, for the enhancement and/or extended duration of the Iberian vegetation changes (Desprat et al., 2005, 2009; Margari et al., 2010; Oliveira el al., 2016), although lower $\delta^{18}O_b$ thresholds (3.2‰ and 3.3‰) have been suggested for the early Pleistocene (Raymo et al., 1998; McIntyre et al., 2001; Bailey et al., 2012; Hodell et al., 2015; Birner at al., 2016). Because changes in the $\delta^{18}O_b$ are not only driven by ice volume but also by deep-water temperature (Shackleton, 1987; Skinner and Shackleton, 2005), caution is required when applying the concept of ice volume thresholds.

5.3.2 Intra-interglacial climate variability during MIS 31

Our pollen record shows pervasive millennial-scale atmospherically driven changes in SW Iberian vegetation throughout MIS 31 (Fig. 4), which contrasts with the proposed suppression of suborbital variability during interglacial stages ($\delta^{18}O_b$ >~3.3–3.5‰) over the past 1.5 My (Hodell et al., 2015; Birner et al., 2016). Six temperate forest declines (U1385-31-fe3 to -fe8) indicate repeated atmospheric cooling and drying episodes, whereas SST remained warm off the western Iberia (Fig. 4). The observed land-sea decoupling at millennial timescales during MIS 31 is supported by the absence of coincident SST reversals in the Uk'_{37}-SST reconstruction of the nearby Site U1387 (Fig. 4) (Voelker et al., 2015). The only exception is the cold spell that appears associated with the forest event U1385-31-fe8, however this SST decrease is characterized by a single sample at Site U1387 while in our $U^{k'}_{37}$-SST record the warming trend is well-resolved (Fig. 4). Moreover, it is noticeable that no Si/Sr peaks at Site U1308 occur during MIS 31 (Fig. 4), suggesting that the SW Iberian millennial-scale forest declines during the Sado interglacial are not driven by North Atlantic freshwater forcing. Regrettably, comparison with the other currently available North Atlantic and Mediterranean records is hampered by their lack of temporal resolution (i.e., centennial-scale) to investigate in detail the MIS 31 intra-interglacial climate variability (Ruddiman et al., 1989; Helmke et al., 2003; Tzedakis et al., 2006; Joannin et al., 2008, 2011; McClymont et al., 2008; Toucanne et al., 2009; Lawrence et al., 2010; Maiorano et al., 2010; Hillaire-Marcel et al., 2011; Girone et al., 2013; Naafs et al., 2013; Hodell et al., 2015).

The spectral analysis of the TF record carried out to explore the nature of MIS 31 variability on millennial timescales revealed a significant dominant cyclicity around 6 ky (Fig. 6a, b), which may be linked to the fourth harmonic of the precessional component of the insolation forcing (5.5 ky cycles) (Berger et al., 2006). Although it has been argued that the amplitude of precessional-derived cyclicity decreases rapidly from the equator to high-latitudes (Short et al., 1991; Berger et al., 2006), the cycles related to the half and fourth precessional components have been recognized in palaeoclimate records from the mid-to-high latitudes in the North Atlantic throughout the Pleistocene (Wara et al., 2000; Weirauch et al., 2008; Ferretti et al., 2010, 2015; Billups et al., 2011; Amore et al., 2012; Hernández-Almeida et al., 2012; Palumbo et al., 2013; Billups and Scheinwald, 2014). Most particularly, based on a new land-sea comparison of MIS 19 at Site U1385, Sánchez Goñi et al. (2016) revealed the

occurrence of 5 ky cycles of cooling and drying in the SW Iberian region associated with warm SSTs in the eastern North Atlantic subtropical gyre also related to the fourth harmonic of precession. The suggestion for a low-latitude insolation forcing is primarily based on the fact that in low-latitudes the incoming daily irradiation over a year is characterized by a double maximum, which leads to a larger latitudinal thermal gradient and results in enhanced poleward atmospheric and oceanic transport of heat and moisture (Short et al., 1991; McIntyre and Molfino, 1996; Berger et al., 2006). As for the MIS 19 (Sánchez Goñi et al., 2016), we observe that the MIS 31 TF dataset filtered in the fourth harmonic of precession frequency (6 ky Gaussian bandpass filter) closely agrees with the largest amplitude in the seasonal cycle at the equator, Δ, calculated from the daily mean irradiance of the winter and summer solstices and autumn and spring equinoxes (Berger et al., 2006) (Fig. 7). Because the Δ index represents a measure of the largest seasonal contrast at the equator that is anticipated to drive the climate system behavior (Berger et al., 2006), its good correlation with the 6 ky-filtered TF record supports the hypothesis of a low-latitude forcing in the trajectory and intensity of the atmospheric westerlies transporting warmth and moisture to the SW Iberian region. It is noteworthy that the most dramatic collapse of temperate forest recorded at Site U1385, forest decline event U1385-32-fe-7, which is not associated with either the glacial inception or any evidence of SST cooling, ice-rafting or wider AMOC perturbation (Fig. 4), correspond, within age uncertainties, to one of the largest amplitude increases of the seasonal cycle at the Equator (Fig. 7). This observation highlights that forest collapses can occur due to hydrological forcing originating in the low-latitudes under prevailing warm (globally ~"superwarm") conditions.

As this low-latitude forcing also involves enhanced oceanic circulation, we expected a surface water response to the fourth harmonic of precession, yet significant suborbital periodicities are not found in the spectral analysis of the Uk'_{37}-SST record at Site U1385 (Fig. S1). This result can be explained by the existence of additional physical mechanism, namely the dominant influence of the subtropical Azores Current and Iberian Poleward Current waters at the Iberian margin over MIS 31, as suggested for MIS 11 (Voelker et al., 2010; Oliveira et al., 2016). These mechanisms that are not considered explicitly in the hypothesis of a low-latitude forcing in the land-sea decoupling at millennial timescales may have dwarfed the impact of a precessional-related cyclicity on local SSTs. Even though further work in the marine and terrestrial realm is needed to confirm the nature of millennial-scale

changes occurring at precession harmonics frequencies during MIS 31, this study supports a growing body of evidence that outlines the importance of the low-latitude forcing in the North Atlantic suborbital variability throughout the Pleistocene, regardless of the baseline climate states of the 41- and 100-ky worlds (e.g. Weirauch et al., 2008; Ferretti et al., 2010, 2015; Billups et al., 2011; Hernández-Almeida et al., 2012; Sánchez Goñi et al., 2016)

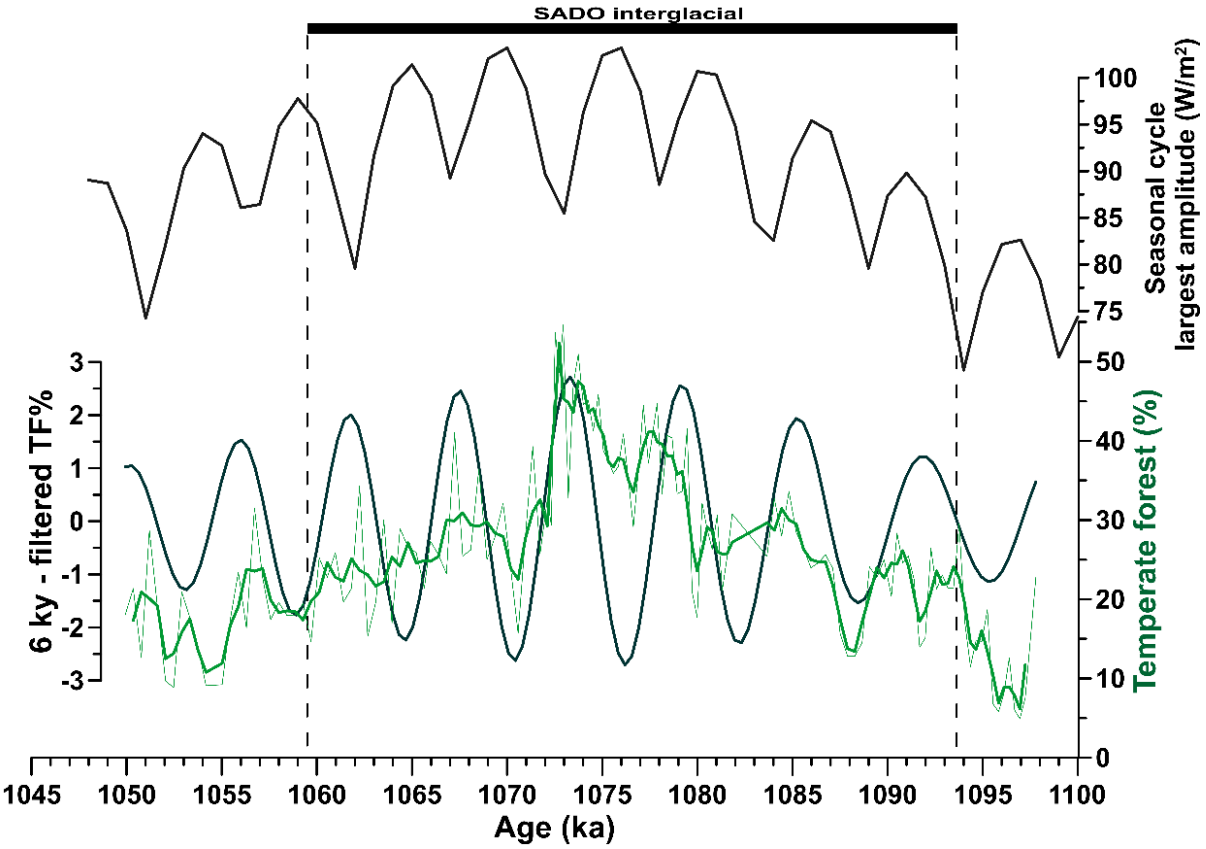

Fig. 7. Comparison of the temperate forest (TF) pollen percentages (green, bold 3-point moving average) and its 6 ky filtered record (dark green) with the largest amplitude in the seasonal cycle at the equator (Berger et al., 2006) (black). Gaussian bandpass filtering (0.02 bandwidth) performed using Analyseries (Paillard et al., 1996). Vertical dashed lines indicate the terrestrial counterpart of MIS 31 in SW Iberia named Sado interglacial.

6. Conclusions

This new multiproxy record of the early Pleistocene at Site U1385, is the first to document the SW Iberian vegetation and surface oceanic conditions in the eastern subtropical gyre at orbital and suborbital timescales over the 1100-1050 ka interval (from MIS 32 to early MIS 30), which includes the "super interglacial" MIS 31.

The MIS 31 extreme insolation (precession) forcing was favorable for an anomalously warm interglacial characterized by enhanced seasonality in the SW Iberia region. However, our study shows that, unlike other locations at higher latitudes, atmospheric and sea-surface temperatures were not exceptionally high in the context of other middle- to late Pleistocene interglacials. Moreover, the Site U1385 pollen-based vegetation record reveals for the first time an unexpected temperate and humid climate regime marked by low abundance of Mediterranean sclerophylls and the development of diverse summer drought-intolerant trees. This muted seasonality during MIS 31 is consistent with analysis of vegetation dynamics and cross-correlation coefficients showing a dominant influence of obliquity on the forest development rather than precession. Prevailing obliquity-driven vegetation and climatic changes, in agreement with modeling experiments, are likely associated to a decrease in the seasonal distribution of rainfall in SW Iberia resulting from higher summer precipitation associated to obliquity maxima rather than to precession minima. The response of Ericaceae (heathland), in contrast to the temperate forest, is strongly imprinted by precession forcing, with major expansions occurring during the two precession maxima of the studied interval. Apart from revealing both obliquity and precession forcing during MIS 31 in SW Iberia, our study shows an unusual prolonged period of interglacial conditions starting ~13 ky earlier than defined in the LR04 stack, which supports the need for a redefinition of the lower boundary of MIS 31.

Superimposed on the orbital-scale driven changes, persistent millennial-scale climate variability is shown by ten forest decline events reflecting cooling and drying episodes in SW Iberia from MIS 32 to early MIS 30. The Site U1385 direct land–sea comparison reveals the different expression of the millennial-scale cooling, in terms of magnitude, character and duration, under the distinct glacial/interglacial boundary conditions. The particularly long,

coldest and driest atmospheric events are synchronously detected in the marine realm by large SST decreases and concur with the larger ice volume conditions of glacial MIS 32 and MIS 30. These extreme events are related to North Atlantic cooling and enhanced iceberg discharges, supporting the key role of northern ice-sheet instability and associated changes in the deep-water circulation in amplifying the intensity and duration of suborbital cooling in SW Iberia throughout the Pleistocene. Comparison of the high intensity MIS 32 and MIS 30 events with Heinrich events reveals close similarities regarding the imprint on terrestrial and marine Iberian ecosystems and the tripartite climatic structure. In the light of this strong resemblance, we suggest that Heinrich-type mechanisms, despite the source of the icebergs, may have also been operating during the glacial climate of the 41-ky world. Finally, our work provides detailed evidence for MIS 31 intra-interglacial instability in SW Iberia. Rapid forest decline events indicating recurring cool and dry atmospheric episodes with no concurrent SST change reveal a land-sea decoupling during MIS 31. Spectral analysis results show that these repeated atmospheric shifts contain a significant suborbital variability at periods of 6 ky, likely corresponding to the fourth harmonic of the precession cycle. We propose that the observed millennial-scale climate variability at Site U1385 during MIS 31 might have been driven by low-latitude insolation forcing, which led to meridional tilts in the temperate westerlies and consequent cooling and drying in SW Iberia. To better constrain the processes and mechanisms involved in rapid climate change during the different background climate states of early Pleistocene, additional high-resolution studies in key regions from the North Atlantic are required.

Supplementary data

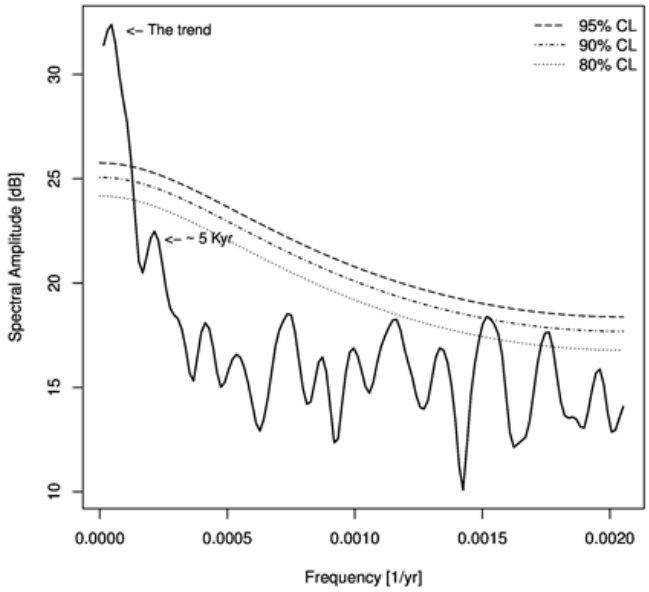

Supplementary Fig. S1. Spectral analysis (smoothed Lomb–Scargle peridogram with 8 degrees of freedom) (Schulz and Mudelsee, 2002) of Site U1385 $U^{k'}_{37}$-SST reconstruction on precession-tuned timescale. Dashed lines represent the significance levels (CL).

Acknowledgments

Financial support was provided by WarmClim, a LEFE-INSU IMAGO project, and the Portuguese Foundation for Science and Technology (FCT) through the project CLIMHOL (PTDC/AAC-CLI/100157/2008), D. Oliveira's doctoral grant (SFRH/BD/9079/2012), F. Naughton's postdoctoral grant (SFRH/BPD/108712/2015) and A. Voelker's IF contract. JM. Polanco-Martínez was funded by a Basque Government post-doctoral fellowship (Ref. No. POS_2015_1_0006) and B. Martrat by a Ramón y Cajal contract (RYC-2013-14073). This research used samples provided by the Integrated Ocean Drilling Program (IODP), Expedition 339. We would like to thank the scientists and technicians of IODP Expedition 339 and the Bremen Core Repository, L. Devaux for technical assistance and A. Rebotim for comments and editing. The editor, José Carrión, and an anonymous reviewer are acknowledged for their constructive and insightful comments.

References

Amore, F.O., Flores, J.A., Voelker, A.H.L., Lebreiro, S.M., Palumbo, E., Sierro, F.J., 2012. A Middle Pleistocene Northeast Atlantic coccolithophore record: Paleoclimatology and paleoproductivity aspects. Marine Micropaleontology 90-91, 44–59. doi:10.1016/j.marmicro.2012.03.006.

Aubry, A.M.R., de Vernal, A., Hillaire-Marcel, C., 2016. The "warm" Marine Isotope Stage 31 in the Labrador Sea: Low surface salinities and cold subsurface waters prevented winter convection. Paleoceanography 31, 1206–1224. doi:10.1002/2015PA002903.

Bailey, I., Foster, G.L., Wilson, P.A., Jovane, L., Storey, C.D., Trueman, C.N., Becker, J., 2012. Flux and provenance of ice-rafted debris in the earliest Pleistocene sub-polar North Atlantic Ocean comparable to the last glacial maximum. Earth and Planetary Science Letters 341-344, 222–233. doi:10.1016/j.epsl.2012.05.034.

Bard, E., Rostek, F., Turon, J. L., Gendreau, S., 2000. Hydrological impact of Heinrich events in the subtropical northeast Atlantic. Science 289(5483), 1321-1324. doi:10.1126/science.289.5483.1321.

Berger W.H., Jansen, E., 1994. Mid-Pleistocene climate shift: The Nansen connection. In: Johanessen OM, Muench RD, Overland JE (eds) The Polar Oceans and Their Role in Shaping the Global Environment: The Nansen Centennial Volume. AGU Geophysical Monograph 84:295-311.

Berger, A., 1978. Long-Term variations of daily insolation and Quaternary climatic changes. Journal of Atmospheric Science, 35, 2362–2367.

Berger, A., Loutre, M.F., Mélice, J.L., 2006. Equatorial insolation: from precession harmonics to eccentricity frequencies. Climate of the Past 2, 131–136. doi:10.5194/cp-2-131-2006.

Billups, K., Rabideaux, N., Stoffel, J., 2011. Suborbital-scale surface and deep water records in the subtropical North Atlantic: implications on thermohaline overturn. Quaternary Science Reviews 30, 2976–2987. doi:10.1016/j.quascirev.2011.06.015.

Billups, K., Scheinwald, A., 2014. Origin of millennial-scale climate signals in the subtropical North Atlantic. Paleoceanography 29, 612–627. doi:10.1002/2014PA002641.

Birks, H., Birks, H., 1980. Quaternary palaeoecology. London: Edward Arnold.

Birner, B., Hodell, D.A., Tzedakis, P.C., Skinner, L.C., 2016. Similar millennial climate variability on the Iberian margin during two early Pleistocene glacials and MIS 3. Paleoceanography 31, 203–217. doi:10.1002/2015PA002868.

Blanco Castro, E., Casado González, M.A., Costa Tenorio M., Escribano Bombín, R., García Antón, M., Génova Fuster, M., Gómez Manzaneque, F., Moreno Sáiz, J.C., Morla Juaristi, C., Regato Pajares, P., Sáiz Ollero, H., 1997. Los bosques ibéricos: una Interpretación Geobotánica. Editorial Planeta, 572 p., Barcelona.

Bosmans, J.H.C., Drijfhout, S.S., Tuenter, E., Hilgen, F.J., Lourens, L.J., Rohling, E.J., 2015. Precession and obliquity forcing of the freshwater budget over the Mediterranean. Quaternary Science Reviews 123, 16–30. doi:10.1016/j.quascirev.2015.06.008.

Brassell, S.C., Eglinton, G., Marlowe, I.T., Pflaumann, U., Sarnthein, M., 1986. Molecular stratigraphy: a new tool for climatic assessment. Nature 320, 129–133. doi:10.1038/320129a0.

Brayshaw, D.J., Rambeau, C.M.C., Smith, S.J., 2011. Changes in Mediterranean climate during the Holocene: Insights from global and regional climate modelling. The Holocene 21, 15–31. doi:10.1177/0959683610377528.

Byrami, M.L., Newnham, R.M., Alloway, B. V., Pillans, B., Ogden, J., Westgate, J., Mildenhall, D.C., 2005. A late Early Pleistocene tephrochronological and pollen record from Auckland, New Zealand. Geological Society, London, Special Publications 247, 183–208. doi:10.1144/GSL.SP.2005.247.01.10.

Chabaud, L., Sánchez Goñi, M.F., Desprat, S., Rossignol, L., 2014. Land-sea climatic variability in the eastern North Atlantic subtropical region over the last 14,200 years: atmospheric and oceanic processes at different timescales. The Holocene 24, 787–797. doi:10.1177/0959683614530439.

Clark, P.U., Archer, D., Pollard, D., Blum, J.D., Rial, J.A., Brovkin, V., Mix, A.C., Pisias, N.G., Roy, M., 2006. The middle Pleistocene transition: characteristics, mechanisms, and implications for long-term changes in atmospheric pCO_2. Quaternary Science Reviews 25, 3150–3184. doi:10.1016/j.quascirev.2006.07.008.

Coletti, A.J., DeConto, R.M., Brigham-Grette, J., Melles, M., 2015. A GCM comparison of Pleistocene super-interglacial periods in relation to Lake El'gygytgyn, NE Arctic Russia. Climate of the Past 11, 979–989. doi:10.5194/cp-11-979-2015.

de Wet, G.A., Castañeda, I.S., DeConto, R.M., Brigham-Grette, J., 2016. A high-resolution mid-Pleistocene temperature record from Arctic Lake El'gygytgyn: a 50 kyr super interglacial from MIS 33 to MIS 31? Earth and Planetary Science Letters 436, 56–63. doi:10.1016/j.epsl.2015.12.021.

DeConto, R.M., Pollard, D., Kowalewski, D., 2012. Modeling Antarctic ice sheet and climate variations during Marine Isotope Stage 31. Global and Planetary Change 88-89, 45–52. doi:10.1016/j.gloplacha.2012.03.003.

Desprat, S., Guilhem, G., Yin, Q.Z., Morales-Molino, C., Sánchez Goñi, M.F., 2016. Regional expression of the MIS 9e interglacial in southwestern Europe. The 12th International conference on Paleoceanography (ICP12), 29 August-2 September 2016, Utrecht, The Netherlands.

Desprat, S., Sanchez Goni, M. F., Naughton, F., Turon, J.-L., Duprat, J., Malaize, B., Cortijo, E., Peypouquet, J.-P., 2007. Climate variability of the last five isotopic interglacials: Direct land-sea-ice correlation from the multiproxy analysis of North-Western Iberian margin deep-sea cores, in: The Climate of Past Interglacials, Developments in Quaternary Science, edited by: Sirocko, F., Litt, T., Claussen, M., Sánchez Goñi M. F., Elsevier, 375–386, 2007.

Desprat, S., Sánchez Goñi, M.F., McManus, J.F., Duprat, J., Cortijo, E., 2009. Millennial-scale climatic variability between 340000 and 270000 years ago in SW Europe: evidence from a NW Iberian margin pollen sequence. Climate of the Past 5, 53–72. doi:10.5194/cp-5-53-2009.

Desprat, S., Sánchez Goñi, M.F., Turon, J.L., McManus, J.F., Loutre, M.F., Duprat, J., Malaizé, B., Peyron, O., Peypouquet, J.P., 2005. Is vegetation responsible for glacial inception during periods of muted insolation changes? Quaternary Science Reviews 24, 1361–1374. doi:10.1016/j.quascirev.2005.01.005.

Duplessy, J.C., Shackleton, N.J., Fairbanks, R.G., Labeyrie, L., Oppo, D., Kallel, N., 1988. Deepwater source variations during the last climatic cycle and their impact on the global deepwater circulation. Paleoceanography 3, 343–360. doi:10.1029/PA003i003p00343.

Dyez, K.A., Ravelo, A.C., 2014. Dynamical changes in the tropical Pacific warm pool and zonal SST gradient during the Pleistocene. Geophysical Research Letters 41, 7626–7633. doi:10.1002/2014GL061639.

Elderfield, H., Ferretti, P., Greaves, M., Crowhurst, S., McCave, N., Hodell, D., Piotrowski, A.M., 2012. Evolution of ocean temperature and ice volume through the Mid- Pleistocene climate transition. Science 377, 704–709. doi:10.1126/science.1221294.

Expedition 339 Scientists, 2013. Site U1385. In: Stow, D.A.V., Hernández-Molina, F.J., Alvarez Zarikian, C.A., the Expedition 339 Scientists (Eds.), Proceedings IODP 339. Integrated Ocean Drilling Program Management International, Inc., Tokyo. http://dx.doi.org/10.2204/iodp.proc.339.103.201.

Ferretti, P., Crowhurst, S.J., Hall, M.A., Cacho, I., 2010. North Atlantic millennial-scale climate variability 910 to 790 ka and the role of the equatorial insolation forcing. Earth and Planetary Science Letters 293, 28–41. doi:10.1016/j.epsl.2010.02.016.

Ferretti, P., Crowhurst, S.J., Naafs, B.D.A., Barbante, C., 2015. The Marine Isotope Stage 19 in the mid-latitude North Atlantic Ocean: astronomical signature and intra-interglacial variability. Quaternary Science Reviews 108, 95–110. doi:10.1016/j.quascirev.2014.10.024.

Fiúza, A. F. G., 1984. Hidrologia e Dinâmica das Águas Costeiras de Portugal, Ph.D. thesis, 294 pp., Univ. de Lisboa, Lisbon.

Fiúza, A. F. G., Hamann, M., Ambar, I., del Rio, G. D., Gonzalez, N., Cabanas, J. M., 1998. Water masses and their circulation off western Iberia during May 1993. Deep Sea Research Part I 45(7), 1127–1160.

Fletcher, W.J., Sánchez Goñi, M.F., 2008. Orbital- and sub-orbital-scale climate impacts on vegetation of the western Mediterranean basin over the last 48,000 yr. Quaternary Research 70, 451–464. doi:10.1016/j.yqres.2008.07.002.

Flores, J.-A., Sierro, F.J., 2007. Pronounced mid-Pleistocene southward shift of the Polar Front in the Atlantic sector of the Southern Ocean. Deep Sea Research Part II: Topical Studies in Oceanography 54, 2432–2442. doi:10.1016/j.dsr2.2007.07.026.

Gallardo-Lancho, J.F., 2001. Distribution of chestnut (*Castanea sativa* Mill.) forests in Spain: possible ecological criteria for quality and management (focusing on timber coppices). Forest Snow and Landscape Research 76, 477–481.

Gimeno, L., Nieto, R., Trigo, R.M., Vicente-Serrano, S.M., López-Moreno, J.I., 2010. Where Does the Iberian Peninsula Moisture Come From? An Answer Based on a Lagrangian Approach. Journal of Hydrometeorology 11, 421–436. doi:10.1175/2009JHM1182.1.

Girone, A., Capotondi, L., Ciaranfi, N., Di Leo, P., Lirer, F., Maiorano, P., Marino, M., Pelosi, N., Pulice, I., 2013. Paleoenvironmental changes at the lower Pleistocene Montalbano Jonico section (southern Italy): Global versus regional signals. Palaeogeography, Palaeoclimatology, Palaeoecology 371, 62–79. doi:10.1016/j.palaeo.2012.12.017.

Grützner, J., Higgins, S.M., 2010. Threshold behavior of millennial scale variability in deep water hydrography inferred from a 1.1 Ma long record of sediment provenance at the southern Gardar Drift. Paleoceanography 25, PA4204. doi:10.1029/2009PA001873.

Head, M.J., Gibbard, P.L., 2015. Early–Middle Pleistocene transitions: Linking terrestrial and marine realms. Quaternary International 389, 7–46. doi:10.1016/j.quaint.2015.09.042.

Helmke, J.P., Bauch, H.A., Erlenkeuser, H., 2003. Development of glacial and interglacial conditions in the Nordic seas between 1.5 and 0.35 Ma. Quaternary Science Reviews 22, 1717–1728. doi:10.1016/S0277-3791(03)00126-4.

Herbert, T.D., Peterson, L.C., Lawrence, K.T., Liu, Z., 2010. Tropical ocean temperatures over the past 3.5 million years. Science 328, 1530–4. doi:10.1126/science.1185435.

Hernández-Almeida, I., Sierro, F.J., Cacho, I., Flores, J.A., 2012. Impact of suborbital climate changes in the North Atlantic on ice sheet dynamics at the Mid-Pleistocene Transition. Paleoceanography 27, PA3214. doi:10.1029/2011PA002209.

Hernández-Almeida, I., Sierro, F.J., Flores, J.-A., Cacho, I., Filippelli, G.M., 2013. Palaeoceanographic changes in the North Atlantic during the Mid-Pleistocene Transition (MIS 31-19) as inferred from planktonic foraminiferal and calcium carbonate records. Boreas 42, 140–159. doi:10.1111/j.1502-3885.2012.00283.x.

Heusser, L., Balsam, W.L., 1977. Pollen distribution in the northeast Pacific Ocean. Quaternary Research 7, 45–62. doi:10.1016/0033-5894(77)90013-8.

Hillaire-Marcel, C., de Vernal, A., McKay, J., 2011. Foraminifer isotope study of the Pleistocene Labrador Sea, northwest North Atlantic (IODP Sites 1302/03 and 1305), with emphasis on paleoceanographical differences between its "inner" and "outer" basins. Marine Geology 279, 188–198. doi:10.1016/j.margeo.2010.11.001.

Hodell, D., Lourens, L., Crowhurst, S., Konijnendijk, T., Tjallingii, R., Jimenez-Espejo, F., Skinner, L., Tzedakis, P.C., 2015. A reference time scale for Site U1385 (Shackleton Site) on the SW Iberian Margin. Global and Planetary Change 1385, 49–64. doi:10.1016/j.gloplacha.2015.07.002.

Hodell, D.A., Channell, J.E.T., Curtis, J.H., Romero, O.E., Röhl, U., 2008. Onset of "Hudson Strait" Heinrich events in the eastern North Atlantic at the end of the middle Pleistocene transition (~640 ka)? Paleoceanography 23, 1–16. doi:10.1029/2008PA001591.

Hodell, D.A., Lourens, L., Stow, D. V, Hernández-Molina, J., Alvarez Zarikian, C., Shackleton Site Project Members, 2013. The "Shackleton Site" (IODP Site U1385) on the Iberian Margin. Proceedings of the Integrated Ocean Drilling Program 16, 13–19. doi:10.5194/sd-16-13-2013.

Hönisch, B., Hemming, N.G., Archer, D., Siddall, M., McManus, J.F., 2009. Atmospheric carbon dioxide concentration across the Mid-Pleistocene Transition. Science 324, 1551–4. doi:10.1126/science.1171477.

Hurrell, J.W., 1995. Decadal trends in the North Atlantic Oscillation: regional temperatures and precipitation. Science 269, 676–9. doi:10.1126/science.269.5224.676.

Joannin, S., Bassinot, F., Nebout, N.C., Peyron, O., Beaudouin, C., 2011. Vegetation response to obliquity and precession forcing during the Mid-Pleistocene Transition in Western Mediterranean region (ODP site 976). Quaternary Science Reviews 30, 280–297. doi:10.1016/j.quascirev.2010.11.009.

Joannin, S., Ciaranfi, N., Stefanelli, S., 2008. Vegetation changes during the late Early Pleistocene at Montalbano Jonico (Province of Matera, southern Italy) based on pollen analysis. Palaeogeography, Palaeoclimatology, Palaeoecology 270, 92–101. doi:10.1016/j.palaeo.2008.08.017.

Joannin, S., Quillévéré, F., Suc, J.-P., Lécuyer, C., Martineau, F., 2007. Early Pleistocene climate changes in the central Mediterranean region as inferred from integrated pollen and planktonic foraminiferal stable isotope analyses. Quaternary Research 67, 264–274. doi:10.1016/j.yqres.2006.11.001.

Juggins, S., 2009. Package "rioja" – Analysis of Quaternary Science Data. The Comprehensive R Archive Network.

Konijnendijk, T.Y.M., Ziegler, M., Lourens, L.J., 2014. Chronological constraints on Pleistocene sapropel depositions from high-resolution geochemical records of ODP Sites 967 and 968. Newsletters on Stratigraphy 47, 263–282. doi:10.1127/0078-0421/2014/0047.

Laskar, J., Robutel, P., Joutel, F., Gastineau, M., Correia, A.C.M., Levrard, B., 2004. A long-term numerical solution for the insolation quantities of the Earth. Astronomy & Astrophysics 428, 261–285. doi:10.1051/0004-6361:20041335.

Lawrence, K.T., Sosdian, S., White, H.E., Rosenthal, Y., 2010. North Atlantic climate evolution through the Plio-Pleistocene climate transitions. Earth and Planetary Science Letters 300, 329–342. doi:10.1016/j.epsl.2010.10.013.

Lionello, P., Malanotte-Rizzoli, P., Boscolo, R., Alpert, P., Artale, V., Li, L., Luterbacher, J., May, W., Trigo, R., Tsimplis, M., Ulbrich, U., Xoplaki, E., 2006. The Mediterranean climate: An overview of the main characteristics and issues. Developments in Earth and Environmental Sciences 4, 1–26. doi:10.1016/S1571-9197(06)80003-0.

Lisiecki, L.E., Raymo, M.E., 2005. A Pliocene–Pleistocene stack of 57 globally-distributed benthic $\delta^{18}O$ records. Paleoceanography 20, PA1003. http://dx.doi.org/10.1029/ 2004PA001071.

Loidi, J., Biurrun, I., Campos, J. A., Garcıa-Mijangos, I., Herrera, M., 2007. A survey of heath vegetation of the Iberian Peninsula and Northern Morocco: a biogeographical and bioclimatic approach. Phytocoenologia 37, 341-370.

Maasch, K.A., Saltzman, B., 1990. A low-order dynamical model of global climatic variability over the full Pleistocene. Journal of Geophysical Research 95, 1955. doi:10.1029/JD095iD02p01955.

Magri, D., 2012. Quaternary History of *Cedrus* in Southern Europe. Annali Di Botanica 57–66. doi:10.4462/annbotrm-10022.

Magri, D., Tzedakis, P.C., 2000. Orbital signatures and long-term vegetation patterns in the Mediterranean. Quaternary International 73-74, 69–78. doi:10.1016/S1040-6182(00)00065-3.

Maiorano, P., Capotondi, L., Ciaranfi, N., Girone, A., Lirer, F., Marino, M., Pelosi, N., Petrosino, P., Piscitelli, A., 2010. Vrica–Crotone and Montalbano Jonico sections: a potential unit-stratotype of the Calabrian Stage. Episodes 33, 218–233.

Maiorano, P., Marino, M., Balestra, B., Flores, J.-A., Hodell, D.A., Rodrigues, T., 2015. Coccolithophore variability from the Shackleton Site (IODP Site U1385) through MIS 16-10. Global and Planetary Change 133, 35–48. doi:10.1016/j.gloplacha.2015.07.009.

Maiorano, P., Marino, M., Flores, J.-A., 2009. The warm interglacial Marine Isotope Stage 31: Evidences from the calcareous nannofossil assemblages at Site 1090 (Southern Ocean). Marine Micropaleontology 71, 166–175. doi:10.1016/j.marmicro.2009.03.002.

Margari, V., Skinner, L. C., Tzedakis, P. C., Ganopolski, A., Vautravers, M., Shackleton, N. J., 2010. The nature of millennial-scale climate variability during the past two glacial periods. Nature Geoscience 3, 127-131.

Margari, V., Skinner, L.C., Hodell, D. A., Martrat, B., Toucanne, S., Grimalt, J.O., Gibbard, P.L., Lunkka, J.P., Tzedakis, P.C., 2014. Land-ocean changes on orbital and millennial time scales and the penultimate glaciation. Geology 42, 183–186. doi:10.1130/G35070.1.

Margari, V., Tzedakis, P.C., Shackleton, N.J., Vautravers, M., 2007. Vegetation response in SW Iberia to abrupt climate change during MIS 6: direct land-sea comparisons. Quaternary International 167–168 (Supplement 1), 267–268.

Marino, M., Maiorano, P., Tarantino, F., Voelker, A., Capotondi, L., Girone, A., Lirer, F., Flores, J.A., Naafs, B.D.A, 2014. Coccolithophores as proxy of seawater changes at orbital-to-millennial scale during middle Pleistocene Marine Isotope Stages 14-9 in North Atlantic core MD01-2446. Paleoceanography 29, 518–532. doi:10.1002/2013PA002574.

Martrat, B., Grimalt, J.O., Shackleton, N.J., de Abreu, L., Hutterli, M. A, Stocker, T.F., 2007. Four climate cycles of recurring deep and surface water destabilizations on the Iberian margin. Science 317, 502–507. doi:10.1126/science.1139994.

Maslin, M.A., Brierley, C.M., 2015. The role of orbital forcing in the Early Middle Pleistocene Transition. Quaternary International 389, 47–55. doi:10.1016/j.quaint.2015.01.047.

Maslin, M.A., Ridgwell, A.J., 2005. Mid-Pleistocene revolution and the "eccentricity myth." Geological Society, London, Special Publications 247, 19–34. doi:10.1144/GSL.SP.2005.247.01.02.

Mc Intyre, K., Delaney, M.L., Ravelo, A.C., 2001. Millennial-scale climate change and oceanic processes in the Late Pliocene and Early Pleistocene. Paleoceanography 16, 535–543. doi:10.1029/2000PA000526.

McClymont, E.L., Rosell-Melé, A., Haug, G.H., Lloyd, J.M., 2008. Expansion of subarctic water masses in the North Atlantic and Pacific oceans and implications for mid-Pleistocene ice sheet growth. Paleoceanography 23, PA4214. doi:10.1029/2008PA001622.

McIntyre, A., Molfino, B., 1996. Forcing of Atlantic Equatorial and Subpolar Millennial Cycles by Precession. Science 274, 1867–1870. doi:10.1126/science.274.5294.1867.

McKay, R., Naish, T., Powell, R., Barrett, P., Scherer, R., Talarico, F., Kyle, P., Monien, D., Kuhn, G., Jackolski, C., Williams, T., 2012. Pleistocene variability of Antarctic Ice Sheet extent in the Ross Embayment. Quaternary Science Reviews 34, 93–112. doi:10.1016/j.quascirev.2011.12.012.

McManus, J.F., Oppo, D.W., Cullen, J.L., 1999. A 0.5-Million-Year Record of Millennial-Scale Climate Variability in the North Atlantic. Science 283, 971–974.

Medina-Elizalde, M., Lea, D.W., 2005. The Mid-Pleistocene Transition in the tropical Pacific. Science 310, 1009–12. doi:10.1126/science.1115933.

Melles, M., Brigham-Grette, J., Minyuk, P.S., Nowaczyk, N.R.,Wennrich, V., DeConto, R.M., Anderson, P.M., Andreev, A.A., Coletti, A., Cook, T.L., Haltia-Hovi, E., Kukkonen, M., Lozhkin, A.V., Rosen, P., Tarasov, P., Vogel, H., Wagner, B., 2012. 2.8 million years of Arctic climate change from Lake El'gygytgyn, NE Russia. Science 337, 315–320. doi:10.1126/science.1222135.

Moore, P.D., Webb, J.A., Collinson, M.E., 1991. Pollen analysis. Oxford, Blackwell scientific publication, 2nd edition, 216 p.

Mudelsee, M., Schulz, M., 1997. The Mid-Pleistocene climate transition: onset of 100 ka cycle lags ice volume build-up by 280 ka. Earth and Planetary Science Letters 151, 117–123. doi:10.1016/S0012-821X(97)00114-3.

Mudelsee, M., Stattegger, K., 1997. Exploring the structure of the mid-Pleistocene revolution with advanced methods of time-series analysis. Geologische Rundschau 86, 499–511. doi:10.1007/s005310050157.

Müller, P.J., Kirst, G., Ruhland, G., Von Storch, I., Rosell-Melé, A., 1998. Calibration of the alkenone paleotemperature index $U^{k'}_{37}$- based on core-tops from the eastern South Atlantic and the global ocean (60°N-60°S). Geochimica et Cosmochimica Acta 62, 1757–1772.

Naafs, B.D.A., Hefter, J., Stein, R., 2013. Millennial-scale ice rafting events and Hudson Strait Heinrich (-like) Events during the late Pliocene and Pleistocene: a review. Quaternary Science Reviews 80, 1–28. doi:10.1016/j.quascirev.2013.08.014.

Naish, T., Powell, R., Levy, R., Wilson, G., Scherer, R., Talarico, F., Krissek, L., Niessen, F., Pompilio, M., Wilson, T., Carter, L., DeConto, R., Huybers, P., McKay, R., Pollard, D., Ross, J., Winter, D., Barrett, P., Browne, G., Cody, R., Cowan, E., Crampton, J., Dunbar, G., Dunbar, N., Florindo, F., Gebhardt, C., Graham, I., Hannah, M., Hansaraj, D., Harwood, D., Helling, D., Henrys, S., Hinnov, L., Kuhn, G., Kyle, P., Läufer, A., Maffioli, P., Magens, D., Mandernack, K., McIntosh, W., Millan, C., Morin, R., Ohneiser, C., Paulsen, T., Persico, D., Raine, I., Reed, J., Riesselman, C., Sagnotti, L., Schmitt, D., Sjunneskog, C., Strong, P., Taviani, M., Vogel, S., Wilch, T., Williams, T., 2009. Obliquity-paced Pliocene West Antarctic ice sheet oscillations. Nature 458, 322–8. doi:10.1038/nature07867.

Naughton, F., Sánchez Goñi, M.F., Desprat, S., Turon, J.L., Duprat, J., Malaizé, B., Joli, C., Cortijo, E., Drago, T., Freitas, M.C., 2007. Present-day and past (last 25 000 years) marine pollen signal off western Iberia. Marine Micropaleontology 62, 91–114. doi:10.1016/j.marmicro.2006.07.006.

Naughton, F., Sánchez Goñi, M.F., Kageyama, M., Bard, E., Cortijo, E., Desprat, S., Duprat, J., Malaizé, B., Joli, C., Rostek, F., Turon, J.-L., 2009. Wet to dry climatic trend in north western Iberia within Heinrich events. Earth and Planetary Science Letters 284, 329–342.

Naughton, F., Sanchez Goñi, M.F., Rodrigues, T., Salgueiro, E., Costas, S., Desprat, S., Duprat, J., Michel, E., Rossignol, L., Zaragosi, S., Voelker, A.H.L., Abrantes, F., 2016. Climate variability across the last deglaciation in NW Iberia and its margin. Quaternary International 414, 9–22. doi:10.1016/j.quaint.2015.08.073.

Oliveira, D., Desprat, S., Rodrigues, T., Naughton, F., Hodell, D., Trigo, R., Rufino, M., Lopes, C., Abrantes, F., Sánchez Goñi, M.F., 2016. The complexity of millennial-scale variability in southwestern Europe during MIS 11. Quaternary Research 86, 373-387. doi:10.1016/j.yqres.2016.09.002.

Paillard, D., Labeyrie, L., Yiou, P., 1996. Macintosh Program performs time-series analysis. Eos, Transactions American Geophysical Union 77, 379–379. doi:10.1029/96EO00259.

Palumbo, E., Flores, J.-A., Perugia, C., Petrillo, Z., Voelker, A.H.L., Amore, F.O., 2013. Millennial scale coccolithophore paleoproductivity and surface water changes between 445 and 360 ka (Marine Isotope Stages 12/11) in the Northeast Atlantic. Palaeogeography, Palaeoclimatology, Palaeoecology 383-384, 27–41. doi:http://dx.doi.org/10.1016/j.palaeo.2013.04.024.

Peinado Lorca, M., Martinez-Parras, J.M., 1987. Castilla-La Mancha. In: Peinado Lorca, M. and Rivas-Martinez, S. (eds) La vegetación de España. Alcala de Henares: Universidad de Alcala de Henares, pp. 163–196.

Peliz, Á., Dubert, J., Santos, A. M.P., Oliveira, P.B., Le Cann, B., 2005. Winter upper ocean circulation in the Western Iberian Basin - Fronts, Eddies and Poleward Flows: An overview. Deep-Sea Research Part I 52(4), 621–646. doi:10.1016/j.dsr.2004.11.005.

Pérez, F.F., Castro, C., Álvarez-Salgado, X.A., Ríos, A., F., 2001. Coupling between the Iberian basin-scale circulation and the Portugal boundary current system: a chemical study. Deep-Sea Research Part I 48, 1519–1533.

Pollard, D., DeConto, R.M., 2009. Modelling West Antarctic ice sheet growth and collapse through the past five million years. Nature 458, 329–32. doi:10.1038/nature07809.

Polunin, O., Walters, M., 1985. A Guide to the Vegetation of Britain and Europe. Oxford University Press, New York 238pp.

Prada, C., 1986._Isoetes_ L. In: Castroviejo, S., Laìnz, M., Lòpez Gonzàlez, G., Montserrat, P., Muñoz Garmendia, F., Paiva, J., Villar, L. (Eds.), Flora Iberica: Plantas Vasculares de la Penìnsula Ibérica e Islas Baleares, vol. 1, Real Jardìn Botànico, CSIC, Madrid, pp. 15-20.

Prahl, F.G., Wakeham, S.G., 1987. Calibration of unsaturation patterns in long-chain ketone compositions for palaeotemperature assessment. Nature 330, 367–369. doi:10.1038/330367a0.

Prentice, C., Guiot, J., Huntley, B., Jolly, D., Cheddadi, R., 1996. Reconstructing biomes from palaeoecological data: a general method and its application to European pollen data at 0 and 6 ka. Climate Dynamics 12, 185–194. doi:10.1007/BF00211617.

Quezel, P., 1989. Les grandes structures de végétation en région méditerranéenne: Facteurs déterminants dans leur mise en place post-glaciaire. Geobios, 32, 19-32.

R Core Team, 2014. R: A language and environment for statistical computing. R Foundation for Statistical Computing, Vienna, Austria. URL http://www.R-project.org/.

Raymo, M.E., Ganley, K., Carter, S., Oppo, D.W., McManus, J., 1998. Millennial-scale climate instability during the early Pleistocene epoch 392, 699–702. doi:10.1038/33658.

Raymo, M.E., Lisiecki, L.E., Nisancioglu, K.H., 2006. Plio-Pleistocene ice volume, Antarctic climate, and the global $\delta^{18}O$ record. Science 313, 492–5. doi:10.1126/science.1123296.

Reille, M., 1992. Pollen et spores d'Europe et d'Afrique du Nord. Marseille, Laboratoire de botanique historique et palynologie, 520 p.

Rios, A.F., Perez, F.F., Fraga, F., 1992. Water Masses in the Upper and Middle North-Atlantic Ocean East of the Azores. Deep-Sea Research Part A-Oceanographic Research Papers 39, 645-658.

Rodrigues, T., Alonso-Garcia, M., Hodell, D.A., Rufino, M., Naughton, F., Grimalt, J.O., Voelker, A. H. L., Abrantes, F., 2016. A 1 Ma record of Sea Surface Temperature and extreme cooling events in the North Atlantic: a perspective from the Iberian Margin "Shackleton site". Submitted to Quaternary Science Reviews, Manuscript number JQSR_2016_117.

Rodrigues, T., Voelker, A.H.L., Grimalt, J.O., Abrantes, F., Naughton, F., 2011. Iberian Margin sea surface temperature during MIS 15 to 9 (580–300 ka): Glacial suborbital variability versus interglacial stability. Paleoceanography 26, PA1204. doi:10.1029/2010PA001927.

Roucoux, K.H., Tzedakis, P.C., de Abreu, L., Shackleton, N.J., 2006. Climate and vegetation changes 180,000 to 345,000 years ago recorded in a deep-sea core off Portugal. Earth and Planetary Science Letters 249, 307–325. doi:10.1016/j.epsl.2006.07.005.

Ruddiman, W.F., McIntyre, A., 1984. Ice-age thermal response and climatic role of the surface Atlantic Ocean, 40°N to 63°N. Geol. Soc. Am. Bull.95, 381–396.

Ruddiman, W.F., Raymo, M.E., Martinson, D.G., Clement, B.M., Backman, J., 1989. Pleistocene evolution: Northern hemisphere ice sheets and North Atlantic Ocean. Paleoceanography 4, 353–412. doi:10.1029/PA004i004p00353.

Russon, T., Elliot, M., Sadekov, A., Cabioch, G., Corrège, T., De Deckker, P., 2011. The mid-Pleistocene transition in the subtropical southwest Pacific. Paleoceanography 26, PA1211. doi:10.1029/2010PA002019.

Salvo Tierra, E., 1990. Guía de helechos de la Península Ibérica y Baleares. Pirámide, Madrid.

Sánchez Goñi, M.F., Eynaud, F., Turon, J.L., Shackleton, N.J., 1999. High resolution palynological record off the Iberian margin: Direct land-sea correlation for the Last Interglacial complex. Earth and Planetary Science Letters 171, 123–137.

Sánchez Goñi, M.F., Landais, A., Fletcher, W.J., Naughton, F., Desprat, S., Duprat, J., 2008. Contrasting impacts of Dansgaard-Oeschger events over a western European latitudinal transect modulated by orbital parameters. Quaternary Science Reviews 27, 1136–1151. doi:10.1016/j.quascirev.2008.03.003.

Sánchez Goñi, M.F., Rodrigues, T., Hodell, D.A., Polanco-Martínez, J.M., Alonso-García, M., Hernández-Almeida, I., Desprat, S., Ferretti, P., 2016. Tropically-driven climate shifts in southwestern Europe during MIS 19, a low eccentricity interglacial. Earth and Planetary Science Letters 448, 81–93. doi:10.1016/j.epsl.2016.05.018.

Sánchez Goñi, M.F., Turon, J.L., Eynaud, F., Gendreau, S., 2000. European climatic response to millennial-scale changes in the atmosphere-ocean system during the last glacial period. Quaternary Research 54, 394–403. doi:10.1006/qres.2000.2176.

Scherer, R.P., Bohaty, S.M., Dunbar, R.B., Esper, O., Flores, J.-A., Gersonde, R., Harwood, D.M., Roberts, A.P., Taviani, M., 2008. Antarctic records of precession-paced insolation-driven warming during early Pleistocene Marine Isotope Stage 31. Geophysical Research Letters 35, L03505. doi:10.1029/2007GL032254.

Schulz, M., Mudelsee, M., 2002. REDFIT: estimating red-noise spectra directly from unevenly spaced paleoclimatic time series. Computers & Geosciences 28, 421–426. doi:10.1016/S0098-3004(01)00044-9.

Shackleton, N.J., 1987. Oxygen isotopes, ice volume and sea level. Quaternary Science Reviews 6, 183–190. doi:10.1016/0277-3791(87)90003-5.

Shackleton, N.J., Hall, M.A., Vincent, E., 2000. Phase relationships between millennial-scale events 64,000-24,000 years ago. Paleoceanography 15, 565–569. doi:10.1029/2000PA000513.

Short, D.A., Mengel, J.G., Crowley, T.J., Hyde, W.T., North, G.R., 1991. Filtering of Milankovitch cycles by Earth's geography. Quaternary Research 35, 157–173. doi:10.1016/0033-5894(91)90064-C.

Skinner, L.C., Elderfield, H., 2007. Rapid fluctuations in the deep North Atlantic heat budget during the last glacial period. Paleoceanography 22, 1–9. doi:10.1029/2006PA001338.

Skinner, L.C., Shackleton, N.J., 2005. An Atlantic lead over Pacific deep-water change across Termination I: implications for the application of the marine isotope stage stratigraphy. Quaternary Science Reviews 24, 571–580. doi:10.1016/j.quascirev.2004.11.008.

Skinner, L.C., Waelbroeck, C., Scrivner, A.E., Fallon, S.J., 2014. Radiocarbon evidence for alternating northern and southern sources of ventilation of the deep Atlantic carbon pool during the last deglaciation. Proceedings of the National Academy of Sciences of the United States of America 111, 5480–4. doi:10.1073/pnas.1400668111.

Sousa, P., Barriopedro, D., Trigo, R.M., Ramos, A.M., Nieto, R., Gimeno, L., Turkman, K.F., Liberato, M.L.R., 2016. Impact of Euro-Atlantic blocking patterns in Iberia precipitation using a novel high resolution dataset. Climate Dynamics, 46: 2573. http://dx.doi.org/10.1007/s00382-015-2718-7.

Tallantire, P.A., 2002. The early-Holocene spread of hazel (*Corylus avellana* L.) in Europe north and west of the Alps: an ecological hypothesis. The Holocene 12, 81–96. doi:10.1191/0959683602hl523rr.

Tarasov, P.E., Andreev, A.A., Anderson, P.M., Lozhkin, A. V., Leipe, C., Haltia, E., Nowaczyk, N.R., Wennrich, V., Brigham-Grette, J., Melles, M., 2013. A pollen-based biome reconstruction over the last 3.562 million years in the Far East Russian Arctic – new insights into climate–vegetation relationships at the regional scale. Climate of the Past 9, 2759–2775. doi:10.5194/cp-9-2759-2013.

Teitler, L., Florindo, F., Warnke, D.A., Filippelli, G.M., Kupp, G., Taylor, B., 2015. Antarctic Ice Sheet response to a long warm interval across Marine Isotope Stage 31: A cross-latitudinal study of iceberg-rafted debris. Earth and Planetary Science Letters 409, 109–119. doi:10.1016/j.epsl.2014.10.037.

Toucanne, S., Zaragosi, S., Bourillet, J.F., Cremer, M., Eynaud, F., Van Vliet-Lanoë, B., Penaud, A., Fontanier, C., Turon, J.L., Cortijo, E., Gibbard, P.L., 2009. Timing of massive "Fleuve Manche" discharges over the last 350 kyr: insights into the European ice-sheet oscillations and the European drainage network from MIS 10 to 2. Quaternary Science Reviews 28, 1238–1256. doi:10.1016/j.quascirev.2009.01.006.

Trigo, R.M., Pozo- Vázquez, D., Osborn, T.J., Castro-Díez, Y., Gamiz-Fortis, S., Esteban-Parra, M.J., 2004. North Atlantic Oscillation influence on precipitation, river flow and water resources in the Iberian Peninsula. International Journal of Climatology 24, 925–944. doi:10.1002/joc.1048.

Tripati, A.K., Roberts, C.D., Eagle, R.A., Li, G., 2011. A 20 million year record of planktic foraminiferal B/Ca ratios: Systematics and uncertainties in pCO_2 reconstructions. Geochimica et Cosmochimica Acta 75, 2582–2610. doi:10.1016/j.gca.2011.01.018.

Tzedakis, P. C., Roucoux, K. H., de Abreu, L., Shackleton, N. J., 2004. The Duration of Forest Stages in Southern Europe and Interglacial Climate Variability. Science 306, 2231–2235. doi:10.1126/science.1102398.

Tzedakis, P.C., Hooghiemstra, H., Pälike, H., 2006. The last 1.35 million years at Tenaghi Philippon: revised chronostratigraphy and long-term vegetation trends. Quaternary Science Reviews 25, 3416–3430. doi:10.1016/j.quascirev.2006.09.002.

Tzedakis, P.C., Margari, V., Hodell, D.A., 2015. Coupled ocean–land millennial-scale changes 1.26 million years ago, recorded at Site U1385 off Portugal. Global and Planetary Change 135, 83–88. doi:10.1016/j.gloplacha.2015.10.008.

Tzedakis, P.C., Pälike, H., Roucoux, K.H., de Abreu, L., 2009. Atmospheric methane, southern European vegetation and low-mid latitude links on orbital and millennial timescales. Earth and Planetary Science Letters 277, 307–317. doi:10.1016/j.epsl.2008.10.027.

Tzedakis, P.C., Wolff, E.W., Skinner, L.C., Brovkin, V., Hodell, D.A., McManus, J.F., Raynaud, D., 2012. Can we predict the duration of an interglacial? Climate of the Past 8, 1473–1485. doi:10.5194/cp-8-1473-2012.

Villa, G., Persico, D., Wise, S.W., Gadaleta, A., 2012. Calcareous nannofossil evidence for Marine Isotope Stage 31 (1 Ma) in Core AND-1B, ANDRILL McMurdo Ice Shelf Project (Antarctica). Global and Planetary Change 96-97, 75–86. doi:10.1016/j.gloplacha.2009.12.003.

Villanueva, J., Pelejero, C., Grimalt, J.O., 1997. Clean-up procedures for the unbiased estimation of C_{37} alkenone sea surface temperatures and terrigenous n-alkane inputs in paleoceanography. Journal of Chromatography A 757, 145–151.

Voelker, A.H.L., Rodrigues, T., Billups, K., Oppo, D., McManus, J., Stein, R., Hefter, J., Grimalt, J.O., 2010. Variations in mid-latitude North Atlantic surface water properties during the mid-Brunhes (MIS 9–14) and their implications for the thermohaline circulation. Climate of the Past 6, 531–552. doi:10.5194/cp-6-531-2010.

Voelker, A.H.L., Salgueiro, E., Rodrigues, T., Jimenez-Espejo, F.J., Bahr, A., Alberto, A., Loureiro, I., Padilha, M., Rebotim, A., Röhl, U., 2015. Mediterranean Outflow and surface water variability off southern Portugal during the early Pleistocene: A snapshot at Marine Isotope Stages 29 to 34 (1020–1135 ka). Global and Planetary Change 133, 223–237. doi:10.1016/j.gloplacha.2015.08.015.

Wara, M.W., Ravelo, A.C., Revenaugh, J.S., 2000. The pacemaker always rings twice. Paleoceanography 15, 616–624. doi:10.1029/2000PA000500.

Weirauch, D., Billups, K., Martin, P., 2008. Evolution of millennial-scale climate variability during the mid-Pleistocene. Paleoceanography 23, PA3216. doi:10.1029/2007PA001584.

Chapter 4

Unraveling the forcings controlling the magnitude and climate variability of the best orbital analogues for the present interglacial in SW Europe

Unraveling the forcings controlling the magnitude and climate variability of the best orbital analogues for the present interglacial in SW Europe

Dulce Oliveira (1) (2) (3) (4); Stéphanie Desprat (1) (2); Qiuzhen Yin (5); Filipa Naughton (3) (4); Ricardo Trigo (6); Teresa Rodrigues (3) (4); Fátima Abrantes (3) (4); Maria Fernanda Sánchez Goñi (1) (2)

(1) EPHE, PSL Research University, F-33615 Pessac, France

(2) Univ. Bordeaux, EPOC, UMR 5805, F-33615 Pessac, France

(3) Divisão de Geologia e Georecursos Marinhos, Instituto Português do Mar e da Atmosfera (IPMA), Avenida de Brasília 6, 1449-006 Lisboa, Portugal

(4) CCMAR, Centro de Ciências do Mar, Universidade do Algarve, Campus de Gambelas, 8005-139 Faro, Portugal

(5) Georges Lemaître Center for Earth and Climate Research, Earth and Life Institute, Université catholique de Louvain, Louvain-la-Neuve, Belgium

(6) Instituto Dom Luiz, Universidade de Lisboa, 1749-016 Lisboa, Portugal

Under review in CLIMATE DYNAMICS

Abstract

The suitability of MIS 11c and MIS 19c as analogues of our present interglacial and its natural evolution is still debated. Here we examine the regional expression of the Holocene and its orbital analogues over SW Iberia using a model–data comparison approach. Regional climate based on snapshot and transient experiments using the LOVECLIM model is evaluated against the atmospheric and oceanic climatic records from IODP Site U1385. The pollen-based reconstructions show a larger forest optimum during the Holocene compared to MIS 11c and MIS 19c, putting into question their analogy in SW Europe. Snapshot experiments indicate reduced MIS 11c forest cover compared to the Holocene, primarily driven by lower winter precipitation which is critical for Mediterranean forest development. Decreased precipitation was possibly induced by the amplified MIS 11c latitudinal insolation and temperature gradient. In contrast, the reconstructed lower forest optimum at MIS 19c is not reproduced by the simulations probably due to the lack of Eurasian ice sheets and its related feedbacks in the model.

Transient experiments with time-varying insolation and CO_2 reveal that the SW Iberian forest dynamics over the interglacials are closely coupled to changes in summer temperature and winter precipitation mainly controlled by precession, CO_2 playing a negligible role. Model simulations reproduce the observed persistent suborbital atmospherically-driven vegetation changes in SW Iberia and the dramatic forest reductions marking the end of the interglacial "optimum". This observation highlights the potential role of the interactions between long-term and millennial-scale climate dynamics in amplifying the climate and vegetation response.

Keywords: Orbital Holocene analogues; Model–data comparison; Mediterranean vegetation; Marine pollen analysis; Insolation; CO_2.

1 Introduction

Past warm intervals are critical experiments for testing how the natural climate system responds to different forcing factors under reduced ice sheets. Two Quaternary interglacials, the Marine Isotope Stage (MIS) 11 (425-374 ka; MIS 11c, 425–395 ka) and MIS 19 (790-761 ka; MIS 19c, 790–774 ka), have received particular attention from the scientific community owing to their relatively similar orbital characteristics with the Holocene (e.g. Berger and Loutre 2002, 2003; Candy et al. 2014; Tzedakis et al. 2012). Such analogy is based on similar low eccentricity and weak precession variations, albeit when the summer half-year insolation is considered, both interglacials appear less analogous to MIS 1 (Tzedakis et al. 2017). MIS 11c has long been considered the most appropriate astronomical analogue for the Holocene and its climatic progression since it displays a similar seasonal and latitudinal distribution of insolation, which is largely responsible for the climatic structure and duration of interglacials (e.g. Droxler and Farrell 2000; Berger and Loutre 2002, 2003; Loutre and Berger 2003; Candy et al. 2014). Based on this similarity, the current interglacial was predicted to be exceptionally long, lasting for more 50,000 years (Berger and Loutre 2002). However, MIS 11c orbital analogy with the Holocene and its future remains complex and controversial mainly due to the uncertainties in the precise alignment of the two interglacials (e.g. EPICA 2004; Ruddiman 2005; Masson-Delmotte et al. 2006; Tzedakis 2010) and the seemingly contradictory evidence in both the climatic structure and greenhouse gas (GHG) concentrations (e.g. Bauch et al. 2000; McManus et al. 2003; de Abreu et al. 2005; Ruddiman 2007; Helmke et al. 2008; Dickson et al. 2009; Pol et al. 2011; Kandiano et al. 2012; Melles et al. 2012; Candy et al. 2014; Ganopolski et al. 2016). Regardless of MIS 11c suitability as an orbital analogue of the Holocene, this interglacial presents additional key features, including its higher than present sea-level probably associated to the collapse of Greenland and West Antarctica ice sheets (e.g. de Vernal and Hillaire-Marcel 2008; Raymo and Mitrovica 2012; Roberts et al. 2012; Reyes et al. 2014; Dutton et al. 2015) and its GHG-driven climate warming (Raynaud et al. 2005; Yin and Berger 2012). MIS 19c phasing between precession and obliquity is more similar to MIS 1 than MIS 11c, a reason why it has been suggested as an even better analogue for the Holocene in terms of orbital configuration, insolation distribution pattern and palaeoclimatic signatures (Tzedakis et al. 2009a, 2012; Pol et al. 2010; Rohling et al. 2010; Tzedakis 2010; Yin and Berger 2012, 2015; Giaccio et al. 2015). Considering MIS 19c as an analogue and assuming that ice growth mainly responds to

insolation and CO_2 forcing, with [CO_2] maxima of 240 ppmv, Tzedakis et al. (2012) propose 1500 additional years to the current interglacial, However, recent work also challenges this analogy based on the different millennial-scale climatic cyclicity observed throughout the two interglacials that appears to interact with the long-term variability in triggering glacial inception (Sanchez Goñi et al. 2016).

Yin and Berger (2012, 2015) have evaluated, using the LOVECLIM model, the individual contributions of the primary forcings (insolation and GHG) to the variability of distinct climate-related parameters (temperature, tree fraction, sea ice) of the interglacials. Their analysis focused at the interglacial climate "optimum" but also over the entire periods of each interglacial. Those authors found that MIS 11c and MIS 19c can be considered as the best analogues, particularly MIS 19c, for the present interglacial from an astronomical point of view and as far as annual and seasonal temperatures under the combined effect of the primary forcings are concerned (Yin and Berger 2012, 2015). The major difference of MIS 11c would be related to its higher GHG-driven warming that results in a warmer interglacial than MIS 1 and MIS 19c (Yin and Berger 2012, 2015). As highlighted by Yin and Berger (2015), looking for analogues implies the intercomparison of the interglacials not only at the global scale but also at the regional scale. The regional expression of these past interglacials remains, however, poorly documented due to the scarcity of proxy data and model experiments. This study aims at filling this gap for the western Mediterranean region by comparing new and published terrestrial and marine climate profiles of MIS 1 (this work) to MIS 11c (Oliveira et al. 2016) and MIS 19c (Sánchez Goñi et al. 2016) from Site U1385. This site covers the last 1.45 Ma, and is located on the SW Iberian margin, a region particularly sensitive to climate change and the effect of precession (Ruddiman and McIntyre 1984). Based on proxy records and model simulations, here we compare the regional expression, i.e. intensity and climatic variability, of the three interglacials MIS 1, MIS 11c and MIS 19c marked by low eccentricity to identify the relative importance of insolation and CO_2 on the magnitude and evolution of the Mediterranean tree fraction and climate.

2 Modern setting

IODP Site U1385 (37°34.285′N, 10°7.562′W; 2578 m water depth) was recovered on the SW Iberian margin (Fig. 1), located on the eastern edge of the North Atlantic subtropical gyre (Expedition 339 Scientists 2013; Hodell et al. 2013). The modern surface hydrography off western Iberia is mainly influenced by the Portugal Current and the Azores Current, depending on the meridional displacements of the subtropical Azores High and the large-scale wind regimes (Fiúza 1984; Peliz et al. 2005). During the summer, the climate of southern Iberia is directly affected by the northeastward expansion of the Azores High, while the dynamics of the North Atlantic westerlies dominate in wintertime (Trigo et al. 2004; Lionello et al. 2006). These complex atmospheric interactions result in the high-seasonality of the Mediterranean climate (warm/dry summers and cool/wet winters), which promotes the development of a Mediterranean vegetation in SW Iberia (Blanco Castro et al. 1997). As shown by Naughton et al. (2007), the pollen signature from the SW Iberian deep-sea sediments reflects the regional vegetation of the adjacent landmasses, in particular the vegetation colonizing the hydrographic basins of the Tagus and Sado rivers. Because the vegetation distribution of these basins is closely related to precipitation and thermal gradients, conifers (*Pinus* woodland with *Juniperus)* generally dominate the highest elevations and deciduous oak the mid-altitude areas (Peinado Lorca and Martínez-Parras 1987; Blanco Castro et al. 1997). Evergreen oak and Mediterranean sclerophylls (*Olea sylvestris*, *Pistacia lentiscus*, *Phillyrea*) occupy the warmest zones at lower elevations (Blanco Castro et al. 1997). Heathlands (Ericaceae) are naturally confined to zones with relatively high humidity (Pann>600) and rockrose shrublands (Cistaceae) expand in drier environments (Peinado Lorca and Martínez-Parras 1987; Loidi et al. 2007).

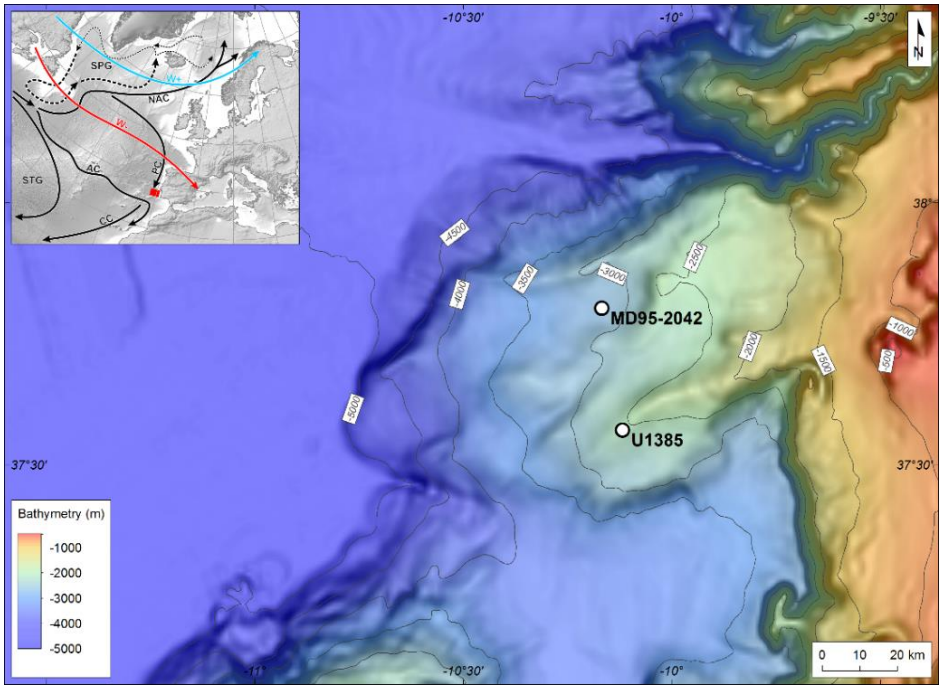

Fig. 1 Map of the SW Iberian margin showing the detailed bathymetry and location of Site U1385 and the core MD95-2042. Left inset: General geographical map showing the Iberian Peninsula. The zonal (red arrow) and meridional (blue arrow) trajectory the atmospheric westerlies is shown. Black arrows represent the surface water circulation (SPG: subpolar gyre, NAC: North Atlantic Current, AC: Azores Current, STG: Subtropical Gyre, CC: Canary Current, PC: Portugal Current).

3 Material and methods

3.1 Chronology

MIS 1 chronology was established from five AMS radiocarbon dates converted to calendar year before present (cal yr BP) using the Marine13 curve (Reimer et al. 2013) with Calib 7.1 (Stuiver and Reimer 1993; http://calib.qub.ac.uk/calib/) (Fig. 2, Table S1). The lower part of the age-depth model was constrained by one additional control point from the age model "Age_Depth_Radiocarbon" of Hodell et al. (2015) that is based on correlating the Ca/Ti record of Site U1385 to the $CaCO_3$ record of the nearby MD99-2334 core, which has a robust radiocarbon chronology (Fig. 2). The age-depth model was obtained using linear interpolation between each of the six control points (Fig. 2). The studied core section encompasses the last 17.5 ka and the average temporal resolution for the pollen and SST record is ~465 yr (Fig. 3). MIS 11c and MIS 19c palaeoclimate records are presented on their original LR04-derived chronology (Hodell et al. 2015; Oliveira et al. 2016; Sánchez Goñi et al. 2016) with an average temporal resolution of ~475 yr (Fig. 4).

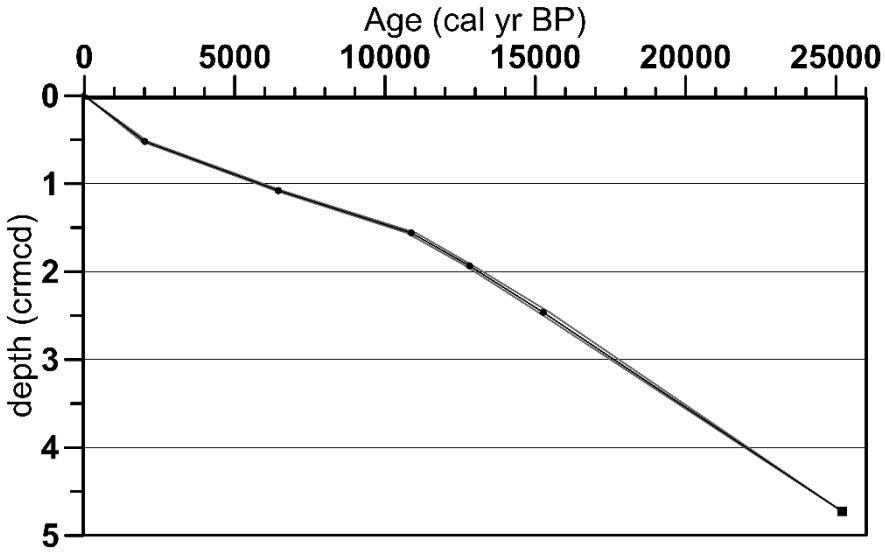

Fig. 2 Age–depth model based on five calibrated AMS radiocarbon ages (black circles, Table S1) and one control point from the radiocarbon age model of Site U1385 (black square, Hodell et al. 2015). Grey lines indicate the 2σ uncertainty envelope.

3.2 Pollen and alkenones analyses

Five holes (A–E) were drilled at Site U1385 using an advanced piston corer system during the IODP Expedition 339 (Mediterranean Outflow) (Fig. 1) (Hodell et al. 2013). Correlation among holes was performed based on X-ray fluorescence core scanning at 1-cm resolution, which allowed the construction of a continuous spliced stratigraphic section spanning the last 1.45 Ma (Hodell et al. 2015).

Thirty-eight levels were sampled from Holes E and D every 5 to 10 cm between 0.05 and 2.92 corrected revised meter composite depth (crmcd). The new pollen and biomarkers analyses followed the methodology described by Oliveira et al. (2016) and Sánchez Goñi et al. (2016) for the study of MIS 11c and MIS 19c. Pollen samples were processed using the standard protocol for marine samples including coarse-sieving (150 μm mesh), treatment with cold HCl and cold HF, micro-sieving (10 μm mesh) and slide preparation in glycerol (http://ephe-paleoclimat.com/ephe/Pollen%20sample%20preparation.htm). A minimum of 20 pollen morphotypes and 100 pollen grains excluding *Pinus*, *Cedrus*, aquatics and Pteridophyta spores were counted in each sample. Pollen percentages are based on the main sum, which includes all pollen except *Pinus*, *Cedrus*, aquatics and Pteridophyta spores. The

Mediterranean forest (MF) pollen percentage record comprises the Mediterranean taxa and all temperate tree and shrub taxa excluding *Pinus*, *Cedrus* and Cupressaceae. Alkenone-based sea surface temperature ($U^{k'}_{37}$-SST) reconstruction was based on the proportion of long chain di- and tri- unsaturated C_{37} alkenones. Alkenones sediment extraction procedure followed Villanueva et al. (1997). $U^{k'}_{37}$-SST was estimated using the $U^{k'}_{37}$ index (Prahl and Wakeham 1987) and the global core-top calibration of annual SST (Müller et al. 1998).

3.3 Model and experimental setup

The climate model experiments were performed with the LOVECLIM three-dimensional Earth system model of intermediate complexity (Goosse et al. 2010). In these simulations, the atmospheric component (ECBilt), sea-ice-ocean model (CLIO) and terrestrial biosphere (VECODE) were interactively coupled while the carbon cycle and the ice sheets were fixed to their present-day values (Yin and Berger 2012, 2015). VECODE is a model of reduced complexity in which the vegetation dynamics, defined as a fractional distribution of desert, tree and grassland, are simulated as a function of the climatic conditions, in particular the growing degree-days above 0 °C (GDD0) and the annual mean precipitation (Brovkin et al. 1997). An extensive description of the model and experiment design used in this study is provided in Yin and Berger (2012, 2015).

The climate "optimum" of each interglacial was simulated with two sets of snapshot experiments using the astronomical parameters (1) at times when Northern Hemisphere summer occurs at perihelion (NHSP) (12 ka, 409 ka and 788 ka) (Yin and Berger 2015) (Figs. 5 and 6a, b) and (2) at the interglacial benthic $\delta^{18}O$ peaks of the LR04 stack from Lisiecki and Raymo (2005) (6 ka, 405 ka and 780 ka) defined by Yin and Berger (2012, 2015). The peak interglacial greenhouse gas (GHG) concentrations were used in the simulations and ice sheets were prescribed to their present-day configuration. Alpert–Stein factor separation method (Stein and Alpert 1993) was performed to evaluate the individual contributions of insolation and GHG as well as their combined and synergistic effects on the tree fraction (%) over the southern Iberian region (35N°-41°N, 0-8°W) (Fig. 7). The seasonal and latitudinal distribution of insolation at the climate "optimum" of MIS 1 was compared to one of MIS 11c (Fig. 8). Comparison between proxy data and model results of transient experiments covering at least one precessional cycle (Yin and Berger 2015) was also carried out to investigate the

regional vegetation and climate dynamics under the varying astronomical configurations and CO_2 concentrations of MIS 1 (last 15 ka), MIS 11c (425-394 ka) and MIS 19c (793-773 ka) (Fig. 9a, b). In these simulations, the ice sheets were prescribed to their Pre-Industrial (PI) levels.

4 Results and discussion

4.1 Direct land-sea comparison for MIS 1

The new direct land-sea comparison from Site U1385 identifies the last 17.5 ka climatic periods, well-documented in the SW Iberian terrestrial and marine environments (e.g. Bard et al. 2000; Rodrigues et al. 2009; Naughton et al. 2016; Chabaud et al. 2014; Salgueiro et al. 2014): (1) the cold/dry Oldest Dryas (OD)/Heinrich Stadial 1; (2) the temperate/humid Bølling-Allerød (B-A); (3) the cool/relatively dry Younger Dryas (YD); and (4) the warm/humid Holocene marked by a major expansion of the MF between ~ 11.6 and 8.5 ka, followed by a progressive contraction toward the late Holocene (Fig. 3, for pollen percentage diagram and summary description see Fig. S1 and Table S2). The comparison of the pollen records from Site U1385 and the nearby core MD95-2042 (Chabaud et al. 2014) during the overlapping time interval, i.e. the last 14.2 ka, shows clear evidence for the replicability of the pollen analysis in the SW Iberian margin sediments (Fig. 3). Although the two pollen diagrams diverge in the values of some taxa such as *Pinus* and Ericaceae, they bear strong similarities in terms of vegetation dynamics within the chronological uncertainties and in particular, they present similar Holocene maximal values of Mediterranean taxa and forest (Fig. 3, Table S3). Since the results of the marine proxy analyses are also in good agreement (Fig. 3) and the chronology from core MD95-2042 is more accurate (twice as many radiocarbon dates than Site U1385), hereafter we also use the higher time-resolution MD95-2042 dataset for MIS 1 (150 yr average for pollen and 340 yr for SST) (Figs. 3, 4 and 9a, b).

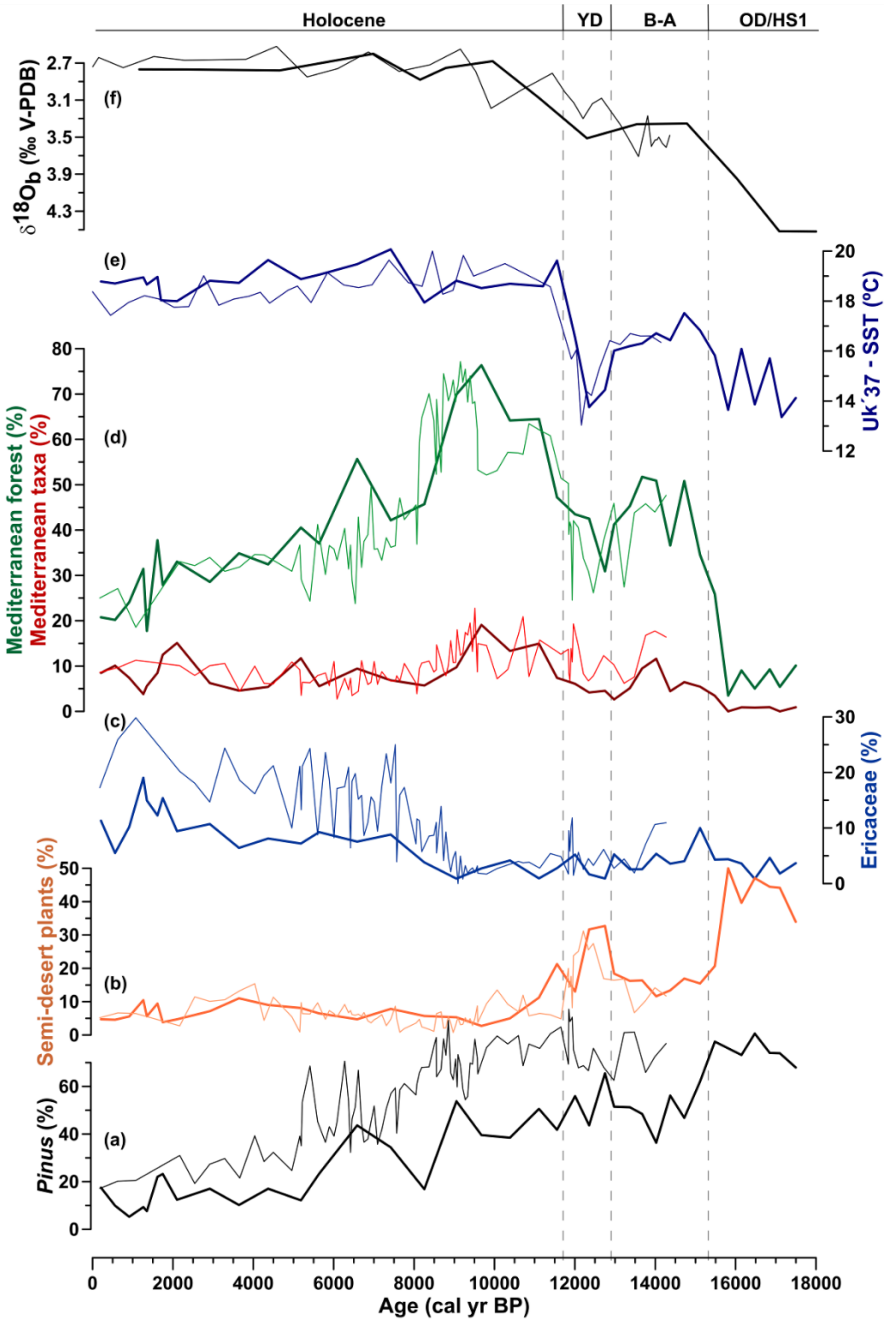

Fig. 3 Vegetation and climatic changes from Site U1385 (bold lines) and the nearby marine core MD95-2042 (thin lines) over the last 17.5 ka. From bottom to top: Percentages of selected pollen taxa or group of taxa (U1385: this study; MD95-2042: Chabaud et al. 2014): (a) *Pinus* (black), (b) semi-desert plants (*Artemisia*, Chenopodiaceae, *Ephedra distachya*-type and *Ephedra fragilis*-type) (orange), (c) Ericaceae (blue), (d) Mediterranean taxa (*Quercus evergreen*-type, *Cistus*, *Olea*, *Phillyrea* and *Pistacia*) (red) and MF (mainly deciduous *Quercus* and Mediterranean taxa) (green); (e) Uk'_{37}-SST (dark blue) (U1385: this study; MD95-2042: Pailler and Bard 2002); (f) $\delta^{18}O_b$ records (black) (U1385: Hodell et al. 2015; MD95-2042: Shackleton et al. 2000). Upper bar indicates the North Atlantic climatic phases: Oldest Dryas (OD)/Heinrich Stadial 1 (HS1), Bølling-Allerød (B-A) interstadial, Younger Dryas (YD) stadial and the Holocene interglacial.

4.2 Interglacial intensity in the SW Iberian region

4.2.1 Comparing reconstructed and simulated interglacial vegetation and climate "Optima" for MIS 1, 11c and 19c

The "optimum" forest development of each interglacial in SW Iberia was determined following recent compilations that defined the interglacial intensity based on the maximum values achieved in a range of climatic proxies within the interglacials (Lang and Wolff 2011; Candy and McClymont 2013; Past Interglacials working group of PAGES 2016). Here, we started by identifying the interval with the highest percentages of Mediterranean taxa and MF (Fig. 4, Table S3) because it represents the optimal expression of the Mediterranean climate (Polunin and Walters 1985). Second, we calculated the mean pollen percentages of Mediterranean taxa and MF maxima during these intervals (Fig. 4, Table S3). Because the maximal expansion of MF and Mediterranean taxa occurred at the same date during MIS 1 and MIS 11c at Site U1385, to avoid the effect of potential outliers, the averaged interval included not only the absolute maximum value but also the values of the samples before and after it (Fig. 4, Table S3).

Site U1385 pollen record shows that MIS 1 stands out in terms of MF "optimum" development, displaying the highest MF values (72 % average) (Fig. 4, Table S3). In contrast, the MF maxima values of MIS 11c and MIS 19c although very similar (40% and 39% average, respectively) are substantially below the average of MIS 1 (Fig. 4, Table S3). Interglacial sea surface conditions off SW Iberia are characterized by overall warm and relatively stable SST (Fig. 4). Nevertheless, the peak warmth of MIS 1 (maximum SST: 20 °C) is slightly higher than that of MIS 11c (18.6 °C) and MIS 19c (19.4 °C), although these differences are close to the limit of the $U^{k'}_{37}$-SST estimated uncertainty (~0.5 °C) (Villanueva et al. 1997) (Fig. 4). At the MF "optimum" development, MIS 1 SST also reached maxima ~ 1.6 and 1 °C higher than MIS 11c and MIS 19c, respectively, in line with the atmospherically-driven MF averaged percentages (Fig. 4).

At present, the MF composition and development critically depend on warm conditions and in particular on the moisture availability during the winter season (Quezel 2002; Gouveia et al. 2008). These ecological requirements coupled with the low-amplitude variations in the $U^{k'}_{37}$-SST profiles of MIS 1, 11c and 19c (Fig. 4) lead to the hypothesis that the different magnitude in the forest expansion during these interglacials is primarily driven by the winter precipitation conditions over the SW Iberian region. Comparison between proxy data and

model results allows to test this hypothesis and to evaluate the vegetation and climate sensitivity to astronomical forcing and GHG.

The major expansion of the SW Iberian forest during MIS 1, 11c and 19c shows closer correspondence to NH summer insolation maxima than to LR04 $\delta^{18}O_b$ peaks (Fig. 4), within age uncertainties. Therefore, it appears more appropriate to compare our proxy-based reconstructions with the snapshot simulations of the interglacial climate "optimum" in which the insolation of NHSP is used (Figs. 5 to 8). This approach is further supported by the evidence of the pervasive influence of precession on the long-term Mediterranean vegetation patterns, with Mediterranean plants displaying maxima associated with precession minima (Magri and Tzedakis 2000). In addition, recent work (Yin and Berger 2015) comparing the results of the two sets of snapshot experiments with the proxy data of five warm interglacials, MIS 1, 5e, 9e, 11c and 19c, showed that the simulations using the insolation of NHSP provide a better agreement with the proxy reconstructions than the ones using the insolation at the interglacial $\delta^{18}O_b$ peaks.

The simulated tree fraction during MIS 1 climate "optimum" over southern Iberia was significantly higher than during MIS 11c but not significantly different from MIS 19c (Fig. 5). Based on experimental studies showing that the pollen tree percentages reflect the past tree cover patterns (e.g. Williams and Jackson 2003), we interpret the MF pollen percentages at Site U1385 as an indicator of the SW Iberian tree fraction (Fig. 4). Both pollen-based vegetation records and snapshot experiments agree on reduced MIS 11c forest cover compared to MIS 1, however, the model doesn't reproduce the differences between MIS 19c and MIS 1 (Figs. 4 and 5). The modelled tree fraction using transient simulations, which provide a broader view of the vegetation to a time-varying forcing (insolation and GHG), further shows that the tree fraction peaks of MIS 1 and MIS 19c are similar and larger than MIS 11c (Fig. 9a, b). The simulated differences in precipitation and surface air temperature between MIS 11c and MIS 1 reveal annual and winter surface air temperatures of MIS 11c only slightly warmer than the ones of MIS 1, and point to the relatively lower winter (DJF) precipitation over SW Iberia as the most important factor leading to its lower tree fraction (Fig. 6a). These results support our hypothesis that winter precipitation was critical for the past forest development over SW Iberia, being therefore the primary climatic signal recorded in our MF pollen percentages. Given the results of the simulated tree fraction differences between MIS 19c and MIS 1 (Fig. 5), as anticipated, MIS 19c regional precipitation is not significantly different from MIS 1 although the annual and winter surface air temperatures are slightly higher during MIS 19c (Fig. 6b).

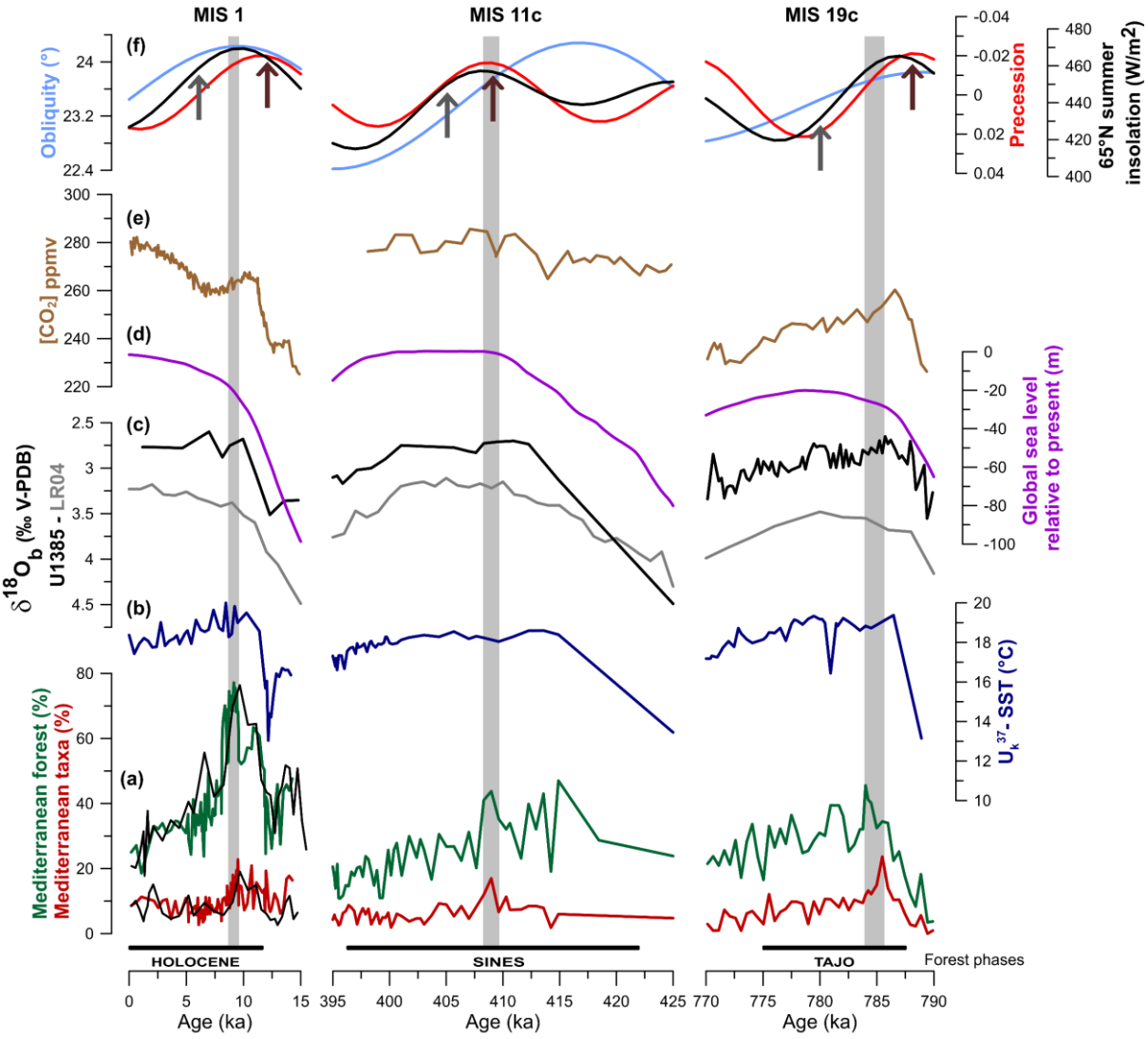

Fig. 4 Vegetation and climatic changes from Site U1385 over MIS 1, MIS 11c (Oliveira et al. 2016) and MIS 19c (Sánchez Goñi et al. 2016). From bottom to top: Selected pollen percentage curves: (a) Mediterranean taxa (MIS 1: red, Chabaud et al. 2014; black, this study) and MF (MIS 1: green, Chabaud et al. 2014; black, this study); (b) Uk'_{37}-SST (MIS 1: Pailler and Bard 2002) (dark blue); (c) $\delta^{18}O_b$ records of Site U1385 (black) (Hodell et al. 2015) and LR04 (grey) (Lisiecki and Raymo 2005); (d) Modeled global sea-level relative to present (m) (purple) (Bintanja and van de Wal 2008); (e) CO_2 concentration (brown) (Lüthi et al. 2008); (f) 65°N summer insolation (black), obliquity (light blue) and precession (red) parameters (Berger 1978). The grey bars mark the interglacial vegetation "optimum", which for the Holocene was based on the MD95-2042 dataset. Arrows indicate the insolation used in the snapshot simulations at the dates when boreal summer occurred at perihelion (NHSP) (dark red) and at the dates of the LR04 $\delta^{18}O_b$ peaks as defined by Yin and Berger 2012, 2015 (grey). Forest phases labeled with local names (bottom) and stratigraphical framework (top) are indicated.

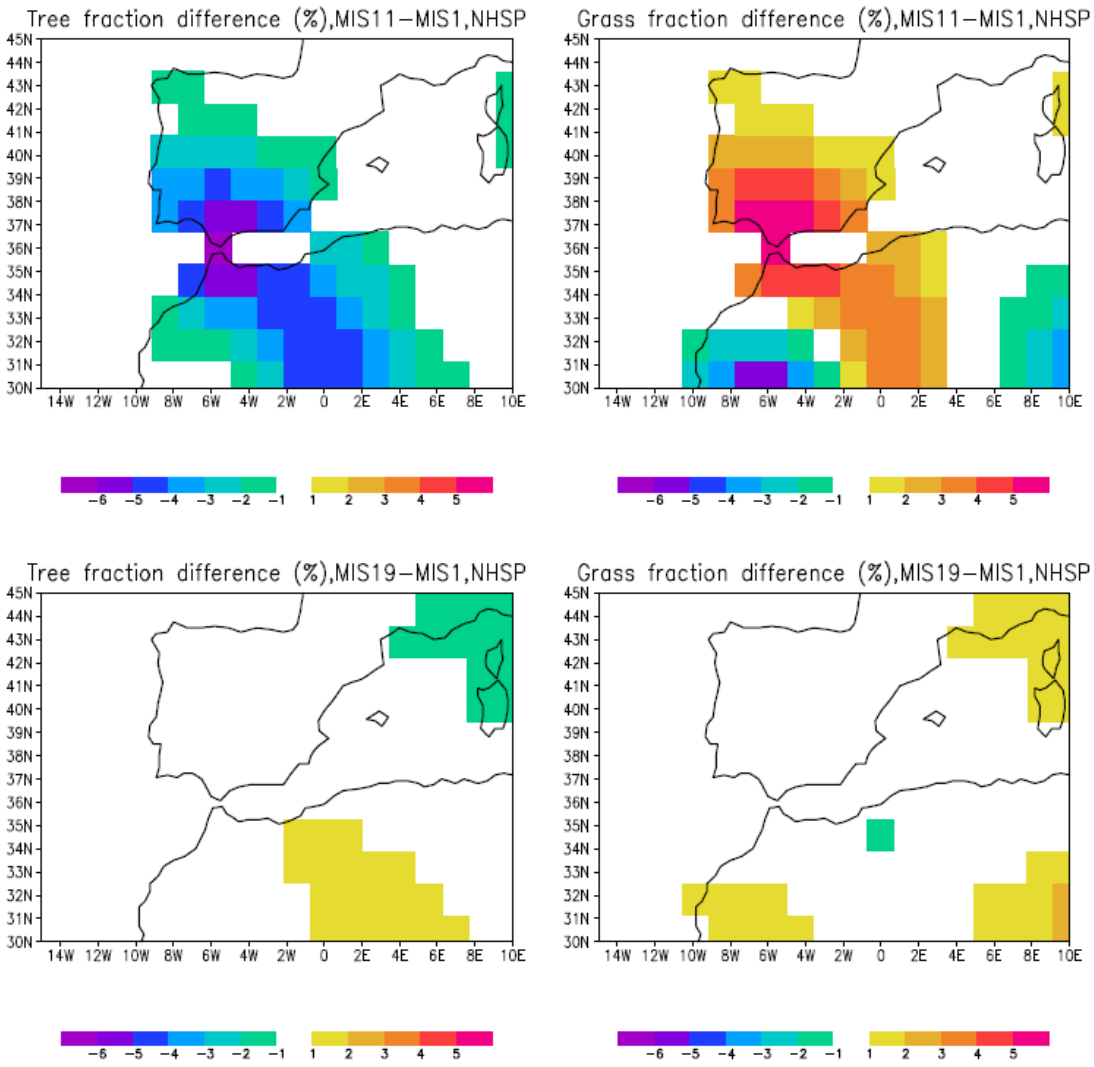

Fig. 5 Differences between MIS 1 and MIS 11c (upper panel) and MIS 19c (lower panel) for the tree and grass fraction change (%) using the snapshot simulations with insolation of NHSP.

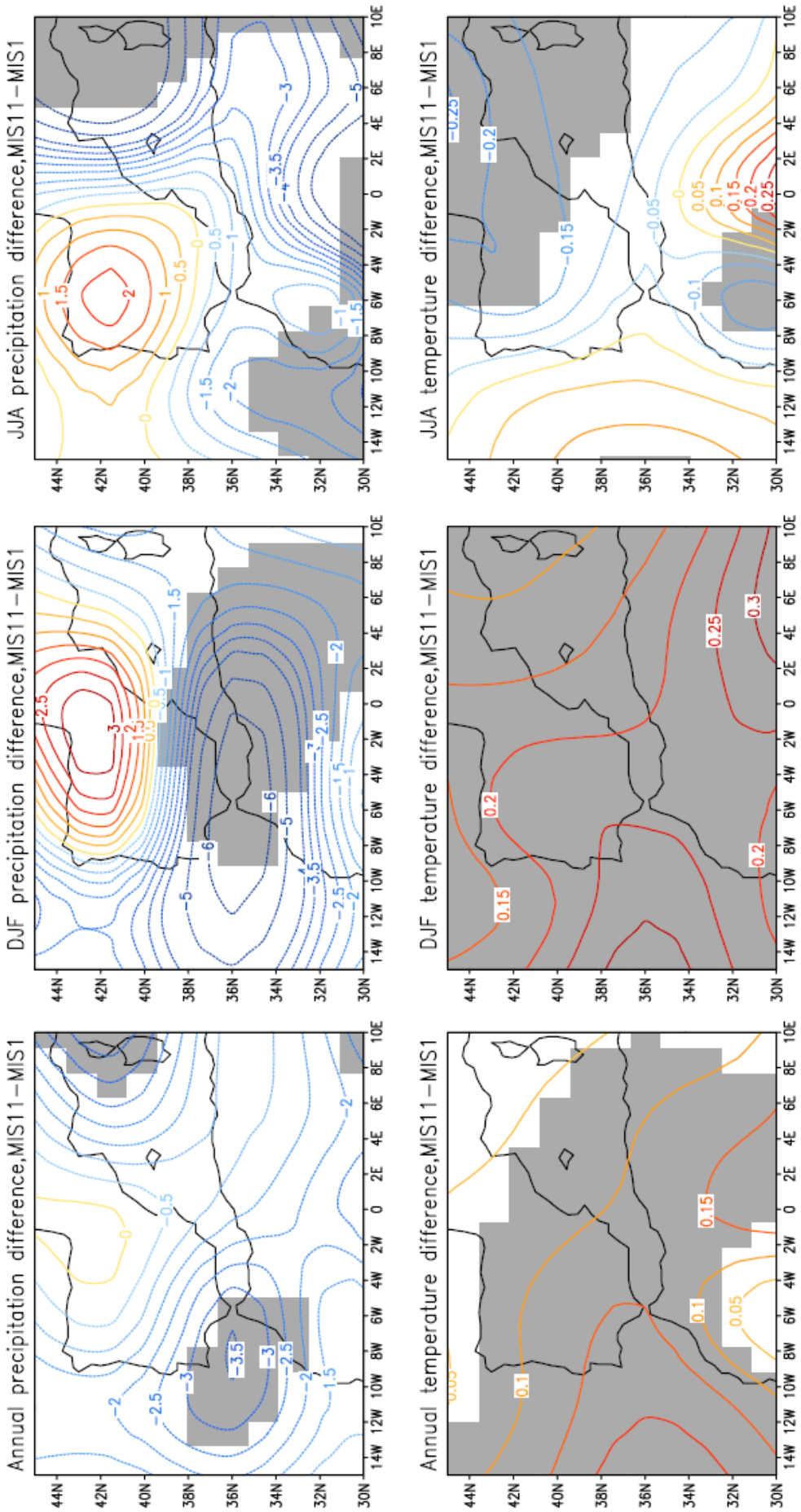

Fig. 6 a Differences between MIS 11c and MIS 1 using the snapshot simulations with insolation of NHSP for the annual mean, DJF and JJA precipitation (cm/year) (upper panel) and annual mean, DJF and JJA surface air temperature (°C) (lower panel). Grey shaded areas indicate the regions for which the simulated anomalies are significantly different at the 90% confidence level based on a t- test.

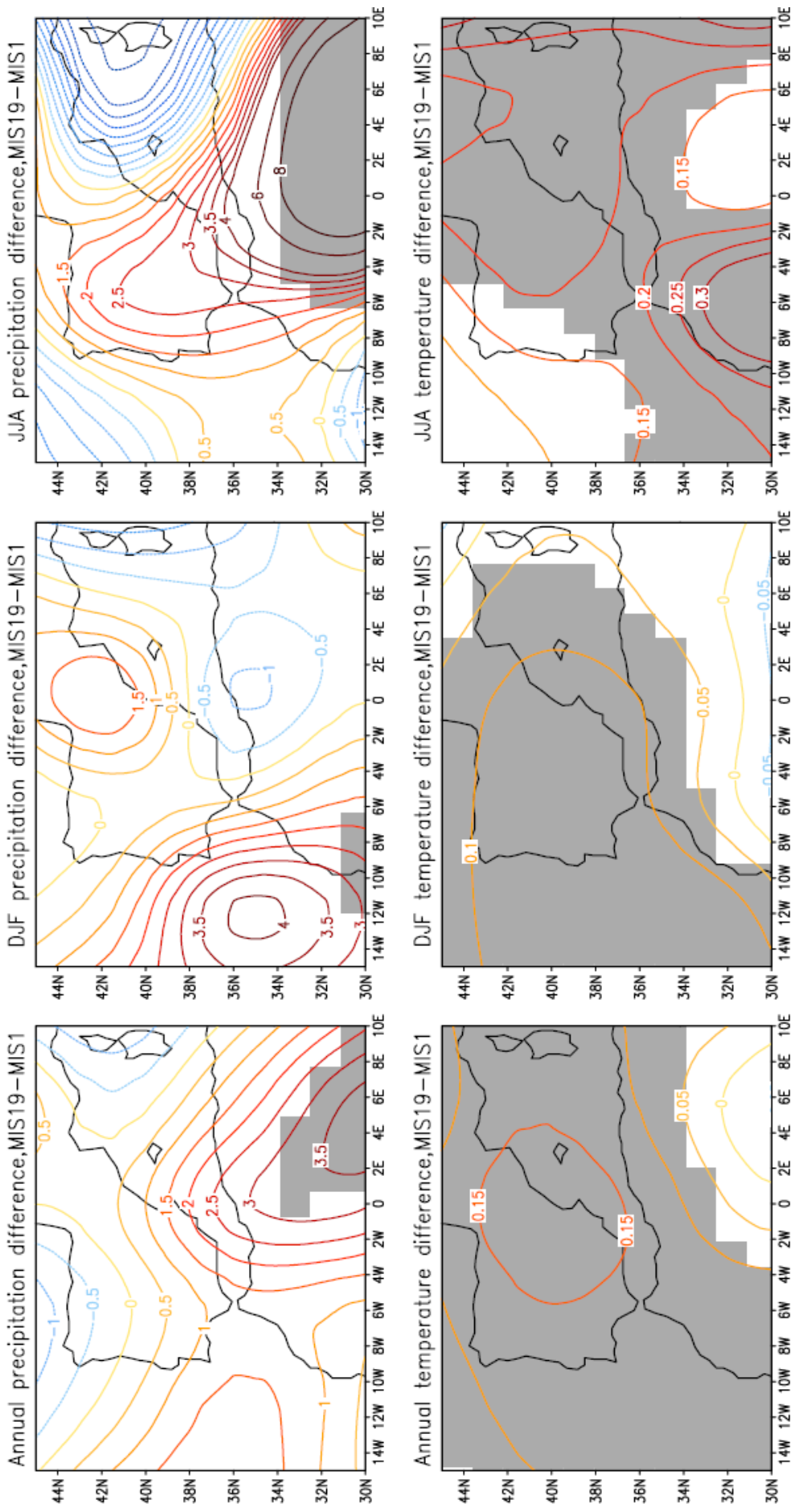

Fig. 6 b Same as Fig. 6a but for the differences between MIS 19c and MIS 1.

4.2.2 What drives the SW Iberian interglacial vegetation at the climate "Optima"?

We used the factor separation method (Stein and Alpert 1993; Yin and Berger 2012) to isolate the effect of the two primary forcings considered, insolation and GHG, on tree fraction over SW Iberia (Fig. 7). These results show that, as expected, under the combined effect of insolation and CO_2 the peak tree fraction of MIS 1 and MIS 19c is comparable and largely higher than that of MIS 11c. Most importantly, this analysis clearly demonstrates that the major factor controlling the interglacial tree fraction maximum over SW Iberia is insolation, whereas GHG plays a smaller role (Fig. 7). The pollen-based vegetation reconstructions and NHSP snapshot simulations show a similar result for the MIS 11c and MIS 1 difference, therefore, our model-data comparison demonstrates the predominant role of insolation on tree fraction in SW Iberia for those stages. These findings extend previous evaluation (Yin and Berger 2012) of the insolation and GHG contribution to the tree fraction changes along the last nine interglacials and at both the global and regional scales, specifically in the low (northern Africa) and high-latitudes (northern Eurasia). Yin and Berger (2012) also showed a dominant effect of insolation on the global tree fraction change and particularly over Northern Africa, which was related to the strong impact of insolation (precession) on precipitation. On the other hand, the CO_2 contribution becomes important in the high-latitudes given that the influence of temperature (GDD0) is larger than in the low-latitudes.

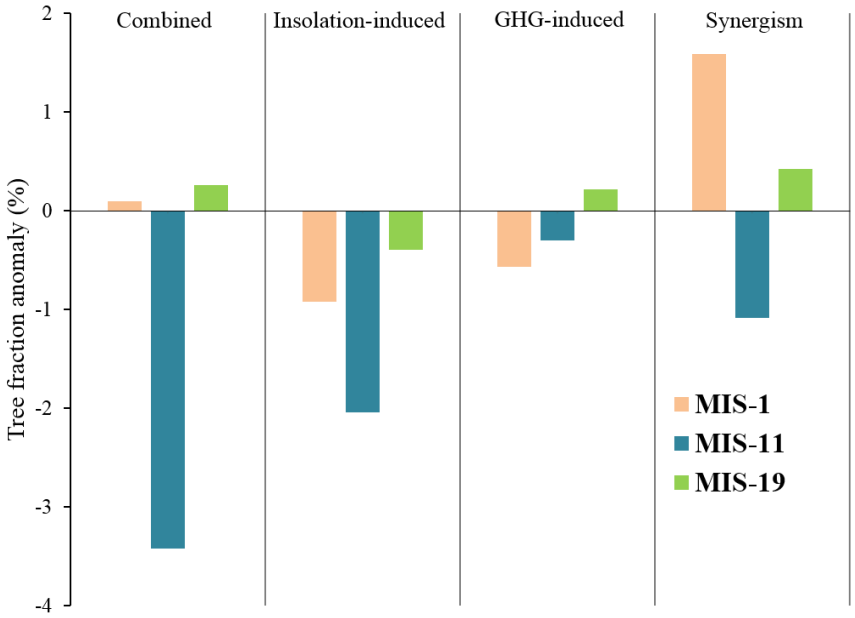

Fig. 7.

Fig. 7 Combined, individual and synergistic effects of GHG and insolation on the NHSP tree fraction peak (%) of MIS 1, MIS 11c and MIS 19c for the southern Iberian region (35N°-41°N, 0-8°W). Combined effect is the total effect of the processes including their interactions and the synergism correspond to the difference between the combined effect and the pure individual effect of each process. The anomalies are deviations from the reference experiment of Yin and Berger (2012) that includes means of the astronomical parameters and of the GHG concentrations of the past nine interglacials.

To understand the role of insolation and underlying mechanisms in inducing the large difference between the tree fraction "optimum" of MIS 1 and MIS 11c over SW Iberia, we calculated the difference in the latitudinal and seasonal distribution of insolation at the NHSP dates (Fig. 8). During boreal winter, MIS 11c insolation over the high-latitudes was not significantly different from MIS 1 but it was higher in the low-latitudes (Fig. 8), a pattern that may have generated a larger latitudinal winter thermal gradient at the MIS 11c peak. Simulations from Yin and Berger (2012, 2015) show that MIS 11c lower obliquity led to an insolation-driven cooling at the interglacial "optimum" that was compensated by the GHG-driven warming during boreal winter, and that in the low-to-mid latitudes MIS 11c was warmer than MIS 1. This hypothesis is further supported by eastern North Atlantic SST reconstructions for MIS 1 and MIS 11c showing a steeper latitudinal temperature gradient during MIS 11c (Kandiano et al. 2012). As the latitudinal temperature gradient has a strong impact on the atmospheric circulation (e.g. Rind 1998), we propose that MIS 11c increased thermal gradient between the low and high-latitudes would have led to the intensification and northward shift of the temperate westerlies with consequent decrease of winter precipitation over the SW Iberia region. These results are compatible with recent precipitation and circulation changes over Europe (IPCC 2013), namely with asymmetrical trends on the number of Atlantic extra-tropical cyclones and precipitation affecting northern and southern Europe (Trigo et al. 2008). Thus, while the northern Atlantic and Europe have suffered a positive trend in Atlantic mid-latitude cyclones, the Mediterranean basin is becoming drier due to fewer low-pressure systems passing through (Sousa et al. 2011). In addition, in line with recent climate model simulations for the obliquity and precession-driven changes in the freshwater budget over the Mediterranean, lower obliquity and slightly lower precession minimum at the MIS 11c "optimum" may have also contributed to its lower winter precipitation by reducing the convective precipitation (Bosmans et al. 2015). These large and

small-scale changes in the atmospheric circulation would explain the reduction of winter moisture availability and the resulting reconstructed and simulated lower tree fraction at the MIS 11c "optimum" in SW Iberia. Moreover, we speculate that MIS 11c lower insolation during the critical spring season for tree growth (Fig. 8) would additionally reduce its tree fraction maximum in comparison to that of MIS 1.

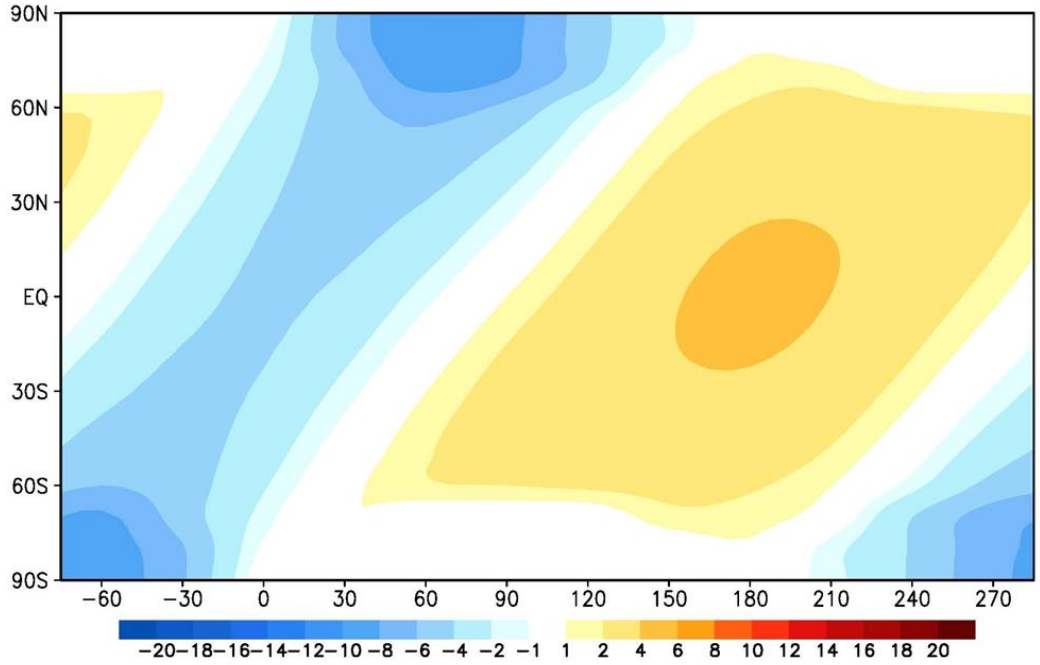

Fig. 8 Differences between MIS 11c and MIS 1 at the NHSP dates for the latitudinal and seasonal distribution of insolation (W m^{-2}). The Y-axis indicates latitude and the X-axis marks the true longitude of the Sun from the beginning to the end of the year (0° and 180° are for the spring and fall equinoxes; 90° and 270° are for the summer and winter solstices). Insolation is determined from the insolation parameters of Berger (1978).

The simulated tree fraction differences between MIS 1 and MIS 19c over southern Iberia show that MIS 19c is the best analogue for the Holocene "optimum". Both snapshot and transient experiments display insignificant differences at the peak of the two interglacials (Fig. 5 and 9a, b), which contrast with Site U1385 pollen records reconstructing a much larger forest cover for MIS 1 (Fig. 4). This model–data discrepancy could result from the fact that only insolation and GHG were taken into account in the simulations, but a possible Eurasian ice sheets during MIS 19c and its influence on the climate and vegetation over SW Iberia were neglected.

According to the LR04 benthic oxygen isotope stack (Lisiecki and Raymo 2005) and marine oxygen isotope records (Hodell et al. 2008; Hodell and Channell 2016), MIS 19c ice volume was relatively higher than during the Holocene (Fig. 4). Although changes in the $\delta^{18}O$ benthic profiles are not only driven by ice volume (Skinner and Shackleton 2005), similar results are showed by modelled global sea-level (Fig. 4) (Bintanja et al. 2005; Bintanja and van de Wal 2008) and a recent sea-level stack (Spratt and Lisiecki 2016). Proxy data and model studies evidence that prior to the Middle Pleistocene Transition (MPT, ~650–1100 ka) the Eurasian ice sheets had an important contribution to the total NH ice volume (e.g. Bintanja and van de Wal 2008; Hodell et al. 2008, Naafs et al. 2013). In particular, studies from the eastern North Atlantic based on organic and inorganic chemistry of ice rafted debris (IRD) demonstrate that the detrital grains of MIS 19 were not derived from the Hudson Strait but rather from northern Europe, Greenland and/or Iceland, which indicates a larger expansion of the Eurasian ice sheets in comparison to the interglacials after MIS 16 (Hodell et al. 2008, Hernández-Almeida et al. 2012; Naafs et al. 2013). We suggest that these differences in ice sheet configuration between MIS 1 and MIS 19c (i.e. NH ice volume baseline conditions and Eurasian ice sheets extent) may have been responsible for the lower SW Iberian forest cover during MIS 19c and additionally explain the discrepancy between pollen-based reconstructions and climate model results. Pollen records off southern Iberia and the Mediterranean region indicate reduced forest cover for the first millennia of the early Holocene that was likely associated with the persistence of relatively large Laurentide and Fennoscandian ice sheets, which may have changed the trajectory of the mid-latitude North Atlantic storm track with consequent reduced penetration into the Mediterranean region (Magny et al. 2011, 2013; Desprat et al. 2013). In analogy to the early Holocene, we suggest that the ice sheet forcing played a major role on winter precipitation over SW Iberia, restricting the maximal forest expansion during MIS 19c. In addition, it is plausible that the volume of the Eurasian ice sheets during MIS 19c reached a significant size to increase the planetary albedo and influence the regional climate, including the SW Iberian region. Compared to MIS 1 and MIS 11c during which the ice sheets in the NH are restricted to Greenland (e.g. Raymo and Mitrovica 2012), this would have promoted regional anticyclonic conditions and led to lower temperature and decreased humidity with consequent lower forest cover and slightly cooler SST as recorded by our multiproxy records (Fig. 4).

It is noteworthy that the factor separation technique shows a striking opposite result when considering the synergistic effects of insolation and of GHG on the tree fraction over SW Iberia (Fig. 7). In agreement with the pollen-based vegetation data (Fig. 4), MIS 1 displays the highest positive tree fraction anomaly followed by MIS 19c and largely above MIS 11c. This suggests that although the insolation is the dominant forcing, the synergism is also very important, particularly at the Holocene "optimum" (Fig. 7). Explaining the synergism is not however straightforward, currently we only can state that a negative synergism, as observed at MIS 11c peak, means that the effect on the tree fraction when insolation and CO_2 play together is smaller than the sum of the effects when they act separately. They are not necessarily counteracting with each other but may co-play on one process (e.g. water vapor, albedo). Nevertheless, the exact physical meaning of the synergism can only be assessed after investigating all the processes, which is not a simple task and is beyond the scope of this study.

Our model–data comparison strengthens previous evidence highlighting the importance for investigating the regional expression of potential past interglacial analogues for the Holocene and future climate (e.g. Lang and Wolff 2011; Candy and McClymont 2013; Yin and Berger 2015; Past Interglacials working group of PAGES 2016). Even though analogies between MIS 1, 11c and 19c have been extensively pointed out (Berger and Loutre 2002, 2003; Droxler et al. 2003; Loutre and Berger 2003; McManus et al. 2003; Tzedakis et al. 2009a, 2012; Masson-Delmotte et al. 2010; Pol et al. 2010; Tzedakis 2010; Yin and Berger 2010, 2012, 2015), our study shows that as far as the vegetation changes in SW Europe (below 40°N) are concerned, they cannot be considered as analogues for the Holocene climate "optimum". Comparison of our pollen-based reconstructions with NW Iberian margin pollen records (Desprat et al. 2007) and the long European records of Praclaux (southern France) (Reille et al. 2000; de Beaulieu et al. 2001) and Tenaghi Phillipon (NE Greece) (van der Wiel and Wijmstra 1987; Tzedakis et al. 2006) further underlines the need for looking for Holocene analogues in terms of climate and environmental impacts at the regional scale. While in the northern sites (only extending until MIS 11) where forest expansion is mainly limited by temperature, the forest "optimum" of the Holocene and MIS 11c are similar (Reille et al. 2000; de Beaulieu et al. 2001; Desprat et al. 2007), the pollen sequence from NE Greece displays the same pattern as Site U1385, showing the strongest temperate tree pollen percentages during MIS 1 and similar temperate forest expansion during MIS 11c and MIS

19c (Tzedakis et al. 2009b). It is therefore crucial to consider the key role of the hydrological changes on the interglacial vegetation and climate dynamics, particularly in regions where the vegetation communities are highly sensitive to moisture availability as the Mediterranean region (Quezel 2002).

4.3 What drives the climate variability during the Holocene and its potential analogues in SW Iberia

To evaluate the main factors contributing to the vegetation and climate variability during the entire MIS 1, 11c and 19c in SW Iberia, we performed a comparison between pollen-based reconstructions and transient experiments with time-varying insolation and GHG. This approach allows us to overcome the problem of using a single peak forcing in the snapshot simulations and explore the major controlling factors of the atmospherically-driven vegetation changes during the different boundary conditions of each interglacial. This comparison shows that, probably due to lack of ice sheet forcing and related feedbacks, the model doesn't reproduce the same deglaciation vegetation change as shown by the pollen records (Fig. 9a, b). The simulated tree fraction during the deglaciations is relatively high, particularly between the last glacial-interglacial transition (B-A and YD) and the early Holocene and during the early MIS 19c, which is not in agreement with the amplitude of the pollen-based vegetation changes recorded at Site U1385 (Fig. 9a, b). As mentioned above, changes in ice sheet size and configuration constitute the strongest forcing of the climate system at both global and regional scale (e.g. Clark et al. 1999; Renssen et al. 2009). Therefore, we suspect that the neglected melting of the ice sheets and associated lack of ice sheet-climate interactions in our model experiments are the explanation for the large model–data discrepancies. Regrettably, this also precludes the precise identification of the onset of the maximal forest expansion and the model–data comparison in terms of the duration of the vegetation "optimum" interval (Fig. 9a, b). Subsequently, both vegetation and model reconstructions show that the major development of the forest cover during all the three interglacials ended rapidly with a strong contraction of the forest, with no ensuing recovery to the previous forest extent (Fig. 9a, b). In addition, there is a clear agreement between the pollen records and the modeled tree fraction for the lower extent and amplitude of the forest over the end of each interglacial. Both proxy and model results display a higher development

of the forest over the end of the optimum period in the Holocene, followed by late MIS 19c and much lower values during the end of MIS 11c (Fig. 9a, b).

To determine the influence of the surface air temperature and precipitation on the vegetation changes during MIS 1, 11c and 19c, we performed simple regression analyses between the tree fraction, annual and seasonal temperature and precipitation, on the 1000-year running mean of the transient simulations original data (Fig. 9a, b, Table 1). In terms of surface air temperature (GDD0), the strongest correlation of the tree fraction is obtained with JJA temperature in all the three interglacials, although the annual temperature is also important during MIS 11c (Fig. 9a, Table 1). As far as the precipitation is concerned, for each interglacial, the tree fraction is highly correlated with the annual precipitation (Fig. 9b, Table 1). As in the terrestrial biosphere model VECODE the tree fraction is a function of GDD0 and annual precipitation (Brovkin et al. 1997), the estimation of the tree fraction does not directly involve the seasonal precipitation. Therefore, the strong correlation of tree fraction with SON precipitation and particularly with DJF precipitation should be due to the high contribution of these two seasons to the annual precipitation (Fig. 9b, Table 1). In accordance with the inferred atmospheric changes, from the pollen-based vegetation records, the expansion (reduction) of the simulated tree fraction was primarily driven by warm (cooler) summer temperatures and moisture availability (deficiency) during the wintertime (Fig. 9a, b). Both proxy and model data indicate that the interglacial vegetation and climate dynamics over SW Iberia have no apparent relationship to atmospheric CO_2 concentration. A prominent example for this negligible CO_2 forcing is given by its relatively high concentrations over the end of the interglacials, in particular for MIS 1 and MIS 11c, while the forest cover, summer temperature and winter precipitation achieved minima values (Fig. 9a, b). We find that the vegetation and climate changes at this time-scale are mainly driven by astronomical forcing, in particular precession, in agreement with the strong impact of precession on the climate of the Mediterranean region south of 40°N (Ruddiman and McIntyre 1984) and with previous pollen studies off southern Iberia (e.g. Fletcher and Sánchez Goñi 2008; Sánchez Goñi et al. 2008, 2016; Margari et al. 2014; Oliveira et al. 2016, 2017). As shown in Fig. 9b, in all the three interglacials the major forest expansion is concurrent with high winter precipitation, and occurs within precession minima forcing. On the contrary, low forest extent over the end of the interglacials is associated to precession maxima. These observations are in line with modeling experiments showing the dominant influence of precession in precipitation

variations in subtropical regions (Yin and Berger 2012; Bounceur et al. 2015), likely driven over southern Iberia by large-scale precipitation and changes in storm track activity (Bosmans et al. 2015).

Superimposed on the long-term vegetation changes, persistent millennial-scale climate variability is revealed by a series of forest reduction events throughout the three interglacials at Site U1385 (Fig. 9a, b). Interestingly, this intra-interglacial variability is also reproduced in the modeled tree fraction, being mainly associated to decreases in the SON and DJF precipitation (Fig. 9b) while the surface air temperatures exhibit low-amplitude and frequency variability (Fig. 9a). This leads to a view that the millennial-scale vegetation changes in SW Iberia under warm climate conditions are essentially generated by hydrological changes mainly induced by insolation, as they are reproduced in the model experiments notwithstanding the absence of ice sheet dynamics and all associated feedbacks (Fig. 9a, b). Although further palaeoclimatic and model work is required to understand the nature of intra-interglacial variability, this study supports a growing body of evidence that outlines the importance of the low-latitude forcing occurring at sub-precessional frequencies not only at the low-latitudes (Berger et al. 2006; Yin and Berger 2015) but also in the subtropical-to-high latitudes of the North Atlantic (e.g. Weirauch et al. 2008; Ferretti et al. 2010, 2015; Billups et al. 2011; Hernández-Almeida et al. 2012; Palumbo et al. 2013; Billups and Scheinwald 2014; Sánchez Goñi et al. 2016; Oliveira et al. 2017).

One of the most conspicuous features of our pollen-based and model results is the magnitude of the forest declines ending the interglacial vegetation "optimum" in SW Iberia and the rapidity with which it is accomplished (Fig. 9a, b). Data and model support that dramatic forest declines can occur under prevailing interglacial warm conditions in SW Iberia, i.e. well before the substantial increase in ice volume marking the end of the Iberian interglacial period, while SST remains high (Fig. 4). The transient simulations show that these changes in forest cover are a response to long-term change mainly in astronomical forcing. However, they appear more rapid in the pollen-based vegetation records than in the model simulations (Fig. 9a, b) and have previously been associated to millennial-scale variability (Sanchez Goñi et al. 2016; Oliveira el al. 2016). Recent interglacial pollen-based vegetation records from Site U1385 revealed millennial cycles driven by the fourth harmonic of the precessional component (Sanchez Goñi et al. 2016; Oliveira el al. 2017). Therefore, we

suggest that these rapid vegetation changes marking the end of the forest maximal extent in SW Iberia may have been a combined response to the long-term and millennial-scale astronomical forcing. Moreover, we suspect that other interactions among internal components of the climate system that are not explicitly represented in the model experiments may have also been involved in the amplification of the primary forcing and the increase of the vegetation change rate, such as vegetation changes due to declining insolation and the associated feedback mechanisms.

Table 1 Correlation coefficient values (R) of simple linear regression between tree fraction and climate variables. The calculation was made on the 1000-year running mean of the original simulated data of the transient experiments.

		MIS 1	MIS 11c	MIS 19c
Surface air temperature	Annual	0.10	0.94	0.70
	JJA	0.85	0.94	0.94
	DJF	-0.44	0.51	-0.28
	MAM	0.24	0.76	0.41
	SON	-0.56	0.17	-0.14
Precipitation	Annual	0.82	0.97	0.96
	JJA	0.51	0.20	0.20
	DJF	0.53	0.94	0.94
	MOM	0.10	0.59	0.46
	SON	0.71	0.84	0.91

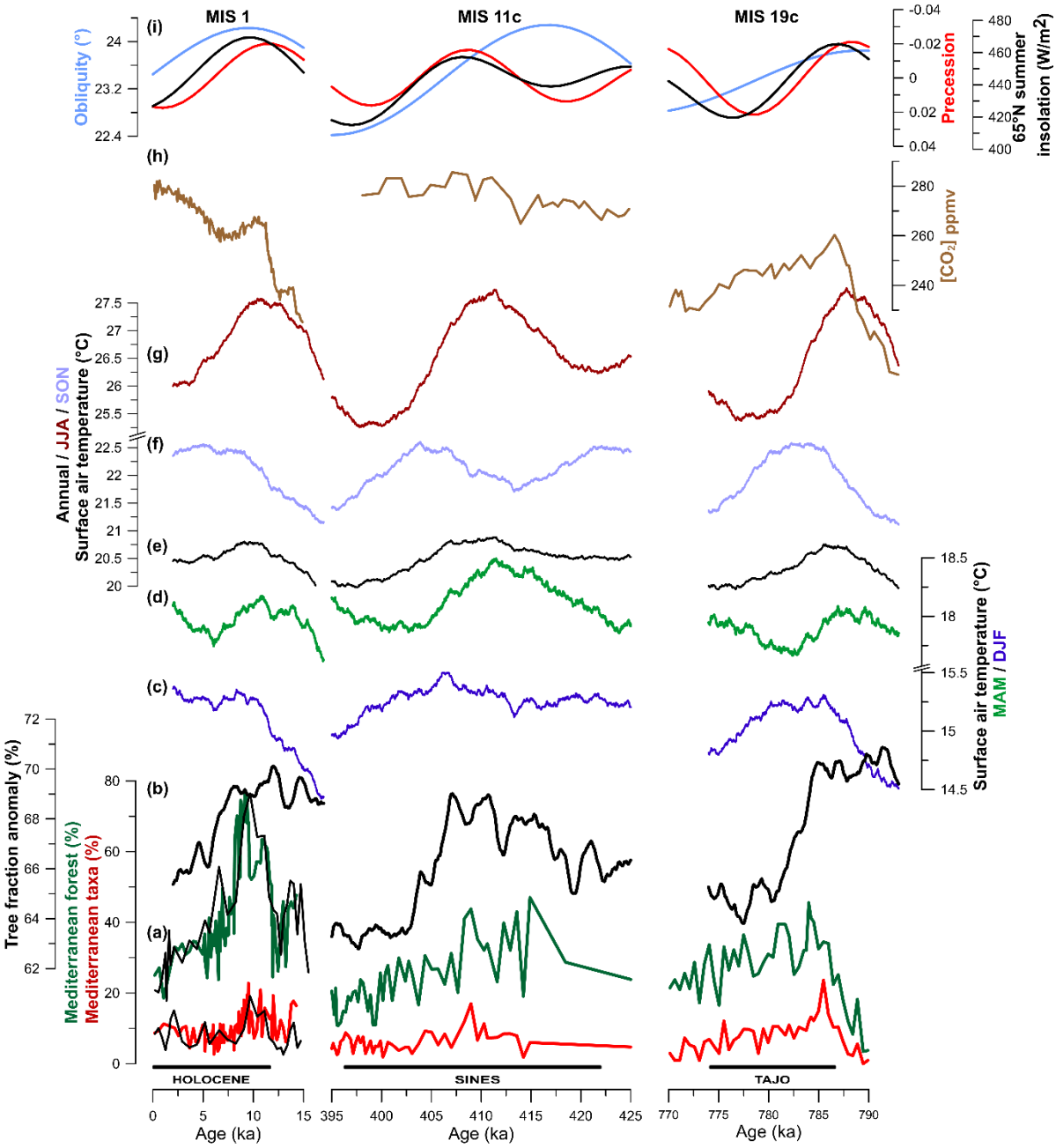

Fig. 9a Vegetation and climatic changes from Site U1385 and results of the transient simulations with time-varying insolation and CO_2 for MIS 1, MIS 11c and MIS 19c for the southern Iberian region (35N°-41°N, 0-8°W). From bottom to top: Selected pollen percentage curves: (a) Mediterranean taxa (MIS 1: red, Chabaud et al. 2014; black, this study) and MF (MIS 1: green, Chabaud et al. 2014; black, this study); (b) Simulated tree fraction anomaly (%) (black); Surface air temperature (°C) (c) DJF (dark blue), (d) MAM (green), (e) annual (black), (f) SON (light blue), (g) JJA (red). The 1000-year running mean of the original simulated data is plotted. (h) CO_2 concentration (brown) (Lüthi et al. 2008); (i) 65°N summer insolation (black), obliquity (light blue) and precession (red) parameters (Berger 1978). Forest phases labeled with local names (bottom) and stratigraphical framework (top) are indicated.

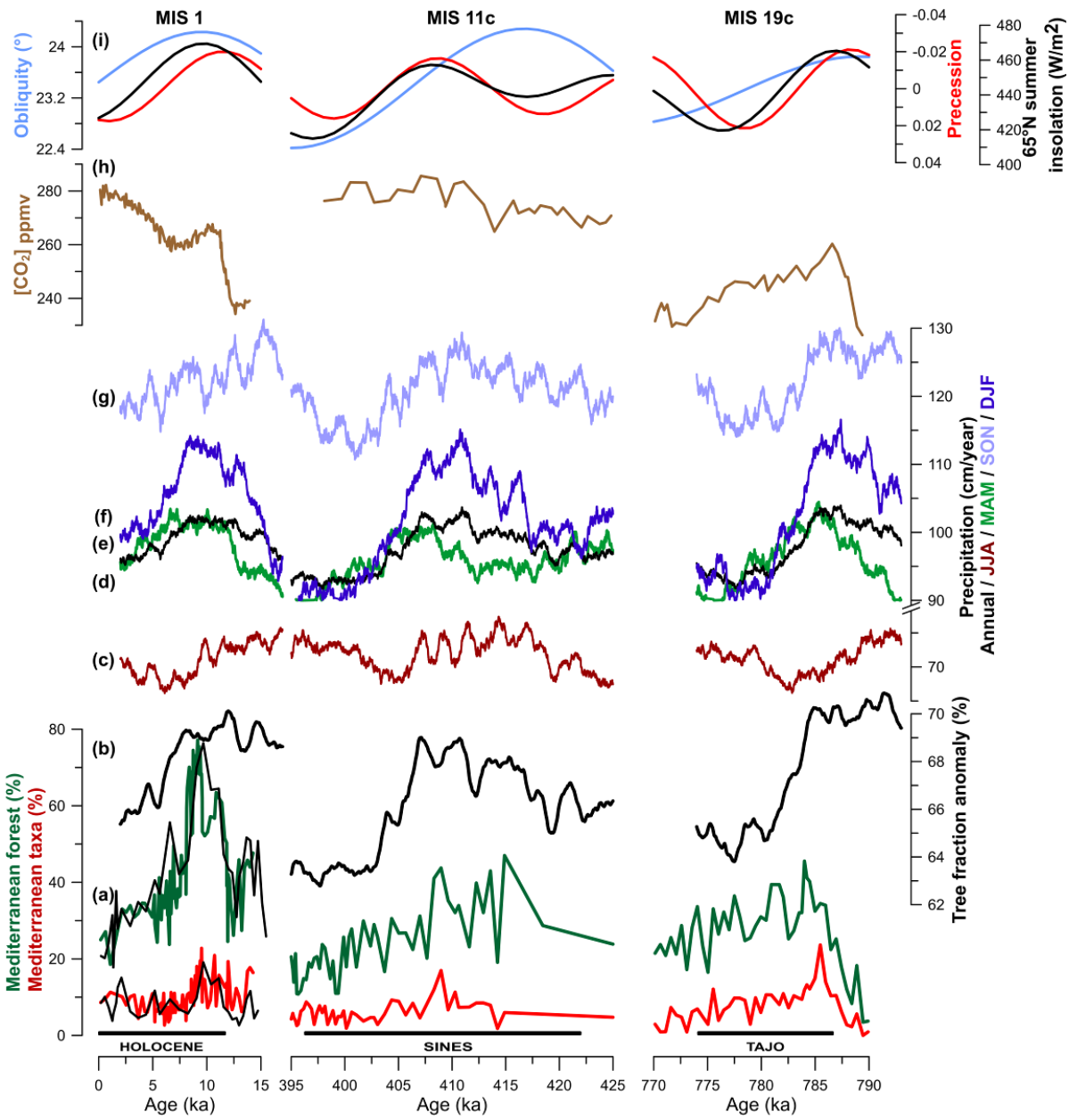

Fig. 9b. Same as Fig. 9a but for precipitation (cm/year): (c) JJA (red), (d) annual (black), (e) MAM (green), (f) DJF (dark blue) and (g) SON (light blue).

5 Conclusions

The forcing mechanisms and regional expression of the Holocene and its potential best interglacial analogues, MIS 11c and MIS 19c, on SW Iberia region are investigated for the first time through comparison of proxy-based reconstructions and climate model experiments. This study relies on the comparison of multiproxy records for regional vegetation, precipitation regime and atmospheric and oceanic temperature variability from IODP Site U1385, with snapshot and transient simulations that concentrate on the interglacial climate "optimum" and the entire interglacial periods, respectively.

1. At the interglacial climate "optimum", the pollen-based vegetation reconstructions show that the Holocene forest expansion was particularly prominent and substantially higher than at MIS 11c and MIS 19c, possibly reflecting the sensitivity of SW Iberian forest development to winter precipitation changes. Therefore, as far as the vegetation and climatic variability in the SW Europe, below 40°N, are concerned, MIS 11c and MIS 19c cannot be considered as straightforward analogues for the Holocene "optimum".

- The model-data comparison confirms that the tree fraction differences between the Holocene and MIS 11c are primarily due to the higher winter precipitation over the SW Iberian region at the Holocene "optimum". Based on factor separation analyses we find that insolation dominates the regional tree fraction changes, whereas GHG plays a minor role. In particular, the differences between the latitudinal and seasonal distribution of insolation at the Holocene and MIS 11c "optimum", mainly related to MIS 11c lower obliquity, may have led to an amplified thermal gradient between low and high northern latitudes at MIS 11c peak with consequent reduction of large-scale winter precipitation in SW Iberia.

- In contrast to the pollen-based vegetation reconstructions, in both snapshot and transient experiments MIS 19c appears to be the best analogue for the Holocene "optimum" in terms of tree fraction in SW Iberia. These large model–data mismatches are probably related to the underestimation of the ice sheet forcing, which is prescribed at PI values. We suggest that MIS 19c lower sea-level/higher ice volume and larger Eurasian ice sheets development in comparison with that of the Holocene may have been responsible for its lower winter precipitation and tree fraction, through its influence in the mid-latitude atmospheric circulation. Interestingly, when considering the synergistic effects of insolation and CO_2 on the tree fraction, which implicates feedbacks processes, the model–data mismatch disappears.

2. The comparison between the pollen-based and simulated interglacial vegetation with time-varying insolation and CO_2 during the entire Holocene and its potential analogues in SW Iberia reveals that the modeled tree fraction match the data reasonably well. A notable exception is noted for the deglaciations and attributed to the lack of ice sheet-climate interactions in the model experiments. We find that the expansion of tree fraction over SW Iberia is highly correlated with warm summer temperatures and high precipitation during the wintertime, with both being mainly controlled by precession and with no obvious relationship with CO_2 trends. Finally, our work provides data and model evidence for intra-interglacial instability in SW Iberia revealed by a series of forest decreases associated to simulated dry atmospheric episodes in winter but no concurrent SST change. Based on the transient simulations, the astronomical forcing is sufficient to drive the observed persistent millennial-scale variability during the three interglacials since ice sheet-climate interactions were neglected in the model. Moreover, it is remarkable that the most dramatic forest reductions ending with the three interglacial "optima", during low ice volume conditions, are also reproduced in the transient experiments although they appear more gradual. This observation highlights the potential role of the interactions between long-term and millennial-scale climate dynamics in amplifying the climate and vegetation response. Further research is clearly required to better understand the interaction between orbital and millennial-scale variability within the different interglacials, including model experiments considering ice sheet configuration and feedbacks within the climate system.

Supplementary data

Table S1 AMS ^{14}C radiocarbon dates from Site U1385 and calibrated ages (cal yr BP) using the Marine13 calibration curve (Reimer et al. 2013) implemented in CALIB 7.1 (Stuiver and Reimer 1993; http://calib.qub.ac.uk/calib/).

Depth (crmcd)	Sample type	^{14}C age (yr BP)	Delta R	Calibrated age (cal yr BP) 2σ range	Median probability (cal yr BP)
0.52	*G. bulloides*	2525±28	143±14	1915:2111	2011
1.08	*G. bulloides*	6181±35	143±14	6345:6568	6454
1.56	*G. bulloides*	10060±33	143±14	10722:11036	10877
1.93	*G. bulloides*	11499±43	143±14	12683:12940	12812
2.46	*G. bulloides*	13355±45	143±14	15097:15470	15257

Fig. S1 Percentage pollen diagram of selected morphotypes and ecological groups from Site U1385 plotted against depth. Ecological groups include Mediterranean forest (MF) which here includes the Mediterranean taxa and all temperate trees and shrub taxa, excluding *Pinus*, *Cedrus* and Cupressaceae; Mediterranean taxa: *Quercus* evergreen-type, *Cistus*, *Olea*, *Phillyrea* and *Pistacia*; and semi-desert plants: *Artemisia*, Chenopodiaceae, *Ephedra distachya*-type and *Ephedra fragilis*-type. On the right of the diagram are represented the pollen zones and results of the cluster analysis.

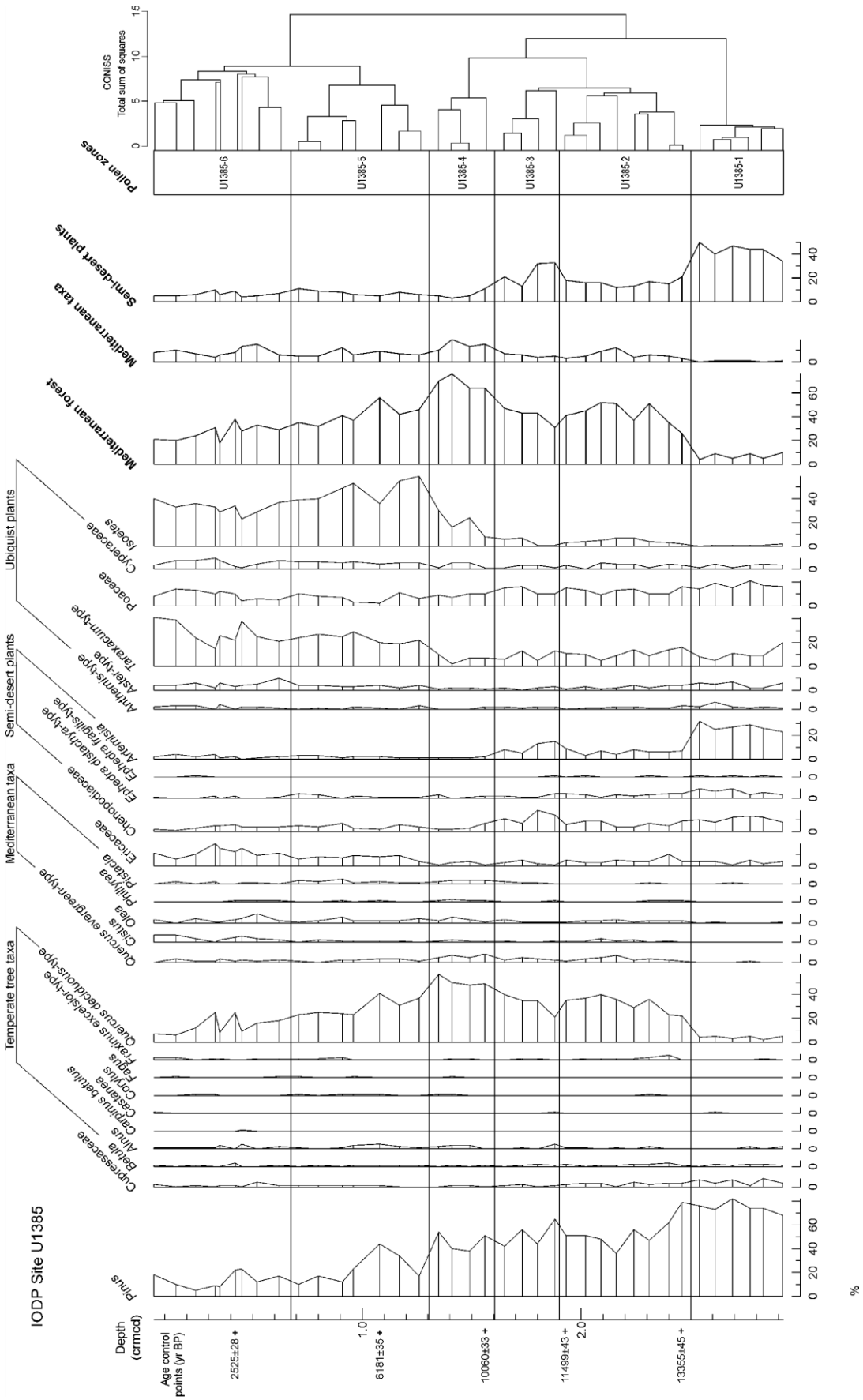
IODP Site U1385
Depth (crmcd)
Age control points (yr BP)
2525±28
6181±35
10060±33
11499±43
13355±45
Pollen zones
U1385-6
U1385-5
U1385-4
U1385-3
U1385-2
U1385-1
CONISS
Total sum of squares
Pinus
Cupressaceae
Betula
Alnus
Carpinus betulus
Castanea
Corylus
Fagus
Taxinus excelsior-type
Quercus deciduous-type
Temperate tree taxa
Quercus evergreen-type
Cistus
Olea
Phillyrea
Pistacia
Ericaceae
Chenopodiaceae
Ephedra distachya-type
Ephedra fragilis-type
Artemisia
Semi-desert plants
Anthemis-type
Asteraceae-type
Tataxacum-type
Poaceae
Cyperaceae
Isoetes
Ubiquist plants
Mediterranean forest
Mediterranean taxa
Mediterranean taxa
Semi-desert plants
%

Fig. S1.

Table S2 Description and interpretation of the pollen record from Site U1385 for last 17.5 ka. Pollen zones are designated as following: U1385 (site name) - number of the pollen zone. MF: Mediterranean forest.

Pollen zonation (Basal depth in crmcd; age in cal yr BP)	**Pollen diagram main features**	**Inferred climate changes**
U1385-6 (0.62; 2 918)	Decreasing abundances of MF values (33-21%). Decline in *Pinus* and deciduous *Quercus* percentages along with higher frequencies of Ericaceae, *Taraxacum*-type and Poaceae.	Slightly cooler and drier conditions
U1385-5 (1.26; 8 255)	Distinct drop of MF taxa to moderate values (45.7%) followed by decreasing trend. Important decline in *Pinus*, deciduous *Quercus* and Mediterranean taxa percentages while Ericaceae, *Taraxacum*-type and *Isoetes* increase.	Decreased temperature and humidity
U1385-4 (1.56; 11 107)	Marked rise of MF taxa to the highest percentages (average ~70%) counteracted by lower frequencies of semi-desert plants. Higher values of temperate and Mediterranean taxa values (particularly *Alnus*, deciduous and evergreen *Quercus*, *Cistus*, *Olea*, *Phillyrea* and *Pistacia).* Increasing percentages of *Isoetes.*	Mediterranean climate with humid/mild winters, and warm/dry summers
U1385-3 (1.88; 12 750)	Decline of MF taxa values at the beginning (in particular deciduous *Quercus*) followed by an increase towards the top of the zone. Higher abundances of Chenopodiaceae and *Artemisia* but decreasing. Fall in Cupressaceae percentages.	Slightly lower temperature and humidity (increasing trend)
U1385-2 (2.46; 15 483)	Pronounced increase of MF taxa percentages (average of 42%). Particular rise in *Alnus*, *Fraxinus excelsior*-type, deciduous and evergreen *Quercus*, *Cistus*, *Olea* and *Isoetes* while *Pinus* and semi-desert plants values (mainly *Artemisia*) decrease.	Warmer conditions and increased humidity
U1385-1 (2.92; 17 496)	Dominance of semi-desert plants and relatively high values of other non-arboreal pollen taxa, mainly Poaceae. Very low percentages of all tree taxa (MF average < 7%), except Cupressaceae and *Pinus*.	Maximal cold and dry conditions

Table S3 Values of Mediterranean forest (MF) and Mediterranean taxa maxima (averaged and absolute) for each interglacial during the interval comprising the major expansion of both ecological groups. For MIS 1 both values from core MD95-2042 and Site U1385 (*italic*) are given.

	MIS 1	MIS 11c	MIS 19c
Time between the maximal expansion of Mediterranean taxa and MF (ka)	9.15-9.51 ka *9.05-10.39 ka*	408.3-409.6 ka	784-785.5 ka
MF averaged maximum (absolute) (%)	72 (77.2) *70 (76.4)*	40 (43.8)	39 (45.5)
Mediterranean taxa averaged maximum (absolute) (%)	17 (22.8) *14 (19.1)*	11 (17)	15 (23.6)

Acknowledgments

Financial support was provided by WarmClim, a LEFE-INSU IMAGO project, and the Portuguese Foundation for Science and Technology (FCT) through the project CLIMHOL (PTDC/AAC-CLI/100157/2008), CCMAR (FCT Research Unit - UID/Multi/04326/2013), D. Oliveira's doctoral grant (SFRH/BD/9079/2012), F. Naughton's postdoctoral grant (SFRH/BPD/108712/2015) and T. Rodrigues's postdoctoral grant (SFRH/BPD/108600/2015). Q.Z. Yin is Research Associate of the Belgian National Fund for Scientific Research (FRS-FNRS). This research used samples provided by the Integrated Ocean Drilling Program (IODP), Expedition 339. We would like to thank the scientists and technicians of IODP Expedition 339, the Bremen Core Repository, L. Devaux for technical assistance and V. Hanquiez for drawing Fig. 1. Computational resources have been provided by the supercomputing facilities of the Université catholique de Louvain (CISM/UCL) and the Consortium des Equipements de Calcul Intensif en Fédération Wallonie Bruxelles (CECI) funded by FRS-FNRS.

References

Bard E, Rostek F, Turon J-L, Gendreau S (2000) Hydrological impact of Heinrich Events in the Subtropical Northeast Atlantic. Science 289:1321–4. doi: 10.1126/science.289.5483.1321

Bauch HA, Erienkeuser H, Helkme JP, Struck U (2000) A palaeoclimatic evaluation of marine oxygen isotope stage 11 in the high-northern Atlantic (Nordic Seas). Glob. Planet. Change 24, 27–39

Berger A (1978) Long-term variations of daily insolation and quaternary climatic changes. J Atmos Sci 35(12):2362–2367

Berger A, Loutre MF (2002) An exceptionally long interglacial ahead? Science 297:1287–1288

Berger A, Loutre MF (2003) Climate 400,000 years ago, a key to the future? In: Droxler A, Burckle L and Poore A (eds) Earth climate and orbital eccentricity: the marine isotope stage 11 question. Geophysical monograph 137, American Geophysical Union, Washington, pp 17–26

Berger A, Loutre MF, Mélice JL (2006) Equatorial insolation: from precession harmonics to eccentricity frequencies. Clim Past 2:131–136. doi: 10.5194/cp-2-131-2006

Billups K, Rabideaux N, Stoffel J (2011) Suborbital-scale surface and deep water records in the subtropical North Atlantic: implications on thermohaline overturn. Quat Sci Rev 30:2976–2987. doi: 10.1016/j.quascirev.2011.06.015

Billups K, Scheinwald A (2014) Origin of millennial-scale climate signals in the subtropical North Atlantic. Paleoceanography 29:612–627. doi: 10.1002/2014PA002641

Bintanja R, van de Wal RSW (2008) North American ice-sheet dynamics and the onset of 100,000-year glacial cycles. Nature 454:869–872. doi: 10.1038/nature07158

Bintanja R, van de Wal RSW, Oerlemans J (2005) Modelled atmospheric temperatures and global sea levels over the past million years. Nature 437:125–128. doi: 10.1038/nature03975

Blanco Castro E, Casado González MA, Costa Tenorio M, Escribano Bombín R, García Antón M, Génova Fuster M, Gómez Manzaneque F, Moreno Sáiz JC, Morla Juaristi C, Regato Pajares P, Sáiz Ollero H (1997) Los bosques ibéricos: una Interpretación Geobotánica. Editorial Planeta, 572 p., Barcelona

Bosmans JHC, Drijfhout SS, Tuenter E, Hilgen FJ, Lourens LJ, Rohling EJ (2015) Precession and obliquity forcing of the freshwater budget over the Mediterranean. Quat Sci Rev 123:16–30. doi: 10.1016/j.quascirev.2015.06.008

Bounceur N, Crucifix M, Wilkinson RD (2015) Global sensitivity analysis of the climate–vegetation system to astronomical forcing: an emulator-based approach. Earth Syst Dyn 6:205–224. doi: 10.5194/esd-6-205-2015

Brovkin V, Ganapolski A, Svirezhev Y (1997) A continuous climate vegetation classification for use in climate-biosphere studies. Ecol Modell 101:251–261

Candy I, Mcclymont EL (2013) Interglacial intensity in the North Atlantic over the last 800000 years: Investigating the complexity of the mid-Brunhes Event. J Quat Sci 28:343–348. doi: 10.1002/jqs.2632

Candy I, Schreve DC, Sherriff J, Tye GJ (2014) Marine Isotope Stage 11: Palaeoclimates, palaeoenvironments and its role as an analogue for the current interglacial. Earth-Science Rev 128:18–51. doi: 10.1016/j.earscirev.2013.09.006

Chabaud L, Sánchez Goñi MF, Desprat S, Rossignol L (2014) Land-sea climatic variability in the eastern North Atlantic subtropical region over the last 14,200 years: atmospheric and oceanic processes at different timescales. The Holocene 24:787–797. doi: 10.1177/0959683614530439

Clark PU, Alley RB, Pollard D (1999) Northern Hemisphere Ice sheet Influences on Global Climate Change. Science 286, 1104-1111

de Abreu L, Abrantes FF, Shackleton NJ, Tzedakis PC, McManus JF, Oppo DW, Hall MA (2005) Ocean climate variability in the eastern North Atlantic during interglacial marine isotope stage 11: A partial analogue to the Holocene? Paleoceanography 20:1–15. doi: 10.1029/2004PA001091

de Beaulieu JL, Andrieu-Ponel V, Reille M, Grüger E, Tzedakis C, Svobodova H (2001) An attempt at correlation between the Velay pollen sequence and the Middle Pleistocene stratigraphy from central Europe. Quat Sci Rev 20:1593–1602. doi: 10.1016/S0277-3791(01)00027-0

de Vernal A, Hillaire-Marcel C (2008) Natural variability of Greenland climate, vegetation, and ice volume during the past million years. Science 320:1622–5. doi: 10.1126/science.1153929

Desprat S, Combourieu-Nebout N, Essallami L, Sicre MA, Dormoy I, Peyron O, Siani G, Bout Roumazeilles V, Turon JL (2013) Deglacial and holocene vegetation and climatic changes in the southern central Mediterranean from a direct land-sea correlation. Clim Past 9:767–787. doi: 10.5194/cp-9-767-2013

Desprat S, Sánchez Goñi MF, Naughton F, Turon JL, Duprat J, Malaize B, Cortijo E, Peypouquet JP (2007) Climate variability of the last five isotopic interglacials: Direct land-sea-ice correlation from the multiproxy analysis of North-Western Iberian margin deep-sea cores, in: The Climate of Past Interglacials, Developments in Quaternary Science, edited by: Sirocko F, Litt T, Claussen M, Sánchez Goñi MF. Elsevier, 375–386

Dickson AJ, Beer CJ, Dempsey C, Maslin MA, Bendle JA, McClymont EL, Pancost RD (2009) Oceanic forcing of the Marine Isotope Stage 11 interglacial. Nat Geosci 2:428–433. doi: 10.1038/ngeo527

Droxler AW, Farrell JW (2000) Marine Isotope Stage 11 (MIS 11): new insights for a warm future. Glob. Planet. Change 24, 1–5

Droxler AW, Poore RZ, Burckle LH (eds) (2003) Earth's Climate and Orbital Eccentricity: The Marine Isotope Stage 11 Question. Geophysical Monograph Series. American Geophysical Union, Washington, D. C., ISBN 0-87590-996-5, p. 240

Epica CM (2004) Eight glacial cycles from an Antarctic ice core. Nature 429:623–628

Expedition 339 Scientists (2013) Site U1385. In: Stow DAV, Hernández-Molina FJ, Alvarez Zarikian CA, the Expedition 339 Scientists (Eds.), Proceedings IODP 339. Integrated Ocean Drilling Program Management International, Inc., Tokyo. http://dx.doi.org/10.2204/iodp.proc.339.103.201

Ferretti P, Crowhurst SJ, Hall MA, Cacho I (2010) North Atlantic millennial-scale climate variability 910 to 790ka and the role of the equatorial insolation forcing. Earth Planet Sci Lett 293:28–41. doi: 10.1016/j.epsl.2010.02.016

Ferretti P, Crowhurst SJ, Naafs BDA, Barbante C (2015) The Marine Isotope Stage 19 in the mid-latitude North Atlantic Ocean: astronomical signature and intra-interglacial variability. Quat Sci Rev 108:95–110. doi: 10.1016/j.quascirev.2014.10.024

Fiúza AFG (1984) Hidrologia e Dinâmica das Águas Costeiras de Portugal, Ph.D. Dissertation, 294 pp., University of Lisbon

Fletcher WJ, Sánchez Goñi MF (2008) Orbital- and sub-orbital-scale climate impacts on vegetation of the western Mediterranean basin over the last 48,000 yr. Quat Res 70:451–464. doi: 10.1016/j.yqres.2008.07.002

Fletcher WJ, Sanchez Goñi MF, Peyron O, Dormoy I (2010) Abrupt climate changes of the last deglaciation detected in a Western Mediterranean forest record. Clim Past 6:245–264. doi: 10.5194/cp-6-245-2010

Ganopolski A, Winkelmann R, Schellnhuber HJ (2016) Critical insolation–CO2 relation for diagnosing past and future glacial inception. Nature 529:200–203. doi: 10.1038/nature16494

Giaccio B, Regattieri E, Zanchetta G, Nomade S, Renne PR, Sprain CJ, Drysdale RN, Tzedakis PC, Messina P, Scardia G, Sposato A, Bassinot F (2015) Duration and dynamics of the best orbital analogue to the present interglacial. Geology 43:603–606. doi: 10.1130/G36677.1

Goosse H, Brovkin V, Fichefet T, Haarsma R, Huybrechts P, Jongma J, Mouchet A, Selten F, Barriat PY, Campin JM, Deleersnijder E, Driesschaert E, Goelzer H, Janssens I, Loutre MF, Morales Maqueda MA, Opsteegh T, Mathieu PP, Munhoven G, Petterson JE, Renssen H, Roche D, Schaeffer M, Tartinville B, Timmermann A, Weber SL (2010) Description of the earth system model of intermediate complexity LOVECLIM version 1.2. Geosci. Model Dev. 3, 603-633

Gouveia C, Trigo RM, DaCamara CC, Libonati R, Pereira JMC (2008) The North Atlantic Oscillation and European vegetation dynamics. International Journal of Climatology, 28, 1835-1847

Helmke JP, Bauch HA, Röhl U, Kandiano ES (2008) Uniform climate development between the subtropical and subpolar Northeast Atlantic across marine isotope stage 11. Clim Past 4:181–190. doi: 10.5194/cp-4-181-2008

Hernández-Almeida I, Sierro FJ, Cacho I, Flores JA (2012) Impact of suborbital climate changes in the North Atlantic on ice sheet dynamics at the Mid-Pleistocene Transition. Paleoceanography 27:n/a–n/a. doi: 10.1029/2011PA002209

Hodell D, Lourens L, Crowhurst S, Konijnendijk T, Tjallingii R, Jimenez-Espejo F, Skinner L, Tzedakis PC (2015) A reference time scale for Site U1385 (Shackleton Site) on the SW Iberian Margin. Glob Planet Change 1385:49–64. doi: 10.1016/j.gloplacha.2015.07.002

Hodell DA, Channeil JET, Curtis JH, Romero OE, Röhl U (2008) Onset of "Hudson Strait" Heinrich events in the eastern North Atlantic at the end of the middle Pleistocene transition (~640 ka)? Paleoceanography 23:1–16. doi: 10.1029/2008PA001591

Hodell DA, Channell JET (2016) Mode transitions in Northern Hemisphere glaciation: co-evolution of millennial and orbital variability in Quaternary climate. Clim Past 12:1805–1828. doi: 10.5194/cp-12-1805-2016

IPCC (2013) Climate Change 2013: The Physical Science Basis. Contribution of Working Group I to the Fifth Assessment Report of the Intergovernmental Panel on Climate Change [Stocker TF, Qin D, Plattner GK, Tignor M, Allen SK, Boschung J, Nauels A, Xia Y, Bex V and Midgley PM (eds.)]. Cambridge University Press, Cambridge, United Kingdom and New York, NY, USA, 1535 pp. doi:10.1017/CBO9781107415324

Kandiano ES, Bauch HA, Fahl K, Helmke JP, Röhl U, Pérez-Folgado M, Cacho I (2012) The meridional temperature gradient in the eastern North Atlantic during MIS 11 and its link to the ocean–atmosphere system. Palaeogeogr Palaeoclimatol Palaeoecol 333-334:24–39. doi: 10.1016/j.palaeo.2012.03.005

Lang N, Wolff EW (2011) Interglacial and glacial variability from the last 800 ka in marine, ice and terrestrial archives. Clim Past 7:361–380. doi: 10.5194/cp-7-361-2011

Lionello P, Malanotte-Rizzoli P, Boscolo R, Alpert P, Artale V, Li L, Luterbacher J, May W, Trigo R, Tsimplis M, Ulbrich U, Xoplaki E (2006) The Mediterranean climate: An overview of the main characteristics and issues. Dev Earth Environ Sci 4:1–26. doi: 10.1016/S1571-9197(06)80003-0

Lisiecki LE, Raymo ME (2005) A Pliocene-Pleistocene stack of 57 globally distributed benthic δ 18 O records. Paleoceanography 20:n/a–n/a. doi: 10.1029/2004PA001071

Loidi J, Biurrun I, Campos JA, Garcia-Mijangos I, Herrera M (2007) A survey of heath vegetation of the Iberian Peninsula and Northern Morocco: a biogeographical and bioclimatic approach. Phytocoenologia 37, 341-370

Loutre MF, Berger AL (2003) Marine Isotope Stage 11 as an analogue for the present interglacial. Glob Planet Change 36:209–217. doi: 10.1016/S0921-8181(02)00186-8

Lüthi D, Le Floch M, Bereiter B, Blunier T, Barnola JM, Siegenthaler U, Raynaud D, Jouzel J, Fischer H, Kawamura K, Stocker TF (2008) High-resolution carbon dioxide concentration record 650,000-800,000 years before present. Nature 453:379–82. doi: 10.1038/nature06949

Magny M, Combourieu-Nebout N, De Beaulieu JL, Bout-Roumazeilles V, Colombaroli D, Desprat S, Francke A, Joannin S, Ortu E, Peyron O, Revel M, Sadori L, Siani G, Sicre MA, Samartin S, Simonneau A, Tinner W, Vannière B, Wagner B, Zanchetta G, Anselmetti F, Brugiapaglia E, Chapron E, Debret M, Desmet M, Didier J, Essallami L, Galop D, Gilli A, Haas JN, Kallel N, Millet L, Stock A, Turon JL, Wirth S, Vannière B, Calo C, Millet L, Leroux A, Peyron O, Zanchetta G, La Mantia T, Tinner W (2013) North-south palaeohydrological contrasts in the central mediterranean during the holocene: Tentative synthesis and working hypotheses. Clim Past 9:2459–2475. doi: 10.1016/j.quascirev.2011.05.018

Magny M, Vannière B, Calo C, Millet L, Leroux A, Peyron O, Zanchetta G, La Mantia T, Tinner W (2011) Holocene hydrological changes in south-western Mediterranean as recorded by lake-level fluctuations at Lago Preola, a coastal lake in southern Sicily, Italy. Quat Sci Rev 30:2459–2475. doi: 10.1016/j.quascirev.2011.05.018

Margari V, Skinner LC, Hodell DA, Martrat B, Toucanne S, Grimalt JO, Gibbard PL, Lunkka JP, Tzedakis PC (2014) Land-ocean changes on orbital and millennial time scales and the penultimate glaciation. Geology 42:183–186. doi: 10.1130/G35070.1

Masson-Delmotte V, Dreyfus G, Braconnot P, Johnsen S, Jouzel J, Kageyama M, Landais A, Loutre MF, Nouet J, Parrenin F, Raynaud D, Stenni B, Tuenter E (2006) Past temperature reconstructions from deep ice cores: relevance for future climate change. Clim Past 2:145–165. doi: 10.5194/cp-2-145-2006

Masson-Delmotte V, Stenni B, Pol K, Braconnot P, Cattani O, Falourd S, Kageyama M, Jouzel J, Landais A, Minster B, Barnola JM, Chappellaz J, Krinner G, Johnsen S, Röthlisberger R, Hansen J, Mikolajewicz U, Otto-Bliesner B (2010) EPICA Dome C record of glacial and interglacial intensities. Quat Sci Rev 29:113–128. doi: 10.1016/j.quascirev.2009.09.030

McManus J, Oppo D, Cullen J, Healey S (2003) Marine isotope stage 11 (MIS 11): Analog for Holocene and future climate? In: A. W. Droxler RZP and LHB (ed) Earth's Climate and Orbital Eccentricity: The Marine Isotope Stage 11 Question. American Geophysical Union, Washington D. C., pp 69–85

Melles M, Brigham-Grette J, Minyuk PS, Nowaczyk NR,Wennrich V, DeConto RM, Anderson PM, Andreev AA, Coletti A, Cook TL, Haltia-Hovi E, Kukkonen M, Lozhkin AV, Rosen P, Tarasov P, Vogel H, Wagner B (2012) 2.8 Million Years of Arctic Climate Change from Lake El'gygytgyn, NE Russia. Science 337:315–320. doi: 10.1126/science.1222135

Müller PJ, Kirst G, Ruhland G, Von Storch I, Rosell-Melé A (1998) Calibration of the alkenone paleotemperature index $U^{k'}_{37}$- based on core-tops from the eastern South Atlantic and the global ocean (60°N-60°S). Geochimica et Cosmochimica Acta 62, 1757–1772

Naafs BDA, Hefter J, Stein R (2013) Millennial-scale ice rafting events and Hudson Strait Heinrich (-like) Events during the late Pliocene and Pleistocene: a review. Quat Sci Rev 80, 1–28. doi:10.1016/j.quascirev.2013.08.014

Naughton F, Sánchez Goñi MF, Desprat S, Turon JL, Duprat J, Malaizé B, Joli C, Cortijo E, Drago T, Freitas MC (2007) Present-day and past (last 25 000 years) marine pollen signal off western Iberia. Mar Micropaleontol 62:91–114. doi: 10.1016/j.marmicro.2006.07.006

Naughton F, Sanchez Goñi MF, Rodrigues T, Salgueiro E, Costas S, Desprat S, Duprat J, Michel E, Rossignol L, Zaragosi S, Voelker AHL, Abrantes F (2016) Climate variability across the last deglaciation in NW Iberia and its margin. Quat Int 414:9–22. doi: 10.1016/j.quaint.2015.08.073

Oliveira D, Desprat S, Rodrigues T, Naughton F, Hodell D, Trigo R, Rufino M, Lopes C, Abrantes F, Sánchez Goñi MF (2016) The complexity of millennial-scale variability in southwestern Europe during MIS 11. Quat Res. doi: 10.1016/j.yqres.2016.09.002

Oliveira D, Sánchez Goñi MF, Naughton F, Polanco-Martínez JM, Jimenez-Espejo FJ, Grimalt JO, Martrat B, Voelker AHL, Trigo R, Hodell D, Abrantes F, Desprat S (2017) Unexpected weak seasonal climate in the western Mediterranean region during MIS 31, a high-insolation forced interglacial. Quat Sci Rev 161:1–17. doi: 10.1016/j.quascirev.2017.02.013

Pailler D, Bard E (2002) High frequency palaeoceanographic changes during the past 140 000 yr recorded by the organic matter in sediments of the Iberian Margin. Palaeogeogr Palaeoclimatol Palaeoecol 81, 431-452

Palumbo E, Flores J-A, Perugia C, Petrillo Z, Voelker AHL, Amore FO (2013) Millennial scale coccolithophore paleoproductivity and surface water changes between 445 and 360 ka (Marine Isotope Stages 12/11) in the Northeast Atlantic. Palaeogeogr Palaeoclimatol Palaeoecol 383-384:27–41. doi: http://dx.doi.org/10.1016/j.palaeo.2013.04.024

Past Interglacials Working Group of PAGES (2016) Interglacials of the last 800,000 years, Reviews of Geophysics, 54, doi:10.1002/2015RG000482

Peinado Lorca M, Martinez-Parras JM (1987) Castilla-La Mancha. In: Peinado Lorca M, Rivas-Martinez S (eds) La vegetación de España. Alcala de Henares: Universidad de Alcala de Henares, pp. 163–196

Peliz A, Dubert J, Santos AMP, Oliveira PB, Le Cann B (2005) Winter upper ocean circulation in the Western Iberian Basin - Fronts, Eddies and Poleward Flows: An overview. Deep Res Part I Oceanogr Res Pap 52:621–646. doi: 10.1016/j.dsr.2004.11.005

Pol K, Debret M, Masson-Delmotte V, Capron E, Cattani O, Dreyfus G, Falourd S, Johnsen S, Jouzel J, Landais A, Minster B, Stenni B (2011) Links between MIS 11 millennial to sub-millennial climate variability and long term trends as revealed by new high resolution EPICA Dome C deuterium data - A comparison with the Holocene. Clim Past 7:437–450. doi: 10.5194/cp-7-437-2011

Pol K, Masson-Delmotte V, Johnsen S, Bigler M, Cattani O, Durand G, Falourd S, Jouzel J, Minster B, Parrenin F (2010) New MIS 19 EPICA Dome C high resolution deuterium data: Hints for a problematic preservation of climate variability at sub-millennial scale in the "oldest ice." Earth Planet Sci Lett 298:95–103. doi: 10.1016/j.epsl.2010.07.030

Polunin O, Walters M (1985) A Guide to the Vegetation of Britain and Europe. Oxford University Press, New York 238pp

Prahl FG, Wakeham SG (1987) Calibration of unsaturation patterns in long-chain ketone compositions for palaeotemperature assessment. Nature 330, 367–369. doi:10.1038/330367a0

Quezel P (2002) Réflexions sur l'évolution de la flore et de la végétation au Maghreb méditerranéen. Ibis Press, Paris

Raymo ME, Mitrovica JX (2012) Collapse of polar ice sheets during the stage 11 interglacial. Nature 483, 453–456. doi:10.1038/nature10891

Raynaud D, Barnola J-M, Souchez R, Lorrain R, Petit JR, Duval P, Lipenkov VY (2005) Palaeoclimatology: the record for marine isotopic stage 11. Nature 436:39–40. doi: 10.1038/43639b

Reille M, Beaulieu J-L De, Svobodova H, Andrieu-Ponel V, Goeury C (2000) Pollen analytical biostratigraphy of the last five climatic cycles from a long continental sequence from the Velay region (Massif Central, France). J Quat Sci 15:665–685

Reimer PJ, Bard E, Bayliss A, Beck JW, Blackwell PG, Bronk Ramsey C, Buck CE, Cheng H, Edwards RL, Friedrich M, Grootes PM, Guilderson TP, Haflidason H, Hajdas I, Hattté C, Heaton TJ, Hoffmann DL, Hogg AG, Hughen KA, Kaiser KF, Kromer B, Manning SW, Niu M, Reimer RW, Richards DA, Scott M, Southon JR, Staff RA, Turney CSM, van der Plicht J (2013) IntCal13 and Marine13 radiocarbon age calibration curves 0-50,000 years cal BP. Radiocarbon 55, 1869-1887

Renssen H, Seppa H, Heiri O, Roche DM, Goosse H, Fichefet T (2009) The spatial and temporal complexity of the Holocene thermal maximum. Nat. Geosci. 2, 411-414

Reyes A V, Carlson AE, Beard BL, Hatfield RG, Stoner JS, Winsor K, Welke B, Ullman DJ (2014) South Greenland ice-sheet collapse during Marine Isotope Stage 11. Nature 510:525–8. doi: 10.1038/nature13456

Rind D (1998) Latitudinal temperature gradients and climate change. J Geophys Res 103:5943–5971

Roberts DL, Karkanas P, Jacobs Z, Marean CW, Roberts RG (2012) Melting ice sheets 400,000 yr ago raised sea level by 13 m: Past analogue for future trends. Earth Planet Sci Lett 357–358:226–237. doi: http://dx.doi.org/10.1016/j.epsl.2012.09.006

Rodrigues T, Grimalt JO, Abrantes FG, Flores JA, Lebreiro S (2009) Holocene interdependences of changes in sea surface temperature, productivity, and fluvial inputs in the Iberian continental shelf (Tagus mud patch). Geochemistry, Geophys Geosystems 10:1–17. doi: 10.1029/2008GC002367

Rohling EJ, Braun K, Grant K, Kucera M, Roberts AP, Siddall M, Trommer G (2010) Comparison between Holocene and Marine Isotope Stage-11 sea-level histories. Earth Planet Sci Lett 291:97–105. doi: 10.1016/j.epsl.2009.12.054

Ruddiman WF (2005) Cold climate during the closest stage 11 analog to recent millennia. Quat. Sci. Rev. 24, 1111–1121

Ruddiman WF (2007) The early anthropogenic hypothesis: challenges and responses. Rev. Geophys. 45, 1–37

Ruddiman WF, McIntyre A (1984) Ice-age thermal response and climatic role of the surface Atlantic Ocean, 40°N to 63°N. Geol. Soc. Am. Bull.95, 381–396

Salgueiro E, Naughton F, Voelker AHL, de Abreu L, Alberto A, Rossignol L, Duprat J, Magalhães VH, Vaqueiro S, Turon JL, Abrantes F (2014) Past circulation along the western Iberian margin: a time slice vision from the Last Glacial to the Holocene. Quat Sci Rev 106:316–329. doi: 10.1016/j.quascirev.2014.09.001

Sánchez Goñi MF, Eynaud F, Turon JL, Shackleton NJ (1999) High resolution palynological record off the Iberian margin: Direct land-sea correlation for the Last Interglacial complex. Earth Planet Sci Lett 171:123–137. doi: 10.1016/S0012-821X(99)00141-7

Sánchez Goñi MF, Landais A, Fletcher WJ, Naughton F, Desprat S, Duprat J (2008) Contrasting impacts of Dansgaard-Oeschger events over a western European latitudinal transect modulated by orbital parameters. Quat Sci Rev 27:1136–1151. doi: 10.1016/j.quascirev.2008.03.003

Sánchez Goñi MF, Rodrigues T, Hodell DA, Polanco-Martínez JM, Alonso-García M, Hernández-Almeida I, Desprat S, Ferretti P (2016) Tropically-driven climate shifts in southwestern Europe during MIS 19, a low eccentricity interglacial. Earth Planet Sci Lett 448:81–93. doi: 10.1016/j.epsl.2016.05.018

Shackleton NJ, Hall MA, Vincent E (2000) Phase relationships between millennial-scale events 64,000-24,000 years ago. Paleoceanography 15:565–569. doi: 10.1029/2000PA000513

Skinner LC, Shackleton NJ (2005) An Atlantic lead over Pacific deep-water change across Termination I: implications for the application of the marine isotope stage stratigraphy. Quat Sci Rev 24:571–580. doi: 10.1016/j.quascirev.2004.11.008

Sousa PM, Trigo RM, Aizpurua P, Nieto R, Gimeno L, Garcia-Herrera R (2011) Trends and extremes of drought indices throughout the 20th century in the Mediterranean. Nat Hazards Earth Syst Sci 11:33–51. doi: 10.5194/nhess-11-33-2011

Spratt RM, Lisiecki LE (2016) A Late Pleistocene sea level stack. Clim Past 12:1079–1092. doi: 10.5194/cp-12-1079-2016

Stein U, Alpert P (1993) Factor separation in numerical simulations. J Atmos Sci 50(14):2107–2115

Stuiver M, Reimer PJ (1993) Extended ^{14}C database and revised CALIB radiocarbon calibration program, Radiocarbon, 35, 215–230

Trigo RM, Pozo-Vazquez D, Osborn TJ, Castro-Díez Y, Gamiz-Fortis S, Esteban-Parra MJ (2004) North Atlantic oscillation influence on precipitation, river flow and water resources in the Iberian peninsula. Int J Climatol 24:925–944. doi: 10.1002/joc.1048

Trigo RM, Valente MA, Trigo I F, Miranda PMA, Ramos AM, Paredes D, García-Herrera R (2008) The Impact of North Atlantic Wind and Cyclone Trends on European Precipitation and Significant Wave Height in the Atlantic. Ann N Y Acad Sci 1146:212–234. doi: 10.1196/annals.1446.014

Tzedakis PC (2010) The MIS 11 – MIS 1 analogy, southern European vegetation, atmospheric methane and the "early anthropogenic hypothesis." Clim Past 6:131–144. doi: 10.5194/cp-6-131-2010

Tzedakis PC Roucoux, KH, de Abreu L, Shackleton NJ (2004) The Duration of Forest Stages in Southern Europe and Interglacial Climate Variability. Science 306:2231–2235. doi: 10.1126/science.1102398

Tzedakis PC, Channell JET, Hodell DA, Kleiven HF, Skinner LC (2012) Determining the natural length of the current interglacial. Nat Geosci 5:138–141. doi: 10.1038/ngeo1358

Tzedakis PC, Crucifix M, Mitsui T, Wolff EW (2017) A simple rule to determine which insolation cycles lead to interglacials. Nature 542:427–432. doi: 10.1038/nature21364

Tzedakis PC, Hooghiemstra H, Pälike H (2006) The last 1.35 million years at Tenaghi Philippon: revised chronostratigraphy and long-term vegetation trends. Quat Sci Rev 25:3416–3430. doi: 10.1016/j.quascirev.2006.09.002

Tzedakis PC, Raynaud D, McManus JF, Berger A, Brovkin V, Kiefer T (2009a) Interglacial diversity. Nat Geosci 2:751–755. doi: 10.1038/ngeo660

Tzedakis PC, Pälike H, Roucoux KH, de Abreu L (2009b) Atmospheric methane, southern European vegetation and low-mid latitude links on orbital and millennial timescales. Earth Planet Sci Lett 277:307–317. doi: 10.1016/j.epsl.2008.10.027

van der Wiel AM, Wijmstra TA (1987) Palynology of 112.8–197.8m interval of the core Tenaghi Philippon III, Middle Pleistocene of Macedonia. Review of Palaeobotany and Palynology 52, 89–117

Villanueva J, Pelejero C, Grimalt JO (1997) Clean-up procedures for the unbiased estimation of C_{37} alkenone sea surface temperatures and terrigenous n-alkane inputs in paleoceanography. J Chromatogr A 757:145–151. doi: 10.1016/S0021-9673(96)00669-3

Weirauch D, Billups K, Martin P (2008) Evolution of millennial-scale climate variability during the mid-Pleistocene. Paleoceanography 23:PA3216. doi: 10.1029/2007PA001584

Williams JW, Jackson ST (2003) Palynological and AVHRR observations of modern vegetational gradients in eastern North America. The Holocene 13, 485–497. doi:10.1191/0959683603hl613rp

Yin Q, Berger A (2015) Interglacial analogues of the Holocene and its natural near future. Quat Sci Rev 120:28–46. doi: 10.1016/j.quascirev.2015.04.008p

Yin QZ, Berger A (2010) Insolation and CO_2 contribution to the interglacial climate before and after the mid-brunhes event. Nat Geosci 3(4):243–246

Yin QZ, Berger A (2012) Individual contribution of insolation and CO_2 to the interglacial climates of the past 800,000 years. Clim Dyn 38:709–724. doi: 10.1007/s00382-011-1013-

Chapter 5

Synthesis and future research

SYNTHESIS

The three preceding chapters of this PhD thesis concentrate on two main topics: 1. Interglacial SW European vegetation and climate variability during two key analogues for projected warming, MIS 11 and MIS 31 (Chapter 2 and 3: Oliveira et al., 2016, 2017, respectively), and 2. Climate forcings controlling the regional expression of the best orbital analogues (MIS 11c and MIS 19c) for the current interglacial in SW Europe (Chapter 4: Oliveira et al., under review, Clim Dyn). This synthesis provides a concise overview of the key findings and addresses the research questions put forward in Chapter 1. Moreover, the main conclusions attained in three additional publications, for which I have contributed within the framework of the PhD project, are also provided here.

1. SW European vegetation and climate changes during MIS 11 and MIS 31

As stated before, studying the warmer than present-day climate of MIS 11 and MIS 31 is of particular interest for developing reliable scenarios of future climate-driven change in the fragile Mediterranean landscapes and ecosystems. Moreover, these interglacial stages offer the opportunity to understand the interglacial climate variability under contrasting orbital forcing within and after the Middle Pleistocene Transition (MPT): MIS 31 and MIS 11 belonging to the 41- and 100-ky worlds, respectively. Orbital and suborbital vegetation and climate changes were investigated by performing pollen analysis at centennial resolution on the SW Iberian margin Site U1385, which allowed a direct comparison between terrestrial and marine climatic indicators and therefore the reconstruction of vegetation-based regional atmospheric conditions and their relationships with oceanic temperature variability.

1.1 Orbital-driven variability

The interglacial forest phases of MIS 11 and MIS 31 are characterized by arboreal pollen percentages oscillating between 20 and 55% (Fig. 1), indicating overall warm conditions and moisture availability in SW Iberia. Major shifts between forested and open vegetation conditions (warm/humid-cold periods) within these interglacials reflect the influence of the orbital-scale climatic variability on the SW Iberian vegetation.

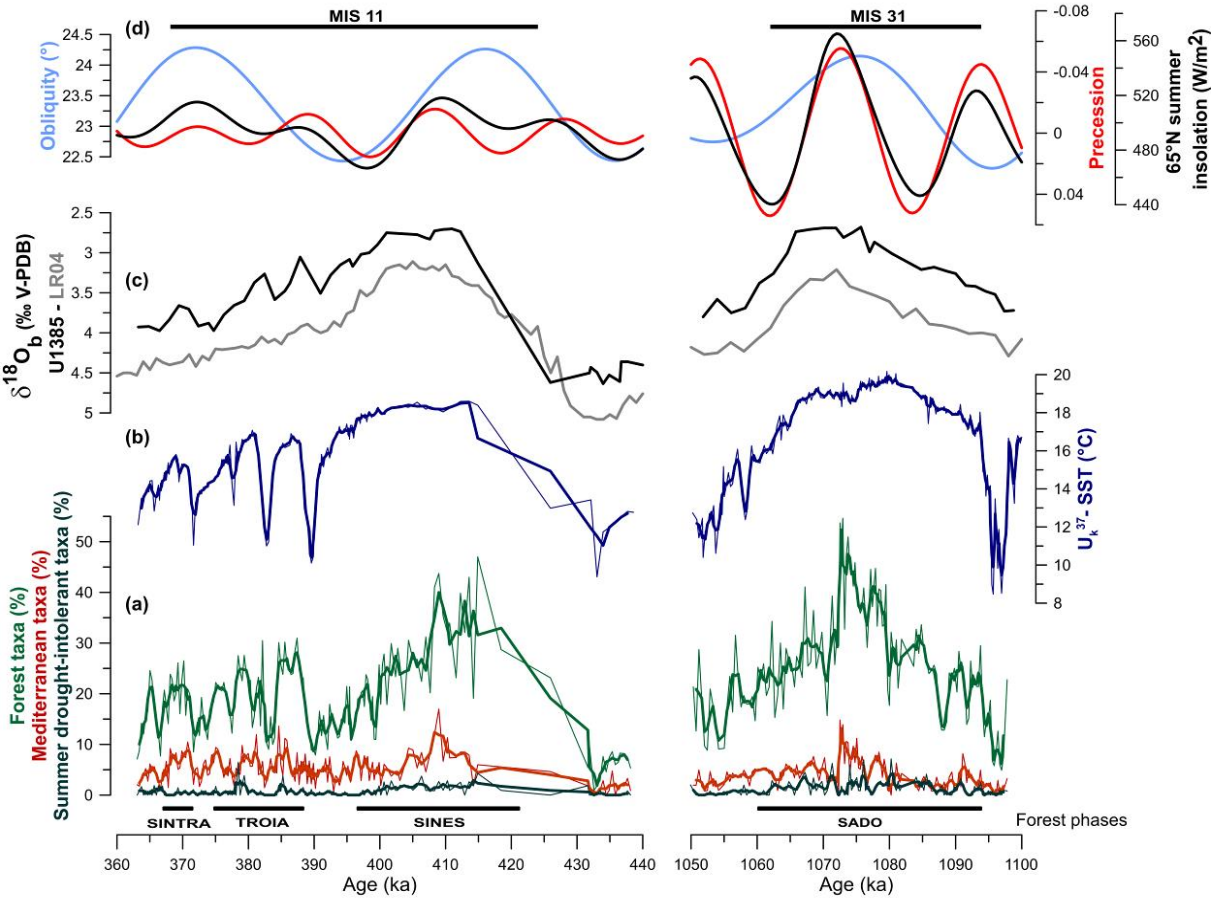

Fig. 1. Long-term vegetation and climatic changes at Site U1385 from MIS 32 to early MIS 30 (Oliveira et al., 2017) and late MIS 12 to early MIS 10 (Oliveira et al., 2016). From bottom to top: Percentages of selected group of taxa: (a) Forest taxa (mainly deciduous *Quercus* and Mediterranean taxa) (green), Mediterranean taxa (red) and summer drought-intolerant taxa (*Carpinus betulus*, *Castanea*, *Corylus*, *Fagus*, *Fraxinus excelsior*-type and *Ulmus*) (dark green). (b) Site U1385 Uk'$_{37}$-SST (blue). Bold lines in (a) and (b) represent 3-point moving averages of data. (c) $\delta^{18}O_b$ records of Site U1385 (Hodell et al., 2015) (black) and LR04 (Lisiecki and Raymo, 2005) (grey); (d) 65°N summer insolation (black), obliquity (blue) and precession (red) parameters (Laskar et al., 2004). SW Iberian forest phases as defined in Oliveira et al. (2016, 2017) and marine isotopic substages (MIS) following Hodell et al. (2015) on bottom and top, respectively.

MIS 11 pollen-based reconstruction shows the response of the vegetation at orbital-scale by detecting a first longest and warmest forest phase (Sines) followed by two forest phases (Troia and Sintra) (Fig. 1). The impact of precession is clearly reflected in the decreasing extent of the three forest maxima, which parallels the magnitude of the three MIS 11 precession minima (Fig. 1). The muted precession forcing of MIS 11, implying less seasonal contrast in SW Iberia, is also noted in the weaker development of the Mediterranean forest and in particular Mediterranean taxa as compared to younger interglacials marked by large precession variations such as during the MIS 5 (Sánchez Goñi et al., 1999).

Considering the strong imprint of precession on the Mediterranean vegetation south of 40°N (e.g. Sánchez Goñi et al., 2008; Oliveira et al., 2016) and the extreme precession forcing of MIS 31, a pronounced development of the forest and Mediterranean taxa was likely to be expected during this stage. However, Site U1385 pollen record reveals that the SW Iberian counterpart of MIS 31 (Sado) does not display an outstanding maximum in temperate forest extent in comparison with other interglacials of the middle-to late Pleistocene, including the ones marked by muted precession changes such as MIS 11 (Fig. 1, Appendix B: Desprat et al, in press). Moreover, given MIS 31 orbital forcing the vegetation composition reveals an unexpected weak Mediterranean character. This is shown by the development of diverse summer drought-intolerant trees and relatively low expansion of Mediterranean taxa (Fig. 1), which reflect a temperate and humid climate regime with reduced seasonality. These observations together with cross-correlation analysis suggest that MIS 31 high precession forcing was dwarfed by the dominant influence of obliquity on the forest development and composition. In line with recent modeling experiments (Bosmans et al., 2015), the predominance of obliquity forcing may have contributed to a reduction in the summer dryness with consequent decrease in the seasonal contrast over the SW Iberian region. Even though obliquity plays a dominant role on the forest development, Ericaceae (heathland) and the fern ally *Isoetes* display a clear precession signal throughout MIS 31 that may relate to a specific response to rainfall seasonality.

The comparison between MIS 11 and MIS 31 reconstructions provides the first evidence for prevailing precession and obliquity-driven vegetation and climatic changes during the interglacials of the 100-ky and 41-ky worlds, respectively, in SW Iberia, a region highly sensitive to precession. In addition, this research reveals that atmospheric and surface oceanic temperatures during MIS 11 and MIS 31 were not exceptionally high in this region (Fig. 1), unlike other locations at higher latitudes, such as the Arctic, where these stages were recognized as "super interglacials" (Melles et al., 2012). Additionally, it is also significant the finding that both stages were characterized by a long duration, although the low sedimentation rate between Termination V and early MIS 11 hampers the precise determination of its length. In particular, Site U1385 multiproxy reconstruction shows that MIS 31 was a 34 ky-long interglacial in the SW Iberia region (Fig. 1), with interglacial conditions starting several thousand years prior to the assigned onset for MIS 31 of Lisiecki and Raymo (2005). This early onset of this interglacial partially echoes recent studies suggesting that the boundaries of MIS 31 should be revised as the warming appears to span the interval from MIS 33 to MIS 31 (Teitler et al., 2015; de Wet et al., 2016). More research is required to confirm whether this is a regional or global feature as it may offer new insights into the duration of interglacials of the 41-ky world and of the MPT.

1.2 Origin and diversity of millennial-scale changes

Superimposed on the long-term variability, the highly resolved pollen records from Site U1385 reveal persistent variability with multiple millennial to- centennial scale shifts in vegetation throughout MIS 11 (Oliveira et al., 2016) and MIS 31 (Oliveira et al., 2017) (Fig. 2). These vegetation changes represent recurring cool/cold and dry atmospheric episodes, which have hitherto not been identified in SW Iberia. The direct comparison between atmospherically-driven vegetation and oceanic changes allows the characterization of different types of millennial-scale cooling events across distinct boundary conditions (Fig. 2). This work proposes that the diversity and complexity of millennial coolings in SW Europe relies on atmospheric and oceanic processes whose predominant role likely depends on baseline climate states.

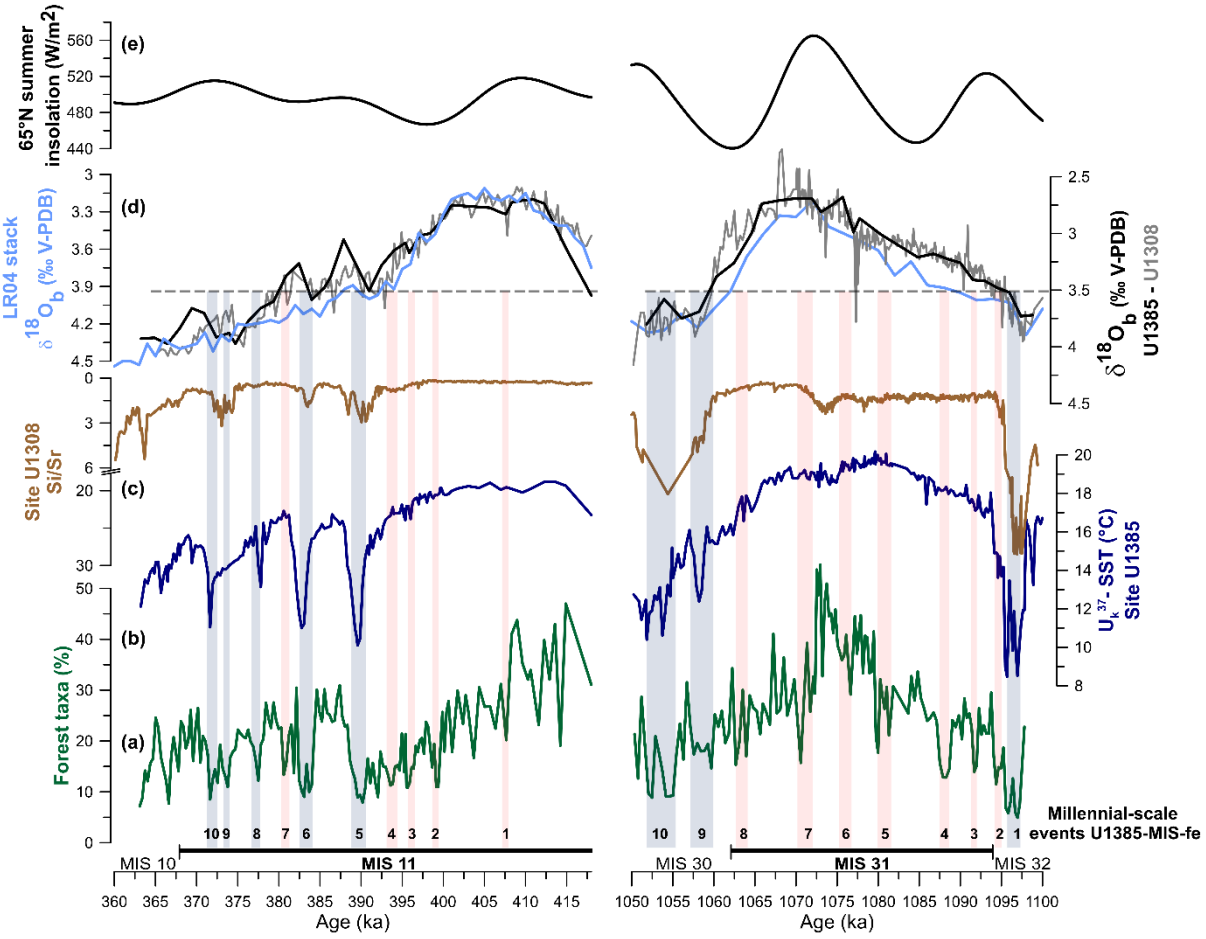

Fig. 2. Millennial-scale variability in the SW Iberia region between MIS 32 and early MIS 30 (Oliveira et al., 2017) and during MIS 11 (Oliveira et al., 2016) in the context of North Atlantic and insolation changes. From the bottom to the top: (a) pollen percentage curves of forest taxa (green); (b) Uk'$_{37}$-SST of Site U1385 (blue); (c) IRD discharges inferred from the Si/Sr ratio of Site U1308 (Hodell et al., 2008) (brown); (d) $\delta^{18}O_b$ records of Site U1385 (Hodell et al., 2015) (black), Site U1308 (Hodell et al., 2008) (grey) and LR04 (Lisiecki and Raymo, 2005) (light blue). Dashed line designates the ice volume threshold of McManus et al. (1999). (e) 65°N summer insolation (Laskar et al., 2004) (black). MIS following Hodell et al. (2015) on bottom. Numbered bands mark the millennial-scale forest decline events labeled as following: Site U1385 - MIS (Marine Isotopic Stage) - number of the event. Blue bands (U1385-32-fe1, -30-fe9, -30-fe10, -11-fe5, -11-fe6, -11-fe8 to -fe10) indicate the atmospheric and oceanic cooling events during large ice volume conditions, while pink bands (U1385-32-fe2 to -31-fe8, -11-fe1 to -fe-4, -11-fe-7) represent the land-sea decoupling during interglacial ice volume minimum and the glacial inception.

1.2.1 Atmospheric and oceanic cooling during large ice volume conditions

The most severe and longer forest decline events, U1385-32-fe1, -30-fe-10, -11-fe5, -11-fe6 and -11-fe10, reflect the coldest and driest atmospheric conditions and are synchronous with strong drops in SSTs down to ~8.5-10°C off SW Iberia (Fig. 2). These extreme events appear to be related with millennial-scale cooling events in the North Atlantic, associated with lithic evidence of iceberg discharges (Fig. 2) and changes in the Atlantic Meridional Oceanic Circulation (AMOC). Moreover, the direct land-sea comparison at Site U1385 reveals that once the 3.5‰ threshold in the $\delta^{18}O_b$ record is exceeded, the intensity and duration of the Iberian cooling and drying events increase not only in the 100-ky world but also in the 41-ky world (Fig. 2). These findings agree with the view that millennial-scale variability throughout the Pleistocene is amplified when ice sheets surpass a critical size (e.g. Raymo et al., 1998; McManus et al., 1999; Hodell et al., 2015), although $\delta^{18}O_b$ variations are not only influenced by ice volume (e.g. Skinner and Shackleton, 2005).

The impact of these high intensity events in SW Iberian ecosystems bear significant similarities to some of the last glacial Heinrich stadials (HS), although they are probably associated with European iceberg discharges into the North Atlantic rather than from the Hudson Strait as the "classic" HS. By analogy to the HS, the drastic events detected at Site U1385 may be linked to atmospheric and oceanic impacts of ice-rafting episodes that led to the intensification and northward displacement of the westerlies with consequent cooling and drying over the SW Iberian region (e.g. Sánchez Goñi et al., 2002).

The forest decline events U1385-30-fe9, -11-fe8 and -11-fe9 also occurred when ice sheets exceeded a critical size (i.e., benthic $\delta^{18}O_b$ >3.5‰), however they are characterized by weaker forest reductions, reflecting less intense cooling and drying episodes on land (Fig. 2). Moreover, while the events U1385-30-fe9 and -11-fe8 are associated to a moderate SST cooling and no evidence for iceberg discharge or change in AMOC, the event -11-fe9 does not appear related to any change in the marine realm (Fig. 2). Thus, although high-latitude ice sheet instability likely produces an amplification of vegetation and climate changes in SW Europe, this research further shows that it is not a straightforward predictive "rule", which underlines the complexity of millennial-scale variability.

1.2.2 Land-sea decoupling during ice volume minimum and the glacial inception

Site U1385 pollen record reveals that a series of millennial-scale cooling and drying events punctuated MIS 11 and MIS 31, U1385-32-fe-2 to -31-fe-8, -11-fe1 to -fe-4 and -11-fe7, during intervals of minimum to intermediate ice volume state ($\delta^{18}O_b$ <3.5‰) (Fig. 2). However, none of these forest decline events has a counterpart in the SST profile from Site U1385 or is associated to a SST cooling in the mid-to-high latitudes of the North Atlantic neither to ice rafting episodes or AMOC perturbation (Fig. 2), suggesting that the observed millennial air-sea contrast is not primarily related to high-latitude ice sheet dynamics.

For MIS 11 events, a first explanation has been proposed associating the air-sea decoupling to a frequent positive mode of NAO-type circulation, which increased dryness in Iberia but affected weakly the local SSTs because of the prevailing influence of subtropical waters (Oliveira et al., 2016). Spectral analyses were subsequently carried out on both MIS 11 and MIS 31 pollen-based forest records to identify potential climatic cyclicities and explore the nature of the intra-interglacial variability. These analyses revealed a dominant cyclicity around 10 ky during MIS 11 (Fig. 3) and around 6 ky during MIS 31 (Oliveira et al., 2017), which are probably linked to the second and fourth harmonic of the precessional component of the insolation forcing (11 and 5.5 ky cycles, respectively) (Berger et al., 2006). Because low-latitudes receive twice the maximum amount of daily irradiation over the course of the year than higher latitudes, they generate a larger latitudinal thermal gradient that results in enhanced poleward transport of heat and moisture by either atmospheric (westerlies) or oceanic circulation (subtropical gyre) (Short et al., 1991; McIntyre and Molfino, 1996; Berger et al., 2006). It is hypothesized, therefore, that the atmospherically-driven forest decline events with no concurrent change in the warm subtropical gyre throughout MIS 11 and MIS 31 may have been driven by the impact of low-latitude forcing on the direction and intensity of the atmospheric westerlies transporting warmth and moisture to the high-latitudes drying the SW Iberian region (Fig. 4). The absence of significant suborbital periodicities in the SST record at Site U1385 may be explained by the persistent influence of the subtropical waters at the Iberian margin, which likely dwarfed the impact of a precessional-related cyclicity on local SSTs.

A particularly interesting feature is that the strongest forest declines marking the end of the forest "optimum" during MIS 31 and MIS 11, U1385-31-fe7 and -11-fe11, occur during ice volume minimum conditions (Fig. 2). These findings demonstrate that dramatic forest contractions in SW Iberia can occur due to hydrological forcing originating in the low-latitudes under globally warm conditions. This increased dependence of Iberian vegetation on water availability is a key characteristic of the Mediterranean-type ecoregions within the context of the present climate (Gouveia et al., 2008, 2016). In addition, the observed decouplings between cold-dry air and warm SST during periods of ice growth appear as important amplifiers of the glacial inception by increasing the regional moisture that is transported northward through intensified storm tracks. As suggested by recent works for the glacial inceptions after the MPT, dominated by 100 ky ice-volume variations (e.g. Sánchez Goñi et al., 2013, 2016a; Cortina et al., 2015), this would have increased the accumulation of snow necessary for the build-up of ice sheets at high-latitudes, which along with the decrease in boreal summer insolation favoured the glaciations. This research underlines the importance of the low-latitude forcing in the North Atlantic millennial-scale variability regardless of the baseline climate states of the 100- and 41-ky worlds.

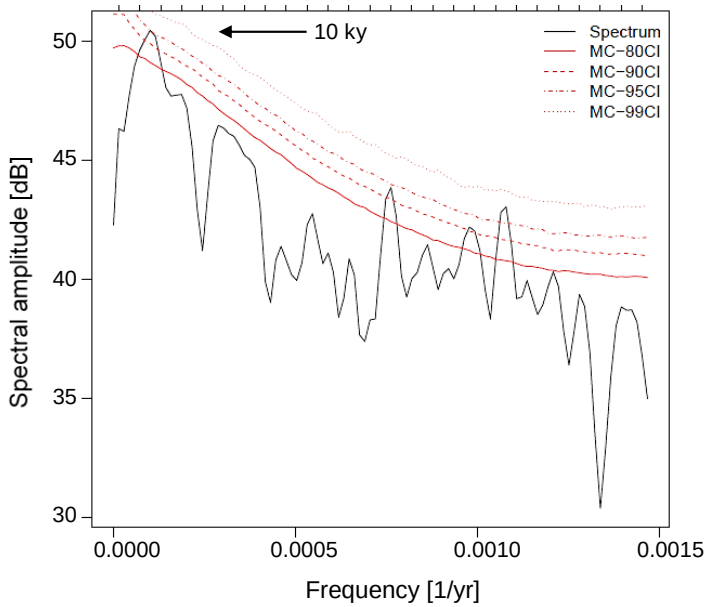

Fig. 3. Spectral analysis (smoothed Lombe Scargle peridogram with 8 degrees of freedom) (Schulz and Mudelsee, 2002) of the MIS 11 Mediterranean forest pollen percentages on the LR04-based chronology (unpublished data). Dashed lines represent the significance levels (CL).

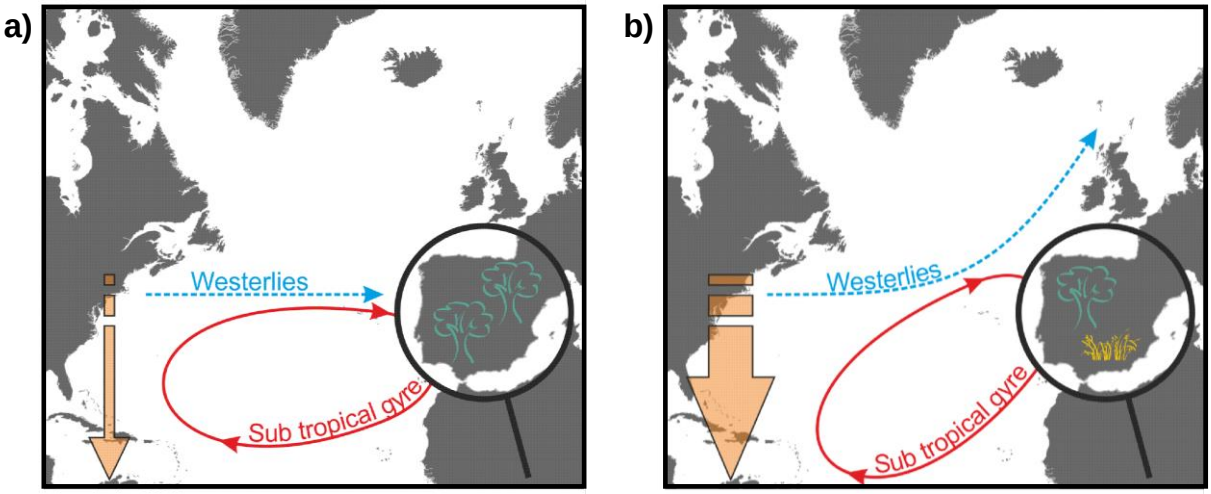

Fig. 4. Schematic representation of the vegetation in the Iberian Peninsula, atmospheric and surface ocean circulations (blue and red arrow, respectively) and latitudinal temperature gradient (orange arrow) in the North Atlantic during a) MIS 11 and MIS 31 forest expansions indicating a zonal configuration of the westerlies and increasing regional precipitation over SW Iberia. b) MIS 11 and MIS 31 millennial-scale forest reductions associated to a land-sea decoupling driven by low-latitude insolation forcing, which probably led to meridional tilts in the westerlies and consequent drying in SW Iberia. (after Desprat et al., in press)

2. Climatic forcings controlling the regional expression of the best orbital analogues (MIS 11c and MIS 19c) for the current interglacial in SW Europe

The interest in MIS 11c and MIS 19c interglacials largely stems from their close orbital analogy with the current interglacial owing to the similarly low values of the eccentricity of Earth's orbit, which led to low-amplitude precessional changes and subdued insolation variations. In Chapter 4 (Oliveira et al., under review, Clim Dyn), the suitability of MIS 11c and MIS 19c as analogues of the Holocene in SW Europe was evaluated and the contributions of the primary forcings (insolation and CO_2) to vegetation and climate changes were explored. This was achieved by performing the first model-data intercomparison between the Holocene and MIS 11c and MIS 19c in SW Iberia. Regional climate snapshot and transient experiments using the LOVECLIM model focusing on the climate "optimum" and the entire interglacial periods, respectively, were compared with new and published terrestrial–marine climate profiles of MIS 1 (Chapter 4), MIS 11c (Chapter 2) and MIS 19c (Sánchez Goñi et al., 2016a) from Site U1385. Proxy-based reconstructions included the high-resolution records of pollen-

based vegetation and atmospheric changes directly compared with alkenone derived-SST changes.

The pollen-based reconstructions show a large discrepancy in forest extent between the forest optimum of MIS 1 and the ones of MIS 11c and MIS 19c, likely reflecting differences in wintertime precipitation which are critical for the Mediterranean forest expansion, and in turn depend on the direction and intensity of the westerlies. These findings demonstrate that MIS 11c and MIS 19c cannot be considered as straightforward analogues for the Holocene "optimum" when considering the vegetation and climatic variability in the SW Europe, south of 40°N.

The results of snapshot simulations confirm a discrepancy in terms of forest expansion at MIS 11c and the Holocene "optimum", with lower and higher forest extent, respectively. We find that these forest differences may be attributed to MIS 11c lower obliquity that generated an amplified latitudinal insolation and thermal gradient between low and high-latitudes during MIS 11c "optimum". This would have favoured the strengthening and northward displacement of the westerlies that led to decreased large-scale winter precipitation in SW Iberia at MIS 11c peak.

Both snapshot and transient simulations exhibit, however, insignificant differences in the tree fraction at the peak of the Holocene and MIS 19c, which contrast with expectations based on Site U1385 pollen records reconstructing a much higher forest cover for MIS 1. The main cause of these large data-model mismatches is probably linked to the absence of ice sheet forcing in the model, which fixed the ice sheets to their present values. We put forward that MIS 19c larger Eurasian ice sheet development and its relatively higher ice volume baseline conditions compared to the Holocene may have influenced the position and strength of the mid-latitude North Atlantic storm track. This would have ultimately triggered the lower winter precipitation and tree fraction at MIS 19c peak in the SW of Iberian Peninsula.

Based on the good agreement between the pollen-based and transient simulations with time-varying insolation and CO_2 during the entire periods of the three interglacials, it was demonstrated that the forest development over SW Iberia is highly correlated with warm summer temperatures and high precipitation during the winter season. In addition, our model-data comparison reveals that these climate parameters in the studied region are primarily driven by precession, with no noticeable relationship with CO_2.

As far as the intra-interglacial instability in SW Iberia is concerned, this study not only confirms previous hypotheses put forward in Chapter 2 and 3 but also provides additional insights. In agreement with the pollen-based reconstructions at Site U1385, the transient simulations of three interglacials reproduce persistent millennial-scale variability in the tree fraction. Moreover, the model experiments confirm that these millennial-scale forest declines are mainly caused by dry atmospheric episodes during winter. As previously hypothesized (see above 1.2.2), the results of the transient simulations also testify that the orbital forcing is sufficient to drive the intra-interglacial variability since ice sheet-climate interactions were neglected in the model simulations. This model-data comparison strengthens, therefore, the suggestion of a low-latitude origin in the observed cold land–warm sea decouplings at millennial timescales in the SW Iberia.

Besides this, it is impressive that the transient experiments are able to reproduce the major forest declines marking the end of the three interglacial "optima" during low ice volume conditions, such as observed during MIS 31 (see above 1.2.2). Because these forest events appear more gradual in the model simulations, it must be acknowledged that the interaction between long-term and millennial-scale climate variability should be further investigated as it may act as an amplifier of the vegetation and climate response.

3. Main findings of the co-authored publications of relevance to the thesis

Sánchez Goñi et al. (2016b) and Eynaud et al. (2016) were published in the Global and Planetary Change Virtual special issue on IODP Expedition 339: The Mediterranean outflow.

Sánchez Goñi et al. (2016b) present grain size and physical property data at three sites from the Gulf of Cadiz (Sites U1388, U1389 and U1390) and compare results with pollen and oxygen isotope data from Site U1385 for two contrasting intervals: MIS 31–30 and MIS 12–11. This study shows that the interval from ~1.1–1.05 Ma (MIS 32–MIS 30) before the MPT (MPT, ~0.9–0.65 Ma, Maslin and Ridgwell, 2005) was marked by wetter climate and weaker bottom current than the interval from 0.47–0.39 Ma (MIS 12–MIS 11), after the MPT. Increasing dryness on land during interglacial to glacial transitions and stronger regional aridity during MIS 12 coincided with an increase in grain size interpreted to represent

stronger Mediterranean Outflow Water (MOW), supporting a link between aridification in the Mediterranean region and MOW intensity.

Eynaud et al. (2016) provide an important dataset of understudied dinoflagellate cyst populations in cores from the Iberian Margin (Site U1385), Gulf of Cadiz and Alboran Sea. This work compares dinoflagellate cysts from several of the past interglacials (MIS 1, 5, 11 and 19). Comparison between the dinocyst bio-indicator observations and other proxy-based reconstructions from the same sequences are performed to evaluate the synchronicity of the marine biota response, as well as the direct comparison between the marine biota and pollen-based terrestrial ecosystem responses. The dinocyst populations were similar on both sides of the Strait of Gibraltar indicating a persistent interchange of populations between the Atlantic and Mediterranean even during sea-level low stands.

Desprat et al. (in press) is accepted for publication in Quaternaire. This study highlights the interest of applying a direct land-sea comparison approach to understand the climatic system. It focuses on the regional expression of the interglacials of the last 800 ky in SW Europe, and it highlights their diversity in terms of duration as well as vegetation and climatic variability, in particular in SW Iberia where changes in precipitation play an important role. This work additionally allows discussing mechanisms involved in glacial inception during orbital analogues of the current interglacial, i.e. MIS 11c (Oliveira et al. 2016) and MIS 19c (Sánchez Goñi et al. 2016a).

FUTURE RESEARCH AND RECOMMENDATIONS

The work presented in this thesis provides a number of new and important insights into the interglacial vegetation and climate dynamics of the 41- and 100-ky worlds in a major "climate change hot spot", the Mediterranean region, and the processes triggering the entering in glaciation. Yet, as often occurs in research, the long process that led to these insights has triggered additional questions that remain to be elucidated. This section is focused on questions that emerged through this PhD project and provides some recommendations for future research.

The chronology of the proxy-based climatic records from Site U1385 is as accurate as present tools allow. In addition, the main conclusions of this research were based on a direct land-sea comparison approach, being therefore independent of the timescale chosen. However, the studies of Site U1385, including the ones present here, would greatly benefit from the improvement of the age models proposed by Hodell et al (2015), in particular between Termination V and early MIS 11 when a condensed section/brief hiatus is suspected. As an example, the LR04-derived chronology could be easily refined by increasing the temporal resolution (20 cm) of the benthic $\delta^{18}O$ record of Site U1385. Similarly, the improvement of the MIS 1 chronology could be achieved by increasing the number of AMS radiocarbon dates.

Although the generated pollen data have proven their ability and efficiency in reconstructing the regional vegetation and terrestrial climate, this thesis research could be complemented in the future by performing quantitative climatic reconstructions based on the pollen dataset using, for instance, the modern analogue technique (MAT). This method considers the relative proportion of the different taxa in each pollen spectrum (Guiot, 1990) and allows reconstructing climate parameters such as the annual, winter and summer temperatures (TANN, MTCO, MTWA) and precipitation (Pann, Pwin, Psum). These quantitative estimations will be particularly important to test if the climate models succeed in reproducing the pollen-based quantitative climatic reconstructions.

In addition, future work should focus on the integration of all datasets from Site U1385, including the ones that are currently in progress:

- Microcharcoal analyses. Microcharcoal is a terrestrial proxy of fire activity at regional scale (Daniau et al., 2007) that is being analyzed on the same sample set used in this thesis and, therefore, can be used as a complementary indicator of summer and winter dryness.

- Site U1385 profiles of ice-rafted debris concentration and benthic $\delta^{13}C$. The integration of pollen data with these records will be particularly important to better characterize Heinrich-type events and assess deep-water circulation changes as recorded by the relative influence of NADW and Antarctic bottom water along the Iberian margin. This would give further support to the hypotheses put forward in this thesis regarding the impacts of high-latitude ice sheet dynamics on the changes in vegetation and climate in SW Europe.

- Dinocyst analysis and quantifications. Complementary sea-surface reconstructions will be obtained from the analysis of this group of microfossils, which is one of the rare tracers giving access to both seasonal SST and surface hydrological parameters such as sea surface salinity and productivity.

The understanding of interglacial climate is strongly biased by the large body of evidence of the middle-to late Pleistocene, therefore one of the most obvious recommendations for future work is to extend this research into other interglacials of the 41-ky world and the transition into the 100-ky world, the intriguing Middle Pleistocene Transition. This would allow testing if the differences reported here between MIS 31 and MIS 11 are also observed when comparing other interglacials of the 41- and 100-ky worlds. In particular, the investigation of interglacials displaying contrasting baseline climate states (insolation/orbital parameters, ice sheet extent and GHG) or intensities (cool versus warm) from both 41- and 100-ky worlds would improve and extend available knowledge on the forcings controlling the character of vegetation and climate changes in SW Europe at orbital and millennial timescales.

As the duration of MIS 31 warming is one of the essential pieces for understanding the interglacials of the 41-ky world, this study should be extended to encompass the entire interval between MIS 33 and MIS 31, recently suggested to be one unique 52-ky long interglacial. This would provide valuable insights into the duration of interglacials within the

MPT. Furthermore, it could increase the understanding about the boundary conditions and mechanisms requested to produce exceptionally long interglacials, and the relationship between the interglacial duration and intensity.

In the course of this PhD research it was recognized the need for other high-resolution studies from strategically located regions. This would be particularly important to support and develop the hypotheses put forward in this thesis involving the impact of latitudinal thermal contrast on the dynamics of the temperate westerlies and NAO-type circulation, which in turn play a major role on the atmospherically-driven vegetation changes. Thus, it would be crucial to examine:

- Palaeoclimate data from key geographic locations in the low and northern latitudes of the North Atlantic allowing to assess latitudinal temperate gradients influencing the SW European hydrological changes. In particular, this may provide key information for better understanding the intra-interglacial climate variability related to low-latitude variations in the seasonal insolation cycle driven by the precession and its harmonics.

- High-resolution records allowing a direct land-sea comparison from other regions sensitive to the temperate westerlies and related North Atlantic storm track such as the western subtropical North Atlantic and higher latitudes than the SW European margin in both the eastern and western North Atlantic.

Comparison of the millennial-scale changes detected in the aforementioned key regions would shed more light into the relationship of SW European climate variability with high and low-latitude forcing depending on the baseline climate states. In addition, it would allow a better understanding of the processes behind the intra-interglacial variability and in particular those controlling the interglacial climate optimum and hastening the glacial inception. This will be, however, a challenging task due to chronological uncertainties, differences in time resolution, biasing in spatial sampling, precise interpretation of the proxy, etc.

Finally, the integration of proxy-based reconstructions from Site U1385 with climate models has greatly improved the knowledge regarding the forcings modulating the interglacial intensity and the vegetation and climate changes at both long and short term in SW Europe. The interaction with the palaeoclimate modelling community needs to be, therefore, reinforced and future work in this context should (1) include dynamical ice sheets

in the models accounting for changes in ice sheet topography and related albedo and freshwater fluxes; and (2) focus on a model-data comparison during other Quaternary interglacials and in particular on the poorly known interglacials of the 41-ky world and of the MPT. Hopefully, this will lead to an improved understanding of the interaction of millennial- and orbital-scale interglacial climate variability under different baseline climate states.

References for Chapters 1 and 5

REFERENCES for Chapters 1 and 5

Abrantes, F., Lebreiro, S., Rodrigues, T., Gil, I., Bartels-Jonsdottir, H., Oliveira, P., Kissel, C. and Grimalt, J.O., 2005. Shallow-Marine sediment cores record climate variability and earthquake activity off Lisbon (Portugal) for the last 2000 years, Quaternary Science Reviews, 24, 2477-2494.

Alcara Ariza, F., Asensi Marfil, A., de Bolos y Capdevilla, O., Costa Tales, M., Arco Aguilar, M., Diaz Gonzales, T.E., Diez Garretas, B., Fernandez Prieto, J.A., Fernandez Gonzales, F., Izco Sevillando, J., Loidi Arregui, J., Martinez Parras, J.M., Navarro Andres, F., Ninot I Sugranes, J.M., Peinado Lorca, M., Rivas Martinez, S., Sanchez Mata, D., Valle Guitierrez, C., Vigo I Bonada, J., Wildpret de la Torre, W., 1987. La vegetacion de Espana. Collection Aula Abierta. Universidad de Alcala de Henares, 544 pp.

Alley, R., Ágústsdóttir, A.M., 2005. The 8k event: cause and consequences of a major Holocene abrupt climate change. Quaternary Science Reviews 24, 1123–1149.

Alonso-Garcia, M., Sierro, F.J., Kucera, M., Flores, J.A., Cacho, I., Andersen, N., 2011. Ocean circulation, ice sheet growth and interhemispheric coupling of millennial climate variability during the mid-Pleistocene (ca 800–400 ka). Quaternary Science Reviews 30, 3234–3247. doi:10.1016/j.quascirev.2011.08.005

Ambar, I., Howe, M.R., 1979. Observations of the Mediterranean Outflow: 1. Mixing in the Mediterranean Outflow, Deep Sea Res., Part A, 26(5), 535–554.

Anav, A., Mariotti, A., 2011. Sensitivity of natural vegetation to climate change in the Euro-Mediterranean area. Climate Research 46, 277–292. doi:10.3354/cr00993.

Bakker, P., Masson-Delmotte, V., Martrat, B., Charbit, S., Renssen, H., Gröger, M., Krebs-Kanzow, U., Lohmann, G., Lunt, D.J., Pfeiffer, M., Phipps, S.J., Prange, M., Ritz, S.P., Schulz, M., Stenni, B., Stone, E.J., Varma, V., 2014. Temperature trends during the Present and Last Interglacial periods – a multi-model-data comparison. Quaternary Science Reviews 99, 224–243. doi:10.1016/j.quascirev.2014.06.031

Bakker, P., Stone, E.J., Charbit, S., Gröger, M., Krebs-Kanzow, U., Ritz, S.P., Varma, V., Khon, V., Lunt, D.J., Mikolajewicz, U., Prange, M., Renssen, H., Schneider, B., Schulz, M., 2013. Last interglacial temperature evolution – a model inter-comparison. Climate of the Past 9, 605–619. doi:10.5194/cp-9-605-2013.

Bard, E., Rostek, F., Turon, J. L., Gendreau, S., 2000. Hydrological impact of Heinrich events in the subtropical northeast Atlantic. Science 289(5483), 1321-1324. doi:10.1126/science.289.5483.1321.

Barker, S., Chen, J., Gong, X., Jonkers, L., Knorr, G., Thornalley, D., 2015. Icebergs not the trigger for North Atlantic cold events. Nature 520, 333–336. doi:10.1038/nature14330.

Barker, S., Knorr, G., Edwards, R.L., Parrenin, F., Putnam, A.E., Skinner, L.C., Wolff, E., Ziegler, M., 2011. 800,000 Years of Abrupt Climate Variability. Science 334, 347–351. doi:10.1126/science.1203580.

Bassinot, F.C., Labeyrie, L.D., Vincent, E., Quidelleur, X., Shackleton, N.J., Lancelot, Y., 1994. The astronomical theory of climate and the age of the Brunhes-Matuyama magnetic reversal. Earth and Planetary Science Letters 126, 91–108.

Bendle, J., Rosell-Melé, A., 2004. Distributions of U^{k}_{37} and $U^{k'}_{37}$ in the surface waters and sediments of the Nordic Seas: Implications for paleoceanography. Geochemistry, Geophysics, Geosystems 5, n/a-n/a.

Bennett, K.D., 2000. Psimpoll and pscomb: computer programs for data plotting and analysis. Uppsala, Sweden: Quaternary Geology, Earth Sciences, Uppsala University. Software available on the internet at http://www.kv.geo.uu.se.

Berger, A. and Loutre, M.F., 2004. Theorie astronomique des paleoclimats. Comptes Rendus Geoscience, 336, 701-709.

Berger, A., 1975. The astronomical theory of paleoclimates: A cascade of accuracy. Proceedings of the WMO-IAMAP Symposium on Long-Term Climatic Fluctuations, 421, 65-72.

Berger, A., 1978. Long-Term variations of daily insolation and Quaternary climatic changes. Journal of Atmospheric Science, 35, 2362–2367.

Berger, A., 2001. The role of CO_2, sea-level and vegetation during the Milankovitch forced glacial-interglacial cycles. Geosphere-Biosphere Interactions and Climate, Cambridge University Press, New York, 119-146.

Berger, A., and Loutre, M. F., 1992. Astronomical solutions for paleoclimate studies over the last 3 million years, Earth Planet. Sci. Lett., 111,369–382.

Berger, A., Loutre, M. F., Yin, Q. Z., 2010. Total irradiation during any time interval of the year using elliptic integrals, Quat. Sci. Rev., 29(17–18), 1968–1982, doi:10.1016/j.quascirev.2010.05.007.

Berger, A., Loutre, M.F., 1996. Modelling the climate response to astronomical and CO_2 forcings. C. R. Acad. Sci. Paris 323, 1-16.

Berger, A., Loutre, M.F., 2002. An exceptionally long interglacial ahead? Science 297, 1287–1288.

Berger, A., Loutre, M.F., 2003. Climate 400,000 years ago, a key to the future? In: Droxler, A., Burckle, L., Poore, A. (Eds.), Earth Climate and Orbital Eccentricity: the Marine Isotope Stage 11 Question, Geophysical Monograph, vol. 137. American Geophysical Union, pp. 17-26.

Berger, A., Loutre, M.F., Mélice, J.L., 2006. Equatorial insolation: from precession harmonics to eccentricity frequencies. Climate of the Past 2, 131–136. doi:10.5194/cp-2-131-2006.

Berger, M., and Loutre, M.F., 1994. Precession, eccentricity, obliquity, insolation and paleoclimates. NATO ASI Series, Long-Term Climatic Variations, 1(22), 145-145.

Bigler, M., Röthlisberger, R., Lambert, F., Wolff, E.W., Castellano, E., Udisti, R., Stocker, T.F., Fischer, H., 2010. Atmospheric decadal variability from high-resolution Dome C ice core records of aerosol constituents beyond the Last Interglacial. Quaternary Science Reviews 29, 324–337. doi:10.1016/j.quascirev.2009.09.009.

Billups, K., Chaisson, W., Worsnopp, M., Thunell, R., 2004. Millennial-scale fluctuations in subtropical northwestern Atlantic surface ocean hydrography during the mid-Pleistocene. Paleoceanography 19(2), PA2017. doi:10.1029/2003pa000990.

Billups, K., Rabideaux, N., Stoffel, J., 2011. Suborbital-scale surface and deep water records in the subtropical North Atlantic: implications on thermohaline overturn. Quaternary Science Reviews 30, 2976–2987. doi:10.1016/j.quascirev.2011.06.015.

Billups, K., Scheinwald, A., 2014. Origin of millennial-scale climate signals in the subtropical North Atlantic. Paleoceanography 29, 612–627. doi:10.1002/2014PA002641.

Bintanja, R., van de Wal, R.S.W., Oerlemans, J., 2005. Modelled atmospheric temperatures and global sea levels over the past million years. Nature 437, 125–128. doi:10.1038/nature03975.

Birks, H., Birks, H., 1980. Quaternary palaeoecology. London: Edward Arnold.

Birner, B., Hodell, D.A., Tzedakis, P.C., Skinner, L.C., 2016. Similar millennial climate variability on the Iberian margin during two early Pleistocene glacials and MIS 3. Paleoceanography 31, 203–217. doi:10.1002/2015PA002868.

Blanco Castro, E., Casado González, M.A., Costa Tenorio M., Escribano Bombín, R., García Antón, M., Génova Fuster, M., Gómez Manzaneque, F., Moreno Sáiz, J.C., Morla Juaristi, C., Regato Pajares, P., Sáiz Ollero, H., 1997. Los bosques ibéricos: una Interpretación Geobotánica. Editorial Planeta, 572 p., Barcelona.

Bosmans, J.H.C., Drijfhout, S.S., Tuenter, E., Hilgen, F.J., Lourens, L.J., Rohling, E.J., 2015. Precession and obliquity forcing of the freshwater budget over the Mediterranean. Quaternary Science Reviews 123, 16–30. doi:10.1016/j.quascirev.2015.06.008.

Bottema, S. and van Straaten, L.M.J.U., 1966. Malacology and palynology of two cores from the Adriatic sea floor. Marine Geolology, 4: 553-564.

Bradshaw, R.H.W., Webb, T., 1985. Relationships between Contemporary Pollen and Vegetation Data from Wisconsin and Michigan, USA. Ecology 66, 721–737. doi:10.2307/1940533.

Brauer, A., Allen, J.R.M., Mingram, J., Dulski, P., Wulf, S., Huntley, B., 2007. Evidence for last interglacial chronology and environmental change from Southern Europe. Proceedings of the

National Academy of Sciences of the United States of America 104, 450–5. doi:10.1073/pnas.0603321104.

Buchdahl, J., 1999. Global Climate Change Student Information Guide: Mesozoic Climates. Manchester, United Kingdom: Atmosphere, Climate and Environment Information Programme.

Candy, I., Mcclymont, E.L., 2013. Interglacial intensity in the North Atlantic over the last 800000 years: Investigating the complexity of the mid-Brunhes Event. Journal of Quaternary Science 28, 343–348. doi:10.1002/jqs.2632.

Candy, I., Schreve, D.C., Sherriff, J., Tye, G.J., 2014. Marine Isotope Stage 11: Palaeoclimates, palaeoenvironments and its role as an analogue for the current interglacial. Earth-Science Reviews 128, 18–51. doi:10.1016/j.earscirev.2013.09.006.

Capron, E., Govin, A., Stone, E. J., Masson-Delmotte, V., Mulitza, S., Otto-Bliesner, B., Sime, L. C., Waelbroeck, C., Wolff, E.W., 2014. Temporal and spatial structure of multi-millennial temperature changes at high latitudes during the Last Interglacial, Quat. Sci. Rev., 103, 116–133.

Chabaud, L., Sánchez Goñi, M.F., Desprat, S., Rossignol, L., 2014. Land-sea climatic variability in the eastern North Atlantic subtropical region over the last 14,200 years: atmospheric and oceanic processes at different timescales. The Holocene 24, 787–797. doi:10.1177/0959683614530439.

Channell, J.E.T., Hodell, D.A., Margari, V., Skinner, L.C., Tzedakis, P.C., Kesler, M.S., 2014. Biogenic magnetite, detrital hematite, and relative paleointensity in Quaternary sediments from the Southwest Iberian margin. Earth Planet. Sci. Lett. 376, 99–109.

Cheddadi, R., Lamb, H.F., Guiot, J., Van Der Kaars, S., 1998. Holocene climatic change in Morocco: A quantitative reconstruction from pollen data. Climate Dynamics 14, 883–890. doi:10.1007/s003820050262.

Chmura, G. L., Eisma, D., 1995. A palynological study of surface and suspended sediments on a tidal flat: implications for pollen transport and deposition in coastal waters. Marine Geology 128 ,183-200.

Clark, P.U., Archer, D., Pollard, D., Blum, J.D., Rial, J.A., Brovkin, V., Mix, A.C., Pisias, N.G., Roy, M., 2006. The middle Pleistocene transition: characteristics, mechanisms, and implications for long-term changes in atmospheric pCO_2. Quaternary Science Reviews 25, 3150–3184. doi:10.1016/j.quascirev.2006.07.008.

Combourieu-Nebout, N., Peyron, O., Dormoy, I., Desprat, S., Beaudouin, C., Kotthoff, U., Marret, F., 2009. Rapid climatic variability in the west Mediterranean during the last 25 000 years from high resolution pollen data. Climate of the Past 5, 503–521. doi:10.5194/cp-5-503-2009.

Cortina, A., Sierro, F. J., Flores, J. A., Martrat, B., Grimalt, J. O., 2015. The response of SST to insolation and ice sheet variability from MIS 3 to MIS 11 in the northwestern Mediterranean Sea (Gulf of Lions). Geophysical Research Letters 42, 10, 366–10, 374. doi:10.1002/2015GL065539.

Cranwell P., 1985. Long-chain unsaturated ketones in recent lacustrine sediments. Geochimica et Cosmochimica Acta, 49: 1545-1551.

Cronin, Thomas M., 1999. Principles of Climatology. New York: Columbia University Press. p. 204.

Daley, T.J., Thomas, E.R., Homes, J.A., Alayne Street-Perrott, F., Chapman, M.R., Tindall, J.C., Valdes, P.J., Loader, N.J., Marshall, J.D., Wolff, E.W., Hopley, P.J., Atkinson, T.C., Barber, K.E., Fisher, E.H., Robertson, I., Hughes, P.D.M., Roberts, C.N., 2011. The 8200 yr BP cold event in stable isotope records from the North Atlantic region. Glob. Planet. Chang. 79, 288–302.

Daniau A.L., Sanchez-Goni M.F., Beaufort L., Laggoun-Defarge F., Loutre M.F., Duprat J., 2007. Dansgaard-Oeschger climatic variability revealed by fire emissions in southwestern Iberia, Quaternary Science Reviews, 26, 1369-1383.

Dansgaard, W., Johnsen, S.J., Clausen, H.B., Dahl-Jensen, D., Gundestrup, N.S., Hammer, C.U., Hvidberg, C.S., Steffensen, J.P., Sveinbjornsdottir, A.E., Jouzel, J., Bond, G., 1993. Evidence for general instability of past climate from a 250-kyr ice-core record. Nature 364, 218–220.

de Vernal, A., Henry, M. and Bilodeau, G., 1996. Techniques de preparation et d'analyse en micropaléontologie. In Les cahiers du GEOTOP 3. Département des Sciences de la terre. Québec University, 16–27.

de Wet, G.A., Castañeda, I.S., DeConto, R.M., Brigham-Grette, J., 2016. A high-resolution mid-Pleistocene temperature record from Arctic Lake El'gygytgyn: a 50 kyr super interglacial from MIS 33 to MIS 31? Earth and Planetary Science Letters 436, 56–63. doi:10.1016/j.epsl.2015.12.021.

DeConto, R.M., Pollard, D., Kowalewski, D., 2012. Modeling Antarctic ice sheet and climate variations during Marine Isotope Stage 31. Global and Planetary Change 88-89, 45–52. doi:10.1016/j.gloplacha.2012.03.003.

Desprat, S., 2005. Réponses climatiques marines et continentales du Sud-Ouest de l'Europe lors des derniers interglaciaires et des entrées en glaciations. PhD Thesis, Bordeaux University, France, 282 pp.

Desprat, S., Naughton, F., Oliveira, D., Sánchez Goñi, M.F., L'étude du pollen des séquences sédimentaires marines pour la compréhension du climat : 1 l'exemple des périodes chaudes passée. in press Quaternaire.

Desprat, S., Sanchez Goni, M. F., Naughton, F., Turon, J.-L., Duprat, J., Malaize, B., Cortijo, E., Peypouquet, J.-P., 2007. Climate variability of the last five isotopic interglacials: Direct land-sea-ice correlation from the multiproxy analysis of North-Western Iberian margin deep-sea cores, in: The Climate of Past Interglacials, Developments in Quaternary Science, edited by: Sirocko, F., Litt, T., Claussen, M., Sánchez Goñi M. F., Elsevier, 375–386, 2007.

Desprat, S., Sánchez Goñi, M.F., McManus, J.F., Duprat, J., Cortijo, E., 2009. Millennial-scale climatic variability between 340000 and 270000 years ago in SW Europe: evidence from a NW Iberian margin pollen sequence. Climate of the Past 5, 53–72. doi:10.5194/cp-5-53-2009.

Desprat, S., Sánchez Goñi, M.F., Turon, J.L., McManus, J.F., Loutre, M.F., Duprat, J., Malaizé, B., Peyron, O., Peypouquet, J.P., 2005. Is vegetation responsible for glacial inception during periods of muted insolation changes? Quaternary Science Reviews 24, 1361–1374. doi:10.1016/j.quascirev.2005.01.005.

Droxler, A.W., Poore, R.Z., Burckle, L.H. (Eds.), 2003. Earth's Climate and Orbital Eccentricity: The Marine Isotope Stage 11 Question, Geophysical Monograph Series. American Geophysical Union, Washington, D. C., ISBN 0-87590-996-5, p. 240.

Duplessy, J.C., Shackleton, N.J., Fairbanks, R.G., Labeyrie, L., Oppo, D., Kallel, N., 1988. Deepwater source variations during the last climatic cycle and their impact on the global deepwater circulation. Paleoceanography 3, 343–360. doi:10.1029/PA003i003p00343.

Dupont, L., Jahns, S., Marret, F. and Ning, S., 2000. Vegetation change in equatorial West Africa: time-slices for the last 150 ka Palaeogeogr. Palaeoclimatol. Palaeoecol. 155 (1-2), 95-122.

Eglinton, T.I., Conte, M.H., Eglinton, G., Hayes, J.M., 2001. Proceedings of a workshop on alkenone-based paleoceanographic indicators. Geochemistry, Geophysics, Geosystems 2, n/a–n/a. doi:10.1029/2000GC000122.

Elderfield, H., Ferretti, P., Greaves, M., Crowhurst, S., McCave, N., Hodell, D., Piotrowski, A.M., 2012. Evolution of ocean temperature and ice volume through the Mid- Pleistocene climate transition. Science 377, 704–709. doi:10.1126/science.1221294.

Emiliani, C., 1955. Pleistocene temperatures, J. Geol., 63(6), 538–578.

EPICA community members, 2004. Eight glacial cycles from an Antarctic ice core. Nature 429, 623–628.

Erdtman, G., 1952. Pollen Morphology and Plant Taxonomy. Angiosperms. Almqvist and Wiksell, Stockholm, 539 pp.

Expedition 339 Scientists, 2013. Site U1385. In: Stow, D.A.V., Hernández-Molina, F.J., Alvarez Zarikian, C.A., the Expedition 339 Scientists (Eds.), Proceedings IODP 339. Integrated Ocean Drilling Program Management International, Inc., Tokyo. http://dx.doi.org/10.2204/iodp.proc.339.103.201.

Eynaud, F., Londeix, L., Penaud, A., Sanchez-Goni, M.-F., Oliveira, D., Desprat, S., Turon, J.-L., 2016. Dinoflagellate cyst population evolution throughout past interglacials: Key features along the

Iberian margin and insights from the new IODP Site U1385 (Exp 339). Glob. Planet. Change 136, 52–64. doi:10.1016/j.gloplacha.2015.12.004.

Faegri, K. and L. van der Pijl, 1979. The Principles of Pollination Ecology (3rd ed.). Pergamon, Oxford, 244 pp.

Faegri, K., 1956. Recent trends in palynology. Bot. Rev., 22, 639-664.

Faegri, K., Kaland, P.E., Krzywinski, K., 1989. Textbook of Pollen Analysis, Fourth ed. John Wiley and Sons, Chichester. 328 p.

Fairbridge, R. W., 1972. Climatology of a glacial cycle, Quat. Res., 2(3), 283–302, doi:10.1016/0033-5894(72)90049-X.

Ferretti, P., Crowhurst, S.J., Hall, M.A., Cacho, I., 2010. North Atlantic millennial-scale climate variability 910 to 790 ka and the role of the equatorial insolation forcing. Earth and Planetary Science Letters 293, 28–41. doi:10.1016/j.epsl.2010.02.016.

Ferretti, P., Crowhurst, S.J., Naafs, B.D.A., Barbante, C., 2015. The Marine Isotope Stage 19 in the mid-latitude North Atlantic Ocean: astronomical signature and intra-interglacial variability. Quaternary Science Reviews 108, 95–110. doi:10.1016/j.quascirev.2014.10.024.

Fiúza, A. F. G., 1984. Hidrologia e Dinâmica das Águas Costeiras de Portugal, Ph.D. thesis, 294 pp., Univ. de Lisboa, Lisbon.

Fiúza, A. F. G., Hamann, M., Ambar, I., del Rio, G. D., Gonzalez, N., Cabanas, J. M., 1998. Water masses and their circulation off western Iberia during May 1993. Deep Sea Research Part I 45(7), 1127–1160.

Fiúza, A. F. G., Macedo, M. E., Guerreiro, M.R., 1982. Climatological space and time variation of the Portuguese coastal upwelling. Oceanologica Acta, 5(1), 31–40.

Flato, G., Marotzke, J., Abiodun, B., Braconnot, P., Chou, S., Collins, W., Cox, P., Driouech, F., Emori, S., Eyring, V., et al., 2013. Evaluation of climate models, in T.F. Stocker (Ed.), et al., Climate Change 2013: The Physical Science Basis. Contribution of Working Group I to the Fifth Assessment Report of the Intergovernmental Panel on Climate Change, pp. 741–866, Cambridge University Press.

Fletcher, W.J., Sánchez Goñi, M.F., 2008. Orbital- and sub-orbital-scale climate impacts on vegetation of the western Mediterranean basin over the last 48,000 yr. Quaternary Research 70, 451–464. doi:10.1016/j.yqres.2008.07.002.

Ganopolski, A., Robinson, A., 2011. The past is not the future. Nat. Geosci. 4, 661-663. http://dx.doi.org/10.1038/ngeo1268.

Ganopolski, A., Winkelmann, R., Schellnhuber, H.J., 2016. Critical insolation–CO_2 relation for diagnosing past and future glacial inception. Nature 529, 200–203. doi:10.1038/nature16494.

Gao, X., Giorgi, F., 2008. Increased aridity in the Mediterranean region under greenhouse gas forcing estimated from high resolution simulations with a regional climate model. Global and Planetary Change 62, 195–209. doi:10.1016/j.gloplacha.2008.02.002.

Giaccio, B., Regattieri, E., Zanchetta, G., Nomade, S., Renne, P.R., Sprain, C.J., Drysdale, R.N., Tzedakis, P.C., Messina, P., Scardia, G., Sposato, A., Bassinot, F., 2015. Duration and dynamics of the best orbital analogue to the present interglacial. Geology 43, 603–606. doi:10.1130/G36677.1.

Gibbard, P. L., and West, R. G., 2000. Quaternary chronostratigraphy: The nomenclature of terrestrial sequences, Boreas, 29(4), 329–336.

Giorgi, F., 2006. Climate change hot-spots. Geophysical Research Letters 33, L08707. doi:10.1029/2006GL025734.

Gouveia, C., Trigo, R.M., DaCamara, C.C., Libonati, R., Pereira, J.M.C., 2008. The North Atlantic Oscillation and European vegetation dynamics. International Journal of Climatology, 28, 1835-1847.

Gouveia, C.M., Trigo, R.M., Beguería, S., Vicente-Serrano, S.M., 2016. Drought impacts on vegetation activity in the Mediterranean region: An assessment using remote sensing data and

multi-scale drought indicators. Glob. Planet. Change 17, 44001. doi:10.1016/j.gloplacha.2016.06.011.

Groot, J.J and Groot, C.R., 1966. Marine Palinology: possibilities, limitations, problems. Marine Geology, 4(6), 387-395.

Grützner, J., Higgins, S.M., 2010. Threshold behavior of millennial scale variability in deep water hydrography inferred from a 1.1 Ma long record of sediment provenance at the southern Gardar Drift. Paleoceanography 25, PA4204. doi:10.1029/2009PA001873.

Guiot, J., 1990. Methodology of the last climatic cycle reconstruction from pollen data, Palaeogeogr. Palaeocl., 80, 49–69.

Guiot, J., Cramer, W., 2016. Climate change: The 2015 Paris Agreement thresholds and Mediterranean basin ecosystems. Science 354, 465–468. doi:10.1126/science.aah5015.

Hays, J. D., Imbrie, J., Shackleton, N. J., 1976. Variations in the Earth's orbit: Pacemaker of the ice ages, Science, 194, 1121–1132.

Head, M.J., Gibbard, P.L., 2015. Early–Middle Pleistocene transitions: Linking terrestrial and marine realms. Quaternary International 389, 7–46. doi:10.1016/j.quaint.2015.09.042.

Heinrich, H., 1988. Origin and consequences of cyclic ice rafting in the Northeast Atlantic Ocean during the past 130,000 years, Quat. Res., 29(2), 142–152, doi:10.1016/0033-5894(88)90057-9.

Hernández-Almeida, I., Sierro, F.J., Cacho, I., Flores, J.A., 2012. Impact of suborbital climate changes in the North Atlantic on ice sheet dynamics at the Mid-Pleistocene Transition. Paleoceanography 27, PA3214. doi:10.1029/2011PA002209.

Hernández-Almeida, I., Sierro, F.J., Flores, J.-A., Cacho, I., Filippelli, G.M., 2013. Palaeoceanographic changes in the North Atlantic during the Mid-Pleistocene Transition (MIS 31-19) as inferred from planktonic foraminiferal and calcium carbonate records. Boreas 42, 140-159. http://dx.doi.org/10.1111/j.1502-3885.2012.00283.x.

Hernández-Molina, F.J., Serra, N., Stow, D.A. V., Llave, E., Ercilla, G., Van Rooij, D., 2011. Along-slope oceanographic processes and sedimentary products around the Iberian margin. Geo-Marine Letters 31, 315–341. doi:10.1007/s00367-011-0242-2.

Herold, N., Yin, Q.Z., Karami, P., Berger, A., 2012. Modeling the climatic diversity of the warm interglacials. Quat. Sci. Rev. 56, 126-141.

Hesse, M., Halbritte, H., Zetter, R., Weber, M., Buchner, R., Frosch-Radivo, A. Ulrich, S., 2009. Pollen Terminology. An illustrated handbook. Springer, Wien. 264 p.

Heusser, C. J., Florer, L. E., 1973. Correlation of marine and continental quaternary pollen records from the Northeast Pacific and Western Washington. Quaternary Research 3, 661-670.

Heusser, L., Balsam, W.L., 1977. Pollen distribution in the northeast Pacific Ocean. Quaternary Research 7, 45–62. doi:10.1016/0033-5894(77)90013-8.

Heusser, L.E. and Stock, C.E., 1984. Preparation techniques for concentrating pollen from marine sediments and other sediments with low pollen density. Palynology, 8, 225-227.

Heusser, L.E., 2005. Spores and pollen in the marine realm. In: Armstrong, H.A. and Brasier, M.D., Microfossils, 2nd ed., Blackwell Publishing, Malden, 296 p.

Hodell, D., Crowhurst, S., Skinner, L., Tzedakis, P.C., Margari, V., Channell, J.E.T., Kamenov, G., MacLachlan, S., Rothwell, G., 2013a. Response of Iberian Margin sediments to orbital and suborbital forcing over the past 420 ka. Paleoceanography 28, 185–199. doi:10.1002/palo.20017.

Hodell, D., Lourens, L., Crowhurst, S., Konijnendijk, T., Tjallingii, R., Jimenez-Espejo, F., Skinner, L., Tzedakis, P.C., 2015. A reference time scale for Site U1385 (Shackleton Site) on the SW Iberian Margin. Global and Planetary Change 1385, 49–64. doi:10.1016/j.gloplacha.2015.07.002.

Hodell, D.A., 2016. The smoking gun of the ice ages. Science 354, 1235–1236. doi:10.1126/science.aal4111.

Hodell, D.A., Channell, J.E.T., Curtis, J.H., Romero, O.E., Röhl, U., 2008. Onset of "Hudson Strait" Heinrich events in the eastern North Atlantic at the end of the middle Pleistocene transition (~640 ka)? Paleoceanography 23, 1–16. doi:10.1029/2008PA001591.

Hodell, D.A., Lourens, L., Stow, D. V, Hernández-Molina, J., Alvarez Zarikian, C., Shackleton Site Project Members, 2013b. The "Shackleton Site" (IODP Site U1385) on the Iberian Margin. Proceedings of the Integrated Ocean Drilling Program 16, 13–19. doi:10.5194/sd-16-13-2013.

Hooghiemstra H., Agwu C.O.C. and Beug H.-J., 1986. Pollen and spore distribution in recent marine sediments: a record of NW-African seasonal wind patterns and vegetation belts. Metero Forschungsergebnisse Reihe C, v. 40, p. 87-135.

Hooghiemstra H., Stalling H., Agwu C.O.C., Dupont L.M., 1992. Vegetational and climatic changes at the northern fringe of the Sahara 250,000-5000 years BP: evidence from 4 marine pollen records located between Portugal and the Canary Islands, Review of Palaeobotany and Palynology, 74, p. 1-53.

Hooghiemstra, H., Lézine, A.M., Leroy, S., Dupont, L. and Marret, F., 2006. Late Quaternary palynology in marine sediments: a synthesis of the understanding of pollen distribution patterns in the NWAfrican setting. Quat. Intern., 148, 29–44.

Hurrell, J., Kushnir, Y., Ottersen, G., and Visbeck, M., 2003. An overview of the North Atlantic Oscillation. In: Hurrel, J., Kushnir, Y., Ottersen, G., and Visbeck, M. (Eds.), The North Atlantic Oscillation: Climatic Significance and Environmental Impact. AGU, Washington, pp.1-35.

Hurrell, J.W., 1995. Decadal Trends in the North Atlantic Oscillation: Regional Temperatures and Precipitation. Science, 269, 676-679.

Hurrell, J.W., Kushnir, Y., Visbeck, M., 2001. The North Atlantic Oscillation. Science, 291, 603-604.

Huybers, P., 2007. Glacial variability over the last two million years: an extended depth-derived age model, continuous obliquity pacing, and the Pleistocene progression. Quaternary Science Reviews 26, 37-55.

Huybers, P., 2011. Combined obliquity and precession pacing of late Pleistocene deglaciations. Nature 480, 229-232.

Iberian Climate Atlas, 2010. Iberian Climate Atlas. Air Temperature and Precipitation (1971-2000). Instituto de Meteorologia de Portugal e Agencia Española de Meteorología, Madrid.

Imbrie J., Berger, A. L., Boyle, E. A., Clemens, S. C., Duffy, A., Howard, W. R., Kukla, G. J., Kutzbach, J., Martinson, D. G., McIntyre, A., Mix, A. C., Molfino, B., Morley, J. J., Peterson, L. C., Pisias, N. G., Prell, W. L., Raymo, M. E., Shackleton, N. J., Toggweiler, J. R., 1992. On the structure and origin of major glaciation cycles. 2. The 100,000-year cycle. Paleoceanography, 8: 699-735.

Imbrie, J., Hays, J. D., Martinson, D. G., McIntyre, A., Mix, A. C., Morley, A. J., Paces, N. G., Prell, W. L., Shackleton, N. J., 1984. The orbital theory of Pleistocene climate: Support from a revised chronology of the marine 18O record, in Milankovitch and Climate. Understanding the Response to Astronomical Forcing, edited by A. L. Berger et al., pp. 607–611, D. Reidel, Dordrecht.

IPCC, 2013. Climate Change 2013: The Physical Science Basis. Contribution of Working Group I to the Fifth Assessment Report of the Intergovernmental Panel on Climate Change [Stocker, T.F., D. Qin, G.-K. Plattner, M. Tignor, S.K. Allen, J. Boschung, A. Nauels, Y. Xia, V. Bex and P.M. Midgley (eds.)]. Cambridge University Press, Cambridge, United Kingdom and New York, NY, USA, 1535 pp. doi:10.1017/CBO9781107415324.

Joannin, S., Bassinot, F., Combourieu Nebout, N., Peyron, O., Beaudouin, C., 2011. Vegetation response to obliquity and precession forcing during the Mid-Pleistocene Transition in Western Mediterranean region (ODP site 976). Quat. Sci. Rev. 30, 280–297.

Joannin, S., Ciaranfi, N., Stefanelli, S., 2008. Vegetation changes during the late early Pleistocene at Montalbano Jonico (Province of Matera, southern Italy) based on pollen analysis. Palaeogeography, Palaeoclimatology, Palaeoecology 270, 92-101.

Joannin, S., Quillévéré, F., Suc, J.-P., Lécuyer, C., Martineau, F., 2007. Early Pleistocene climate changes in the central Mediterranean region as inferred from integrated pollen and planktonic foraminiferal stable isotope analyses. Quat. Res. 67, 264–274.

Jones, P. D., Jonsson, T. and Wheeler, D., 1997. Extension to the North Atlantic Oscillation using early instrumental pressure observations from Gibraltar and south-west Iceland, Int. J. Climatol., 17, 1433–1450.

Jouzel, J., Masson-Delmotte, V., Cattani, O., Dreyfus, G., Falourd, S., Hoffmann, G., Minster, B., Nouet, J., Barnola, J.M., Chappellaz, J., Fischer, H., Gallet, J.C., Johnsen, S., Leuenberger, M., Loulergue, L., Luethi, D., Oerter, H., Parrenin, F., Raisbeck, G., Raynaud, D., Schilt, A., Schwander, J., Selmo, E., Souchez, R., Spahni, R., Stauffer, B., Steffensen, J.P., Stenni, B., Stocker, T.F., Tison, J.L., Werner, M., Wolff, E.W., 2007. Orbital and millennial Antarctic climate variability over the past 800,000 years. Science 317, 793–796. doi:10.1126/science.1141038.

Juggins, S., 2009. Package "rioja" – Analysis of Quaternary Science Data. The Comprehensive R Archive Network.

Kawamura, K., Abe-Ouchi, A., Motoyama, H., Ageta, Y., Aoki, S., Azuma, N., Fujii, Y., Fujita, K., Fujita, S., Fukui, K., Furukawa, T., Furusaki, A., Goto-Azuma, K., Greve, R., Hirabayashi, M., Hondoh, T., Hori, A., Horikawa, S., Horiuchi, K., Igarashi, M., Iizuka, Y., Kameda, T., Kanda, H., Kohno, M., Kuramoto, T., Matsushi, Y., Miyahara, M., Miyake, T., Miyamoto, A., Nagashima, Y., Nakayama, Y., Nakazawa, T., Nakazawa, F., Nishio, F., Obinata, I., Ohgaito, R., Oka, A., Okuno, J., Okuyama, J., Oyabu, I., Parrenin, F., Pattyn, F., Saito, F., Saito, T., Saito, T., Sakurai, T., Sasa, K., Seddik, H., Shibata, Y., Shinbori, K., Suzuki, K., Suzuki, T., Takahashi, A., Takahashi, K., Takahashi, S., Takata, M., Tanaka, Y., Uemura, R., Watanabe, G., Watanabe, O., Yamasaki, T., Yokoyama, K., Yoshimori, M., Yoshimoto, T., 2017. State dependence of climatic instability over the past 720,000 years from Antarctic ice cores and climate modeling. Science Advances 3, e1600446. doi:10.1126/sciadv.1600446.

Kleinen, T., Brovkin, V., Munhoven, G., 2016. Modelled interglacial carbon cycle dynamics during the Holocene, the Eemian and Marine Isotope Stage (MIS) 11. Climate of the Past 12, 2145–2160. doi:10.5194/cp-12-2145-2016.

Kleinen, T., Hildebrandt, S., Prange, M., Rachmayani, R., Müller, S., Bezrukova, E., Brovkin, V., Tarasov, P.E., 2014. The climate and vegetation of Marine Isotope Stage 11 – Model results and proxy-based reconstructions at global and regional scale. Quaternary International 348, 247–265. doi:10.1016/j.quaint.2013.12.028.

Konijnendijk, T.Y.M., Ziegler, M., Lourens, L.J., 2014. Chronological constraints on Pleistocene sapropel depositions from high-resolution geochemical records of ODP Sites 967 and 968. Newsletters on Stratigraphy 47, 263–282. doi:10.1127/0078-0421/2014/0047.

Koutsodendris, A., Brauer, A., Pälike, H., Müller, U.C., Dulski, P., Lotter, A.F., Pross, J., 2011. Sub-decadal- to decadal-scale climate cyclicity during the Holsteinian interglacial (MIS 11) evidenced in annually laminated sediments. Climate of the Past 7, 987–999. doi:10.5194/cp-7-987-2011.

Lambeck, K., Esat, T.M., Potter, E.-K., 2002. Links between climate and sea levels for the past three million years. Nature 419, 199–206. doi:10.1038/nature01089.

Lang, N., Wolff, E.W., 2011. Interglacial and glacial variability from the last 800 ka in marine, ice and terrestrial archives. Climate of the Past 7, 361–380. doi:10.5194/cp-7-361-2011.

Laskar, J., Robutel, P., Joutel, F., Gastineau, M., Correia, A.C.M., Levrard, B., 2004. A long-term numerical solution for the insolation quantities of the Earth. Astronomy & Astrophysics 428, 261–285. doi:10.1051/0004-6361:20041335.

Lézine, A.M. and Vergnaud-Grazzini, C., 1993, Evidence of forest extension in West-Africa since 22,000 BP. A pollen record from eastern tropical Atlantic: Quaternary Science Reviews, v. 12, p. 203-210.

Lionello, P., Malanotte-Rizzoli, P., Boscolo, R., Alpert, P., Artale, V., Li, L., Luterbacher, J., May, W., Trigo, R., Tsimplis, M., Ulbrich, U., Xoplaki, E., 2006. The Mediterranean climate: An overview of the main characteristics and issues. Developments in Earth and Environmental Sciences 4, 1–26. doi:10.1016/S1571-9197(06)80003-0.

Lisiecki, L.E., Raymo, M.E., 2005. A Pliocene–Pleistocene stack of 57 globally-distributed benthic $\delta^{18}O$ records. Paleoceanography 20, PA1003. http://dx.doi.org/10.1029/ 2004PA001071.

Lisiecki, L.E., Stern, J. V., 2016. Regional and global benthic $\delta^{18}O$ stacks for the last glacial cycle. Paleoceanography 31, 1368–1394. doi:10.1002/2016PA003002.

Loidi, J., Biurrun, I., Campos, J. A., Garcıa-Mijangos, I., Herrera, M., 2007. A survey of heath vegetation of the Iberian Peninsula and Northern Morocco: a biogeographical and bioclimatic approach. Phytocoenologia 37, 341-370.

Loulergue, L., Schilt, A., Spahni, R., Masson-Delmotte, V., Blunier, T., Lemieux, B., Barnola, J.-M., Raynaud, D., Stocker, T.F., Chappellaz, J., 2008. Orbital and millennial-scale features of atmospheric CH_4 over the past 800,000 years. Nature 453, 383–386. doi:10.1038/nature06950.

Loutre, M.F., Berger, A.L., 2003. Marine Isotope Stage 11 as an analogue for the present interglacial. Global and Planetary Change 36, 209–217. doi:10.1016/S0921-8181(02)00186-8.

Luque-Espinar, J.A., Chica-Olmo, M., Pardo-Igúzquiza, E., García-Soldado, M.J., 2008. Influence of climatological cycles on hydraulic heads across a Spanish aquifer. Journal of Hydrology 354, 33–52. doi:10.1016/j.jhydrol.2008.02.014.

Lüthi, D., Le Floch, M., Bereiter, B., Blunier, T., Barnola, J.-M., Siegenthaler, U., Raynaud, D., Jouzel, J., Fischer, H., Kawamura, K., Stocker, T.F., 2008. High-resolution carbon dioxide concentration record 650,000-800,000 years before present. Nature 453, 379–382. doi:10.1038/nature06949.

Lynch-Stieglitz J., 2017. The Atlantic Meridional Overturning Circulation and Abrupt Climate Change. Annual Review of Marine Science, 9 (1), 83-104.

Magri, D., 2012. Quaternary History of *Cedrus* in Southern Europe. Annali Di Botanica 57–66. doi:10.4462/annbotrm-10022.

Maher, L.J. Jr., 1981. Statistics for microfossil concentration measurements employing samples spiked with marker grains. Review of Palaeobotany and Palynology, 32, 153-191.

Maher, L.J., 1972. Nomograms for computing 0.95 confidence limits of pollen data, Rev Palaeobot Palyno, 32, 153-191.

Manten, A.A., 1966. Marine palynology in progress. Marine Geology, 4. 385-386.

Marcott, S. A., Shakun, J. D., Clark, P. U., Mix, A. C., 2013. A reconstruction of regional and global temperature for the past 11,300 years, Science (New York, N.Y.), 339(6124), 1198–1201, doi:10.1126/science.1228026.

Margari, V., Skinner, L. C., Tzedakis, P. C., Ganopolski, A., Vautravers, M., Shackleton, N. J., 2010. The nature of millennial-scale climate variability during the past two glacial periods. Nature Geoscience 3, 127-131.

Martinson D. G., Pisias N. G., Hays J. D., Imbrie J., Moore T. C., Shackleton N. J., 1987. Age dating and the orbital theory of ice ages: Development of a high-resolution 0 to 300,000-years chronostratigraphy. Quaternary Research, 27: 1-29.

Martrat, B., Grimalt, J.O., Shackleton, N.J., de Abreu, L., Hutterli, M. A, Stocker, T.F., 2007. Four climate cycles of recurring deep and surface water destabilizations on the Iberian margin. Science 317, 502–507. doi:10.1126/science.1139994.

Maslin, M.A., Brierley, C.M., 2015. The role of orbital forcing in the Early Middle Pleistocene Transition. Quaternary International 389, 47–55. doi:10.1016/j.quaint.2015.01.047.

Maslin, M.A., Ridgwell, A.J., 2005. Mid-Pleistocene revolution and the'eccentrycity myth'. In: Head, M.J., Gibbard, P.L. (Eds.), Early–Middle Pleistocene Transitions: The Land– Ocean Evidence. Geological Society of London, Special Publication 247, pp. 19–34.

Masson-Delmotte, V., Dreyfus, G., Braconnot, P., Johnsen, S., Jouzel, J., Kageyama, M., Landais, A., Loutre, M.-F., Nouet, J., Parrenin, F., Raynaud, D., Stenni, B., Tuenter, E., 2006. Past temperature reconstructions from deep ice cores: relevance for future climate change. Climate of the Past 2, 145–165. doi:10.5194/cp-2-145-2006.

Mc Intyre, K., Delaney, M.L., Ravelo, A.C., 2001. Millennial-scale climate change and oceanic processes in the Late Pliocene and Early Pleistocene. Paleoceanography 16, 535–543. doi:10.1029/2000PA000526.

McAndrews, JH, King, J., 1976. Pollen of the North American Quaternary: the top twenty. Geosciences and Man 15, 41–49.

McClymont, E.L., Rosell-Melé, A., Haug, G.H., Lloyd, J.M., 2008. Expansion of subarctic water masses in the North Atlantic and Pacific oceans and implications for mid-Pleistocene ice sheet growth. Paleoceanography 23, PA4214. doi:10.1029/2008PA001622.

McIntyre, A., Molfino, B., 1996. Forcing of Atlantic Equatorial and Subpolar Millennial Cycles by Precession. Science 274, 1867–1870. doi:10.1126/science.274.5294.1867.

McManus, J., Oppo, D., Cullen, J., Healey, S., 2003. Marine Isotope Stage 11 (MIS 11): analog for Holocene and future climate? In: Droxler, A.W., Poore, R.Z., Burckle, L.H. (Eds.), Earth's Climate and Orbital Eccentricity: The Marine Isotope Stage 11 Question. AGU Geophysical Monograph Series No. 137, pp. 61–6.

McManus, J.F., Oppo, D.W., Cullen, J.L., 1999. A 0.5-Million-Year Record of Millennial-Scale Climate Variability in the North Atlantic. Science 283, 971–974.

Melles, M., Brigham-Grette, J., Minyuk, P.S., Nowaczyk, N.R.,Wennrich, V., DeConto, R.M., Anderson, P.M., Andreev, A.A., Coletti, A., Cook, T.L., Haltia-Hovi, E., Kukkonen, M., Lozhkin, A.V., Rosen, P., Tarasov, P., Vogel, H., Wagner, B., 2012. 2.8 million years of Arctic climate change from Lake El'gygytgyn, NE Russia. Science 337, 315–320. doi:10.1126/science.1222135.

Milankovitch M. M., 1920. Théorie mathématique des phénomènes thermiques produits par la radiation solaire, Gauthier-Villars, Paris.

Milankovitch M. M., 1941. Canon of insolation and the ice-age problem. Royal Serbian Academy, Belgrade.

Milker, Y., Rachmayani, R., Weinkauf, M.F.G., Prange, M., Raitzsch, M., Schulz, M., Kučera, M., 2013. Global and regional sea surface temperature trends during Marine Isotope Stage 11. Climate of the Past 9, 2231–2252. doi:10.5194/cp-9-2231-2013.

Moore, P.D., Webb, J.A., Collinson, M.E., 1991. Pollen analysis. Oxford, Blackwell scientific publication, 2nd edition, 216 p.

Mudie, P. J., McCarthy, M. G., 1994. Late Quaternary pollen transport processes, western North Atlantic: Data from box models, cross-margin and N-S transects. Marine Geology, 118: 79-105.

Mudie, P., McCarthy, F., 2006. Marine palynology: potentials for onshore—offshore correlation of Pleistocene—Holocene records. Transactions of the Royal Society of South Africa 61, 139–157.

Muller, J., 1959. Palynology of recent Orinoco delta and shelf sediments. Micropaleontology, 5, 1–32.

Müller, P.J., Kirst, G., Ruhland, G., Von Storch, I., Rosell-Melé, A., 1998. Calibration of the alkenone paleotemperature index Uk'_{37}- based on core-tops from the eastern South Atlantic and the global ocean (60°N-60°S). Geochimica et Cosmochimica Acta 62, 1757–1772.

Naafs, B.D.A., Hefter, J., Stein, R., 2013. Millennial-scale ice rafting events and Hudson Strait Heinrich (-like) Events during the late Pliocene and Pleistocene: a review. Quaternary Science Reviews 80, 1–28. doi:10.1016/j.quascirev.2013.08.014.

Naish, T., Powell, R., Levy, R., Wilson, G., Scherer, R., Talarico, F., Krissek, L., Niessen, F., Pompilio, M., Wilson, T., Carter, L., DeConto, R., Huybers, P., McKay, R., Pollard, D., Ross, J., Winter, D., Barrett, P., Browne, G., Cody, R., Cowan, E., Crampton, J., Dunbar, G., Dunbar, N., Florindo, F., Gebhardt, C., Graham, I., Hannah, M., Hansaraj, D., Harwood, D., Helling, D., Henrys, S., Hinnov, L., Kuhn, G., Kyle, P., Läufer, A., Maffioli, P., Magens, D., Mandernack, K., McIntosh, W., Millan, C., Morin, R., Ohneiser, C., Paulsen, T., Persico, D., Raine, I., Reed, J., Riesselman, C., Sagnotti, L., Schmitt, D., Sjunneskog, C., Strong, P., Taviani, M., Vogel, S., Wilch, T., Williams, T., 2009. Obliquity-paced Pliocene West Antarctic ice sheet oscillations. Nature 458, 322–8. doi:10.1038/nature07867.

Naughton, F., Sánchez Goñi, M.F., Desprat, S., Turon, J.L., Duprat, J., Malaizé, B., Joli, C., Cortijo, E., Drago, T., Freitas, M.C., 2007. Present-day and past (last 25 000 years) marine pollen signal off western Iberia. Marine Micropaleontology 62, 91–114. doi:10.1016/j.marmicro.2006.07.006.

Nieto-Lugilde, D., Maguire, K.C., Blois, J.L., Williams, J.W., Fitzpatrick, M.C., 2015. Close agreement between pollen-based and forest inventory-based models of vegetation turnover. Global Ecology and Biogeography 24, 905–916. doi:10.1111/geb.12300.

North Greenland Ice Core Project (NGRIP) members, 2004. High-resolution record of northern hemisphere climate extending into the last interglacial period. Nature 431, 147-151.

Oliveira, D., Desprat, S, Yin, Q., Naughton, F., Trigo, R., Rodrigues, T., Abrantes, F., Sánchez Goñi, M.F., Unraveling the forcings controlling the magnitude and climate variability of the best orbital analogues for the present interglacial in SW Europe under review, Climate Dynamics.

Oliveira, D., Desprat, S., Rodrigues, T., Naughton, F., Hodell, D., Trigo, R., Rufino, M., Lopes, C., Abrantes, F., Sánchez Goñi, M.F., 2016. The complexity of millennial-scale variability in southwestern Europe during MIS 11. Quaternary Research 86, 373-387. doi:10.1016/j.yqres.2016.09.002.

Oliveira, D., Sánchez Goñi, M.F., Naughton, F., Polanco-Martínez, J.M., Jimenez-Espejo, F.J., Grimalt, J.O., Martrat, B., Voelker, A.H.L., Trigo, R., Hodell, D., Abrantes, F., Desprat, S., 2017. Unexpected weak seasonal climate in the western Mediterranean region during MIS 31, a high-insolation forced interglacial. Quaternary Science Reviews 161, 1–17. doi:10.1016/j.quascirev.2017.02.013.

Oppo D.W., Mcmanus J.F., Cullen J.L., 2006. Evolution and demise of the Last Interglacial warmth in the subpolar North Atlantic. Quaternary Science Reviews, 25 (23-24), 3268-3277.

Oppo, D.W., McManus, J.F., Cullen, J.L., 1998. Abrupt climate events 500,000 to 340,000 years ago: Evidence from subpolar North Atlantic sediments. Science 279, 1335–1338.

Parrenin, F., Barnola, J.-M., Beer, J., Blunier, T., Castellano, E., Chappellaz, J., Dreyfus, G., Fischer, H., Fujita, S., Jouzel, J., Kawamura, K., Lemieux-Dudon, B., Loulergue, L., Masson-Delmotte, V., Narcisi, B., Petit, J.-R., Raisbeck, G., Raynaud, D., Ruth, U., Schwander, J., Severi, M., Spahni, R., Steffensen, J.P., Svensson, A., Udisti, R., Waelbroeck, C., Wolff, E., 2007. The EDC3 chronology for the EPICA Dome C ice core. Climate of the Past 3, 485–497. doi:10.5194/cp-3-485-2007.

Past Interglacials Working Group of PAGES, 2016. Interglacials of the last 800,000 years, Reviews of Geophysics, 54, doi:10.1002/2015RG000482.

Peinado Lorca, M., Martinez-Parras, J.M., 1987. Castilla-La Mancha. In: Peinado Lorca M and Rivas-Martinez S (eds) La vegetación de España. Alcala de Henares: Universidad de Alcala de Henares, pp. 163–196.

Peliz, Á., Dubert, J., Santos, A. M.P., Oliveira, P.B., Le Cann, B., 2005. Winter upper ocean circulation in the Western Iberian Basin - Fronts, Eddies and Poleward Flows: An overview. Deep-Sea Research Part I 52(4), 621–646. doi:10.1016/j.dsr.2004.11.005.

Pisias N. G., Moore T. C. Jr., 1981. The evolution of the Pleistocene climate: a time series approach. Earth and Planetary Science Letters, 52: 450-458.

Pol, K., Debret, M., Masson-Delmotte, V., Capron, E., Cattani, O., Dreyfus, G., Falourd, S., Johnsen, S., Jouzel, J., Landais, A., Minster, B., Stenni, B., 2011. Links between MIS 11 millennial to sub-millennial climate variability and long term trends as revealed by new high resolution EPICA Dome C deuterium data - A comparison with the Holocene. Climate of the Past 7, 437–450. doi:10.5194/cp-7-437-2011.

Pol, K., Masson-Delmotte, V., Cattani, O., Debret, M., Falourd, S., Jouzel, J., Landais, A., Minster, B., Mudelsee, M., Schulz, M., Stenni, B., 2014. Climate variability features of the last interglacial in the East Antarctic EPICA Dome C ice core. Geophysical Research Letters 41, 4004–4012. doi:10.1002/2014GL059561.

Pol, K., Masson-Delmotte, V., Johnsen, S., Bigler, M., Cattani, O., Durand, G., Falourd, S., Jouzel, J., Minster, B., Parrenin, F., 2010. New MIS 19 EPICA Dome C high resolution deuterium data: Hints for a problematic preservation of climate variability at sub-millennial scale in the "oldest ice." Earth and Planetary Science Letters 298, 95–103. doi:10.1016/j.epsl.2010.07.030.

Pollard, D., DeConto, R.M., 2009. Modelling West Antarctic ice sheet growth and collapse through the past five million years. Nature 458, 329–32. doi:10.1038/nature07809.

Prahl, F.G., Wakeham, S.G., 1987. Calibration of unsaturation patterns in long-chain ketone compositions for palaeotemperature assessment. Nature 330, 367–369. doi:10.1038/330367a0.

Prentice, I.C., Berglund, B.E., Olsson, T., 1987. Quantitative forest composition sensing characteristics of pollen samples from Swedish lakes. Boreas 16, 43–54.

Prokopenko, A.A., Bezrukova, E. V., Khursevich, G.K., Solotchina, E.P., Kuzmin, M.I., Tarasov, P.E., 2010. Climate in continental interior Asia during the longest interglacial of the past 500 000 years: the new MIS 11 records from Lake Baikal, SE Siberia. Climate of the Past 6, 31–48. doi:10.5194/cp-6-31-2010.

Punt, W., 1971. Pollen morphology of the genera Norantea, Souroubea and Ruyschia (Marcgraviaceae). Pollen Spores, 13, 199-232.

Punt, W., Hoen, P.P., Blackmore, S., Nilsson, S. and Le Thomas, A., 2007. Glossary of pollen and spore terminology. Review of Palaeobotany and Palynology, 143 (1-2), 1-81.

Quezel, P., 1989. Les grandes structures de végétation en région méditerranéenne: Facteurs déterminants dans leur mise en place post-glaciaire. Geobios, 32, 19-32.

Quezel, P., 2002. Réflexions sur l'évolution de la flore et de la végétation au Maghreb méditerranéen. Ibis Press, Paris.

R Core Team, 2014. R: A language and environment for statistical computing. R Foundation for Statistical Computing, Vienna, Austria. URL http://www.R-project.org/.

Railsback, L.B., Gibbard, P.L., Head, M.J., Voarintsoa, N.R.G., Toucanne, S., 2015. An optimized scheme of lettered marine isotope substages for the last 1.0 million years, and the climatostratigraphic nature of isotope stages and substages. Quaternary Science Reviews 111, 94–106. doi:http://dx.doi.org/10.1016/j.quascirev.2015.01.012.

Ramos, A.M., Pires, A.C., Sousa, P.M., Trigo, R.M., 2013. The use of circulation weather types to predict upwelling activity along the Western Iberian Peninsula coast. Cont. Shelf Res. 69, 38–51. doi:10.1016/j.csr.2013.08.019.

Raymo, M.E., Ganley, K., Carter, S., Oppo, D.W., McManus, J., 1998. Millennial-scale climate instability during the early Pleistocene epoch 392, 699–702. doi:10.1038/33658.

Raymo, M.E., Lisiecki, L.E., Nisancioglu, K.H., 2006. Plio-Pleistocene ice volume, Antarctic climate, and the global $\delta^{18}O$ record. Science 313, 492–5. doi:10.1126/science.1123296.

Raymo, M.E., Nisancioglu, K., 2003. The 41 ky world: Milankovitch's other unsolved mystery. Paleoceanography 18, 1011-1017.

Reille, M., 1992. Pollen et spores d'Europe et d'Afrique du Nord. Marseille, Laboratoire de botanique historique et palynologie, 520 p.

Rios, A.F., Perez, F.F., Fraga, F., 1992. Water Masses in the Upper and Middle North-Atlantic Ocean East of the Azores. Deep-Sea Research Part A-Oceanographic Research Papers 39, 645-658.

Rivas-Martínez, S., 2007. Mapa de series, geoseries y geopermaseries de vegetacion de España. Memoria del mapa de la vegetación potencial de España, parte 1. Itinera Geobot. 17, 5-435. http://www.globalbioclimatics.org/form/bg_med.htm.

Rivas-Martinez, S., Penas A., Diaz, T. E., 2004. Biogeographic Map of Europe. Cartographic Service. University of Leon, Spain.

Rodrigues, T., Alonso-Garcia, M., Hodell, D.A., Rufino, M., Naughton, F., Grimalt, J.O., Voelker, A. H. L., Abrantes, F., 2016. A 1 Ma record of Sea Surface Temperature and extreme cooling events in the North Atlantic: a perspective from the Iberian Margin "Shackleton site". Submitted to Quaternary Science Reviews, Manuscript number JQSR_2016_117.

Rodrigues, T., Grimalt, J.O., Abrantes, F., Flores, J.A., Lebreiro, S., 2009. Holocene interdependences of changes in sea surface temperature, productivity and fluvial inputs in the Iberian continental shelf (Tagus mud patch). Geochemistry, Geophysics, Geosystems, 10 (7). doi:10.1029/2008GC002367.

Rodrigues, T., Voelker, A.H.L., Grimalt, J.O., Abrantes, F., Naughton, F., 2011. Iberian Margin sea surface temperature during MIS 15 to 9 (580–300 ka): Glacial suborbital variability versus interglacial stability. Paleoceanography 26, PA1204. doi:10.1029/2010PA001927.

Rodríguez-Tovar, F.J., Dorador, J., Grunert, P., Hodell, D., 2015. Deep-sea trace fossil and benthic foraminiferal assemblages across glacial Terminations 1, 2 and 4 at the "Shackleton Site" (IODP Expedition 339, Site U1385). Global and Planetary Change 133, 359–370. doi:10.1016/j.gloplacha.2015.05.003.

Rohling, E. J., Grant, K., Bolshaw, M., Roberts, A. P., Siddall, M., Hemleben, C., Kucera, M., 2009. Antarctic temperature and global sea level closely coupled over the past five glacial cycles. Nature Geoscience 2, 500–504. doi:10.1038/ngeo557.

Rohling, E.J., Braun, K., Grant, K., Kucera, M., Roberts, A.P., Siddall, M., Trommer, G., 2010. Comparison between Holocene and Marine Isotope Stage-11 sea-level; histories. Earth Planet. Sci. Lett. 291, 97–105.

Rosell-Mele A., M.S., Weinelt, M., Sarnthein, N., Koç-Karpuz, E., Jansen, 1998. Variability of the Arctic front during the last climatic cycle: application of a novel molecular proxy. Terra Nova, 10: 86-89.

Ruddiman, W.F., 2001. Earth's Climate: Past and Future, New York.

Ruddiman, W.F., 2006. Orbital changes and climate, Quaternary Science Reviews, 25(23-24), 3092-3112.

Ruddiman, W.F., McIntyre, A., 1981. Oceanic mechanisms for amplification of the 23,000-year ice-volume cycle. Science 212 (4495), 617-627. http://dx.doi.org/10.1126/science.212.4495.617.

Ruddiman,W.F., 2005. Cold climate during the closest stage 11 analog to recent millennia. Quaternary Science Reviews 24, 1111–1121.

Sánchez Goñi M, Cacho I, Turon J, Guiot J, Sierro F, Peypouquet J, Grimalt J, Shackleton N (2002) Synchroneity between marine and terrestrial responses to millennial scale climatic variability during the last glacial period in the Mediterranean region. Clim Dyn 19:95–105. doi: 10.1007/s00382-001-0212-x.

Sánchez Goñi, M.F., Bard, E., Landais, A., Rossignol, L., d'Errico, F., 2013. Air–sea temperature decoupling in western Europe during the last interglacial–glacial transition. Nature Geoscience 6, 837–841. doi:10.1038/ngeo1924.

Sánchez Goñi, M.F., Eynaud, F., Turon, J.L., Shackleton, N.J., 1999. High resolution palynological record off the Iberian margin: Direct land-sea correlation for the Last Interglacial complex. Earth and Planetary Science Letters 171, 123–137.

Sánchez Goñi, M.F., Landais, A., Fletcher, W.J., Naughton, F., Desprat, S., Duprat, J., 2008. Contrasting impacts of Dansgaard-Oeschger events over a western European latitudinal transect modulated by orbital parameters. Quaternary Science Reviews 27, 1136–1151. doi:10.1016/j.quascirev.2008.03.003.

Sánchez Goñi, M.F., Llave, E., Oliveira, D., Naughton, F., Desprat, S., Ducassou, E., Hodell, D.A., Hernández-Molina, F.J., 2016b. Climate changes in south western Iberia and Mediterranean Outflow variations during two contrasting cycles of the last 1 Myrs: MIS 31–MIS 30 and MIS 12–MIS 11. Global and Planetary Change 136, 18–29.

Sánchez Goñi, M.F., Rodrigues, T., Hodell, D.A., Polanco-Martínez, J.M., Alonso-García, M., Hernández-Almeida, I., Desprat, S., Ferretti, P., 2016a. Tropically-driven climate shifts in southwestern Europe during MIS 19, a low eccentricity interglacial. Earth and Planetary Science Letters 448, 81–93. doi:10.1016/j.epsl.2016.05.018.

Sánchez Goñi, M.F., Turon, J.L., Eynaud, F., Gendreau, S., 2000. European climatic response to millennial-scale changes in the atmosphere-ocean system during the last glacial period. Quat. Res. 54, 394–403. doi:10.1006/qres.2000.2176.

Sánchez-Goñi, M.F., Landais, A., Cacho, I., Duprat, J., Rossignol, L., 2009. Contrasting intrainterstadial climatic evolution between high and middle North Atlantic latitudes: A close-up of

Greenland Interstadials 8 and 12. Geochemistry, Geophysics, Geosystems 10. doi:10.1029/2008GC002369.

Santini, M., Collalti, A., Valentini, R., 2014. Climate change impacts on vegetation and water cycle in the Euro-Mediterranean region, studied by a likelihood approach. Regional Environmental Change 14, 1405–1418. doi:10.1007/s10113-013-0582-8.

Scherer, R.P., Bohaty, S.M., Dunbar, R.B., Esper, O., Flores, J.-A., Gersonde, R., Harwood, D.M., Roberts, A.P., Taviani, M., 2008. Antarctic records of precession-paced insolation-driven warming during early Pleistocene Marine Isotope Stage 31. Geophysical Research Letters 35, L03505. doi:10.1029/2007GL032254.

Schulz H. M., Scöner A., Emeis K. C., 2000. Long-chain alkenone patterns in the Baltic sea: an ocean-freshwater transition. Geochimica et Cosmochimica Acta, 64: 469-477

Schulz, M., Mudelsee, M., 2002. REDFIT: estimating red-noise spectra directly from unevenly spaced paleoclimatic time series. Computers & Geosciences 28, 421–426. doi:10.1016/S0098-3004(01)00044-9.

Shackleton N. J., 1969. The last interglacial in the marine and terrestrial records. Proceedings of the Royal Society of London, B174: 135-154

Shackleton, N. J, Fairbanks, R. G., Chiu, T.-C., Parrenin, F., 2004. Absolute calibration of the Greenland time scale: implications for Antarctic time scales and for Δ14C. Quaternary Science Reviews 23, 1513–1522. doi:10.1016/j.quascirev.2004.03.006.

Shackleton, N. J., Berger, A., Peltier, W. R., 1990. An alternative astronomical calibration of the lower Pleistocene timescale based on ODP site 677, Trans. R. Soc. Edinburgh: Earth Sci., 81, 251–261.

Shackleton, N. J., Chapman, M., Sánchez-Goñi, M.F., Pailler, D., Lancelot, Y., 2002. The classic Marine Isotope Substage 5e, Quat. Res., 58(1), 14–16, doi:10.1006/qres.2001.2312.

Shackleton, N. J., Opdyke, N. D., 1973. Oxygen isotope and palaeomagnetic stratigraphy of Equatorial Pacific core V28-238: Oxygen isotope temperatures and ice volumes on a 105 year and 106 year scale, Quat. Res., 3(1), 39–55, doi:10.1016/0033-5894(73) 90052-5.

Shackleton, N.J., 1967. Oxygen isotope analyses and Pleistocene temperatures re-assessed, Nature, 215(5096), 15–17.

Shackleton, N.J., Hall, M.A., Vincent, E., 2000. Phase relationships between millennial-scale events 64,000-24,000 years ago. Paleoceanography 15, 565–569. doi:10.1029/2000PA000513.

Shackleton, N.J., Sánchez-Goñi, M.F., Pailler, D., Lancelot, Y., 2003. Marine Isotope Substage 5e and the Eemian Interglacial. Global and Planetary Change 36, 151–155. doi:10.1016/S0921-8181(02)00181-9.

Short, D.A., Mengel, J.G., Crowley, T.J., Hyde, W.T., North, G.R., 1991. Filtering of Milankovitch cycles by Earth's geography. Quaternary Research 35, 157–173. doi:10.1016/0033-5894(91)90064-C.

Siddall, M., Rohling, E.J., Almogi-Labin, A., Hemleben, C., Meischner, D., Schmelzer, I., Smeed D.A., 2003. Sea-level fluctuations during the last glacial cycle. Nature, 423 (6942), 853-858.

Skinner, L.C., Elderfield, H., 2007. Rapid fluctuations in the deep North Atlantic heat budget during the last glacial period. Paleoceanography 22, 1–9. doi:10.1029/2006PA001338.

Skinner, L.C., Elderfield, H., Hall, M., 2007. Phasing of millennial events and Northeast Atlantic deep-water temperature change since ~50 ka BP. In: Schmittner, A., Chiang, J., Hemming, S.R. (Eds.), Ocean Circulation: Mechanisms and Impacts. AGU Geophysical Monograph 173. AGU, Washington, D.C., pp. 197–208.

Skinner, L.C., Shackleton, N.J., 2005. An Atlantic lead over Pacific deep-water change across Termination I: implications for the application of the marine isotope stage stratigraphy. Quaternary Science Reviews 24, 571–580. doi:10.1016/j.quascirev.2004.11.008.

Skinner, L.C., Waelbroeck, C., Scrivner, A.E., Fallon, S.J., 2014. Radiocarbon evidence for alternating northern and southern sources of ventilation of the deep Atlantic carbon pool during the last deglaciation. Proceedings of the National Academy of Sciences of the United States of America 111, 5480–4. doi:10.1073/pnas.1400668111.

Solomon, S., Plattner, G.-K., Knutti, R., Friedlingstein, P., 2009. Irreversible climate change due to carbon dioxide emissions. Proc. Natl. Acad. Sci. U. S. A. 106, 1704–9. doi:10.1073/pnas.0812721106.

Sousa, P., Trigo, R.M., Pereira, M., Bedia, J., Gutierrez, J.M., 2015. Different approaches to model future burnt area in the Iberian Peninsula. Agricultural and Forest Meteorology 202, 11-25. doi: 10.1016/j.agrformet.2014.11.018.

Stein, R., Hefter, J., Grützner, J., Voelker, A., Naafs, B.D.A., 2009. Variability of surface water characteristics and Heinrich-like events in the Pleistocene midlatitude North Atlantic Ocean: Biomarker and XRD records from IODP Site U1313 (MIS 16–9). Paleoceanography 24, PA2203. doi:10.1029/2008pa001639.

Stockmarr, J., 1971. Tablets with spores used in absolute pollen analysis. Pollen et Spores 13, 615-621.

Suc, J.P., 1984. Origin and evolution of the Mediterranean vegetation and climate in Europe, Nature, 307, 429-432.

Teitler, L., Florindo, F., Warnke, D.A., Filippelli, G.M., Kupp, G., Taylor, B., 2015. Antarctic Ice Sheet response to a long warm interval across Marine Isotope Stage 31: A cross-latitudinal study of iceberg-rafted debris. Earth and Planetary Science Letters 409, 109–119. doi:10.1016/j.epsl.2014.10.037.

Trigo, R. and DaCamara, C.C., 2000. Circulation Weather Types and Influence on the Precipitation Regime in Portugal, International Journal of Climatology, 20, 1559-1581.

Trigo, R.M., Osborn, T.J., and Corte-Real, J., 2002. The North Atlantic Oscilation influence on Europe: Climate impacts and associated physical mechanisms, Climate Research, 20, 9-17.

Trigo, R.M., Pozo- Vázquez, D., Osborn, T.J., Castro-Díez, Y., Gamiz-Fortis, S., Esteban-Parra, M.J., 2004. North Atlantic Oscillation influence on precipitation, river flow and water resources in the Iberian Peninsula. International Journal of Climatology 24, 925–944. doi:10.1002/joc.1048.

Tripati, A.K., Roberts, C.D., Eagle, R.A., Li, G., 2011. A 20 million year record of planktic foraminiferal B/Ca ratios: Systematics and uncertainties in pCO_2 reconstructions. Geochimica et Cosmochimica Acta 75, 2582–2610. doi:10.1016/j.gca.2011.01.018.

Turner, C., 1970. The Middle Pleistocene deposits at Marks Tey, Essex. Philos. Trans. R. Soc. Lond. B 257, 373–440.

Turon, J.L., 1984. Le palynoplankton dans l'environnement actuel de l'Atlantique nord oriental: évolution climatique et hydrologique depuis le dernier maximum glaciale. Thèse de Doctorate ès Sciences, Université de Bordeaux. 313 pp.

Tye, G.J., Sherriff, J., Candy, I., Coxon, P., Palmer, A., McClymont, E.L., Schreve, D.C., 2016. The $\delta^{18}O$ stratigraphy of the Hoxnian lacustrine sequence at Marks Tey, Essex, UK: implications for the climatic structure of MIS 11 in Britain. Journal of Quaternary Science 31, 75–92. doi:10.1002/jqs.2840.

Tzedakis, P. C., Roucoux, K. H., de Abreu, L., Shackleton, N. J., 2004. The Duration of Forest Stages in Southern Europe and Interglacial Climate Variability. Science 306, 2231–2235. doi:10.1126/science.1102398.

Tzedakis, P. C., Wolff, E. W., Skinner, L. C., Brovkin, V., Hodell, D. A., McManus, J. F., Raynaud, D. 2012a. Can we predict the duration of an interglacial?, Clim. Past, 8, 1473–1485.

Tzedakis, P.C., 1994. Hierarchical biostratigraphical classification of long pollen sequences. Jour. Quaternary Science, 9, 257-260.

Tzedakis, P.C., 2007. Seven ambiguities in the Mediterranean palaeoenvironmental narrative. Quaternary Science Reviews 26, 2042-2066.

Tzedakis, P.C., 2010. The MIS 11 – MIS 1 analogy, southern European vegetation, atmospheric methane and the "early anthropogenic hypothesis". Climate of the Past 6, 131–144. doi:10.5194/cp-6-131-2010.

Tzedakis, P.C., Channell, J.E.T., Hodell, D.A., Kleiven, H.F., Skinner, L.C., 2012b. Determining the natural length of the current interglacial. Nature Geoscience 5, 138–141. doi:10.1038/ngeo1358.

Tzedakis, P.C., Crucifix, M., Mitsui, T., Wolff, E.W., 2017. A simple rule to determine which insolation cycles lead to interglacials. Nature 542, 427–432. doi:10.1038/nature21364.

Tzedakis, P.C., Hooghiemstra, H., Pälike, H., 2006. The last 1.35 million years at Tenaghi Philippon: revised chronostratigraphy and long-term vegetation trends. Quat. Sci. Rev. 25, 3416–3430. doi:10.1016/j.quascirev.2006.09.002.

Tzedakis, P.C., Margari, V., Hodell, D.A., 2015. Coupled ocean–land millennial-scale changes 1.26 million years ago, recorded at Site U1385 off Portugal. Global and Planetary Change 135, 83–88. doi:10.1016/j.gloplacha.2015.10.008.

Tzedakis, P.C., Pälike, H., Roucoux, K.H., de Abreu, L., 2009b. Atmospheric methane, southern European vegetation and low-mid latitude links on orbital and millennial timescales. Earth and Planetary Science Letters 277, 307–317. doi:10.1016/j.epsl.2008.10.027.

Tzedakis, P.C., Raynaud, D., McManus, J.F., Berger, A., Brovkin, V., Kiefer, T., 2009a. Interglacial diversity. Nature Geoscience 2, 751–755. doi:10.1038/ngeo660.

Vautravers, M., Shackleton, N.J., 2006. Centennial scale surface hydrology off Portugal during Marine Isotope Stage 3: insights from planktonic foraminiferal fauna variability. Paleoceanography 21, PA3004.

Villanueva, J., Pelejero, C., Grimalt, J.O., 1997. Clean-up procedures for the unbiased estimation of C_{37} alkenone sea surface temperatures and terrigenous n-alkane inputs in paleoceanography. Journal of Chromatography A 757, 145–151.

Voelker, A.H.L., de Abreu, L., 2011. A review of abrupt climate change events in the Northeastern Atlantic Ocean (Iberian Margin): latitudinal, longitudinal, and vertical gradients. In: Rashid, H., Polyak, L., Mosley-Thompson, E. (Eds.), Abrupt Climate Change: Mechanisms, Patterns, and Impacts. Geophysical Monograph Series 193, pp. 15–37.

Walker, M.J.C., Johnsen, S., Rasmussen, S.O., Steffensen, J.P., Popp, T., Gibbard, P., Hoek, W., Lowe, J., Andrews, J., Björck, S., Cwynar, L., Hughen, K., Kershaw, P., Kromer, B., Litt, T., Lowe, D.J., Nakagawa, T., Newnham, R., Schwander, J., 2008. The Global Stratotype Section and Point (GSSP) for the base of the Holocene Series/Epoch (Quaternary System/Period) in the NGRIP ice core. Episodes 31, 264–267.

Wang, Y. J., Cheng, H., Edwards, R. L., Kong, X. G., Shao, X. H., Chen, S. T., Wu, J. Y., Jiang, X. Y., Wang, X. F., An, Z. S., 2008. Millennial and orbital-scale changes in the East Asian monsoon over the past 224,000 years, Nature, 451, 1090–1093, doi:10.1038/nature06692.

Wanner, H., Beer, J., Bütikofer, J., Crowley, T.J., Cubasch, U., Flückiger, J., Goosse, H., Grosjean, M., Joos, F., Kaplan, J.O., Küttel, M., Müller, S.A., Prentice, I.C., Solomina, O., Stocker, T.F., Tarasov, P., Wagner, M., Widmann, M., 2008. Mid- to Late Holocene climate change: an overview. Quaternary Science Reviews 27, 1791–1828. doi:10.1016/j.quascirev.2008.06.013.

Weirauch, D., Billups, K., Martin, P., 2008. Evolution of millennial-scale climate variability during the mid-Pleistocene. Paleoceanography 23, PA3216. doi:10.1029/2007PA001584.

West, R. G., 1970. Pollen zones in the Pleistocene of Great Britain and their correlation. New Phytologist, 69(4), 1179-1183.

West, R. G., 1984. Interglacial, interstadial and oxygen isotope stages, Diss. Bot., 72, 345–358.

Williams, J.W., Jackson, S.T., 2003. Palynological and AVHRR observations of modern vegetational gradients in eastern North America. The Holocene 13, 485–497. doi:10.1191/0959683603hl613rp.

Worldwide Bioclimatic Classification System, 1996-2017, S.Rivas-Martinez & S.Rivas-Saenz, Phytosociological Research Center, Spain. http://www.globalbioclimatics.org.

Wright, A.K., Flower, B.P., 2002. Surface and deep ocean circulation in the subpolar North Atlantic during the mid-Pleistocene revolution. Paleoceanography 17, 20–1–20–16. doi:10.1029/2002PA000782.

Yin, Q.,Z., 2013. Insolation-induced mid-Brunhes transition in Southern Ocean ventilation and deep-ocean temperature. Nature 494, 222–225. doi:10.1038/nature11790.

Yin, Q.Z., Berger, A., 2010. Insolation and CO_2 contribution to the interglacial climate before and after the Mid-Brunhes Event. Nature Geoscience 3, 243–246. doi:10.1038/ngeo771.

Yin, Q.Z., Berger, A., 2012. Individual contribution of insolation and CO_2 to the interglacial climates of the past 800,000 years. Climate Dynamics 38, 709–724. doi:10.1007/s00382-011-1013-5.

Yin, Q.Z., Berger, A., 2015. Interglacial analogues of the Holocene and its natural near future. Quaternary Science Reviews 120, 28–46. doi:10.1016/j.quascirev.2015.04.008p.

Appendix A

Site U1385 detailed percentage pollen diagrams spanning MIS 1, MIS 11 and MIS 31

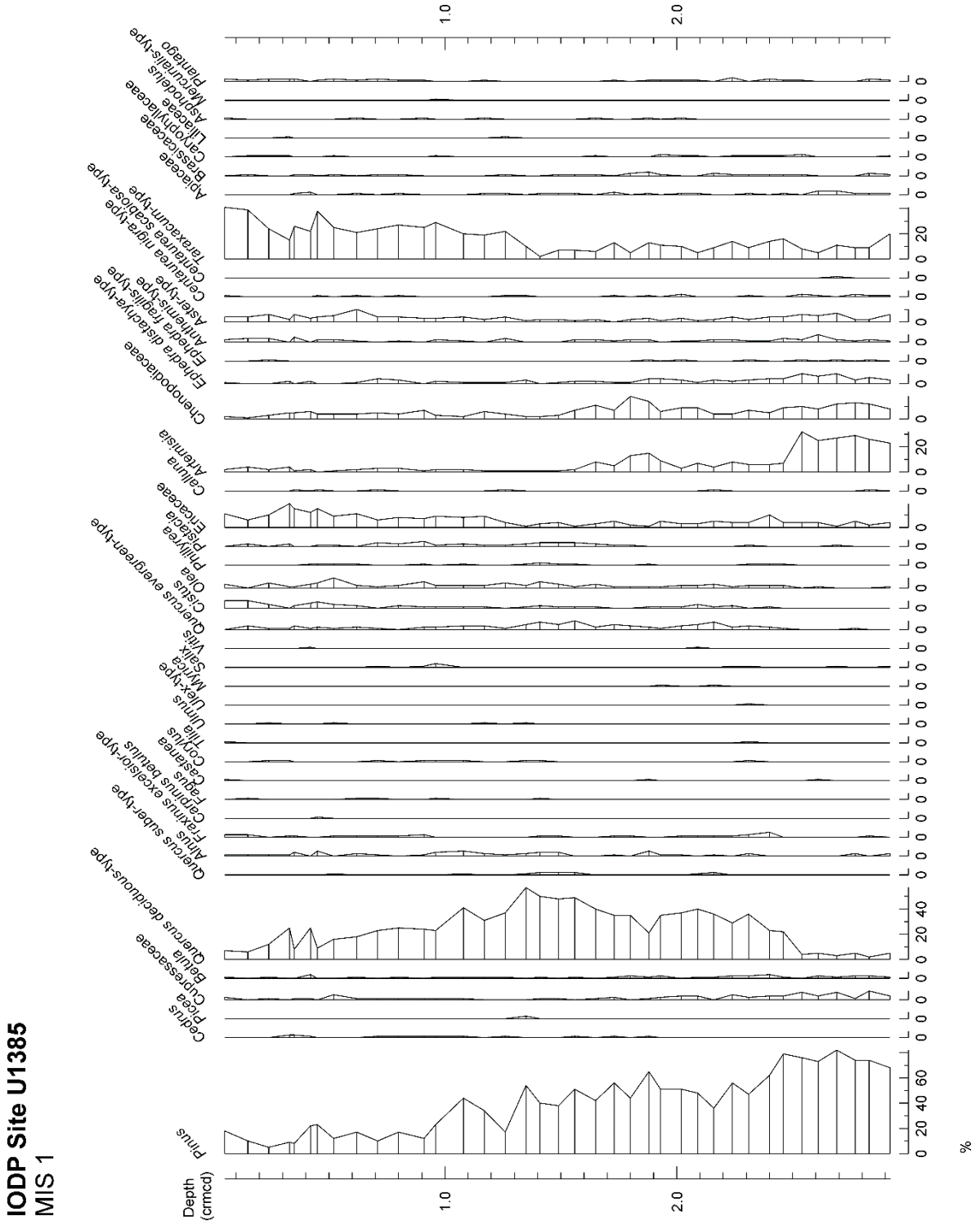
IODP Site U1385
MIS 1
Depth (crmcd)
1.0
2.0
%
Pinus
Cedrus
Picea
Cupressaceae
Betula
Quercus deciduous-type
Quercus subber-type
Alnus
Fraxinus excelsior-type
Carpinus betulus
Fagus
Castanea
Corylus
Tilia
Ulmus
Ulex-type
Myrica
Salix
Vitis
Quercus evergreen-type
Cistus
Olea
Phillyrea
Pistacia
Ericaceae
Cailuna
Artemisia
Chenopodiaceae
Ephedra distachya-type
Ephedra fragilis-type
Aster-type
Centaurea nigra-type
Centaurea scabiosa-type
Tarraxacum-type
Apiaceae
Brassicaceae
Caryophyllaceae
Liliaceae
Asphodelus
Mercurialis
Plantago

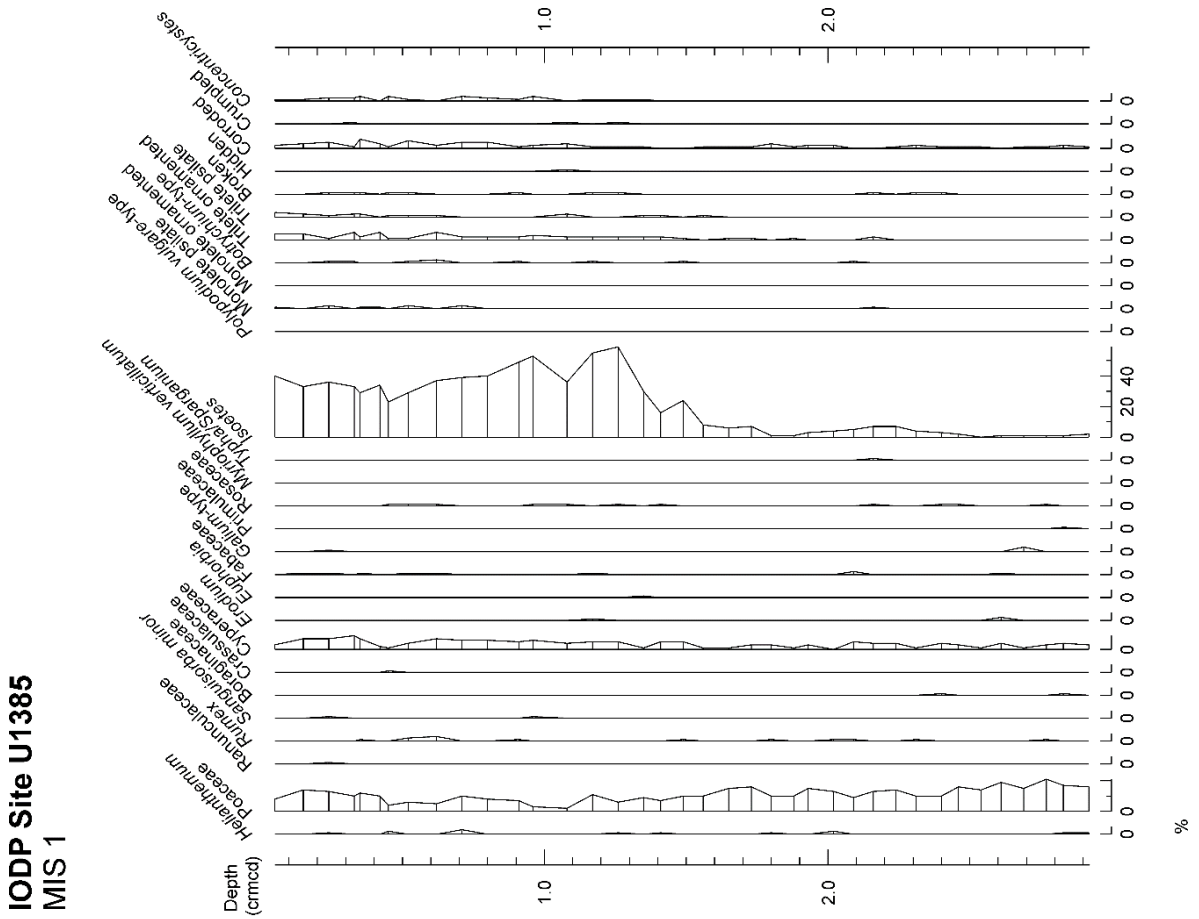
IODP Site U1385
MIS 1
Depth (crmcd)
1.0
2.0
Helianthemum
Poaceae
Ranunculaceae
Rumex
Sanguisorba minor
Brassicaceae
Cyperaceae
Erodium
Euphorbia
Fabaceae
Galium-type
Primulaceae
Rosaceae
Myriophyllum verticillatum
Typha/Sparganium
Isoetes
Polypodium vulgare-type
Monolete psilate-type
Monolete ornamented
Trilete ornamented
Trilete psilate
Broken
Hidden
Corroded
Crumpled
Concentricysts
%
0 20 40

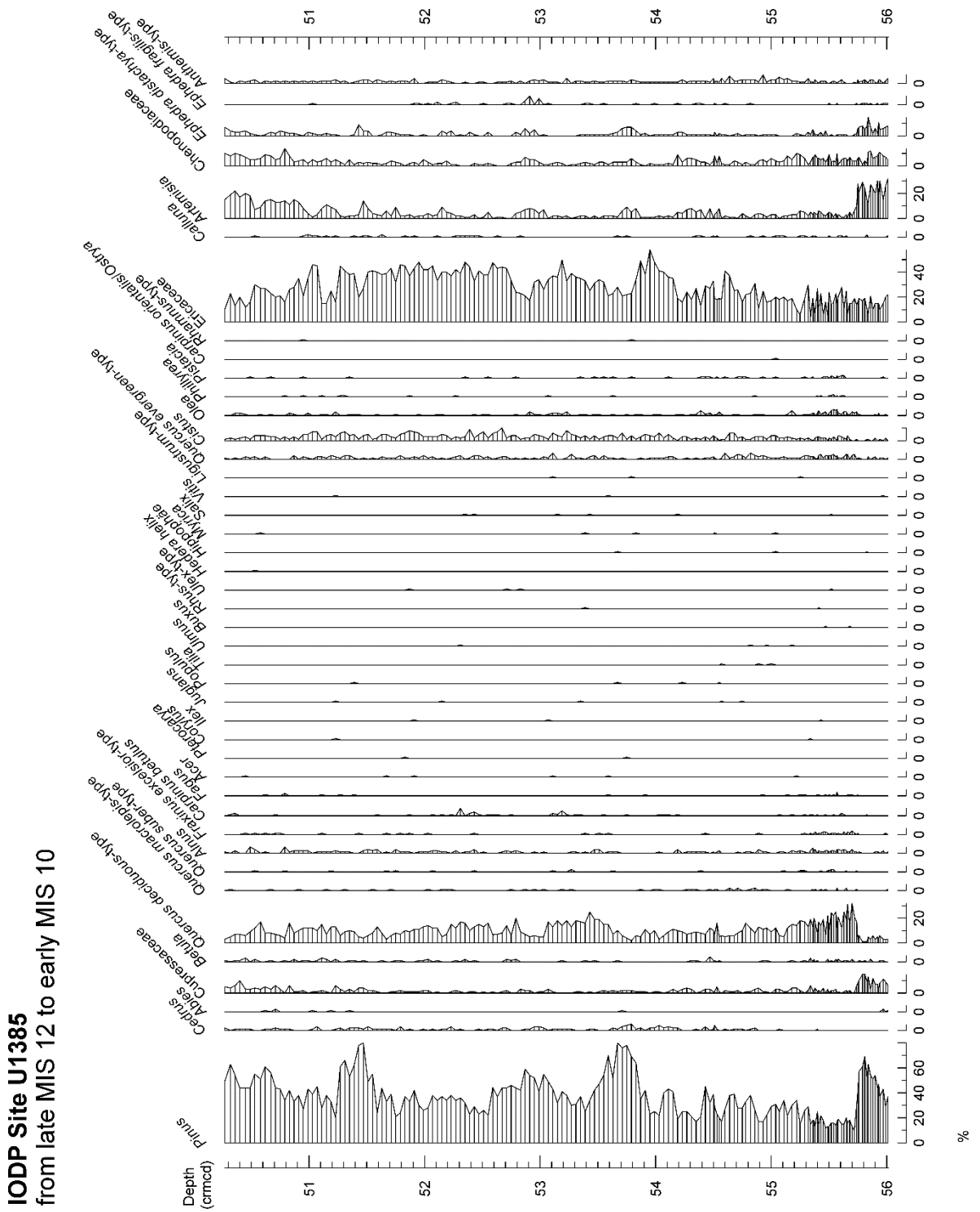
IODP Site U1385
from late MIS 12 to early MIS 10
Depth (crmcd)
51
52
53
54
55
56
Pinus
Cedrus
Abies
Cupressaceae
Betula
Quercus deciduous-type
Quercus macrolepis-type
Alnus
Fraxinus subar-type
Carpinus excelsior-type
Fagus
Acer
Pterocarya
Corylus
Ilex
Juglans
Populus
Tilia
Ulmus
Buxus
Rhus-type
Ulex-type
Hedera helix
Hippophae
Myrica
Salix
Vitis
Ligustrum-type
Quercus evergreen-type
Cistus
Olea
Phillyrea
Pistacia
Carpinus orientalis-type
Rhamnus-type
Ericaceae
Calluna
Artemisia
Chenopodiaceae
Ephedra distachya-type
Ephedra fragilis-type
Anthemis-type
%

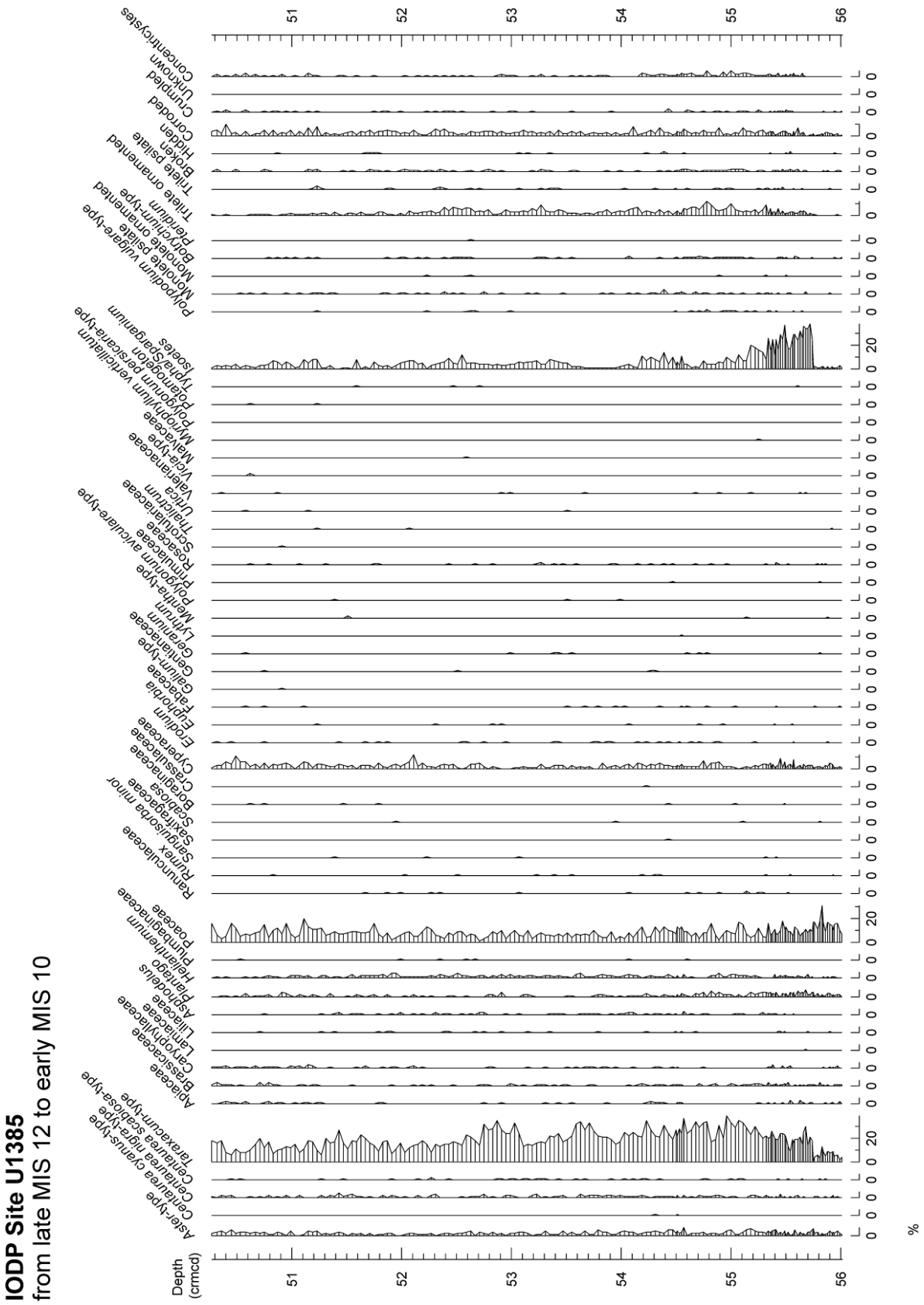
IODP Site U1385
from late MIS 12 to early MIS 10
Depth (crmcd)
51
52
53
54
55
56
Aster-type
Centaurea cyanus-type
Centaurea nigra-type
Centaurea scabiosa-type
Taraxacum-type
Apiaceae
Brassicaceae
Caryophyllaceae
Lamiaceae
Liliaceae
Asphodelus
Plantago
Helianthemum
Plumbaginaceae
Poaceae
Ranunculaceae
Rumex
Sanguisorba minor
Saxifragaceae
Scabiosa
Boraginaceae
Crassulaceae
Cyperaceae
Erodium
Euphorbia
Fabaceae
Galium-type
Gentianaceae
Geranium
Lythrum
Mentha-type
Polygonum aviculare-type
Pinnuliaceae
Rosaceae
Scrofulariaceae
Thalictrum
Urtica
Valerianaceae
Vicia-type
Malvaceae
Myriophyllum
Polygonum
Polygonum verticillatum
Potamogeton
Pteridium
Typha/Sparganium
Isoetes
Polypodium vulgare-type
Monolete psilate
Bolbitiaceae
Monolete ornamented
Tilia
Triletes ornamented
Triletes psilate
Broken
Hidden
Corroded
Crumpled
Unknown
Concentricycloidites
%

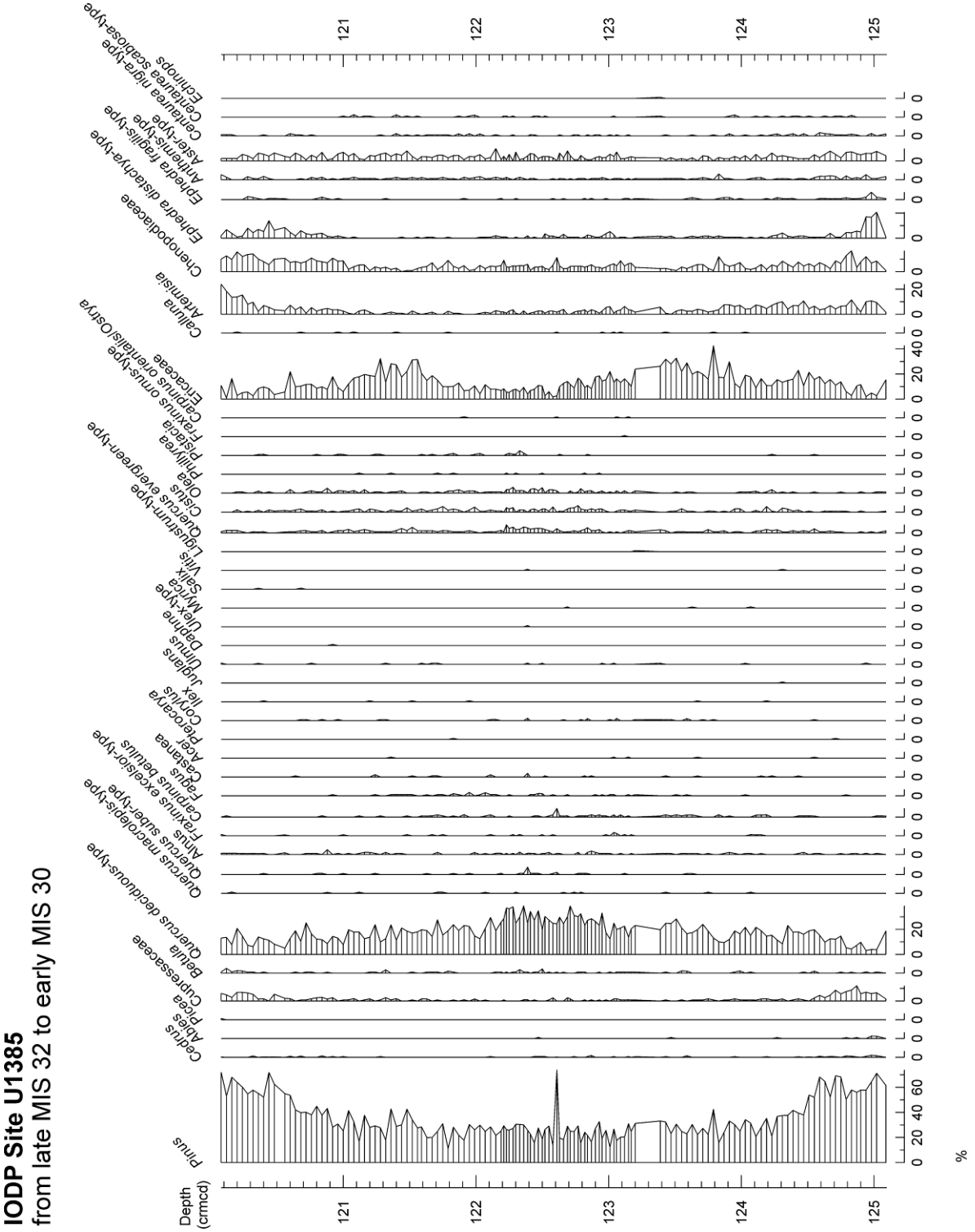
IODP Site U1385
from late MIS 32 to early MIS 30
Depth (crmcd)
121
122
123
124
125
Pinus
Cedrus
Abies
Picea
Cupressaceae
Betula
Quercus deciduous-type
Quercus macrolepis-type
Alnus
Fraxinus subter-type
Carpinus excelsior-type
Fagus
Castanea
Acer
Pterocarya
Corylus
Ilex
Juglans
Ulmus
Daphne
Ulex-type
Myrica
Salix
Vitis
Ligustrum-type
Quercus evergreen-type
Cistus
Olea
Phillyrea
Pistacia
Fraxinus ornus-type
Carpinus orientalis/Ostrya
Ericaceae
Calluna
Artemisia
Chenopodiaceae
Ephedra distachya-type
Ephedra fragilis-type
Asteraceae-type
Centaurea-type
Centaurea nigra-type
Echinops
%

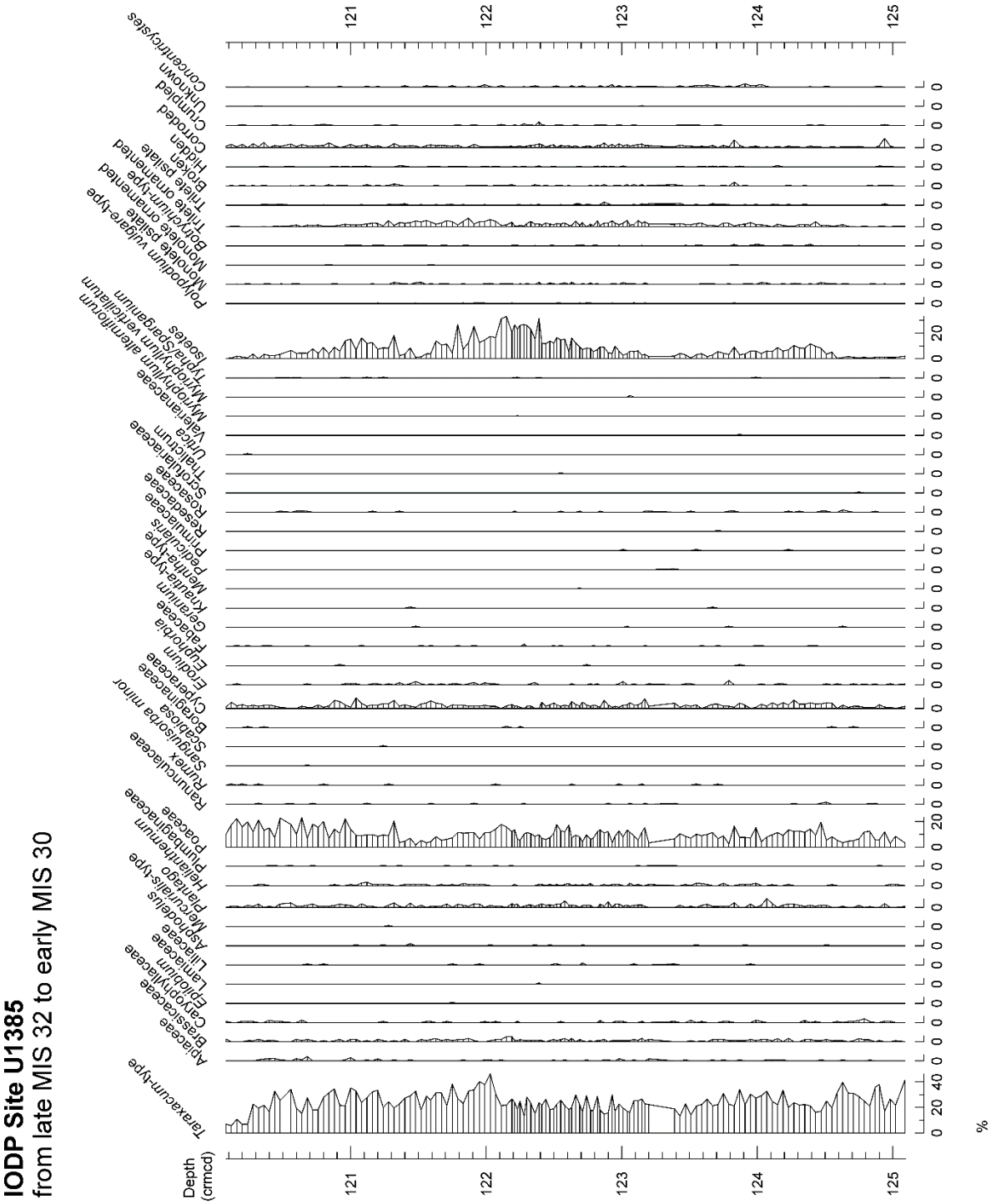
IODP Site U1385
from late MIS 32 to early MIS 30
Depth (crmcd)
121
122
123
124
125
Taraxacum-type
Asteraceae
Brassicaceae
Caryophyllaceae
Ephedra
Lamiaceae
Liliaceae
Apiaceae
Meconopsis
Plantago
Helianthemum
Plumbaginaceae
Poaceae
Ranunculaceae
Rumex
Sanguisorba minor
Scabiosa
Boraginaceae
Cyperaceae
Erodium
Euphorbia
Fabaceae
Geranium
Knautia-type
Mentha-type
Pedicularis
Primulaceae
Resedaceae
Rosaceae
Scrofulariaceae
Thalictrum
Urtica
Valerianaceae
Myriophyllum alterniflorum
Typha/Sparganium
Isoetes
Polypodium vulgare-type
Monolete psilate
Bothrychium-type
Trilete ornamented
Trilete psilate
Botrydium
Hidden
Crumpled
Unknown
Concentricysites
%
0
20
40
0
20
0
20

Appendix B

Co-authored publications of relevance to the thesis

Climate changes in south western Iberia and Mediterranean Outflow variations during two contrasting cycles of the last 1 Myrs: MIS 31–MIS 30 and MIS 12–MIS 11. Sánchez Goñi, M.F., Llave, E., Oliveira, D., Naughton, F., Desprat, S., Ducassou, E., Hodell, D.A., Hernández-Molina, F.J. (2016). Global and Planetary Change 136, 18–29.

Dinoflagellate cyst population evolution throughout past interglacials: Key features along the Iberian margin and insights from the new IODP Site U1385 (Exp 339). Eynaud, F., Londeix, L., Penaud, A., Sánchez Goñi, M.F., Oliveira, D., Desprat, S., Turon, J.-L. (2016). Global and Planetary Change 136, 52–64.

L'étude du pollen des séquences sédimentaires marines pour la compréhension du climat : l'exemple des périodes chaudes passée. [*Pollen in marine sedimentary archives, a key for climate studies: the example of past warm periods*].
Desprat, S., Naughton, F., Oliveira, D., Sánchez Goñi, M.F. (in press). Quaternaire.

Global and Planetary Change 136 (2016) 18–29

Contents lists available at ScienceDirect

Global and Planetary Change

journal homepage: www.elsevier.com/locate/gloplacha

Climate changes in south western Iberia and Mediterranean Outflow variations during two contrasting cycles of the last 1 Myrs: MIS 31–MIS 30 and MIS 12–MIS 11

M.F. Sánchez Goñi [a,*], E. Llave [b], D. Oliveira [a,c,d], F. Naughton [c,d], S. Desprat [a], E. Ducassou [e], D.A. Hodell [f], F.J. Hernández-Molina [g]

[a] Ecole Pratique des Hautes Etudes (EPHE), UMR CNRS 5805 EPOC, Université de Bordeaux, Allée Geoffroy St Hilaire, 33615 Pessac, France
[b] Instituto Geológico y Minero de España, Ríos Rosas 23, 28003 Madrid, Spain
[c] Divisão de Geologia e Georecursos Marinhos, Instituto Português do Mar e da Atmosfera (IPMA), Av. de Brasília 6, 1449-006 Lisbon, Portugal
[d] CCMAR, Center of Marine Sciences, Algarve, Portugal
[e] Université de Bordeaux, UMR CNRS 5805 EPOC, Allée Geoffroy St Hilaire, 33615 Pessac, France
[f] Godwin Laboratory for Palaeoclimate Research, Department of earth Sciences, University of Cambridge, UK
[g] Department of Earth Sciences, Royal Holloway, University of London, Egham, Surrey TW20 0EX, UK

ARTICLE INFO

Article history:
Received 28 April 2015
Received in revised form 10 November 2015
Accepted 16 November 2015
Available online 17 November 2015

Keywords:
Mediterranean Outflow Water
South western Iberia
Grain-size
Pollen
Vegetation
Climate
MIS 31–MIS 30
MIS 12–MIS 11

ABSTRACT

Grain size analysis and physical properties of Sites U1388, U1389 and U1390 collected in the Contourite Depositional System of the Gulf of Cádiz during the Integrated Ocean Drilling Program (IODP) Expedition 339 "Mediterranean Outflow" reveal relative changes in bottom current strength, a tracer of the dynamics of the Mediterranean Outflow Water (MOW), before and after the Middle Pleistocene Transition (MPT). The comparison of MOW behavior with climate changes identified by the pollen analysis and $\delta^{18}O$ benthic foraminifera measurements of Site U1385, the Shackleton Site, collected in the south western Iberian margin shows that the interval MIS 31–MIS 30, ~1.1–1.05 million years ago (Ma), before the MPT, was marked by wetter climate and weaker bottom current than the interval MIS 12–MIS 11 (0.47–0.39 Ma), after the MPT. Similarly, the increase in fine particles from these glacials to interglacials and in coarse fraction from interglacials to glacials was coeval with forest and semi-desert expansions, respectively, indicating the lowering/enhancement of MOW strength during periods of regional increase/decrease of moisture. While these findings may not necessarily apply to all glacial/interglacial cycles, they nonetheless serve as excellent supporting examples of the hypothesis that aridification can serve as a good tracer for MOW intensity. The strongest regional aridity during MIS 12 coincides with a remarkable increase of coarse grain size deposition and distribution that we interpret as a maximum in MOW strength. This MOW intensification may have pre-conditioned the North Atlantic by increasing salinity, thereby triggering the strong resumption of the Meridional Overturning Circulation that could contribute to the great warmth that characterizes the MIS 11c super-interglacial.

1. Introduction

The warm and saline water plume formed by the Mediterranean Outflow exiting the Strait of Gibraltar between 500 and 1400 mbsl is a prominent feature that presently enhances the water density in the North Atlantic, thereby affecting deep convection in the North Atlantic that regulates the Meridional Overturning Circulation (MOC) (Rogerson et al., 2006; Hernández-Molina et al., 2014). Estimates from coarse resolution climate models suggest that without Mediterranean Outflow Water (MOW), the Atlantic Meridional Overturning Circulation (AMOC) would be reduced by ~15% and North Atlantic sea surface temperatures would fall by up to 1 °C (Rogerson et al., 2012; Ivanovic et al., 2013). Other model simulations show that the position of the North Atlantic subtropical and subpolar gyres is very sensitive to MOW intensity (cf. New et al., 2001). For example, an enhanced MOW induces an amplified current crossing the Atlantic from Florida to the Canary Current leading to a more zonal position of the subtropical gyre and a weakening of the North Atlantic Drift that reaches the subpolar gyre and Nordic Seas. In contrast, a strong decrease in MOW might slowdown this current, thus changing the shape of the subtropical gyre and enhancing the North Atlantic Drift. Variations in the strength of MOW can therefore affect not only the AMOC, but also the climate in general and, in particular, that of Europe (e.g. Lohmann et al., 2009). Conversely, climate in high and low latitudes of the North Atlantic region, affects the present-day Gibraltar water exchange (Rogerson et al., 2012). For example, outbursts of cold dry air in winter from the European continent induce surface water cooling and deep convection in the Mediterranean

* Corresponding author.
E-mail address: mf.sanchezgoni@epoc.u-bordeaux1.fr (M.F. Sánchez Goñi).

http://dx.doi.org/10.1016/j.gloplacha.2015.11.006
0921-8181/

Basin that contribute to the formation of MOW (Candela, 2001). Alternatively, reduced evaporation in the Mediterranean region and more northerly and stronger African monsoon rainfall would reduce salinity in the Mediterranean and, therefore, the Gibraltar exchange (Rogerson et al., 2012).

Previous studies suggest strong relationships between changes in MOW intensity and position, and the orbital and millennial scale variability of Greenland and the North Atlantic; e.g., D–O cycles and Heinrich events (Rogerson et al., 2006, 2012; Voelker et al., 2006; Llave et al., 2006; Toucanne et al., 2007). These studies show that repeated MOW increases occurred during decreases in air surface temperature and precipitation in the western Mediterranean region and, particularly during Heinrich events when AMOC decreased (Voelker et al., 2006). However, few studies address the relationships between MOW variability and regional climate during older periods beyond the last climatic cycle (e.g. Llave et al., 2006; Voelker and Lebreiro, 2010), partly because of the scarcity of paleoclimate records (e.g. Joannin et al., 2011) of air surface temperature and precipitation changes during those periods in the Mediterranean region.

During the Early to the Late Pleistocene including the Middle Pleistocene Transition (MPT, ~0.9–0.65 Ma, Maslin and Ridgwell, 2005), when the dominant cyclicity changed from 41,000 to 100,000 year-cycles, the MOW became sequentially shallower suggesting the increase of the density contrast between Atlantic and Mediterranean water (Rogerson et al., 2012). It has been hypothesized that the shoaling of the MOW and its intensification are indicators of ice volume increase and Mediterranean aridity (e.g. Llave et al., 2006; Rogerson et al., 2012). The objective of this work is testing the second hypothesis using several high-resolution sedimentary sequences and focusing on Marine Isotope Stage (MIS) 31–MIS 30 (from 1.1 to 1.05 Ma) and MIS 12–MIS 11c (from 0.47 to 0.39 Ma) collected during the IODP Expedition 339 "Mediterranean Outflow" in the southwestern Iberian margin and Gulf of Cádiz. These intervals are ideally suited to test the aforementioned hypothesis. The LR04 stack record suggests that the most recent interval is characterized on average by larger ice sheets and more marked cold glacial and warm interglacial periods than the MIS 31–MIS 30 interval (Lisiecki and Raymo, 2005). Previous studies additionally show the regional wet character of the cycle before the MPT (Joannin et al., 2011) when compared with the cycles after 400 ka (e.g. Sánchez Goñi et al., 1999; Roucoux et al., 2006). No data are available for MIS 12 and no indicator of aridity, i.e. pollen percentage of semi-desert plants, has been published for MIS 11 so far.

2. Present-day environmental context

Climate in the southern Iberian continental margin, including the Gulf of Cádiz, is directly affected in winter by the North Atlantic westerlies, while a high pressure cell develops in the North Atlantic during summer. This seasonality of climate is characterized by mild winters (m: 5–1 °C; M: 13–8 °C) and hot and dry summers (*P*ann < 600 mm) (Peinado Lorca and Martínez-Parras, 1987), and lead to the development of a Mediterranean vegetation in the adjacent landmasses dominated by deciduous oak at middle elevation, and evergreen oak, olive tree, *Pistacia*, *Phillyrea* and rockroses (*Cistus*) at lower elevations (Blanco Castro et al., 1997). Experimental studies on the pollen representation of western Iberian vegetation in the sediments of its margin (Naughton et al., 2007) show that marine pollen assemblages give an accurate and integrated image of the regional vegetation occupying the adjacent continent. Present-day Mediterranean and Atlantic forest communities of Iberia are well discriminated by south and north marine pollen spectra, respectively (Naughton et al., 2007).

The dynamics of the North Atlantic subtropical gyre dominate the oceanic surface currents on the southern Iberian margin (Stramma and Siedler, 1988). The waters are under the influence of the Portuguese Current, the southern branch of the North Atlantic Current a part of the eastern North Atlantic subtropical gyre (Péliz et al., 2005). The intermediate layers are directly affected by the MOW that causes the formation of contourite deposits along the middle slope (e.g. Llave et al., 2007).

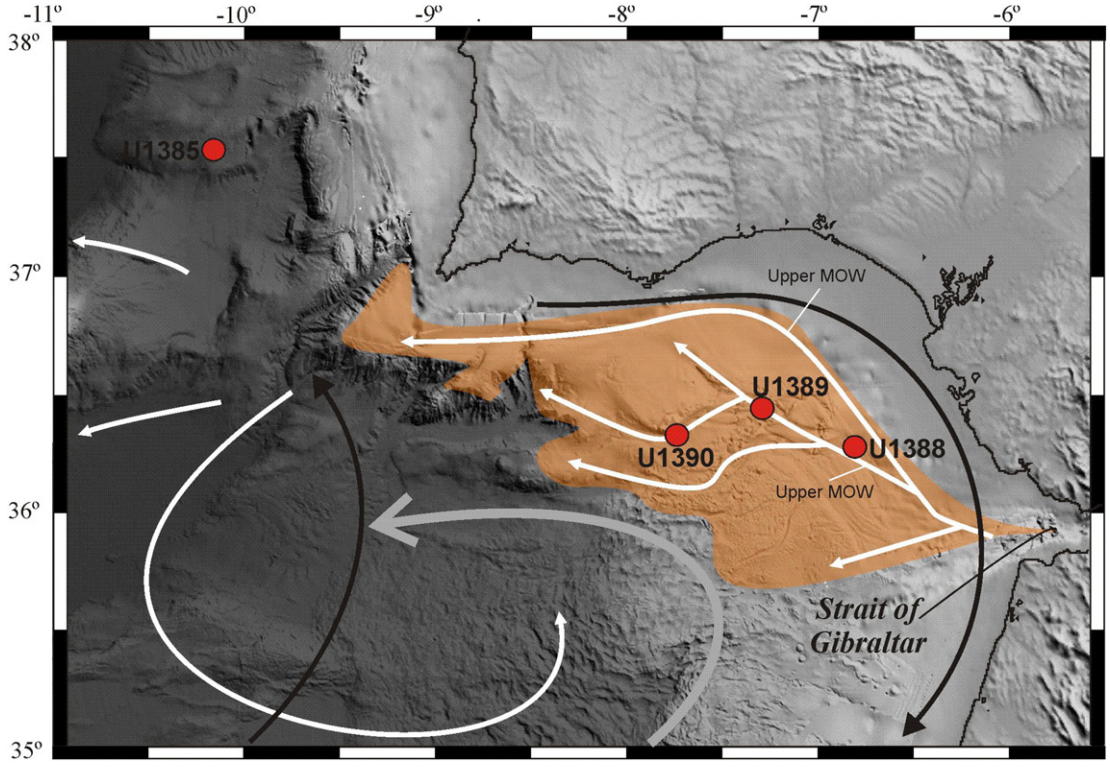

Fig. 1. Location of the cores on the CDS (Contourite Depositional System of the Gulf of Cadiz) (orange area), and circulation of the main water masses. Black arrows: NASW (North Atlantic Surficial Water); white arrows: MOW (Mediterranean Outflow intermediate Water); gray arrow: NADW (North Atlantic deep Water).

Below the MOW, Northeast Atlantic Deep Water (NADW) and Lower Deep Water are found (Baringer and Price, 1999). Seasonal coastal upwelling occurs in summer due to the northerly winds (Fiúza et al., 1982).

3. Material and methods

The evolution of the Mediterranean climate will be documented by the pollen-derived vegetation study of Site U1385, the so-called "Shackleton Site", while the study of contourite deposition in Sites U1388, U1389 and U1390 will provide information on MOW variability. Sites U1388, U1389 and U1390, obtained during the IODP Expedition 339, are located in the proximal and middle sectors of the Gulf of Cádiz Contourite Depositional System (CDS) under the influence of the Lower core of the MOW (Fig. 1). Site U1388 is located about 50 km southwest of the Spanish city of Cádiz (36°16.142 N; 6°47.647 W), in a water depth of 663 mbsl. This site lies within the extensive Cádiz sandy-sheeted drift, which is the proximal part of the larger Cádiz CDS (Hernández-Molina et al., 2003; Llave et al., 2007), and is the closest site to the Strait of Gibraltar gateway drilled during Expedition 339. Site U1389 is placed ~90 km west of the Spanish city of Cádiz (36°25.515 N; 7°16.683 W), in a water depth of 644 mbsl. Site U1390 is situated ~130 km west of the Spanish city of Cádiz (36°19.110 N; 7°43.078 W) in a water depth of 992 mbsl. These last two sites are drilled in the "channels and ridges" sector of the Cádiz CDS, on the Huelva sheeted/patch drift and Guadalquivir drift, respectively.

Site U1385 (37°34.285′ N, 10°7.562′ W), also collected during the IODP Expedition 339, is located on a spur, the Promontorio dos Principes de Avis, along the continental slope of the southwestern Iberian margin, under pelagic/hemipelagic sedimentation and not affected by turbidite processes (Hodell et al., 2013). This site is at a water depth of 2578 mbsl, under the influence of Northeast Atlantic Deep Water at present time, although it was influenced by southern sourced waters during glacial periods (Martrat et al., 2007).

3.1. Chronology

The age models for Sites U1388, U1389 and U1390 are in progress. Age control points presented in Stow et al. (2013) allowed the correlation of these sites to the LR04 isotopic chronology (Lisiecki and Raymo, 2005). A synthesis of the control points used for each site is presented in Table 1. Stratigraphic correlation between the different holes and sites are based on physical and downhole logging data, mainly gamma-ray (Lofi et al., in review). The stratigraphy of Site U1385 was built upon a combination of chemo-stratigraphic proxies (Hodell et al., 2015, this issue). Ca/Ti was measured in all holes by core scanning XRF and was used to construct a complete composite section. Oxygen isotopes of benthic foraminifera were correlated to the marine $\delta^{18}O$ stack of LR04 to provide the age model used in this paper. Additional $\delta^{18}O$ measurements were made of benthic foraminifera to refine the age model over the MIS 12/11 transition.

3.2. Grain-size analysis

A textural study of grain-size distribution parameters has been carried out at Sites U1388, U1389 and U1390. Bulk sediment subsamples in silts and sands were taken for grain-size measurements using a Malvern MasterSizer S (0.05 to 878.67 μm) at the University of Bordeaux. Grain-size statistical parameters (mean, sorting, skewness and kurtosis) have been calculated with GRADISTAT program, using the Folk and Ward (1957) method of geometric (modified) graphical measures (Blott and Pye, 2001). GRADISTAT software provides descriptors as primary, secondary and tertiary modes, the median, and a measure of distribution spread, such as D90–D10, which frequently prove to be more reliable than the standard size statistics, especially when sediments are clearly multimodal. Because D90 oscillations obtained by Malvern MasterSizer are more significant while showing congruent fluctuations with mean > 63 μm, we use this grain-size parameter throughout this study to be compared with the other textural attributes as well as with physical properties: Gamma ray attenuation (GRA) density, Magnetic Susceptibility (MS), Natural gamma radiation (NGR) and color reflectance (L*, a*), obtained during the Expedition 339 (Stow et al., 2013) and with seismic profiles database (Hernández-Molina et al., 2015). This correlation was performed in more detail only in Site U1389. For the other sites, recovery at Site U1388 was generally poor, and the studied intervals (MIS 12–MIS 11 and MIS 31–MIS 30) at Site U1390 coincides with a short hiatus described by Stow et al. (2013)..

3.3. Pollen analysis

Sediment subsamples of 1-cm thickness and 1.5–4.5 cm3 volume were prepared for pollen analysis using the standard protocol for marine samples, http://www.ephe-paleoclimat.com/Files/Other/Pollen%20extraction%20protocol.pdf, employing coarse-sieving at 150 μm, successive treatments with cold HCl, cold HF at increasing strength and micro-sieving (10 μm mesh). Known quantities of *Lycopodium* spores in tablet form were added to permit the calculation of pollen concentrations. Slides were prepared using a mobile mounting medium to permit rotation of the grains and counted using a Nikon light microscope at 500× and 1000× magnifications for routine and identification of pollen and spores, respectively. Pollen counts reached a minimum main sum of 100 terrestrial pollen grains excluding *Pinus*, aquatics and spores and between 20 and 32 taxa excluding four samples from MIS 12 with 19 (3 samples) and 17 (1 sample) taxa. The total sum that includes all terrestrial and aquatic pollen and spores oscillates between 140 and 936 grains per sample. Pollen percentages for terrestrial taxa were calculated against the main sum of terrestrial grains, while

Table 1
Biostratigraphical datums used to build the age model of cores U1388, U1389 and U1390. FO: first occurrence and LO: last occurrence.

Biostratigraphic event	Age (Ma)	Depth (mbsf)									
		U1388B		U1389A		U1389C		U1389E		U1390A	
		Top	Bottom	Top	Bottom	Top	Bottom	Top	Bottom	Top	Bottom
FO *Emiliana huxley*	0.26	47.47	56.14	91.96	93.37	111.64	122.26			189.5	190.5
LO *Pseudoemiliania lacunosa*	0.46	162.82	178.02	208.73	210.56	211.52	221.12			228.65	228.73
LO *Gephyrocapsa omega*	0.57									228.65	228.73
Stilostomella extinction	0.58–0.7									284.61	293.68
LO *Reticulofenestra asanoi*	0.9			322.63	332.55	326.9	327.44				
FO *R. asanoi*	1.07							360.65	362.15		
Top Paracme *Neogloboquadrina pachyderma* (s)	1.21									284.61	293.68
LO *G.* spp.	1.24							377.66	387.99		
LO *Helicosphaera sellii*	1.24										

percentages for *Pinus* were calculated against the main sum plus *Pinus*. Aquatics and spores percentages are based on the total sum.

4. Results

The time intervals studied, MIS 12–MIS 11 and MIS 31–MIS 30, are represented by sediments included in Subunit IA and in the top of Subunit IB as described by Stow et al. (2013), respectively. Site U1389 provides the highest resolution record for MIS 12 and MIS 11 owing to the poor recovery at Site U1388, and the short hiatus (0.3–0.6 Ma) described at Site U1390 (Stow et al., 2013). In the case of MIS 31 and MIS 30, the best site for lithologic and physical properties correlation is Site U1389 as well. Site U1388 is younger than 0.6–0.7 Ma, and there is a second hiatus (0.65–1.2 Ma) at Site U1390 (Stow et al., 2013). However, the correlation of all sites with seismic profiles provides some evidence of the sedimentary evolution during these climatic stages. Site U1385 covers without interruption the last 1.5 Ma but a very low sedimentation rate or a short hiatus is identified during the MIS 12/11 transition (Hodell et al., 2015, this issue).

4.1. Sedimentological changes during MIS 12 and MIS 11

The lithological records differ for sites located along a transect extending from more proximal to distal locations from the Gibraltar Strait. At Site U1388 a coarsening upward (D90 around 350 μm-medium sands) occurs during MIS 12 (between 170 and 160 mbsf), and fining upward (D90 around 50 μm-very coarse silt) during MIS 11 (around 150 mbsf) (Fig. 2). There is a unimodal shape in sand fraction during MIS 12 and bimodal shape during MIS 11, reflecting the mixing of a subordinate sandy coarse silt and a dominant silt population. This is caused by an increasing percentage of sand fraction during MIS 12, and of silt fraction during MIS 11. The binary plots show that coarse grains deposited during MIS 12 are characterized by lower sorting values (very poorly sorted); negative skewness; and greater variations in kurtosis between leptokurtic and platykurtic. The finest grains are deposited during MIS 11 and show positive skewness and better sorting than MIS12, and leptokurtic kurtosis (Fig. 2). The physical properties show a correspondence between higher magnetic susceptibility and density of sandier layers within the more mud-prone sections, but negatively correlated with NGR (Fig. 2).

At Site U1389, MIS 12 is identified between 235 and 205 mbsf and MIS 11 between 205 and 195 mbsf (Fig. 3). The grain size characteristics of the silt/sand fractions of the intervals MIS 12 and MIS 11 were examined in detail to investigate any changes in sedimentology through the period of contourite deposition. Overall, clear differences can be seen between sediments deposited during MIS 12 and MIS 11 in terms of sorting, kurtosis and skewness. The D90 grain size is remarkably constant at around 40 μm for the majority of samples in MIS 11, and more variable but coarser in MIS 12 (80–180 μm-very fine to fine sand) generally showing poorly sorted and negative skewness (Fig. 3). In general, the distribution of the grain size is bimodal during both isotopic intervals, with the very fine sand mode being dominant during MIS 12, and the fine silt fraction during MIS 11. Variations of D90 are positively correlated with sorting and variability, and inversely correlated with skewness and kurtosis. The beds of coarser grain size correspond to higher GRA-density, magnetic susceptibility and a* values than for the otherwise muddy sediment. A remarkable change is observed in the physical properties in the depth interval occurs at the MIS 12/11 transition: The lower part 250–220 mbsf is characterized by relatively high and variable magnetic susceptibilities and GRA-densities as well as widely fluctuating a* values. A distinct second interval can be discerned from 220 to >195 mbsf, which displays high NGR values, low a* (i.e. more greenish colors) as well as magnetic susceptibilities and GRA densities with similar fluctuations as above but a considerably reduced scatter of the data. A plot of sorting against skewness of the sand/silt fractions shows a simple correlation between the two parameters, with more positive skewness corresponding to better sorting (Fig. 3). The binary plots show fine grains, symmetric or positive skewed and poorly sorted, with a dominant mesokurtic modal distribution during MIS 11, and coarser grained and worse sorted during MIS 12, dominantly fine skewed and platykurtic distribution.

Finally at Site U1390, there are some changes related to the hiatus associated to the MIS 12–MIS 11: from gentle coarsening to a general fining upward; from very poorly to poorly sorted; from fine to symmetric skewed; from platykurtic to more constant mesokurtic (Fig. 4). This coarser layer just after the hiatus shows a bimodal distribution, with a

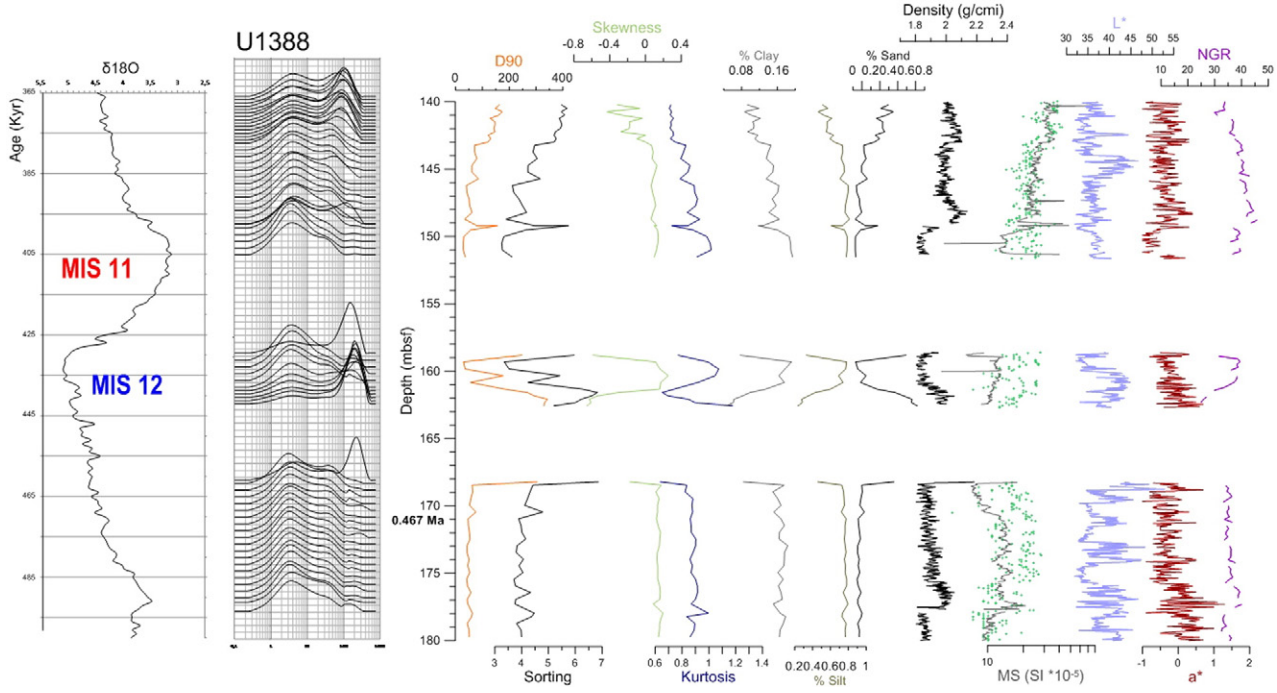

Fig. 2. Grain size parameters and physical properties distribution at Site U1388 compared with the LR04 isotopic chronology (Lisiecki and Raymo, 2005).

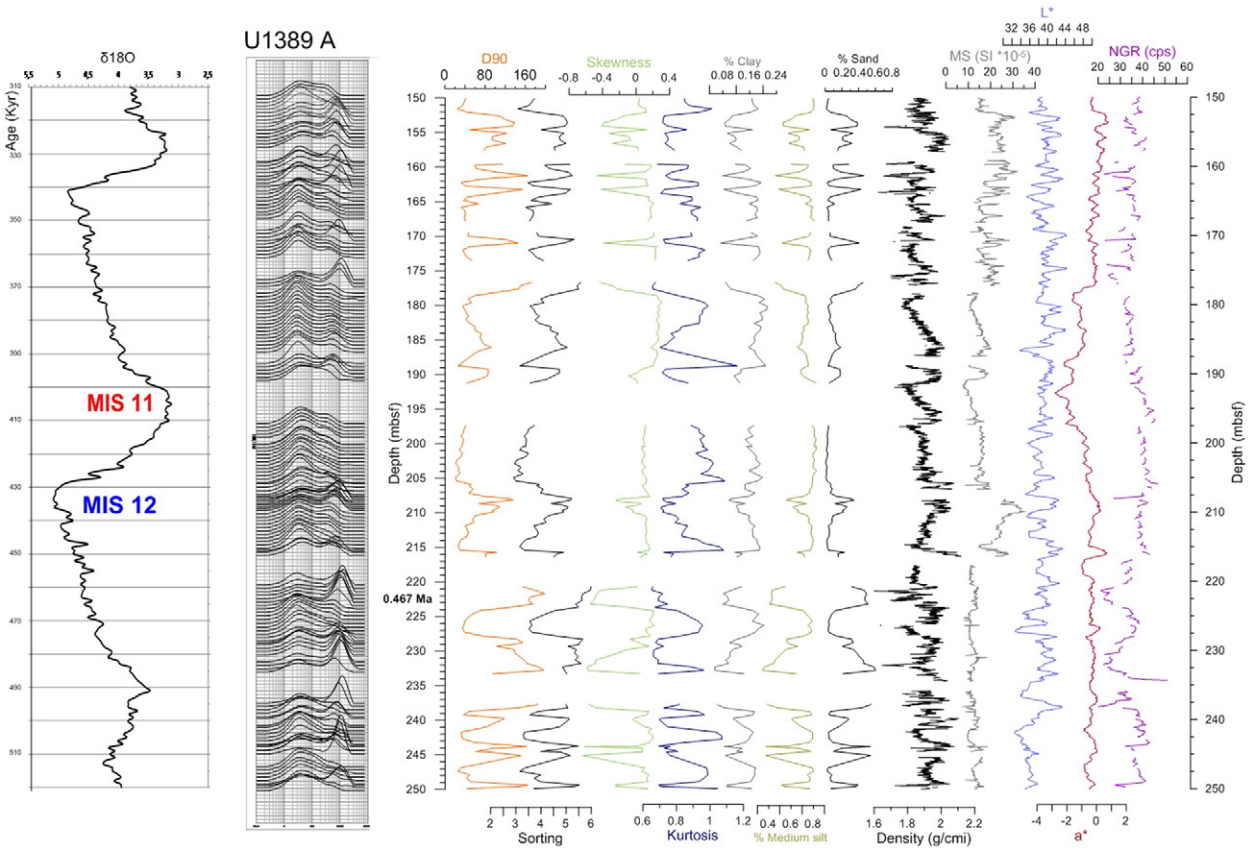

Fig. 3. Grain size parameters and physical properties distribution at Site U1389 compared with the LR04 isotopic chronology (Lisiecki and Raymo, 2005).

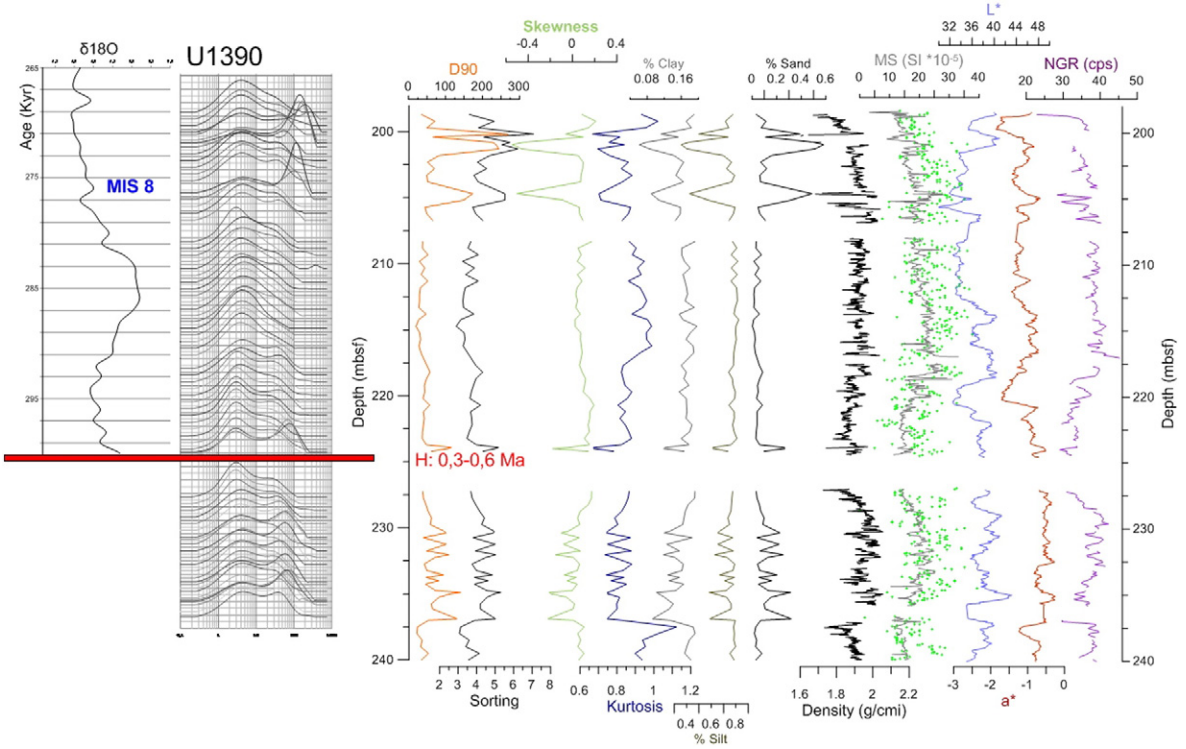

Fig. 4. Grain size parameters and physical properties distribution at Site U1390 compared with the LR04 isotopic chronology (Lisiecki and Raymo, 2005).

main mode at ~100 μm (fine sand) and a subordinate mode at 4 μm (fine silt). As observed in the other studied sites, physical properties data show a positive correlation of magnetic susceptibility and bulk density correlating with the D90 grain size, and a negative correlation with NGR values.

4.2. Sedimentological changes during MIS 31 and MIS 30

This interval was partially recovered between 365 and 355 mbsf at Site U1389 (Fig. 5). Although the clay size fraction is more abundant (47%) than the sand size fraction (20%) in this unit (unit IB) than in the unit where MIS 12–MIS 11 occurred, unit IA, the silt abundance remains similar. Additionally at 363 mbsf, where the transition of MIS 31 to MIS 30 is supposed to be developed, a change occurs from fine silt unimodal distribution to a bimodal distribution with a dominant mode at ~300 μm (medium sand). The same pattern as at the aforementioned sites is observed in physical properties data, showing a positive correlation between magnetic susceptibility and bulk density correlating with the D90 grain size, and negative correlation with NGR values. In the binary plots, mesokurtic, symmetrical skewed and poorly sorted is observed in silty fractions during warm intervals, and very poorly sorted, varied skewed and distributed in sandy fraction during cold intervals, especially during MIS 30 (Fig. 5).

The integration of the studied sites with the geophysical database, have also allowed correlation of these lithological units with the major seismic units. The increase in the amplitude of the reflections during MIS 12 and MIS 30, related to coarsening in the grain size fraction, is higher during MIS 12 than MIS 30 and correlated with one of the main discontinuities identified during the Quaternary (Hernández-Molina et al., 2002; Llave et al., 2007; Marches et al., 2010). No direct data from sites U1388, 1389 and 1390 exist for MIS 31. However, MIS 31 is found in the unit IB which is a clearly distinct lithological subunit from that encompassing MIS 11, unit IA. Unit IB (320–410 mbsf) is largely dominated by calcareous mud (80%) associated with a minor contribution of silty and sandy muds (13% including biogenic carbonate) and 7% of silty sand with biogenic carbonate. In contrast, unit IA (<320 mbsf) is characterized by calcareous mud (60%), silty mud with biogenic carbonate (25%) being the next main lithology; sandy mud with biogenic carbonate (9%), and silty sand with biogenic carbonate making minor contributions to the overall lithology.

4.3. Pollen-based climate changes during MIS 12 and MIS 11

Fig. 6 shows the low resolution pollen and $\delta^{18}O$ benthic foraminifera ($\delta^{18}O_b$) records from Site U1385 along with the LR04 oxygen isotopic stack and insolation and precession changes. The comparison of the $\delta^{18}O_b$ record from Site U1385 (Hodell et al., 2013) with the LR04 stack clearly identifies MIS 12 and MIS 11 with maximum and minimum values by ~4.5 and 2.7‰, respectively (Fig. 6, panel a). These values are however lighter than those observed in the LR04 stack because U1385 values are uncorrected to equilibrium values. MIS 12 is characterized by very high percentages of semi-desert vegetation (30–60%), similar to those observed in the western Mediterranean region from cores MD95-2043 and MD01-2444 during MIS2, MIS4 and MIS6.4 when ice volume was great (Fletcher et al., 2010; Margari et al., 2014). This vegetation indicates extremely dry cold winters and, by analogy with the last glacial period (Moreno et al., 2005), a windy climate. In contrast, during interglacial MIS 11c, the first high sea level stand of MIS 11, a rapid increase in the Mediterranean forest, up to 45% of pollen percentages, suggests an increase in winter precipitation and warmer temperatures as already revealed by the nearby site MD01-2443 (Tzedakis et al., 2009). However, the low pollen representation of the Mediterranean taxa *s.s.* (evergreen *Quercus*, *Olea*, *Pistacia*, *Phillyrea*, *Olea* and *Cistus*), with less than 10%, may indicate a period of muted seasonality contrasting with warmer interglacials in southern Iberia such as the Eemian (~MIS5e) marked by an average of 20% of Mediterranean plants (Sánchez Goñi et al., 1999). This muted seasonality in the Mediterranean region would be in line with the low eccentricity and,

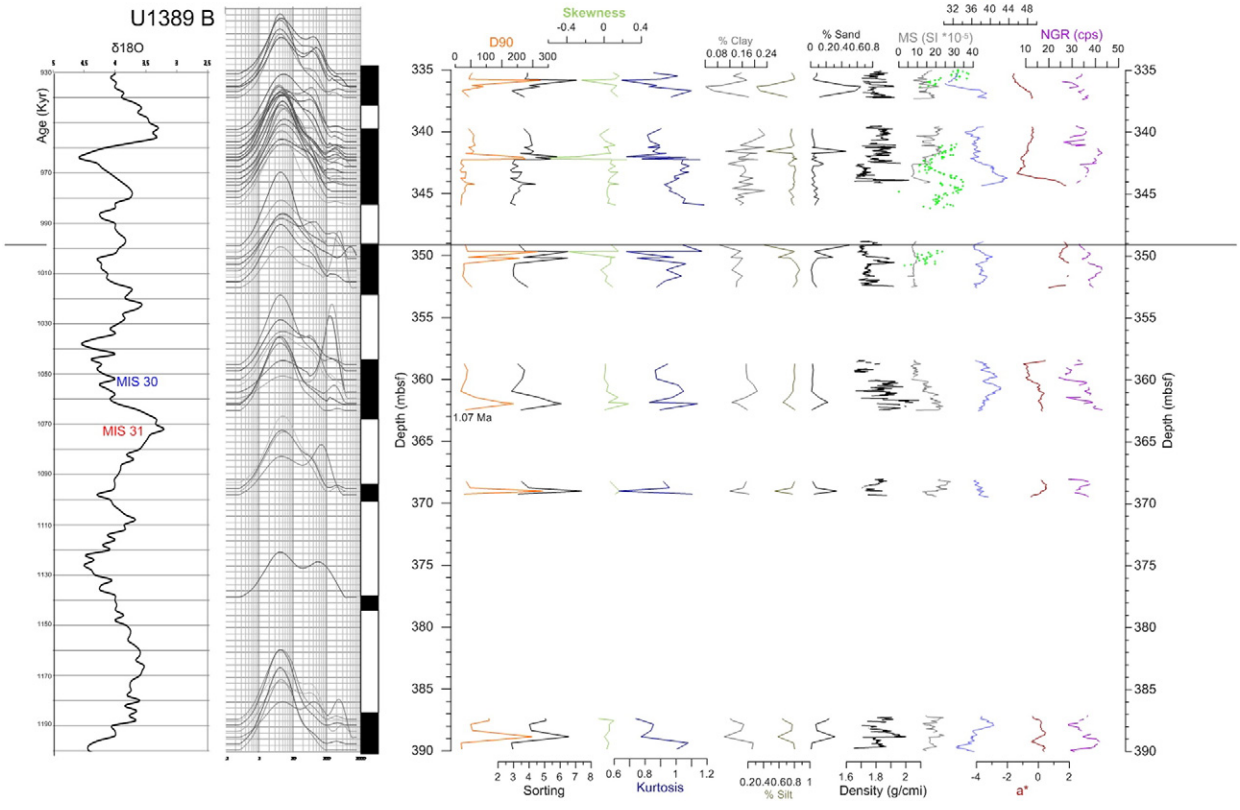

Fig. 5. Grain size parameters and physical properties distribution at Site U1389 B correlated with the LR04 isotopic chronology (Lisiecki and Raymo, 2005).

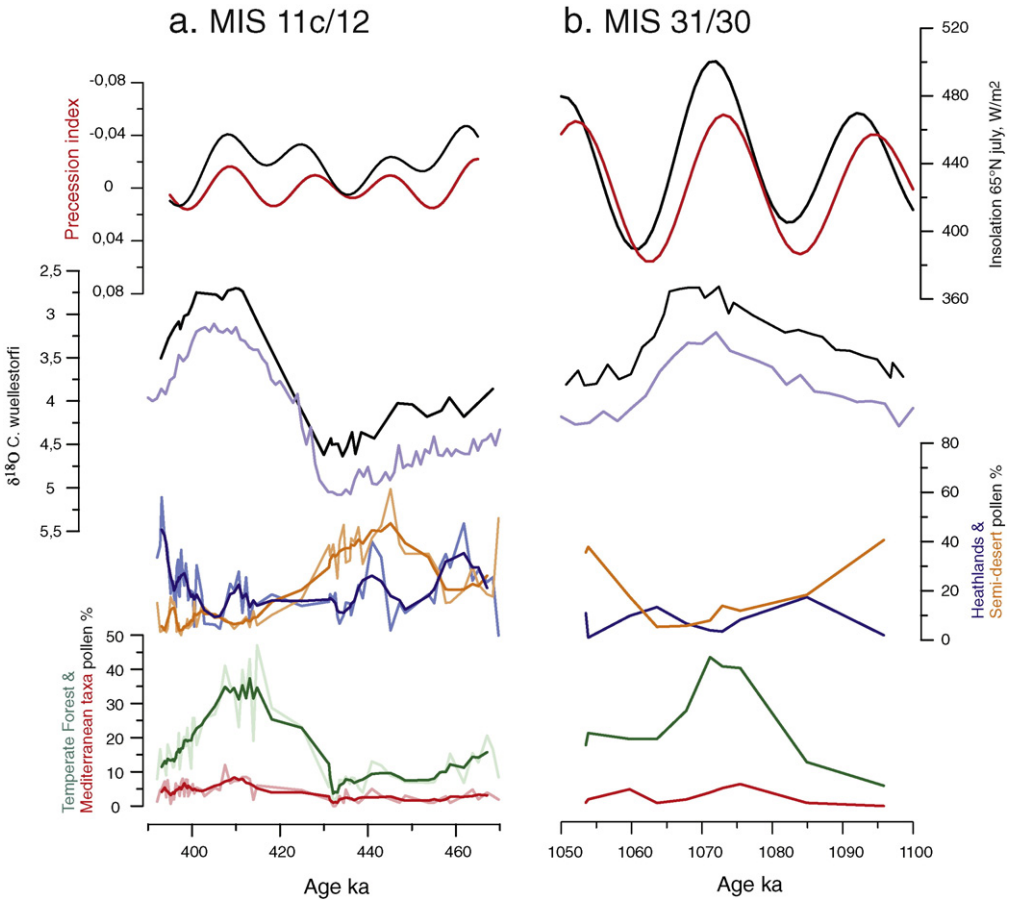

Fig. 6. Insolation at 65° N in July and precession changes during MIS 31–30 and MIS 12–11 (Berger, 1978) plotted along $\delta^{18}O$ benthic foraminifera values (U1385 and LR04 stack in black and purple, respectively) and pollen percentages of Mediterranean forest (green), Mediterranean taxa (red), semi-desert (orange) and heathlands (blue).

therefore muted precession (less seasonal contrast), that characterized MIS 11c in contrast to MIS5e. An alternative hypothesis is that the warmest phase of MIS 11c (Desprat et al., 2005) is not represented at Site U1385 owing to the very low sedimentation rates observed during Termination V and early MIS 11c indicating a condensed section or brief hiatus between 430 and 410 ka (Hodell et al., 2015, this issue)..

4.4. Pollen-based climate changes during MIS 31 and MIS 30

The $\delta^{18}O_b$ anomalies between MIS 31 and MIS 30 are weaker than those observed between MIS 12 and MIS 11 because of the relatively weak glacial state (low oxygen isotopic values) during MIS 30, at ~4.2 and 3.7‰ in the LR04 and U1385 records, respectively (Fig. 6, panel b). Vegetation during MIS 31 was marked by high percentages of forest but low percentages and weak diversity of Mediterranean taxa *s.s.*, and the occurrence of various temperate trees such as deciduous *Quercus*, *Castanea*, *Corylus* and *Carpinus betulus*-type that cannot survive summer drought and develops with relatively high/low mean winter/summer temperatures, above 0 °C and between 15 and 18 °C, respectively (Fig. 7) (Polunin and Walters, 1985; Blanco Castro et al., 1997; Gallardo-Lancho, 2001; Tallantire, 2002). The composition of this forest indicates a warm–cool and wet summer climate with low seasonality. This climate likely implies less evaporation and lower salinity in the Mediterranean Sea than during the younger interglacial MIS 11c marked by a more Mediterranean character (higher diversity of Mediterranean taxa and virtual absence of intolerant-summer drought trees, Fig. 7). The average lower percentages of the fern spore *Isoetes* during MIS 31 than during MIS 11c would also indicate a relatively seasonally wetter climate as the optimal development of *Isoetes* requires periods of flooding alternating with desiccation (Salvo Tierra, 1990). The low amount of heathlands in comparison with that observed during MIS 11c is difficult to explain as the optimal development of European heathlands requires similar climatic conditions as the aforementioned temperate trees (Webb, 1998). MIS 30 is marked by the relatively high forest pollen percentages, at around 20%, when compared with those of MIS 12 indicating a warmer and wetter glacial climate. Pollen-based quantitative climatic reconstructions for MIS 31 in the western Mediterranean region from ODP Site 976 (Alboran Sea) confirm the low seasonality in temperature and precipitation with relatively high/low mean temperature of the coldest/warmest month (MTCO/MTWA) at around 0 °C and 15 °C, respectively, with relatively high summer, ~150 mm, and annual precipitation, 800–1000 mm (Joannin et al., 2011). For MIS 30, these reconstructions revealed a decrease in MTCO, by about 5 °C, and in annual precipitations, by about 500 mm, though MTWA increase resulted in warmer annual temperatures than those prevailing during MIS 31 (Joannin et al., 2011).

5. Discussion

5.1. Grain size and MOW variations

The standard deviation and mean of the coarse fraction are directly correlated throughout our data set. A decrease in the degree of sorting is apparently coupled with higher mean grain-size values. The skewness is, with a few exceptions, negative especially in coarse grain size. This means that almost all samples analyzed have excess coarse particles with respect to a log normal Gaussian distribution. In general, there is a positive correlation between the skewness values and the kurtosis

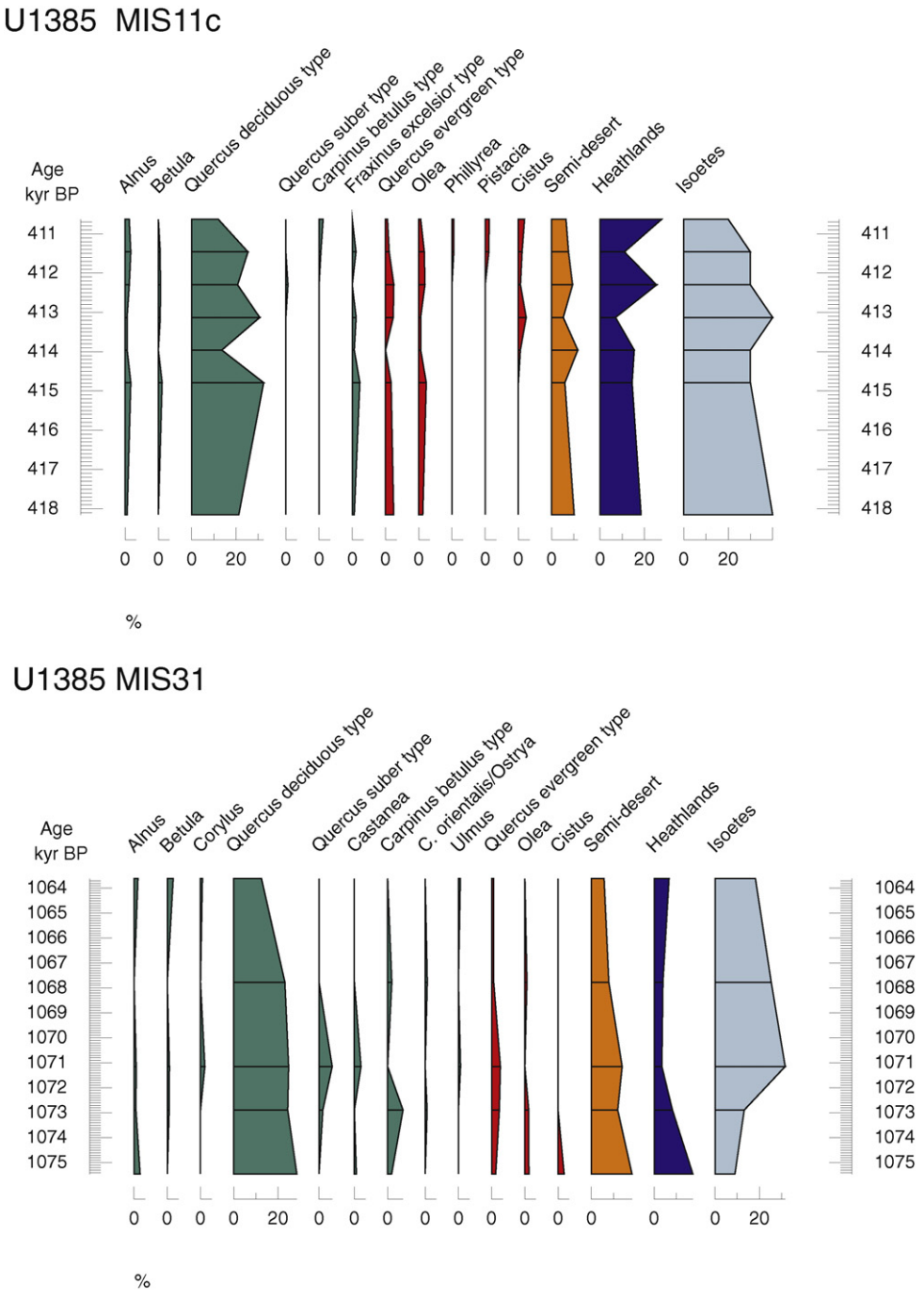

Fig. 7. Pollen diagram with selected taxa of the peak forest interval during MIS 31 and MIS 11c interglacials. Green curves: Eurosiberian tree taxa; red curves: Mediterranean taxa *s.s.* Semi-desert includes *Artemisia*, Chenopodiaceae and *Ephedra*.

values. Fluctuations within the kurtosis values (measure of the peakness of a distribution) indicate highly variable depositional processes (Friedman, 1967). A lithological difference is also observed between the two intervals, before and after the MPT. MIS 31–MIS 30 interval is on average richer in clay fraction than MIS 12–MIS 11 (Fig. 8) indicating weaker bottom currents before the MPT.

These grain-size records of the silt and sand fractions at Sites U1388, U1389 and U1390 are used to reconstruct variations in the history of the MOW strength, especially during the transition between MIS 31–MIS 30 and MIS 12–MIS 11. Although a direct link between bottom current strength and nature of the contourite facies, especially grain size, have been proposed (Ellwood and Ledbetter, 1977; Stow et al., 1986, 2009), it remains difficult to determine whether a change in the mean grain-size is the product of variations in mean speed, in the frequency and/or the amplitude of current velocity, or the result of increase sediment supply by rivers and downslope transport (Mulder et al., 2013). Several attempts have been made to provide grain size parameters that respond to changes in bottom current strength (e.g. Robinson and McCave, 1994; McCave et al., 1995;Bianchi and McCave, 1999; Bianchi et al., 2001). According to McCave et al. (1995) increasing current velocities transport increasingly larger grain sizes. Much of the sediment is dominantly bimodal, comprising fine silt (mode between 8 and 15 μm), coarse silt to fine sand (mode between 39 and 73 μm), and medium sand (mode > 100 μm) components. The position of the mode and the sorting of each component changes through the succession, but the primary variation is the presence or abundance of the coarse silt fraction. This

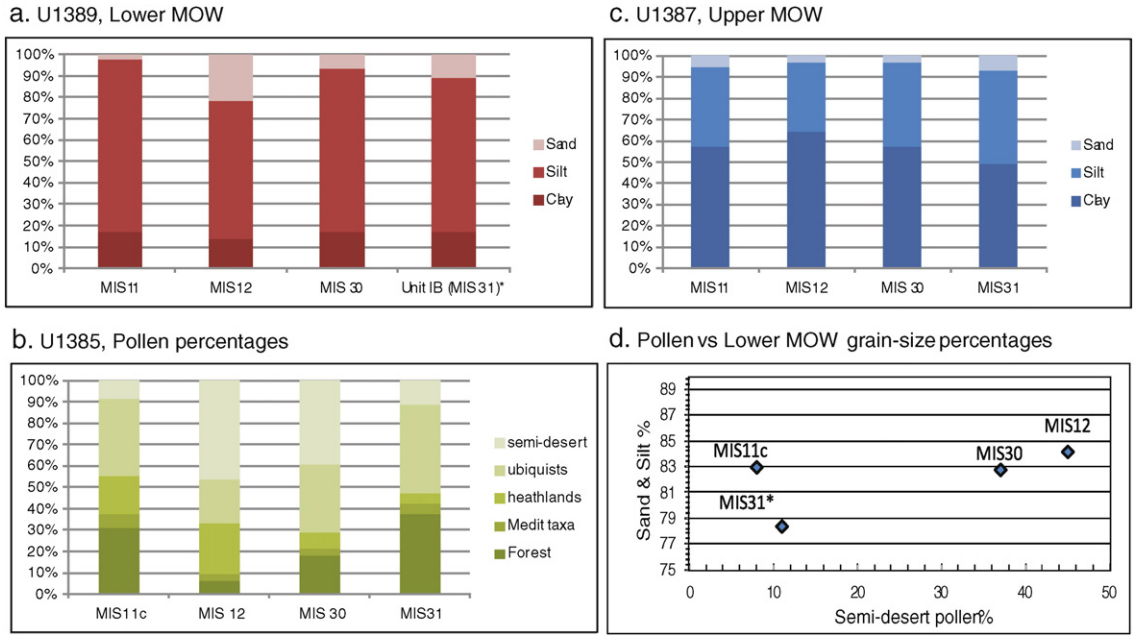

Fig. 8. Panel a) Mean percentages of clay, silt and sand for the MIS 11 interval from Site U1389 Hole A (16 samples, 195–205 mbsf), MIS 12 interval from site U1389 Hole A (56 samples, 205–235 mbsf), and MIS 30 interval from U1389 Hole B (9 samples, 358–363 mbsf). Grain-size percentages for the MIS 31 are not available because this interval corresponds to a major discontinuity. The percentages shown are an average of the percentages from Unit IB. Panel b) Mean percentages of clay, silt and sand for the MIS 11 (9 samples, 96.35–101.49 mbsf), MIS 12 (9 samples, 102.49–111.55 mbsf), MIS 30 (21 samples, 239.08–246.41 mbsf) and MIS 31 (41 samples, 246.86–257.82 mbsf) from site U1387. Site U1389 and Site U1387 are in the Lower and Upper branch of the MOW, respectively. Panel c) Mean pollen percentages of forest, Mediterranean taxa, heathlands, ubiquists and semi-desert plants for the MIS 11c plateau (5 samples, 55.70–55.63 crmcd), MIS 12 (5 samples, 56.01–56.28 crmcd), MIS 30 (3 samples, 120.08–120.84 crmcd) and MIS 31 (3 samples, 122.39–122.87 crmcd) from site U1385. d) Percentages of sand and silt plotted against the semi-desert pollen percentages..

component is the key variable controlling the overall mean grain size and sorting of the entire sample. This typical bimodal distribution of the grain size reflects the mixing of subordinate fine silt and a dominant sandy silt/silty sand population. This bimodal distribution in the terrigenous silt fraction was already underscored by Robinson and McCave (1994); Bianchi et al. (2001) and more recently by Mulder et al., 2013.

The observed changes in the studied silt/sand fractions are most likely related to the MOW variability, decreasing from the proximal (U1388) to the distal (U1389) sites, and increasing from MIS 30 to MIS 12. A general up-core increase in the abundance of fine silt to fine sand sizes during the Quaternary and from the distal to proximal sites to the Strait of Gibraltar, is interpreted as an increase in the average MOW velocity. Several authors (Llave et al., 2006; Voelker et al., 2006; Toucanne et al., 2007; Rogerson et al., 2010) inferred changes in MOW intensity paced by millennial scale climate changes from grain-size fluctuations. A higher MOW velocity prevailed during Greenland stadials, Heinrich events and the Younger Dryas whereas a lower MOW velocity was inferred for Greenland interstadials, Bølling-Allerød and Early Holocene. Cold climatic intervals, favorable to deep-sea water formation in Mediterranean Sea, increased the salinity of the Mediterranean Sea and thus the density and the downslope velocity of the MOW (Schönfeld and Zahn, 2000), thus intermittently increased the MOW intensity during the last 50 kyr.

5.2. MOW variation versus Mediterranean aridity: testing the hypothesis

During MIS 31–MIS 30 prior to the MPT, we have identified weaker bottom currents than those of the post-MPT interval, MIS 12–MIS 11, at the time of a regional wetter climate and less global ice volume. At glacial–interglacial scale, deep water currents during MIS 31 and MIS 11 interglacials were less intense than those of MIS 30 and MIS 12 glacials, respectively. Both interglacials are considered to be "super interglacials" because they are characterized by extremely warm conditions in the Arctic region (summer temperatures 3 to 5 °C above present interglacial values) (Masson-Delmotte et al., 2006; Melles et al., 2012; Cronin et al., 2013 for MIS 11). Additionally, during MIS 31 the dynamics of the East Antarctic ice sheet were dominated by ablation processes (Maiorano et al., 2009). MIS 11c was one of the warmest interglacials in Antarctica (Masson-Delmotte et al., 2010) when boreal coniferous forest developed in southern Greenland indicating a nearly ice-free Greenland (De Vernal and Hillaire-Marcel, 2008), supported by isotopic studies of Eirik Drift sediments and numerical models (Reyes et al., 2014). In the western Mediterranean region, MIS 31 and MIS 11c interglacials are thus characterized by lower bottom current strength at periods were regional climate was generally wet and the low evaporation and low salinity likely reduced deep convection in the Mediterranean basin and, therefore, MOW strength. The $\delta^{18}O_{seawater}$-based relative sea level change record suggests that at the time of MIS 31 ice caps were more developed than during MIS 11c (Elderfield et al., 2012). The climatic difference between the two interglacials is reflected regionally in the grain-size and pollen records (Fig. 8a, b, d). MIS 31 is marked by larger clay fraction than MIS 11, weaker bottom water currents, and a wetter climate reflected by a forest less Mediterranean in character also indicating lower temperatures, at least in summer, and less evaporation. With larger ice-sheets more zonal westerlies could be deflected towards the Mediterranean region bringing more moisture during MIS 31 than during MIS 11c and weakening the MOW.

By contrast, larger mean grain sizes during MIS 30 and MIS 12, indicate enhanced circulation during glacials when regional climate was marked by dry and cold winter outbursts that enhanced MOW (Fig. 8a, b, d). The remarkable increase in grain size observed during MIS 12 at Site U1390, being the most distal site of the studied sites and where a decreasing influence of the MOW is expected, can be coeval to sediment supply by gravity processes related to neotectonic events (Llave et al., 2007; Hernández-Molina et al., 2015). The increase and larger distribution of the coarse fraction can be also the result of the particularly strong glacial climate during MIS12. The LR04 benthic oxygen isotope record and the $\delta^{18}O_{seawater}$ record show very high ice volume for MIS 12 in comparison with that characterizing MIS 30 (Lisiecki and Raymo, 2005; Elderfield et al., 2012). Actually, MIS 12 was one of the

most extensive glaciations with widespread lowland ice-sheets in the northern hemisphere (Ehlers et al., 2011), onset of perennial sea ice in the Arctic (Cronin et al., 2013) and long-lasting and very severe Heinrich stadial in the North Atlantic Ocean (Vázquez Riveiros et al., 2013) associated with one of the lowest temperature values in Antarctica (Masson-Delmotte et al., 2006). In the southwestern Iberian margin a clear mean grain size maxima during the MIS 12 coincides with warmer bottom water temperature, by at around 5.1 °C, than the modern one when the MOW replaced northeast Atlantic deep water (Voelker and Lebreiro, 2010). Our pollen study additionally shows that strong arid conditions prevailed in the western Mediterranean region during MIS 12. The high coarse fraction and its large distribution suggest an enhanced MOW-related salt accumulation during MIS 12. This salty water would be exported to the North Atlantic, perhaps triggering the large resumption of the MOC that lead to the strong global warmth of MIS 11c (Lang and Wolff, 2011), one of the strongest of the last 800,000 years. The magnitude of this warmth is difficult to explain by orbital parameters alone as it occurred during a time of reduced eccentricity modulation (Imbrie and Imbrie, 1980; Vázquez Riveiros et al., 2013).

The present study allows interpreting coarse grain-size variations as relative bottom current intensity changes, rather than permitting absolute estimates of current speed. The hydrographic and depositional background in the study area, however, is complex because of the various flow and transport regimes of deep water masses and surface currents (Rogerson et al., 2012): (1) changes in mean grain size could reflect different sources of sediment supply associated with the distinct flow regimes of MOW and NADW; (2) climatically induced changes in the rivers sediment discharge may disturb or overprint the normal marine bottom current signal; and (3) additional variability of sediment supply may be encountered via the erosion of MOW before and after the Gibraltar Strait. Moreover, the paleoceanographic significance of sandy contourites indicating periods of enhance bottom currents has not been widely investigated. This lack of studies is mainly because sandy contourites that often occur in thin sheets with low deposition rates are intensively bioturbated, and are usually believed to contain material reworked from older deposits (Rebesco et al., 2014).

It is still unclear how much of the overall variation in grain size and sorting is caused by changes in the relative contribution of hemipelagic, turbidite sedimentation or by variations in bottom current strength and in situ hydrodynamic sorting. However, the variations through time of the regional climate identified from the pollen record and particularly the degree of aridity parallel the variations of the sand-silt percentages. We observe that the driest conditions of MIS 12 coincide with the highest proportion of coarse sediments and the wettest climate of MIS 31 is associated with the finer material. Before the MPT the relatively wet MIS 31 and MIS 30 periods are marked by finer sediments than the MI 12–MIS 11 interval after the MPT. If we interpret grain size and sorting variations as the result of changes in bottom current strength from changes in the MOW, our study supports that the intensification of the MOW is a tracer of Mediterranean aridification.

The comparison with the grain-size fraction of the cores located in the upper core of the MOW, U1386 and U1387, shows that the deposition of clay particles dominated during MIS 30 and MIS 12 glacial periods (Fig. 8c), and that the coarse fraction was predominant during the interglacials MIS 31 and MIS 11 (Lofi et al., in review). This apparent contradiction is well explained by the fact that the lower core of the MOW is more intense during glacial periods whereas the upper core of the MOW prevails during warm periods.

6. Conclusions

Variations of grain size, sorting and physical properties of the sedimentary sequences from Sites U1388, U1389 and U1390 retrieved during IODP Expedition 339, “Mediterranean Outflow”, in the Gulf of Cádiz have been interpreted as relative changes of the bottom current variation during two contrasting periods before and after the MPT, MIS 31-MIS 30 and MIS 12-MIS 11. This reconstruction has been compared with the pollen-derived regional climate changes identified from Site U1385 also collected during the same expedition in the southwestern margin of Iberia. We recognize that the interpretation of the coarse grain-size variations is not always straightforward in the hydrologically and sedimentologically complex area of the Gulf of Cádiz. However, our work shows for the first time that the MIS 31–MIS 30 interval, and particularly MIS 31, was marked in the south western Iberian region by wetter conditions and lower seasonality than the interval MIS 12–MIS 11c. The MIS 31–MIS 30 interval was associated with less proportion of sand-silt fraction when MOW was weaker. At glacial-interglacial time scale, we identified finer particles during interglacials reflecting a weakening of the MOW associated with a wetting climate. Conversely, higher Mediterranean aridity during glacial periods coincided with stronger bottom water current when more evaporation leads to the increase in the density of the Mediterranean Sea and MOW intensity. Our work clearly shows that MIS 12 was one of the driest and coldest periods of the Pleistocene in the western Mediterranean region and that coincided with enhanced bottom currents with a clear impact in the distal sites. This finding suggests that climate played a substantial role in the deposition of the coarse grain-size fraction found in the distal part of the Cádiz CDS. The strong export of salt during MIS 12 likely entrained North Atlantic freshwater into the Mediterranean Sea and triggered a large resumption of the MOC that lead to one of the global warmest interglacial of the last 800,000 years, i.e. MIS 11c, that it is difficult to explain by orbital parameters alone. Future work integrating other proxies and a more detail age control will be essential for a higher resolution sedimentary analysis of sandy contourites to better compare with the regional climate and infer MOW paleocirculation.

Acknowledgments

This research used samples and data collected through the Integrated Ocean Drilling Program (IODP). The research was partially supported through the CTM 2012-39599-C03, CGL2011-16057-E, IGCP-619, and INQUA 1204 Projects. This work has been funded by WarmClim, a LEFE-INSU IMAGO project. NERC is acknowledged for the chronostratigraphy of Site U1385. Research was conducted in the framework of the Continental Margins Research Group of the Royal Holloway University of London.

References

Baringer, M.O.N., Price, J.F., 1999. A review of the physical oceanography of the Mediterranean outflow. Mar. Geol. 155, 63–82.
Berger, A., 1978. Long-term variations of daily insolation and Quaternary climatic changes. J. Atmos. Sci. 35, 2362–2367.
Bianchi, G.G., McCave, I.N., 1999. Holocene periodicity in North Atlantic climate and deep-ocean flow south of Iceland. Nature 397, 515–517.
Bianchi, G.G., Vautravers, M.J., Shackleton, N.J., 2001. Deep flow variability under apparently stable North Atlantic Deep Water production during the last interglacial of the subtropical NW Atlantic. Paleoceanography 16, 306–316.
Blanco Castro, E., Casado González, M.A., Costa Tenorio, M., Escribano Bombín, R., García Antón, M., Génova Fuster, M., Gómez Manzaneque, F., Moreno Sáiz, J.C., Morla Juaristi, C., Regato Pajares, P., Sáiz Ollero, H., 1997. Los bosques ibéricos. Planeta, Barcelona (572 p).
Blott, S.J., Pye, K., 2001. GRADISTAT: a grain size distribution and statistics package for the analysis of unconsolidated sediments. Earth Surf. Process. Landf. 26, 1237–1248.
Candela, J., 2001. Mediterranean water and global circulation. In: Siedler, G., Church, J., Gould, J. (Eds.), Ocean Circulation and Climate-Observing and Modelling the Global OceanInt. Geophys. Ser. 77. Academic Press, San Diego, London, pp. 419–429.
Cronin, T.M., Polyak, L., Reed, D., Kandiano, E.S., Marzen, R.E., Council, E.A., 2013. A 600-ka Arctic sea-ice record from Mendeleev Ridge based on ostracodes. Quat. Sci. Rev. 79, 157–167.
De Vernal, A., Hillaire-Marcel, C., 2008. Natural variability of Greenland climate, vegetation, and ice volume during the past million years. Science 320, 1622–1625.
Desprat, S., Sánchez Goñi, M.F., Turon, J.-L., McManus, J.F., Loutre, M.F., Duprat, J., Malaizé, B., Peyron, O., Peypouquet, J.-P., 2005. Is vegetation responsible for glacial inception during periods of muted insolation changes? Quat. Sci. Rev. 24, 1361–1374.

Ehlers, J., Gibbard, P.L., Hugues, P.D., 2011. Quaternary glaciations — extent and chronology. In: Van der Meer, J.J.M. (Ed.)Developments in Quaternary Science 15. Elsevier.
Elderfield, H., Ferretti, P., Greaves, M., Crowhurst, S., McCave, I.N., Hodell, D., Piotrowski, A.M., 2012. Evolution of ocean temperature and ice volume through the Mid-Pleistocene climate transition. Science 337, 704–709.
Ellwood, B.B., Ledbetter, M.T., 1977. Antarctic bottom water fluctuations in the Vema Channel: effects of velocity changes on particle alignment and size. Earth Planet. Sci. Lett. 35, 189–198.
Fiúza, A.F.d.G., Macedo, M.E.d., Guerreiro, M.R., 1982. Climatological space and time variation of the Portuguese coastal upwelling. Oceanol. Acta 5, 31–40.
Fletcher, W.J., Sánchez Goñi, M.F., Allen, J.R.M., Cheddadi, R., Combourieu-Nebout, N., Huntley, B., Lawson, I., Londeix, L., Magri, D., Margari, V., Müller, U.C., Naughton, F., Novenko, E., Roucoux, K., Tzedakis, P.C., 2010. Millennial-scale variability during the last glacial in vegetation records from Europe. Quat. Sci. Rev. 29, 2839–2864.
Folk, R.L., Ward, W.C., 1957. Brazos River bar: a study in the significance of grain size parameters. J. Sediment. Petrol. 27, 3–26.
Friedman, G.M., 1967. Dynamic process and statistical parameters compared for size frequency distribution of beach and river sands. J. Sediment. Petrol. 37, 327–354.
Gallardo-Lancho, J.F., 2001. Distribution of chestnut (*Castanea sativa* Mill.) forests in Spain: possible ecological criteria for quality and management (focusing on timber coppices). Forest Snow and Landscape Research 76, 477–481.
Hernández-Molina, F.J., Somoza, L., Vazquez, J.T., Lobo, F., Fernandez-Puga, M.C., Llave, E., Diaz-del Rio, V., 2002. Quaternary stratigraphic stacking patterns on the continental shelves of the southern Iberian Peninsula: their relationship with global climate and palaeoceanographic changes. Quat. Int. 92, 5–23.
Hernández-Molina, F.J., Stow, D.A.V., Alvarez-Zarikian, C.A., Acton, G., Bahr, A., Balestra, B., Ducassou, E., Flood, R., Flores, J.A., Furota, S., Grunert, P., Hodell, D., Jimenez-Espejo, F., Kim, J.K., Krissek, L., Kuroda, J., Li, B., Llave, E., Lofi, J., Lourens, L., Miller, M., Nanayama, F., Nishida, N., Richter, C., Roque, C., Pereira, H., Sanchez Goñi, M.F., Sierro, F.J., Singh, A.D., Sloss, C., Takashimizu, Y., Tzanova, A., Voelker, A., Williams, T., Xuan, C., 2014. Onset of Mediterranean Outflow into the North Atlantic. Science 344, 1244–1250.
Hernández-Molina, F.J., Sierro, F.J., Llave, E., Roque, C., Stow, D.A.V., Williams, T., Lofi, J., Van der Schee, M., Arnáiz, A., Ledesma, S., Rosales, C., Rodríguez-Tovar, F.J., Pardo-Igúzquiza, E., Brackenridge, R.E., 2015. Evolution of the gulf of Cadiz margin and southwest Portugal contourite depositional system: tectonic, sedimentary and paleoceanographic implications from IODP expedition 339. Mar. Geol. http://dx.doi.org/10.1016/j.margeo.2015.09.013.
Hernández-Molina, F.J., Llave, E., Somoza, L., Fernández-Puga, M.C., Maestro, A., León, R., Medialdea, T., Barnolas, A., García, M., Díaz del Río, V., Fernández-Salas, L.M., Vázquez, J.T., Alveirinho Dias, J.M., Rodero, J., Gardner, J., 2003. Looking for clues to paleoceanographic imprints: a diagnosis of the Gulf of Cadiz contourite depositional systems. Geology 31, 19–22.
Hodell, D.A., Lourens, L., Stow, D.A.V., Hernández-Molina, J., Alvarez Zarikian, C.A., Shackleton Site Project Members, 2013. The "Shackleton Site" (IODP Site U1385) on the Iberian Margin. Sci. Drill. 16, 13–19.
Hodell, D.A., Lourens, L., Crowhurst, S., Konijnendijk, T., Tjallingii, R., Jiménez-Espejo, F., Skinner, L., Tzedakis, P.C., Shackleton Site Project Members, 2015. A reference time scale for site U1385 (Shackleton Site) on the Iberian Margin. Glob. Planet. Chang. 133, 49–64.
Imbrie, J., Imbrie, J.Z., 1980. Modeling the climatic response to orbital variations. Science 207, 943–953.
Ivanovic, R.F., Valdes, P.J., Gregoire, L., Flecker, R., Gutjahr, M., 2013. Sensitivity of modern climate to the presence, strength and salinity of Mediterranean–Atlantic exchange in a global general circulation model. Clim. Dyn. 42, 859–877.
Joannin, S., Bassinot, F., Combourieu-Nebout, N., Peyron, O., Beaudin, C., 2011. Vegetation response to obliquity and precession forcing during the Mid-Pleistocene Transition in Western Mediterranean region (ODP site 976). Quat. Sci. Rev. 30, 280–297.
Lang, N., Wolff, E.W., 2011. Interglacial and glacial variability from the last 800 ka in marine, ice and terrestrial archives. Clim. Past 7, 361–380.
Lisiecki, L., Raymo, M.E., 2005. A Pliocene-Pleistocene stack of 57 globally distributed benthic δ 18 O records. Paleoceanography 20, PA1003.
Llave, E., Schönfeld, J., Hernández-Molina, F.J., Mulder, T., Somoza, L., Díaz del Río, V., Sánchez-Almazo, I., 2006. High-resolution stratigraphy of the Mediterranean outflow contourite system in the Gulf of Cadiz during the late Pleistocene: the impact of Heinrich events. Mar. Geol. 227, 241–262.
Llave, E., Hernández-Molina, F.J., Stow, D., Fernández-Puga, M.C., García, M., Vázquez, J.T., Maestro, A., Somoza, L., Díaz del Río, V., 2007. Reconstructions of the Mediterranean Outflow Water during the Quaternary since the study of changes in buried mounded drift stacking pattern in the Gulf of Cádiz. Mar. Geophys. Res. 28, 379–394.
Lofi, J., Voelker, A., Ducassou, E., Hernandez Molina, F.J., Sierro, F.J., Bahr, A., Galvani, A., Lourens, L., Pardo-Iguzquiza, E., Rodriguez Tovar, F.J., Williams, T., 2015. Quaternary regional contourite signal record in the Gulf of Cadiz and Portuguese Contourite Depositional Systems. Marine Geology (VSI) (in review).
Lohmann, K., Drange, H., Bentsen, M., 2009. Response of the North Atlantic subpolar gyre to persistent North Atlantic oscillation like forcing. Clim. Dyn. 32, 273–285.
Maiorano, P., Marino, M., Flores, J.A., 2009. The warm interglacial Marine Isotope Stage 31: evidences from the calcareous nannofossil assemblages at Site 1090 (Southern Ocean). Mar. Micropaleontol. 71, 166–175.
Marches, E., Mulder, T., Gonthier, E., Cremer, M., Hanquiez, V., Garlan, T., Lecroart, R., 2010. Perched lobe formation in the Gulf of Cádiz: interactions between gravity processes and contour currents (Algarve Margin, Southern Portugal). Sediment. Geol. 229, 81–94.
Margari, V., Skinner, L.C., Hodell, D.A., Martrat, B., Toucanne, S., Grimalt, J.O., Gibbard, P.O., Lunkka, J.P., Tzedakis, P.C., 2014. Land-ocean changes on orbital and millennial timescales and the penultimate glaciations. Geology 42, 183–186.
Martrat, B., Grimalt, J.O., Shackleton, N.J., De Abreu, L., Hutterli, M.A., Stocker, T.F., 2007. Four cycles of recurring deep and surface water destabilizations on the Iberian margin. Science 317, 502–507.
Maslin, M.A., Ridgwell, A.J., 2005. Mid-Pleistocene revolution and the'eccentrycity myth'. In: Head, M.J., Gibbard, P.L. (Eds.), Early–Middle Pleistocene Transitions: The Land–Ocean Evidence. Geological Society of London, Special Publication 247, pp. 19–34.
Masson-Delmotte, V., Dreyfus, G., Braconnot, P., Johnsen, J., Jouzel, J., Kageyama, M., Landais, A., Loutre, M.-F., Nouet, J., Parrenin, F., Raynaud, D., Stenni, B., Tuenter, E., 2006. Past temperature reconstructions from deep ice cores: relevance for future climate change. Clim. Past 2, 145–165.
Masson-Delmotte, V., Stenni, B., Pol, K., Braconnot, P., Cattani, O., Falourd, S., Kageyama, M., Jouzel, J., Landais, A., Minster, B., Barnola, J.M., Chappellaz, J., Krinner, G., Johnsen, S., Röthlisberger, R., Hansen, J., Mikolajewicz, U., Otto-Bliesner, B., 2010. EPICA Dome C record of glacial and interglacial intensities. Quat. Sci. Rev. 29, 113–128.
McCave, I.N., Manighetti, B., Beveridge, N.A.S., 1995. Circulation in the glacial North Atlantic inferred from grain-size measurements. Nature 374, 149–152.
Melles, M., Brigham-Grette, J., Minyuk, P.S., Nowaczyk, N.R., Wennrich, V., DeConto, R.M., Anderson, P.M., Andreev, A.A., Coletti, A., Cook, T.L., Haltia-Hovi, E., Kukkonen, M., Lozhkin, A.V., Rosén, P., Tarasov, P., Vogel, H., Wagner, B., 2012. 2.8 million years of Arctic climate change from Lake El'gygytgyn, NE Russia. Science 337, 315–320.
Moreno, A., Cacho, I., Canals, M., Grimalt, J.O., Sánchez-Goñi, M.F., Shackleton, N., Sierro, F.J., 2005. Links between marine and atmospheric processes oscillating on a millennial time-scale. A multi-proxy study of the last 50,000 yrs from the Alboran Sea (Western Mediterranean Sea). Quat. Sci. Rev. 24, 1623–1636.
Mulder, T., Hassan, R., Ducassou, E., Zaragosi, S., Gonthier, E., Hanquiez, V., Marchès, E., Toucanne, S., 2013. Contourites in the Gulf of Cadiz: a cautionary note on potentially ambiguous indicators of bottom current velocity. Geo-Mar. Lett. 33, 357–367.
Naughton, F., Sánchez Goñi, M.F., Desprat, S., Turon, J.-L., Duprat, J., Malaizé, B., Joli, C., Cortijo, E., Drago, T., Freitas, M.C., 2007. Present-day and past (last 25000 years) marine pollen signal off western Iberia. Mar. Micropaleontol. 62, 91–114.
New, A.L., Jia, Y., Coulibaly, M., Dengg, J., 2001. On the role of the Azores current in the ventilation of the North Atlantic Ocean. Prog. Oceanogr. 48, 163–194.
Peinado Lorca, M., Martínez-Parras, J.M., 1987. Castilla-La Mancha. In: Peinado Lorca, M., Rivas Martínez, S. (Eds.), La vegetación de España. Universidad de Alcalá de Henares, Alcalá de Henares, pp. 163–196.
Péliz, Á., Dubert, J., Santos, A.M.P., Oliveira, P.B., Le Cann, B., 2005. Winter upper ocean circulation in the western Iberian basin—fronts, eddies and poleward flows: an overview. Deep-Sea Res. II 52, 621–646.
Polunin, O., Walters, M., 1985. A Guide to the Vegetation of Britain and Europe. Oxford University Press, New York (238 p).
Rebesco, M., Hernández-Molina, F.J., Van Rooij, D., Wahlin, A., 2014. Contourites and associated sediments controlled by deep-water circulation processes: state of the art and future considerations. Mar. Geol. 352, 111–154 (SI: 50th anniversary).
Reyes, A.V., Carlson, A.E., Beard, B.L., Hatfield, R.G., Stoner, J.S., Winsor, K., Welke, B., Ullman, D.J., 2014. South Greenland ice-sheet collapse during Marine Isotope Stage 11. Nature 510, 525–528.
Robinson, S.G., McCave, I.N., 1994. Orbital forcing of bottom-current enhanced sedimentation on Feni Drift, NE Atlantic, during the mid-Pleistocene. Paleoceanography 9, 943–972.
Rogerson, M., Rohling, E.J., Bigg, G.R., Ramirez, J., 2012. Paleoceanography of the Atlantic–Mediterranean exchange: overview and first quantitative assessment of climatic forcing. Rev. Geophys. 50, RG2003. http://dx.doi.org/10.1029/2011RG000376.
Rogerson, M., Colmenero-Hidalgo, E., Levine, R.C., Rohling, E.J., Voelker, A.H.L., Bigg, G.R., Schönfeld, J., Cacho, I., Sierro, F.J., Löwemark, L., Reguera, M.I., de Abreu, L., Garrick, K., 2010. Enhanced Mediterranean–Atlantic exchange during Atlantic freshening phases. Geochem. Geophys. Geosyst. 11, Q08013. http://dx.doi.org/10.1029/2009GC002931.
Rogerson, M., Rohling, E.J., Weaver, P.P.E., 2006. Promotion of meridional overturning by Mediterranean-derived salt during the last deglaciation. Paleoceanography 21, PA4101. http://dx.doi.org/10.1029/2006PA001306.
Roucoux, K.H., Tzedakis, P.C., de Abreu, L., Shackleton, N.J., 2006. Climate and vegetation changes 180000 to 345000 years ago recorded in a deep-sea core off Portugal. Earth Planet. Sci. Lett. 249, 307–325.
Salvo Tierra, E., 1990. Guía de helechos de la Península Ibérica y Baleares, Madrid.
Sánchez Goñi, M.F., Eynaud, F., Turon, J.-L., Shackleton, N.J., 1999. High resolution palynological record off the Iberian margin: direct land–sea correlation for the Last Interglacial complex. Earth Planet. Sci. Lett. 171, 123–137.
Schönfeld, J., Zahn, R., 2000. Late Glacial to Holocene history of the Mediterranean Outflow. Evidence from benthic foraminiferal assemblages and stable isotopes at the Portuguese margin. Palaeogeogr. Palaeoclimatol. Palaeoecol. 159, 85–111.
Stow, D.A.V., Faugères, J.-C., Gonthier, E., 1986. Facies distribution and drift growth during the late Quaternary (Gulf of Cadiz). Mar. Geol. 72, 71–100.
Stow, D.A.V., Hernández-Molina, F.J., Alvarez Zarikian, C.A., the Expedition 339 Scientists, 2013, Proceedings IODP, 339, Tokyo (Integrated Ocean Drilling Program Management International, Inc.).
Stow, D.A.V., Hernández-Molina, F.J., Llave, E., Sayago, M., Díaz del Río, V., Branson, A., 2009. Bedform-velocity matrix: the estimation of bottom current velocity from bedform observations. Geology 37, 327–330.
Stramma, L., Siedler, G., 1988. Seasonal changes in the North Atlantic subtropical gyre. Journal of Geophysical Research: Oceans 93, 8111–8118.
Tallantire, P.A., 2002. The early-Holocene spread of hazel (*Corylus avellana* L.) in Europe north and west of the Alps: an ecological hypothesis. The Holocene 12, 81–96.
Toucanne, S., Mulder, T., Schönfeld, J., Hanquiez, V., Gonthier, E., Duprat, J., Cremer, M., Zaragosi, S., 2007. Contourites of the Gulf of Cadiz: a high-resolution record of the

paleocirculation of the Mediterranean outflow water during the last 50,000 years. Palaeogeogr. Palaeoclimatol. Palaeoecol. 246, 354–366.
Tzedakis, P.C., Pälike, H., Roucoux, K.H., de Abreu, L., 2009. Atmospheric methane, southern European vegetation and low-mid latitude links on orbital and millennial timescales. Earth Planet. Sci. Lett. 277, 307–317.
Vázquez Riveiros, N., Waelbroeck, C., Skinner, L., Duplessy, J.-C., McManus, J.F., Kandiano, E.S., Bauch, H.A., 2013. The "MIS 11 paradox" and ocean circulation: role of millennial scale events. Earth Planet. Sci. Lett. 371-372, 258–268.
Voelker, A.H.L., Lebreiro, S.M., 2010. Millennial-scale changes in deep water properties at the middepth western Iberian margin linked to Mediterranean Outflow Water activity. Geotemas 175-176.
Voelker, A.H.L., Lebreiro, S.M., Schönfeld, J., Cacho, I., Erlenkeuser, H., Abrantes, F., 2006. Mediterranean outflow strengthening during northern hemisphere coolings: a salt source for the glacial Atlantic? Earth Planet. Sci. Lett. 245, 39–55.
Webb, N.R., 1998. Study of Biotopes and Habitats Losing Wildlife Interest as a Result of Ecological Succession. European Council.

Global and Planetary Change 136 (2016) 52–64

Contents lists available at ScienceDirect

Global and Planetary Change

journal homepage: www.elsevier.com/locate/gloplacha

Dinoflagellate cyst population evolution throughout past interglacials: Key features along the Iberian margin and insights from the new IODP Site U1385 (Exp 339)

Frédérique Eynaud [a,*], Laurent Londeix [a], Aurélie Penaud [b], Maria-Fernanda Sanchez-Goni [a,c], Dulce Oliveira [a,c,d,e], Stéphanie Desprat [a,c], Jean-Louis Turon [a]

[a] Université de Bordeaux, UMR CNRS 5805 EPOC (Environnements et Paleoenvironnements Oceaniques et Continentaux), Allée Geoffroy St Hilaire, 33615 Pessac Cedex, France
[b] UMR 6538 CNRS Laboratoire Domaines Océaniques, Université de Brest (UBO), Institut Universitaire Européen de la Mer (IUEM), Place Nicolas Copernic, Plouzané, France
[c] EPHE, UMR CNRS 5805 EPOC (Environnements et Paleoenvironnements Oceaniques et Continentaux), 33615 Pessac Cedex, France
[d] Divisão de Geologia e Georecursos Marinhos, Instituto Português do Mar e da Atmosfera (IPMA), Av. de Brasília 6, 1449-006 Lisbon, Portugal
[e] CIMAR, Associate Laboratory, Porto, Portugal

ARTICLE INFO

Article history:
Received 2 March 2015
Received in revised form 19 November 2015
Accepted 4 December 2015
Available online 9 December 2015

Keywords:
Dinocysts
Interglacials
Biodiversity and climate shifts
Southern Iberian margin

ABSTRACT

IODP 339 Site U1385 ("Shackleton site", e.g. Hodell et al., 2013a), from the SW Iberian margin, offers the opportunity to study marine microfossil population dynamics by comparing several past interglacials and to test natural shifts of species that occurred across these warm periods, in a subtropical context. Here, more specifically, we present results obtained for the dinoflagellate cyst (dinocyst) population integrated at a regional scale thanks to the addition of data from proximal sites from southern Iberian margin. When possible, observations made using the dinocyst bio-indicator are compared to additional proxies from the same records in order to test the synchronicity of the marine biota response. Pollen data available for some of the compiled marine sequences also offer the opportunity to directly compare marine biota with terrestrial ecosystem responses. This spatio-temporal compilation reveals that, over the last 800 ka, surface waters around Iberia were tightly coupled to (rapid) climate changes and were characterised by coherent dinocyst assemblage patterns, highlighting a permanent connection between Atlantic and Mediterranean waters as evidenced through a continuous exchange of dinocyst populations. Some index species well illustrate the evolution of the regional hydrographic context along time, as for instance *Spiniferites* and *Impagidinium* species, together with *Lingulodinium machaerophorum*, *Bitectatodinium tepikiense* and heterotrophic brown cysts. They constitute key bio-indicators in context of natural environmental shifts at long and short timescales.

1. Introduction

Drastic marine biodiversity changes that occurred over the last century raise key questions today in connection with the concept of ecosystem resilience to environmental changes (e.g. Millenium Ecosystem Assessment synthesis reports, 2005). This is especially true for neritic ecosystems that encountered major perturbations especially related to the geochemical balances of sea-surface waters (e.g. eutrophication, pollution contaminants, acidification, see Crutzen, 2002) but also to physical parameters (e.g. SST warming, sea-level changes, river nutrient loads). At present, natural environmental trends are hidden by anthropogenic forcings and reference points are lacking. The natural state is only found in the recent past, outside of the modern instrumental period (i.e. the last century), thus preventing actualistic studies from defining robust baselines for environmental predictions and trajectories. Paleostudies carried out on fossil sediment archives thus provide invaluable information (e.g. Willis et al., 2010) even if they are integrating only a partial view of the paleo-biodiversity, being only indirectly and incompletely representative of past biomes and biotopes. Interglacial optima, and especially their surrounding transitional periods (both deglaciations and glacial inceptions), represent key intervals where ecosystems, comparable to modern ones, could be tested along large amplitude ecological shifts (e.g. Willis et al., 2010). They permit us to test if the marine biota offers the same recurrent kind of transient populations during such shifts and if so, to picture characteristic patterns that could be recognized within the assemblages. Are there typical species that could be considered as pioneers, opportunistic or pre-adapted, and so repetitive scenarios that could provide us with a predictive ecological model for the marine biota evolution?

For this study we based our approach on the dinoflagellate cyst (dinocyst) proxy, an organic-walled bio-indicator related to the phytoplankton realm which constitutes sexual reproduction remains of some dinoflagellate species (e.g. de Vernal and Marret, 2007; Ellegaard et al.,

* Corresponding author.
E-mail address: f.eynaud@epoc-u-bordeaux1.fr (F. Eynaud).

http://dx.doi.org/10.1016/j.gloplacha.2015.12.004
0921-8181/

2013). Fossil dinocysts have long been used in Mesozoic–Cenozoic paleoceanographic studies to reconstruct past hydrographical patterns qualitatively as well as quantitatively through transfer functions (e.g. Williams, 1971; Turon, 1978; de Vernal et al., 2001; Houben et al., 2013; de Schepper et al., 2013; Mertens et al., 2014). They constitute a robust planktic group to document past sea-surface ecological changes (e.g. Marret and Zonneveld, 2003; Zonneveld et al., 2013) and are especially powerful in neritic environments where their motile thecal forms proliferate preferentially (e.g. Dale, 1983; Dodge and Harland, 1991).

Here we compare the evolution of dinocyst relative abundances across four of the most studied interglacials with regard to their climate dynamics: Marine Isotopic Stages (MIS) 1, 5, 11 and 19. We thus gathered sedimentary sequences (along which dinocyst assemblages have been analysed at high resolution) from the south-western European margin (Iberia), from its Atlantic side as well as from the inner Alboran Sea. This compilation, providing an integrated view of dinocyst assemblage evolution in space and time from a sensitive subtropical area (e.g. Giorgi, 2006), includes new original analyses on the IODP 339 Site U1385 (Hodell et al., 2013a, 2013b). It gives us the opportunity to: i) document poorly known dinocyst populations from the interglacial MIS 19 and 11, and ii) study ecological interactions through several climate cycles of the Quaternary between two end-member environments on either sides of the Gibraltar strait: the Mediterranean Basin (residual Tethys) and the North Atlantic.

2. Environmental setting: key features

The modern hydrography of the southern Iberian margin is mainly forced by water mass exchanges with North-Atlantic waters penetrating the Alboran Sea at the surface, whereas deep saltier waters exit the Mediterranean at depth (Mediterranean Overflow Water or MOW). This scheme is mainly related to contrasted density budgets in between the two respective basins, however modulated by atmospheric forcing throughout the transfer of wind stress to surface currents, such as the Azores and Portugal currents for the Atlantic, or the western/eastern anticyclonic gyres associated with the Algerian current for the Alboran (e.g. Rohling et al., 1995; Johnson, 1997; Font, 2002; Mauritzen et al., 2001; Arístegui et al., 2005, 2009, see Fig. 1). This dynamical pattern evolves seasonally/yearly according to meridional shifts/contractions — extensions of the subtropical North Atlantic gyre, inducing changes in the temporality of upwelling cells and thus major modifications of the sea-surface productivity conditions (Arístegui et al., 2005; Peliz et al., 2005; Relvas et al., 2007). At millennial time scales, significant modulations of the MOW have been recorded during major climate transitions associated with boreal ice-sheet collapses (i.e. the well-known Heinrich events, e.g. Heinrich, 1988) with a consensus supporting synchronous accelerations of MOW during these cold episodes (e.g. Cacho et al., 2000; Voelker et al., 2006; Rogerson et al., 2010). This also resulted in drastic consequences in water mass surface exchanges with the reorganisation of the Alboran gyres and obvious impacts on sea-surface productivity on either sides of Gibraltar (Penaud et al., 2011).

3. Methods

This study relies on new unpublished data (IODP 339 Site U1385 MIS 19 and 11 sections — i.e. from the 788–749 ka and 410–384 ka age intervals respectively — from the "Shackleton site", e.g. Hodell et al., 2013a,) and also gathers several previously published and unpublished dinocyst records from the Southern Iberian margin (Fig. 1; see Table 1 for key elements concerning each studied core). We selected marine sequences that could provide us a fine enough analytical resolution regarding dinocyst assemblage patterns through time and where comparative data exists from other paleoenvironmental proxies (mainly derived from planktic foraminiferal and pollen assemblages, mono-specific foraminifera $\delta^{18}O$).

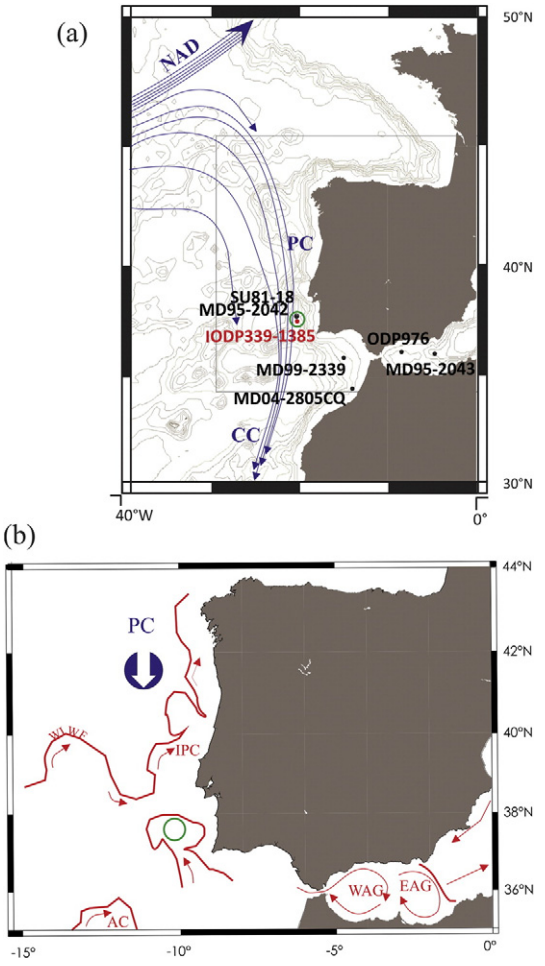

Fig. 1. (a) location of the cores of interest (IODP 339 U1385, SU81-18, MD95-2042, MD99-2339, MD04-2805CQ) with a sketch of the modern sea-surface hydrological dynamics (main currents, PC = Portugal current, CC = Canary current, NAD = North Atlantic drift); (b) detailed view of the modern surface dynamic structures, with: IPC: Iberian Poleward Current, AC: Azores Current, WIWF: Western Iberia Winter Front, after Peliz et al. (2005); and WAG: Western Alboran Gyre, EAG: Eastern Alboran Gyre, AOF: Almería–Oran Front after Hauschildt et al. (1999). Green empty circle: "SHACK area" identifying the location of twin and/or proximal cores (i.e. SU81-18/MD95-2042) of the "Shackleton site" — IODP 339 U1385.

Site U1385 was drilled from the SW Iberian Margin during IODP Expedition 339 (e.g. Hodell et al., 2013a) with the aim of extending further back in time the range of the exceptional piston cores previously retrieved in this area (including those listed in Table 1). Its stratigraphy was built upon a combination of chemo-stratigraphic proxies (Hodell et al., 2013a; 2015-this volume), i.e. Ca/Ti ratio, measured in all holes by XRF core scanning to construct a composite section, coupled to benthic foraminifera oxygen isotopes which were correlated to the marine $\delta^{18}O$ LR04 stack (Lisiecki and Raymo, 2005). More details regarding this stratigraphical work can be found in Hodell et al. (2013a, 2013b); 2015-this volume). Concerning the other published paleoceanographical records used in this study, we strictly used the age models as initially established and published by the authors (cf. Table 1).

Palynological preparations were conducted on IODP 339 Site U1385, Hole D, Core 10H between Sections 3 and 6 which encompass MIS 19 and on Hole D, Core 7H Section 1 and Hole E, Core 6H Sections 5 and 6 for MIS 11. The preparation techniques follow standard procedures and can be found at http://www.epoc.u-bordeaux.fr/index.php?lang=fr&page=eq_paleo_pollens. Acetolysis was not employed to avoid destruction of heterotrophic dinocyst taxa such as Polykrikaceae and *Brigantedinium* cysts (Marret, 1993; Combourieu-Nebout et al., 1998;

Table 1
Key information regarding the set of cores used for this study.

Core	Latitude	Longitude	Water depth (m)	Marine isotopic stage	References, data sources
IODP339 1385 D10H	37.8	−10.02	3146	11, 19	This work, Oliviera et al., in preparation, Sànchez-Goñi et al., 2016-this volume
SU81-18	37.77	−10.18	3155	1	Le coeur, in press; Turon et al. (2003)
ODP976	36.20	−4.30	1108	1, 5, 11, 19	Combourieu-Nebout et al. (1999, 2002), Levi, (1999), Rattinacannou (2007)
MD95-2042	37.80	−10.17	3146	3, 5	Eynaud (1999); Eynaud et al. (2000)
MD95-2043	36.14	−2.62	1841	1, 3	Rouis-Zargouni (2010), Penaud (2009)
MD99-2339	35.89	−7.53	1177	1, 3	Penaud (2009), Penaud et al. (2011), Penaud et al. submitted
MD04-2805CQ	34.52	−7.02	859	1	Penaud et al. (2010)

Kodrans-Nsiah et al., 2008). The samples were used together for dinocyst and pollen analyses (Sànchez-Goñi et al., 2016-this volume) with two set of slides mounted independently to facilitate each kind of observations (i.e. glycerine jelly coloured with fushine for dinocysts and bidistilled glycerine for pollen). Dinocysts were counted on the fraction 10–150 μm (from 47 to 365 – average 187 – specimens per sample) using a Zeiss PrimoStar light microscope at ×400 magnifications. Identifications were based on Turon (1984), de Vernal et al. (1992) and Rochon et al. (1999). The nomenclature conforms to Fensome et al. (1998) and Fensome and Williams (2004), and dinocyst assemblages were described by the percentages of each species calculated on the basis of the total dinocyst sum including unidentified taxa and excluding pre-Quaternary specimens. Palynomorph absolute concentrations (number of dinocysts/cm^3) were calculated using the marker grain method (Stockmarr, 1971; de Vernal et al., 1999; Mertens et al., 2009).

A composite sequence was built (for what we have called the "SHACK area", i.e. green circle on Fig. 1) using relative abundances of dinocysts from the twin cores SU81-18 (MIS 1 to 2), MD95-2042 (MIS 2 to 6) and IODP 339 Site U1385 (MIS 11 and 19, "Shackleton site" sensu Hodell et al., 2013a). A Principal component analysis (PCA) was applied to this raw data set (non- transformed relative abundances) using the XLSTAT software (XLSTAT Version 2015.4.01.19992 @ Addinsoft 1995–2015, http://www.xlstat.com/en/). The training dataset and the PCA results can be downloaded on line as Supplementary information (SI). Additionally, some coherency tests were done using the XLSTAT and PAST (Hammer et al., 2001) softwares for the comparison of thermophilous indexes derived from pollen (Mediterranean forest) and from dinocysts. Two indexes were used for dinocysts: (a) the warm *Impagidinium* sum: $\Sigma W_{Impagidinium}$, cumulating relative abundances of the tropical/subtropical *I patulum* and *I. aculeatum* species and of the subtropical/temperate *I. paradoxum* and *I. sphaericum* species; (b) the warm/cold dinocyst ratio as defined in Combourieu-Nebout et al. (1999), i.e. [W/(W + C)], where (W) cumulates warm-water indicator species: i.e. *Spiniferites mirabilis* s.l. (= *S. mirabilis* + *S. hyperacanthus*), *Selenopemphix nephroides*, *Impagidinium patulum*, *Impagidinium strialatum*, *Operculodinium israelianum*, *Spiniferites delicatus*, and *Spiniferites membranaceus*, excluding *Operculodinium centrocarpum* considered to be too ubiquitous, whereas (C) gathers cold-water indicators, namely: *Nematosphaeropsis labyrinthus*, *Bitectatodinium tepikiense*, *Spiniferites elongatus*, *Impagidinium pallidum*, *Pentapharsodinium dalei* and *Islandinium minutum*.

4. Trends and common features in dinocyst communities during climatic optima and their transitions

For the following discussion, we consider the main features detected in the assemblages over time. Our interpretations are based on dominant dinocyst species and also, in some cases, on biostratigraphically significant ones. A detailed picture of selected significant dinocyst species is provided for the SHACK area (MD95-2042/SU81-18 and IODP 339; Fig. 2) since MIS 11 (from 410–384 ka) and MIS 19 (788–749 ka) analyses constitute new dinocyst results for this area.

The compilation made for the Southern Iberian margin is mainly based on the comparison of three specific/index groups, that dominate alternatively dinocyst assemblages and showed a sensitive response to climate shifts through time (Fig. 3): i) heterotrophic taxa (sum established after the taxa list of Marret and Zonneveld, 2003), ii) warm *Impagidinium* species (sum of subtropical *I. patulum* and *I. aculeatum* species, also grouped with temperate *I. paradoxum* and *I. sphaericum* species), and iii) the species *Lingulodinium machaeorophorum*.

In the SHACK area, autotrophic taxa are marked by the dominance of well-known temperate to cosmopolite species: *L. machaeorophorum*, *N. labyrinthus*, *O. centrocarpum* sensu Wall and Dale (1966), cysts of *P. dalei* together with numerous species from the *Spiniferites* group, including *S. mirabilis* s. l. and *S ramosus* s. s. (Fig. 2). Heterotrophic dinocysts are mainly represented by *Brigantedinium* species (*B cariacoense* and *Brigantedinium simplex* included) together with *Peridinioid* taxa such as *Selenopemphix quanta* or *Selenopemphix nephroides* (Plate 1). In this group, it is worth noting the common occurrence of cysts of *Protoperidinium stellatum*, which will herein be refer to the usual binomial name "*Stelladinium stellatum*" (Plate 1) for practical reasons and in order to be consistent with reference recent works (e.g. Zonneveld et al., 2013) and with the Sprangers et al. (2004) dinocyst inventory study from modern sediments of the Iberian margin. In the MIS 19 section of IODP339 1385, *S. stellatum* abundances reach up to 7% of the total dinocyst assemblage (Fig. 2), while this taxa was not observed in any of the most recent interglacials MIS 11, 5 and 1 from the twin cores MD95-2042 and SU81-18 (Eynaud, 1999; Turon et al., 2003). A similar assemblage pattern was also observed for the Alboran site ODP976 over a longer time scale (see Fig. 2 in Combourieu-Nebout et al., 1999), with also an almost disappearance of *S. stellatum* for time periods following the Mid-Brunhes Event (MBE). On the basis of our compilation, the highest occurrences of *S. stellatum* observed during MIS 19 (between roughly 750 and 800 ka BP) could thus sign a specific biostratigraphic event. At present, this species is characteristic of hypertrophic environments and was used as a marker of eutrophication in historical times (e.g. Shin et al., 2010 in the East China and Japan seas; Zonneveld et al., 2012 in the Adriatic and Ionan seas). Furthermore, on the basis of sediment trap analyses from the Mauritanian upwelling zone, Zonneveld et al. (2010) related the ecology of *S. stellatum* and its seasonal dynamics to those of *L. machaeorophorum*. It has also been described from modern sediments of the Gulf of Mexico (Limoges et al., 2013), in Brittany Bays (Larrazabal et al., 1990), and identified as a potential proxy of sea-level rise over the last glacial-interglacial period by marked increases of this species detected at 16 ka BP in near-equatorial latitudes of the Western African margin (Hardy et al., in prep).

Among the *Spiniferites* species, *S. ramosus* and the rare taxa *S rubinus* (e.g. Harland, 1992; Head, 1996) also display noticeable biostratigraphic trends in relation to MIS 19: Between 750 and 800 ka, *S. ramosus* shows percentages two times higher than modern values recorded in the area (e.g. Rochon et al., 1999), and then shows a progressive decline until present (Figs. 2 and 4). *S. rubinus* appears as specifically related to the beginning of MIS 19. Their cumulative abundances reached up to 30% of the assemblage at 784 ka.

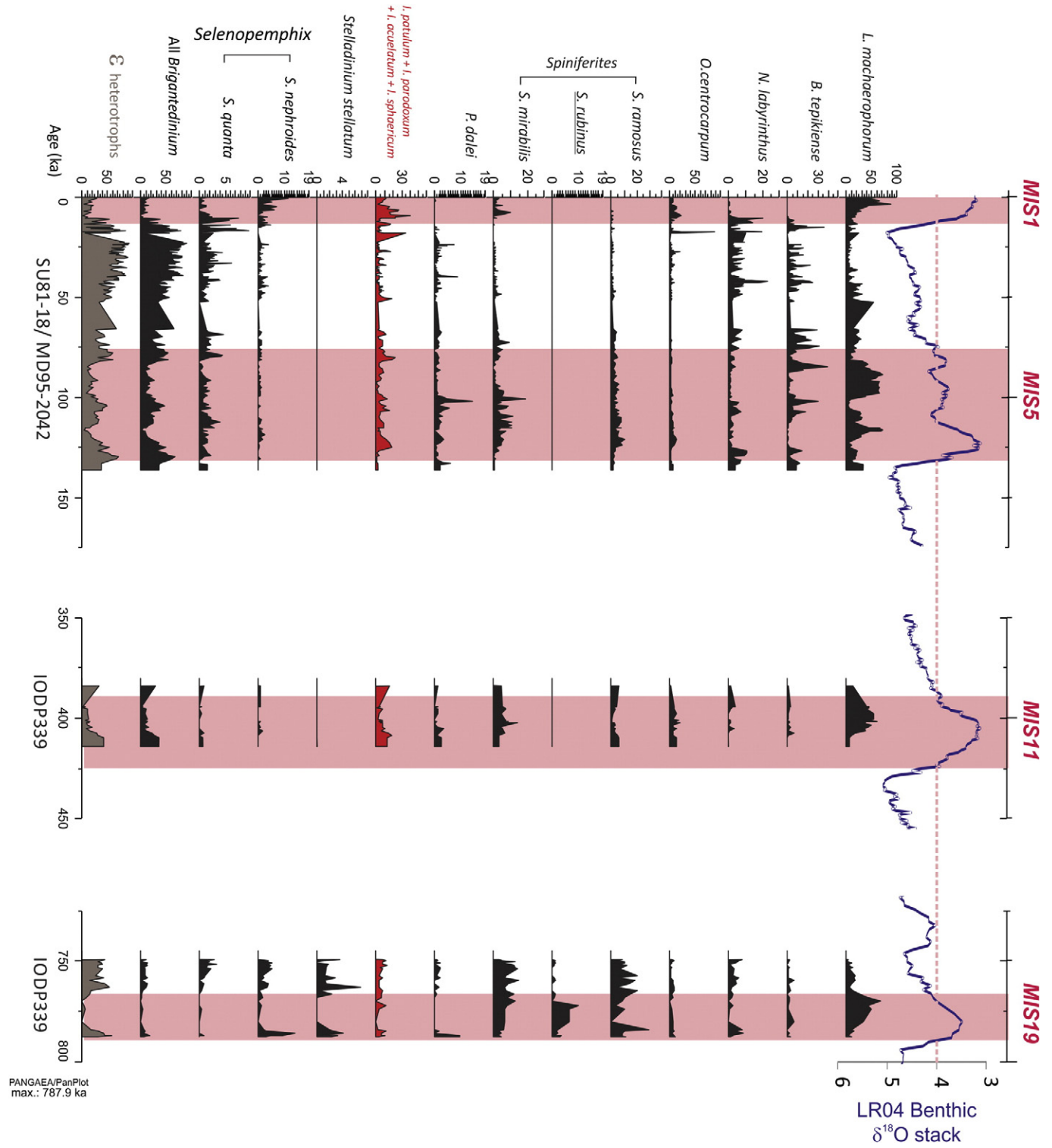

Fig. 2. Main dinocyst taxa shifts (relative abundances) over the "SHACK area" for the last one million years as depicted by a composite sequence consisting of interglacials from cores SU81-18 (e.g. Turon et al., 2003), MD95-2042 (e.g. Eynaud, 1999; Eynaud et al., 2000) and IODP 339 U1385 (this work). Full interglacial conditions are highlighted by pink bands for LR04 Benthic $\delta^{18}O$ stack (Lisiecki and Raymo, 2005) values under 4‰.

4.1. L. machaeorophorum and heterotrophic dinocysts: when past data put to test modern ecology knowledge

Fig. 3a provides an integrated peri-Iberian picture of dinocyst specific changes that occurred during interglacials and surrounding glacials in order to identify coherent ecological adaptations of this group through time. Climate changes are illustrated in parallel through planktonic $\delta^{18}O$ signals obtained on the same cores (when available), the global LR04 benthic stack (Lisiecki and Raymo, 2005), and summer insolation values at 65°N (Berger and Loutre, 1991).

Especially obvious in all studied records is the opposition observed between the occurrence of heterotrophic dinocysts and *L. machaeorophorum*, which seem to exclude each other. Except during MIS 1, these two species show opposite patterns with

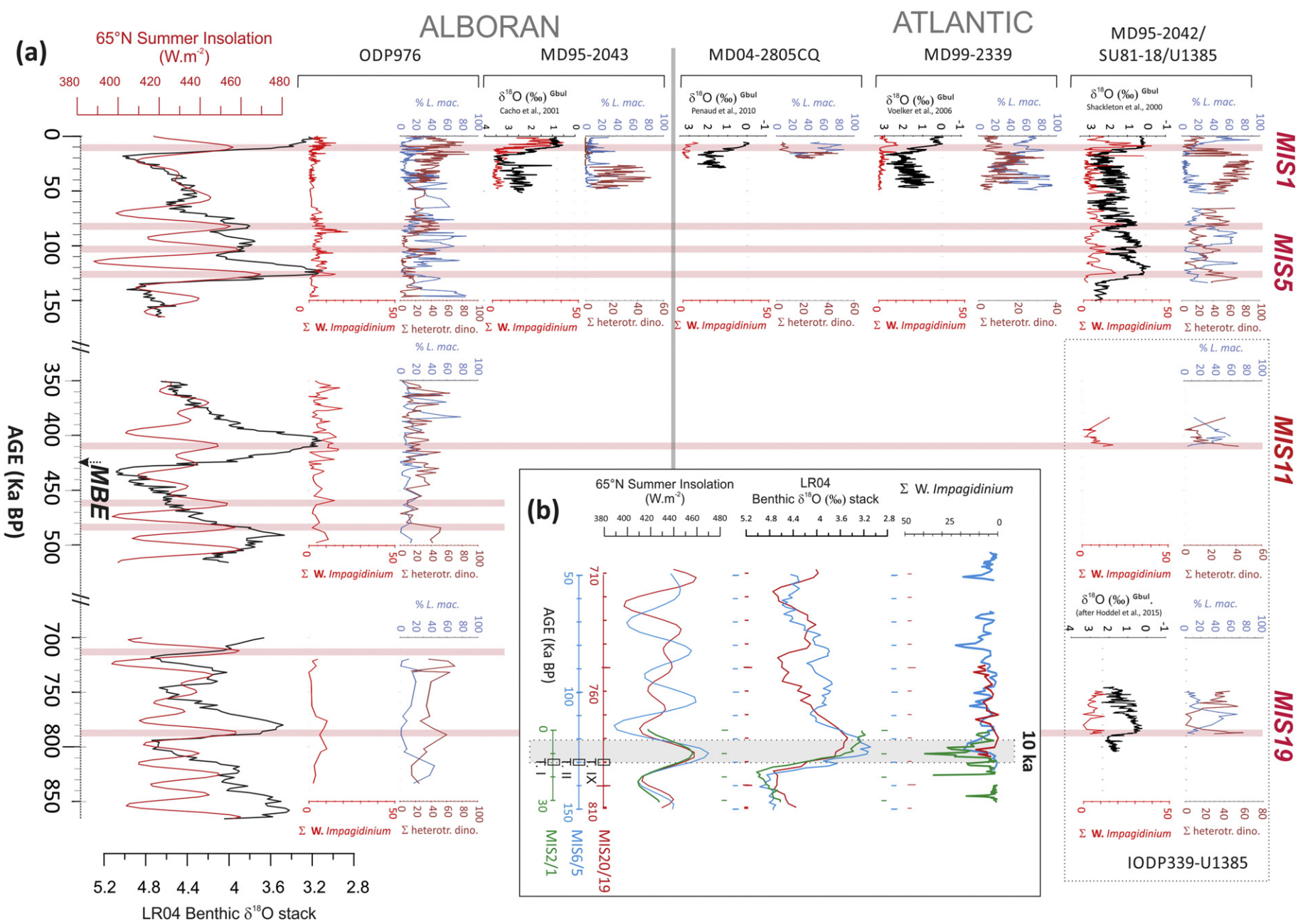

Fig. 3. (a) Comparison of interglacial signals along time and space of some selected dinocyst groups and species plotted versus isotopic $\delta^{18}O$ data of the respective cores (Cacho et al., 2001; Penaud et al., 2010; Voelker et al., 2006; Shackleton et al., 2000; Hodell et al., 2015), the LR04 Benthic $\delta^{18}O$ stack (Lisiecki and Raymo, 2005) and the 65°N summer insolation data (Berger and Loutre, 1991; pink band locate insolation values ≥ 450 W.m^{-2}). Mid-Brunhes Event (MBE) after Candy et al., 2010. % *L.mac.* = relative abundances, i.e. percentages of *Lingulodinium machaerophorum*; Σheterotr. dino. = sum of the relative abundances of heterotrophic dinocysts (taxa list after Marret and Zonneveld, 2003); Σ W. *Impagidinium* = sum of the relative abundances of the warm *Impagidinium*: *I. patulum*, *I. paradoxum*, *I. aculeatum* and *I. sphaericum*). **(b)** synchronisation of the Σ W. *Impagidinium* signals from cores SU81-18 (e.g. Turon et al. 2003) , MD95-2042 (e.g. Eynaud 1999; Sànchez-Goñi et al., 1999; Eynaud et al. 2000; Sànchez-Goñi et al., 2008) and IODP 339 U1385 (this work) over Terminations 1, 2 and 9 in concordance with the LR04 Benthic $\delta^{18}O$ stack (Lisiecki and Raymo, 2005). Note the good coherency of dinocyst derived data (suborbital events included) along comparable sections.

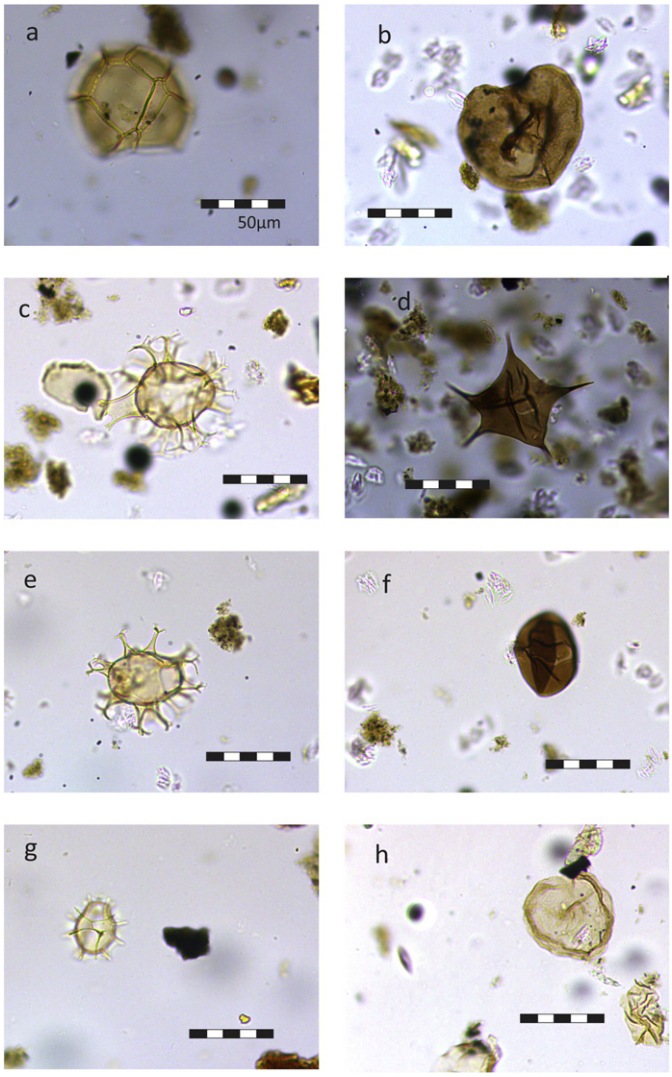

Plate 1. Some common specimens from IODP 339 1385 (HoleD). Scale bar = 50 µm. (a) *Impagidinium patulum*; (b, h) *Selenopemphix nephroides*; (c) *Spiniferites membranaceus*; (d) *Stelladinium stellatum*; (e) *Spiniferites lazus*; (f) *Brigantedinium carioense*; (g) *Impagidinium aculeatum.*

the expansion of heterotrophic species during cold periods (percentages ≥80% reached during the last glacial) and of *L. machaeorophorum* during transitional periods (comparable high near monospecific values only recorded during glacial inceptions). This is especially evident for MIS 19, 11 and 5 but should be shaded for MIS 1 where the *L. machaerophorum* high abundances occur early just after the Termination I. The species *L. machaerophorum* (related to the motile dinoflagellate *Lingulodinium polyedrum*) is a widely distributed dinocyst (e.g. Rochon et al., 1999) but is especially concentrated today in coastal/neritic sediments around the Gibraltar strait (Williams, 1971; Marret and Zonneveld, 2003; Zonneveld et al., 2013; Penaud et al., submitted). This local high occurrence is particularly interesting as this species could then be used as a peculiar taxa index for the present study. *L. machaerophorum* also colonizes estuarine environments (Morzadec-Kerfourn, 1977, 1992) and is frequently associated with eutrophic areas (fjords especially, e.g. Sætre et al., 1997; Dale et al., 1999, but not restrictively e.g. Zonneveld et al., 2012). As such, Leroy et al. (2013) recently considered its highest occurrences in the Caspian Sea as a biostratigraphical marker for the Anthropocene. Finally, it was interpreted as a proxy for past huge river discharges into the Ocean (Zaragosi et al., 2001; Eynaud et al., 2007; Penaud et al., submitted) and even considered as allochtonous in marine waters by Turon and Londeix (1988). Blooms of its motile form can be responsible for toxic red tides (Moorthi et al., 2006) and some culture experiments demonstrated that this species is highly sensitive to the water column stratification (Thomas and Gibson, 1990, 1992).

At present, *L. machaerophorum* distribution in modern sediments matches fairly well with the distribution of heterotrophic species, with high abundances preferentially found in coastal regions and close to upwelling cells (e.g. Zonneveld et al., 2013). It questions the observed patterns in our records where these species rather seem to oppose: (1) are they related to nuanced ecological patterns such as seasonality, i.e. shifts from permanent to seasonal upwelling regimes (or vice-versa) which could have induced major changes in dinocyst communities, or (2) are they due to preservation and/or cyst transportation changes along time? Preservation is especially a critical issue as dinocyst species are not equally impacted by oxydation in the water-column and after deposition (e.g. Zonneveld et al., 1997; Zonneveld et al., 2012; Zonneveld and Brummer, 2000; Bogus et al., 2012): some of them being very sensitive to water oxygen concentrations and thus water sources and dynamics. It is generally accepted that brown cysts, mainly produced by heterotrophic dinoflagellates (i.e. *Protoperidinium*) are more sensitive to aerobic degradation than *Gonyaulacoid* derived cysts (e.g. Dale, 1976). Among our index taxa for this comparative study, *L. machaerophorum* and warm *Impagidinium* species are respectively classified as moderately sensitive and resistant to oxygen availability in bottom waters (de Vernal and Marret, 2007).

Does the observed pattern thus signify a difference in bottom water-mass properties (and thus circulation) rather than a sea-surface productivity change, or is it a combination of both processes? In our study, the inter-basin comparison can provide some clues to solve this question, as the opposition between heterotroph cysts and *L. machaerophorum* are systematically observed whatever the considered period and basin. Such a coherent pattern suggests a similar way of cyst production and/or preservation despite distinct local surface and bottom conditions. It is highly improbable that interglacial/glacial changes cancelled these hydrographical differences since dinocyst population changes are not perfectly synchronized between the two basins, thus also underlining their own specificities through time. Therefore, the alternative solution would be to consider that the observed downcore antiphase between heterotroph cysts and *L. machaerophorum* is not a matter of post-production/preservation biases. Then, how to reconcile quite similar modern biogeographies which, in past times, seemed to exclude each other? Modern *L. machaerophorum* ecological requirements are still far from being correctly identified and this species may represent simply an opportunistic species. Interestingly, *L. machaerophorum* dynamics observed from our compilation (Fig. 3) reveals that this species follows or precedes maximal expansion of warm sea-surface taxa during interglacial optima. This shift is then discussed below.

4.2. Warm Impagidinium species along interglacials: what do they reveal?

In this study, the probable most significant dinocyst assemblage we retained is the one associated with *Impagidinium*. These typical oceanic taxa, often thermophilous, are among the common dinocysts found in the area (e.g., Turon et al., 2003; Penaud et al., 2011). For this work, we have lumped together abundances of warm Impagidinium ($\Sigma W_{Impagidinium}$) to define a specific index of warm sea-surface conditions,for which we have tested coherency through time and from one basin to another (Figs. 3 and 4, see also SI for further details regarding this group). At present, maximum abundances of these species are recorded in sediments of the equatorial Atlantic Ocean with a preference for full marine waters (Zonneveld et al., 2013). In the studied records, highest $\Sigma W_{Impagidinium}$ values (i.e. >10%) are associated with the onset of warm conditions during climatic optima (as defined from low isotopic values plateau, Fig. 3a). Their expansion is noticeable during short periods only, of maximum

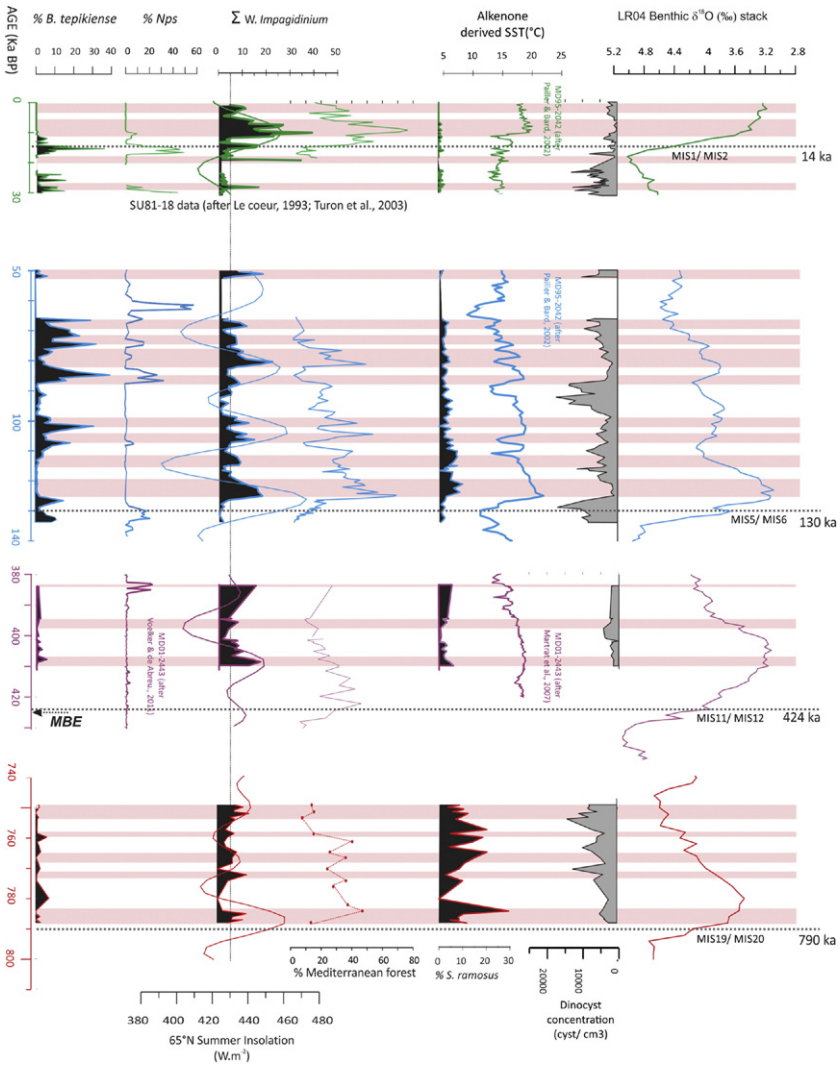

Fig. 4. Sea-surface key proxies (from dinocysts, foraminifera and alkenones) compared to continental ones (Mediterranean forest) over a composite sequence gathering data from cores SU81-18 (e.g. Le coeur, in press; Turon et al., 2003), MD95-2042 (e.g. Sànchez-Goñi et al., 1999; Eynaud et al., 2000; Sànchez-Goñi et al., 2008) and IODP 339 1385 (this work, Sánchez Goñi et al., 2016-this volume, Oliviera et al., in preparation). Derived SST from alkenone data: for MIS 1 and 5 from core MD95-2042 after Pailler and Bard (2002), for core MD01-2443 after Martrat et al. (2007). Percentages of the polar taxa *Neogloboquadrina pachyderma* sinistral (Nps) after Turon et al. (2003) for core SU81-18, after Sànchez-Goñi (2006) for core MD95-2042 and after Voelker and de Abreu (2011) for core MD01-2443. Marine isotopic stage limits after Lisiecki and Raymo (2005). Note the progressive regression of the *S. ramosus* through time.

duration of 10 ka, in close phasing with negative shifts in the planktonic $\delta^{18}O$ signal. They seem specifically to mark post-glacial warm conditions rather than hypsithermal periods (Fig. 3). The relative short duration of expansion of these warm *Impagidinium* is easily explained by competition stress with other thermophilous taxa such as *S. mirabilis* (see Turon and Londeix, 1988; Eynaud et al., 2000; Penaud et al., 2008, 2011 for discussions). It could also typify a peculiar ecological strategy as a pioneer group and/or as accompanying a change in the oceanic circulation as it was already suggested by Londeix et al. (2007).

For MIS 5, $\Sigma W_{Impagidinium}$ increases parallel the three isotopic substage lightening and coincide well with insolation maxima (pink bands on Fig. 3a). When comparing the intrinsic dynamics of each interglacial optima in the SHACK area (Fig. 3b) by synchronizing Terminations (here Terminations I, II and IX after Lisiecki and Raymo, 2005), and despite differences in temporal resolution analysis, trends in the $\Sigma W_{Impagidinium}$ show similar pacing along interglacials. This is especially obvious for peaks observed just after Terminations and for the glacial inception following interglacial optima.

Furthermore, the multi-phased interglacial complexes MIS 19 and MIS 5 are also well reflected in the $\Sigma W_{Impagidinium}$ evolution. Amplitudes for MIS 1 (green curve; Fig. 3b) are noticeably largest than those of previous warm MIS (blue and red curves; Fig. 3b), probably resulting from a major dinocyst community change through time, implying a growing presence of *Impagidinium* species associated with a synchronous general decline of *Spiniferites* species (as previously pointed out).

Fig. 4 synthesizes the most salient features provided by dinocysts and pollen (here the Mediterranean forest) for a composite sequence consisting of cores SU81-18 (e.g. Turon et al., 2003), MD95-2042 (e.g. Eynaud et al., 2000; Shackleton et al., 2003) and IODP 339 1385 (this work, Sànchez-Goñi et al., 2016–this volume). Additionally we plotted alkenone-derived SST from core MD95-2042 (MIS 1 and 5 sections after Pailler and Bard, 2002) and from the proximal core MD01-2443 (MIS 11 section after Martrat et al., 2007). Percentages of the polar taxa *Neogloboquadrina pachyderma* sinistral (*Nps*) are also shown (from core SU81-18 MIS 1 after Turon et al., 2003, for core MD95-2042 MIS 5 after Sànchez-Goñi, 2006; for core MD01-2443 MIS 11 after Voelker and de Abreu, 2011). This data set is also compared to the Marine $\delta^{18}O$ stack LR04 (Lisiecki and Raymo, 2005) and to summer insolation at 65°N (Berger and Loutre, 1991). Periods of maximum values of $\Sigma W_{Impagidinium}$ are marked by pink bands. They provide evidence of discrete warming episodes that took place near Terminations I, II and IX, that we can also directly compare with synchronous proximal

continental responses regarding Mediterranean forest evolution. From this compilation, sea-surface warming events appear synchronous with warming detected on land at millennial scales. A test of correlation was done to check this synchronicity giving a r^2 of 0.270 (results obtained with the Past software, see SI). The reader should keep in mind that pollen and dinocyst preparations are observed from same slides, coming from identical laboratory procedures, thus implying no artefact when correlating palynological ocean-continent data. Such a result confirms previous observations made for MIS 5 and 3 on the same site (Sànchez-Goñi et al., 1999, 2000; Eynaud et al., 2000) and permits us here to confirm and extend the continental/ocean relationship up to 800 ka.

In contrast to $\Sigma W_{Impagidinium}$, high abundances of *B. tepikiense* are observed during cold phases, also characterised by high *Nps* percentages. A strong representation of *B. tepikiense* is especially noticeable during cold MIS 5 interglacial substages. Cold phases are also marked by high absolute abundances of dinocysts (i.e. concentrations in nb of cysts/dry cm^3) in sediments. These high concentrations were already noted by several authors on this margin during cold climatic events (e.g. Zippi, 1992; Eynaud, 1999; Eynaud et al., 2009; Penaud et al., 2010, 2011) and interpreted as representing changes in the local upwelling dynamics (from seasonal to year-round) in response to atmospheric re-organisations. This interpretation was based on the distribution of modern dinocyst concentrations in the sediments from the proximal North Canary Basin, which show high dinocyst concentrations within zones marking upwelling filaments (e.g. Targarona et al., 1999; Bouimetarhan et al., 2009b). Conversely, on the SW Iberian Margin (Fig. 1), Zippi (1992) noted an opposite relation between carbonate content and dinocyst concentrations in the sediment and attributed that observation to the preferential dissolution of carbonate under cold climate (and thus the artificial increase of cysts) in concordance to a high index of fragmentations of planktonic foraminifera shells. However, Zippi (1992) did not introduce any consideration about the paleoproductivity issue. Indeed, for calcareous (foraminifera) as well as for organic-walled (dinocysts) material, the residual concentration of microfossils in sediments is the result of a complex balance between production, dissolution and preservation. Thanks to the close correlation made in this study between marine and pollen data, we directly attribute the modulation of dinocyst concentrations to climate.

5. The significance of population shifts: from ecology to oceanic circulation patterns

The dinocyst compilation made in this study provides important biodiversity information that could be tied to changes in the local and/or regional hydrographical dynamics in response to climate changes. Population shifts occur repetitively and coherently through time with some index groups that could be used to evaluate the adaptation capability of the marine flora. They illustrate a constant population interchange between the western Mediterranean and the subtropical North Atlantic despite sea-level changes and the temporal physiographic barrier of the Strait of Gilbraltar, which should have reduced water exchanges during low sea-levels of the last million years. These latter processes have had important echoes on planktonic populations, as demonstrated by Rohling et al. (1995) for planktonic foraminifera, something also detected with some dinocyst key taxa.

Strong modulations of the MOW have already been pointed out by several studies for the last glacial (e.g. Cacho et al., 2000; Voelker et al., 2006; Rogerson et al., 2010), showing an acceleration of the outflow during cold phases. Their impact on the distribution of dinoflagellate and their cysts has certainly been important. A southward migration of biogeographical provinces in the North Atlantic and even the invasion of the Alboran Sea waters by *B. tepikiense* from where this species is absent at present (Turon and Londeix, 1988; Combourieu-Nebout et al., 2002; Penaud et al., 2011; Fig. 3) have been observed concomitantly. This invasion, in a configuration of accelerated MOW, attests to an extensive North Atlantic intrusion in the Alboran Sea, probably as a way to compensate the MOW export and its associated deficit. This thus supposes vigorous Atlantic/Mediterranean exchanges at those times and thus enhanced exportation/importation of cysts.

Cold sub-stages within interglacial complexes (MIS 19 and 5) demonstrate the same biotic pattern with also high occurrences of *B. tepikiense* (this work, Combourieu-Nebout et al., 1999; Eynaud et al., 2000). The context is however different here even if some analoguous hydrographical mechanisms could be at play, i.e. due to acceleration of the MOW also, but in this case rather forced by a reduction of the Gibraltar strait section during cold sub-stages and associated sea-level low stands (the reader should keep in mind that at the opposite HEs record a rising sea-level with an estimated magnitude of up to 30 m, e.g. Siddall et al., 2003). The synchronous regression of warm species and of *L. machaerophorum* furthermore documents a severe cooling and a major change of the water column stability; a vital requirement for this later species as deduced from culture (e.g. Thomas and Gibson, 1990). Turbulence at the Gibraltar strait due to the acceleration of currents, thus preventing a soft settling of cysts and inhibiting a complete life cycle, could explain the *L. machaerophorum* disappearance. This turbulence could be amplified by atmospheric processes, i.e. winds, the regression of the Mediterranean forest on Iberia being also noticed (Fig. 3).

The past population shifts observed in this part of the sub-tropical North-Atlantic provide some new insights regarding the known modern ecology and biogeography of cysts and their related theca (i.e. Marret and Zonneveld, 2003; de Vernal and Marret, 2007). They show a strong potential for dinoflagellates to adapt, even when facing abrupt ecological changes. Two taxa would especially be considered as super-adapted to transient periods: one is a common typical cyst from the studied area, *L. machaerophorum*; the other, *B. tepikiense*, is a taxa rather distributed in the cool temperate Atlantic but especially adapted to strong seasonality (i.e. cold winters and warm summers), as those which characterize waters from the St Laurent outlet at present (e.g. Rochon et al., 1999). These two species are found at the transition boundaries of interglacial optima and could thus be qualified of opportunistic, as conditions accompanying transition phases (glacial inception and termination) are especially unstable and contrast with the relative equilibrium of warm optima. However the local high occurrence of *L. machaerophorum* rather argues for a pre-adaptation to the sea-surface conditions surrounding the Gibraltar strait. Conversely, its presence with nearly mono-specific abundances in the modern sediments from the Iberian and North Canary regions since 5 ka at least (Fig. 2) questions the hydrographic and associated climatic modes of the last millennia. When comparing its specific dynamics during previous interglacials, this species does not mark hypsithermal modes but rather cooler conditions. This supports previous findings showing that modern conditions around Iberia already shifted toward a late Holocene Neoglacial state (e.g. Jerardino, 1995). For the Atlantic side, it seems to have already implied changes in the seasonality of the modern Canary Current upwelling (e.g. Abrantes et al., 2011; McGregor et al., 2007; Bouimetarhan et al., 2009a).

6. The nine past and current interglacials: new insights from dinocyst data of the "Shackleton" site

Even if not continuous, the dinocyst data produced for this compilation gathering cores from the SHACK area (Fig. 1) offer the possibility to test the significance of this phyto-planktonic population regarding long term records over the last 800 ka. The purpose of our approach was to test interglacial periods in low eccentricity contexts first, explaining why, up to date, our focus and records are thus restricted to some snapshots. To present a comprehensive view of these results and simplify the message brought by dinocyst assemblages, we ran a PCA on the composite "SHACK" sequence (SU81-18/MD95-2042/IODP339 U1385, see Methods and SI). The coordinates of the first three axis obtained

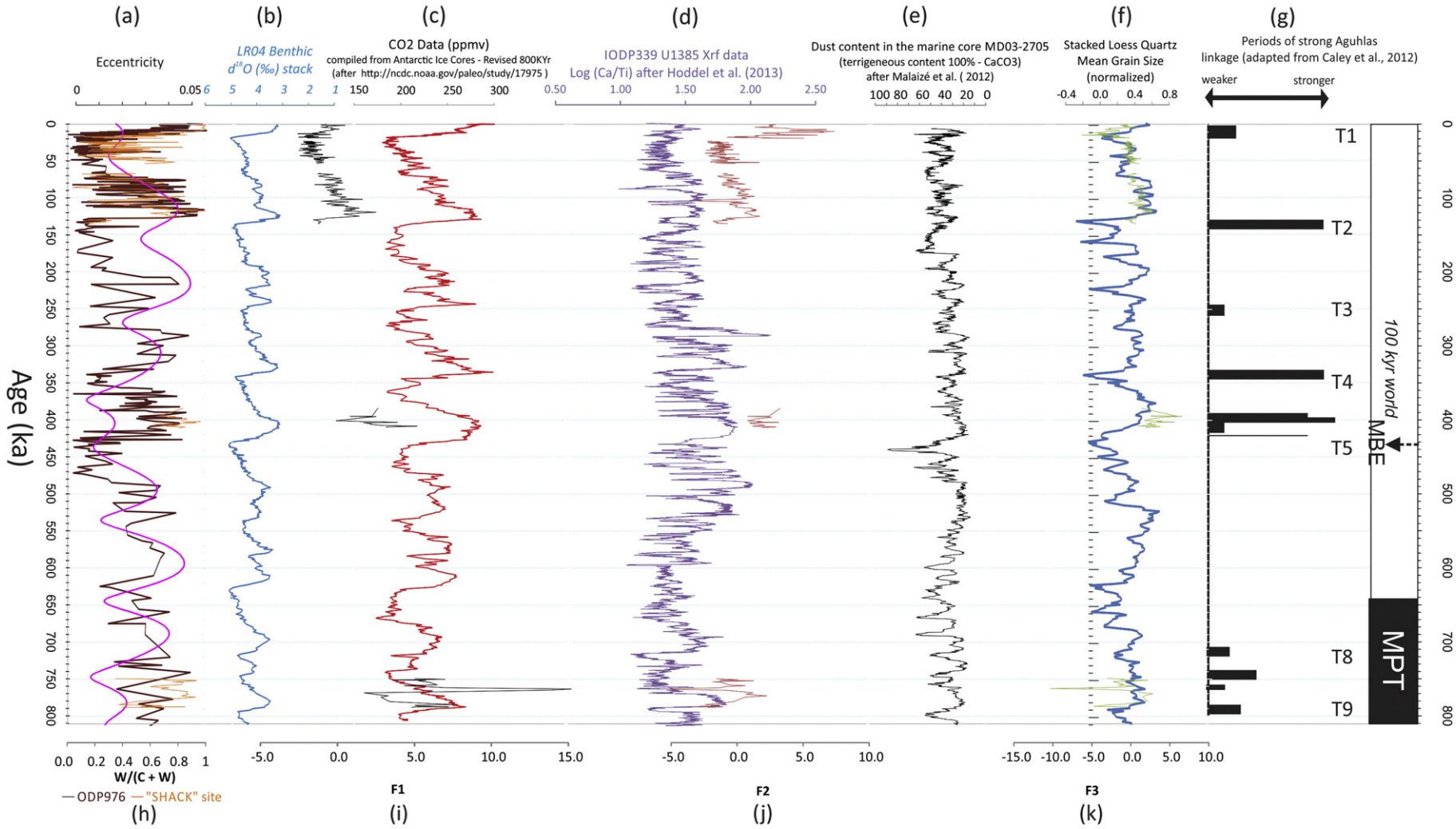

Fig. 5. Compilation of some archives of interest along the last 810 ka with: (a) Eccentricity cycles (after Berger & Loutre, 1991), (b) LR04 Benthic $\delta^{18}O$ stack (Lisiecki and Raymo, 2005), (c) CO_2 data (ppmv) compiled from Antarctic Ice Cores (from http://ncdc.noaa.gov/paleo/study/17975), (d) IODP339 U1385 XRF data Log (Ca/Ti) after Hodell et al. (2013a, 2013b), (e) Dust content in the marine core MD03-2705 (terrigeneous content 100% - CaCO3) after Malaizé et al. (2012), (f) Mean Grain Size (normalized) after Clemens et al. (2008), (g) periods of strong Aguhlas linkage (adapted from Caley et al., 2012). These sequences are compared to (h) the dinocyst W/(W + C) ratio from the Alboran ODP976 site and from the "SHACK" area (SU81-18/MD95-2042 and IODP 339 U1385), together with the PCA analysis results of this composite dinocyst record (see Methods) as seen throughout the first 3 components (from F1 (i) to F3 (k), representing 30% of the total variance).

from this PCA are plotted along time on Fig. 5 and compared to selected 800 ka-long-sequences of interest, along with the [W/(C + W)] dinocyst ratio for the SHACK area and for the Alboran ODP976 record which, even if of lowest resolution, encompasses the last 810 ka (Combourieu-Nebout et al., 1999). A schematic index reflecting qualitatively the Aguhlas linkage dynamics (as redrawn from Caley et al., 2012) is also plotted to further document inter-oceanic exchanges.

This comparison reveals very distinctive patterns and specific signatures (Fig. 5 and SI) for each of the first three PCA-axis (these 3 axis representing nearly 30% of the total variance, see methods and the excel file provided in SI for detailed results of the PCA). *These signatures could be summarized as follow*: (a) a first axis F1 (13.6% of the total variance), positively related to warm eutrophic species but negatively related to cold eutrophic ones (see species/variables distribution in SI), thus bearing the double and coupled environmental signal of SST and upwelling dynamics. Considering a paleoceanographic perspective, this axis clearly relates to global changes as seen throughout the (ice-volume/sea-level linked) LR04 record and the CO_2 atmospheric content.

(b) A second axis F2 (7.65% of the total variance), also bearing a strong SST/upwelling signature but for which species positively correlated to, are representative of the typical Iberian margin modern dinocyst assemblage (i.e. Sprangers et al., 2004). Its time distribution shows a close matching with the Ca content (vs terrigeneous components) of marine sediments from the subtropical North Atlantic western margin as derived from XRF data, both for the same "Shackleton site" (Log (Ti/Ca) from Hodell et al., 2013a, 2013b) and from the southern core MD03-2705 (Malaizé et al., 2012).

(c) A third axis F3 (7.33% of the total variance), which plainly separates autotrophic from heterotrophic dinocyst species, and is interestingly closely mirroring the monsoon index along time (after the stack produced by Clemens et al., 2008).

From this 810 ka long perspective, arise some noticeable points which shed light on the high sensitivity of dinocyst communities regarding climate changes. First of all, it is worth noting the good reproducibility of the [W/(C + W)] ratio at the regional scale except during MIS 19 where the "Shackleton site" reveals much more contrasted responses. Differences in time resolution are at the origin of this discrepancy but other evidences are brought by the PCA that this MIS 19 interval is clearly atypical. This is well expressed in the F1 component which registers large and sharp amplitude shifts (not seen later in the Pleistocene neither in the Holocene) and additionally shows poor matching with other 810 ka records as plotted on Fig. 5. Conversely, F2 and F3 during MIS 19 closely mirror the Ca sedimentary content and the monsoon index respectively, recording synchronous and consistent transitions, thus suggesting that the message brought by dinocyst populations from the Iberian margin is however comprehensive enough to be assimilated to large scale environmental changes over the last 810 ka. The link between the Ca content and PCA axis 2 is easily understandable at the scale of the North Atlantic basin (including its marginal seas) as it reflects mainly biogenic carbonate content and thus the pelagic production, well known to be favoured, during warm periods (e.g. Chapman and Shackleton, 1998; Richter et al., 2006; Hodell et al., 2013b). In the same way, consistency between the stacked monsoon index vs the PCA axis 3 could be explained by the fact that this axis is mainly representing the weight of autotrophic species which thereby need sea-surface fertilisation and thus dust arrival to proliferate.

Most problematic is the signal detected with the PCA axis 1 during MIS 19, which if it does echo the [W(/(C + W)] ratio and the Ca content within the "Shackleton site", is not completely attributable to long term and global trends as stated previously. Is this difference related to the specific assemblage we encountered during MIS 19, with the occurrence of atypical species such as *S. stellatum* and *S. rubinus*, and the high percentages of *S. ramosus* as previously underlined? Could the drastic climatic transitions occurring between MIS 19 and modern times, i.e. the MPT and the MBE, have impacted dinocyst population of this area so significantly? This is highly possible, as these two climatic temporal nodes are known to sign major oceanic reorganisations, with especially a strong impact on the Atlantic meridional oceanic circulation (e.g. Poirier and Billups, 2014; Bell et al., 2015), a key component for the Iberian margin oceanography and its associated upwelling dynamics. To valid such an assumption we urgently need to further extend our record up and back in time, putting a focus not only on past interglacials but also on glacials, including the atypical MIS 13 and MIS 6 ones, so as to detect an optimal set of contrasted features.

7. Conclusions

This study was designed to provide new biogeographical and stratigraphical patterns for the Iberian margin by compiling micropaleontological records derived from the study of dinoflagellate cysts during past interglacials. This effort has revealed that surface waters around Iberia were characterised over the last million years by the repetitive occurrence of the same dinocyst assemblage; however, some discrepancies in the response of this marine protist community shade its adaption to glacial and interglacial cycles. Very coherent features occur on both sides of the Gibraltar strait indicating a constant interchange of populations and a permanent connection between Atlantic and Mediterranean marine biomes, even during sea-level low stands. Regarding dinocysts, this interchange is easily attributed to sea-surface water exchanges, but the Mediterranean Outflow Waters could also be considered as a vector of settled cysts. Some index groups could be used to evaluate the adaptation capability and the dynamics of the marine dinoflagellate flora, especially the autotrophic cysts: *Lingulodinium machaerophorum*, *Bitectatodinium tepikiense*, together with some species from the *Spiniferites* and the *Impagidinium* groups, which swing with heterotrophic dinocysts along time. Changes detected in the dinocyst community appeared to be coherent at sub-orbital and orbital scales with those detected with other sea-surface proxies and continental bio-indicators (pollen), demonstrating a close connection between sea-surface environments and the Iberian continent over the last 800 ka.

Acknowledgements

The crews, together with the scientific and technical staffs of the RV JOIDES Resolution are thanked for work accomplished during the IODP leg 339 and the recovery of site U1385. This study was conducted in the frame of the INSU (OA-LEFE-IMAGO and TS-INTERRVIE) French CNRS programmes within the "IceBioRAM", "Warmclim" & "Pulse" projects and grants which supported palynological analyses of the IODP339 U1385 site. We wish to thank L Devaux for preparing the samples and MC Gasparotto for her help on MIS 11 data acquisition. We gratefully acknowledge reviewers, whose anonymous comments have contributed to increase the quality of this manuscript. This is an UMR-EPOC contribution.

Appendix A. Supplementary data

Supplementary data to this article can be found online at http://dx.doi.org/10.1016/j.gloplacha.2015.12.004.

References

Abrantes, F., Rodrigues, T., Montanari, B., Santos, C., Witt, L., Lopes, C., Voelker, A., 2011. Climate of the last millennium at the southern pole of the North Atlantic Oscillation: an inner-shelf sediment record of flooding and upwelling. Clim. Res. 48, 261–280. http://dx.doi.org/10.3354/cr01010.

Arístegui, J., Ãlvarez-Salgado, X.A., Barton, E.D., Figueiras, F.G., Hernandez-Leon, S., Roy, C., Santos, A.M.P., 2005. Oceanography and fisheries of the canary current/Iberian region of the eastern north Atlantic (18a, E). In: Robinson, A.R., Brink, K.H. (Eds.), The Sea.

Arístegui, J., Barton, E.D., Álvarez-Salgado, X.A., Santos, A.M.P., Figueiras, F.G., Kifani, S., Hernández-León, S., Mason, E., Machú, E., Demarcq, H., 2009. Sub-regional ecosystem variability in the canary current upwelling. Prog. Oceanogr. 83, 33–48. http://dx.doi.org/10.1016/j.pocean.2009.07.031.

Bell, D.B., Jung, S.J.A., Kroon, D., 2015. The Plio-Pleistocene development of Atlantic deep-water circulation and its influence on climate trends. Quat. Sci. Rev. 123, 265–282. http://dx.doi.org/10.1016/j.quascirev.2015.06.026.

Berger, A., Loutre, M.F., 1991. Insolation values for the climate of the last 10 millions years. Quat. Sci. Rev. 10, 297–317.

Bogus, K.A., Zonneveld, K.A.F., Fischer, D., Kasten, S., Bohrmann, G., Versteegh, G.J.M., 2012. The effect of meter-scale lateral oxygen gradients at the sediment–water interface on selected organic matter based alteration, productivity and temperature proxies. Biogeosciences 9, 1553–1570.

Bouimetarhan, I., Dupont, L., Schefuß, E., Mollenhauer, G., Mulitza, S., Zonneveld, K., 2009a. Palynological evidence for climatic and oceanic variability off NW Africa during the late Holocene. Quat. Res. 72, 188–197. http://dx.doi.org/10.1016/j.yqres.2009.05.003.

Bouimetarhan, I., Marret, F., Dupont, L., Zonneveld, K., 2009b. Dinoflagellate cyst distribution in marine surface sediments off West Africa (17–6°N) in relation to sea-surface conditions, freshwater input and seasonal coastal upwelling. Mar. Micropaleontol. 71, 113–130. http://dx.doi.org/10.1016/j.marmicro.2009.02.001.

Cacho, I., Grimalt, J.O., Sierro, J.F., Shackleton, N., Canals, M., 2000. Evidence for enhanced Mediterranean thermohaline circulation during rapid climatic coolings. Earth Planet. Sci. Lett. 183, 417–429.

Cacho, I., Grimalt, J.O., Canals, M., Sbaffi, L., Shackleton, N.J., Schönfeld, J., Zahn, R., 2001. Variability of the western Mediterranean Sea surface temperature during the last 25,000 years and its connection with the Northern Hemisphere climatic changes. Paleoceanography 16, 40–52. http://dx.doi.org/10.1029/2000PA000502.

Caley, T., Giraudeau, J., Malaizé, B., Rossignol, L., Pierre, C., 2012. Agulhas leakage as a key process in the modes of Quaternary climate changes. Proc. Natl. Acad. Sci. 109, 6835–6839.

Candy, I., Coope, G.R., Lee, J.R., Parfitt, S.A., Preece, R.C., Rose, J., Schreve, D.C., 2010. Pronounced warmth during early Middle Pleistocene interglacials: investigating the Mid-Brunhes Event in the British terrestrial sequence. Earth Sci. Rev. 103, 183–196. http://dx.doi.org/10.1016/j.earscirev.2010.09.007.

Chapman, M.R., Shackleton, N.J., 1998. What level of resolution is attainable in a deep-sea core? Results of a spectrophotometer study. Paleoceanography 13, 311–315.

Clemens, S.C., et al., 2008. Plio-Pleistocene East Asian monsoon proxy data. IGBP PAGES/World Data Center for Paleoclimatology Data Contribution Series # 2008–119. USA, NOAA/NCDC Paleoclimatology Program, Boulder CO.

Combourieu-Nebout, N., Londeix, L., Baudin, F., Turon, J.-L., von Grafenstein, R., Zahn, R., 1999. Chap. 36: Quaternary marine and continental paleoenvironments in the western Mediterranean (site 976, Alboran sea): palynological evidence. In: Zahn, R., Comas, M.C., Klaus, A. (Eds.), Proceedings of the Ocean Drilling Program Scientific Results 161, pp. 457–468.

Combourieu-Nebout, N., Paterne, M., Turon, J.-L., Siani, G., 1998. A high resolution record of the last deglaciation in the central Mediterranean sea: palaeovegetation and palaeohydrological evolution. Quat. Sci. Rev. 17, 303–317.

Combourieu-Nebout, N., Turon, J.-L., Zahn, R., Capotondi, L., Londeix, L., Pahnke, K., 2002. Enhanced aridity and atmospheric high-pressure stability over the western Mediterranean during the North Atlantic cold events of the past 50 k.y. Geology 30, 863–866.

Crutzen, P.J., 2002. The "anthropocene." J Phys. IV France, EDP Sciences, Les Ulis 12. http://dx.doi.org/10.1051/jp4:20020447.

Dale, B., 1976. Cyst formation, sedimentation, and preservation: factors affecting dinoflagellate assemblages in recent sediments from Trondheimsfjord, Norway. Rev. Palaeobot. Palynol. 22, 39–60.

Dale, B., 1983. Dinoflagellate resting cysts: "benthic plankton". In: Fryxell, G.A. (Ed.), Survival Strategies of the Algae. Cambridge University Press, pp. 69–1367.

Dale, B., Thorsen, T.A., Fjellså, A., 1999. Dinoflagellate cysts as indicators of cultural eutrophication in the Oslofjord, Norway. Estuar. Coast. Shelf Sci. 48, 371–382.

De Schepper, S., Groeneveld, J., Naafs, B.D.A., Van Renterghem, C., Hennissen, J., Head, M.J., Louwye, S., Fabian, K., 2013. Northern hemisphere glaciation during the globally warm Early Late Pliocene. PLoS One 8, e81508. http://dx.doi.org/10.1371/journal.pone.0081508.

de Vernal, A., Marret, F., 2007. Chapter nine : organic-walled dinoflagellate cysts : tracers of sea-surface conditions. In: Hillaire-Marcel, C., de Vernal, A. (Eds.), Developments in Marine Geology, pp. 371–408.

de Vernal, A., Henry, M., Bilodeau, G., 1999. Techniques de préparation et d'analyse en micropaléontologie. Cah. GEOTOP 3, 1–29.

de Vernal, A., Henry, M., Matthiessen, J., Mudie, P.J., Rochon, A., Boessenkool, K.P., Eynaud, F., Grösfjeld, K., Guiot, J., Hamel, D., Harland, R., Head, M.J., Kunz-Pirrung, M., Levac, E., Loucheur, V., Peyron, O., Pospelova, V., Radi, T., Turon, J.L., Voronina, E., 2001. Dinoflagellate cyst assemblages in surface sediments of the Laptev Sea region (Arctic Ocean) and their relationship to hydrographic conditions. J. Quat. Sci. 16, 637–649.

de Vernal, A., Londeix, L., Mudie, P.J., Harland, R., Morzadec-Kerfourn, M.-T., Turon, J.L., Wrenn, J.H., 1992. Quaternary organic-walled dinoflagellate cysts of the North Atlantic Ocean and adjacent seas : ecostratigraphy and biostratigraphy. In: Head, M.J., Wrenn, J.H. (Eds.), Neogene and Quaternary Dinoflagellate Cyst of the North Atlantic Ocean and Adjacent Seas : Ecostratigraphy and Biostratigraphy. AASP Foundation, pp. 289–328.

Dodge, J.D., Harland, R., 1991. The distribution of planktonic dinoflagellates and their cysts in the eastern and northeastern Atlantic ocean. New Phytol. 118, 593–603.

Ellegaard, M., Figueroa, R., Versteegh, G.J.M., 2013. Dinoflagellate life cycles, strategy and diversity: key foci for future research. In: Lewis, J.M., Marret, F., Bradley, L. (Eds.), Biological and Geological Perspectives of DinoflagellatesThe Micropalaeontological Society, Special Publications. Geological Society, London, pp. 249–261.

Eynaud, F., 1999. Kystes de Dinoflagellés et Evolution paléoclimatique et paléohydrologique de l'Atlantique Nord au cours du Dernier Cycle Climatique du Quaternaire (Thèse de 3e cycle). Université de Bordeaux I.

Eynaud, F., De Abreu, L., Voelker, A., Schönfeld, J., Salgueiro, E., Turon, J.L., Penaud, A., Toucanne, S., Naughton, F., Sànchez-Goñi, M.F., Malaizé, B., Cacho, I., 2009. Position of the polar front along the western Iberian margin during key cold episodes of the last 45 ka. Geochem. Geophys. Geosyst. 10. http://dx.doi.org/10.1029/2009GC002398.

Eynaud, F., Turon, J.L., Sànchez-Goñi, M.F., Gendreau, S., 2000. Dinoflagellate cyst evidence of "Heinrich-like events" off Portugal during the marine isotopic stage 5. Mar. Micropaleontol. 40, 9–21.

Eynaud, F., Zaragosi, S., Scourse, J.D., Mojtahid, M., Bourillet, J.F., Hall, I.R., Penaud, A., Locascio, M., Reijonen, A., 2007. Deglacial laminated facies on the NW European continental margin: the hydrographic significance of British–Irish ice sheet deglaciation and fleuve manche paleoriver discharges. Geochem. Geophys. Geosyst. 8.

Fensome, R.A., Williams, G.L., 2004. The Lentin and Williams index of fossil dinoflagellates. AASP Foundation Contributions Series. 42 (909 pp. Ed.).

Fensome, R.A., MacRae, R.A., Williams, G.L., 1998. DINOFLAJ. Geological Survey of Canada Open File 3653.

Font, J., 2002. Mesoscale variability in the Alboran sea: synthetic aperture radar imaging of frontal eddies. J. Geophys. Res. 107. http://dx.doi.org/10.1029/2001JC000835.

Giorgi, F., 2006. Climate change hot-spots. Geophys. Res. Lett. 33, L08707. http://dx.doi.org/10.1029/2006GL025734.

Hammer, Ø., Harper, D.A.T., Ryan, P.D., 2001. PAST: paleontological statistics software package for education and data analysis. Palaeontol. Electron. 4 (1) (9 pp. http://palaeo-electronica.org/2001_1/past/issue1_01.htm).

Harland, R., 1992. Dinoflagellate biostratigraphy of Neogene and Quaternary sediments at holes 400/400A in the Bay of Biscay (Deep Sea Drilling Project Leg 48). DSDP Initial Reports Volume XLVIII http://dx.doi.org/10.2973/dsdp.proc.48.1979.

Hauschildt, M., Rinna, J., Rullkötter, J., 1999. Chap. 30: molecular indicators of the supply of marine and terrigenous organic matter to a pleistocene organic-matter-rich layer in the Alboran Basin (Western Mediterranean Sea). In: Zahn, R., Comas, M.C., Klaus, A. (Eds.), Proceedings of the Ocean Drilling Program Scientific Results 161, pp. 391–400.

Head, M.J., 1996. Modern dinoflagellate cysts and their biological affinities. Palynol. Princ. Appl. 3, 1197–1248.

Heinrich, H., 1988. Origin and consequences of cyclic ice rafting in the northeast Atlantic ocean during the past 130,000 years. Quat. Res. 29, 142–152.

Hodell, D., Crowhurst, S., Skinner, L., Tzedakis, P.C., Margari, V., Channell, J.E.T., Kamenov, G., Maclachlan, S., Rothwell, G., 2013b. Response of Iberian margin sediments to orbital and suborbital forcing over the past 420 ka. Paleoceanography 28, 185–199. http://dx.doi.org/10.1002/palo.20017.

Hodell, D., Lourens, L., Crowhurst, S., Konijnendijk, T., Tjallingii, R., Jiménez-Espejo, F., Skinner, L., Tzedakis, P.C., 2015. A reference time scale for Site U1385 (Shackleton Site) on the SW Iberian Margin. Glob. Planet. Chang. 133, 49–64. http://dx.doi.org/10.1016/j.gloplacha.2015.07.002 (this volume).

Hodell, D.A., Lourens, L., Stow, D.A.V., Hernández-Molina, J., Alvarez Zarikian, C.A., the Shackleton site project members, 2013a. The "Shackleton Site" (IODP Site U1385) on the Iberian Margin. Sci. Drill. 16, 13–19. http://dx.doi.org/10.5194/sd-16-13-2013.

Houben, A.J.P., Bijl, P.K., Pross, J., Bohaty, S.M., Passchier, S., Stickley, C.E., Röhl, U., Sugisaki, S., Tauxe, L., van de Flierdt, T., Olney, M., Sangiorgi, F., Sluijs, A., Escutia, C., Brinkhuis, H., the Expedition 318 Scientists, 2013. Reorganization of Southern Ocean Plankton Ecosystem at the Onset of Antarctic Glaciation. Science 340, 341–344. http://dx.doi.org/10.1126/science.1223646.

Jerardino, A., 1995. Late Holocene Neoglacial episodes in southern South America and southern Africa: a comparison. The Holocene 5, 361–368.

Johnson, R.G., 1997. Ice age initiation by an ocean-atmospheric circulation change in the Labrador Sea. Earth Planet. Sci. Lett. 148, 367–379.

Kodrans-Nsiah, M., de Lange, G.J., Zonneveld, K.A.F., 2008. A natural exposure experiment on short-term species-selective aerobic degradation of dinoflagellate cysts. Rev. Palaeobot. Palynol. 152, 32–39.

Larrazabal, M.E., Lassus, P., Maggi, P., Bardouil, M., 1990. Kystes modernes de dinoflagellés en baie de Vilaine-Bretagne sud (France). Cryptogam. Algol. 11, 171–185.

Le coeur, L., 2015. Reconstitution quantitative des paléotempératures et des paléosalinités de surface depuis le dernier maximum glacaire, au large du Portugal, à partir des asssemblages de kystes de dinoflagellés (DEA, U. Bordeaux 1, 1993) (in press).

Leroy, S.A.G., Lahijani, H.A.K., Reyss, J.-L., Chalié, F., Haghani, S., Shah-Hosseini, M., Shahkarami, S., Tudryn, A., Arpe, K., Habibi, P., Nasrollahzadeh, H.S., Makhlough, A., 2013. A two-step expansion of the dinocyst *Lingulodinium machaerophorum* in the Caspian Sea: the role of changing environment. Quat. Sci. Rev. 77, 31–45. http://dx.doi.org/10.1016/j.quascirev.2013.06.026.

Levi, C., 1999. Les variations paléo-climatiques et paléo-hydrologiques en Méditerranée occidentale (Mer d'Alboran) entre -70 000 et -130 000 ans (Stade isotopique 5). (DEA Environnements et paléoenvironnements océaniques report, Univ. Bordeaux 1).

Limoges, A., Londeix, L., de Vernal, A., 2013. Organic-walled dinoflagellate cyst distribution in the Gulf of Mexico. Mar. Micropaleontol. 102, 51–68. http://dx.doi.org/10.1016/j.marmicro.2013.06.002.

Lisiecki, L.E., Raymo, M.E., 2005. A Pliocene–Pleistocene stack of 57 globally distributed benthic $\delta^{18}O$ records. Paleoceanography 20, 1–17.

Londeix, L., Benzakour, M., Suc, J.-P., Turon, J.-L., 2007. Messinian palaeoenvironments and hydrology in Sicily (Italy): the dinoflagellate cyst record. Geobios 40, 233–250. http://dx.doi.org/10.1016/j.geobios.2006.12.001.

Malaizé, B., Jullien, E., Tisserand, A., Skonieczny, C., Grousset, E.F., Eynaud, F., Kissel, C., Bonnin, J., Karstens, S., Martinez, P., Bory, A., Bout-Roumazeilles, V., Caley, T., Crosta, X., Charlier, K., Rossignol, L., Flores, J.-A., Schneider, R., 2012. The impact of African aridity on the isotopic signature of Atlantic deep waters across the

Middle Pleistocene transition. Quat. Res. 77, 182–191. http://dx.doi.org/10.1016/j.yqres.2011.09.010.
Marret, 1993. Les effets de l'acétolyse sur les assemblages de kystes de dinoflagellés. Palynosciences 2, 267–272.
Marret, F., Zonneveld, K.A.F., 2003. Atlas of modern organic-walled dinoflagellate cyst distribution. Rev. Palaeobot. Palynol. 125, 1–200.
Martrat, B., Grimalt, J.O., Shackleton, N.J., de Abreu, L., Hutterli, M.A., Stocker, T.F., 2007. Four climate cycles of recurring deep and surface water destabilizations on the Iberian margin. Science 317, 502–507. http://dx.doi.org/10.1126/science.1139994.
Mauritzen, C., Morel, Y., Paillet, J., 2001. On the influence of Mediterranean water on the central waters of the North Atlantic Ocean. Deep-Sea Res. I Oceanogr. Res. Pap. 48, 347–381.
McGregor, H.V., Dima, M., Fischer, H.W., Mulitza, S., 2007. Rapid 20th-Century Increase in Coastal Upwelling off Northwest Africa. Science 315, 637–639. http://dx.doi.org/10.1126/science.1134839.
Mertens, K.N., Takano, Y., Head, M.J., Matsuoka, K., 2014. Living fossils in the Indo-Pacific warm pool: a refuge for thermophilic dinoflagellates during glaciations. Geology 42, 531–534. http://dx.doi.org/10.1130/G35456.1.
Mertens, K.N., Verhoeven, K., Verleye, T., Louwye, S., Amorim, A., Ribeiro, S., Deaf, A.S., Harding, I., De Schepper, S., Kodrans-Nsiah, M., de Vernal, A., Radi, T., Dybkjaer, K., Poulsen, N.E., Feist-burkhardt, S., Chitolie, J., González Arango, C., Heilmann-Clausen, C., Londeix, L., Turon, J.-L., Marret, F., Matthiessen, J., McCarthy, F.M.G., Prasad, V., Pospelova, V., Kyffin Hughes, J.E., Riding, J.B., Rochon, A., Sangiorgi, F., Welters, N., Sinclair, N., Thun, C., Soliman, A., Van Nieuwenhove, N., Vink, A., Young, M., 2009. Determining the absolute abundance of dinoflagellate cysts in recent marine sediments: the *Lycopodium* marker-grain method put to the test. Rev. Palaeobot. Palynol. 157, 238–252.
Millennium Assessment Synthesis Reports, 2005. Chap 4. Ecosystems and human well–being: biodiversity synthesis. http://www.millenniumassessment.org/en/Synthesis.html.
Moorthi, S.D., Countway, P.D., Stauffer, B.A., Caron, D.A., 2006. Use of quantitative real-time PCR to investigate the dynamics of the red tide dinoflagellate *Lingulodinium polyedrum*. Microb. Ecol. 52, 136–150. http://dx.doi.org/10.1007/s00248-006-9030-3.
Morzadec-Kerfourn, M.-T., 1977. Les kystes de dinoflagellés dans les sédiments récents le long des côtes Bretonnes. Rev. Micropaléontol. 20, 157–166.
Morzadec-Kerfourn, M.-T., 1992. Estuarine Dinoflagellate cysts among oceanic assemblages of Pleistocene Deep-Sea sediments from the west African Margin and their paleoenvironmental significance. In: Head, M.J., Wrenn, J.H. (Eds.), Neogene and Quaternary Dinoflagellate Cyst of the North Atlantic Ocean and Adjacent Seas: Ecostratigraphy and Biostratigraphy. AASP Foundation, pp. 133–146.
Oliviera D., Desprat S., Rodrigues T., Naughton F., Hodell D., Trigo R., Abrantes F., Sánchez Goñi M.F., in preparation. Land-sea millennial and sub-millennial climate changes in southwestern Europe during MIS 11. 2015.
Pailler, D., Bard, E.U., 2002. High frequency palaeoceanographic changes during the past 140000 yr recorded by the organic matter in sediments of the Iberian Margin. Palaeogeogr. Palaeoclimatol. Palaeoecol. 181, 431–452. http://doi.pangaea.de/10.1594/PANGAEA.736599.
Peliz, Á., Dubert, J., Santos, A.M.P., Oliveira, P.B., Le Cann, B., 2005. Winter upper ocean circulation in the Western Iberian Basin—Fronts, eddies and poleward flows: an overview. Deep-Sea Res. I Oceanogr. Res. Pap. 52, 621–646. http://dx.doi.org/10.1016/j.dsr.2004.11.005.
Penaud, A., 2009. Interactions climatiques et hydrologiques du système Méditerranée/Atlantique au Quaternaire. Bordeaux 1.
Penaud, A., Eynaud, F., Sanchez Goni, M.F., Malaizé, B., Turon, J.L., Rossignol, L., 2011. Contrasting sea-surface responses between the western Mediterranean Sea and eastern subtropical latitudes of the North Atlantic during abrupt climatic events of MIS 3. Mar. Micropaleontol. 80, 1–17.
Penaud, A., Eynaud, F., Turon, J.L., Blamart, D., Rossignol, L., Marret, F., Lopez-Martinez, C., Grimalt, J.O., Malaizé, B., Charlier, K., 2010. Contrasting paleoceanographic conditions off Morocco during Heinrich events (1 and 2) and the last glacial maximum. Quat. Sci. Rev. 29, 1923–1939.
Penaud, A., Eynaud, F., Turon, J.L., Zaragosi, S., Marret, F., Bourillet, J.F., 2008. Interglacial variability (MIS 5 and MIS 7) and dinoflagellate cyst assemblages in the Bay of Biscay (North Atlantic). Mar. Micropaleontol. 68, 136–155.
Penaud, A., Eynaud F., Voelker A., Ganne, A., Hardy, W., Turon, J.L., submitted. Phytoplanktonic productivity over the last 50 ky BP in the subtropical NE Atlantic Ocean: complex forcing mechanisms mixing multi-scale processes.
Poirier, R.K., Billups, K., 2014. The intensification of northern component deepwater formation during the mid-Pleistocene climate transition: Mid-Pleistocene deep water circulation. Paleoceanography 29, 1046–1061. http://dx.doi.org/10.1002/2014PA002661.
Rattinacannou, J.-E., 2007. Paléoclimat et paléocirculation hydrologique à Gibraltar lors de la transition MIS 12-11; enregistrement des dinokystes et comparaison avec les transitions vers l'Eémien et vers l'Holocène (Master 2 Envolh report, Univ. Bordeaux 1).
Relvas, P., Barton, E.D., Dubert, J., Oliveira, P.B., Peliz, Á., da Silva, J.C.B., Santos, A.M.P., 2007. Physical oceanography of the western Iberia ecosystem: latest views and challenges. Prog. Oceanogr. 74, 149–173. http://dx.doi.org/10.1016/j.pocean.2007.04.021.
Richter, T.O., Van Der Gaast, S., Koster, B., Vaars, A., Gieles, R., de Stigter, H.C., de Haas, H., Van Weering, T.C.E., 2006. The Avaatech XRF Core Scanner: technical description and applications to NE Atlantic sediments. In: Rothwell, R.G. (Ed.), New Techniques in Sediment Core Analysis. Geological Society Special Publications, London, pp. 39–50.
Rochon, A., de Vernal, A., Turon, J.-L., Matthiessen, J., Head, M.J., 1999. Distribution of Dinoflagellate Cysts in Surface Sediments From the North Atlantic Ocean and Adjacent Basins and Quantitative Reconstruction of sea-Surface Parameters. AASP special pub.
Rogerson, M., Colmenero-Hidalgo, E., Levine, R.C., Rohling, E.J., Voelker, A.H.L., Bigg, G.R., Schönfeld, J., Cacho, I., Sierro, F.J., LÃwemark, L., Reguera, M.I., De Abreu, L., Garrick, K., 2010. Enhanced Mediterranean-Atlantic exchange during Atlantic freshening phases. Geochem. Geophys. Geosyst. 11.
Rohling, E.J., Pujol, C., Den Dulk, M., Vergnaud-Grazzini, C., 1995. Abrupt hydrographic change in the Alboran Sea (western Mediterranean) around 8000 yrs BP. Deep-Sea Res. I Oceanogr. Res. Pap. 42, 1609–1619.
Rouis-Zargouni, I., 2010. Evolution paléoclimatique et paléohydrologique de la Méditerranée Occidentale au cours des derniers 30 000 ans; contribution des dinokystes et des foraminifères planctoniques Ph.D. thesis Bordeaux I- Sfax Univ. 210 pp.
Sætre, M.M.L., Dale, B., Abdullah, M.I., Sætre, G.-P., 1997. Dinoflagellate cysts as potential indicators of industrial pollution in a Norwegian Fjord. Mar. Environ. Res. 44, 167–189.
Sànchez-Goñi, M.F., 2006. Interactions végétation-climat au cours des derniers 425.000 ans en Europe occidentale. Le message du pollen des archives marines. Quaternaire. Rev. Assoc. Fr. Etud. Q. 17, 3–25.
Sànchez-Goñi, M.F., Eynaud, F., Turon, J.L., Shackleton, N.J., 1999. High resolution palynological record off the Iberian margin: direct land-sea correlation for the last interglacial complex. Earth Planet. Sci. Lett. 171, 123–137.
Sànchez-Goñi, M.F., Landais, A., Fletcher, W.J., Naughton, F., Desprat, S., Duprat, J., 2008. Contrasting impacts of Dansgaard–Oeschger events over a western European latitudinal transect modulated by orbital parameters. Quat. Sci. Rev. 27, 1136–1151.
Sánchez Goñi, M.F., Llave, E., Oliveira, D., Naughton, F., Desprat, S., Ducassou, E., Hodell, D.A., Hernández-Molina, F.J., 2016. Climate changes in south western Iberia and Mediterranean Outflow variations during two contrasting cycles of the last 1Myrs: MIS 31–MIS 30 and MIS 12–MIS 11. Glob. Planet. Chang. 136, 18–29. http://dx.doi.org/10.1016/j.gloplacha.2015.11.006.
Sànchez-Goñi, M.F., Turon, J.-L., Eynaud, F., Gendreau, S., 2000. European climatic response to millennial-scale changes in the atmosphere–ocean system during the last glacial period. Quat. Res. 54, 394–403.
Shackleton, N.J., Chapman, M., Sanchez-Goni, M.F., Pailler, D., Lancelot, Y., 2000. The classic marine isotope substage 5e. Quat. Res. 58, 14–16.
Shackleton, N.J., Sanchez-Goni, M.F., Pailler, D., Lancelot, Y., 2003. Marine isotope substage 5e and the Eemian interglacial. Glob. Planet. Chang. 36, 151–155.
Shin, H.H., Mizushima, K., Oh, S.J., Park, J.S., Noh, I.H., Iwataki, M., Matsuoka, K., Yoon, Y.H., 2010. Reconstruction of historical nutrient levels in Korean and Japanese coastal areas based on dinoflagellate cyst assemblages. Mar. Pollut. Bull. 60, 1243–1258. http://dx.doi.org/10.1016/j.marpolbul.2010.03.019.
Siddall, M., Rohling, E.J., Almogi-Labin, A., Hemleben, C., Meischner, D., Schmelzer, I., Smeed, D.A., 2003. Sea-level fluctuations during the last glacial cycle. Nature 423, 853–858. http://dx.doi.org/10.1038/nature01690.
Sprangers, M., Dammers, N., Brinkhuis, H., van Weering, T.C., Lotter, A.F., 2004. Modern organic-walled dinoflagellate cyst distribution offshore NW Iberia; tracing the upwelling system. Rev. Palaeobot. Palynol. 128, 97–106. http://dx.doi.org/10.1016/S0034-6667(03)00114-3.
Stockmarr, J., 1971. Tablets with spores used in absolute pollen analysis. Pollen et Spores XIII 4, pp. 615–621.
Targarona, J., Warnaar, J., Boessenkool, K.P., Brinkhuis, H., Canals, M., 1999. Recent dinoflagellate cyst distribution in the North Canary Basin, NW Africa. Grana 38, 170–178. http://dx.doi.org/10.1080/00173139908559225.
Thomas, W.H., Gibson, C.H., 1990. Quantified small-scale turbulence inhibits a red tide dinoflagellate *Gonyaulax polyedra* Stein. Deep-Sea Res. 37, 1583–1593.
Thomas, W.H., Gibson, C.H., 1992. Effects of quantified small-scale turbulence on the dinoflagellate, *Gymnodinium sanguineum* (splendens): contrasts with *Gonyaulax* (*Lingulodinium*) *polyedra*, and the fishery implication. Deep-Sea Res. 39, 1429–1437.
Turon, J.-L., 1978. Les dinoflagellés témoins des paléoenvironnements durant l'Holocène dans l'Atlantique Nord Oriental. Signification paléohydrologique et paléoclimatique. C.R. Acad. Sci. Paris 286, 1861–1864.
Turon, J.-L., 1984. Le palynoplancton dans l'environnement actuel de l'Atlantique Nord-oriental. Evolution climatique et hydrologique depuis le dernier maximum glaciaire. Mémoires de l'Institut de Géologie du Bassin d'Aquitaine 17 (313 pp.).
Turon, J.-L., Londeix, L., 1988. Les asssemblages de kystes de dinoflagellés en méditerranée occidentale (Mer d'alboran) : mise en evidence de l'évolution des paléoenvironnement depuis le dernier maximum glaciaire. Bull. Centres Rech. Explor. Prod. Elf-Aquitaine 12, 313–344.
Turon, J.-L., Lezine, A.-M., Denefle, M., 2003. Land-sea correlations for the last glaciation inferred from a pollen and dinocyst record from the Portuguese margin. Quat. Res. 59, 88–96.
Voelker, A.H.L., de Abreu, L., 2011. A review of abrupt climate change events in the northeastern Atlantic ocean (Iberian Margin): latitudinal, longitudinal, and vertical gradients. In: Rashid, H., Polyak, L., Mosley-Thompson, E. (Eds.), Geophysical Monograph Series. American Geophysical Union, Washington, D. C., pp. 15–37.
Voelker, A.H.L., Lebreiro, S.M., SchÃ¶nfeld, J., Cacho, I., Erlenkeuser, H., Abrantes, F., 2006. Mediterranean outflow strengthening during northern hemisphere coolings: a salt source for the glacial Atlantic? Earth Planet. Sci. Lett. 245, 39–55.
Wall, D., Dale, B., 1966. Living fossils in western Atlantic plankton. Nature 211, 1025–1027. http://dx.doi.org/10.1038/2111025a0.
Williams, D.B., 1971. In: Funnel, B.M., Riedel, W.R. (Eds.), The distribution of marine dinoflagellates in relation to physical and chemical conditions. Cambridge University Press, pp. 91–95.
Willis, K.J., Bailey, R.M., Bhagwat, S.A., Birks, H.J.B., 2010. Biodiversity baselines, thresholds and resilience: testing predictions and assumptions using palaeoecological data. Trends Ecol. Evol. 25, 583–591. http://dx.doi.org/10.1016/j.tree.2010.07.006.
Zaragosi, S., Eynaud, F., Pujol, C., Auffret, G.A., Turon, J.L., Garlan, T., 2001. Initiation of the European deglaciation as recorded in the northwestern Bay of Biscay slope environments (Meriadzek Terrace and Trevelyan escarpment): a multi-proxy approach. Earth Planet. Sci. Lett. 188, 493–507.

Zippi, P.A., 1992. Dinoflagellate cyst stratigraphy and climate fluctuations in the eastern North Atlantic during the last 150,000 years. In: Head, M.J., Wrenn, J.H. (Eds.), Neogene and Quaternary Dinoflagellate Cyst of the North Atlantic Ocean and Adjacent Seas: Ecostratigraphy and Biostratigraphy, pp. 55–68.

Zonneveld, K.A.F., Versteegh, G.J.M., De Lange, G.J., 1997. Dinoflagellate cyst distribution in surface sediments from the Arabian Sea (northwestern Indian Ocean) in relation to temperature and salinity gradients in the upper water column. Deep-Sea Res. II Top. Stud. Oceanogr. 44, 1411–1443.

Zonneveld, K.A.F., Brummer, G.A., 2000. (Palaeo-)ecological significance, transport and preservation of organic-walled dinoflagellate cysts in the Somali Basin, NW Arabian Sea. Deep-Sea Res. II Top. Stud. Oceanogr. 47, 2229–2256.

Zonneveld, K.A.F., Chen, L., Elshanawany, R., Fischer, H.W., Hoins, M., Ibrahim, M.I., Pittauerova, D., Versteegh, G.J.M., 2012. The use of dinoflagellate cysts to separate human-induced from natural variability in the trophic state of the Po River discharge plume over the last two centuries. Mar. Pollut. Bull. 64, 114–132. http://dx.doi.org/10.1016/j.marpolbul.2011.10.012.

Zonneveld, K.A.F., Marret, F., Versteegh, G.J.M., Bogus, K., Bonnet, S., Bouimetarhan, I., Crouch, E., de Vernal, A., Elshanawany, R., Edwards, L., Esper, O., Forke, S., Grøsfjeld, K., Henry, M., Holzwarth, U., Kielt, J.F., Kim, S.Y., Ladouceur, S., Ledu, D., Chen, L., Limoges, A., Londeix, L., Lu, S.H., Mahmoud, M.S., Marino, G., Matsouka, K., Matthiessen, J., Mildenhal, D.C., Mudie, P., Neil, H.L., Pospelova, V., Qi, Y., Radi, T., Richerol, T., Rochon, A., Sangiorgi, F., Solignac, S., Turon, J.L., Verleye, T., Wang, Y., Wang, Z., Young, M., 2013. Atlas of modern dinoflagellate cyst distribution based on 2405 datapoints. Rev. Palaeobot. Palynol. 191, 1–197. http://dx.doi.org/10.1016/j.revpalbo.2012.08.003.

L'étude du pollen des séquences sédimentaires marines pour la compréhension du climat : l'exemple des périodes chaudes passées

---

Pollen in marine sedimentary archives, a key for climate studies: the example of past warm periods.

S. Desprat[1,2], D. Oliveira[1,2] , F. Naughton[3,4] et M.F. Sánchez Goñi[1,2]

1. EPHE, PSL Research University

2. EPOC UMR 5805, Université de Bordeaux, Allée Geoffroy St Hilaire, 33615 Pessac

3. Divisão de Geologia e Georecursos Marinhos, Instituto Português do Mar e da Atmosfera (IPMA), Avenida de Brasília 6, 1449-006 Lisboa, Portugal

4. CCMAR, Centro de Ciências do Mar, Universidade do Algarve, Campus de Gambelas, 8005-139 Faro, Portugal

Adresse électronique : stephanie.desprat@u-bordeaux.fr

RESUME

Les interglaciaires des derniers 800 000 ans sont tous des périodes chaudes comme celle dans laquelle nous vivons, l'Holocène, mais présentent une diversité marquée en termes d'intensité, de durée, de variabilité et d'expression régionale ainsi que de forçages (astronomique et gaz à effet de serre). Dans ce travail, nous nous attachons à examiner la réponse régionale de la végétation et du climat dans le sud-ouest de l'Europe lors des interglaciaires passés. Pour cela, nous faisons une synthèse des études récentes basées sur l'analyse du pollen préservé dans les sédiments marins de la marge ibérique permettant de comparer directement les processus atmosphériques et océaniques. Ce travail met en évidence la diversité des interglaciaires des derniers 400 000 ans dans le sud-ouest de l'Europe en termes de durée mais aussi de végétation et de climat, en particulier dans le sud-ouest de la péninsule Ibérique où les changements de précipitation jouent un rôle important. Il permet aussi de discuter des mécanismes jouant un rôle potentiel dans les entrées en glaciation lors de périodes caractérisées par un forçage astronomique semblable à notre interglaciaire (Marine Isotopic Stages 19c et 11c).

ABSTRACT

The interglacials of the last 800,000 years are all warm periods comparable to the current interglacial, called the Holocene. However, their intensity, duration, variability and regional expression are different as the result of different astronomical and greenhouse gases forcing. The work presented here focuses on the regional expression of these interglacials in southwestern Europe, and it is based on recent studies using pollen from Iberian margin sedimentary sequences that enables a direct comparison of atmospheric and marine processes. This work highlights the diversity of these interglacials in southwestern Europe in terms of duration as well as vegetation and climatic variability, in particular in southwestern Iberia where changes in precipitation play an important role. This work additionally allows discussing mechanisms involved in glacial inception during orbital analogs of the current interglacial (i.e. Marine Isotopic Stages 19c and 11c).

1- INTRODUCTION

Les archives géologiques montrent qu'au cours des derniers 2.5 millions d'années, la Terre a connu de grands changements environnementaux se traduisant par des oscillations entre périodes glaciaires et interglaciaires forcées à l'origine par les variations de l'insolation (Hays *et al.*, 1976; Shackleton & Opdyke, 1973). Pendant les périodes glaciaires, les calottes de glace couvraient les deux tiers de l'hémisphère nord avec pour corollaire un niveau marin bas alors que pendant les périodes interglaciaires, elles étaient très restreintes, la glace se retrouvant confinée au Groenland et le niveau marin étant élevé. Ces changements de volume de glace sont identifiés dans les séquences sédimentaires marines par les mesures du rapport isotopique de l'oxygène contenu dans les carbonates des foraminifères benthiques ($\delta^{18}O_b$), constituant la base de la stratigraphie isotopique marine. Des valeurs légères définissent les périodes interglaciaires *sensu lato* (*s.l.*) ou stades isotopiques marins (MIS = *Marine Isotope Stages*) avec des chiffres impairs tandis que des valeurs lourdes marquent les périodes glaciaires, correspondant à des MIS pairs. A l'intérieur des périodes interglaciaires, une alternance de périodes chaudes, nommées « e », « c » et « a », et plus froides, « d » et « b », est observée, résultant aussi du forçage orbital. La période interglaciaire *sensu stricto* (*s.s.*) correspond au sous-stade comportant le plus fort minimum de volume de glace qui se retrouve souvent être le minimum suivant la déglaciation.

Surimposée à cette variabilité orbitale, des changements climatiques abrupts ayant une périodicité millénaire ont ponctué les derniers 800 000 ans. Ces changements sont globaux et se reflètent notamment dans les températures des eaux de surface de l'Atlantique Nord (Martrat *et al.*, 2007) et dans les températures atmosphériques du Groenland (Barker *et al.*, 2011; NGRIP members, 2004) et de l'Antarctique (EPICA community members, 2004). Ils se produisent indépendamment de l'état de base du système climatique, c'est-à-dire en période glaciaire et interglaciaire. Ces changements sont généralement associés à des variations du volume de glace (Siddall *et al.*, 2003), de la concentration des gaz à effet de serre (Knutti *et al.*, 2004; Loulergue *et al.*, 2008) et de la circulation thermohaline (Lynch-Stieglitz, 2017; Oppo *et al.*, 2006). Néanmoins, leur amplitude est plus

importante lorsque les calottes de glace ont atteint une taille critique (McManus *et al.*, 1999). Les oscillations étant relativement ténues pendant les périodes interglaciaires, la variabilité millénaire intra-interglaciaire reste peu documentée lorsqu'on s'intéresse aux périodes chaudes antérieures à l'Holocène. Néanmoins, les récents enregistrements haute résolution révèlent qu'en Europe, en Atlantique Nord et en Antarctique des oscillations millénaires ponctuent les périodes chaudes du dernier million d'années (Billups *et al.*, 2011; Ferretti *et al.*, 2010; Ferretti *et al.*, 2015; Koutsodendris *et al.*, 2012; Pol *et al.*, 2011; Pol *et al.*, 2014).

Nous savons actuellement que les interglaciaires du dernier million d'années qui sont tous des périodes chaudes comme celle dans laquelle nous vivons, sont néanmoins très variables en terme d'intensité, de durée, de variabilité millénaire et de forçage (Past Interglacials Working Group of Pages, 2016; Tzedakis *et al.*, 2009). Certains interglaciaires se démarquent par un fort réchauffement, en particulier aux hautes latitudes; c'est le cas du MIS 11c (~400 000 ans avant le présent), du MIS 9e (~300 000 ans) et du MIS 5e (~125 000 ans) (Barker *et al.*, 2011; Masson-Delmotte *et al.*, 2010; Past Interglacials Working Group of Pages, 2016). Des enregistrements localisés dans les hautes latitudes de l'hémisphère nord montrent même que le MIS 11 est un « super-interglaciaire » c'est-à-dire un interglaciaire particulièrement chaud, se révélant être le plus chaud du dernier million d'années (de Vernal & Hillaire-Marcel, 2008; Melles *et al.*, 2012). Durant ce stade, les calottes de glace du Groenland et de l'Antarctique Ouest ont subi une fonte quasi-totale (Raymo & Mitrovica, 2012; Reyes *et al.*, 2014) entraînant un niveau marin de 6 à 13 m plus élevé qu'à l'actuel (Dutton *et al.*, 2015). Le réchauffement des MIS 5e et 9e est aussi associé à une forte régression de la calotte de glace du Groenland bien que moins importante que pendant le MIS 11 (Hatfield *et al.*, 2016). Le niveau marin de l'interglaciaire du MIS 5e était lui aussi particulièrement élevé, 6 à 9 m au-dessus de l'actuel (Dutton *et al.*, 2015). Bien que le forçage orbital (insolation) soit à l'origine des cycles glaciaires-interglaciaires en dictant notamment le « timing » des déglaciations, il ne peut expliquer à lui seul la variabilité de l'intensité des interglaciaires. Par exemple, l'insolation d'été aux hautes latitudes nord présente un fort maximum pendant les MIS 9e et MIS 5e mais un maximum de faible intensité

pendant le MIS 11c. Les modèles paléoclimatiques peuvent être utilisés pour examiner les facteurs forçant le climat des interglaciaires passés. Les simulations de températures de Yin & Berger (2012; 2015), faisant partie des rares travaux qui ont tenté l'exercice de simuler le climat des interglaciaires des derniers 800 000 ans, montrent que le fort réchauffement des MIS 9e et 5e aux hautes latitudes serait le résultat du forçage combiné de l'insolation et des gaz à effet de serre (GES) qui sont tous deux particulièrement importants au cours de ces stades alors que pendant le MIS11, les GES seraient le forçage dominant. En effet, pendant ces interglaciaires, les concentrations de CO_2 dans l'atmosphère étaient particulièrement élevées avec les valeurs les plus fortes des derniers 800 000 ans pendant le MIS 9e (Bereiter *et al.*, 2015; Petit, 1999; Siegenthaler *et al.*, 2005). Néanmoins, les simulations de modèles réalisées par Yin & Berger (2012) ne reproduisent pas les conditions particulières du MIS 11c révélées par les enregistrements des hautes latitudes de l'hémisphère nord.

Les compilations de données (Lang & Wolff, 2011; Past Interglacials Working Group of Pages, 2016) ainsi que les simulations de Yin & Berger (2012, 2015) montrent également une forte variabilité régionale de l'intensité des périodes interglaciaires des derniers 800 000 ans. Par exemple, contrairement aux hautes latitudes, les températures dans le sud de l'Europe apparaissent dans les simulations équivalentes pour tous les interglaciaires. Néanmoins, ceci doit encore être confirmé par les données. Par ailleurs, l'intensité d'un interglaciaire et son expression régionale sont très souvent évaluées en terme de température en portant peu d'intérêt aux précipitations. Or certaines régions apparaissent aujourd'hui très sensibles au réchauffement climatique du point de vue de la disponibilité en eau, c'est le cas de la région méditerranéenne. Pour déterminer l'expression régionale des interglaciaires dans le sud-ouest de l'Europe, il apparaît donc essentiel d'évaluer les changements de précipitations.

Quant à la durée des interglaciaires des derniers 800 000 ans, elle est généralement comprise entre 10 000 et 30 000 ans (Past Interglacials Working Group of Pages, 2016). Cette durée est implicitement liée aux déglaciations et entrées en glaciations et donc aux mécanismes qui déclenchent ces deux périodes de transition. Si le forçage orbital prescrit grossièrement le « timing »

des entrées en glaciation, il ne peut expliquer précisément le déclenchement des entrées en glaciation et donc la durée des périodes chaudes. Certains travaux proposent que la variabilité millénaire a pu jouer un rôle dans les entrées en glaciation (Past Interglacials Working Group of Pages, 2016). Les oscillations millénaires sont souvent imputées au forçage des « hautes latitudes » c'est à dire à la dynamique de la glace associées aux changements de circulation océanique (AMOC, Atlantic Meridional Overturning Circulation). Néanmoins, certains travaux proposent une origine tropicale en démontrant que ces oscillations présentent une cyclicité correspondant aux harmoniques de la précession qui se retrouve seulement dans l'insolation équatoriale (Berger *et al.*, 2006; Billups *et al.*, 2011; Ferretti *et al.*, 2010).

Les mécanismes contrôlant l'intensité, la durée, la variabilité et l'expression régionale des interglaciaires restent à ce jour mal connus. Déterminer ces mécanismes apparaît pourtant essentiel pour comprendre l'évolution naturelle de notre interglaciaire qui a commencé il y a 11 700 ans. Dans ce travail, nous nous intéressons aux questions suivantes : quelle est l'intensité des interglaciaires passés dans le sud-ouest de l'Europe et qu'en est-il des changements de précipitations en particulier dans la région méditerranéenne ? La variabilité millénaire intra-interglaciaire est-elle détectée dans les enregistrements de cette région et si oui, comment se caractérise-t-elle en termes d'amplitude et de cyclicité? Quels sont les mécanismes déterminant la durée des interglaciaires, c'est-à-dire, forçant les entrées en glaciation ? Pour répondre à ces questions, nous présentons une synthèse des études récentes portant sur les changements de la végétation et du climat dans le sud-ouest de l'Europe pendant les interglaciaires passés reconstitués à partir du pollen de carottes de la marge ibérique (Figure 1). L'analyse du pollen préservé dans les sédiments marins couplée à celle de traceurs paléoclimatiques marins est une approche originale qui permet d'évaluer la réponse des différentes composantes du système climatique (atmosphère/végétation, océan) à un changement climatique donné. Nous nous focalisons sur l'expression régionale des interglaciaires des derniers 425 000 ans. Finalement nous discutons des interactions océaniques et atmosphériques forçant les entrées en glaciation en nous intéressant tout particulièrement aux interglaciaires des MIS 11 (vers 425 000 ans)

et MIS 19 (vers 800 000 ans) qui sont les meilleurs analogues à l'interglaciaire actuel d'un point de vue des paramètres astronomiques.

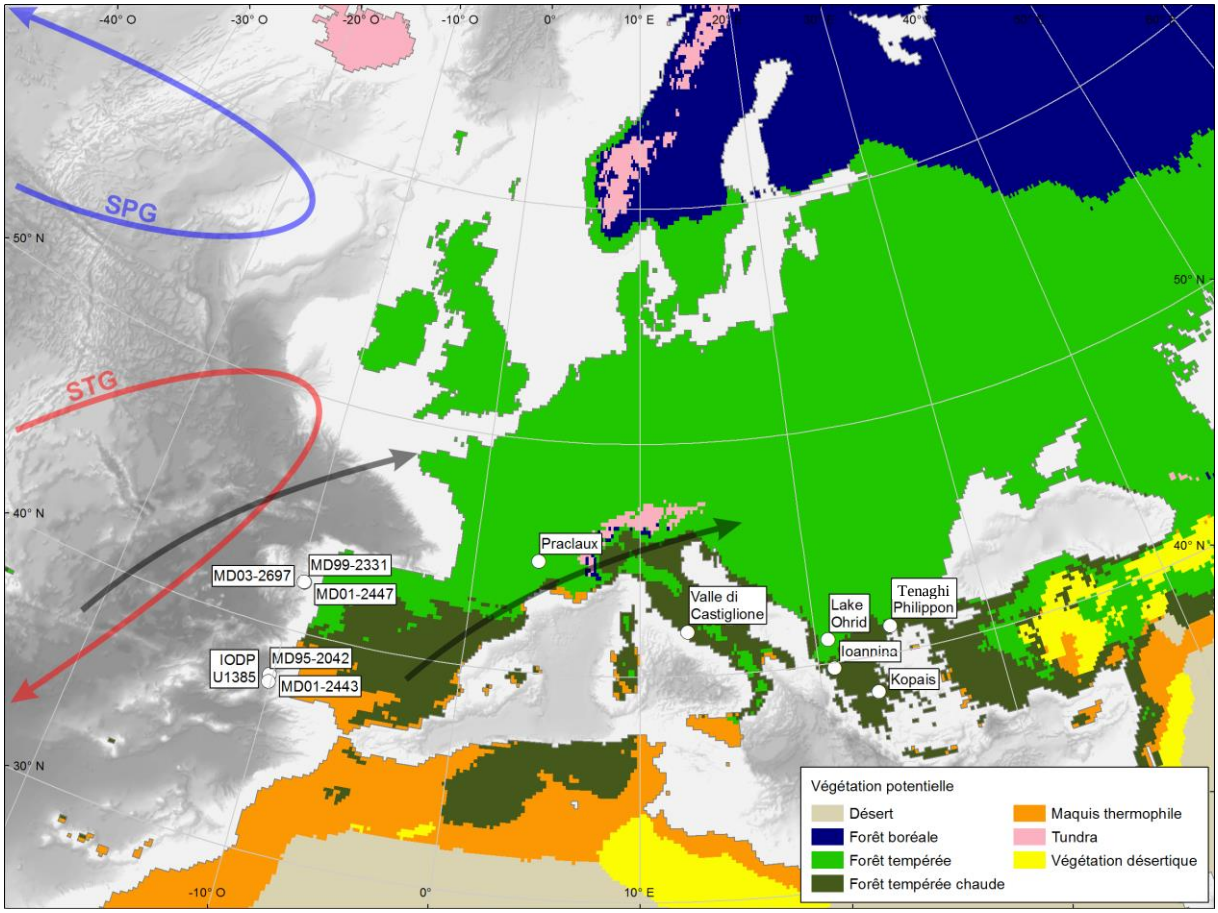

Figure 1 – Localisation des carottes marines étudiées ainsi que des séquences terrestres discutées dans le texte. La distribution de la végétation en Europe (Levavasseur *et al.*, 2012), le système atmosphérique (flèches grises : vents d'ouest, i.e. les vents dominants) et les principaux courants océanographiques (flèche rouge : gyre subtropicale nommée STG) affectant la marge et la péninsule Ibérique sont également présentés (cf. figure couleur en ligne pour plus de détails).

Figure 1 – Location of the studied marine cores and of the terrestrial sequences mentioned in the text. Vegetation distribution in Europe (Levavasseur et al., 2012), atmospheric system (grey arrows: Westerlies, i.e. prevailing winds) and main oceanic currents (red arrow: subtropical gyre named here STG) influencing the Iberian margin are also presented. See online version for color details.

2- COMMENT ETUDIER LES VARIATIONS CLIMATIQUES ?

Les variations du climat résultent de l'influence de forçages climatiques externes, en particulier le forçage astronomique/orbital (insolation) qui est lié à la position de la Terre par rapport au Soleil et à la constante solaire, sur les différentes composantes du système climatique que sont l'atmosphère, l'hydrosphère, notamment les océans, la cryosphère, en particulier les calottes de glace polaires, la lithosphère et la biosphère. Ces différents réservoirs agissent à leur tour sur le climat au travers de rétroactions négatives ou positives qui, respectivement, atténuent ou amplifient le signal climatique. Un changement climatique se caractérise notamment par une fréquence, une durée et une amplitude qui résultent du forçage astronomique auquel s'ajoutent divers forçages internes liés aux différents réservoirs (AMOC, mécanique interne de la glace, végétation, éruptions volcaniques, concentrations du CO_2, albédo, etc.). Les enregistrements paléoclimatiques marins, de glace et continentaux permettent de reconstituer son impact sur ces cinq réservoirs dans le passé. Toutefois pour comprendre ces trois caractéristiques et les mécanismes associés au changement climatique naturel, il est nécessaire de comparer les changements enregistrés dans les séquences terrestres avec les archives marines mais leur corrélation est difficile en raison du manque de précision des différents cadres chronologiques. En effet, ces séquences dispersées géographiquement, ont des modèles d'âge différents, certains basés sur des datations radiométriques (^{14}C, U/Th…), d'autres sur des datations relatives (stratigraphie isotopique, calage orbital…), comportant tous des incertitudes chronologiques pouvant aller de quelques décennies à plusieurs milliers d'années. Une façon de contourner ce problème est de travailler sur des carottes marines à sédimentation continue et non perturbée, riches en pollen et spores, qui nous renseignent sur l'histoire de la végétation et par conséquent, sur le climat du proche continent. Ces carottes renferment par ailleurs des indicateurs paléoclimatiques marins permettant d'estimer la température et la salinité des eaux de surface (foraminifères planctoniques, kystes de dinoflagellés, alcénones, coccolithes, diatomées, etc.), les caractéristiques des eaux du fond (Mg/Ca des ostracodes ou des foraminifères benthiques, $\delta^{13}C$, etc.), la dynamique des icebergs et l'instabilité des calottes polaires (IRD, « Ice Rafted Debris » qui sont des éléments

grossiers apportés par les icebergs) et le volume de glace stocké aux pôles ($\delta^{18}O$ des foraminifères benthiques ; il est toutefois à noter que d'autres facteurs comme la température des eaux de fond et la salinité influencent ce rapport isotopique et donc biaisent la relation avec le volume de glace dans ces enregistrements). La comparaison directe de ces différents types d'enregistrements paléoclimatiques dans une même archive permet d'une part d'identifier les changements climatiques qui ont affecté le continent/l'atmosphère et de les comparer directement avec la réponse d'autres composantes du système climatique comme l'océan. Ceci permet aussi de documenter d'éventuels déphasages dans la réponse de ces réservoirs à un même changement climatique et enfin de discuter de la fréquence et de la nature de ces changements. Une comparaison entre données et sorties de modèles paléoclimatiques permet en plus de tester la validité de ces dernières et donc, le réalisme des mécanismes impliqués dans les différents modèles pour reproduire le changement climatique.

3- LES ARCHIVES POLLINIQUES MARINES

Depuis une cinquantaine d'années, plusieurs campagnes océanographiques réalisées dans le cadre de programmes internationaux tels que IMAGES ou ODP/IODP (International Ocean Drilling Program), ont permis de collecter des carottes marines sur la marge européenne dont les sédiments sont riches en pollen. Le pollen produit par la végétation du proche continent arrive à l'océan par les vents et les fleuves. Il est alors ingéré par les organismes planctoniques et par ce biais intégré dans des pelotes fécales, ou bien aggloméré avec les argiles (Mudie & McCarthy, 2006). Grâce à ces processus, la flottabilité du pollen diminue et il est peu influencé par les courants océaniques. Il devient donc partie intégrante de la neige marine et traverse la colonne d'eau avec une vitesse de sédimentation relativement importante (estimée à ~100 m/jour dans la colonne d'eau atlantique) avant de se déposer au fond des océans (Hooghiemstra *et al.*, 1992). Des études portant sur la pluie pollinique récente en domaine marin que ce soit sur la marge ibérique (Naughton *et al.*, 2007; Turon, 1984b) mais aussi dans le Golfe de Gascogne (Turon, 1984a), en Méditerranée (Koreneva, 1971), sur

la marge africaine (Dupont & Wyputta, 2003; Hooghiemstra *et al.*, 1986), ou sur les marges ouest et est de l'Amérique du Nord et dans le golfe du Mexique (Heusser, 1985; Heusser & Balsam, 1977; Heusser & Van de Geer, 1994) montrent que le pollen des sédiments océaniques reflète une image intégrée de la végétation régionale du proche continent et, par conséquent, les paramètres climatiques sous lesquels cette végétation s'est développée. En particulier, Naughton et al. (2007) démontrent par la comparaison de spectres polliniques actuels de l'océan profond, d'estuaires et d'échantillons de surface continentaux que le signal pollinique de la marge ibérique représente de façon fiable la végétation du proche continent. En effet, les spectres polliniques du nord de la marge reflètent la forêt tempérée, dite atlantique, se développant dans le nord-ouest de la péninsule Ibérique, et plus particulièrement la chênaie caducifoliée, alors que ceux du sud de la marge discriminent la forêt méditerranéenne, e.g. la forêt tempérée chaude et le maquis thermophile, caractéristique de la partie méridionale de la péninsule (Figure 1). Cette représentation fiable est liée à l'origine fluviatile prédominante de l'apport pollinique. En effet, dans cette zone, l'apport fluviatile est favorisé car les vents dominants sont du nord-ouest et les bassins hydrographiques des rivières de la péninsule Ibérique sont importants, ce qui favorise le transport fluviatile (Dupont & Wyputta, 2003; Naughton *et al.*, 2007).

4- LA DIVERSITE DES INTERGLACIAIRES DES DERNIERS 425 000 ANS DANS LE SUD-OUEST DE L'EUROPE

La séquence du sud-ouest de la marge ibérique est un enregistrement sédimentaire composite de trois sites jumeaux (MD95-2042, MD01-2443 et IODP U1385), localisés vers 37°N (Figures 1 & 2; Chabaud *et al.*, 2014; Oliveira *et al.*, 2016; Sánchez Goñi *et al.*, 1999; Sánchez Goñi *et al.*, 2016; Tzedakis *et al.*, 2004; données non publiées). Le pollen de ce site provient de la végétation du sud-ouest de la péninsule Ibérique, dominée par la forêt méditerranéenne. Cette région est influencée par un climat méditerranéen qui se distingue par des étés chauds et secs et des hivers doux et humides (Figure 1).

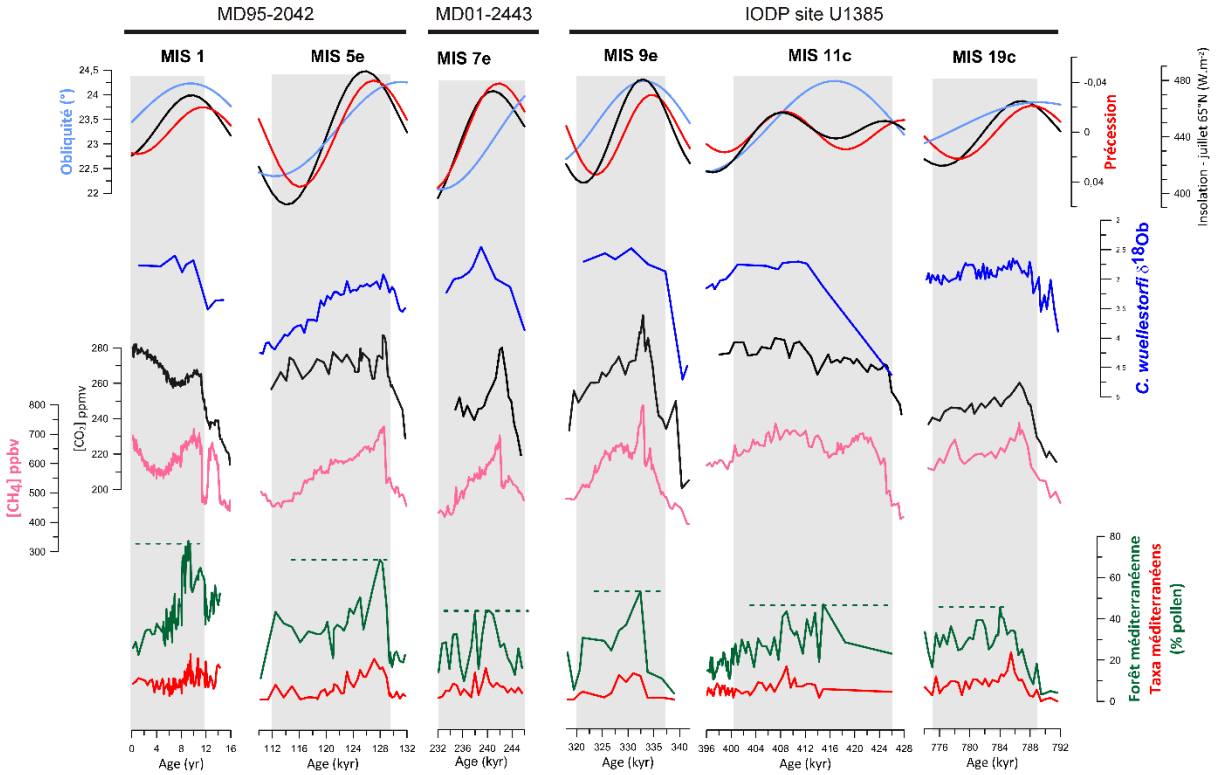

Figure 2 – Enregistrements pollinique et isotopique ($\delta^{18}O_b$) du sud-ouest de la marge ibérique (Chabaud *et al.*, 2014; Hodell *et al.*, 2015; Oliveira *et al.*, 2016; Sánchez Goñi *et al.*, 1999; Sánchez Goñi *et al.*, 2016; Tzedakis *et al.*, 2004; données non publiées). La forêt méditerranéenne est composée principalement de chênes caducifoliés et de taxons méditerranéens (chêne sclérophylle, olivier, filaire, pistachier et ciste). Les données polliniques sont comparées aux concentrations des gaz à effet de serre CO_2 et CH_4 (Loulergue *et al.*, 2008; Lüthi *et al.*, 2008; Siegenthaler *et al.*, 2005; Spahni *et al.*, 2005) et au forçage astronomique (Berger, 1978).

Figure 2 – Pollen and isotopic ($\delta^{18}O_b$) records from the southwestern Iberian margin (Chabaud et al., 2014; Hodell et al., 2015; Oliveira et al., 2016; Sánchez Goñi et al., 1999; Sánchez Goñi et al., 2016; Tzedakis et al., 2004; unpublished data). The Mediterranean forest is mainly composed of deciduous oaks and Mediterranean plants such as evergreen oaks, olive trees, phillyreas, pistachios and rockroses. Pollen data are compared to CO_2 and CH_4 records from ice cores (Loulergue et al., 2008; Lüthi et al., 2008; Siegenthaler et al., 2005; Spahni et al., 2005) and astronomical forcing (Berger, 1978).

Quant à l'enregistrement du nord-ouest de la marge ibérique, c'est un composite issu de trois carottes (MD99-2331, MD01-2447 et MD03-2697) prélevées à 42°N permettant de retracer les changements de végétation dans le nord-ouest de la péninsule Ibérique au cours des derniers 425 000 ans (Figure 1 & 3; Desprat *et al.*, 2009; Desprat *et al.*, 2007; Desprat *et al.*, 2006; Desprat *et al.*, 2005; Naughton *et al.*, 2007; Naughton *et al.*, 2009; Sánchez Goñi *et al.*, 2008; Sánchez Goñi *et al.*, 2005; données non publiées). La végétation caractéristique de cette région est la forêt atlantique (ou

forêt tempérée humide) se développant sous l'influence d'un climat atlantique, c'est-à-dire tempéré et humide avec une faible saisonnalité (Figure 1). En hiver, ces deux régions sont influencées par les vents d'ouest qui amènent les précipitations. Par contre, en été la région méditerranéenne est influencée par le système tropical au travers de la branche descendante de la cellule de Hadley et des anticyclones subtropicaux associés qui produisent la sécheresse estivale alors que le nord-ouest de la péninsule reste sous l'influence des vents d'ouest.

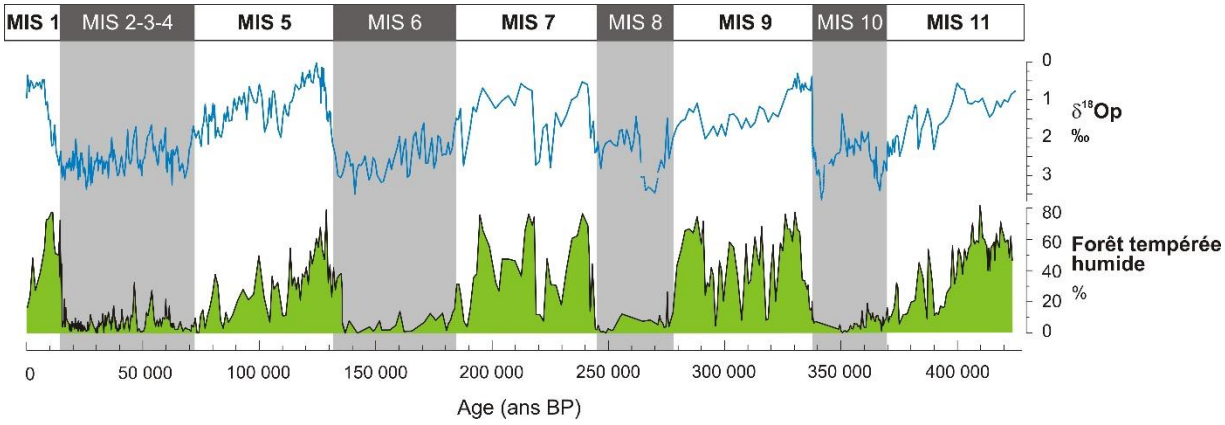

Figure 3 - Enregistrements pollinique et isotopique ($\delta^{18}O_p$) du nord-ouest de la marge ibérique (Desprat *et al.*, 2009; Desprat *et al.*, 2007; Desprat *et al.*, 2006; Desprat *et al.*, 2005; Naughton *et al.*, 2007; Naughton *et al.*, 2009; Sánchez Goñi *et al.*, 2008; Sánchez Goñi *et al.*, 2005; données non publiées). La forêt atlantique est composée principalement de chênes caducifoliés, de charmes, de noisetiers et de hêtres. Les MIS impairs caractéristiques des périodes avec un faible volume de glace/haut niveau marin correspondent aux bandes blanches. Les données de $\delta^{18}O$ des foraminifères planctoniques (*Globigerina bulloides* principalement et *Neogloboquadrina pachyderma* senestre en pointillé) représentent principalement les variations des températures des eaux de surface sur la marge ibérique.

Figure 3 - Pollen and isotopic ($\delta^{18}O_p$) records from the northwestern Iberian margin (Desprat et al., 2009; Desprat et al., 2007; Desprat et al., 2006; Desprat et al., 2005; Naughton et al., 2007; Naughton et al., 2009; Sánchez Goñi et al., 2008; Sánchez Goñi et al., 2005; unpublished data). The Atlantic forest is mainly composed of deciduous oaks, hazels, hornbeams and beeches. $\delta^{18}O$ data of planktonic foraminifera, Globigerina bulloides mainly (bold line) and Neogloboquadrina pachyderma left coiling (dashed line), mainly represent sea surface temperature variations on the Iberian margin.

Les deux enregistrements montrent que les stades isotopiques interglaciaires sont marqués par l'augmentation du pollen d'arbres, caractérisant la forêt tempérée humide dans le nord et la forêt méditerranéenne dans le sud, au détriment du pollen d'herbacées et plus particulièrement des plantes semi-désertiques. Ces changements de végétation indiquent un réchauffement et une

augmentation des précipitations (Figure 3). Néanmoins, chacun de ces stades comportent deux à trois phases majeures d'expansion de la forêt correspondant chacun à un minimum de volume de glace marquant les sous-stades isotopiques « a », « c » et « e » pour les MIS 5, 7 et 9 et « a » et « c » pour le MIS 11. Généralement, la première phase de développement de la forêt de chaque MIS correspond à l'interglaciaire *s.s.* (même si un doute subsiste pour le MIS 7) sachant qu'elle est contemporaine du minimum de volume de glace le plus important du stade. L'intensité de l'interglaciaire dans ces deux régions du sud de l'Europe peut être estimée grâce aux pourcentages de pollen d'arbres. Plus particulièrement, dans le sud de la péninsule, l'expansion de la forêt méditerranéenne qui comporte des éléments méditerranéens (chêne verts, oliviers, pistachiers…) à basse altitude et des éléments tempérés se développant sous des conditions plus humides au niveau des reliefs, indique l'installation d'un climat méditerranéen, saisonnier, caractérisé par des hivers doux et humides et des étés chauds et secs. Il faut noter que le développement de cette forêt est principalement limité par les précipitations hivernales, et donc que l'amplitude d'expansion de la forêt d'un interglaciaire traduira l'importance des précipitations. Dans le nord-ouest de la péninsule Ibérique, l'expansion de la forêt atlantique pendant les périodes chaudes est principalement limitée par les températures hivernales. Des différences d'expansion maximale d'un interglaciaire à l'autre reflèteront alors un réchauffement plus ou moins important dans le nord-ouest de la péninsule. Les enregistrements polliniques de la marge ibérique montrent que l'amplitude du développement de la forêt méditerranéenne est spécifique à chaque interglaciaire tandis que l'expansion de la forêt atlantique est similaire, les pourcentages de pollen d'arbres atteignant les 80%, pour les cinq interglaciaires des derniers 400 000 ans (Figures 2 & 3). Cela suggère des températures maximales interglaciaires équivalentes dans le nord-ouest de la péninsule Ibérique mais des précipitations différentes dans le sud, l'Holocène et le dernier interglaciaire, le MIS 5e, étant les plus humides, les MIS 9e, 11c et 19c étant moins humides et le MIS 7e le plus sec.

Il existe six séquences polliniques continentales longues dans le sud de l'Europe : Tenaghi Philippon, Ioanina et Kopais localisées en Grèce (Okuda *et al.*, 2001; Tzedakis, 1993; Tzedakis *et al.*,

1997; Tzedakis *et al.*, 2006), Praclaux dans le Massif Central (de Beaulieu *et al.*, 2001; Reille *et al.*, 2000), Lake Ohrid en Albanie (Sadori *et al.*, 2016), et Valle di Castiglione en Italie (Follieri *et al.*, 1988). Néanmoins, nous ne comparerons nos données ni avec la séquence Valle di Castiglione qui n'atteint que le MIS7, ni avec Kopais et Ioanina qui n'ont pas une résolution temporelle suffisante. Tenaghi Philippon et Praclaux montrent, comme la séquence de la marge nord-ouest ibérique, très peu de différences dans l'amplitude d'expansion de la forêt entre les interglaciaires des derniers 400 000 ans. Comme pour le nord-ouest de la péninsule Ibérique, la végétation dans le Massif central n'est pas limitée par les précipitations mais principalement par les températures. Quant au site de Tenaghi Philippon, bien que situé dans la région méditerranéenne, il se trouve à la limite nord-orientale de cette zone où les hivers sont plus froids et les étés moins secs (Saaroni *et al.*, 1996; Xoplaki *et al.*, 2003) ; la végétation se développant alentours est donc moins limitée par les précipitations. Les pourcentages de pollen arboréen de ces séquences terrestres étant très proches d'un stade à l'autre, cela confirme que les différences de températures dans le sud de l'Europe entre les interglaciaires des derniers 425 000 ans sont faibles, du moins pas assez importantes pour avoir des conséquences sur l'extension de la forêt. La séquence du lac Ohrid qui couvre les derniers 500 000 ans montre qu'en Albanie la forêt était plus ouverte indiquant un climat plus chaud et plus sec pendant l'Holocène et le dernier interglaciaire que pendant les interglaciaires plus anciens (Sadori *et al.*, 2016). Dans le sud-ouest de la péninsule Ibérique, les interglaciaires récents sont au contraire marqués par un couvert forestier plus important attestant de conditions hivernales plus humides. Il faut toutefois noter que le lac Ohrid est soumis à un climat continental (Popovska & Bonacci, 2007) avec des étés chauds et des hivers très froids et une sécheresse estivale moins marquée que celle typique du régime méditerranéen, régime qui caractérise le climat du sud-ouest de la péninsule ibérique; ceci pourrait expliquer des différences locales au sein même du sud de l'Europe.

La variabilité régionale des changements climatiques est particulièrement illustrée par la comparaison avec les changements observés aux hautes latitudes. Précédemment, nous avons mentionné que les interglaciaires MIS 5e, 9e et 11c apparaissent comme les périodes plus chaudes

aux hautes latitudes résultant d'un forçage orbital et/ou des GES importants (Figure 2; Yin & Berger, 2012; Yin & Berger, 2015). Par conséquent, nous pouvons dire que même si un interglaciaire est marqué par un réchauffement et une fonte des calottes de glace importants dans les hautes latitudes de l'hémisphère nord, il n'est pas forcément associé à une forte augmentation des températures dans le sud-ouest de l'Europe. Par contre, des différences notables de précipitations sont détectées d'un interglaciaire à l'autre mais pour autant aucune relation ne semble évidente entre réchauffement des hautes latitudes en relation avec de fortes concentrations de GES et augmentation de la sècheresse en région méditerranéenne contrairement à ce qu'indique les simulations du climat futur (Hoerling *et al.*, 2012). Les forçages responsables de la diversité des interglaciaires en terme d'intensité des précipitations dans la région méditerranéenne restent encore à définir. Un bon candidat serait un des paramètres orbitaux déterminant l'insolation, la précession, qui a une influence importante sur le climat des régions situées à des latitudes inférieures à 40°N (Ruddiman & McIntyre, 1984). La précession contrôle l'amplitude de la saisonnalité et donc la quantité de précipitations hivernales dans les régions subtropicales comme suggéré par des simulations récentes (Yin & Berger, 2012) et les observations (e.g. Oliveira *et al.*, 2016; Sánchez Goñi *et al.*, 2008).

5- LA DUREE ET LA VARIABILITE MILLENAIRE DES INTERGLACIAIRES ET LES MECANISMES FORÇANT LES ENTREES EN GLACIATION

La durée des phases forestières dans la péninsule Ibérique et en particulier de la première phase qui correspond à la période interglaciaire *s.s.* varie entre ~9 000 ans pour l'interglaciaire du MIS 7 et ~31 000 ans pour celui du MIS 11 alors que l'Holocène a commencé il y a 11 700 ans. Il est intéressant de noter que les interglaciaires des MIS 11 et 19 qui sont semblables à l'interglaciaire actuel d'un point de vue du forçage astronomique (Loutre & Berger, 2000) sont caractérisés par un couvert forestier persistant pendant des durées très différentes, 30 000 ans pour le MIS 11 et 12 300 ans pour le MIS 19 (interglaciaire Tajo, Figure 3), respectivement (Figure 2). Néanmoins, il est connu que même si le MIS11 est marqué par une insolation variant avec une amplitude similaire à notre

interglaciaire, il présente une caractéristique atypique. Il comporte en son milieu un minimum d'insolation, certes faible, qui n'a pas engendré d'entrée en glaciation, ne mettant donc pas fin à l'interglaciaire et générant un interglaciaire particulièrement long sur un cycle et demi de précession. Néanmoins, il reste un bon analogue pour examiner les mécanismes associés à l'entrée en glaciation qui a eu lieu avec la diminution d'insolation suivante. Nous allons maintenant nous focaliser sur la variabilité climatique des analogues orbitaux à notre interglaciaire, les MIS 11c et MIS 19c, et son rôle potentiel dans les entrées en glaciations.

L'analyse pollinique des MIS 11 et 19 du site U1385 montre qu'une succession d'épisodes d'expansion et de contraction de la forêt méditerranéenne a eu lieu tout au long de ces stades même pendant les périodes interglaciaires *s.s.*, MIS 11c et MIS 19c (Oliveira *et al.*, 2016; Sánchez Goñi *et al.*, 2016) (Figure 4a, MIS 19 pris comme exemple). Les expansions sont interprétées comme une augmentation des précipitations hivernales et donc des vents d'ouest avec une direction plus zonale influençant d'avantage le sud de la péninsule Ibérique. Une direction plus méridionale de ces vents d'ouest apporterait moins de précipitations dans cette région et expliquerait la diminution du couvert forestier.

Ces données polliniques peuvent être comparées avec les SST-alcénones et les pourcentages du biomarqueur $C_{37:4}$ du site U1385 indiquant les apports d'eau douce, ainsi qu'avec le contenu en IRD de sites situés plus au nord permettant de retracer les débâcles d'icebergs en Atlantique Nord. Nous constatons que seuls les événements les plus froids et secs sur le continent (plus fortes réductions de forêt) mais aussi les plus longs sont associés à une diminution des températures des eaux de surface et à des débâcles d'icebergs en Atlantique Nord (Figure 4, Oliveira *et al.*, 2016; Sánchez Goñi *et al.*, 2016). En effet, les épisodes de réduction de forêt au sein des MIS 19c et 11c ne sont pas associés à un refroidissement des eaux de surface sur la marge ibérique, ni à des décharges d'icebergs en Atlantique Nord (Figure 4b). Ceci confirme que des épisodes millénaires froids et secs peuvent avoir lieu quel que soit le volume de glace (Desprat *et al.*, 2009; Oppo *et al.*, 1998). Par contre, leur intensité et leur durée sont modulées par des mécanismes de rétroactions

positives sur l'AMOC associées à la dynamique de la glace et en particulier à l'apport d'eau douce issu du vêlage et dispersion des icebergs (Barker *et al.*, 2015; Oliveira *et al.*, 2016).

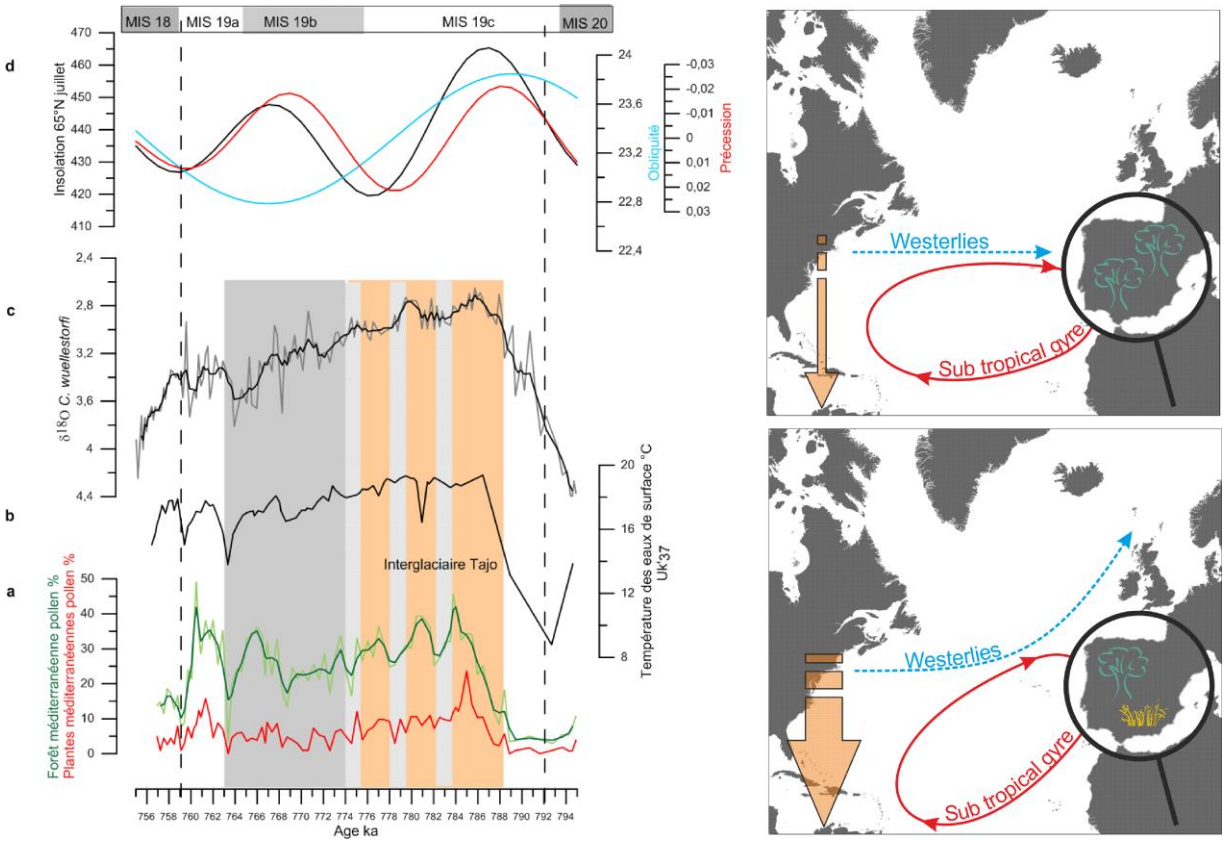

Figure 4 – La variabilité millénaire pendant les interglaciaires (*s.l.*) : I) Exemple : le MIS 19 dans sud-ouest de la marge ibérique d'après les enregistrements polliniques (a), SST-alcénones (b) et $\delta^{18}O$ benthique (c) du site IODP U1385 (Sánchez Goñi *et al.*, 2016) comparés au forçage astronomique (d) (Berger, 1978). II) Représentation schématique de la végétation dans la péninsule Ibérique, de la circulation atmosphérique et de la circulation océanique de surface ainsi que du gradient de température en Atlantique Nord (flèche orange) pendant les épisodes millénaires du MIS 19c et MIS 11c.

Figure 4 – Millennial-scale variability during interglacials (s.l.): I) Example: the southwestern Iberian margin records of MIS 19 : pollen (a), SST-alkenones (b), benthic $\delta^{18}O$ (c) from the IODP site U1385 (Sánchez Goñi et al., 2016) compared to astronomical forcing (Berger, 1978). II) Schematic representation of the vegetation in the Iberian Peninsula, atmospheric and surface ocean circulations and temperature gradient in the North Atlantic during millennial events of MIS 19c and MIS 11c.

Pendant les MIS 19c et 11c, l'enregistrement des SST de la marge ibérique indique que les eaux de la gyre subtropicale restent chaudes quelles que soient les conditions d'humidité sur le continent. La récurrence d'épisodes de sécheresse dans le sud-ouest de la péninsule Ibérique

impliquerait donc des augmentations périodiques d'arrivée d'air humide et chaud associé au courant ouest de la gyre subtropicale, aux hautes latitudes de l'Atlantique Nord (Figure 4). Dans la gyre subpolaire, nous observons également des températures qui restent chaudes au cours du MIS 19c ainsi que l'absence de décharges d'icebergs (Alonso-Garcia *et al.*, 2011). Le découplage répété entre une mer chaude et une atmosphère plus froide et sèche observé au niveau de la marge sud-ouest ibérique pendant les MIS 19c et 11c n'est donc pas associé à la dynamique des calottes polaires, et donc au climat des hautes latitudes.

Les données polliniques du MIS 19 ont fait l'objet d'une analyse spectrale qui révèle que la variabilité climatique millénaire de ce stade a une cyclicité de 5 000 ans. Cette cyclicité semble être associée aux changements d'insolation à l'équateur, en particulier au quatrième harmonique de la précession (Berger *et al.*, 2006) qui génère des périodes de surplus de chaleur dans les basses latitudes, avec par conséquent, un gradient des températures des eaux de surface plus important entre cette région et les pôles. Cette augmentation répétée du gradient thermique dirige les vents d'ouest vers le nord, augmentant la sécheresse dans la péninsule Ibérique et favorisant l'apport d'humidité dans les hautes latitudes. Cette humidité qui tombe sous forme de neige est nécessaire pour l'accumulation de glace aux hautes latitudes au moment où l'insolation d'été diminue graduellement, favorisant l'entrée en glaciation (Figure 4d). Les épisodes de découplage SST-forêt s'observent d'ailleurs en même temps qu'une augmentation des valeurs de $\delta^{18}O_b$ suggérant des augmentations de volume de glace (Figure 4c). La variabilité millénaire pendant le MIS 19c serait donc liée au forçage tropical et pourrait avoir joué un rôle prépondérant dans l'entrée en glaciation sous des conditions de forçage astronomique très semblable à notre interglaciaire. Néanmoins, l'analyse spectrale des données polliniques de l'Holocène (marge ibérique) montre que notre interglaciaire est caractérisé par une variabilité climatique ayant une cyclicité dominante de 2 500 ans et donc différente de celle du MIS 19c. Si la variabilité climatique millénaire est un facteur important dans les entrées en glaciation comme montré dans ce travail, le MIS 19c ne serait pas un bon analogue de l'interglaciaire actuel et leur durée ne serait donc pas nécessairement la même.

6- CONCLUSIONS

L'analyse du pollen préservé dans les sédiments marins de la marge ibérique permet de recueillir des informations uniques sur le climat des interglaciaires des cycles climatiques passés. Deux séquences longues prélevées sur la marge ibérique, la plus septentrionale couvrant les derniers 425 000 ans et la plus méridionale les derniers 800 000 ans, ont été étudiées afin d'évaluer l'intensité, la durée et la variabilité des interglaciaires passés dans le sud-ouest de l'Europe. Ces études montrent que les interglaciaires sont tous marqués par le développement d'une forêt atlantique au nord de la Péninsule et d'une forêt méditerranéenne au sud mais ils présentent effectivement une diversité importante et des caractéristiques différentes dans les deux régions. Nos données montrent que contrairement aux hautes latitudes où les différences de températures d'un interglaciaire à l'autre sont importantes, dans le nord de la péninsule Ibérique elles ne semblent pas significatives. Par contre, les différences d'intensité des interglaciaires sont très marquées dans le sud mais ici associées aux précipitations. Nous n'avons néanmoins pas observé de concordance entre températures très chaudes aux hautes latitudes et sècheresse accentuée en région méditerranéenne comme le suggèrent les simulations du climat futur. Notre approche de comparaison directe entre les traceurs atmosphériques (pollen) et marins a aussi permis de discuter des mécanismes jouant un rôle dans les entrées en glaciation, et en particulier du rôle de la variabilité millénaire, lors de périodes caractérisées par un forçage astronomique semblable à notre interglaciaire (MIS 19c et 11c). Effectivement, ces deux interglaciaires sont marqués par une forte variabilité millénaire traduisant le passage récurrent d'une configuration de vents d'ouest zonale à une configuration méridionale, amenant l'humidité nécessaire aux hautes latitudes pour l'accumulation de glace et donc favorisant les entrées en glaciation. Cette variabilité millénaire de la circulation atmosphérique ayant une cyclicité de 5000 ans (MIS 19c) serait liée au forçage tropical d'origine astronomique et non au forçage des hautes latitudes.

REMERCIEMENTS

Ce travail a été réalisé dans le cadre des projets LEFE-IMAGO *WarmClim* et *PuLSE* financés par l'INSU-CNRS et de projets PNEDC. La FCT (Agence de financement portugaise pour la science et la technologie) a contribué au financement de cette étude au travers du projet CLIMHOL (PTDC/AAC-CLI/10 0157/20 08), de la bourse doctorale de D. Oliveira (SFRH/BD/9079/2012), et de la bourse postdoctorale de F. Naughton (SFRH/BPD/108712/2015). Nous tenons à remercier l'IPEV (Institut Polaire Francais Paul Emile Victor) et IODP (Integrated Ocean Drilling Program) ainsi que l'équipe logistique à bord du R/V Marion Dufresne II et du Joides Resolution pour le prélèvement des carottes sédimentaires de la marge ibérique. Nous remercions également V. Hanquiez pour la réalisation d'illustrations et l'équipe technique (M.H. Castéra, L. Devaux et M. Georget) du laboratoire EPOC pour la préparation des échantillons.

RÉFÉRENCES

ALONSO-GARCIA M., SIERRO F.J., KUCERA M., FLORES J.A., CACHO I. & ANDERSEN N., 2011 - Ocean circulation, ice sheet growth and interhemispheric coupling of millennial climate variability during the mid-Pleistocene (ca 800-400ka). *Quaternary Science Reviews* **30** (23-24), 3234-3247.

BARKER S., KNORR G., EDWARDS R.L., PARRENIN F., PUTNAM A.E., SKINNER L.C., WOLFF E. & ZIEGLER M., 2011 - 800,000 Years of Abrupt Climate Variability. *Science*, **334** (6054), 347-351.

BARKER S., CHEN J., GONG X., JONKERS L., KNORR G. & THORNALLEY D., 2015 - Icebergs not the trigger for North Atlantic cold events. *Nature* **520** (7547), 333-336.

BEREITER B., EGGLESTON S., SCHMITT J., NEHRBASS-AHLES C., STOCKER T.F., FISCHER H., KIPFSTUHL S. & CHAPPELLAZ J., 2015 - Revision of the EPICA Dome C CO_2 record from 800 to 600 kyr before present. *Geophysical Research Letters* **42** (2), 542-549.

BERGER A., LOUTRE M.F. & MÉLICE J.L., 2006 - Equatorial insolation: From precession harmonics to eccentricity frequencies. *Climate of the Past Discussions*, **2** (4), 519-533.

BERGER A.L., 1978 - Long-Term Variations of Daily Insolation and Quaternary Climatic Changes. *Journal of the Atmospheric Sciences*, **35** (12), 2362-2367.

BILLUPS K., RABIDEAUX N. & STOFFEL J., 2011 - Suborbital-scale surface and deep water records in the subtropical North Atlantic: implications on thermohaline overturn. *Quaternary Science Reviews* **30** (21–22), 2976-2987.

CHABAUD L., SÁNCHEZ GOÑI M.F., DESPRAT S. & ROSSIGNOL L., 2014 - Land-sea climatic variability in the eastern North Atlantic subtropical region over the last 14,200 years: atmospheric and oceanic processes at different timescales. *The Holocene*, **24**, 787-797.

DE BEAULIEU J.-L., ANDRIEU-PONEL V., REILLE M., GRÜGER E., TZEDAKIS C. & SVOBODOVA H., 2001 - An attempt at correlation between the Velay pollen sequence and the Middle Pleistocene stratigraphy from central Europe. *Quaternary Science Reviews*, **20**, 1593-1602.

DE VERNAL A. & HILLAIRE-MARCEL C., 2008 - Natural variability of Greenland climate, vegetation, and ice volume during the past million years. *Science*, **320** (5883), 1622-1625.

DESPRAT S., SÁNCHEZ GOÑI M.F., TURON J.L., MCMANUS J.F., LOUTRE M.F., DUPRAT J., MALAIZÉ B., PEYRON O. & PEYPOUQUET J.P., 2005 - Is vegetation responsible for glacial inception during periods of muted insolation changes? *Quaternary Science Reviews* **24** (12-13), 1361-1374.

DESPRAT S., SÁNCHEZ GOÑI M.F., TURON J.L., DUPRAT J., MALAIZÉ B. & PEYPOUQUET J.P., 2006 - Climatic variability of Marine Isotope Stage 7: direct land-sea-ice correlation from a multiproxy analysis of a north-western Iberian margin deep-sea core. *Quaternary Science Reviews* **25** (9-10), 1010-1026.

DESPRAT S., SÁNCHEZ GOÑI M.F., NAUGHTON F., TURON J.L., DUPRAT J., MALAIZÉ B., CORTIJO E. & PEYPOUQUET J.P., 2007 - 25. Climate variability of the last five isotopic interglacials: Direct land-sea-ice correlation from the multiproxy analysis of North-Western Iberian margin deep-sea cores. *In*: Frank Sirocko, M.C.M.F.S.G., Thomas, L. (Eds.), *Developments in Quaternary Sciences*. Elsevier, **Volume 7**, 375-386.

DESPRAT S., SANCHEZ GOÑI M.F., MCMANUS J.F., DUPRAT J. & CORTIJO E., 2009 - Millennial-scale climatic variability between 340 000 and 270 000 years ago in SW Europe: Evidence from a NW Iberian margin pollen sequence. *Climate of the Past*, **5** (1), 53-72.

DUPONT L. & WYPUTTA U., 2003 - Reconstructing pathways of aeolian pollen transport to the marine sediments along the coastline of SW Africa. *Quaternary Science Reviews*, **22**, 157-174.

DUTTON A., CARLSON A.E., LONG A.J., MILNE G.A., CLARK P.U., DECONTO R., HORTON B.P., RAHMSTORF S. & RAYMO M.E., 2015 - Sea-level rise due to polar ice-sheet mass loss during past warm periods. *Science*, **349** (6244), aaa4019.

EPICA COMMUNITY MEMBERS, 2004 - Eight glacial cycles from an Antarctic ice core. *Nature*, **429**, 623-628.

FERRETTI P., CROWHURST S.J., HALL M.A. & CACHO I., 2010 - North Atlantic millennial-scale climate variability 910 to 790ka and the role of the equatorial insolation forcing. *Earth and Planetary Science Letters* **293** (1-2), 28-41.

FERRETTI P., CROWHURST S.J., NAAFS B.D.A. & BARBANTE C., 2015 - The Marine Isotope Stage 19 in the mid-latitude North Atlantic Ocean: astronomical signature and intra-interglacial variability. *Quaternary Science Reviews* **108**, 95-110.

FOLLIERI M., MAGRI D. & SADORI L., 1988 - 250.000-year pollen record from valle di Castiglione (Roma). *Pollen et Spores*, **30** (3/4), 329-356.

HATFIELD R.G., REYES A.V., STONER J.S., CARLSON A.E., BEARD B.L., WINSOR K. & WELKE B., 2016 - Interglacial responses of the southern Greenland ice sheet over the last 430,000 years determined using particle-size specific magnetic and isotopic tracers. *Earth and Planetary Science Letters* **454**, 225-236.

HAYS J.D., IMBRIE J. & SHACKLETON N.J., 1976 - Variations in the Earth's orbit: Pacemaker of ice ages. *Science*, **194**, 1121-1132.

HEUSSER L., 1985 - Quaternary palynology of marine sediments in the northeast Pacific, northwest Atlantic, and Gulf of Mexico. *Pollen records of Late-Quaternary North American sediments*. AASP Foundation, 385-403.

HEUSSER L.E. & BALSAM W.L., 1977 - Pollen distribution in the N.E. Pacific ocean. *Quaternary Research*, **7**, 45-62.

HEUSSER L.E. & VAN DE GEER G., 1994 - Direct correlation of terrestrial and marine paleoclimatic records from four glacial-interglacial cycles-DSDP site 594 Southwest Pacific. *Quaternary Science Reviews*, **13**, 273-282.

HODELL D., LOURENS L., CROWHURST S., KONIJNENDIJK T., TJALLINGII R., JIMÉNEZ-ESPEJO F., SKINNER L., TZEDAKIS P.C., ABRANTES F., ACTON G.D., ALVAREZ ZARIKIAN C.A., BAHR A., BALESTRA B., BARRANCO E.L., CARRARA G., DUCASSOU E., FLOOD R.D., FLORES J.-A., FUROTA S., GRIMALT J., GRUNERT P., HERNÁNDEZ-MOLINA J., KIM J.K., KRISSEK L.A., KURODA J., LI B., LOFI J., MARGARI V., MARTRAT B., MILLER M.D., NANAYAMA F., NISHIDA N., RICHTER C., RODRIGUES T., RODRÍGUEZ-TOVAR F.J., ROQUE A.C.F., SANCHEZ GOÑI M.F., SIERRO SÁNCHEZ F.J., SINGH A.D., SLOSS C.R.,

STOW D.A.V., TAKASHIMIZU Y., TZANOVA A., VOELKER A., XUAN C. & WILLIAMS T., 2015 - A reference time scale for Site U1385 (Shackleton Site) on the SW Iberian Margin. *Global and Planetary Change* **133**, 49-64.

HOERLING M., EISCHEID J., PERLWITZ J., QUAN X.W., ZHANG T. & PEGION P., 2012 - On the Increased Frequency of Mediterranean Drought. *Journal of Climate*, **25**, 2146–2161.

HOOGHIEMSTRA H., AGWU C.O.C. & BEUG H.-J., 1986 - Pollen and spore distribution in recent marine sediments: a record of NW-African seasonnal wind patterns and vegetation belts. *Meteor Forsch.-Ergebnisse*, **40**, 87-135.

HOOGHIEMSTRA H., STALLING H., AGWU C.O.C. & DUPONT L.M., 1992 - Vegetational and climatic changes at the northern fringe of the Sahara 250,000-5000 years BP: evidence from 4 marine pollen records located between Portugal and the Canary Islands. *Review of Palaeobotany and Palynology*, **74**, 1-53.

KNUTTI R., FLUCKIGER J., STOCKER T.F. & TIMMERMANN A., 2004 - Strong hemispheric coupling of glacial climate through freshwater discharge and ocean circulation. *Nature* **430**, 851-856.

KORENEVA E.V., 1971 - Spores and pollen in Mediterranean bottom sediments. *In*: Funnel, B.M., Reidel, R.M. (Eds.), *The micropaleontology of Oceans*, Cambridge, 361-371.

KOUTSODENDRIS A., PROSS J., MÜLLER U.C., BRAUER A., FLETCHER W.J., KÜHL N., KIRILOVA E., VERHAGEN F.T.M., LÜCKE A. & LOTTER A.F., 2012 - A short-term climate oscillation during the Holsteinian interglacial (MIS 11c): An analogy to the 8.2ka climatic event? *Global and Planetary Change* **92-93**, 224-235.

LANG N. & WOLFF E.W., 2011 - Interglacial and glacial variability from the last 800 ka in marine, ice and terrestrial archives. *Climate of the Past*, **7** (2), 361-380.

LEVAVASSEUR G., VRAC M., ROCHE D.M. & PAILLARD D., 2012 - Statistical modelling of a new global potential vegetation distribution. *Environmental Research Letters*, **7** (4), 044019.

LOULERGUE L., SCHILT A., SPAHNI R., MASSON-DELMOTTE V., BLUNIER T., LEMIEUX B., BARNOLA J.M., RAYNAUD D., STOCKER T.F. & CHAPPELLAZ J., 2008 - Orbital and millennial-scale features of atmospheric CH4 over the past 800,000 years. *Nature* **453** (7193), 383-386.

LOUTRE M.F. & BERGER A., 2000 - Future climatic changes: Are we entering an exceptionally long interglacial? *Climatic Change*, **46** (1-2), 61-90.

LÜTHI D., LE FLOCH M., BEREITER B., BLUNIER T., BARNOLA J.M., SIEGENTHALER U., RAYNAUD D., JOUZEL J., FISCHER H., KAWAMURA K. & STOCKER T.F., 2008 - High-resolution carbon dioxide concentration record 650,000-800,000 years before present. *Nature* **453** (7193), 379-382.

LYNCH-STIEGLITZ J., 2017 - The Atlantic Meridional Overturning Circulation and Abrupt Climate Change. *Annual Review of Marine Science*, **9** (1), 83-104.

MARTRAT B., GRIMALT J.O., SHACKLETON N.J., DE ABREU L., HUTTERLI M.A. & STOCKER T.F., 2007 - Four climate cycles of recurring deep and surface water destabilizations on the Iberian margin. *Science*, **317** (5837), 502-507, doi: 510.1126/science.1139994.

MASSON-DELMOTTE V., STENNI B., POL K., BRACONNOT P., CATTANI O., FALOURD S., KAGEYAMA M., JOUZEL J., LANDAIS A., MINSTER B., BARNOLA J.M., CHAPPELLAZ J., KRINNER G., JOHNSEN S., RÖTHLISBERGER R., HANSEN J., MIKOLAJEWICZ U. & OTTO-BLIESNER B., 2010 - EPICA Dome C record of glacial and interglacial intensities. *Quaternary Science Reviews* **29** (1-2), 113-128.

MCMANUS J.F., OPPO D.W. & CULLEN J.L., 1999 - A 0.5-million-year record of millennial-scale climate variability in the North Atlantic. *Science*, **283**, 971-975.

MELLES M., BRIGHAM-GRETTE J., MINYUK P.S., NOWACZYK N.R., WENNRICH V., DECONTO R.M., ANDERSON P.M., ANDREEV A.A., COLETTI A., COOK T.L., HALTIA-HOVI E., KUKKONEN M., LOZHKIN A.V., ROSÉN P., TARASOV P., VOGEL H. & WAGNER B., 2012 - 2.8 Million Years of Arctic Climate Change from Lake El'gygytgyn, NE Russia. *Science*, **337** (6092), 315-320.

MUDIE P.J. & MCCARTHY F.M.G., 2006 - Marine palynology: potentials for onshore–offshore correlation of Pleistocene–Holocene records. *Transactions of the Royal Society of South Africa*, **61** (2), 139-157.

NAUGHTON F., SANCHEZ GOÑI M.F., DESPRAT S., TURON J.L., DUPRAT J., MALAIZÉ B., JOLI C., CORTIJO E., DRAGO T. & FREITAS M.C., 2007 - Present-day and past (last 25 000 years) marine pollen signal off western Iberia. *Marine Micropaleontology* **62** (2), 91-114.

NAUGHTON F., SÁNCHEZ GOÑI M.F., KAGEYAMA M., BARD E., DUPRAT J., CORTIJO E., DESPRAT S., MALAIZÉ B., JOLY C., ROSTEK F. & TURON J.L., 2009 - Wet to dry climatic trend in north-western Iberia within Heinrich events. *Earth and Planetary Science Letters* **284** (3-4), 329-342.

NORTH GREENLAND ICE CORE PROJECT (NGRIP) MEMBERS, 2004 - High-resolution record of northern hemisphere climate extending into the last interglacial period. *Nature* **431**, 147-151.

OKUDA M., YASUDA Y. & SETOGUCHI T., 2001 - Middle to Late Pleistocene vegetation history and climatic changes at Lake Kopais, Southeast Greece. *Boreas*, **30**, 73-82.

OLIVEIRA D., DESPRAT S., RODRIGUES T., NAUGHTON F., HODELL D., TRIGO R., RUFINO M., LOPES C., ABRANTES F. & SÁNCHEZ GOÑI M.F., 2016 - The complexity of millennial-scale variability in southwestern Europe during MIS 11. *Quaternary Research (United States)*, **86** (3), 373-387.

OPPO D.W., MCMANUS J.F. & CULLEN J.L., 1998 - Abrupt climate events 500,000 to 340,000 years ago: evidence from subpolar North Atlantic sediments. *Science*, **279**, 1335-1338.

OPPO D.W., MCMANUS J.F. & CULLEN J.L., 2006 - Evolution and demise of the Last Interglacial warmth in the subpolar North Atlantic. *Quaternary Science Reviews*, **25** (23-24), 3268-3277.

PAST INTERGLACIALS WORKING GROUP OF PAGES, 2016 - Interglacials of the last 800,000 years. *Reviews of Geophysics* **54** (1), 162-219.

PETIT J.R., 1999 - Climate and atmospheric history of the past 420,000 years from the Vostok ice core, Antarctica. *Nature*, **399**, 429-436.

POL K., DEBRET M., MASSON-DELMOTTE V., CAPRON E., CATTANI O., DREYFUS G., FALOURD S., JOHNSEN S., JOUZEL J., LANDAIS A., MINSTER B. & STENNI B., 2011 - Links between MIS 11 millennial to sub-millennial climate variability and long term trends as revealed by new high resolution EPICA Dome C deuterium data - A comparison with the Holocene. *Climate of the Past*, **7** (2), 437-450.

POL K., MASSON-DELMOTTE V., CATTANI O., DEBRET M., FALOURD S., JOUZEL J., LANDAIS A., MINSTER B., MUDELSEE M., SCHULZ M. & STENNI B., 2014 - Climate variability features of the last interglacial in the East Antarctic EPICA Dome C ice core. *Geophysical Research Letters* **41** (11), 4004-4012.

POPOVSKA C. & BONACCI O., 2007 - Basic data on the hydrology of Lakes Ohrid and Prespa. *Hydrological Processes*, **21** (5), 658-664.

RAYMO M.E. & MITROVICA J.X., 2012 - Collapse of polar ice sheets during the stage 11 interglacial. *Nature* **483** (7390), 453-456.

REILLE M., DE BEAULIEU J.-L., SVOBODOVA V., ANDRIEU-PONEL V. & GOEURY C., 2000 - Pollen analytical biostratigraphy of the last five climatic cycles from a long continental sequence from the Velay region (Massif Central, France). *Journal of Quaternary Science*, **15** (7), 665-685.

REYES A.V., CARLSON A.E., BEARD B.L., HATFIELD R.G., STONER J.S., WINSOR K., WELKE B. & ULLMAN D.J., 2014 - South Greenland ice-sheet collapse during Marine Isotope Stage[thinsp]11. *Nature* **510** (7506), 525-528.

RUDDIMAN W.F. & MCINTYRE A., 1984 - Ice-age thermal response and climatic role of the surface Atlantic Ocean, 40oN to 63oN. *Geological Society of America Bulletin*, **95** (4), 381-396.

SAARONI H., BITAN A., ALPERT P. & ZIV B., 1996 - Continental polar outbreaks into the levant and eastern mediterranean. *International Journal of Climatology*, **16** (10), 1175-1191.

SADORI L., KOUTSODENDRIS A., PANAGIOTOPOULOS K., MASI A., BERTINI A., COMBOURIEU-NEBOUT N., FRANCKE A., KOULI K., JOANNIN S., MERCURI A.M., PEYRON O., TORRI P., WAGNER B., ZANCHETTA G., SINOPOLI G. & DONDERS T.H., 2016 - Pollen-based paleoenvironmental and paleoclimatic change at Lake Ohrid (south-eastern Europe) during the past 500 ka. *Biogeosciences*, **13** (5), 1423-1437.

SÁNCHEZ GOÑI M.F., EYNAUD F., TURON J.-L. & SHACKLETON N.J., 1999 - High resolution palynological record off the Iberian margin: direct land-sea correlation for the Last Interglacial complex. *Earth and Planetary Science Letters*, **171**, 123-137.

SÁNCHEZ GOÑI M.F., LOUTRE M.F., CRUCIFIX M., PEYRON O., SANTOS L., DUPRAT J., MALAIZÉ B., TURON J.L. & PEYPOUQUET J.P., 2005 - Increasing vegetation and climate gradient in Western Europe over the Last Glacial Inception (122-110 ka): Data-model comparison. *Earth and Planetary Science Letters* **231** (1-2), 111-130.

SÁNCHEZ GOÑI M.F., LANDAIS A., FLETCHER W.J., NAUGHTON F., DESPRAT S. & DUPRAT J., 2008 - Contrasting impacts of Dansgaard-Oeschger events over a western European latitudinal transect modulated by orbital parameters. *Quaternary Science Reviews* **27** (11-12), 1136-1151.

SÁNCHEZ GOÑI M.F., RODRIGUES T., HODELL D.A., POLANCO-MARTÍNEZ J.M., ALONSO-GARCÍA M., HERNÁNDEZ-ALMEIDA I., DESPRAT S. & FERRETTI P., 2016 - Tropically-driven climate shifts in southwestern Europe during MIS 19, a low eccentricity interglacial. *Earth and Planetary Science Letters* **448**, 81-93.

SHACKLETON N.J. & OPDYKE N.D., 1973 - Oxygen isotope and paleomagnetic stratigraphy of Equatorial Pacific core V28-238: oxygen isotope temperatures and ice volumes on a 10^5 year and 10^6 year scale. *Quaternary Research*, **3**, 39-55.

SIDDALL M., ROHLING E.J., ALMOGI-LABIN A., HEMLEBEN C., MEISCHNER D., SCHMELZER I. & SMEED D.A., 2003 - Sea-level fluctuations during the last glacial cycle. *Nature*, **423** (6942), 853-858.

SIEGENTHALER U., STOCKER T.F., MONNIN E., LÜTHI D., SCHWANDER J., STAUFFER B., RAYNAUD D., BARNOLA J.M., FISCHER H., MASSON-DELMOTTE V. & JOUZEL J., 2005 - Atmospheric science: Stable carbon cycle-climate relationship during the late pleistocene. *Science*, **310** (5752), 1313-1317.

SPAHNI R., CHAPPELLAZ J., STOCKER T.F., LOULERGUE L., HAUSAMMANN G., KAWAMURA K., FLÜCKIGER J., SCHWANDER J., RAYNAUD D. & JOUZEL J., 2005 - Atmospheric methane and nitrous oxide of the late Pleistocene from Antarctic ice cores. *Science*, **310**, 1317-1321.

TURON J.-L., 1984a - *Le palynoplancton dans l'environnement actuel de l'Atlantique nord-oriental. Evolution climatique et hydrologique depuis le dernier maximum glaciaire*. Université de Bordeaux I, Bordeaux.

TURON J.-L., 1984b - Direct land/sea correlations in the last interglacial complex. *Nature*, **309**, 673-676.

TZEDAKIS P.C., 1993 - Long-term tree populations in northwest Greece through multiple Quaternary cycles. *Nature*, **364**, 437-440.

TZEDAKIS P.C., ANDRIEU V., DE BEAULIEU J.L., CROWHURST S., FOLLIERI M., HOOGHIEMSTRA H., MAGRI D., REILLE M., SADORI L., SHACKLETON N.J. & WIJMSTRA T.A., 1997 - Comparison of terrestrial and marine records of changing climate of the last 500,000 years. *Earth and Planetary Science Letters* **150** (1-2), 171-176.

TZEDAKIS P.C., ROUCOUX K.H., DE ABREU L. & SHACKLETON N.J., 2004 - The duration of forest stages in southern Europe and interglacial climate variability. *Science*, **306** (5705), 2231-2235.

TZEDAKIS P.C., HOOGHIEMSTRA H. & PÄLIKE H., 2006 - The last 1.35 million years at Tenaghi Philippon: revised chronostratigraphy and long-term vegetation trends. *Quaternary Science Reviews* **25** (23-24), 3416-3430.

TZEDAKIS P.C., RAYNAUD D., MCMANUS J.F., BERGER A., BROVKIN V. & KIEFER T., 2009 - Interglacial diversity. *Nature Geoscience*, **2** (11), 751-755.

XOPLAKI E., GONZÁLEZ-ROUCO J.F., LUTERBACHER J. & WANNER H., 2003 - Mediterranean summer air temperature variability and its connection to the large-scale atmospheric circulation and SSTs. *Climate dynamics* **20** (7-8), 723-739.

YIN Q.Z. & BERGER A., 2012 - Individual contribution of insolation and CO2 to the interglacial climates of the past 800,000 years. *Climate dynamics* **38** (3-4), 709-724.

YIN Q.Z. & BERGER A., 2015 - Interglacial analogues of the Holocene and its natural near future. *Quaternary Science Reviews* **120**, 28-46.